Queensland Government
Department of Natural Resources and Mines
Department of Emergency Services
Environmental Protection Agency

Queensland Climate Change and Community Vulnerability to Tropical Cyclones

OCEAN HAZARDS ASSESSMENT

- Stage 1

March 2001

SEA Systems Engineering Australia Pty Ltd

Bureau of Meteorology

JCU James Cook University

SEA Doc. No. J0004-PR001C

Department of Natural Resources and Mines, Queensland
Department of Emergency Services, Queensland
Environmental Protection Agency, Queensland
Bureau of Meteorology, Queensland
Systems Engineering Australia Pty Ltd, Queensland

QNRM01019
ISBN: 0 7345 1765 3

General Disclaimer

Front cover images have been provided courtesy of the Department of Emergency Services, from the Brisbane Storm Chasers Homepage and the Queensland State Library

Enquiries should be addressed to:

Steven Crimp
Department of Natural Resources and Mines
80 Meiers Road, Indooroopilly
Brisbane, QLD 4068

Contents

List of Tables

List of Figures

List of Contributors

Systems Engineering Australia Pty Ltd
7 Mercury Ct Bridgeman Downs Qld 4035
ACN 073 544 439

Bruce Harper BE PhD FIEAust CPEng RPEQ
Director
Editor
P*rincipal author all Chapters except 6, 7 and 8.2 to 8.4.*

James Cook University
Department of Civil and Environmental Engineering

Thomas Hardy BS MS PhD
Assoc. Prof. and Principal Academic Adviser
Director, Marine Modelling Unit
Chapters 6, part 9 and 11.

Luciano Mason BE MIEAust
Research Engineer, Marine Modelling Unit
Chapters 6, part 10 and 11, Appendix D and F.

James Cook University
Department of Mathematics and Statistics

Lance Bode BSc PhD
Senior Lecturer
Oceanographer, Marine Modelling Unit
Chapter 6, Appendix D.

Adelaide University
Faculty of Engineering, Computer and Mathematical Sciences

Ian Young BE MEngSc PhD FIEAust
Professor and Executive Dean
Chapter 7.

The University of Queensland
Department of Civil Engineering

Peter Nielsen ME PhD DE
Associate Professor
Chapter 8 sections 8.2 to 8.4.

Acknowledgements

This project was funded through a Greenhouse Special Treasury Initiative managed by the Queensland Department of Natural Resources and Mines. Project management was provided by the Bureau of Meteorology Queensland Regional Office (Jim Davidson, Supervising Meteorologist) assisted by a Project Management Committee with representatives from the Department of Natural Resources and Mines (Steven Crimp), the Department of Emergency Services (Leslie Galloway) and the Environmental Protection Agency (David Robinson and Michael Allen).

The cooperation of Bureau of Meteorology staff in the Queensland Regional Office is gratefully acknowledged, especially Jim Davidson, Jeff Callaghan, Michael Berechree, Sue Oates and Matt Saunderson. Jeff Kepert (Bureau of Meteorology Research Centre) provided comment on the identified issue of asymmetry of tropical cyclone windfields. In addition, John Broadbent (Queensland Transport) greatly assisted through the supply of recorded water level data. Michael Gourlay and Jennifer Hacker (University of Queensland) assisted through provision of historical information regarding the *Mackay 1918* storm. Ken Granger (AGSO) provided information on ground elevations in the Mackay area as well as a diagram of the flooded area during the *Mackay 1918* event. Peter Croker (Caloundra) assisted in the locating of the family home "Bona Vista" in Mackay during 1918 and provided extracts from a letter written by his mother who described the cyclone effects at the Eimeo Hotel. David Robinson (EPA) provided Department of Harbours and Marine archive material in regard to tropical cyclone *Ted* in 1976. Jason McConochie (James Cook University) assisted in developing the numerical model documentation and Wesley Bailey assisted in model domain generation.

The Project Management Committee particularly wishes to acknowledge the significant contribution by Rex Falls, former Regional Director of the Bureau of Meteorology, Queensland, whose efforts led to the establishment of the project.

B. Harper
T. Hardy

1. Executive Summary

The Bureau of Meteorology, in conjunction with a number of Queensland Government agencies and with financial support from the Greenhouse Special Treasury Initiative, commissioned the present study to assess the magnitude of the ocean threat from tropical cyclones in Queensland. The overall project is intended to update and extend the present understanding of the threat of storm tide inundation in Queensland on a state-wide scale including the effects of storm wave conditions in selected areas, and estimates of potential Greenhouse impacts.

The overall project scope is outlined in Appendix A, while the present report addresses only Stage 1 of the project, which is limited to:

a) A review of technical requirements in order to further develop the project;
- Reviewing current knowledge and making technical recommendations for the overall project.
- Appraising and adapting the James Cook University (JCU) storm surge model (MMUSURGE) software for the purposes of the project.

b) State-wide numerical simulations of tropical cyclone storm surge;
- Installing the MMUSURGE storm surge modelling software on the Bureau's computer system in Brisbane.
- Assisting the Bureau in undertaking storm surge modelling for the Queensland coast.

The specific work items under Stage 1 were:

Part A: Review of Project Technical Requirements.
A-1 Assessment of Greenhouse climate change and sea level rise.
A-2 Review the technical requirements for numerical modelling of cyclone storm surge.
A-3 Review the technical requirements for numerical modelling of cyclone wind waves.
A-4 Database design.
A-5 Review the technical requirements for an operational MEOWs system.
A-6 Dissemination of results.

Part B: Numerical Modelling of Tropical Cyclone Storm Surge.
B-1 Establishment of the storm surge modelling system and database.
B-2 Production of numerical simulation data.

The above scope items have been addressed within a developmental context which aims to provide a complete overview of the technical needs for assessment of ocean hazards for tropical cyclones in Queensland, taking account of climate change and community vulnerability issues. Each report chapter provides its own specific recommendations, which are brought together in **Chapter 14** as a series of major recommendations, re-framed to address the original workscope items as listed above.

It is concluded that much of the work requiring to be done under subsequent stages of the project can be achieved with existing tools and methodologies. There are some items however which will greatly benefit from modest but immediate research and development efforts.

2. Tropical Cyclone Induced Ocean Hazards in Queensland

This study is concerned with the risk assessment of ocean hazards associated with tropical cyclones throughout Queensland. This chapter provides a brief contextual overview of the problem and introduces the various hazard elements, which are addressed more completely in subsequent chapters.

2.1 Overview

Figure 2.1 provides a schematic overview of the inter-relationships between the tropical cyclone hazard and its impacts, firstly in terms of directly-induced hazards in the ocean environment and secondly in terms of indirect impacts on community, infrastructure and the environment. Some of the potential tactical and strategic outcomes from these relationships are indicated and all these aspects are considered in the development of the report sections which follow. These include:

Tropical Cyclone Climatology

Essential knowledge of the incidence and behaviour of tropical cyclones affecting the Queensland region, intrinsically related to:

- Climatic variability
- Climate change

Issues include:

- Data quality
- Parameterisation
- Statistical descriptions
- Current knowledge

Tropical Cyclone Forcing

The link between the tropical cyclone and its impacts in the ocean environment:

- Extreme winds
- Extreme waves
- Extreme currents
- Storm surge

Issues include:

- Air-sea interaction
- Model parameterisation
- Accuracy and verification

Tropical Cyclone Storm Tide

The culmination of impacts from a landfalling tropical cyclone, including:

- Predictive tools
- Long term statistics

Issues Include:

- Coastal bathymetry
- Surge - tide interaction

- Localised wave effects
- Inundation
- Statistical representation

Vulnerability

The various elements at risk from the tropical cyclone hazard:

- Community
- Infrastructure
- Environment

Issues include:

- Predictive tools
- Communication
- Logistics and organisation
- Planning and legislation

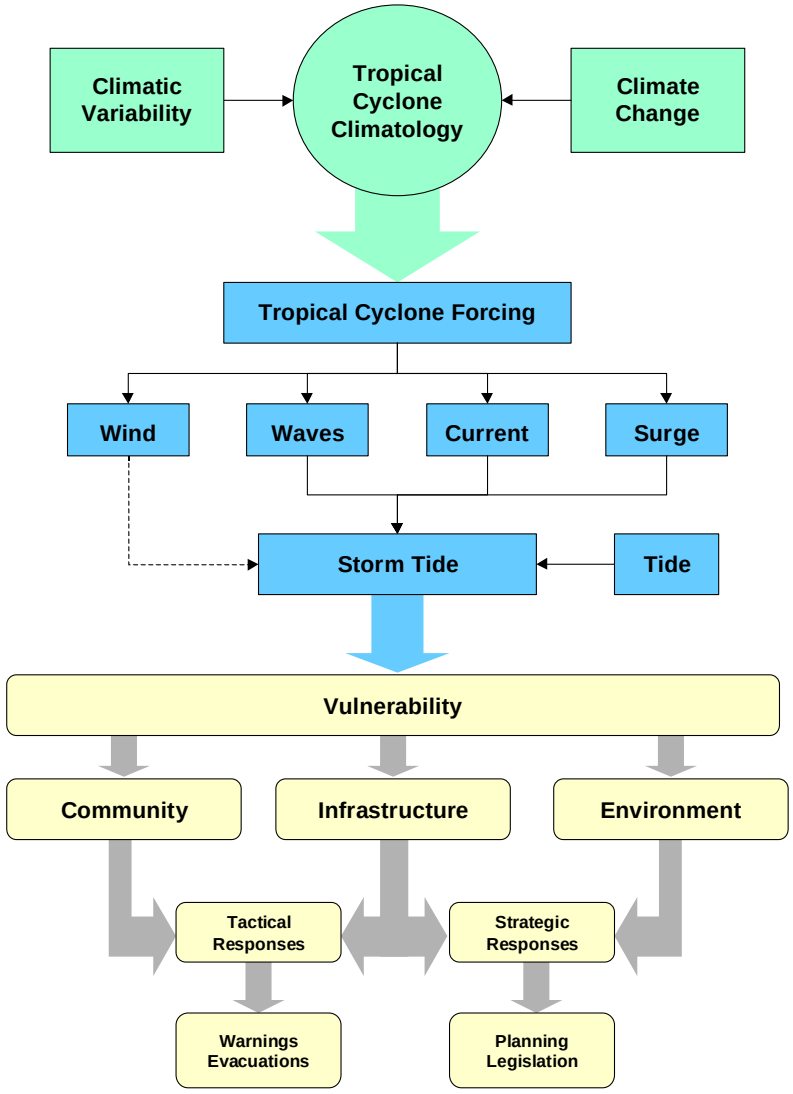

Figure 2.1 The tropical cyclone storm tide hazard assessment process.

2.2 Tropical Cyclones

Tropical cyclones are large scale and potentially very severe low pressure weather systems that affect the Queensland region typically between November and April, with an average incidence of 5.2 storms per year since 1959/60 (refer Chapter 3).

The strict definition of a tropical cyclone (WMO, 1997) is:

> *A non-frontal cyclone of synoptic scale developing over tropical waters and having a definite organized wind circulation with average wind of 34 knots (63 km h^{-1}) or more surrounding the centre.*

The tropical cyclone is an intense tropical low pressure weather system where, in the southern hemisphere, winds circulate clockwise around the centre. In Australia, such systems are upgraded to *severe* tropical cyclone status (referred to as hurricanes or typhoons in some countries) when average, or sustained, surface wind speeds exceed 120 kmh^{-1}. The accompanying shorter-period destructive wind *gusts* are often 50 per cent or more higher than the *sustained* winds.

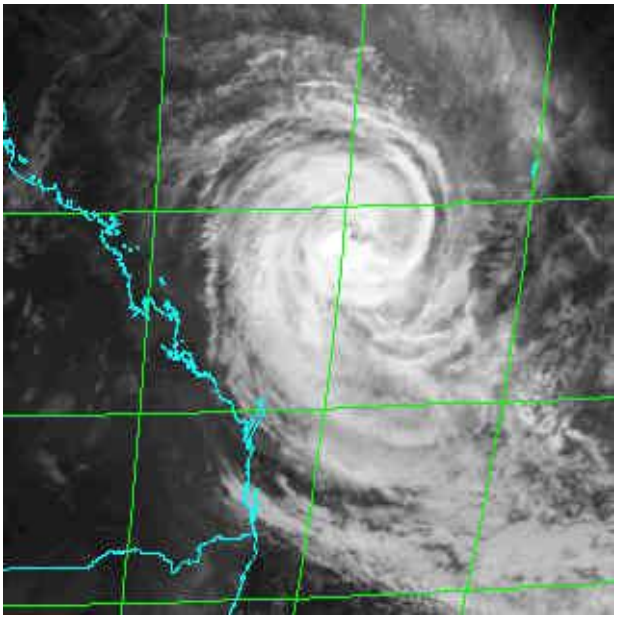

Figure 2.2 Tropical cyclone Fran approaching the Queensland coast in March 1992.

There are three components of a tropical cyclone that combine to make up the total cyclone hazard - strong winds, intense rainfall and induced ocean effects including extreme waves, currents, storm surge and resulting storm tide. The destructive force of cyclones is usually expressed in terms of the strongest wind *gusts* experienced. Maximum wind gust is related to the central pressure and structure of the system, whilst extreme waves and storm surge, are linked more closely to the combination of the *mean* surface winds, central pressure and regional bathymetry.

The Bureau of Meteorology (BoM 1999) uses the five-category system shown in Table 2.1 for classifying tropical cyclone intensity in Australia. *Severe* cyclones are those of Category 3 and above.

Table 2.1 Australian tropical cyclone category scale.

Category	Maximum Wind Gust ($km\ h^{-1}$)	Potential Damage
1	<125	minor
2	125-170	moderate
3	170-225	major
4	225-280	devastating
5	>280	extreme

Tropical cyclone development is complex, but various authors (e.g. WMO 1995), have identified the general conditions necessary for their formation and intensification. Requisite dynamic parameters include low-level *relative vorticity*, exceedence of a threshold value of the *Coriolis* effect of the earth's rotation, and minimal *vertical shear* of the horizontal wind between the upper and the lower troposphere. Ideal thermodynamic parameters include *sea surface temperature* (SST) above 26°C through the *oceanic mixed layer* to a depth of about 60 m, *moist instability* between the surface and the 500 hPa level (approximately 5600 m above sea level), high values of middle tropospheric *relative humidity*, and warm upper troposphere air.

The main structural features of a severe tropical cyclone at the earth's surface are the eye, the eye wall and the spiral rainbands (refer satellite image in Figure 2.2). The eye is the area at the centre of the cyclone at which the surface atmospheric pressure is lowest. It is typically 20 to 50 km in diameter, skies are often clear and winds are light. The eye wall is an area of cumulonimbus clouds, which swirls around the eye. Recent studies (e.g. Wakimoto and Black 1994) suggest that unusually high winds can occur in the vicinity of the eye wall due to instabilities as the cyclone makes landfall. Tornado-like vortices of even more extreme winds may also occur associated with the eye wall and outer rain bands. The rain bands spiral inwards towards the eye and can extend over 1000 km or more in diameter. The heaviest rainfall and the strongest winds, however, are usually associated with the eye wall.

For any given central pressure, the spatial size of individual tropical cyclones can vary enormously. Generally, smaller cyclones occur at lower latitudes and larger cyclones at higher latitudes but there are many exceptions. For example, because it is difficult for a cyclone to form south of 25ºS in the Queensland region, the vast majority affecting south-east Queensland have travelled from further north and are likely to be either fully *mature*, undergoing decay or tending *extra-tropical*. In those circumstances, small cyclones are relatively rare. Large cyclones can have impacts far from their track, especially on waves and storm tide. For example, *David* crossed the coast near Yeppoon in 1976 and caused significant coastal impacts in southeastern Queensland.

Cyclonic winds circulate clockwise in the Southern Hemisphere. The windfield within a moving cyclone, however, is generally asymmetric so that, in the Southern Hemisphere, winds are typically stronger to the left of the direction of motion of the system (the 'track'). This is because on the left-hand side the direction of cyclone movement and circulation tends to act together; on the right-hand side, they are opposed. During a coast crossing in the

Southern Hemisphere, the cyclonic wind direction is onshore to the left of the eye (seen from the cyclone) and offshore to the right.

Given specifically favourable conditions, tropical cyclones can continue to intensify until they are efficiently utilising all of the available energy from the immediate atmospheric and oceanic sources. This *maximum potential intensity* (MPI) is a function of the climatology of regional SST and atmospheric temperature and humidity profiles. When applying a thermodynamic MPI model for the Queensland coast (Holland 1997, *pers. comm.*), indicative values for the MPI increase northwards from about 940 hPa near Brisbane to 895 hPa for regions north of Mackay. Thankfully, it is rare for any cyclone to reach its MPI because environmental conditions often act to limit intensities in the Queensland region.

Chapter 3 examines the climatology of tropical cyclones in Queensland while Chapter 5 discusses methods for modelling their effects on the ocean and nearshore environment.

2.3 Extreme Waves

Ocean waves are generated as a result of the transfer of momentum from the wind to the sea. The air-sea energy transfer is a complex function of the near-surface wind profile, the turbulence of the wind and the vector difference between wind and wave velocities. The growth of wave height is most rapid for higher wave frequencies (shorter periods or wavelengths) and when the wind speed matches the wave speed. This latter effect means that any existing waves, which have a propagation speed close to the wind speed, will absorb the energy very effectively and quickly grow in height. As the wave field grows, complex wave-wave mechanisms then act to transfer the energy derived from the wind towards lower frequency (higher period or longer wavelength) components.

Combined with the variability of wind strength and direction over an area, these wave growth mechanisms result in the complex seastates, which subsequently impact the coastline. If a constant wind speed persists for long enough, the wave growth process becomes self-limiting across the range of wave frequencies because wave breaking (e.g. white caps) prevents the sea from absorbing any more energy at that specific transfer frequency. This equilibrium condition is known as a *fully-arisen* or *fully-developed* sea and most commonly occurs under broad frontal storm conditions in open ocean environments at higher latitudes. In tropical waters, this condition may also occur during monsoons or periods of persistent trade winds. Fully-developed seas are rarer close to the centre of tropical cyclones because of the constantly varying wind speed and direction which accompanies these smaller scale but severe weather events.

In the nearshore environment, the local coastal topography limits the available *fetch* (or distance acted on by the wind) to generate waves from various directions. For many parts of the eastern coast of Queensland north of Mackay, wave growth is essentially *fetch-limited* by the presence of the Great Barrier Reef, various island chains and large sand shoals. South from Mackay the influence of the reef decreases as the available fetch increases and fully-developed seas are often associated with strong SE wind conditions. In this situation, the wave height growth is termed *duration-limited* because it depends only on the time over which the wind acts. Large, slow moving tropical cyclones, particularly in association with high-pressure ridge effects to their south, can create such conditions over extensive regions of the southern Queensland coast. In the Gulf of Carpentaria, the region is essentially land-

bounded but the available fetch under tropical cyclone conditions can be quite large and extreme waves can result.

Individual ocean waves will propagate through and away from the area of wind generation at speeds dependent upon their wavelength and the local depth and at directions set by the mean angle of the wind. Propagation continues subject to the influence of bottom friction or the effects of an opposing wind. Waves that are still subject to growth by the wind will tend to be of relatively shorter periods to those that have travelled away from the area of generation. The former characteristic is due to the wave growth mechanism; the latter is due to the subsequent wave-wave interaction. Traditionally the term *sea* is given to the shorter period wave and *swell* to the longer period wave. These two basic wave components commonly exist together, the swell having propagated from a remote wave generating weather system, the sea being generated locally, relative to the swell component. Because of these differing sources, the mean direction of the two components is often also different.

Because wave speed depends on depth of water, any wave which approaches contours of changing depth at an angle will experience small changes in speed along its crest. The outcome of these small changes is that the crest will be seen to bend toward alignment with the bed contours. This process is termed *refraction* and has the potential to either concentrate wave energy at specific locations along the coast or to diffuse energy, depending on the seabed characteristics. In classic terms, embayments tend to experience *divergence* of energy whereas headlands experience *convergence*. Refraction can also be caused by the effects of currents. Accompanying refraction is *shoaling* which results in a change in the height of the wave relative to its original condition because of either convergence or divergence of energy having occurred relative to the *deepwater* condition. *Diffraction* is an additional process whereby energy is transferred laterally along a wave crest after experiencing a disturbance or impediment to its process. Typically, this occurs when waves encounter manmade structures such as breakwaters but diffraction can also occur due to interaction with natural features. Diffraction is the reason why, even in water of constant depth, waves will "bend" around behind a barrier and may produce complex wave interference patterns within harbours, between breakwater entrances or behind islands or reefs.

As a wave enters increasingly shallow water it will eventually reach a point of gravitational instability and wave breaking will occur. This is the point where the water particle velocity at the wave crest begins to exceed the wave speed. Wave breaking characteristics are typically classified as *spilling* (mild slopes), *plunging* (medium slopes) or *surging* (steep slopes). During the wave shoaling and breaking processes, the wave *potential energy* and *kinetic energy* is redistributed in response to the retarding effects of the shallow coastal waters. Ultimately much of the energy of the wave is dissipated as *turbulence* and *heat* during the breaking process. However, some of the energy is transferred into a forward momentum within the surf zone. This results in a quasi-steady superelevation of the local water level above the still water level that would otherwise occur in the absence of any waves. This phenomenon is termed *wave setup*. Great Barrier Reef cays and atolls can be especially susceptible to wave setup effects.

In addition to wave setup, any residual kinetic energy of waves is manifested as vertical *runup* of the upper beach face. This allows some wave energy to attack at higher levels than just implied through the setup level alone. Since setup and runup are essentially part of the same energy dissipation process, it follows that their influences are typically complementary. For example, very flat beaches will experience the majority of the energy dissipation as setup

while very steep beaches experience higher levels of runup. The absolute vertical level of runup though will typically exceed that of setup and allow erosion of the upper beach or possible dune overtopping to occur. The time for which the sensitive portion of the beach is exposed to severe runup is therefore critical in determining the degree of damage that might result.

Chapter 7 discusses methods for estimating the growth and propagation of extreme ocean waves while Chapter 9 specifically addresses nearshore processes and estimating wave setup and runup.

2.4 Storm Surge

All tropical cyclones on or near the coast are capable of producing a *storm surge*, which can increase coastal water levels for periods of several hours and significantly affect over 100 km of coastline (Harper 1999). The storm surge (or *meteorological tide*), is an atmospherically forced ocean response caused by extreme surface winds and low surface pressures associated with severe and/or persistent offshore weather systems. In the Queensland context, the tropical cyclone represents the principal threat to life and property in respect of storm surge. Other intense large-scale weather systems are also capable of producing storm surges but the effects of these are less significant and generally limited to the SE corner of the State. An individual storm surge is measured relative to the tide level at the time. It is generated by the combined action of the severe surface winds circulating around the storm centre, generating ocean currents, and the decreased atmospheric pressure, causing a local rise in sea level (the so-called *inverted barometer effect*). When a severe tropical cyclone crosses the coast, the strong currents impinging against the land are normally responsible for the greater proportion of the surge.

The highly organised structure of the near-surface wind field and atmospheric pressure forcing in a tropical cyclone, together with forward motion of the system, results in a complex and transient long-wave motion of the underlying ocean. This motion initially lags behind the moving cyclone (due to the effect of mass inertia) but can then travel large distances along a coastline before gradually decaying over time. Complex coastal bathymetry can significantly interact with the storm surge, affecting both its generation and propagation in a region. The storm surge arrives as a prolonged and generally gradual increase in coastal water levels, followed by a similar decline after the event has passed. A storm surge may influence normal water levels for several hundred or even thousands of kilometres along a coastline but the region of peak and potentially destructive surge levels is associated with the region of maximum wind speeds of the tropical cyclone. Typically, relative to the centre of a tropical cyclone, this is of the order of 50 to 100 km in diameter. Close to the position of the peak surge level, the rate of increase in water height can at times be quite rapid, e.g. several metres in one hour.

The potential magnitude of the surge is affected by many factors - principally the intensity of the tropical cyclone, its size and forward speed. In deep water far from the coast the main contribution to the total surge comes from the inverted barometer effect - which is broadly a mirror image of the cyclone's own surface pressure profile in the underlying ocean. The local magnitude of the rise in elevation is approximately 10 mm per hPa of pressure deficit, relative to the ambient surface pressure far removed from the storm centre. Consequently, a Category 5 cyclone (e.g. 910 hPa) would only produce a maximum pressure-induced surge component of about 1m directly below the eye of the cyclone in deep water, decreasing further away from

the centre. Islands with narrow continental shelves and in deep water away from the coast normally only experience the static effects of the pressure-induced surge. In such situations, breaking wave-induced *setup* may represent the highest component of increased water levels. In shallow waters, the pressure surge component interacts with the bathymetry and coastal forms, and may become dynamically amplified at the coastline to levels approximately twice the offshore levels.

By contrast, the influence of the severe surface wind shear on surge levels is confined largely to the shallower waters of the continental shelf. The wind-induced surge component is depth dependent, increasing with decreasing ocean depth and normally responsible for the greater proportion of surge height at the coastline. Flat, shallow continental shelf regions are therefore much more effective in assisting the generation of large storm surges than are narrow, steep shelf regions. Storm surge magnitude can often be regarded as directly proportional to the cyclone intensity for a given coastal site, over the range of intensities likely to be experienced at that site. It can also be highly site specific due to local factors. The relative horizontal scale (eg. diameter of maximum winds) of the cyclone is also important in determining the length of affected coastline.

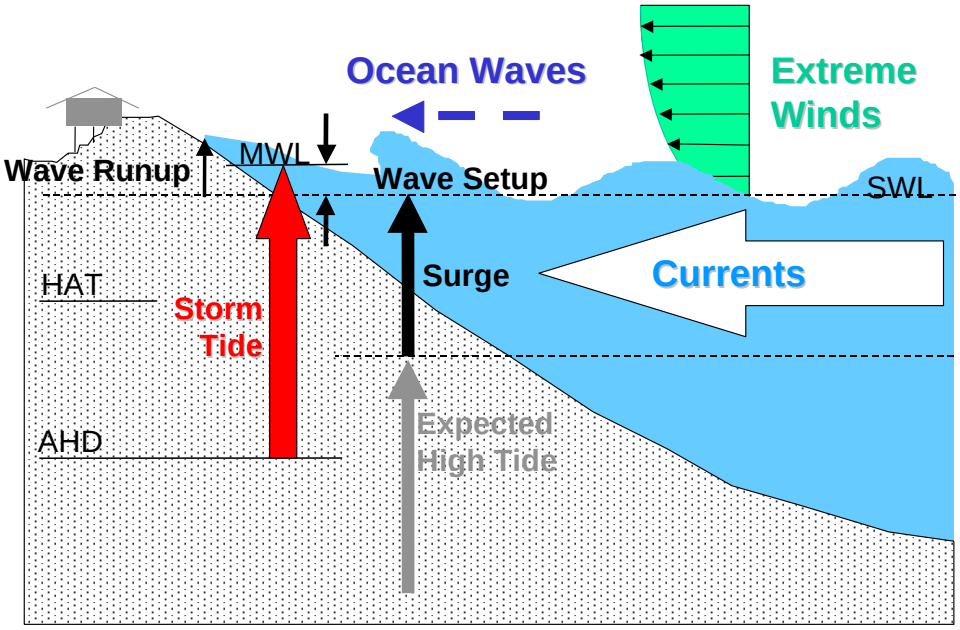

Figure 2.3 Water level components of a storm tide.

In general, the highest surge will be generated for the case of a coast-crossing or *landfalling* cyclone. However, a cyclone that moves nearly parallel to the coast at a distance offshore close to the radius of maximum winds can produce an equivalent surge in some situations. In practice, coastal features such as bays, capes and offshore islands often reduce the influence of the parallel-moving case and increase the influence of the coast-crossing situation. Because of inertial effects in the ocean, it is also difficult for a system that forms close to land to generate a large surge. Speed of forward motion can also affect the peak surge, generally tending to increase with faster moving cyclones. Theoretically, a resonance situation is possible between the forward speed and the surge generation process, but this requires particularly special conditions in time and space. Some *non-linear interaction* between the *astronomical tide* and the generation of the surge can also occur in some areas. This refers to the fact that surge generation is dependent on the water depth. Usually this effect is quite

small and so the linear addition of storm surge levels calculated at *mean sea level (MSL)* and the actual astronomical tide levels can often be assumed when estimating the total *storm tide*.

Chapter 6 presents the mathematical basis for estimating the generation and propagation of storm surge in coastal environments with particular reference to Australian conditions.

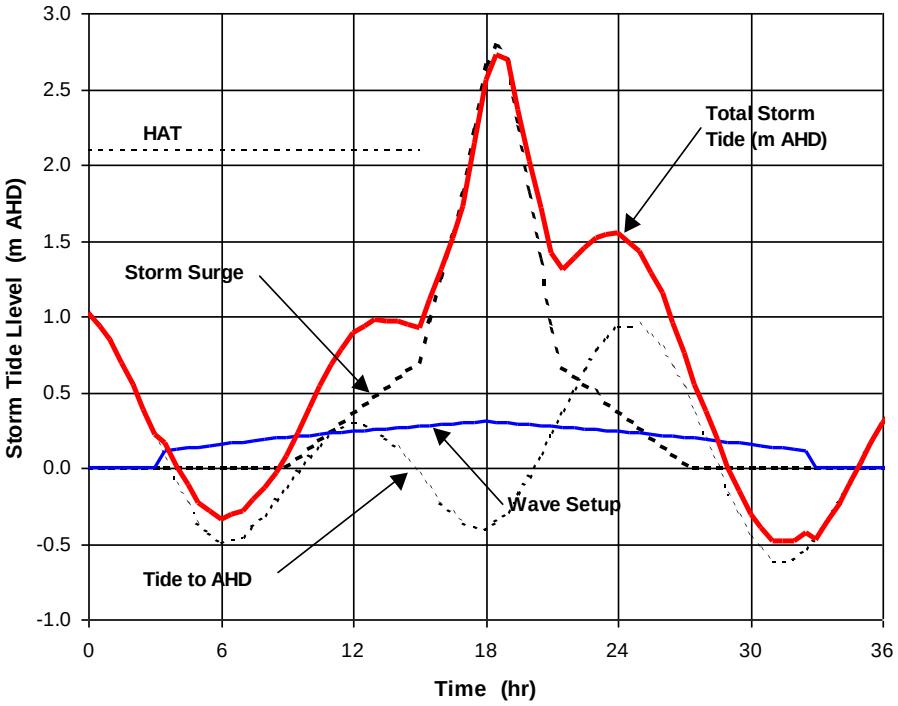

Figure 2.4 Effect of tide, storm surge and wave setup phasing on storm tide level.

2.5 Storm Tide

When the *storm surge* is combined with the *astronomical tide* variation and the *wave setup* contribution at the coast, the absolute combined *mean water level (MWL)* reached is called the *storm tide* level[1]. Because it includes the tide, the *storm tide* level can be referenced to a specific ground contour and is given as an absolute level such as *Australian Height Datum (AHD)*. It is the *storm tide* level which must be accurately predicted and conveyed to emergency managers to enable timely evacuation of low lying areas prior to storm landfall. Loss of life through drowning is the principal community threat caused by the extreme storm tide.

Figure 2.3 summarises the various components which work together to produce an extreme storm tide. Firstly, the *storm surge*, mainly caused by the interaction of the extreme wind-driven currents and the coastline, raises coastal water levels above the normally expected tide at the time - producing the so-called *stillwater level (SWL)*. Meanwhile, extreme wind-generated ocean waves, combinations of swell and local sea, are also driven before the strong winds and ride upon the SWL. As part of the process of wave breaking, a portion of their energy is transferred to vertical *wave setup*, yielding a slightly higher *mean water level*

[1] For completeness, this study considers wave setup as an integral part of the storm tide level, whereas some earlier studies e.g. Harper (1999) treated wave setup as a separate additional component.

(MWL). Additionally, individual waves will run-up sloping beaches to finally expend their forward energy and, when combined with the elevated SWL, this allows them to attack foredunes or nearshore structures to cause considerable erosion or destruction of property.

The principal role of the astronomical tide is then in providing a background modulation in coastal water levels. The relative phasing of the arrival of the storm surge and associated wave setup relative to the tide determines the actual variation in storm tide levels, as illustrated in Figure 2.4. The example shown is similar to the storm tide response during cyclone *Althea* in Townsville in 1971, where the peak surge arrived fortunately close to the time of low tide.

The first critical phase of a storm tide is when the MWL commences to exceed the local *Highest Astronomical Tide (HAT),* which represents the normal landward extent of the sea at any coastal location (Queensland Transport 1999). By this time, depending on the coastal features, it is likely that extensive beach and dune erosion will have occurred due to wave runup effects alone. If the water level rises further, inundation of normally dry land will commence and the storm tide will be capable of causing loss of life through drowning and significant destruction of nearshore buildings and facilities if large ocean swell penetrate the foreshore regions.

Table 2.2, extracted from Harper (1999), provides a summary of some of the more significant storm tide events known to have occurred in Queensland, caused by tropical cyclones. This list should be regarded as indicative only but shows that at least 34 separate surge events occurred during the past 100 years which resulted in storm tide levels reaching above the HAT level. As significant as this record might appear, it is of little value in estimating the long-term hazard of storm tide inundation at any specific part of the coastline. Accordingly, extensive numerical and statistical modelling is required to provide the guidance needed for planning and warning activities.

Chapter 9 addresses techniques for estimating the long-term risk of inundation by storm tide at any specific coastal location and traces the development of various methods.

Chapter 10 demonstrates the current state-of-the-art ability to reproduce (or hindcast) the actual storm tides from a selection of historical cyclones on the Queensland coast using the MMUSURGE modelling system.

Table 2.2 Summary of significant Queensland storm tides.

Date	Place	Event	Reference Central Pressure	Storm Surge	Storm Tide Level	Inundation Above HAT
			hPa	m	m AHD	m
1858	Green Is		?	?	2?	"awash"
04-Mar-1887	Albert R Heads		"cyc"	5.5?	7.8	5.1
08-Jun-1891	Brisbane		?	?	1.8	0.3
19-Feb-1894	Brisbane		"cyc"	0.6	1.6	0.2
26-Jan-1896	Townsville	*Sigma*	"hur"	>2?	4?	2?
05-Mar-1899	Bathurst Bay	*Mahina*	914	13.7?	13?	11?
09-Mar-1903	Cairns	*Leonta*	965<	?	2+?	0.7
27-Jan-1910	Cairns		"hur"	?	2+?	0.7
21-Jan-1918	Mackay		933	3.8	5.5	2
10-Mar-1918	Mission Beach		926	>7?	8?	3.5?
04-Feb-1920	Cairns		988	>1.5	2.5?	0.7?
30-Mar-1923	Albert R Heads	*Douglas Mawson*	974	>3	5?	2.3?
16-Jun-1928	Brisbane		?	?	1.7	0.2
11-Mar-1934	Cape Tribulation		968	>9?	>7?	>6?
17-Mar-1945	Cairns		994	>0.8	?	?
28-Jan-1948	Brisbane		?	0.5	1.8	0.3
23-Feb-1948	Bentinck Is		996	>3.7	4.7?	3.2?
02-Mar-1949	Gladstone		988	>1.2	2.2	0.2
18-Jan-1950	Brisbane		?	0.6	1.8	0.3
21-Feb-1954	Coolangatta		973	>1?	2?	?
03-Feb-1964	Edward River	*Dora*	974	5?	?	?
29-Jan-1967	Moreton Bay	*Dinah*	945	2?	2.8?	1.5?
19-Feb-1971	Inkerman Station	*Fiona*	960	>4?	?	?
24-Dec-1971	Townsville	*Althea*	952	2.9	2.6	0.4
11-Feb-1972	Fraser Island	*Daisy*	959	3?	?	?
07-Feb-1974	Brisbane	*Pam*	965	0.7	1.9	0.4
19-Dec-1976	Albert River	*Ted*	950	4.6?	6.3?	3.6?
31-Dec-1978	Weipa	*Peter*	980	1.2	2.3	0.6
26-Apr-1989	Beachmere	*Charlie*	972	0.6	1.5	0.2
04-Apr-1989	Molongle Creek	*Aivu*	935	3.2?	3.7?	1.7?
16-Mar-1992	Burnett Heads	*Fran*	980	1	2.1	0.2
06-Jan-1996	Gilbert River	*Barry*	950	4.5?	6?	3.4?
09-Mar-1996	Weipa	*Ethel*	980	1.2	3.6	0.3
08-Mar-1997	Cairns	*Justin*	975	0.7	1.9	0.2
27-Feb-2000	Cairns	*Steve*	975	0.99	1.07	-
3-Apr-2000	Townsville	*Tessi*	980	1.05	1.73	-

2.6 References

BoM (1999) Tropical cyclone warning directive (eastern region) 1999-2000. Queensland Regional Office, *Bureau of Meteorology.*

Harper B.A. (1999) Storm tide threat in Queensland: History, prediction and relative risks. Conservation Technical Report No. 10, *Dept of Environment and Heritage,* Jan, ISSN 1037-4701.

Holland G.J. (1997) The maximum potential intensity of tropical cyclones. *J. Atmos. Sci.,* 54, Nov, 2519-2541.

Queensland Transport (1999) The official tide tables and boating safety guide 2000. *Queensland Department of Transport.*

Wakimoto W. and Black P.G. (1994) Damage survey of Hurricane Andrew and its relationship to the eyewall. *Bull. Amer. Met. Soc.,* 75 (2), 189-200.

WMO (1995) Global perspectives on tropical cyclones. TD-No. 693, Tropical Cyclone Programme Report No. TCP-38, *World Meteorological Organization,* Geneva.

WMO (1997) Tropical cyclone operational plan for the South Pacific and South-East Indian Ocean. TD-No. 292, Tropical Cyclone Programme Report No. TCP-24, *World Meteorological Organization,* Geneva.

3. Tropical Cyclone Climatology of Queensland

3.1 Historical Summary of Incidence and Intensity

Recent historical research into the impacts of tropical cyclones affecting the Queensland region has uncovered significant community impacts as early as the mid-1800s (Callaghan 2000). The most significant impact recorded to date is the 1889 "*Mahina*" or "*Bathurst Bay*" cyclone (Whittingham 1958) which destroyed a pearling fleet in Princess Charlotte Bay with the loss of over 300 lives. The 914 hPa central pressure attributed to this event is based on a reading of 27" Hg from a schooner that was almost sunk and, if accurate, represents a record intensity for landfalling cyclones on the Queensland coast. The storm is also reported to have produced a massive storm surge of the order of 12 m (refer Table 2.2 entry), although that is less supportable based on present-day surge estimation techniques. A recent site debris survey (Nott and Hayne, 2000) has also failed to confirm evidence of such a significant surge event and it is concluded for the moment that wave runup may have been a significant contributor to the historical account. Nevertheless, the 1899 cyclone remains as an extreme example of the potential severity of tropical cyclones impacting the Queensland coast.

The official tropical cyclone record maintained in electronic form by the Bureau of Meteorology *National Climate Centre (NCC)* begins in the 1906/07 season. This database derives from climatological summaries by Coleman (1972) and later Lourensz (1977, 1981) with updates of "best track" information from the Regional Offices since that time. An overview of this 94 year official record is given below, summarising cyclone activity within a radius of 1500 km from Mackay, which includes all cyclones that entered the 138ºE to 160ºE jurisdictional area of the Queensland Regional Office[2]. A complete summary of all storm details is included as Appendix B.

Figure 3.1 summarises the historical trends in frequency of occurrence on an annual (or seasonal) basis and also the intensity, based on minimum recorded central pressure. There have been a total of 404 storms recorded in the region since 1906/07. This averages to 4.3 storms per year, but occurrences have varied between a low of 1 and a high of 12 (1956/57) in any one season. The 5-year running mean occurrence is also indicated on the figure, rising from a low of about 3 storms per season pre-1930, up to a high of almost 8 from 1955 through to 1970 and then reducing to around 4 per season during the 1990s. While this is an extensive period of record, Holland (1981) advises caution in utilising records prior to 1959/60 in any detailed statistical analysis of frequency of occurrence or intensity because of the major changes in observing technology, standards of reporting and increasing scientific understanding over that time. For example, experimental satellite imagery first became available in 1960, leading to the adoption of objective intensity estimating methods from 1968 onwards. The later Dvorak technique (Dvorak 1975) is still in regular usage today, albeit undergoing recalibration and automation. There is evidence from Figure 3.1, for example, that the advent of WW2 probably led to a sudden increase in the detection of tropical storms from around 1939 onwards. The first radiosonde ascents were used in 1943; weatherwatch radars were installed at Townsville, Gladstone and Mackay over the period 1955 to 1959, with Cairns added in 1961.

[2] The present study has removed 12 storms from the official NCC record for the 1962/63 season which are believed to be erroneous. This was done in conjunction with Regional Office staff (J. Callaghan).

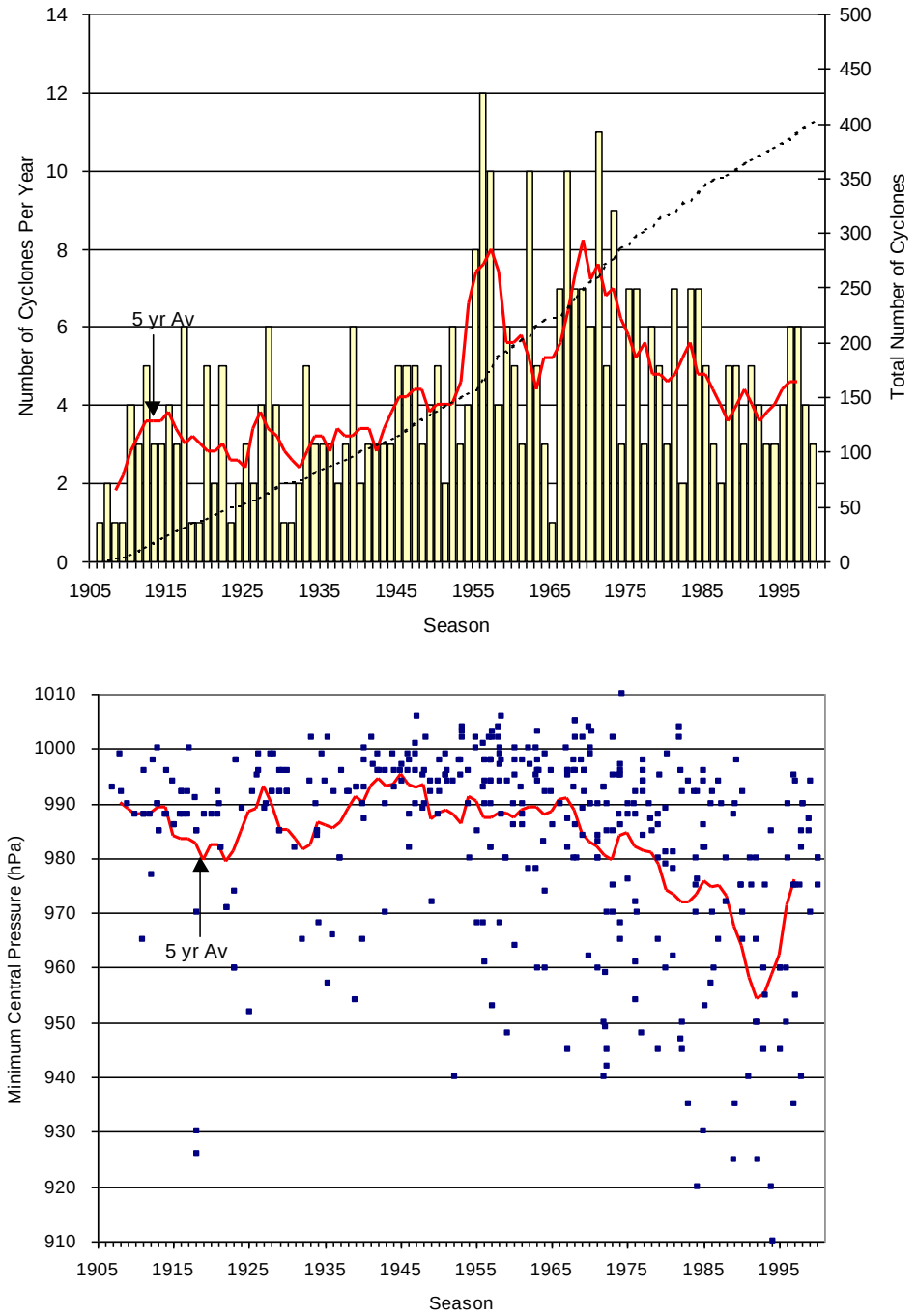

Figure 3.1 Historical trends for tropical cyclones in the Queensland region

Offshore *automatic weather stations (AWS)* were then gradually installed from 1970 onwards, initially at Flinders Reef and Lihou Reef, followed by Creal Reef, Gannet Cay and Holmes Reef in 1972. Prior to this time the staffed Willis Island station provided the only fixed remote offshore observations. Routine infrared satellite observations only became available in 1972 and geostationary satellites in 1978 provided fixed reference points.

The time series of minimum storm central pressure underpins the need for caution in selecting a representative period for statistical analysis. With the exception of the influence of the 1918 season, which witnessed two very severe landfalling storms (Mackay and Innisfail), the 5-year average central pressures rarely fell below 980 hPa until the late 1960s, when the early Dvorak technique was becoming established. From then until the early 1990s, the incidence of more intense storms continued to increase and the average pressure fell to a low of 955 hPa, before rising again over the past decade. The extent to which this variability is entirely due to climate or due to interpretation and classification remains unknown. However, the availability of satellite data clearly had a considerable impact at least in detection of the systems. The degree to which satellite influenced classification is perhaps harder to assess, although adoption of the newly developing intensity estimation methods was probably gradual and there may still be a bias towards lower intensities over the first decade after its introduction. For example, Callaghan (2000) suggests there may have been a reluctance amongst many forecasters to "overstate" a storm's intensity without reasonable groundtruth being available, even as late as the mid-1970s. If such a bias exists, then it is probably more pronounced furthest from the coast or in the more remote regions. The quantitative data quality assessment by Holland (1981) is summarised in Table 3.1 for the Eastern Region (nominally 142ºE to 165ºE). Here "coastal" refers to < 500 km of the coast and "Group 1" refers to situations with an observation within 100 km and 12 h of the place and time of maximum intensity. His analysis concludes the possibility of at least 10 to 15 hPa errors in estimating intensity over the period 1959 to 1979.

Table 3.1 Data base quality assessment for the Eastern Region (after Holland 1981)

Statistic	Situation	1909-1939	1939-1959	1959-1969	1969-1979
Occurrence:	Coastal	15% to 30% low	5% to 15% low	< 5% low	< 5% low
	Open Ocean	> 50% low	> 50% low	15% to 30% low	< 5% low
Coast Crossing:		5% to 15% low	< 5% low	< 5% low	< 5% low
Location Accuracy:	Coastal	< 250 km	< 150 km	<100 km	< 50 km
	Open Ocean	no idea	< 250 km	150 - 100 km	<100 km
Intensity:	Group 1	< 15 hPa	< 15 hPa	< 15 hPa	< 10 hPa
	Group 2	no idea	no idea	< 30 hPa	< 20 hPa

Another source of bias which is known to exist in the historical data is the inclusion of some "winter cyclones", which have a Category 1 level of severity and would now be classed as *east coast lows*. Their inclusion in the tropical cyclone dataset would tend to increase the apparent frequency of tropical cyclones but also reduce the average intensity estimates.

3.2 Statistical Analysis of Post 1959/60 Data

Restricting the data set to post-1959/60 more than halves the available record but results in a total of 213 storms in a 41 year period, giving an average occurrence rate of 5.2 per season, an increase of more than one per year compared with the full record. Figure 3.2 shows the basic occurrence statistics and intensity histogram for this reduced dataset.

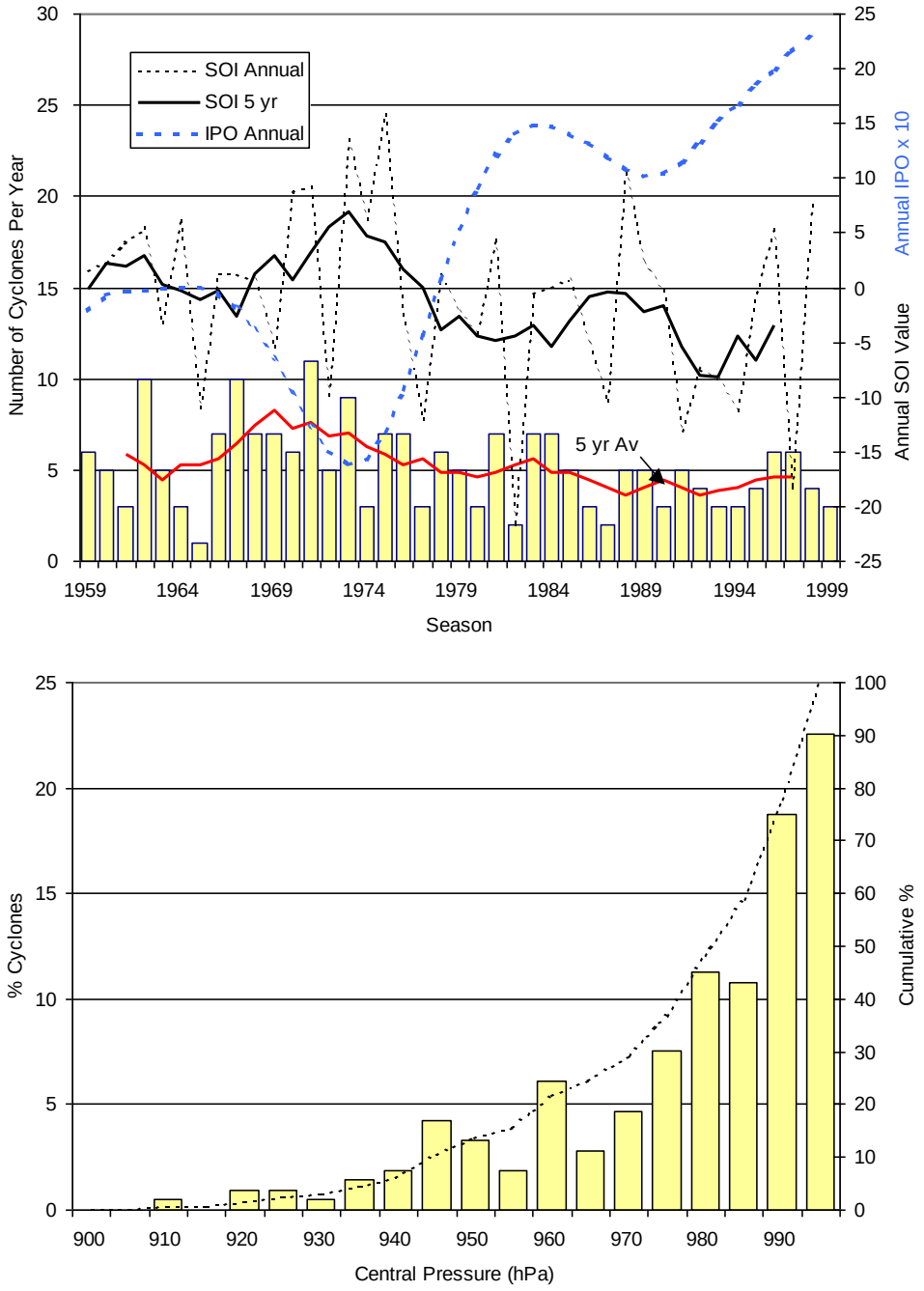

Figure 3.2 The post-1959/60 tropical cyclone dataset for Queensland.

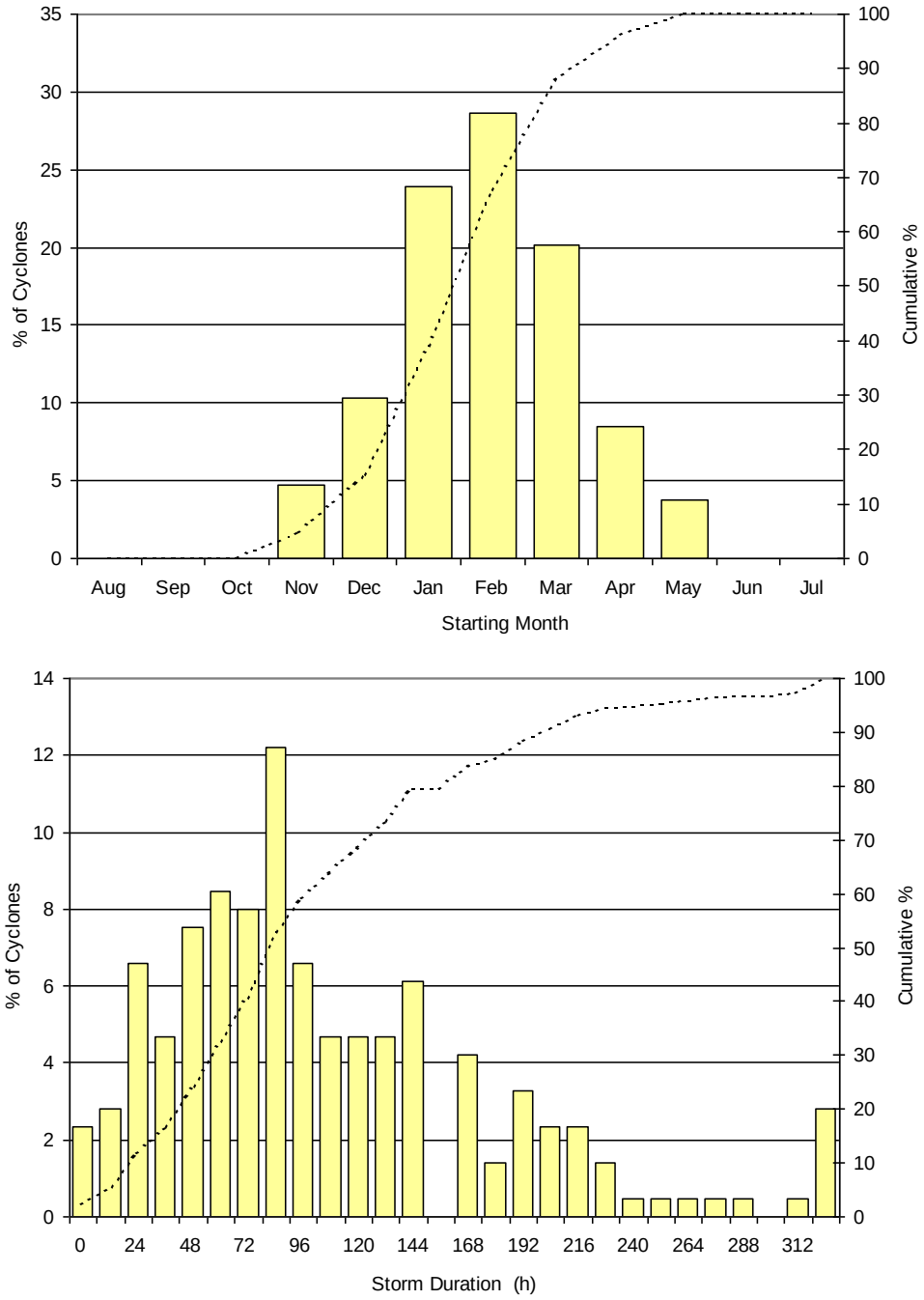

Figure 3.3 Tropical cyclone seasonal occurrence and duration post 1959/60.

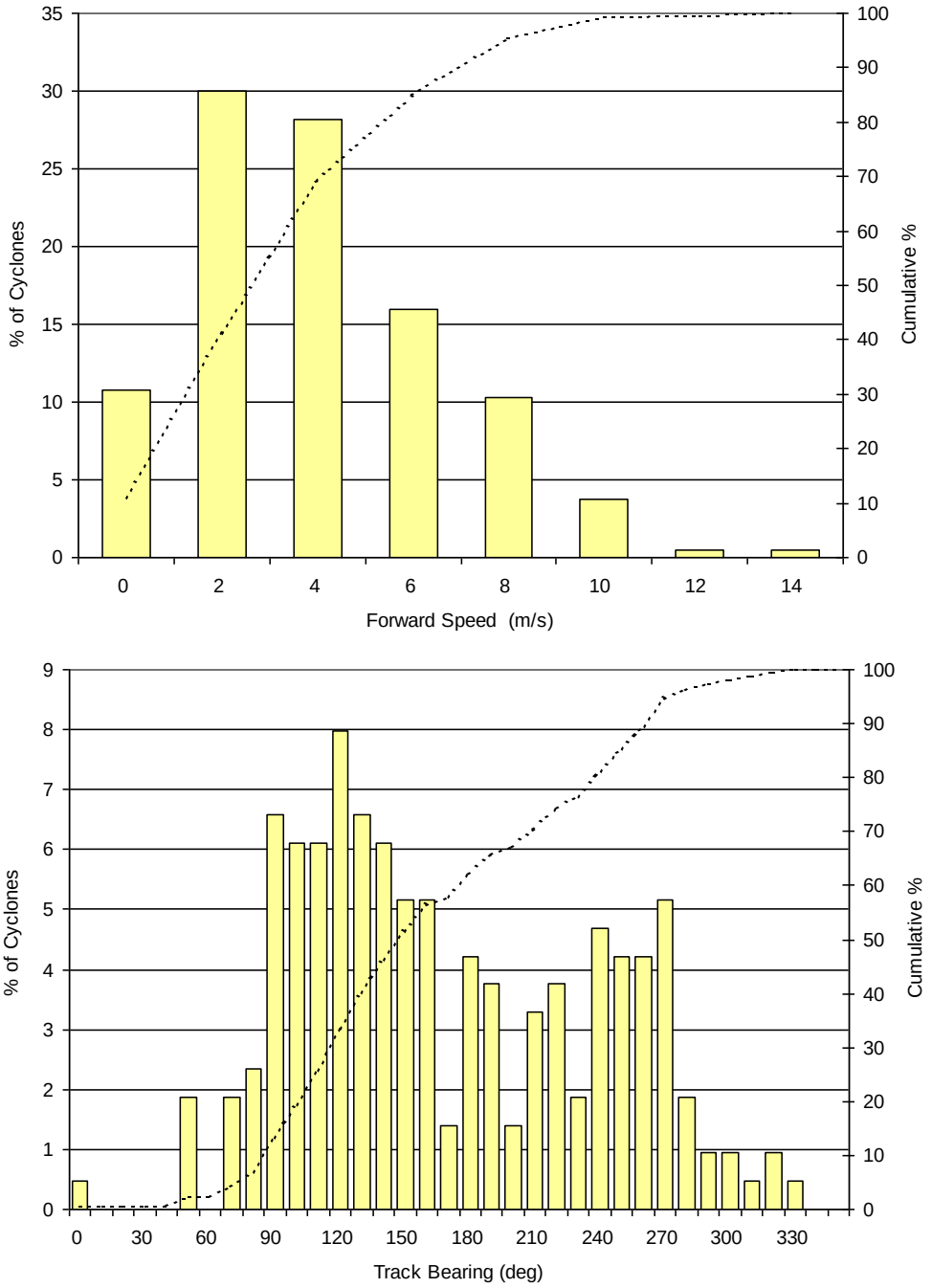

Figure 3.4 Tropical cyclone forward speed and direction post-1959.

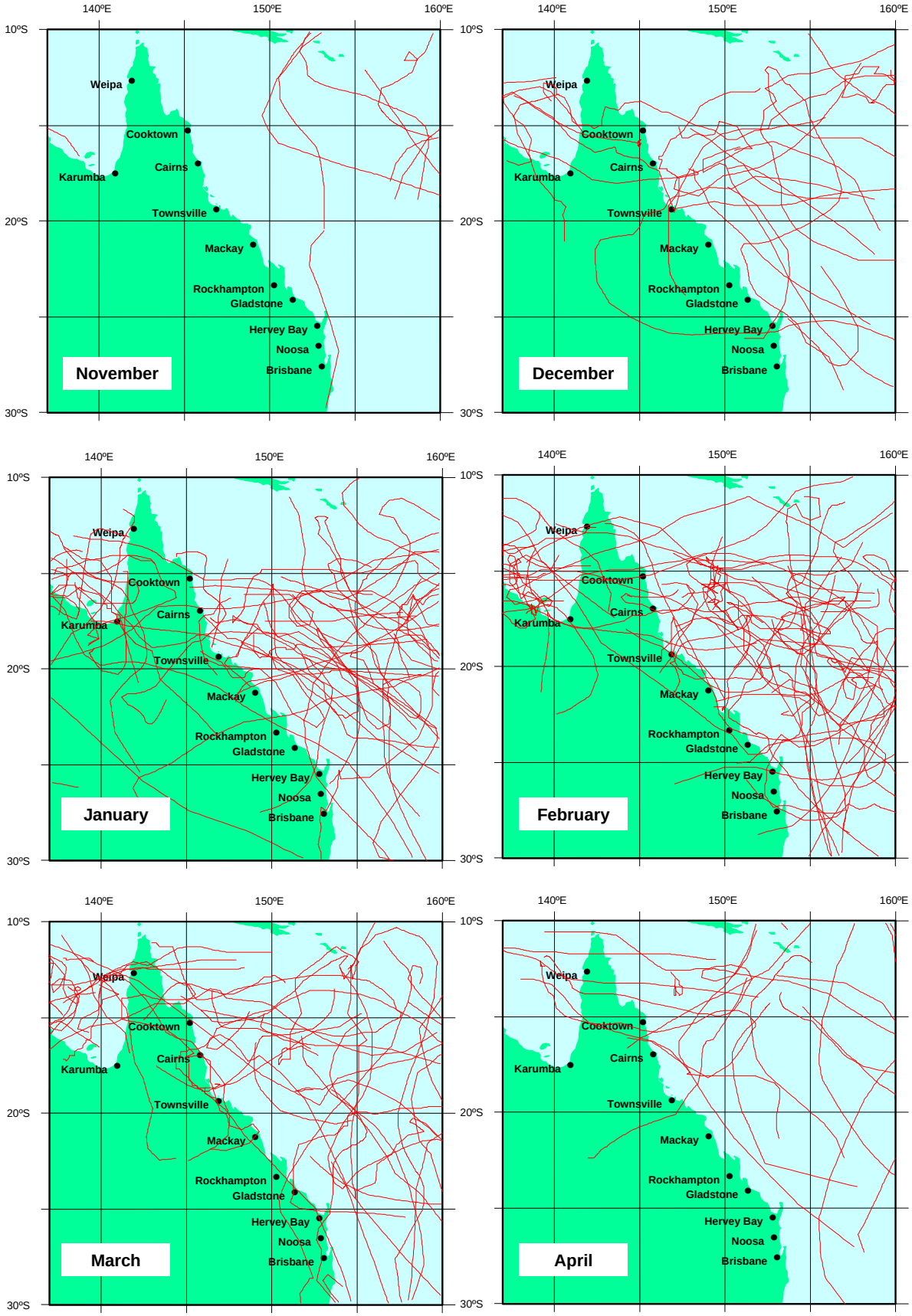

Figure 3.5 Seasonal track variation of tropical cyclones post-1959.

Figure 3.2 also shows time history comparisons against the annual and 5 year averaged *Southern Oscillation Index (SOI)* and the *Inter-decadal Pacific Oscillation (IPO)*. Further discussion on these points is provided later in regard to climatic variability.

Figure 3.3 shows the seasonal analysis of cyclone start date by month, indicating most tropical cyclones in the region (83%) occur during the period from December through to March, although November with 4.7% of the total is acknowledged as the start of the season. February can be seen to have the highest proportion at 28%, followed by January with 24% and March with about 20%. December and April are similar with only 10% and 8% respectively. The small incidence in May mainly represents dataset contamination from *east coast lows*, as mentioned previously.

The histogram of duration shows that cyclone lifetimes can be highly variable. Approximately 60% of all cyclones exist for less than 4 days, but 10% may persist for 8 days or more. This variation is dictated to a large extent by the forward speed and track of individual storms, as summarised at the time of their maximum intensity in Figure 3.4. In this case the most likely forward speed is about 2 m s^{-1}, with the average being about 3 m s^{-1}. The very highest speeds (> 10 m s^{-1}) are normally associated with those cyclones undergoing extra-tropical transition at higher latitudes.

The distribution of track bearing (direction towards) at time of maximum intensity shows predominance in the E to SSE band, peaking near SE and tending to represent the shape of the east coast. There are also other bands near the SSW and between SW and W. After their formation in low latitudes, cyclones tend to move westwards and polewards under combined easterly steering currents and dynamical effects, although individual tracks can be erratic. South of latitude 15°S on the Queensland coast, the major direction of movement is southeastward. This is caused by interaction with the northwesterly winds to the east of deep mid-latitude troughs that tend to steer tropical cyclones southeastward parallel to the coast (Callaghan 2000). The continental east coast itself participates in this process by influencing the evolution and structure of these trough systems. As tropical cyclones move into temperate latitudes they begin to interact with troughs in the middle to upper westerlies. There are three possibilities in South East Queensland as a result of this interaction. The cyclone may remain sufficiently removed from the westerlies to retain tropical cyclone characteristics; the westerlies may interfere destructively with the cyclone circulation and weaken it or the cyclone may interact favourably with an upper trough to form an intense temperate latitude cyclone – collectively termed extra-tropical cyclones in the literature. These processes, combined with unfavourable SST, tend to place a limit on the southerly extent of severe tropical cyclones.

Figure 3.5 provides an overview of tracks in the Queensland region, summarised on the basis of the starting month. The season can be seen to develop in all areas as the season progresses, although by April the activity in the Gulf of Carpentaria appears to have reduced significantly. January appears to have the greatest proportion of overland tracks, principally being sourced from the Gulf region.

Although the tracks of Figure 3.5 appear essentially randomised, it is possible to undertake systematic statistical analyses to yield summary parameters that can be used in risk assessment studies. The results from one such analysis (after Harper 1999) are given in Figure 3.6. The technique applied in this case is to analyze samples of track parameters within a given radius (500 km) of a number of coastal locations - which are indicated on the figure.

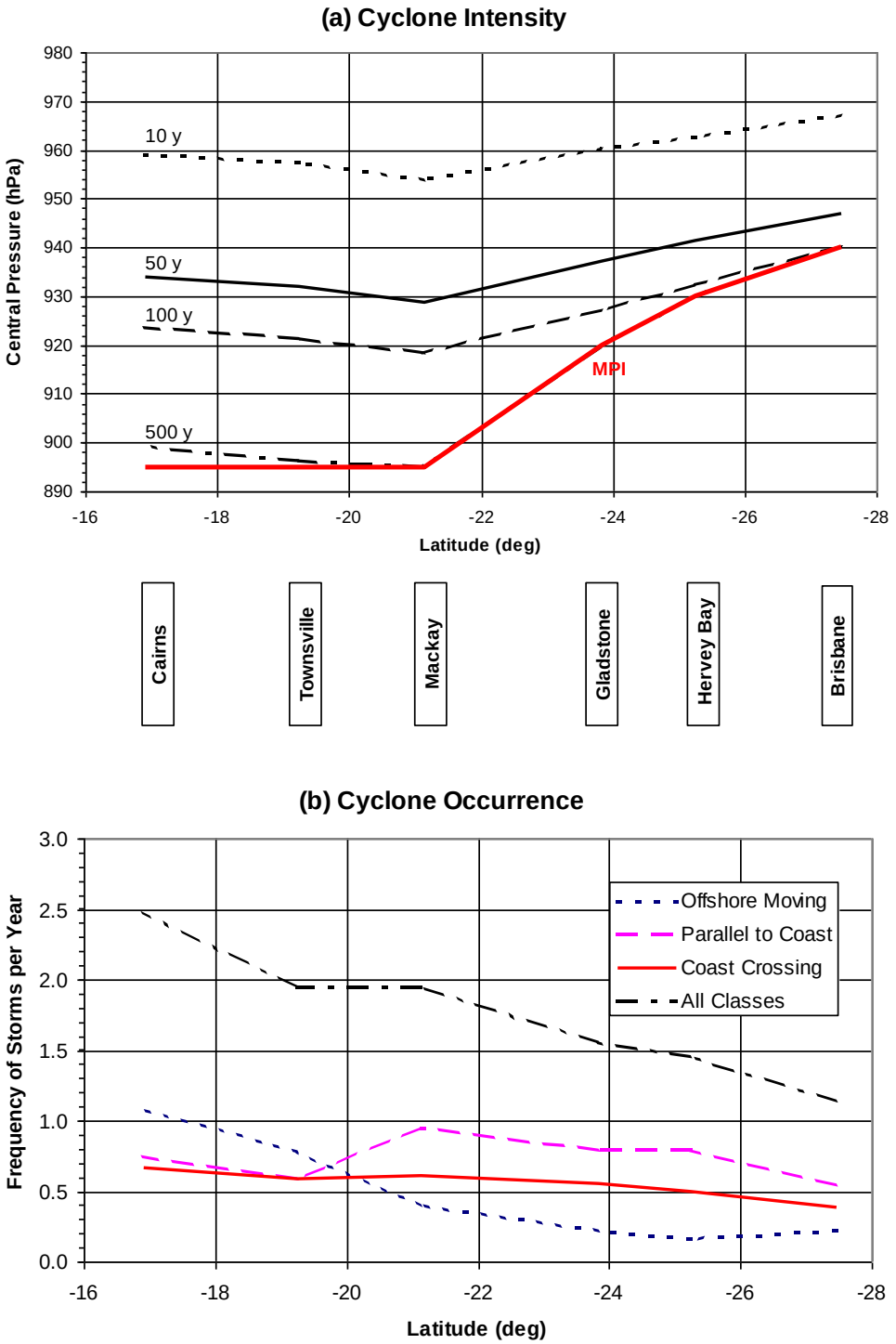

Figure 3.6 Smoothed statistical analyses of post-1959 tropical cyclone track data

(based on a 500 km radius at each 2° latitude ; analyses after Harper 1999).

Firstly, an extreme value analysis of the minimum central pressures yields a latitudinal variation in intensity, peaking in the vicinity of Mackay. Curves are shown for average return periods of 10, 50, 100 and 500 y applicable to the 500 km radius sample zones. These are limited by an assumed MPI curve (Holland 1997, *pers. comm.*) which lies close to the 500 y intensity curve north of Mackay, but reduces to the 100 y curve nearer to Brisbane. Clearly, different return period variations will be obtained with different sample radii. The choice of radii in this case being guided by the need to maintain an adequate data set for analysis but also to ensure capture of those storms which could affect the central location within 24 h.

Using the same sampling concept, but separating the cyclones into population classes based on characteristic paths, Figure 3.6b shows how the various track class contributions vary with latitude. The "offshore moving" class tends to decrease towards the south, while the "parallel to coast" tends to be relatively small north of Townsville, rising to a peak near Mackay and then staying relatively constant as far south as Hervey Bay. The "coast crossing" class tends to decrease slowly towards the south. The combined threat from tropical cyclones at any point along the coast is then a combination of the frequency of occurrence and the intensity variation. On this basis the Townsville - Mackay region tends to represent the greatest risk.

It should be noted that the available cyclone database is deficient in the recording of horizontal scale information, such as radius to maximum wind estimates and wind peakedness. Accordingly, present hazard assessment studies need to develop statistical descriptions of such parameters.

3.3 Climatic Variability

Figure 3.2 shows that the incidence of tropical cyclones can be quite variable from one year to the next and this is because of the complex set of factors that influence their genesis (WMO 1995). The data also suggests changes that are associated more with a decadal timescale. In Figure 3.7, for example, the distribution of tracks is shown for each of the decades since 1959/60, where there are some strong differences evident. For example, the 1969-1978 decade appears to have many more coastal crossings than the preceding and following periods. Also, the later 1989-1999 period shows a marked decrease in activity south from Townsville.

For many years one of the most frequently used indicators of seasonal cyclonic activity has been the so-called *El Niño - Southern Oscillation (ENSO)* phenomenon (Nicholls 1992). This is the name given to a near-periodic (between one and three year) cycle of alternating cold and warm ocean temperatures between one side of the Pacific Ocean and the other. The El Niño phase sees abnormally warm ocean temperatures off the coast of South America and along the central and eastern Pacific equatorial zone and simultaneously cooler ocean temperatures in the western Pacific and the Coral Sea. During the reverse cycle, or La Niña, ocean temperatures near the Queensland coast are typically above average. Ocean temperature is not the only factor causing cyclone variability but it is a prime contributor. When combined with associated shifts in large-scale zones of atmospheric convergence (Basher and Zheng 1995), the regions of tropical cyclone genesis in the South Pacific tend, as a result, to move further towards the east (El Niño) or the west (La Niña).

There are several techniques used for determining the state or strength of the ENSO condition. One of the most widely used methods is the *Southern Oscillation Index (SOI)*, which compares differences in the mean monthly sea level pressure between Darwin and Tahiti. The annual and 5-year averaged SOI time series is shown in Figure 3.2, compared with the

occurrence of tropical cyclones in the Queensland region. The SOI has been shown to be a strong indicator of rainfall and tropical cyclone activity in northern Australia and Queensland (e.g. Nicholls, 1992). Another common method is to use ocean surface temperature readings (SSTs) from various zones in the Pacific. These data have become routinely available from satellite as well as ships, drifting buoys and from moored buoy networks positioned along the equator. Using an accepted SST-based sequence from 1959 to 1997 (e.g. from Pielke and Landsea, 1999), Figure 3.8 shows that when the historical record is separated into El Niño, neutral and La Niña periods, there is a quite noticeable effect on the tracks of tropical cyclones in the Coral Sea. During La Niña (the positive SOI phase) cyclone activity tends to be located closer to the east coast of Queensland and further south than during the El Niño (negative SOI phase). The Gulf of Carpentaria appears to be less affected.

While the ENSO phenomenon appears to be somewhat random, El Niño years have outnumbered La Niña years by about a factor of 3 since the mid-1970s. This has been reflected along much of the east coast of Queensland by a corresponding reduction in frequency of cyclone occurrence and Figure 3.2 indicates this effect from the 1970s onwards, which becomes much magnified if only the area south of Mackay is considered. Exactly why this preference for El Niño episodes has persisted during this period is not entirely clear but it may be related to longer period climatic variability as discussed below, or even global climate change. From 1998 to early 2000 there has been a return to mild La Niña and near-neutral conditions. Latest SOI results (Nov-Dec 2000) suggest a stronger La Niña could be developing for 2001.

Interestingly, as shown in the following table, neutral years actually have the highest frequency of occurrence of cyclones in the Queensland region, although the number of El Niño, neutral and La Niña years is approximately equal over the 41 year record. Numbers of neutral years alone account for nearly 40% of all occurrences. Importantly, neutral years show a 53% increase in occurrences compared with El Niño years and a 5.5% increase compared with La Niña years.

Table 3.2 Summary ENSO statistics for Queensland.

ENSO Condition	Years Experienced	Total Cyclone Numbers	Frequency of Occurrence	Proportion of Occurrences
El Niño	14	55	3.93	25.8%
Neutral	14	84	6.00	39.4%
La Niña	13	74	5.69	34.7%
Total	**41**	**213**	**5.20**	**100%**

Power *et al.* (1999) recently highlighted the potential importance for Australian climate of apparent 10 to 30 year longer-term cycles of ocean temperatures in the Pacific Ocean. This oscillation is also measured in terms of relative SST heating or cooling but relates more to the whole of the tropical Pacific Ocean region rather than just differences between the eastern and western limits. Termed the Inter-decadal Pacific Oscillation (IPO), this long-term variation in mean SST appears to modulate the effect of ENSO on rainfall in Australia. When the IPO is positive, the tropical ocean is slightly warmer than average while to the north and south the temperatures are slightly less than average. During this period the effect of ENSO on rainfall appears to be less significant. When the IPO is “negative”, the tropical ocean is slightly cooler and ENSO seems to be much more strongly correlated with Australian rainfall. The IPO effect

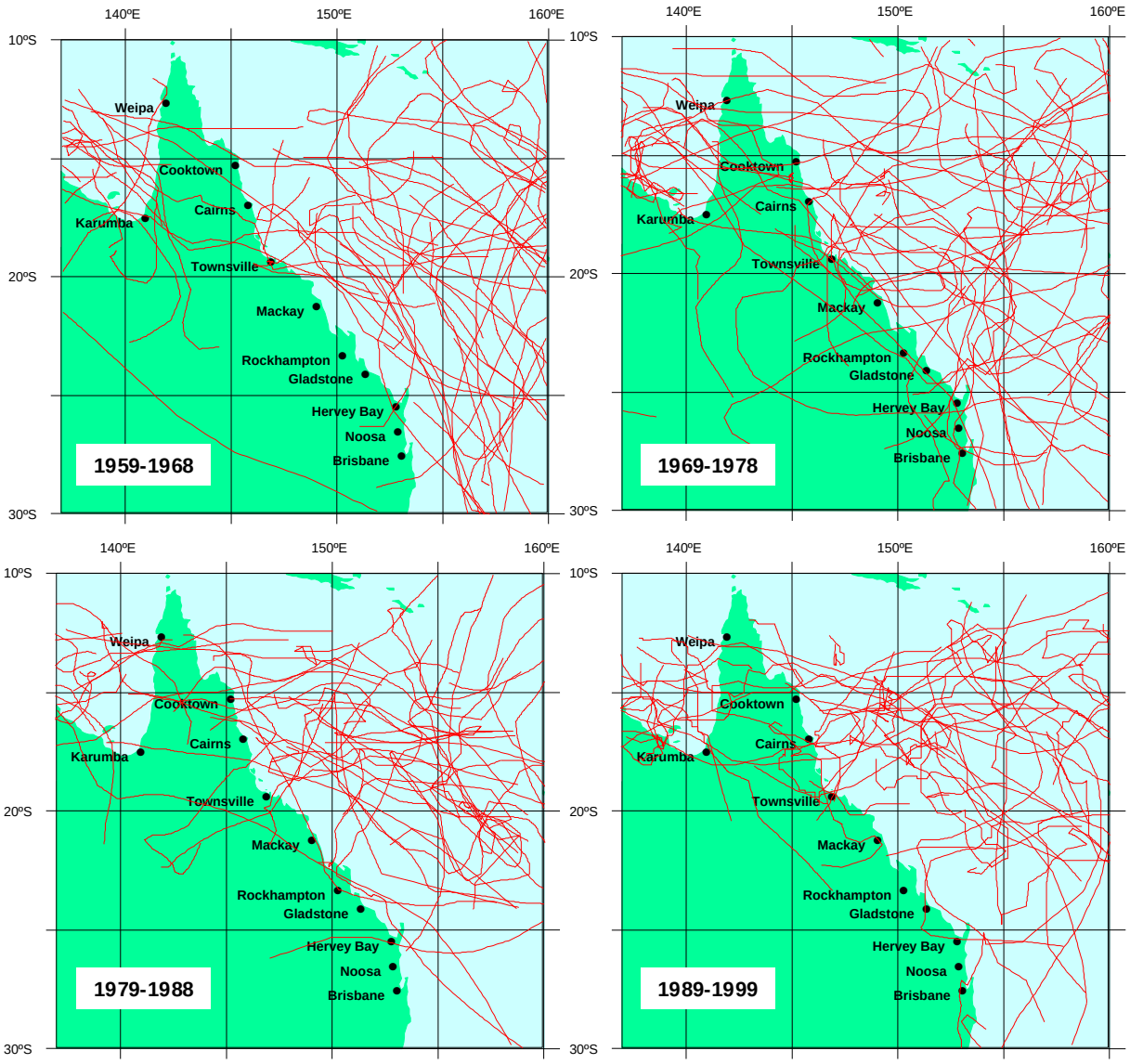

Figure 3.7 Decadal tropical cyclone track variability post-1959.

may also be related to the large-scale thermo-haline circulation between the Atlantic and the Pacific Ocean that has been identified as a potential indicator of hurricane incidence in the Atlantic (Landsea *et al.*, 1994). Callaghan and Power (submitted AMM) describe a possible modulating effect of the IPO on Australian tropical cyclone activity which suggests that damaging impacts in Queensland are more likely during negative (cooler) phases of the IPO, which is associated with warmer ocean temperatures near Queensland. Since the mid-1970s, there has been a prolonged positive phase of the IPO that is only now (1999-2000) showing some possible signs of reversal. If this is correct, recent trends may suggest that cyclone incidences along the Queensland coast could increase, especially in the SE region. However, these outcomes remain speculative at this time since it will require several further years of observations to confirm whether the IPO phase is changing. The annual IPO index x 10 is plotted as a time series in Figure 3.2 for comparison with the SOI and cyclone occurrences. Generally the IPO can be seen to inversely mimic the SOI, except from around 1985 to 1990 where the IPO failed to reverse when the SOI rose and it is now thought the IPO is at or near its peak positive phase.

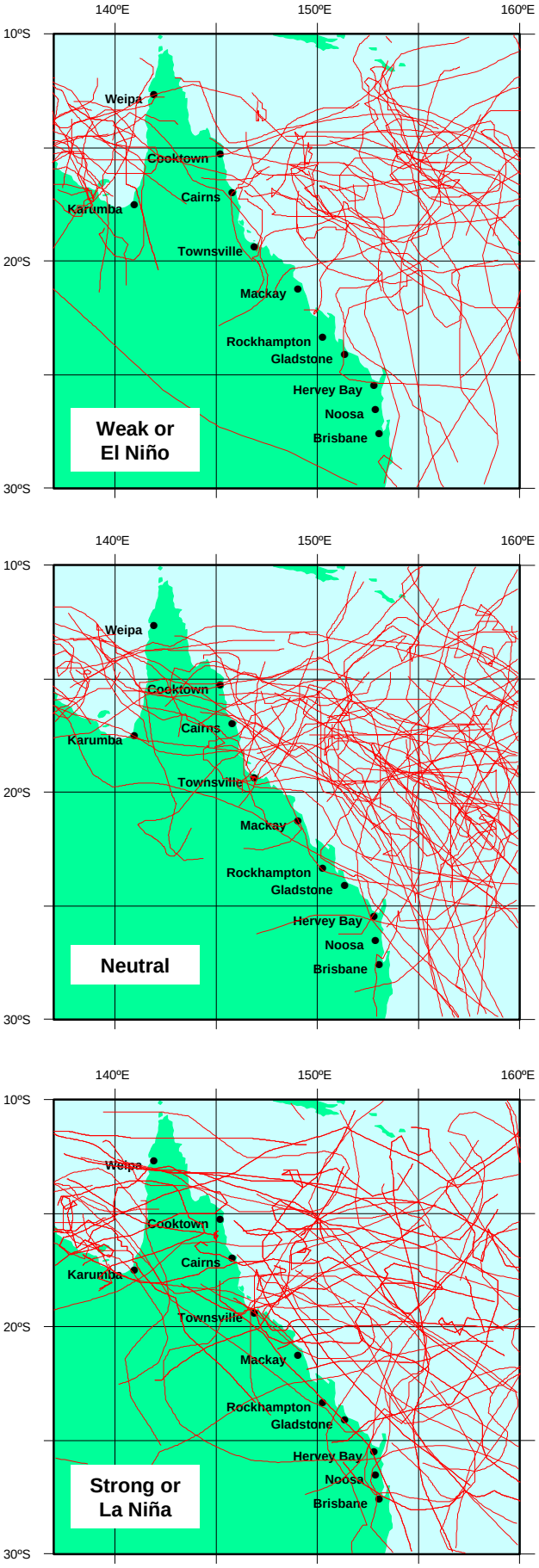

Figure 3.8 ENSO variation in tropical cyclone tracks post-1959.

3.4 Conclusions and Recommendations

Any assessment of ocean hazards due to the effects of tropical cyclones in Queensland needs to assimilate the many climatological factors that affect cyclone frequency and intensity, on a variety of time and space scales. However, errors and inaccuracies exist in the available datasets (this includes the "official" national Climate Centre records) and not all of the necessary information is readily available. This requires development of robust statistical models of the climatology that can be applied in hazard assessments and provide the means for sensitivity testing of the many necessary assumptions.

It is recommended that a complete review of tropical cyclone climatology be undertaken for Queensland that can be used to support future stages of the present ocean hazard assessment project. This should include inter-seasonal, inter-decadal and long-term climate change issues. Synoptic scale interactions with tropical cyclone vortices should also be considered, together with decay after landfall, recurvature and regeneration issues.

3.5 References

Basher R.E. and Zheng X. (1995) Tropical cyclones in the Southwest Pacific: spatial patterns and relationships to southern oscillation and sea surface temperature, *Journal of Climate*, Vol 8, May, 1249-1260.

Callaghan J. and Power, S. (to appear) Long term changes in the occurrence of damaging cyclonic storms in tropical and sub tropical eastern Australia. Submitted *Aust. Met. Magazine* 1999.

Coleman F. (1972) Frequencies, tracks and intensities of tropical cyclones in the Australian region, 1909 - 1969. Bureau of Meteorology, *Meteorological Summary*. July.

Dvorak V.F. (1975) Tropical cyclone intensity analysis and forecasting from satellite imagery. *Mon. Weath. Rev*., 103, 420-430.

Harper B.A. (1999) Numerical modelling of extreme tropical cyclone winds. APSWE Special Edition, *Journal of Wind Engineering and Industrial Aerodynamics*, 83, 35 - 47.

Holland G.J. (1981) On the quality of the Australian tropical cyclone data base. *Aust. Met. Mag*., 29, 169-181.

Holland G.J. (1997) The maximum potential intensity of tropical cyclones. *J. Atmos. Sci*., 54, Nov, 2519-2541.

Lourensz R.S. (1977) Tropical Cyclones in the Australian Region July 1909 to June 1975. *Bureau of Meteorology*.

Lourensz R.S. (1981) Tropical cyclones in the Australian region July 1909 to June 1980. *Bureau of Meteorology*. Oct.

Nicholls N. (1992) Historical El Nino / Southern Oscillation variability in the Australian region. In Diaz, H.F. and Margraf, V. (Eds), El Nino, historical and paleoclimate aspects of the Southern Oscillation. *Cambridge Uni. Press*, Cambridge, UK, 51-174.

Nott J. and Hayne M. (2000) How high was the storm surge from tropical cyclone Mahina? *Aust Jnl of Emergency Management*, Autumn, 11-13.

Pielke R.A. (Jr) and Landsea C.W. (1999) La Niña, El Niño, and Atlantic hurricane damages in the United States, *Bull. Amer. Meteor. Soc*., 80, 2027-2033.

Power S., Casey T., Folland C., Colman A. and Mehta V. (1999) Inter-decadal modulation of the impact of ENSO on Australia. *Climate Dynamics*, 15, 319-324.

Whittingham H.E. (1958) The Bathurst Bay hurricane and associated storm surge. *Aust. Met. Mag*., 23, Dec.

WMO (1995) Global perspectives on tropical cyclones. *World Meteorological Organization* TD-No. 693, Tropical Cyclone Programme Report No. TCP-38, Geneva.

4. Greenhouse Climate Change and Sea Level Rise

The Intergovernmental Panel on Climate Change (IPCC) provides the primary consensus reference on this subject. The IPCC was jointly established by the World Meteorological Organisation (WMO) and the United Nations Environment Programme (UNEP) in 1988. Its role is to (i) assess available scientific information on climate change, (ii) assess the environmental and socio-economic impacts of climate change, and (iii) formulate response strategies.

The IPCC First Assessment Report was completed in August 1990 and served as the technical basis for the United Nations Framework Convention on Climate Change (UNFCC). This convention seeks to minimise and reduce the adverse human impacts on the global climate system through internationally agreed controls on so-called greenhouse gas production. The greatest single contribution to global warming is due to increases in atmospheric CO_2 since the industrial revolution. The revised and updated IPCC Second Assessment Report was completed in late 1995 and formally published in 1996, as well as an interim update of regional vulnerabilities completed more recently (IPCC 1998). The next full IPCC review (Third Assessment Report) is planned for completion by early 2001 with expectations of conclusions similar to the 1995 study. The Australian Government interpretation of the IPCC predictions and impacts is provided in *Climate Change: Australia's Second National Report under the United Nations Framework on Climate Change* (Dept of the Environment 1997).

Much of the development here follows NCCOE (2001), which in turn is derived essentially from IPCC (1996ab).

4.1 The Global Warming Process

The earth absorbs radiation from the Sun, mainly at the surface. This energy is then redistributed by the atmospheric and oceanic circulation and radiated to space at longer ("terrestrial" or "infrared") wavelengths. On average, for the Earth as a whole, the incoming solar radiation is balanced by the outgoing terrestrial radiation. Any factor that alters the radiation received from the Sun or lost to space, or that alters the redistribution of energy within the atmosphere, and between the atmosphere, land and ocean, can affect climate. A change in the energy available to the Earth/atmosphere system is termed a *radiative forcing*.

Figure 4.1 summarises the earth's energy balance. Some of the infrared radiation that leaves the atmosphere originates near the Earth's surface and is transmitted through the atmosphere relatively unimpeded. The bulk of the radiation, however, is intercepted and absorbed by the atmosphere, which in turn emits radiation both up and down. Most of the atmosphere consists of nitrogen and oxygen (99% of dry air) which are transparent to infrared radiation. However, water vapour (0 to 2%), carbon dioxide, ozone and some other minor gases absorb some of the surface thermal radiation. These *radiatively active* gases are also termed *greenhouse* gases because they act as a partial blanket increasing the surface temperature of the Earth above what it would otherwise be, analogous to the effects of a greenhouse. Water vapour (as clouds) is radiatively active but also reflects solar radiation, leading to a net small cooling effect overall. The natural presence of greenhouse gases has been a positive and necessary feature of the development of life on Earth. Without heat-trapping greenhouse gases, the Earth's surface would have an average temperature of -18°C rather than our current average of 15°C. Synthetic aerosol gases such as CFCs and HCFCs are also radiatively active, but

because they act to deplete stratospheric ozone levels, their net radiative forcing effect is relatively low.

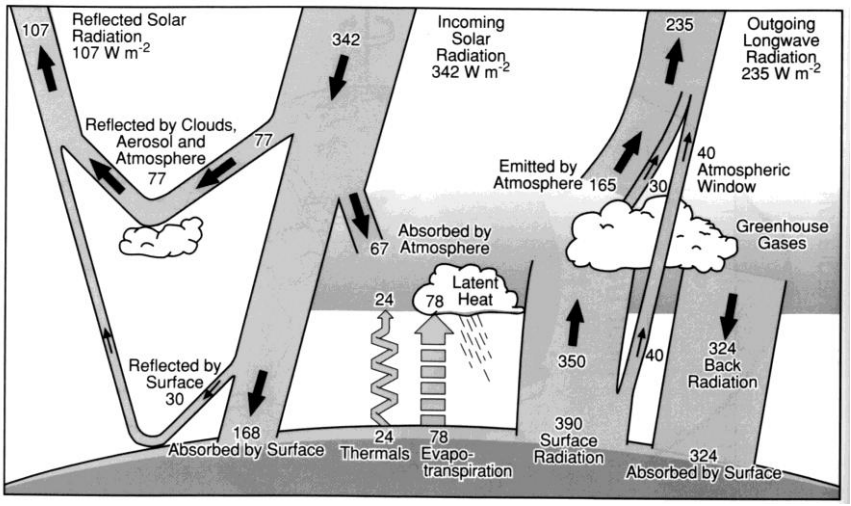

Figure 4.1 The Earth's radiation and energy balance in W m^{-2} (After IPCC (1996a, fig 1.3)

The climate can vary for many reasons but human activities, in particular, can lead to changes in atmospheric composition and hence radiative forcing. For example, changes can occur through the burning of fossil fuels, wide-scale deforestation or through processes which increase the number and distribution of manmade aerosols. Large-scale changes in land uses that alter properties of the Earth's surface can also give rise to changes in climate.

4.2 Evidence of Climate Change

The balance of evidence now suggests there has been a discernible human influence on global climate since the late 19th century. Evidence for this is supported by the following:

- Recent years have been the warmest since 1860
- Global mean surface air temperature has increased by between about 0.3 and 0.6°C and night-time temperatures over land have generally increased more than daytime temperatures (Figure 4.2)
- Regional changes of precipitation have been observed
- Global sea level has risen by between 0.10 m and 0.25 m and may be related to the increase in mean global temperature (Figure 4.3)
- The atmospheric concentrations of greenhouse gases, *inter alia* carbon dioxide (CO_2), methane (CH_4) and nitrous oxide (N_2O), have grown significantly: by about 30%, 145% and 15% respectively (1992 values) since pre-industrial times, i.e. since about 1750.

The Australian National Tidal Facility has been collecting, archiving and disseminating sea level and related material for over 30 years, and an extract of data from some long-term Australian tidal stations is presented in Figure 4.3 (PCTMSL 1999). The longest reliable record is from Fremantle in Western Australia spanning 100 years, followed by Fort Denison in Sydney Harbour with over 80 years. The mean sea level trend in mm per year is indicated against each record, together with the standard deviation. Three of these four records show an increasing trend while Port Pirie in South Australia shows a negative trend with some marked variability. The Adelaide Outer Harbour site has the highest positive trend but this is thought

to be due to local land subsidence. Taking all 27 sites in Australia where the record is at least 23 years long, the average trend in sea level is +0.3 mm per year, but with 11 sites showing a negative trend. Of particular significance for many of these records is the high variability on a decadal timescale, with many stations recording lowering sea levels in the past few years.

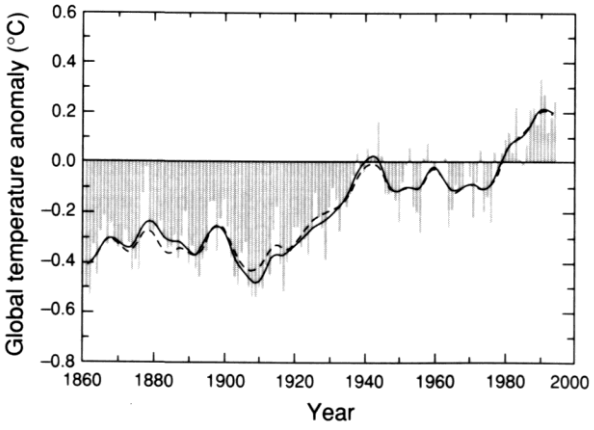

Figure 4.2 Combined trends in land-surface air and sea-surface temperature anomalies (after IPCC 1996a, fig 8)

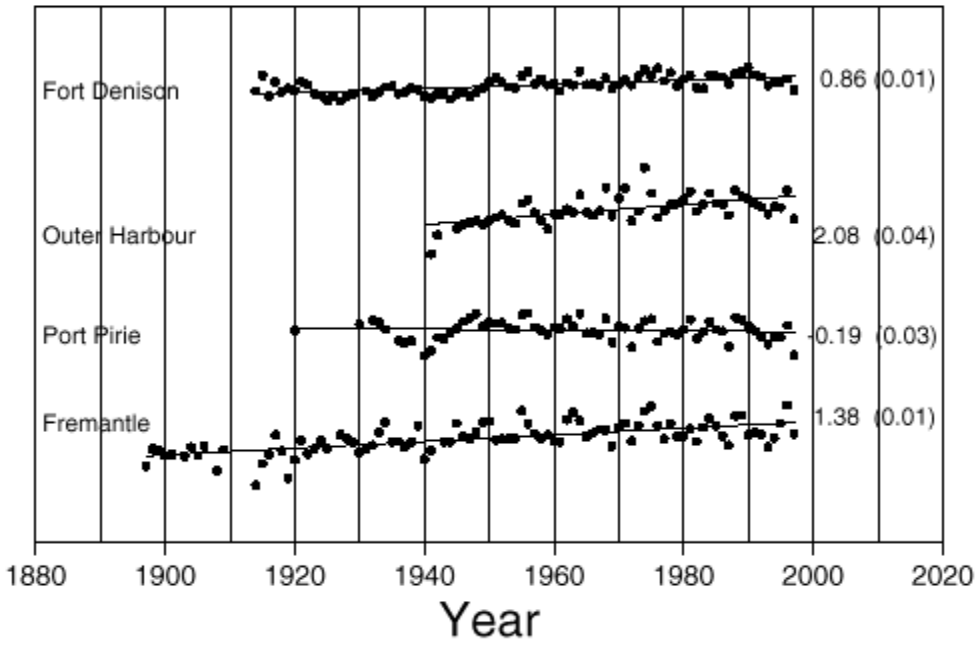

Figure 4.3 Australian long-term sea level records (after PCTMSL 1999)

The additional surface heating component of human-induced (or anthropogenic) origins is referred to as the *enhanced greenhouse* effect. Because of the relative radiative forcing potential of each of the primary gases, the principal contributing effect is from CO_2, the excess amounts of which can be expected to remain in the atmosphere for many decades to centuries. If CO_2 emissions were maintained at 1994 levels, it is estimated that they would lead to a nearly constant rate of increase in atmospheric concentrations for at least two

centuries, reaching about 500 ppm (approaching twice the pre-industrial concentration of 280 ppm) by the end of the 21st century. This prediction is the basis of the commonly referred to "$2 \times CO_2$" scenario.

4.3 Latest Global Projections

Many of the existing numerical global climate models (GCMs) have had some success in reproducing broad climate behaviour but assume an equilibrium condition between the atmosphere and the ocean (the so-called *slab model* approach) which has limited their predictive capability. Meanwhile, the increasing realism of simulations of present and past climate by the more complex *coupled atmosphere-ocean* climate models has increased the confidence in their use for predicting climate change. Important uncertainties remain, but the IPCC believes these have been taken into account in the full range of projections of global mean temperature and sea level change. These are described by a series of modelled greenhouse gas emission scenarios, termed IS92a through to IS92f, which are predicated on world population estimates, economic growth and consequent energy usage patterns. The range of temperature increases predicted by these scenarios varies between 1.5°C and 4.5°C by the year 2100. Within each base scenario, model sensitivity testing has then been undertaken using a range of model parameter assumptions.

The most-often quoted scenario is the IS92a, which is typically termed the "business as usual" outcome and implicitly assumes limited success of UNFCC plans. The IS92a scenario produces an increase in mean global temperature of 2.5°C by the year 2100. The key projections of sea level increase by the year 2100 are presented in Table 4.1. These results also reflect sub-scenarios regarding sulfate aerosol emissions and are plotted in Figure 4.4 as a varying function of time.

Table 4.1 IS92a projected sea level increases to 2100

IS92a Scenario	Sea level Rise	
	1990 Aerosols	Increasing Aerosols
"low"	0.23 m	0.20 m
"mid-range"	0.55 m	0.49 m
"high"	0.96 m	0.86 m

The IS92a temperature estimate is approximately one third lower than the "best estimate" in 1990. This is due primarily to lower emission scenarios, the inclusion of the cooling effect of increasing aerosols, and improvements in the model treatments of the carbon cycle. It should be noted however that regional temperature changes might vary substantially from the global mean value. In addition, because of the thermal inertia of the oceans, temperature would continue to increase beyond 2100, even if concentrations of greenhouse gases were stabilised by that time.

The IS92a sea level rise estimate is approximately 25% lower than the "best estimate" in 1990 due to the lower temperature prediction, but also reflecting improvements in the climate and ice melt models. Likewise, sea level is expected to continue to rise beyond 2100 and even beyond the point of mean temperature stabilisation.

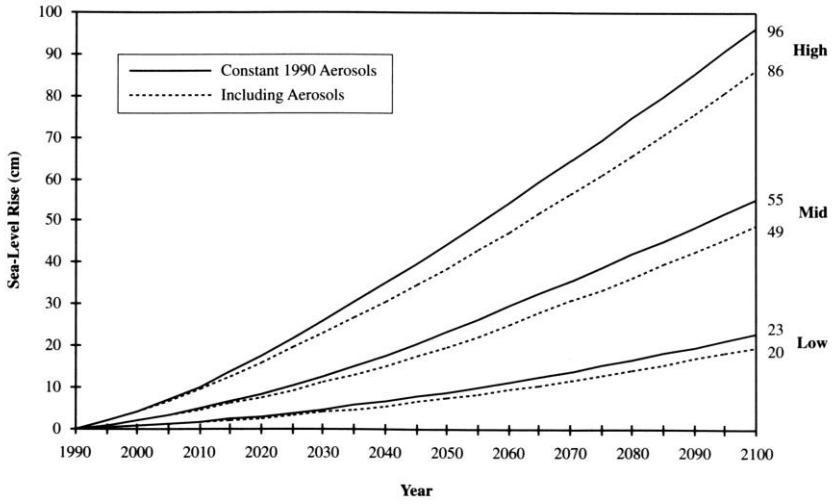

Figure 4.4 1990 to 2100 sea level rise for scenario IS92a (after IPCC 1996b, fig 9-3)

4.4 Major Weather Systems and Global Climate Change

El Niño - Southern Oscillation

IPCC (1996a) notes that some of the more sophisticated climate models predict a continuation of the ENSO-like SST (sea surface temperature) phenomenon under enhanced greenhouse conditions, with possible increases in precipitation variability over tropical regions. These conclusions are supported by Nicholls (1993) and Smith *et al.* (1997).

Tropical Cyclones

Any significant modifications to the behaviour of tropical cyclones in a changed climate could have especially damaging impacts for regions of northern Australia. In the context of coastal and ocean hazards, the potential exists for changing extreme wind, wave and current environments to perhaps adversely affect existing infrastructure where design conditions have been based on estimates from the historical dataset. In terms of loss of life, storm surge generation and their resulting storm tides represent the single greatest threat to our rapidly growing coastal populations (Harper 1999).

The current IPCC statement on the possible effects of climate change on tropical cyclones (IPCC 1996a, p334) states that "it is not possible to say whether the frequency, area of occurrence, time of occurrence, mean intensity or maximum intensity of tropical cyclones will change". This circa-1994/5 statement was based primarily on acknowledged difficulties in the ability of coarse resolution GCMs to correctly represent the conditions necessary for tropical cyclone development, plus a lack of skill in ENSO representation under current climate.

This position has been under review in the intervening years (e.g. Holland 1996) and recently updated by the specialist Tropical Marine Research Program sub-committee of the WMO Commission for Atmospheric Sciences (Henderson-Sellers *et al.* 1998) which has provided more definitive guidance on a number of specific issues. This later update draws upon a wider source of information than was considered by the IPCC and has directly involved the peak world expertise on tropical cyclones.

The major conclusions of this later assessment are as follows:

- Long-term reliable data on tropical cyclone intensity and frequency (which are largely limited to the North Atlantic and Western North Pacific regions) show substantial multi-decadal variability but there is no clear evidence of any long term trends in number, intensity or location.
- Attempts to extend this record through analysis of geological and geomorphological records to establish a paleoclimate have so far not produced definitive results.
- Recent thermodynamic modelling attempts to estimate the maximum potential intensity (MPI) of tropical cyclones in present climate has shown good agreement with observations (e.g. Holland 1997).
- Application of MPI techniques to changed climate indicate the MPI of cyclones will remain the same or undergo a modest increase of up to 10 - 20% at the extreme end of the scale.
- The broad geographic regions of cyclogenesis and therefore the regions affected by tropical cyclones are not expected to change significantly.
- The region of cyclogenesis is unlikely to expand with the 26°C isotherm, i.e. the 28°C isotherm is likely to become the new proxy reference temperature under present scenarios. The very modest available evidence points to an expectation of little or no change in global frequency.
- Regional or local frequency of occurrence may however change substantially, in either direction, because of the dependence of cyclone genesis and track on other phenomena (e.g. ENSO) that are not yet predictable.

Mid-Latitude Systems

IPCC (1996a) notes that there is little agreement between climate models at present as to the likely changes in "storminess" which might occur in a warmer world. In the regional sense, some numerical studies (e.g. McInnes *et al.* 1992; Hopkins and Holland, 1997) have attempted to explore possible changes to the behaviour of severe low-pressure systems such as "east coast lows".

In addition to the possible changes in frequency or severity of intense large-scale storms there may also be shifts in the mean synoptic patterns which could affect regional wind speeds and directions. This in turn could change the distribution of the wave-energy flux presently impacting the coastline. As explored by Gordon (1988), when combined with sea level rise, these more subtle changes may have a significant impact on the stability of coastal margins. Some potential evidence for changes in long term significant wave height is presented in Cox and Horton (1998).

4.5 Impact on the Oceans

Oceans occupy about 70% of the earth's surface. They provide an important component of the climate system, due to their role in controlling the distribution and transfer of heat and CO_2 and in the transfer of freshwater back to the continents as precipitation. The oceans function as regulators of the Earth's climate and sustain planetary biogeochemical cycles. They have significant capacity to store heat and are the largest reservoir of the two most important greenhouse gases - water vapour and carbon dioxide. About 60% of the Earth's radiative energy from the Sun is received by the oceans, 80% of that being absorbed within the top 10 m. Winds and waves mix down a seasonal surface layer of nearly uniform temperature, salinity and other properties which extends to tens of metres in the tropics and to several

hundred metres in higher latitudes (the so-called upper thermocline). The permanent (lower) thermocline lies below the seasonal surface layer, down to about 1000 m. While wind-driven circulation dominates the upper ocean mixing, manifesting as basin-scale gyres and intensive western boundary currents, the deeper ocean circulation is controlled by thermohaline processes (density currents). The lower thermocline and abyssal ocean represents nearly 90% of the volume of the oceans and most of this water is colder than 5°C. The oceans contain about 60 times more carbon than the atmosphere and variations in atmospheric carbon dioxide could result from even minor changes in the ocean's carbon cycling process, which is related to the ocean circulation. Conversely however, carbonate chemistry dictates that the ocean is not an especially efficient sink for human-induced increases in atmospheric carbon dioxide concentrations. Sea ice covers about 11% of the ocean and affects surface reflection of energy, salinity and ocean-atmosphere thermal exchange.

In the oceans, climate change will be accompanied by changes in temperature, circulation, sea level, ice coverage, wave climate and possibly extreme events:

- Sea surface temperature (SST) increases are likely to be less than air temperature increases and to lag continental air temperature increases by as much as 10 years, before rising at a similar rate
- Changes in SST gradients are expected to lead to a decrease in trade wind intensity, a reduction in strength of upper ocean currents and a decrease in areas and intensity of upwelling
- Due to a lack of basic understanding of the present interactions, it is still premature to project the behaviour of ENSO events for different climate changes
- Available estimates of sea level changes are rather preliminary but will likely occur due to ocean thermal expansion, changing volumes of polar and glacial ice sheets, dynamical ocean circulation effects, altered wind and weather patterns and differences in regional ocean density
- Even the lower estimates of sea level rise are about 2 to 4 times the rate of sea level rise experienced in the last 100 years
- Projected changes in climate should produce large reductions in the extent, thickness and duration of sea ice
- Present numerical weather models are not yet capable of objectively estimating whether there is likely to be an increase in the frequency or intensity of severe tropical cyclones
- Some corals are likely to be impacted through increased SST and possibly UVB exposure due to ozone depletion, leading to increased bleaching and a reduction in coral production
- Increased loading of land-based pollutants is expected as a result of increased precipitation and atmospheric transport

4.6 Impact on Coastal Zones and Small Islands

It is estimated that 50 - 70% of the global human population (86% of Australians) live in the coastal zone, where important socioeconomic activities include resource exploitation (living and non-living), industry and commerce, infrastructure development, tourism, recreation and nature conservation. In most coastal nations, a considerable part of gross national product is derived from activities connected with the coastal zone. Many coastal problems presently being experienced worldwide can be attributable to the unsustainable use and unrestricted development of coastal areas and resources. Climate change is likely to pose an additional stress on these areas, with sea level rise and possible changes in the frequency and intensity of extreme events being of prime concern. In addition to the physical changes that are possible,

climate change has the potential to significantly affect coastal biological diversity through alteration of habitat.

The following are the major aspects of concern to the coastal zone and small islands:

- Any changes in sea level are expected to vary from the global mean over regional and local scales due to (1) vertical land movement e.g. subsidence, upheaval and (2) dynamical ocean effects due to circulation patterns, wind and pressure distributions and density differences. These are effects, which already dictate global variation in mean sea level, but the possible changes caused by a warming climate are unknown at this stage.
- A 2°C change in mean SST would mean that values presently considered anomalous (of the order of peak ENSO fluctuations) could well be normal occurrences, with resultant long-term stress on natural ecosystems that are unable to effectively adapt.
- Increased precipitation is expected throughout the year in high-latitudes and during the winter in mid-latitudes, possibly increasing coastal deposition rates. Some increase in Asian monsoon rainfall is also predicted.
- Changes in storm patterns or general shifts in mean weather conditions (windiness, wave energy and direction) are not able to be reliably estimated at this time but could have significant long term impacts on coastal stability and alignments.
- Any potential increase in the frequency, magnitude or extent of very severe weather systems such as tropical cyclones would severely impact coastal regions, with the potential for enormous loss of life and devastating impacts on coastal ecosystems and morphology. Fortunately, the present predictions show a low likelihood of significant changes occurring to these systems.

The possibility of sea level rise alone forms a basis for considering a number of major impacts for the coastal zone, such as:

- inundation and displacement of wetlands and lowlands
- eroded shorelines
- increased coastal flooding by storms
- salinity intrusion of estuaries and aquifers
- altered tidal ranges, prisms and circulation in estuarine systems
- changed sedimentation patterns
- decreased light penetration

Coral reefs and reef islands appear especially susceptible to climate change and associated sea level rise. The erosion of the coastline, inundation and flooding of low lying areas and seawater intrusion into groundwater lenses will all act to reduce the habitability of such regions. However, individual responses are likely to vary greatly because of sediment availability, available freeboard, aquifer characteristics and general resilience of the natural systems.

Normal rates of coral growth are thought sufficient to keep pace with projected rates of sea level rise and in some situations may even benefit from an increased water level. It is also conjectured that coral biota may be able to adjust to the projected rate of water temperature increases without succumbing to bleaching effects. However, reduced resilience caused by UVB increases may restrict this ability. Additionally, many coral reef areas are already thought to be adversely affected by rainfall and urban runoff, which may increase in some areas under a changed climate.

4.7 Australian Regional Predictions and Impacts

The most recent regional climate change projections for Australia are presented in CSIRO (1996). Potential broad-scale impacts of these projections form the basis of a national vulnerability assessment by Basher and Pittock (1998) in IPCC (1998). CSIRO scenarios for Australia indicate possible temperature increases of 0.3°C to 1.4°C by 2030, approximately doubling by 2070. Total rainfall trends vary across the continent and have seasonal aspects but with changes up to 10% in magnitude relative to present norms, the overall tendency being for decreases. In spite of this, an increase in intensity of heavy rainfall events is predicted. There are no specific projections of regional sea level rise in addition to IPCC (1996a) nor are there any trends for tropical cyclone effects which are at variance with Hendersen-Sellers *et al.* (1998), e.g. Walsh and Pittock (1998), McInnes *et al.* (2000), Walsh and Ryan (2000). These predictions must still be viewed within the context that, relative to their assessed global performance, existing climate models are considered to have reduced skill at subcontinental scales. CSIRO (1996) also relies on a combination of slab model and coupled models because of some doubts about the reliability of scenarios from the coupled models versus latitudinal warming gradients and trends in summer rainfall across Australia.

A wide range of vulnerability and impact studies have been undertaken for various areas of Australia and the South Pacific over the past ten years. Some early studies (e.g. Pearman *et al.* 1988) which predate IPCC (1996a) must be reinterpreted in terms of the revised climate projections, but otherwise still contain useful guidance on some specific regional issues. The majority of studies have been undertaken by and for State and Commonwealth authorities through research grants under the Australian Greenhouse Office and also with specific State funding, e.g. Bouma *et al.* (1996). A number of regional climate change scenarios are also available, which are essentially the same as the overall Australian view but with localised commentary, e.g. CSIRO (1998), specific climate change scenarios for northern Australia. In regard to specific coastal vulnerability issues, Waterman (1996) summarises a number of studies undertaken for the Commonwealth Department of Environment, Sport and Territories from 1994 to 1996, although in the Queensland context this is limited to DEH (1996) for Mackay. The earliest storm tide study that included a Greenhouse assessment is due to Hardy *et al.* (1987), while McInnes *et al.* (2000) provides a more recent assessment for Cairns. Henderson-Sellers (1996) provides an overview of issues and possible adaptive options confronting Oceania in general.

4.8 Conclusions and Recommendations

NCCOE (2001) concurs that the weight of scientific opinion suggests that baseline changes to climate may occur within the design life of much of our coastal and ocean community infrastructure. Consequently, consideration of the possible impacts of climate change should be included in the design processes and in long term planning. The overall response to "greenhouse" though should be seen as an expansion of current methodologies where natural variability of climate still dominates considerations of risk. In spite of the enormous and growing body of scientific literature and knowledge of global warming, there are unlikely to be definite predictions of its effects or panaceas for its possible impacts. It is therefore essential that good judgement be also exercised at all times.

In regard to the impacts of climate change on storm tide risks caused by tropical cyclones, it is recommended that consideration should be given to:

1. *Mean sea level rise scenarios over time (e.g. 0.49 m by 2100)*

2. *Some increase (e.g. 10% to 20%) in the maximum potential intensity of individual cyclones (MPIs)*

It is important to note the latter recommendation should be introduced as a lowering of the MPI physical limit rather than an across-the-board lowering of central pressures.

It is not considered essential to allow for any specific change in the frequency of occurrence or geographical limit of tropical cyclone activity in the Queensland region since there is insufficient analysis upon which to draw a conclusion.

Until such analyses prove otherwise, it is recommended that model sensitivity to the frequency of occurrence or geographical limit of tropical cyclones should be tested as part of a comprehensive hazard assessment methodology, i.e. inclusion of a nominal 10% variation.

4.9 References

Basher R.E. and Pittock A.B. (1998) Australasia. In: The regional impacts of climate change - an assessment of vulnerability. [IPCC, 1998], *Cambridge University Press*, ISBN 0-521-634555, 106-148.

Bouma W.J, Pearman G.I. and Manning M.R. (eds.) (1996) Greenhouse: coping with climate change, *CSIRO Publishing*, Collingwood, Vic.

Cox R.J. and Horton, P.R. (1998) Managing climate change in the coastal zone. Proc. Australian Global Warming Conf..

CSIRO (1996) Climate change scenarios for the Australian region. Climate Impact Group, *CSIRO Div Atmospheric Research*, Melb, Nov, 8pp.

CSIRO (1998) Climate change under enhanced greenhouse conditions in northern Australia - Final report 1994-1997. *CSIRO Div of Atmospheric Research*, Jan, 49pp, ISBN 0643060170.

DEH (1996) Methodology for climate change vulnerability assessment of Mackay coast. Coastal Resource Assessment Section, Coastal management branch. Prep by Qld Dept of Environment and Heritage for the Commonwealth *Dept of Environment, Sport and Territories.*

Dept of the Environment (1997) Climate change: Australia's second national report under the United Nations framework on climate change. *Commonwealth of Australia*, Nov, ISBN 0642194610, 125 pp.

Gordon, A.D. (1988) A tentative but tantalizing link between sea-level rise and coastal recession in New South Wales,. In *Greenhouse: Planning for Climate Change* [Pearman, G.I. (ed.)], CSIRO Publishing, Collingwood, VIC, 121-134.

Harper B.A. (1999) Storm tide threat in Queensland: History, prediction and relative risks. Conservation Technical Report No. 10, *Dept of Environment and Heritage,* Jan, ISSN 1037-4701.

Henderson-Sellers A., Zhang H., Bertz G., Emanuel K., Gray W., Landsea C., Holland G., Lighthill J., Shieh S-L.,Webster P. and McGuffie K. (1998) Tropical cyclones and global climate change: a post-IPCC assessment. *Bull. of the Amer Met. Soc.*, 79, 1, January, 19-38.

Henderson-Sellers A. (1996) Adaptation to climate change: its future role in Oceania. In: Greenhouse: Coping with Climate Change [Bouma, W.J, Pearman, G.I. and Manning M.R. (eds.)]. *CSIRO Publishing*, Collingwood, VIC, 349-376.

Holland G.J. (1996) Tropical cyclone intensity and intensity change: A review and outlook. ONR Symposium on Tropical Cyclones: State of Understanding and Future Directions, *Bureau of Meteorology*, Melb, Dec 9-13.

Holland G.J. (1997) The maximum potential intensity of tropical cyclones. *J. Atmos. Sci.*, Vol 54, Nov, 2519-2541.

Hopkins L.C. and Holland G.J. (1997) Australian heavy-rain days and associated east coast cyclones: 1958-92. *Journal of Climate*, 10, 621-635.

IPCC (1996a) Climate change 1995 - the science of climate change. Contribution of working group I to the second assessment report of the intergovernmental panel on climate change, *Cambridge University Press*, ISBN 0 521 56436 0, 572pp.

IPCC (1996b) Climate change 1995 - impacts, adaptations and mitigation of climate change: scientific-technical analyses. Contribution of working group II to the second assessment report of the intergovernmental panel on climate change, *Cambridge University Press*, ISBN 0 521 56437 9, 879pp.

IPCC (1996c) Climate change 1995 - economic and social dimensions of climate change. Contribution of working group III to the second assessment report of the intergovernmental panel on climate change, *Cambridge University Press*, ISBN 0 521 568544.

IPCC (1998) The regional impacts of climate change - an assessment of vulnerability. A special report of IPCC Working Group II, *Cambridge University Press*, ISBN 0-521-634555.

McInnes K. L., Leslie L. M. and McBride J. L. (1992) Numerical simulation of cut-off lows on the Australian east coast: sensitivity to sea-surface temperature. *J. Climate*, 12, 783-795.

NCCOE (2001) Guidelines for responding to the effects of climate change in coastal and ocean engineering. National Committee on Coastal and Ocean Engineering, *IEAust.* (in preparation)

Nicholls N. (ed.) (1993) Climate change and El Niño southern oscillation, BMRC Res. Rep No 36, Bureau of Meteorology, Melbourne, 31pp.

PCTMSL (1999) Permanent committee on tides and mean sea level - circular 43. *Defence Publishing Service*, Department of Defence, May, 8pp.

Pearman G.I. (ed.) (1988) Greenhouse: planning for climate change. *CSIRO Publishing*, Collingwood, VIC, 752pp, ISBN 0 643 04863 4.

Smith I.N., Dix M. and Allan R.J. (1997) The effect of greenhouse SSTs on ENSO simulations with an AGCM. *Journal of Climate*, 10, 342-352.

Walsh K. and Pittock A.B. (1998) Potential changes in tropical storms, hurricanes, and extreme rainfall events as a result of climate change. *Climatic Change*, 39, 199-213.

Walsh K.J.E. and Ryan B.F. (2000) Tropical cyclone intensity increase near Australia as a result of climate change. Jnl. Climate (to appear).

Waterman P. (ed.) (1996) Australian coastal vulnerability assessment project report. *Dept of the Environment Sport and Territories*, Australian Government, Canberra, 2 Vols / CDROM.

5. Tropical Cyclone Wind and Pressure Modelling

5.1 The Need for Simplified Models

This section introduces the need for simplified parametric models for hazard studies and presents some of the technical bases for a typical model in popular usage. An example wind field pattern is also presented for reference purposes. Areas where there are opportunities for model results to significantly differ are highlighted in the discussion. The development here is drawn from WMO (1988) and also the subsequent work by Harper and Holland (1998), a state-of-the-art review commissioned by the Risk Prediction Initiative, Bermuda.

The tropical cyclone (hurricane or typhoon) is an extremely complex meteorological phenomenon but from a descriptive viewpoint is still amenable to analytical simplification, provided that the essential time and space scales of motion are preserved. This descriptive reconstruction process is separate from the very difficult questions of prediction of intensification and movement of tropical cyclones that beset forecasters. These questions continue to be the subject of intensive research into the basic physics and dynamic interaction of the storm with its environment, both atmosphere, ocean and land, throughout its life. Some very complex numerical models of tropical cyclone behaviour are now available which attempt to represent the full 3-dimensional interactions of the storm (e.g. Kurihara *et al.* 1995; Wang and Holland 1996; Kepert 2000; Kepert and Wang 2000). As these models continue to be developed and computer power increases it is likely that these deterministic models will, in association with better environmental data sets and improved physical parameterisations, continue to gain accuracy and skill. However, such models are presently too cumbersome and computationally expensive to be applied to the types of studies required for long-term risk assessment. This is because a large number of storm scenarios need to be considered across wide areas to develop the statistical basis required for risk estimation. In addition, deterministic models will eventually reach a limit of representation where stochastic processes begin to dominate the prediction of storm behaviour. It is likely that these stochastic elements remain very important in individual storm scenarios and the appropriate statistical representation of their occurrence may become the single most important factor in the estimation of insured losses from tropical cyclones. Techniques utilising simplified parametric models already have the capacity to incorporate this type of stochastic variability into risk assessments, albeit at a lower level of representation.

Since we are interested in impacts of tropical cyclones at the surface (land or ocean), the emphasis is on the representation of the near-surface (horizontal) wind and pressure field as it evolves with time. Developments over several years have resulted in such models furnishing simplified descriptions of the essential wind (and pressure) profiles that provide spatial and temporal surface forcing for use in a variety of complex engineering, numerical modelling and risk assessment studies such as

- offshore facilities wind, wave, continental shelf current and storm surge design criteria
- onshore infrastructure design (eg ports, public housing, wind sensitive structures)
- public evacuation and disaster planning (wind and storm surge)
- insurance risk assessment

5.2 Basic Model Characteristics

A tropical cyclone is described by WMO (1997) as a non-frontal cyclone of synoptic scale developing over tropical waters and having a definite organized wind circulation with average wind of 34 kn (63 km h^{-1} or 17.5 m s^{-1}) or more surrounding the centre. The averaging period for defining the winds varies between countries, being 1 minute in the USA, and 10 minutes in most other regions (e.g. Neumann 1993). Unless otherwise stated, a 10-minute *mean* wind is assumed throughout this document.

The common approach in representing the fully developed features of tropical cyclones over the open ocean is to begin with the surface wind field derived from a steady axisymmetric vortex that is stationary in a fluid at rest. The vortex solution is based on the Eulerian equations of motion in a rotating frame of reference (Smith 1968). The analysis begins with a consideration of the force balance at the geostrophic, or gradient, wind level above the influence of the planetary boundary layer. Following the pioneering work of Schloemer and collaborators from the US Army Corps of Engineers (e.g. Schloemer 1954), the radial profiles of both the surface pressure and gradient wind speed can then be expressed as a function of storm central pressure, spatial size, air density and latitude. The gradient wind speed is then reduced to the standard surface reference level over the ocean of +10m MSL (mean sea level) by consideration of boundary layer effects. This includes wind inflow towards the vortex centre, and asymmetric effects due to storm forward motion or surrounding synoptic pressure gradients. This permits description of the near-surface wind and pressure fields as a function of radial and azimuthal offsets from the centre of the storm.

This approach provides an analytical representation of a fully developed storm based essentially on four time-varying parameters:

1. Storm central pressure; $p_0(t)$
2. Ambient or environmental pressure; $p_n(t)$
3. Radius to maximum winds; $R(t)$
4. Track or forward motion vector; $V_{fm}(t)$; $\theta_{fm}(t)$

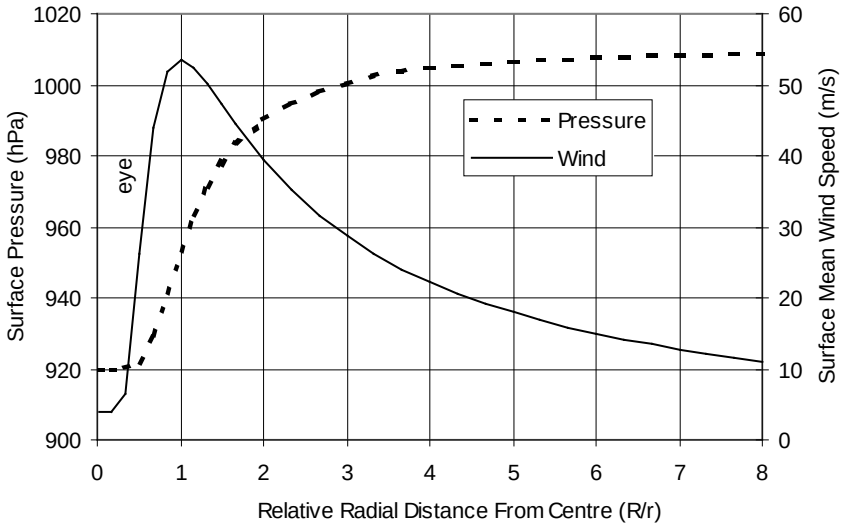

Figure 5.1 Basic radial wind and pressure profiles in a tropical cyclone.

Figure 5.1 illustrates the basic radial wind and pressure profile that results from such an analysis; the MSL pressure decreases exponentially towards the centre and levels-off to a

relatively flat region of lowest pressure inside the cyclone "eye" (920 hPa in this example). The winds initially increase exponentially towards the centre, driven by the increasing pressure gradient and reach a maximum at the so-called radius of maximum winds, before rapidly dropping to calm in the centre. While many real storms may not always exhibit such symmetry and form throughout their full life cycle, this basic model does appear to well represent the essential force balance and spatial variability of the tropical cyclone. In more sophisticated models additional parameters are often added, as detailed in the following sections.

For the purpose of illustration, the Holland (1980) model development is followed here, but replacing the Holland *A* parameter by its equality R^B. The model relies on the primary assumption of a radially symmetric pressure field derived from Schloemer (1954) but with a modified rectangular hyperbola to give the pressure *p* at any radius (*r*) from the centre as:

$$p(r) = p_0 + (p_n - p_0)\ exp\ (-R/r)^B \tag{5.1}$$

Here an additional fifth parameter "*B*" is introduced to add to the basic set of descriptive storm parameters previously listed. Holland recognised that the basic Schloemer profile lacked sufficient dynamic range to match many steep storm pressure profiles such as *Tracy* and subsequently added the *B* parameter - the so-called profile "peakedness". When *B* is set to the lower limit of 1, the profile is equivalent to the classic Schloemer formulation and Holland nominally limited its range based on simple physical arguments to lie within $1 < B < 2.5$.

The gradient level winds are then derived by considering the balance between the centrifugal and Coriolis forces acting outwards and the pressure force acting inwards, leading to the gradient wind balance equation:

$$V_g^2(r)/r + f\,V_g = 1/\rho_a\ dp(r)/dr \tag{5.2}$$

where V_g = gradient level wind
ρ_a = air density
f = Coriolis parameter ($2\omega \sin \phi$)

and the pressure gradient from differentiation of (5.1) is given by:

$$dp(r)/dr = (p_n - p_0)\ (B/r)\ (R/r)^B\ exp\ (-R/r)^B \tag{5.3}$$

which substitutes into (5.2) to yield the gradient wind at any radius as:

$$V_g\,(r) = \sqrt{(p_n - p_0)\ B/\rho_a\ (R/r)^B\ exp\ (-R/r)^B + r^2f^2/4\ )} - rf/2 \tag{5.4}$$

At $r = R$ the maximum gradient wind speed is given by:

$$V_g max = \sqrt{(p_n - p_0)\ B\ /\ (e\ \rho_a) + R^2f^2/4\ )} - rf/2 \tag{5.5}$$

but since the Coriolis terms are normally negligible at $r = R$, this reduces effectively to:

$$V_g max = \sqrt{(p_n - p_0)\ B\ /(e\ \rho_a)} \tag{5.6}$$

where it can be seen that for the Holland model, the pressure differential is further modulated by $\sqrt{B}$ over the original Schloemer estimate for $V_g max$, thus providing a further dynamic range up to a factor of 1.6. Based on the climatological work by Atkinson and Holliday (1977) and Dvorak (1975), Holland also suggested "standard" *B* values might be inferred of the form:

$$B = 2 - (p_0 - 900)/160 \quad (5.7)$$

making B a direct function of storm intensity. To allow for possible climatological variability in such a trend this can also be generalised to a "family" of like curves which might apply to a specific storm's lifetime, e.g.

$$B = B_0 - p_0(t)/160 \quad (5.8)$$

where B_0 is the intercept value of the trend.

A potentially important component missing from both the Holland and other wind profile formulations, is the variation of air density with pressure towards the cyclone centre. Introducing this variation changes the wind peakedness significantly and might lead to more easily defined values of *B*.

5.3 Boundary Layer Representation

Equation (5.4) provides a radially symmetric profile of estimated gradient level winds which must be transferred to be representative at the surface. Traditionally, this adjustment to the surface (+10m) has been based on similarity theory and the logarithmic deficit law approach, whereby the near-surface boundary layer profile at any height *z* is a function of the surface roughness z_0 and the reference wind speed. This is clearly an oversimplification of the complex dynamics of the tropical cyclone boundary layer, many aspects of which are still emerging (e.g. Kepert and Wang 2000). However, in the absence of better information this approach has permitted reasonable calibration against a range of measured results under tropical cyclone conditions. This assumption results in the mean near-surface wind V_m, under assumed neutral stability conditions, being estimated by an equation of the form:

$$V_m = Km\, V_g \quad (5.9)$$

where $K_m = ln(10/z_0)/ln(z_g/z_0)$ (5.10)

and z_g = gradient wind height V_g $(z=z_g)$

Over the open ocean, the surface roughness is dynamically a function of wave growth with time, while over land it varies spatially according to the natural and built environment. Open ocean roughness values are generally accepted as ultimately reaching levels similar to lightly timbered savanna.

Application of this theoretical approach is strictly limited to stationary wind conditions where the peak gust is related to a mean wind reference by a Gaussian distribution function. Accordingly, a representative mean wind-averaging period of 10 minutes is often used to establish the mean profile and then gust factors are re-applied to suit various applications such as 2 or 3 sec gusts. In this context V_m is to be considered as a 10 minute averaged wind sample. A basic limitation of this theory is that convective storm elements, especially within

rainbands, are thought capable of allowing gradient winds to penetrate to the surface without the assumed vertical mixing processes occurring. Also, microburst and vortex breakdown components can simply add horizontal wind at the surface as localised transient features. These essentially convective elements are becoming recognised as at least partially responsible for relatively high gust factors often being reported in landfalling tropical cyclones (Holland and Black *pers. comm.* 1997).

A variety of values for K_m exist in the literature and some of the early choices are mentioned later, the differences being complicated by the often unstated choice of averaging period for the surface wind. For example, Powell (1980) proposed 0.8 but his later observational studies (e.g. Powell and Black 1989; Powell *et. al.* 1991; 1998) have reported variability over the range 0.7 to 0.9, which has normally been attributed to vertical stability differences. As an order of magnitude, it is believed that K_m can be considered as approximately 0.7 over the ocean which, when combined with a peak gust factor of order 1.4, typically delivers 2 to 3 sec gusts basically equivalent to the gradient speed. Microbursts and other transient features might further cause super-gradient winds to develop locally for short periods. Kepert (2000) also introduces the possibility that K_m may in fact be azimuthally varying due to the complex vertical structure of the boundary layer. The potentially arbitrary choice of K_m and associated wind averaging periods is typically a major source of variation between "similar" parametric models and can have significant impact on predicted surface stress magnitudes and distributions.

In addition to the scalar reduction in wind speed, surface friction and continuity demand that the wind must flow inward across the isobars. The angle of inflow is taken to be approximately 25° in the outer region (e.g. Shea and Gray 1973), but reduces to zero near the radius of maximum winds. For example, Sobey *et al.* (1977) adopted the following, based on US Weather Bureau (1968):

$$\beta = \begin{cases} (10\ (r/R) & 0 \le r < R \\ (10 + 75\ (r/R\text{-}1) & R \le r < 1.2\,R \\ (25 & r \ge 1.2\,R \end{cases} \qquad (5.11)$$

5.4 Forward Motion Asymmetry

Tropical cyclone motion produces complex changes to the surface wind field that are intrinsically related to the 3-dimensional structure of the storm, the underlying surface conditions, and the atmospheric environment within which the cyclone is embedded. Parametric models to date have sought to reproduce only the first-order effects of the observed forward motion on the surface windfield. In some cases, the forward motion vector has been added to the wind field at the gradient level, then reduced to the surface by the standard techniques described above. The preference here though is that the forward speed is directly added at the surface since it is a manifestation of movement at the surface. This provides a left-right asymmetry, with the maximum winds to the left (right) when looking in the direction of motion of the cyclone in the Southern (Northern) Hemisphere. The actual location of the region of maximum surface winds in individual storms can occur almost anywhere (Jelesnianski and Holland 1993; Kepert 2000).

This asymmetry is thus achieved by various models such that some proportion of the forward speed δ_{fm} (typically 0.5 or 1) is added at the surface along an assumed line of maximum winds θ_{max} (measured upwind relative to the cyclone movement direction) and then azimuthally adjusted about the storm, e.g.

$$V_m(r,\theta) = K_m V_g(r) + \delta_{fm} V_{fm} \cos(\theta_{max} - \theta) \quad (5.12)$$

and when $\theta = \theta_{max}$ and $r = R$, the maximum surface wind speed in the storm is:

$$V_m max = K_m V_g max + \delta_{fm} V_{fm} \quad (5.13)$$

This is perhaps the least satisfactory aspect of the current empirical approaches to modelling the cyclone surface wind field. Values chosen for θ_{max} have varied, with early estimates being 115º (rear left) based inferred from Graham and Nunn (1959) with later values being around 65º (front left) consistent with, for example, Shapiro (1983) and now Kepert (2000).

5.5 A Typical Parametric Wind Field Representation

Based on the foregoing description, Figure 5.2 presents an example parametric mean wind field of a fully developed tropical cyclone over the ocean, together with a crossection of mean wind and pressure normal to the direction of movement. The storm is presented as a Southern Hemisphere example moving south. The full set of parameters used is listed in Table 5.1 below.

Table 5.1 Example Storm Parameter Set

Parameter	Symbol	Value	Units
Latitude	ϕ	-20	°
Central Pressure	p_0	920	hPa
Ambient Pressure	p_n	1010	hPa
Radius to Max Wind	R	30	km
Forward Speed	V_{fm}	4	m s^{-1}
Bearing	θ_{fm}	180	°
Peakedness	B	1.5	-
Asymmetry Factor	δ_{fm}	1.0	-
Line of Max Wind	θ_{max}	65	°
Air Density	ρ_a	1.15	kg m^{-3}
B/L Coefficient	K_m	0.67	-

The $V_m max$ resulting from this combination at $r = R$ along the line of maximum winds is 47.5 m s^{-1} located in the front left stormwise quadrant (65° left or upwind of the forward motion vector).

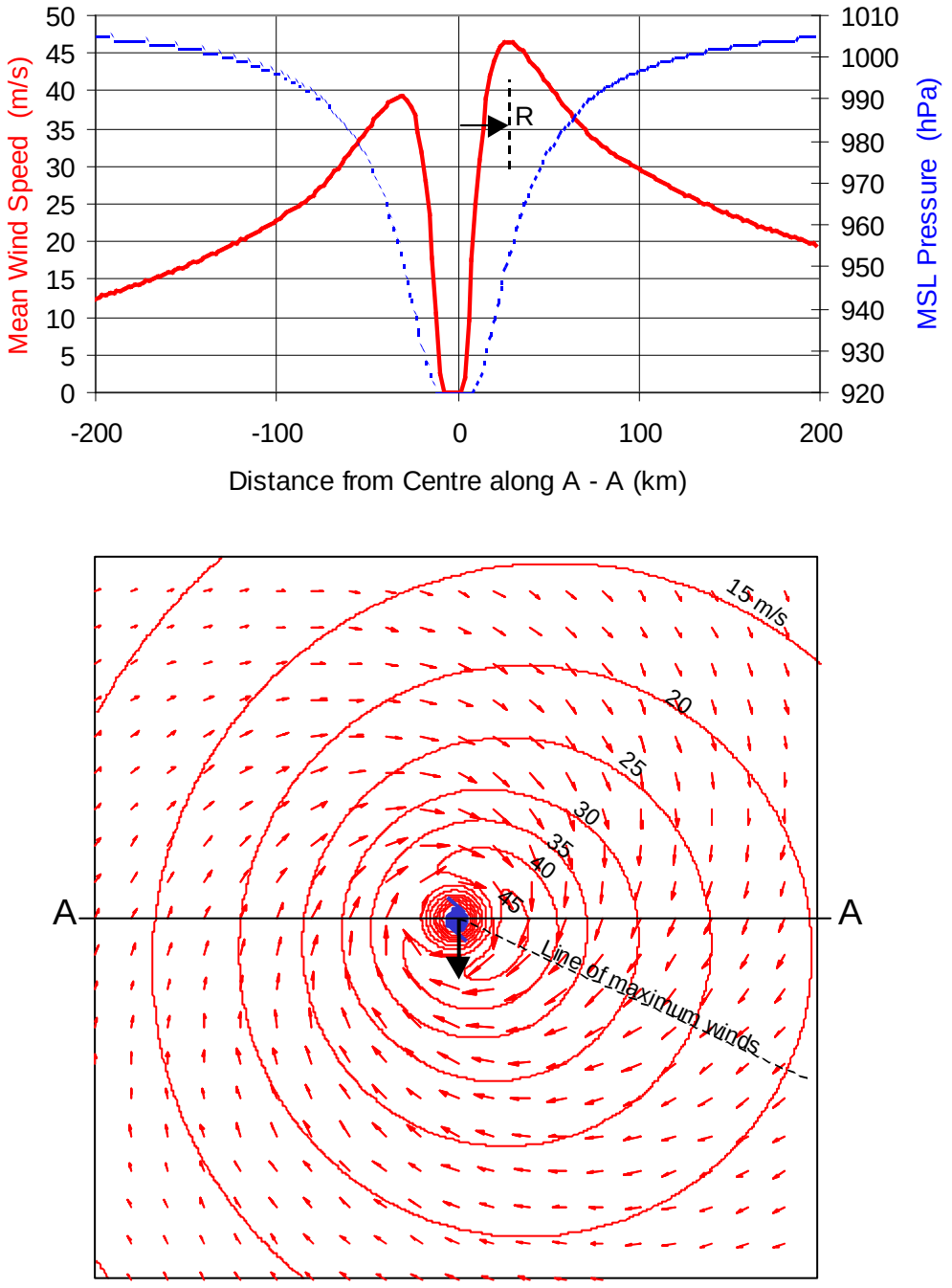

Figure 5.2 Example surface mean wind field for a moving storm.

5.6 Historical Development of Windfield Models

Some of the early development presented here follows essentially the work by Lovell (1990) who identified 24 separate parametric wind field model descriptions that had been published up until the late 1980s. His conclusion was that almost all popular formulations were essentially variations on those first developed by either the US Weather Bureau and the US Army Corps of Engineers in the 1950s (firstly by the Hydrometeorological Section and then by the joint National Hurricane Research Program (NHRP)) or by Holland (1980). The apparent proliferation of models in various forms over the years has resulted mainly because many authors failed to adequately acknowledge the original sources for the parametric formulations or inadvertently disguised the pedigrees by the introduction of simplifying constants, non-dimensionalising of equations and the like.

5.6.1 Earliest Studies

Takahashi (1939, 1952) and Hughes (1952) were instrumental in proposing some early empirical methods while perhaps the earliest attempt at describing the full wind field in a parametric manner dates to Depperman (1947) in a study of Philippine typhoons. This is the so-called Rankine-combined or modified potential vortex, where the radial wind field at gradient height is given by:

$$V_g = V_g max\ (r/R) \qquad r < R \qquad (5.14a)$$

$$V_g = V_g max\ (r/R)^{-x} \qquad r > R \qquad (5.14b)$$

The shape parameter x allows the outer wind profile beyond R to be modified to fit available data. For physical reasons $0 < x < 1$ with a practical range $0.3 < x < 0.8$ and a typical application value of 0.5. The Rankine vortex model is mentioned for completeness rather than practical application. This is because practitioners find it often produces a profile that generally under or over shoots measured winds.

5.6.2 US Army Corps of Engineers Impetus

A number of specific studies were undertaken by the US Weather Bureau on behalf of the US Army Corps of Engineers over the period 1954 through to the early 1960s, which were aimed at producing objective techniques for estimating hurricane intensities.

The first study was by Schloemer (1954), who developed a model pressure profile to plan levee heights for storm surge impacts on Lake Okeechobee in Florida. Although the profile was based on limited pressure data from only nine storms it appears to have captured the essential broad-scale form of the radial pressure relationship. His exponential pressure profile was based on the general principle that:

$$(p-p_0) / (p_n-p_0) = \mathbf{f}(r) \qquad (5.15)$$

Schloemer applied the exponential pressure profile to the cyclostrophic wind balance equation to provide a radial wind profile and derived a value for $V_g max$. He also proposed a value for K_m and the surface inflow angle. His work was significant in being the first to specify a continuous radial wind profile in pressure balance and to recognise the significance of the

environmental pressure, an *R* scale and the surface boundary layer effects. Fletcher (1955) provided further dissemination of Schloemer's work for general application in estimating maximum surface winds.

Myers (1954) extended Schloemer's work in applying it to a statistical analysis to establish design criteria. He replaced the cyclostrophic balance by the gradient balance (i.e. including Coriolis effects) to obtain better data matches at outer radii. He also further examined the K_m issue and considered the difference in roughness regimes and transition lengths between onshore and offshore winds. Out of this work came the recommendation to apply the (much quoted to three significant figures) K_m of 0.865 for transfer of gradient winds to off-water V_m. This was predicated on the assumption that the peak 3 second gust approximately equalled the gradient wind *V*. Myers also examined the possible relationship between *R* and storm intensity, noting that the highest wind speeds in very intense hurricanes tended to become more spatially limited.

This work continued with the National Hurricane Research Project (NHRP) in 1955 and Graham and Nunn (1959) developed the so-called Standard Project Hurricane (SPH) indices for seven differing geographic zones along the East and Gulf coasts of the US. These indices were based on applying Myer's equations to a database of storms over the period 1900 to 1956. They also introduced forward motion asymmetry allowances using a δf_m of 0.5 and selected θ_{max} as -115° based on observational studies. Finally, they made recommendations in regard to transition zones and, although generally applying the Myer's K_m of 0.865, were swayed by one set of measurements to allow 0.885 for one of the Gulf regions. Their recommendations were published as a series of nomograms for forecaster use, the radial wind profiles not exactly following the theoretical curve but allowing for empirical shape variations on a regional basis.

Graham and Hudson (1960) continued the work by looking at further cases in detail, including extra-tropical storms, and adjudged Schloemer's pressure profile considerably in error in the outer portions of the profiles. They were the first to consider introducing the *B* exponent to objectively address this, Graham and Nunn already having empirically adjusted the regional outer wind profiles to suit. Ironically, the *B* parameter here was proposed for reasons opposite to that later to be considered by Holland in regard to the peak portion of the profile.

Over this period a number of theoretical and observational studies of hurricane wind fields contributed to increasing knowledge. These included Colon (1961), Miller (1958,1962), Kraft (1961), Rhiel (1962) and Rosenthal (1961,1962). Further updates of the NHRP followed over time with US Weather Bureau (1968) first introducing the *probable maximum hurricane (PMH)*, with later updates by Schwerdt (1972) and finally Schwerdt *et al.* (1979).

5.6.3 Growth of Applications

Subsequent works then concentrated on the application of these techniques for planning and warning purposes, especially in regard to storm surge prediction (Harris 1958; Harris and Jelesnianski 1964; Marinas and Woodward 1968) and the burgeoning Gulf of Mexico offshore oil and gas developments.

Jelesnianski (1965,1966) adopted the Schloemer pressure profile for incorporation into his numerical hydrodynamic model for storm surge but chose not to apply the balanced wind

profile. This may have been more for computational convenience at the time, his formula being:

$$V_m(r) = (2\ V_m max + V_{fm})\ R\ r\ /\ (R^2 + r^2) \qquad (5.16)$$

This later led to the development of the US Weather Service SPLASH storm surge prediction model (Jelesnianski and Taylor 1973) and the SLOSH model (Jelesnianski *et al.* 1992).

Many other workers continued to explore variations on the NHRP theme, increasingly targeted now at computer application of the SPH nomograms, and to try to accommodate the additional dynamic range needed from the Schloemer profile. Collins and Viehman (1971) presented a re-examination of unpublished NHRP data (Goodyear and Nunn 1965) correlating R vs $V/V_m max$, ostensibly to provide a "simplified" model but arguably not succeeding. Patterson (1972) provided an (ill-conditioned polynomial) variant for use in early numerical wave models, in conjunction with work by Wilson (1961,1966). Bretschneider (1972) had considerable impact in ocean engineering application but merely provided a non-dimensional form of Graham and Nunn's work with an added climatological variation based on ρ_a. His nomogram wind field was widely adopted for coastal and offshore engineering design through incorporation into various editions of the US Army Corps of Engineers design manual issued by CERC (1984). This has now been supplanted by the Holland (1980) model in the new CERC design manual (not yet released).

Cardone *et al.* (1976) introduced the next most dramatic change in approach to the problem by applying a numerical boundary layer solution targeted at wave prediction improvements. Their model still contained aspects of the Schloemer recommendations and utilised a form of R in specifying the symmetric vortex pressure profile. Their resulting model, used extensively in offshore design criteria work, is essentially numerical rather than parametric, based on earlier work by Chow (1971) and Cardone (1969).

Other oceanographers and ocean engineers adopted a number of different model approaches over this period. Russell (1971) published a further variant; Overland (1977) provided a review of methods; Ross (1979) modified Patterson (1972) in conjunction with the JONSWAP wave experiment (Hasselmann *et al.* 1973); Forristall (1980) adopted Patterson (1972), attributing it to Wilson (1961); Wang (1987) adopted Patterson (1972) but attributed it to Forristall (1980).

Wind engineers at this time also took advantage of the increasing availability of parametric models and applied them to the estimation of design wind speeds for construction. Typical applications of the Schloemer-Myers form included Martin (1974), Simiu *et al.* (1976), Gomes and Vickery (1976) and Batts *et al.* (1980).

In developing the first numerical storm surge model for Australian conditions, Sobey *et al.*(1977) and Harper (1980), adopted the Schloemer pressure profile and $V_m max$ estimates. They also fitted a separate B parameter to match the range of Graham and Nunn (1959) empirical wind profiles, the outer region equation being:

$$V(r) = V_g max\ exp(\ B(1-r/R)\ ) \qquad r > R \qquad (5.17a)$$

where $B = 0.0025R + 0.05$ for R in km. (5.17b)

A separate inner region wind equation was also developed and surface inflow angles established. A K_m of 1.0 was nominally adopted as a deliberate conservative response to the conflicting advice from a number of sources at that time.

5.6.4 Improving Theory and Observations

Landmark studies by Shea and Gray (1973) and Gray and Shea (1973) provided comprehensive data sets for further analysis and interpretation. Dvorak (1975) introduced the extremely powerful satellite cloud pattern recognition system for estimating intensity, based on the Atlantic basin, but still finding a wide application globally (and now being formalised in a new automatic and objective method).

Atkinson and Holliday (1977) analysed 28 years of data (76 typhoons) from the Western North Pacific to develop a relationship between maximum surface wind gusts and minimum storm pressure:

$$V_3 = 3.4\ (1010\text{-}p_0)^{0.644} \tag{5.18}$$

However, their methodology relied on making anemometer height and gust factor adjustments that may have compromised the final analysis. Guard (1998), for example, believes their results were biased, lacking data close to many of the storm centres.

The Schwerdt *et al.* (1979) revision to the SPH criteria recommended a modified asymmetry factor formulation and a more conservative K_m of between 0.9 and 0.95. An overland filling rate based on time after landfall was also developed. Wang (1978) applied the Schloemer form to typhoons near Taiwan.

Holland (1980) addressed the ability to fit wind profiles to a number of specific storms of record in the Australian region (*Tracy* and *Kerry*), especially in regard to matching the peak wind region critical for assessing impacts. He formalised the use of the "peakedness" parameter B (Equation 3.1) to provide increased dynamic range and acknowledged the potential benefit of climatological work by Atkinson and Holliday and also Dvorak (1975) in providing possible predictive capacity. He showed that the enhanced pressure and wind profiles produced better data fits to three Australian and nine Florida storms than either the Schloemer or the modified-Rankine profile.

Powell (1980), while not proposing a parametric wind field model, addressed the associated problem of predicting the boundary layer effects for estimating the surface winds. He compared four alternative numerical boundary layer models and two simple estimation techniques, concluding that a simple 0.8 K_m factor applied to flight level winds gave comparable results to the more sophisticated methods for the three hurricanes studied in detail.

The advent of routine aerial reconnaissance from the mid 1970s lead to significant improvements in data quality and quantity, such as reported by Willoughby and Shoreibah (1982) and Willoughby and Gray (1988), while Gray (1985) provided the first fully global view of tropical cyclone climatology.

5.6.5 More Contemporary Developments

Georgiou (1985) presented a comprehensive record of progress in this field and with additional analysis formulated a sophisticated two-level parametric model (700 hPa to 500 hPa and 500 hPa to surface). The upper-level is based on gradient wind balance essentially following Holland but with more sophisticated forward motion asymmetry. The lower level was parameterised from the numerical boundary layer model by Shapiro (1983) resulting in a radially varying K_m with typical values of 0.75 at $r/R > 5$, increasing towards the centre to 0.83 for $0.5 < r/R < 2$ and equalling the gradient speed at the storm centre. Georgiou also presented an overland storm decay model based on 26 storms, updating earlier estimates such as by Goldman and Ushijima (1974). He recommended the best-fit relationships based on distance travelled overland for several of US geographic zones. Water/land surface speed transitions were also considered.

During the early 1980s, much progress was also made in the interpretation of ocean surface wind stress relationships, which are intrinsically linked to the boundary layer issue. This topic has not been expressly addressed here but, for example, Hsu (1986) provides a summary.

Weatherford and Gray (1988ab) presented analyses of flight level profiles from 66 typhoons in the North West Pacific, noting the wide variability in pressure-wind relationship and scale radius.

Emanuel (1988), using steady-state thermodynamic arguments, provided an updated view of the maximum possible wind speeds that might be experienced in a tropical cyclone.

Powell and Black (1989) presented 11 years of aerial reconnaissance data and surface buoy wind data and provided updated K_m estimates for a range of boundary layer stability conditions. For neutral stability, a value of 0.7 was found generally representative for "mean" winds at the surface.

The Holland model profile, combined with asymmetry and inflow geometry, was used extensively for establishing engineering design criteria for the Goodwyn 'A' oil and gas production platform offshore Western Australia by Harper *et al.* (1989, 1993). Based on 17 storms and 23 anemometer sites, peak wind speed error was less than 4% for 21 of the cases, with bias error less than 12% in 19 cases. Among the many parametric forms of storm behaviour investigated for these studies, the Myers (1954) proposition of size being proportional to intensity was applied in the Australian context, i.e.

$$R(t) = R_c / (p_n - p_0(t)) \tag{5.19}$$

with values of R_c varying between 640 to 3000 and a mean of 1850. This relationship was then used in statistical simulation of storm climatologies to provide realistic variation in R, rather than a strict latitude-based assumption used in many previous studies.

Brown and Swail (1991) provided one of the most comprehensive analyses of over-water wind gust data yet available but only for North Atlantic conditions. Krayer and Marshall (1992) update this for hurricane conditions and propose special consideration for the eye wall region.

Powell *et al.* (1991) provide the first of many detailed surface wind analyses for landfalling cyclones based on flight level and surface wind data composites.

De Maria *et al.* (1992) recently proposed a model for incorporation into a numerical spectral model of storm movement. Their radial wind profile is of the form:

$$V_g(r) = V_g max\ (r/R)\ exp[\ (1-(r/R)^b)/b] \tag{5.20}$$

where b is a profile shape parameter, $0.2 < b < 0.8$ which is derived by consideration of matching with an assumed outer radius of storm influence. No estimate of $V_m max$ is independently provided but this model produces essentially the same profile shapes as that of Holland (1980).

The wind engineering discipline has also seen developments in recent years. Twisdale and Vickery (1992), Vickery and Twisdale (1994, 1995a, 1995b) charts the development of a modified form of the Georgiou (1985) model. They contend that the Batts *et al.* (1980) approach based on Schloemer underpredicts peak winds near the centre and overestimates winds at inland locations. They also developed an overland decay model of the form:

$$\Delta p(t) = \Delta p_0\ exp^{-\alpha t} \tag{5.21a}$$

where the filling constant α is given by:

$$\alpha = \alpha_0 + \alpha_1 \Delta p_0 + \varepsilon \tag{5.21b}$$

with ε a normally distributed error term and α_0 and α_1 varying to suit each of three geographic zones for the Florida, Gulf and Atlantic coasts of the US. Peterka and Shahid (1998) utilised these and other results in compiling the latest update of design gust wind speeds for the US. By comparison, Rupp and Lander (1996) present the results of a technique for estimating the recurrence interval of tropical cyclone winds in the Guam region.

Houston and Powell (1994) compares flight level and composited surface wind profiles with those assumed by the SLOSH storm surge model after Jelesnianski and Taylor (1973) and Jelesnianski *et al.* (1992). The wind model performed reasonably well except for offshore wind conditions, which were significantly overestimated.

Kaplan and De Maria (1995) present an additional empirical model for estimating the filling rate of landfalling storms. Their method predicts wind speed decay directly without inference from a pressure decay, unlike the Georgiou (1985) and Vickery and Twisdale (1995b) approach, but does account for distance travelled over land. Results are presented for the US Gulf and Atlantic Coasts. Their relationship has the form:

$$V(t) = V_b + (C_0 V_0 - V_b) exp^{-\alpha t} - C_1 \tag{5.22}$$

where V_0 is the starting intensity (maximum winds), V_b a base reference wind speed, C_0 an initial reduction coefficient, α a decay constant and C_1 is a correction for the proportion of the eyewall still over water.

A recent contribution from the coastal and ocean engineering field by Thompson and Cardone (1996) extends the use of parametric descriptions of the surface pressure field based on Holland to incorporate a broad or double wind maxima as follows:

$$p(r) = p_n + \sum dp_i \exp[-(R_i/r)^{bi}] \quad (5.23)$$

where dp_i is the pressure anomaly for the ith component, R_i and b_i similarly, so that

$$\sum dp_i = p_n - p_0 \quad (5.24)$$

with (p_n-p_c) and a value of dp_1 being needed to specify a value for a second dp_2 etc. Encouraging results fitted against the Hurricane Gilbert flight-level wind profiles are presented for comparison. The actual surface wind field is computed by a numerical planetary boundary layer model and so unfortunately is not available in a parametric form.

Callaghan and Smith (1997) present a re-examination of the possible relationships between $V_g max$, storm size and translation speed using a number of case histories and a theoretical development based on an idealised profile. Their conclusion is that large, intense tropical cyclones appear to have lower central pressures than small cyclones of similar intensity, especially when in the midst of a concentric eye cycle. In association with this, they further consider the possible form of a radial pressure profile where there may be a region of dead calm in the inner part of the vortex core. No specific profile form is provided.

Carr and Elsberry (1997) developed a tangential wind formula based on the principle of conservation of absolute angular momentum but including frictional dissipation. Their study was concerned with basic numerical modelling of how the circulation of the tropical cyclone interacts with its environment to affect its motion. Their wind speed profile is used for initialisation of a numerical storm motion model and has a modified Rankin form:

$$V_g(r) = M/r^X - 0.5 f r \quad (5.25a)$$

where

$$M = 0.5 f R_o^{(1+X)} \quad (5.25b)$$

and R_o is the average radius at which the tangential winds are zero and X is a parameter to account for frictional dissipation. Their profile is targeted at reproducing the outer core winds most accurately and, with winds increasing to infinity at r=0, does not include an eye. A technique is provided for forcing an eye based on a nominal spatial scale parameter but is not a practical solution to the estimation of peak winds near the eye wall. They find support also for the work by Merrill (1984).

Bode and Hardy (1997) updated the status of numerical modelling of tropical cyclone storm surge. It reviewed many aspects of the wind field and boundary layer problem and offered the Holland (1980) model as a most viable technique for this field of work.

McConochie *et al.* (1999) recently adopted the Thompson and Cardone (1996) multi-vortex approach in conjunction with the Holland (1980) parametric model, specifically for modelling of waves in the Great Barrier Reef. The multi-vortex is primarily used in this context to enhance outer wind fields rather than represent eye-replacement of the inner vortex, thus providing better control over the outer wind strength than available from the Holland *B* parameter alone.

Houston *et al.* (1999) revisited the performance of the SLOSH model wind field for 10 cases in five recent hurricanes. They found good agreement between the peak wind speeds in most cases (<6%) but more significant differences for the general region of strongest winds, where the SLOSH model mean wind speed was 14% greater than the reconstructed HRD winds.

The increasing availability of high resolution satellite imagery, Doppler radar and dropsonde data together with increasing computational ability continues to lead to new insights into tropical cyclone structure and behaviour. A number of more recent studies derive from these and other advances. Holland and Lander (1993) looks at scale interactions; Barnes and Powell (1995), Dobos *et al.* (1995) and Samsury and Zipser (1995) address detailed structural features of tropical cyclones; Donelan *et al.* (1997) and Fairall *et al.* (1994) consider the air-sea interface; Emanuel (1995), Kalishnik (1995) and Holland (1997) re-examine the question of maximum potential intensity (MPI); Quilfen *et al.* (1998) present new high-resolution surface winds based on scatterometry; Powell and Houston (1998) provide further composited surface wind fields for the 1995 US hurricane season.

5.6.6 Transient Wind Features

There was been mounting speculation over many years as to the possible role of high speed convectively-linked wind transients associated with tropical cyclones, especially at or near landfall (Willoughby and Black 1996, Wakimoto and Black 1994). Likewise, observed building damage at catastrophic levels that occurred during *Tracy*, where the anemograph also failed at the peak of the storm, lends conjecture to whether small-scale high-speed transients coexist within the maximum wind region of the cyclone circulation. Flight-level data combined with satellite and radar has now provided tantalising glimpses of just such convective systems within a number of rapidly deepening storms (Bluestein and Marks 1987, Marks and Houze 1984, Black and Marks 1991).

It is now clear that some of these meso-vortex features are linked to supercell thunderstorm formation close to the eyewall, circulating within the larger cyclone vortex, and forming and dissipating over timescales as small as 15 minutes. The rotational translation of these systems then appears outwardly as a time-varying eyewall asymmetry and, where the meso-vortex circulation adds to the cyclonic circulation, a wind speed asymmetry can result. More speculative, but supported by modelling studies and observed features of cyclones at landfall, is the potential for vortex breakdown. Under this scenario, the strong winds surrounding the eye can fold inwards and come to the surface as an intense localised jet of air. Such features may have existed within both *Tracy* and *Andrew* where radar and satellite information indicates a potential eye breakdown that corresponds with damage patterns.

It is also possible that local microbursts (Fujita 1981) could also be active, especially in rainbands outside the maximum wind region. These microbursts result when the rain-laden convective downdrafts develop and descend rapidly to the surface. The behaviour of the microburst is then similar to that of a vertical jet impinging on a horizontal surface, spreading radially with an exponential decay in magnitude but also translating with the speed of the parent convective cell (Hjelmfelt 1988). The resulting speed at the surface may then be the combined speed of the cyclonically-advecting mesoscale vortex and the radially-spreading microburst component. This could lead to local high-speed transients of perhaps only hundreds of metres in width, but extended longitudinally because of the high translation speed. This mechanism provides an explanation for the possible occurrence of “super-

gradient" surface wind speeds within tropical cyclones and could result in tornado-like damage swathes at the surface. Whether tornadoes could also coexist within this complex scale interaction is unknown, although tornadoes are known to be associated with at least the periphery of such systems (Novlan and Gray 1974).

In regard to storm surge modelling, the presence of transients is relevant only in regard to how their presence might contaminate historical anemometer records that are being used for model calibration. However, Kepert and Wang (2000) provide numerical evidence for the existence of persistent mid-level super-gradient jets in the vicinity of the eyewall which are apparently consistent with recent GPSsonde data. These jets coexist within an azimuthally and radially varying K_m, which does have significant potential to alter surface wind stress distributions compared with present constant K_m assumptions.

5.6.7 Summary of Model Developments

The foregoing condensed history of developments in this field highlights a number of specific points:

1. A very large number of alternative parametric representations have been proposed over the past 50 years (in excess of 30 specific identifiable types), although many of these are highly interdependent.

2. Most models have been based either on a limited number of high quality data samples or on larger numbers of lower quality samples.

3. All researchers have sought to improve the ensemble performance of their models by seeking more generalised forms at the risk of over-complicating the simpler parametric forms.

4. Significant differences in detail exist between the various models, especially in regard to the estimation of peak surface wind magnitudes and spatial distribution.

An example is given in Figure 5.3 of how several of the more popular and recent model wind profiles compare when set to "typical" parameter values. To avoid the issue of gradient to surface adjustment, only the radial gradient level wind speed profiles are shown. The example parameter values are Rankin (X=0.5), Holland (B=1.5), De Maria *et al.* (b=0.5), Schloemer (B=1), Jelesnianski and Carr *et al.* (X=0.4, R_o=800). A nominal p_0 of 960 hPa and p_n of 1010 hPa is used in this example, with an R of 30 km. To simplify the figure, each curve has been normalised to give the same peak wind at $r=R$ and even with this adjustment, the resulting range of speed variability is typically between 10 and 15 m s^{-1} along the radial, or 20 to 30 % of the peak value. After application of K_m assumptions and asymmetry factors, these differences can increase further. Radially integrated damage values obtained from these curves therefore will consequently vary dramatically, depending on the choice of parameters.

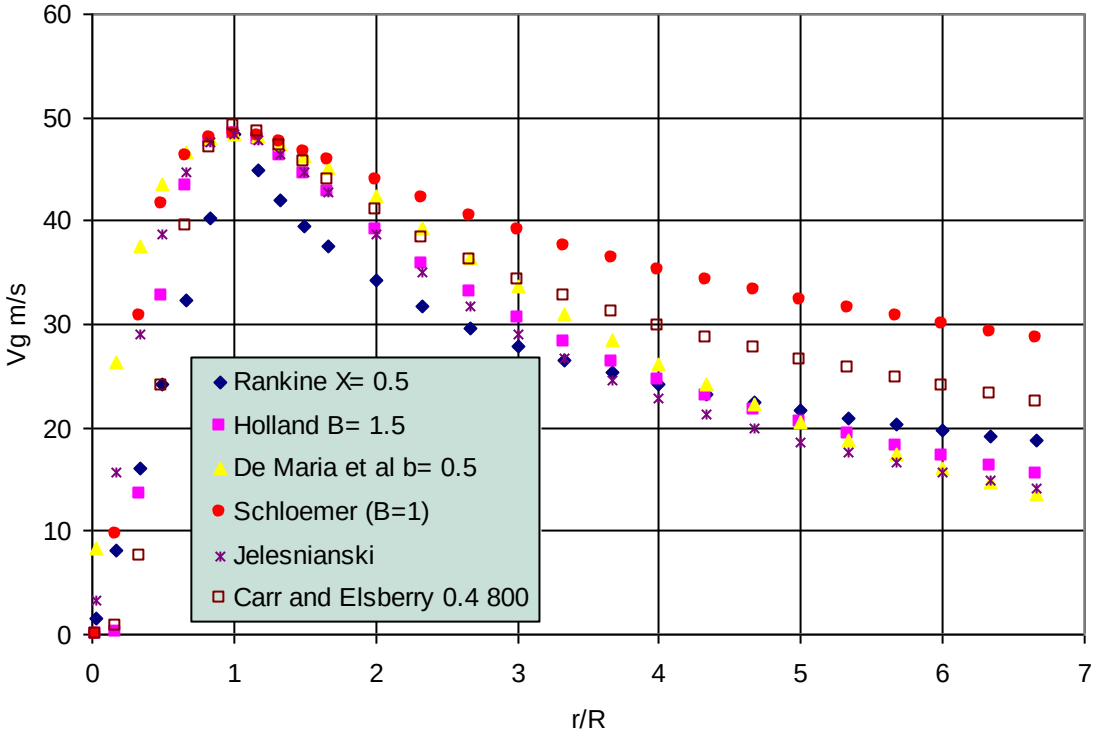

Figure 5.3 Some example parametric radial wind profiles.

Parametric wind field models of tropical cyclones need to address a wide range of application-specific needs (Harper and Holland 1998). These vary considerably from the open marine environment to coastal, landfall and post-landfall conditions. Unfortunately, much of the high-quality flight-level reconnaissance data that has been collected over the past 25 years is yet to be systematically analysed in a manner that could lead to more powerful parametric representations. A comprehensively-updated parametric wind and pressure field model of tropical cyclones is well overdue (Harper and Holland 1999).

5.7 Conclusions and Recommendations

The present study timeframe unfortunately did not permit a radical re-examination of the performance of parametric wind and pressure models. Since interest concentrates on over-ocean conditions, this simplifies the needs to some extent, although near-coastal convergence and topographic shielding may remain a significant issue for storm surge determination.

The results of storm surge hindcasts reported in Chapter 10 cast considerable doubt as to the most appropriate choice of windfield asymmetry that should be applied for storm tide modelling in the Queensland context. It is believed that this relates to the integrated effect of surface wind stress over (say) 2 to 5 *R* from the storm centre, where the vortex winds are merged with the background synoptic condition. In the simple parametric models described here, the only control of asymmetry is via application of a first-order forward speed effect. However, the dynamics of the boundary layer are extremely complex and actual sea surface wind asymmetry is likely due to a number of interactions which can manifest as varying gradient-to-surface wind factors and wind inflow angle etc. It is therefore potentially dangerous to treat the vortex in isolation from the larger scale flow when storm tide is of interest, rather than simply destructive winds. An extensive climatology review, as

recommended in Chapter 3, would assist greatly in resolving this issue since some form of climatology parameterisation at the synoptic scale will be desirable even to describe these influences.

It is recommended that further sensitivity testing of the impact of the latest tropical cyclone boundary layer research (e.g. BMRC modelling) be undertaken using existing Australian wind data before committing to an extensive storm tide modelling project.

If the above review is not achievable, it is recommended that the present study proceed with a parametric model essentially based on Holland (1980), as presented earlier in this chapter.

The model is described in detail in Appendix C but the essential features are summarised as follows:

- An axisymmetric wind and pressure field at gradient height
- A speed-dependent boundary layer reduction to +10 m
- Radially variable frictional inflow at the surface
- First-order forward speed asymmetry (variable, e.g. left front through to left rear)
- Synoptic scale interactions through application of merged vortices
- Overland decay based on distance travelled

5.8 References

Atkinson, G.D., and Holliday, C.R. (1977) Tropical cyclone minimum sea level pressure/maximum sustained wind relationship for the Western North Pacific. *Mon. Wea. Rev.,* 105, 421-427.

Barnes, G.M. and Powell, M.D. (1995) Evolution of the inflow boundary layer of Hurricane Gilbert (1988). *Mon. Wea. Rev.,* 123 (8), 2348-2368.

Batts, M.E., Russell, L.R., and Simiu, E. (1980) Hurricane wind speeds in the United States. *J. Structural Div.,* ASCE., Paper 15744, October 1980, 2001-2016.

Black, P.G. and Marks, F.D. (1991) The structure of an eyewall meso-vortex in Hurricane Hugo (1989). 19th Conf. on Hurr. and Trop. Meteor., AMS, May 6-10, Miami, FL, 579-582.

Bluestein, H.B. and Marks, F.D. (1987) On the structure of the eyewall of Hurricane Diana (1984)) Comparison of radar and visual characteristics. *Mon. Wea. Rev*., 115, 2542-2552.

Bode, L. and Hardy, T.A. (1997) Progress and recent developments in storm surge modelling. *J. of Hydraulic Engineering*, ASCE, 123(4), April, 315-331.

Bretschneider, C.L. (1972a)A non-dimensional stationary hurricane wave model. *Offshore Technology Conf.,* Houston, Tex., May 1972, Paper No. OTC 1417.

Bretschneider, C.L. (1972b) Revisions to hurricane design wave practices. *Proc. 13th Coastal Eng. Conf.,* Vancouver, July 1972, 167-195.

Brown, R.D. and Swail, V.R. (1991) Over-water gust factors. *Ocean Engng.*, 18(4), 363-394.

Callaghan, J. and R. K. Smith (1998) The relationship between surface wind speeds and central pressure in tropical cyclones. *Aust Meteorological Magazine*, (to appear).

Cardone, V.J. (1969) Specification of the wind distribution in the marine boundary layer for wave forecasting. *New York Univ.*, Geophysical Sciences Laboratory TR69-1, December 1969.

Cardone, V.J., Pierson, W.J., and Ward, E.G. (1976) Hindcasting the directional spectra of hurricane generated waves. *J. Petroleum Technology*, April 1976, 385-394.

Carr, L. E., III, and R. L. Elsberry (1997) Models of tropical cyclone wind distribution and beta-effect propagation for application to tropical cyclone track forecasting. *Mon. Wea. Rev*., 125, 3190-3209.

CERC (1984) Shore protection manual. U.S. Army Corps of Engrs., Coastal Engineering Research Centre, *Dept. of Army*,Vol. 1, 3-81 to 3-84.

Chow, S. (1971) A study of the wind field in the planetary boundary layer of a moving tropical cyclone. *MS thesis*, Dept. of Meteorology and Oceanography, New York Univ.

Collins, J.I., and Viechman, M.J. (1971) A simplified empirical model for hurricane wind fields. *Offshore Technology Conf.*, Houston, Tex., April 1971, Paper No. OTC 1346.

Colon, J.A. (1961) On the structure of Hurricane Daisy (1958). *U.S. Weather Bureau*, Natl. Hurr. Res. Proj., Rept. No. 48.

De Maria, M., S.D. Aberson, and K.V. Ooyama (1992) A nested spectral model for hurricane track forecasting. *Mon. Wea. Rev.*, 120, 1628-1640.

Depperman, C.E. (1947) Notes on the origin and structure of Philippine typhoons. *Bull. Amer. Meteor. Soc.*, 28, 399-404.

Dobos, P.H., Lind, R.J. and Elsberry, R.L. (1995) Surface wind comparisons with radar profiler observations near tropical cyclones. *Weather and Forecasting*, 10 (3), 564-575.

Donelan, M.A., Drennan, W.M. and Katsaros, K.B. (1997) The air-sea momentum flux in conditions of wind sea and swell. *J. Physical Oceanography*, 27, Oct, 2087-2099.

Dvorak, V.F. (1975) Tropical cyclone intensity analysis and forecasting from satellite imagery. *Mon. Wea. Rev.*, 103, 420-430.

Emanuel, K.A. (1988) The maximum intensity of hurricanes. *J. Atmos. Sci*., 45, 1143-1155.

Emanuel, K.A. (1995) Sensitivities of tropical cyclones to surface exchange coefficients and a revised steady state model incorporating eye dynamics. *J. Atmos. Sci*., 52(22), 3969-3976.

Fairall, C.W., Kepert, J.D. and Holland, J.D. (1994) The effect of sea spray on surface energy transports over the ocean. *The Global Atmosphere and Ocean System*, Vol 2, 121-142.

Fletcher, R.D. (1955) Computation of maximum surface winds in a hurricane, *Bull. Amer. Meteor. Soc*., 36, 246-250.

Forristall, G.Z. (1980) A two-layer model for hurricane-driven currents on an irregular grid. *J. Phys. Oceanogr*., 10, 1417-1438.

Fujita, T.T. (1981) Tornadoes and downbursts in the context of generalised planetary scales. *J. Atmos Sciences*, 38(8), Aug, 1511-1534.

Garratt, J.R. (1977) Review of drag coefficients over oceans and continents. *Monthly Weather Review*, 105, 915-929.

Georgiou, P.N. (1985) Design wind speeds in tropical-cyclone prone areas. PhD Thesis. *The University of Western Ontario*, London, Sept.

Goldman, J.L. and Ushijima, T. (1974) Decrease in hurricane winds after landfall. *Jnl Structural Div.*, ASCE, 100(ST1), Jan, 129-141.

Gomes, L., and Vickery, B.J. (1976) On the prediction of tropical cyclone gust speeds along the Northern Australian Coast. Dept. of Civil Engineering, *Univ. Sydney*, Australia, Research Report No. R278.

Goodyear, H.V., and Nunn, D.E. (1965) Memo. No. 7-85. Natl. Hurr. Res. Proj., *U.S. Weather Bureau* (unpublished).

Graham, H.E., and Hudson, G.N. (1960) Surface winds near the center of hurricanes (and other cyclones). *U.S. Weather Bureau*, Natl. Hurr. Res. Proj., Rept. No. 39, September 1960.

Graham, H.E., and Nunn, D.E. (1959) Meteorological consideration pertinent to standard project hurricane, Atlantic and Gulf coasts of the United States. Natl. Hurr. Res. Proj., Rept. No. 33, *U.S. Weather Bureau*, Nov.

Gray, W.M. (1985) Tropical cyclone global climatology. *World Meteor. Org.*, Tech. Doc. No. 72, Vol. 1, 3-19.

Guard, C.P. (1998) Personal communication. University of Guam.

Harper, B.A. (1980) Numerical simulation of tropical cyclone storm surge. Ph.D. thesis, *James Cook Univ*., Queensland, Australia, September 1980. (also as Sobey *et al.*, 1977, Dept Civil and Systems Engin, Research Bulletin CS14, May.)

Harper, B.A., Lovell, K.F., Chandler, B.D. and Todd D J (1989) The derivation of environmental design criteria for Goodwyn 'A' platform, Proc. 9th Aust Conf. Coastal and Ocean Engin., *IEAust*, Adelaide, Dec.

Harper, B.A., Mason, L.B. and Bode, L. (1993) , Tropical cyclone Orson - a severe test for modelling, Proc. 11th Australian Conf. on Coastal and Ocean Engin., *IEAust*, Townsville, Aug, 59-64.

Harper B.A. (1996a) Risk modelling of cyclone losses, Proc. IEAust Annual Engin Conf., *IEAust*, Darwin, April, 53-88.

Harper B.A. (1996b) The application of numerical modelling in natural disaster risk management, Proc. Conf. on Natural Disaster Reduction NDR'96, *IEAust*, Gold Coast, Sept, 107-114, ISBN 0 85825 662 2.

Harper B.A (1997) Numerical modelling of extreme tropical cyclone winds, Proc 4th Asia-Pacific Conf. on Wind Engin., *The University of Queensland*, Gold Coast, July, 49-52, ISBN 0 86776 7316.

Harper B A and Holland G J (1998) Development of a public wind field model for tropical cyclones - scoping study. Report prepared by Systems Engineering Australia Pty Ltd in association with the Bureau of Meteorology Research Centre, *The Risk Prediction Initiative*, Bermuda Biological Station for Research, St Georges.

Harper B A and Holland G J (1999) An updated parametric model of the tropical cyclone. Proc. 23rd Conf. Hurricanes and Tropical Meteorology, *AMS*, Dallas, Texas, 10-15 Jan.

Harris, D.L. (1958) Meteorological aspects of storm surge generation. *J. Hydraulics Div.*, ASCE, Paper 1859, Dec.

Harris, D.L., and Jelesnianski, C.P. (1964) Some problems involved in the numerical solution of tidal hydraulics equations. *Mon. Wea. Rev.*, 92, 409-422.

Hasselmann, K., *et al.* (1973)) Measurements of wind-wave growth and swell decay during the Joint North Sea Wave Project (JONSWAP). *Deut. Hydrogr. Z.*, Suppl. A, 8(12).

Hjelmfelt, M.R. (1988) Structure and life cycle of microburst outflows observed in Colorado., *J. Appl. Meteor*., 27, Aug, 900-927.

Holland, G.J. (1980) An analytic model of the wind and pressure profiles in hurricanes. *Mon. Wea. Rev.*, 108, 1212-1218.

Holland, G.J. and Lander, M.A. (1993) On the interaction of tropical cyclone scale vortices. Part I: Observations. *Qtly. J. Royal Met. Soc*., 119, 1347-1361.

Holland, G.J. (1997) The maximum potential intensity of tropical cyclones. *J. Atmos. Sci.*, 54, Nov, 2519-2541.

Houston, S.H. and Powell, M.D. (1994) Observed and modeled wind and water-level response from tropical storm Marco (1990). Weather and Forecasting, 9(3), Sept, 427-439.

Houston, S.H., Shaffer, W.A., Powell, M.D. and Chen, J. (1999) Comparisons of HRD and SLOSH surface wind fields in hurricanes: Implications for storm surge modeling. Weather and Forecasting, 14, Oct, 671-686.

Hughes, L.A. (1952) On the low-level wind structure of tropical storms. *J.. Meteor.*, 9, 422-428.

Hsu, S.A. (1986) Mechanism for the increase of wind stress (drag) coefficient with wind speed over water surfaces: a parametric model. *J. Physical Oceanography*, 16 (1), Jan, 144-150.

Ishizaki, H. (1983) Wind profiles, turbulence intensities and gust factors for design in typhoon-prone regions. *J. Wind Engin. and Indust. Aerodynamics*, 13, 55-66.

Jelesnianski, C.P. (1965) A numerical calculation of storm tides induced by a tropical storm impinging on a continental shelf. *Mon. Wea. Rev.*, 93, 343-358.

Jelesnianski, C.P. (1966) Numerical computations of storm surges without bottom stress. *Mon. Wea. Rev.*, 94, 379-394.

Jelesnianski, C.P. and Taylor, A.D. (1973) A preliminary view of storm surges before and after storm modifications. *NOAA Tech Memo*., ERL WMPO-3, Boulder, CO, 33pp.

Jelesnianski, C.P., Chen, J. and Shaffer, W.A. (1992) SLOSH: sea, lake and overland surges from hurricanes. *NOAA Tech. Rep*., NWS 48, Silver Spring, MD, 71pp.

Jelesnianski, C.P. (1993) The habitation layer. Chapter 4 of the Global Guide to Tropical Cyclone Forecasting WMO/TD-560 (Ed. G.J. Holland), *World Meteorological Organization*, Geneva, pp4.1-4.29.

Kalashnik, M.V. (1995) On the maximum wind velocity in the tropical cyclone. *Izvestiya Atmospheric and Oceanic Physics*, 30 (1), 23-27.

Kaplan, J. and M. De Maria (1995) A simple empirical model for predicting the decay of tropical cyclone winds after landfall. *J. Applied Meteorology*, 34(11), Nov, 2499-2512.

Kepert, J. (2000) The dynamics of boundary layer jets within the tropical cyclone core - part I: linear theory. *Jnl Atmospheric Sciences* (to appear).

Kepert, J. and Wang Y. (2000) The dynamics of boundary layer jets within the tropical cyclone core - Part II: nonlinear enhancement. *Jnl Atmospheric Sciences* (to appear).

Kraft, R.H. (1961) The hurricane's central pressure and highest wind. *Mar. Wea. Log*., 5, 157.

Krayer, W.R. and Marshall R.D. (1992) Gust factors applied to hurricane winds. *Bull. Amer. Met. Soc.*, 73, 613-617.

Kurihara, Y., M..A. Bender, R.E. Tuleya and R.J. Ross (1995) Improvements in the GFDL hurricane prediction system. *Mon. Wea. Rev., **123***, 2791-2801.

Lovell, K.F. (1990) Review of tropical cyclone wind and pressure field models. Master of Engin Stud. Thesis, Dept of Civil Engin., *Univ of Western Australia*, Perth.

McConochie, J.D., Mason, L.B. and Hardy, T.A. (1999) A Coral Sea wind model intended for wave modelling. Proc. 14th Australasian Conf. Coastal and Ocean Engineering, *IEAust*, Perth, April, 413-418.

Marinas, D. and Woodward, J.W. (1968) Estimation of hurricane surge hydrographs. *J. Waterways, and Harbors*, ASCE, WW2, 189-216.

Marks, F.D. and Houze, R.A. (1984) Airborne doppler radar observations in Hurricane Debby. *Bul. Amer. Meteor. Soc*., 65, 569-582.

Martin, G.S. (1974) Probability distributions for hurricane wind gust speeds on the Australian coast. Proc. Conf. Applications of Probability Theory to Structural Design, *IEAust*, Melbourne, Australia, 55-56.

Merrill, R. T. (1984) A comparison of large and small tropical cyclone. *Mon. Wea. Rev.*, 112, 1408-1418

Miller, B.I. (1958) On the maximum intensity of hurricanes. *J. Meteor*.,15(2), Apr, 184-195.

Miller, B.I. (1962) On the momentum and energy balance of Hurricane Helene, 1958. *U.S. Weather Bureau*, Natl. Hurr. Res. Proj., Rept. No. 53.

Myers, V.A. (1954) Characteristics of United States hurricanes pertinent to levee design for Lake Okeechobee, Florida. *U.S. Weather Bureau*, Hydrometeor. Rept. No. 32, Mar.

Neumann, C.J. (1993) Global Overview. Chapter 1 of the Global Guide to Tropical Cyclone Forecasting WMO/TD-560 (Ed. G.J. Holland), *World Meteorological Organization*, Geneva, pp1.1-1.43.

Novlan, D.J. and W.M. Gray (1974) Hurricane spawned tornadoes. *Mon. Wea. Rev*., 102, 476-488

Overland, J.E. (1977) Providing winds for wave models. *Proc. Ocean Wave Symposium*, Herndon, Va.

Patterson, M.M. (1972) Hindcasting hurricane waves in the Gulf of Mexico. *J. Petroleum Eng*., 12, 321-328.

Peterka, J.A. and Shahid, A. (1998) Design gust wind speeds in the United States. *J. Struct. Engin*., ASCE, 124(2), 207-213.

Powell, M.D. (1980) Evaluations of diagnostic marine boundary-layer models applied to hurricanes. *Mon. Wea. Rev.*, 108, 757-766.

Powell, M.D. and Black P.G. (1989) The relationship of hurricane flight level wind measurements to winds measured by NOAA's oceanic platforms. *Proc. 6th US Nat. Conf. on Wind Engin*., March.

Powell, M.D., Dodge, P.P. and Black M.L. (1991) The landfall of Hurricane Hugo in the Carolinas: surface wind distribution. *Weather and Forec*asting, 6, Sep, 379-399.

Powell, M.D., Houston, S.H. and Reinhold, T.A. (1993) Standardizing wind measurements for documentation of surface wind fields in Hurricane Andrew. Proc Symp. Hurricanes of 1992, *ASCE*, Miami, Dec, ISBN 0-7844-0046-6, 52-69.

Powell, M.D. and Houston, S.H. (1998) Surface wind fields of 1995 hurricanes Erin, Opal, Luis, Marilyn and Roxanne at landfall. Mon. Wea. Rev., 126, May, 1259-1273.

Quilfen, Y., Chapron, B., Elfouhaily, T., Katsaros, K. and Tournadre, J. (1998) Observation of tropical cyclones by high-resolution scatterometry. *J. Geophys. Res*., 103(C4), Apr, 7767-7786.

Riehl, H. (1962) Surface processes in Hurricane Donna. Natl. Hurr. Res. Proj., Rept. No. 50, *U.S. Weather Bureau*, 314-316.

Rosenthal, S.L. (1961) Concerning the mechanics and thermodynamics of the inflow layer of mature hurricanes. Natl. Hurr. Res. Proj., Rept. No. 47, *U.S. Weather Bureau*.

Rosenthal, S.L. (1962) A theoretical analysis of the field of motion in the hurricane boundary layer. Natl. Hurr. Res. Proj., Rept. No. 56, *U.S. Weather Bureau*.

Ross, D. (1979) Observing and predicting hurricane wind and wave conditions. *Seminar on Ocean Products and IGOSS Data Processing and Service System*, Moscow, U.S.S.R., 407-420.

Rupp, J.A. and Lander, M.A. (1996) A technique for estimating recurrence intervals of tropical cyclone-related high winds in the tropics: results for Guam. *J. Appl Meteorology*, May.

Russell, L.R. (1971) Probability distributions for hurricane effects. *J. Waterways, Harbors and Coastal Eng. Div.,* ASCE, Paper 7886, Feb.

Samsury, C.E. and Zipser, E.J. (1995) Secondary wind maxima in hurricanes: airflow and relationship to rainbands. *Mon. Wea. Rev.*, 123, 3502-3517.

Schloemer, R.W. (1954) Analysis and synthesis of hurricane wind patterns over Lake Okeechobee, Florida. Hydromet. Rep., 31, *Dept of Commerce*, Washington D.C., Mar, 49pp.

Schwerdt, R.W. (1972) Revised Standard Project Hurricane criteria for the Atlantic and Gulf coasts of the United States. *Natl. Wea. Serv.*, Silver Spring, Md., Memo. HUR 7-120.

Schwerdt, R.W., Ho, F.P., and Watkins, R.R. (1979) Meteorological criteria for Standard Project Hurricane and Probable Maximum Hurricane windfields, Gulf and East coasts of the United States. *N.O.A.A.,* Tech. Rept. NWS-23, Sep.

Shapiro, L.J. (1983) The asymmetric boundary-layer flow under a translating hurricane. *J. Atmos. Sci.*, 40, 1984 - 1998.

Shea, D.J. and Gray, W.M. (1973) The hurricane's inner core region: symmetric and asymmetric structure. *J. Atmos. Sci.*, 30, 1544-1564.

Simpson, R.H. (1974) The hurricane disaster potential scale. *Weatherwise*, 27, 167-186.

Simiu, E., Patel, V.C., and Nash, J.F. (1976) Mean speed profiles of hurricane winds. *J. Eng. Mechanics Div.* ASCE, 102, 265-273.

Smith, R.K. (1968) The surface boundary layer of a hurricane. *Tellus*, 0, 473-484.

Standards Australia (1989) AS1170.2 - 1989 SAA Loading Code. Part 2: Wind Loads. 96p.

Systems Engineering Australia (1998) Tropical cyclone wind and pressure model. *Unpublished.*

Takahashi, K. (1939) Distribution of pressure and wind in a typhoon. *J. Meteor. Soc. Japan*, Ser. 2, 17, 417-421.

Takahashi, K. (1952) Techniques of the typhoon forecast in Japan. *3rd Ann. Typhoon Conf.*, Tokyo, Feb 1952.

Thompson, E.F. and V.J. Cardone (1996) Practical modeling of hurricane surface wind fields. *Journal of Waterways, Port, Coastal and Ocean Engineering*, ASCE, 122(4), 195-205.

Twisdale, L.A. and Vickery P.J. (1992) Predictive methods for hurricane winds in the United States - Final Report, *SBIR Grant ISI 916035, National Science Foundation*, Washington, DC, Sept.

Twisdale, L.A., Vickery, P.J. and Hardy, M.B. (1993) Uncertainties in the prediction of hurricane windspeeds. ***Proc. Symp. Hurricanes of 1992,*** *ASCE*, Miami, Dec, ISBN 0-7844-0046-6, 706-715.

US Weather Bureau (1968) Interim report - Meteorological characteristics of the Probable Maximum Hurricane, Atlantic and Gulf Coasts of the United States. *Dept. of Commerce*, Silver Spring, Md., Memo HUR 7-97 (unpublished).

Vickery, P.J. and Twisdale, L.A. (1994) Hurricane windspeeds at inland locations. *Proc Structures Congress, ASCE*, April.

Vickery, P.J. and Twisdale, L.A. (1995a) Prediction of hurricane wind speeds in the United States. *J. Struct. Engin.*, ASCE, 121(11), 1691-1699.

Vickery, P.J. and Twisdale, L.A. (1995b) Wind-field and filling models for hurricane wind speed prediction. *J. Struct. Engin.*, ASCE, 121(11), 1700-1709.

Wakimoto, W. and Black, P.G. (1994) Damage survey of Hurricane Andrew and its relationship to the eyewall. *Bull. Amer. Met. Soc.*, 75 (2), 189-200.

Wang, G.C. (1978) Sea level pressure profile and gusts within a typhoon circulation. *Mon. Wea. Rev.*, 106, 954-960.

Wang, J.D. (1987) Hurricane effects on surface Gulf Stream currents. *Ocean Eng.*, 14, 165-180.

Wang, Y., and G.J. Holland (1996) Tropical cyclone motion and evolution in vertical shear. *J. Atmos. Sci.*, 53, 3737-3756.

Weatherford, C.L. and Gray, W.M. (1988a) Typhoon structure as revealed by aircraft reconnaissance. Part I: Data analysis and climatology. *Mon. Wea. Rev*., 116, 1032-1043.

Weatherford, C.L. and Gray, W.M. (1988b) Typhoon structure as revealed by aircraft reconnaissance. Part II: Structural variability. *Mon. Wea. Rev*., 116, 1044-1056.

Willoughby, H.E., Clos J.A. and Shoreibah (1982) Concentric eye walls, secondary wind maxima, and the evolution of the hurricane vortex. *J. Atmos. Sci.*, 39,395-411.

Willoughby, H.E. and Gray W.M. (1988) Typhoon structure as revealed by aircraft reconnaissance. Part II : Structural variability. *Mon. Wea. Rev.*, 116, 1044-1056.

Willoughby, H.E. and Black P.G. (1996) Hurricane Andrew in Florida: dynamics of a disaster. *Bull Amer. Met. Soc*., 77 (3), 543-549.

Wilson, B.W. (1961) Deep water wave generations by moving wind systems. *J. Waterways and Harbours Div.* ASCE, 87, 113-141.

Wilson, B.W. (1966) Design sea and wind conditions for offshore structures. *Proc. Offshore Exploration Conf.*, 1966.

Wilson, K.J. (1979a) Characteristics of the subcloud layer wind structure in tropical cyclones. *Proc. Int. Conf. on Tropical Cyclones*, Perth.

Wilson, K.J. (1979b) Wind observations from an instrumented tower during tropical cyclone Karen, 1977. Proc. 12th Tech Conf on Hurricanes and Tropical Meteorology, *AMS*, New Orleans, Apr.

WMO (1997) Tropical cyclone operational plan for the South Pacific and South-East Indian Ocean. TD-No. 292, Tropical Cyclone Programme Report No. TCP-24, *World Meteorological Organization*, Geneva.

WMO (1998) Topic chairman and rapporteur reports of the fourth WMO international workshop on tropical cyclones (IWTC-IV). *World Meteorological Organisation*, WMO/TD - No. 875., Apr.

6. Numerical Modelling of Tropical Cyclone Storm Surge

6.1 Background and Introduction

A storm surge is a meteorologically forced long wave motion, which can produce sustained elevations of the water surface above the normal levels due to the astronomical tides. It results from the combined action of wind stress and, to a lesser extent reduced atmospheric pressure, on shallow coastal shelf seas. The precise impact of the storm surge at any particular location is sensitive to an often complex combination of meteorological and topographic parameters. These include: intensity and path of the storm, and its spatial and temporal scales; the width and slope of the continental shelf, along with the presence and geometry of local coastal and shelf features (bays, headlands, inlets, barrier islands, offshore islands and reefs). The most potentially critical situation arises when the total sustained water level surge and tide combined) exceeds the highest astronomical tide. In this report, many of the theoretical aspects are relatively standard, but we also assess the significance and relevance of some more recent developments to have been incorporated into storm surge modelling (SSM).

SSM plays an important role in coastal engineering design, coastal land planning, and emergency management. It is important to realise, however, that the storm surge is only one component of total water level. Also present are the effects associated with wind waves: setup, runup, and overtopping. These additional components are important for their direct contribution to total water levels, but they also produce nonlinear interactions with the storm surge. We do not treat nearshore wave effects in any detail in this section, but it should be noted that the subject of nonlinear interactions forms a research area of growing importance in SSM. As well as extreme water levels, there has lately been more interest in recent times in computing storm-induced currents on the continental shelf. Such work remains outside the scope of this report.

In Europe, where surges associated with mid-latitude storms have caused several major catastrophes, operational storm surge warning systems have been developed (Proctor and Flather 1983, De Vries 1991, Flather *et al.* 1991, Verboom *et al.* 1992, Vested *et al.* 1992, 1995, Pratt 1993). Less such development is found for tropical cyclone surge prediction, although this is to some extent a reflection of the magnitude and difficulty of the problem.

An early summary of the state-of-the-art was provided by a pioneer of mid-latitude SSM, Norman Heaps (1983), who covered the area of nonlinear interactions between the storm surge and astronomical tides. It is now standard practice for storm surge models to simultaneously include tidal calculations. Predicted water levels are significantly more accurate as a result (Prandle and Wolf 1978, Flather 1981). Heaps also pointed towards an area that is treated in this report, the dynamical interactions between the (long) surge and (short) surface wind waves. Descriptive material on storm surges can be found in Murty (1984), Murty *et al.* (1986), and Pugh (1987). Other reviews of TC-induced storm surges include Harris (1982), Bode and Sobey (1984), Reid (1990), and Westerink and Gray (1991). Murty (1984) gives an extended treatment of numerical SSM, while De Vries *et al.* (1994) provides an inter-comparison of several 2D surge models. A number of modelling studies have treated the disastrous 1970 Bangladesh cyclone and other Bay of Bengal storms, as summarised in Murty *et al.* (1986); a more recent perspective is Flather (1994). Bode and Hardy (1997) review the current status of SSM, providing also a perspective on more recent and innovative developments, such as inverse modelling, which is not covered here.

In our own region, tropical cyclone *Althea*, which struck Townsville in December 1971, provided a major impetus to research into storm surges in the Australian tropics. *Althea* caused a reasonably pronounced storm surge that fortunately rose only just above the predicted highest astronomical tides, largely because of timing.

6.2 Essential Physics – The Long Wave Equations

While there are some compelling reasons to move towards 3D modelling for more general applications, the main effort in this study is focused on extreme coastal water levels. In this situation, barotropic (2D, or depth-averaged) modelling suffices, as discussed below. The importance of 3D modelling lies in its ability to provide information on the vertical structure of storm-induced currents. Such treatments also allow a more physically based specification of bottom stress at the seabed than in 2D models. This can clearly affect the calculation of nonlinear surge-tide (and, presumably in the future, surge-wave) interactions in shallow water. From the engineering perspective, 3D models enable design studies for offshore structures (platforms, pipelines) in which currents, rather than water levels, are the significant physical design factor. However, 2D models still form the backbone of state-of-the-art operational storm surge prediction systems, for which coastal water levels are the prime concern (Gerritsen *et al.* 1995).

Although the use of stratified (baroclinic) 3D models on the continental shelf is now relatively common, they have rarely been applied to the computation of storm surge currents and water levels. Stratified models are much more computationally expensive than homogeneous (or barotropic) 3D models, which assume a vertically well-mixed water column, and for which the computational cost is often not much more than that of corresponding 2D models. Importantly, baroclinic SSM is still essentially untested against observations.

Homogeneous 3D storm surge models include Cooper and Pearce (1982) and Hearn and Holloway (1990). For some time there was a vogue for the use of so-called 2.5D models, which mathematically couple horizontal 2D and vertical 1D sub-models (Welander 1961, Jelesnianski 1970, Forristall 1974). These have essentially been superseded by 3D models as a serious hydrodynamic modelling tool: homogeneous 3D models generally perform better, invoke fewer assumptions, and avoid the evaluation of numerically awkward convolution integrals needed for 2.5D models.

6.2.1 Equations of Motion

For simplicity only, the equations of motion are expressed here in Cartesian form. However, SSM involves computations which, increasingly, extend over significant portions of the earth's surface, so that it is advisable to express the equations in a spherical coordinate system rotating with the earth (e.g., Haltiner and Williams 1980). This approach is adopted in more recent storm surge models (Flather 1981, 1994; Harper *et al.* 1993; Blain *et al.* 1994; Gerritsen *et al.* 1995). It is also the approach to SSM that has been adopted for some years at JCU, as well as for hydrodynamic modelling in general (Bode and Mason 1992, 1994; Bode *et al.*, 1997).

The long wave equations are obtained from the Reynolds equations for a turbulent fluid, under the usual hydrostatic and Boussinesq approximations. As outlined and justified by standard scaling arguments (Gill, 1982), these equations assume an incompressible fluid; vertical accelerations can be ignored and density variations affect the buoyancy of the fluid only. In a right-handed Cartesian system (x,y,z), where z is vertically upwards from Mean Sea Level (MSL), and with the further assumption of a homogeneous fluid (constant density, ρ_w), the momentum equations for horizontal velocity, $\mathbf{u} = (u,v)$ can be expressed vectorially (in flux form) as:

$$\frac{\partial \mathbf{u}}{\partial t} + \nabla_h \cdot (\mathbf{uu}) + \frac{\partial (w\mathbf{u})}{\partial z} + f\mathbf{k} \times \mathbf{u} = -\nabla_h [g(\eta - \bar{\eta}) + P_s / \rho_w] + \frac{\partial}{\partial z}\left(K_m \frac{\partial \mathbf{u}}{\partial z} \right) + \mathbf{F} \ , \qquad (6.1)$$

where ∇_h is the horizontal gradient operator, $(\partial/\partial x, \partial/\partial y)$. Mass conservation is expressed by the incompressible continuity equation:

$$\frac{\partial \eta}{\partial t} + \nabla_h \cdot \mathbf{u} + \frac{\partial w}{\partial z} = 0 \ . \qquad (6.2)$$

Equations (6.1) and (6.2) apply from the seabed at $z = -h(x,y)$ to the free water surface at $z = \eta(x,y,t)$, both measured w.r.t. the MSL datum. Other notation is standard: t is time; f is the Coriolis parameter, with $f \approx -4.8\ 10^{-5}\ s^{-1}$ at, for example, the latitude of Townsville; $\mathbf{k}$ is the local vertical unit vector; g is gravitational acceleration; w is the vertical velocity component; and P_s is atmospheric pressure at the free surface. The equilibrium tide, $\bar{\eta}$, associated with external astronomical forcing (by the moon and sun), can be assumed negligible for most limited area modelling and will be ignored here. Vertical turbulent transfer of momentum is parameterised here by the eddy viscosity, K_m. $\mathbf{F}$ represents additional horizontal forces (chiefly dissipative), which are clearly sometimes introduced in certain models to aid numerical stability, rather than to improve the physics!

The vertical momentum equation describes hydrostatic balance: $\partial P/\partial z = -\rho_w g$, where P is total pressure, consistent with the long wave assumption of quasi-horizontal flow ($w \ll u,v$). If $D = h + \eta$ is the total water depth, integration of the continuity equation, using Leibniz's theorem for differentiation under an integral and some standard assumptions on depth-averaged structure (Welander 1961) yield the conventional equations for 2D storm surge models in familiar Cartesian component form:

$$\frac{\partial \bar{u}}{\partial t} + \bar{u}\frac{\partial \bar{u}}{\partial x} + \bar{v}\frac{\partial \bar{u}}{\partial y} - f\bar{v} = -\frac{\partial}{\partial x}(g\eta + P_s/\rho_w) + \frac{1}{\rho_w D}(\tau_{sx} - \tau_{bx}) \ , \qquad (6.3)$$

$$\frac{\partial \bar{v}}{\partial t} + \bar{u}\frac{\partial \bar{v}}{\partial x} + \bar{v}\frac{\partial \bar{v}}{\partial y} + f\bar{u} = -\frac{\partial}{\partial y}(g\eta + P_s/\rho_w) + \frac{1}{\rho_w D}(\tau_{sy} - \tau_{by}) \ , \qquad (6.4)$$

$$\frac{\partial \eta}{\partial t} + \frac{\partial (D\bar{u})}{\partial x} + \frac{\partial (D\bar{v})}{\partial y} = 0 \ . \qquad (6.5)$$

Depth-averaging replaces vertical eddy friction terms by the difference in shear stress between the free surface and sea floor. Here, $\boldsymbol{\tau}_s = (\tau_{sx}, \tau_{sy})$ is the specified surface stress, the

key forcing in SSM; $\boldsymbol{\tau}_b = (\tau_{bx}, \tau_{by})$ is bottom frictional stress, which can be defined in terms of turbulent flow near the bottom. Equations (6.3)–(6.5) form the basis of most SSM. For homogeneous fluids, the horizontal pressure force depends only on sea surface elevation and atmospheric pressure. The basic geometric layout is depicted in the schematic diagram below (Figure 6.1).

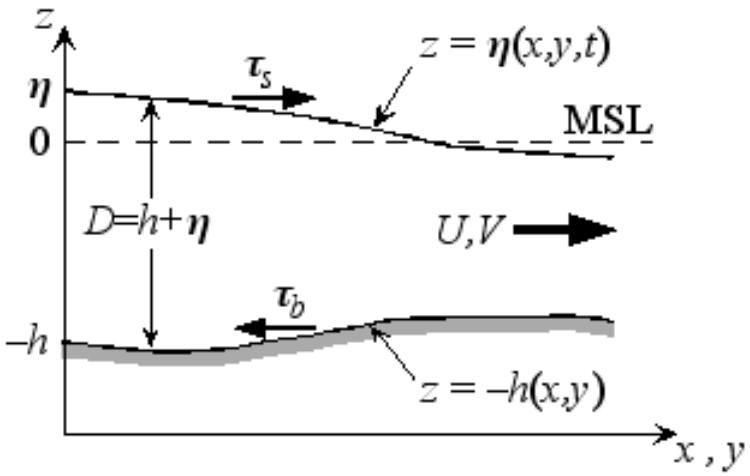

Figure 6.1 Schematic layout of model geometry in Cartesian coordinates (x,y,z).

The water column of total depth *D* extends from the free surface, $z = \eta(x,y,t)$, to the sea floor, $z = -h(x,y)$. The vertical datum is depicted here as Mean Sea Level (MSL), $z = 0$. Also shown are the surface and bottom stresses, τ_s and τ_b, and the transport, $\mathbf{U} = (U,V)$.

6.2.2 Boundary Conditions

Boundary conditions constitute an integral part of the formulation and solution of partial differential equations. Horizontal or lateral boundary conditions are essentially those that apply for 2D models: i.e., no flow normal to solid coastal boundaries, with so-called open boundary conditions (OBCs) required elsewhere. The important area of OBCs is discussed separately in the section on numerical methodologies. In some areas, flooding of deltas and near-coastal lowlands is often a major consequence of storm surges. For such cases the simple no-flow coastal boundary condition is not appropriate, and a separate numerical treatment is required, as discussed in Section 6.4.4. For the present, a brief discussion is given of vertical boundary conditions, concentrating on the specification of frictional resistance at the seabed. More attention to the important free surface boundary condition is given subsequently.

At the free surface, shear stress is equal to the applied (wind) stress, so that

$$K_m \left(\frac{\partial u}{\partial z}, \frac{\partial v}{\partial z} \right)_{z=\eta} = \frac{1}{\rho_w} (\tau_{sx}, \tau_{sy}) \ . \qquad (6.6)$$

The important issue of how the surface stress is parameterised in SSM is discussed separately below.

At the sea floor, the corresponding relationship for bottom stress $\boldsymbol{\tau}_b$ is typically obtained by applying the quadratic bottom friction law, expressed in terms of the near-bottom velocity, $\mathbf{u}_b = (u_b , v_b)$:

$$K_m\left(\frac{\partial u}{\partial z},\frac{\partial v}{\partial z}\right)_{z=-h}=\frac{1}{\rho_w}(\tau_{bx},\tau_{by})=C_b\,|\mathbf{u}_b|\,(u_b,v_b)\ , \tag{6.7}$$

where C_b is a quadratic bottom friction coefficient. Subscript b denotes values 'near' the bottom. In 3D numerical models, this is usually defined as the first grid point, at distance z_b above the seabed. Physically, Equation (6.7) should be consistent with the observed logarithmic velocity profile in the immediate vicinity of the seabed. Provided the vertical grid can resolve this logarithmic sublayer, $\boldsymbol{\tau}_b$ can be expressed by the usual quadratic friction law, Equation (6.7), where the drag coefficient is then given by

$$C_b=\left[\frac{1}{\kappa}\ln\left(\frac{z_b}{z_0}\right)\right]^{-2}. \tag{6.8}$$

Here, z_b is the height of the first grid point above the sea floor, z_0 is the aerodynamic roughness length, and $\kappa \approx 0.4$ is von Karman's constant. The usual 2D parameterisation, which applies for Equations (6.3) and (6.4), is

$$\boldsymbol{\tau}_b=(\tau_{bx},\tau_{by})=C_f\,\rho_w\,|\bar{\mathbf{u}}|\,(\bar{u},\bar{v}), \tag{6.9}$$

where C_f is the friction factor appropriate to a depth-averaged treatment. For fully developed turbulence, C_f remains dependent on bottom roughness, in a manner described by, for example, the Colebrook-White formula (ASCE Task Force 1963),

$$\frac{1}{\sqrt{C_f}}=4\sqrt{2}\log_{10}\left(\frac{14.8D}{k_b}\right). \tag{6.10}$$

This is consistent with the definition of C_b in (6.8). A default value for the physical roughness height of $k_b \approx 25$ cm (so that z_0 is of order 1 cm) is typical (Sobey *et al.* 1977, 1982). Note that Equation (6.10) does model the increased influence of friction in shallow water, whereas common 2D modelling practice often simply sets C_f to a constant value, in the range 0.002–0.003. With k_b = 25 cm, C_f values from (6.10) range from 0.0014 (D = 100 m) to 0.0033 (D = 2 m).

In the 2D case, however, the imposition of $\boldsymbol{\tau}_b$ is instantaneous, and hence this ignores the natural frictional time scale $T_f = O(h/C_f\,|\mathbf{u}|)$, associated with momentum transfer through the water column. Suitable values for the passage of a tropical cyclone (hurricane) across a continental shelf (h = 50 m, C_f = 0.0025, $|\mathbf{u}|$ = 2 ms^{-1}), yield $T_f \approx 3$ h, which could be the same order as the time scale of the passage of the core of a moving hurricane. Equation (6.9) also ignores other 3D effects (Reid 1957). The simplest such example occurs for steady, linear wind-driven flow in a closed 1D channel, for which the depth-averaged velocity from Equation (6.5) is $u \equiv 0$. From Equation (6.3), however, this implies that $\partial\eta/\partial x = (\boldsymbol{\tau}_s - \boldsymbol{\tau}_b)/(\rho_w g h)$. From Equation (6.9), the depth-averaged formulation gives $\boldsymbol{\tau}_b = 0$. However, since $\boldsymbol{\tau}_s \neq 0$, near-surface flow is directed by the wind stress, so that there must necessarily be a return flow, of opposite sign, near the bottom, in order to guarantee that $u = 0$. From the above

expression for η, surface and bottom stress contributions are additive for this case, so that water levels calculated from the zero depth-averaged velocity must under-estimate surface slope. Although such cases raise questions about overall validity, 2D models continue to be used widely and to generally perform well. This is especially so for computed water levels, which are largely insensitive to the vertical structure of the water column, even in 3D baroclinic models (Slordal *et al.* 1994).

6.2.3 Surge-tide Interactions

In many parts of the world, the presence of significant astronomical tides adds further complications to storm surge dynamics (e.g., Bay of Bengal, North Sea, tropical Australia). Clearly, the relative phases of the surge and tidal components affect the peak sustained water levels, as seen to disastrous effect in Bangladesh (Flather 1994). It has long been recognised (e.g., Prandle and Wolf 1978, Heaps 1983) that simple superposition of these two components (i.e., ignoring their interaction), can lead to substantial errors in both the magnitude and timing of the peak surge. For the Queensland situation, these errors are expected to be much smaller due to the narrower continental shelf and the fewer regions with extensive flood plains.

The water depth, particularly in shallow waters significantly affects the nonlinear interaction of tide and surge. A further major contributor to this interaction is quadratic friction (Prandle and Wolf 1978). Consequently, simply adding the computed surge to the tide produces a conservative result for the total water level. In operational forecasting schemes, tidal and meteorological forcing is now routine, and this practice has been standard over a long period of time in the SSM carried out at JCU (e.g., Stark *et al.*, 1985).

6.3 External Forcing

The effects of surface pressure and, particularly, surface stress, are the principal agents that act to generate the storm surge. Atmospheric pressure acts on the entire water column, contributing to the barotropic dynamic pressure. Assuming atmospheric pressure is known accurately, its incorporation presents no problems for SSM. In the shallow waters of the continental shelf, the effects of the surface wind stress are so profound, yet so complex physically, that the results of model calculations depend critically on the manner in which $\boldsymbol{\tau}_s$ is specified. This has lately become an active area of research through incorporation of the effects of surface waves, a topic to which some attention is given below. For the present, we consider only the traditional method of parameterising surface stress in terms of the surface wind speed, but it is evident, even in this area, that many uncertainties remain.

6.3.1 Wind field modelling

The foremost requirement for SSM is an accurate wind field model, and the divide between the mid-latitude and tropical cases is most pronounced here. Mid-latitude models take their wind (and pressure) fields from operational NWP models, which generally perform well. Current developments involve the use of finer-scale meteorological models (e.g., Gerritsen *et al.* 1995, Vested *et al.* 1995). The same does not apply for tropical cyclones, where the task of path and intensity prediction remains an active and developing field (e.g., Kurihara *et al.*, 1995). Some sophisticated predictive modelling has been attempted, using moving nested grids and assimilated data from storm-penetrating aircraft, but such work is still experimental and is likely to remain beyond the operational capabilities of most areas subject to tropical

cyclones. Tropical SSM relies on synthetic wind and pressure field models, of a relatively simple nature, characterised by a small set of parameters.

Computed responses of the ocean are found to be critically dependent on a tropical cyclone's velocity of forward movement, V_{fm}, both in the deep ocean (Price *et al.* 1994) and over the continental shelf (Sobey *et al.* 1977, Fandry and Steedman 1994). The storm track is influenced by synoptic-scale meteorology, but the tropical cyclone also generates its own self-steering mechanisms, due to interactions between its intense vorticity field and the meridionally varying planetary vorticity field in which it is embedded (Chan and Williams, 1987). Despite this, the practical modelling issues of cyclonic wind and pressure fields for tropical SSM are generally limited to the simplified parametric models described earlier in Chapter 5. Obtaining sufficiently accurate values for these parameters is another matter, although advances in remote sensing offer increasingly improved estimates.

Hydrodynamic forcing is due to the transfer of momentum to the marine boundary layer (BL) from the frictional inflow surface layer of the tropical cyclone. Surface wind shear stress $\boldsymbol{\tau}_s$ and atmospheric pressure P_s act on the water body across massive scales, generating complex forced and free modes of motion, which can persist for days after a storm.

The considerable uncertainty that accompanies the specification of the tropical cyclone velocity field, V_m, is evidenced by the prescriptive nature of such formulations. This uncertainty must automatically be transferred, through further assumptions about air-sea interaction processes, to the storm surge models. Given the lack of detailed knowledge of the tropical cyclone BL, it is perhaps not surprising that such simple and empirical approaches have been adopted. Nevertheless, there is wide agreement that the correct specification of wind speed is a crucial first step in providing forcing to storm surge models (Heaps 1983, Proctor and Wolf 1990, Hardy *et al.*, 2000). The present approach remains a weak link in the overall parameterisation of the physics of tropical SSM.

Extensive use has been made of the Holland (1980) profile in storm surge and wave modelling on the North West Shelf of Western Australia (Harper *et al.* 1993). Approximately 30 cyclones were hindcast, using objectively analysed best estimates of the storm tracks. The main parameter varied was Holland's peakedness factor, *B*, with some tuning of the reported *R* (radius to maximum winds) value also used. Many of these hindcasts were able to fit the measured data extremely well (see Figure 1 in Bode and Hardy, 1997) for intense tropical cyclone *Orson*, of April 1989, in which a minimum central pressure of 905 hPa was recorded. Excellent agreement between measured and modelled winds at one of the anemometer sites was observed; the fit to data at six other sites was almost equally convincing. The best-fit value of the *B* factor for *Orson* was $B = 1.94$.

6.3.2 Parameterisation of surface stress

Assuming the wind field is adequately known, the final step in specifying atmospheric forcing for most storm surge models is the calculation of surface shear stress via the quadratic drag law:

$$\boldsymbol{\tau}_s = (\tau_{sx}, \tau_{sy}) = C_{10}\,\rho_a \left|\mathbf{U}_{10}\right| \mathbf{U}_{10}\,. \tag{6.11}$$

where U_{10} is equivalent to V_m from Chapter 5. The drag coefficient used here applies for neutral atmospheric conditions, appropriate for the high wind speeds of a tropical cyclone (in which the BL can be expected to be essentially well-mixed). Although it is generally agreed that C_{10} is a non-decreasing function of wind speed, debate remains about the quantitative details of its relationship to U_{10}. Indeed, the question of whether Equation (6.11) can be used universally, particularly at tropical cyclone wind speeds, needs more attention. We adopt the viewpoint that C_{10} can be specified with certainty. Typical of such formulae is that of Wu (1980, 1982), based on the amalgamation and averaging of a number of data sets, for which

$$10^3 C_{10} = 0.8 + 0.065 U_{10}, \tag{6.12}$$

with the wind speed magnitude given in units of ms^{-1}. Wu (1982) claimed that Equation (6.12) applies for wind speeds from light (2 ms^{-1}) to tropical cyclone force (52 ms^{-1}). At speeds of U_{10} = 50 ms^{-1} (not excessive by the standards of very intense storms), the calculated τ_s is well in excess of 12 Pa! While expressing some caution about its use for very high winds, where the physics of the air-sea interface are largely unknown, Wu (1982) argues that the data support such formulae, as does Garratt (1977). Others such as Smith (1988) express strong caution about extrapolating formulae like Equation (6.12) to such high wind speeds. A more conservative but equally arbitrary approach is to modify the linear C_{10} relationship above an assumed critical wind speed, e.g., by using a constant maximum value (Fandry and Steedman 1994). Large and Pond (1981) assume constant C_{10} for wind speeds below 11 ms^{-1}, although differences among the various formulations at such low speeds will have negligible effects for SSM. An early expression for sea surface roughness comes from Charnock (1955), who postulated that a dimensionless roughness z_* is given by

$$z_* = \frac{g z_0}{u_*^2} = \alpha , \tag{6.13}$$

where α is a constant. This is equivalent to stating that z_0, which provides a measure of the aerodynamic roughness associated with the surface wave field, varies linearly with the surface stress, $\tau_s = \rho_a u_*^2$.

There is a close relationship between formulae such as Equation (6.12) and the Charnock model, Equation (6.13), as noted by Garratt (1977), Wu (1982), and others. From the assumption of a near-surface atmospheric log layer, these can be combined to give

$$C_{10} = \left[\frac{1}{\kappa} \ln\left(\frac{10g}{\alpha C_{10} U_{10}^2} \right) \right]^{-2} . \tag{6.14}$$

A brief selection of drag laws for neutral atmospheric conditions is given in Table 6.1. Some of these relationships are also plotted in Figure 2, along with the Charnock curves for α = 0.011 (Smith 1980), 0.0185 (Wu 1980, 1982) and 0.035 (Powell 1980). Note that the Charnock relationship is almost perfectly linear, except at low wind speeds.

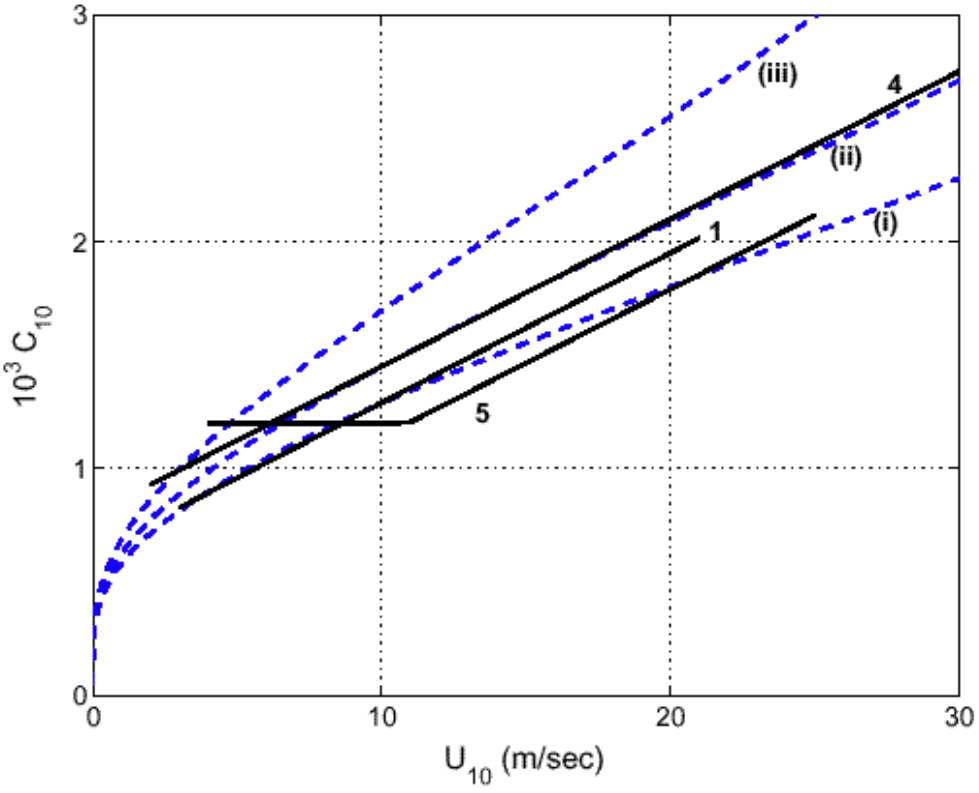

Figure 6.2 C_{10} as a function of U_{10} for formulations 1, 4 and 5 of Table 6.1. Dashed curves show the Charnock formulation for constant α: (i) α = 0.011, (ii) α = 0.0185, (iii) α = 0.035.

Table 6.1 Various formulations for surface drag coefficient C_{10}

Investigators	$10^3 C_{10}$	Range (ms^{-1})	α
1.Smith and Banke (1975)	$0.63 + 0.065U_{10}$	$3 \le U_{10} \le 21$	
2. Garratt (1977)	$0.75 + 0.067U_{10}$	$4 \le U_{10} \le 21$	0.017
3. Smith (1980)	$0.61 + 0.063U_{10}$	$6 \le U_{10} \le 22$	0.011
4. Wu (1982)	$0.80 + 0.065U_{10}$	$2 \le U_{10}$	0.0185
5. Large and Pond (1981)	1.2 $0.49 + 0.065U_{10}$	$4 \le U_{10} \le 11$ $U_{10} \le 26$	

6.4 Solution Procedures

Numerical solution procedures are obligatory for realistic SSM. Closed form solutions in any realistic geometry to the 2D equations (6.3)–(6.5), are out of the question, and numerical methods are essential. Details of numerical procedures are available in the literature, and only the barest details are offered here, although we do address the important subject of open boundary conditions (OBCs). We note also the important role of solutions that use idealised shelf geometries, both analytical and numerical. In spite of their limitations, these illustrate some of the essential dynamical aspects of storm surge response. Three recent numerical works can be consulted for details: Fandry and Steedman (1994) discuss various aspects of idealised 2D storm surge response; Tang and Grimshaw (1995) use a mode fitting analysis to study barotropic storm-generated continental shelf waves; and Slordal *et al.* (1994) model the baroclinic response on a deep continental shelf, for which the dominant response is in the currents due to shelf waves.

Whether 2D or 3D models are used, the numerical solution of the equations of motion essentially comprises a coupled set of 2D (horizontal) equations. The particular algorithm used can be chosen from a myriad of available methods. A number of significant questions then arise, including whether to use a finite difference (FD) or finite element (FE) algorithm. This choice almost invariably influences the nature of the spatial discretisation and the areal extent of the model domain, with consequent impact on the representation of OBCs. The time differencing scheme may be explicit or implicit. Other topics, such as the treatment of the nonlinear advective terms (simple scaling shows these should not be ignored for the extremes of tropical cyclone forcing), lead to a further range of numerical representations, beyond the scope of this review.

6.4.1 Finite Difference versus Finite Element

Much has been written on the formulation (and relative merits) of FD and FE solutions to the long wave equations. Works where specific details and summaries can be found include Abbott and Basco (1989), Foreman (1984), Haltiner and Williams (1980), Heaps (1983), and Murty (1984). Both methods produce large sets of matrix equations, and grids with 10^5 or more unknowns are no longer uncommon. In FD schemes, grids are generally rectangular; larger-domain models should be formulated in spherical polar coordinates (Flather, 1994). In general, the staggered Arakawa ‘C’ spatial grid is used (Mesinger and Arakawa 1976), allowing easy imposition of the zero normal flow coastal boundary condition. Increased spatial resolution in key areas (e.g. inlets) has been claimed through the use of stretched and curvilinear grid systems, although they can introduce unusual open boundary geometry. Similar techniques have been used to transform irregular coastlines onto rectangular horizontal model domains (Reid *et al.* 1977, Johns *et al.* 1981, Bentsen *et al.* 1999). FE equations are invariably derived via a Galerkin approach (Foreman 1984), and tend to use triangular grids to conform with irregularly shaped boundaries and to selectively enhance spatial resolution. FE triangulations are usually generated semi-automatically by specialised software – Henry and Walters (1993).

Finite element SSM is relative new. Such methods first solved the primitive equations (6.3)–(6.5) (Taylor and Davis 1975). Thacker (1978) argued that on the grounds of computational economy, FE methods were uncompetitive with FDs, but a more fundamental concern was the generation of noisy solutions. This originated from the nature of the numerical wave

dispersion relationship for primitive equation FEs (Lynch and Gray, 1979), thereby giving possible multiple solutions. Lynch and Gray recast the problem in the form of a generalised wave equation to remove the noise problem (Foreman 1984). The wave equation approach is now the dominant method for FE models. Near-coastal 3D models are still almost exclusively cast in FD form (Blumberg and Mellor, 1987). Both FD and FE methods are valid approaches, and no fundamental advantage should necessarily be ascribed to either one or the other, despite some partisan claims in the literature. However, FD methods have so far been the predominant choice in SSM, dating from the pioneering efforts of Hansen (1956), and continued by Jelesnianski (1965), Leendertse (1967), Reid and Bodine (1968), and many others.

6.4.2 Explicit vs Implicit

The simplicity of explicit time differencing schemes has seen them retain their popularity for SSM, despite an increase in the use of implicit methods. The discussion here concentrates on the simpler FD schemes. FE methods, although inherently implicit, can also be formulated explicitly (Foreman 1984). Explicit methods lead to simple time-stepping schemes; the main advantage is the ease and speed with which error-free code can be produced. Their obvious shortcoming lies with the CFL criterion, which for the 2D case is given by

$$\Delta t < \frac{\Delta s}{\sqrt{2gD_{\max}}}\ , \tag{6.15}$$

with Δt the time step and $D_{\max}$ the maximum depth. Thus for explicit 2D models, not only is $\Delta t \sim 1/\sqrt{D_{\max}}$, but (6.15) also implies the total CPU time, $T_{\mathrm{CPU}} \sim N^3$, where N is the total number of active grid cells (with $T_{\mathrm{CPU}} \sim N^4$ for 3D models). Simple arithmetic thus shows that timesteps for high-resolution FD models can be extremely restrictive if, as is ideal, the model domain extends into deep water. JCU experience has concentrated on problems in the GBR, with a consequent need for relatively fine spatial grids, and all models have been converted to implicit methods (Bode and Mason 1994). This is despite the fact that earlier modelling (Sobey *et al.*, 1977) used explicit schemes exclusively.

Implicit models are not in general bound by stability criteria such as Equation (6.15), but we stress the need to consider model *accuracy* as the prime requirement, rather than stability. Inverting large matrices is required in implicit models, and although they are extremely sparse and highly structured, the resulting computational task is usually very demanding. Early implicit models favoured the alternating direction implicit (ADI) algorithm (Leendertse 1967), with its need to invert only tridiagonal matrices. However, ADI can lead to problems in regions of complex geometry (Wilders *et al.* 1988), and semi-implicit and fully implicit models are being adopted more widely. Traditional methods for matrix inversion such as successive over-relaxation, although simple to implement, suffer from prohibitively slow convergence rates for large problems. Advantage can be taken of operator splitting, and the adoption of more modern sparse matrix techniques, such as pre-conditioned conjugate gradients (Wilders *et al.* 1988, Bode and Mason 1994) and multigrid methods. In semi-implicit methods, the critical timestep restriction Equation (6.15) is removed through implicit formulation of the gravity wave terms.

In early models, the lack of CPU resources led to a need for relatively coarse grids, and model domains that were limited in spatial extent. The constraint applied by Equation (6.15) was thus not excessive and, with the accompanying ease of programming, made explicit methods an attractive option. Increasingly now, high spatial resolution is demanded, while is it also clear that model domains should be made as large as possible to aid with the problems of OBCs (below). The resulting minuscule values of Δt demanded by Equation (6.15) now make implicit modelling much more attractive, in spite of its inherent complexity. For high resolution grids, it has been shown in certain circumstances that Δt values, many times the traditional CFL limit, can be used while still retaining stability and accuracy (Wilders *et al.* 1988, Bode and Mason 1994). Clearly, there is a trade-off between small Δt values for explicit models and the cost of matrix inversion in the implicit case.

6.4.3 Sizes for spatial step and time step

Standard application of Fourier analysis to numerical schemes for the long wave equations (e.g., Abbott and Basco 1989) leads to a resolution criterion that states approximately

$$\Delta s \leq \frac{L}{20} \ . \tag{6.16}$$

Here, Δs and L are representative length scales for the numerical grid resolution and the shortest inertia-gravity wavelengths expected to be generated by the storm (or tides). This essentially states that the long waves must be sufficiently well resolved by the grid (i.e., by 20 grid points or better per wavelength). Provided this rule-of-thumb is adhered to, few problems should be expected in numerical integrations, especially in the calculation of water levels, η. Note, however, that additional length scale criteria are imposed in the coastal SSM problem.

The model must be capable of resolving the following:

(i) The strong spatial gradients in the cyclone wind field cause rapid spatial changes in magnitude and direction of surface stress. The band of maximum winds can reverse direction over a distance equal to about twice the radius to maximum winds of the cyclone. This indicates that the appropriate ocean response wavelength should be set at four times the radius. This is also consistent with the need to resolve the surface wind gradients, as highlighted by Sobey *et al.* (1977) who suggested $R/\Delta s > 4$ as a suitable rule for preserving the forcing wavelength.

(ii) The gradient of water surface elevation is largest in shallow water and the primary interest of SSM is to provide coastal surge values. If the computational point nearest to the actual shoreline is some distance offshore, the surge may be underpredicted, since this gradient will not apply all the way to the true shoreline location. Likewise, the surge would be overpredicted if the grid point were onshore from the true shoreline position. Simplifying Equation (6.3) to 1D, steady state, and ignoring pressure and Coriolis effects, the gradient of the surface elevation is approximately 2×10^{-4} for a wind speed of 50 ms^{-1} normal to shore and a water depth of 4 m. Thus if the grid point is 1000 m offshore, the surge is underpredicted by approximately 0.2 m ($2 \times 10^{-4} \times 1000$ m = 0.2 m).

(iii) Coastal features such as headlands, islands or shoals and channels can trap and or direct water movements, thus changing coastal surge levels.

(iv) Stream or drain pathway widths and changes in the elevation of dunes and roadways will determine the timing and extent of inland flooding. The overland topography may be more variable than offshore bathymetry, so these features may be difficult to resolve in a storm surge model.

These last two items are difficult to quantify, but obviously the better the resolution of bathymetry and coastal geometry, the more accurate the surge prediction.

An argument similar to that posed by Equation (6.16) can be used to determine a suitable time step. In the same manner as the spatial step has to be able to resolve the spatial signal, the time step has to be able to resolve the temporal variation of the storm surge. Thus Equation (6.16) could be recast for time step by substituting Δt and T (wave period) for Δs and L, so that

$$\Delta t \leq \frac{T}{20} \, . \qquad (6.17)$$

To estimate the wavelength and period for use of Equations (6.16) and (6.17), we suggest using $L = 4 \times R$ (four times the radius of maximum winds of the cyclone) and $T = L/V_{fm}$ (wavelength divided by the forward speed of the cyclone). Example calculations using Equations (6.16) and (6.17) for an average storm (R = 30 km and V_{fm} = 18 km/h) and an extreme storm (R = 10 km and V_{fm} = 35 km/h) are included in Table 6.2. This second storm is an extreme example and such a combination of radius and forward speed has a small probability of occurrence. It is important to realise that a change of spatial step requires the construction of a new grid, whereas a change in time step is much easier to implement.

Table 6.2 Example calculations of space and time steps

Example	R (km)	V_{fm} (km h^{-1})	L (km)	T (h)	Δs (km)	Δt (min)
"average"	30	18	120	6.67	6	20
"extreme"	10	35	40	1.14	2	3.4

6.4.4 Open Boundary Conditions

The storm surge response is a forced long wave mode, accompanied by a family of free modes, consisting of rotationally modified gravity waves. The precise mix of waveforms is determined by the storm forcing and continental shelf geometry. In a numerical model, interpretation of the storm response is complicated by the necessarily limited extent of the solution domain and the resulting need to specify open boundary conditions. For limited-area modelling, the OBC problem remains one of *the* computational challenges. Ideally, these boundaries must allow interior waves to pass through unhindered, without reflections or other

unrealistic behaviour; additionally, they should also permit any information associated with external forcing to pass into the region.

The true open coast situation is one where OBCs can exert an identifiable impact on the computed solution. In general, such models have two transverse or cross-shelf open boundaries, and one in deep water off the shelf edge. The first step along all boundaries should be to incorporate the inverted barometer effect. Atmospheric pressure can essentially be removed from the momentum equations (6.3) and (6.4) by defining an adjusted sea level elevation,

$$\eta' = \eta - \frac{\Delta P}{\rho_w g} \ , \tag{6.18}$$

where $\Delta P = (p_n - p_s)$ is the local atmospheric pressure deficit. This gives the well-known rule that a 1 hPa pressure drop leads approximately to a 1 cm rise in static sea level. From Equation (6.3) or (6.4), the ratio of surface stress to atmospheric pressure forcing is $O(\tau_s L/(D \Delta P))$, where L is a length scale for horizontal pressure variations (e.g., 400 km). For parameters appropriate to strong hurricanes such as *Camille* (Table 1, Bode and Hardy 1997), this ratio is of the order of 10 for h = 20 m, but only 0.01 for h = 2,000 m. The dominating influence in deep water of the inverted barometer effect is obvious in many modelling studies from the near-circular η-contours which mirror the radially symmetric form of p_s that is often imposed for idealised storms (Bunpapong *et al.* 1985, Blain *et al.* 1994, Fandry and Steedman 1994). Given the importance of surge-tide interactions, tidal elevations are also generally added to the OBCs; this is largely a routine matter.

On transverse boundaries, however, the use of Equation (6.18) plus tidal modifications is insufficient. Unless OBCs are further modified, they will act along these cross-shelf boundaries to produce total internal reflection of any waves generated within the model domain (subtraction of the forced tidal and inverse barometer solutions means that such models effectively apply a condition of zero elevation). Instead of this 'clamped' ($\eta' = 0$) OBC, Jelesnianski (1965) and Forristall (1974), adopted a condition of zero normal velocity derivative along transverse open boundaries – e.g., for an x-directed boundary,

$$\frac{\partial \overline{v}}{\partial y} = 0 \ . \tag{6.19}$$

Either the clamped condition or Equation (6.19) is computationally trivial to apply, but both were shown by Reid (1975) to produce total internal reflection of wave energy, thus preventing free modes from passing unrestricted out of the model region. Reid advocated a 'radiation' condition and showed that for 1D gravity waves, these internal reflections are prevented if the velocity and surface elevation are in phase, as with a travelling wave. Specifically, the Reid radiation condition is

$$\overline{v} = \pm \frac{c\eta}{D} \ , \tag{6.20}$$

a condition originating with Reid and Bodine (1968). The default value for the velocity is the celerity of free gravity waves, $c = (gD)^{1/2}$, the sign depending on the direction of the outward

normal. Modifications for combined tidal and surge modelling are given in Flather (1981). Strictly, (6.20) allows progressive waves in the computational domain to pass through the open boundaries in the absence of forcing and rotation (f = 0), and with quiescent initial conditions. Problems with the performance of Equation (6.20) on cross-shelf boundaries for steady wind-driven shelf flow (Bode and Sobey 1983), have led to the adoption of the kinematic 'Sommerfeld' condition (Orlanski 1976):

$$\frac{\partial \phi}{\partial t} + c\frac{\partial \phi}{\partial x} = 0 \ , \tag{6.21}$$

where ϕ denotes any variable to be 'radiated' through the boundary, and c is a suitable velocity. A number of such schemes, chiefly involving variations in the definition of c, are investigated by Chapman (1985). Further variants of Equation (6.21) are described by Tang and Grimshaw (1996), whose main concern was to ensure the correct propagation of continental shelf waves.

Another approach is the Flow Relaxation Scheme (FRS) of Martinsen and Engedahl (1987). It blends the results of fine-scale, near coastal models with those from larger domain external models, in which the fine-scale model is nested, according to the 'convex combination':

$$\phi = \beta\phi_{ext} + (1-\beta)\phi_{int} \, , \tag{6.22}$$

where β is the relaxation parameter ($0 < \beta < 1$). Martinsen and Engedahl (1987) show that FRS performs well on nested problems, and can also be used as a pure OBC. OBCs continue to exercise the interest of modellers, but as summarised by Chapman (1985), the fact remains that for wind-driven flows, *no* OBC performs satisfactorily in a general sense for open coast wind-driven models. If these are to be used, then experimentation and compromise are essential.

Tropical cyclone SSM leads to an essential conflict of scales that affects OBCs: at one extreme, the storm's eye radius (the scale of the dominant forcing) together with prominent coastal and bathymetric features must be resolved adequately; at the other, the model domain should encompass the extent of the storm. Ideally, a model should accommodate both ends of this spectrum (even now an often-impossible demand with realistic CPU resources), and the compromise of limited-area models and OBC problems are usually an immediate consequence. Non-uniform grids, as used by the FE modellers offer one solution, as do boundary-fitted and other transformed mesh approaches for FDs. If fixed resolution FD grids apply, recourse should be made to nested grids (Haltiner and Williams 1980), using methods such as FRS to couple the boundary interfaces. Multiple-stage nesting provides an effective and affordable means of obtaining extra accuracy at smaller scales, especially for the regions of major interest near coastlines, while still incorporating the effects of distant forcing in the deep ocean, where resolution requirements are not so crucial.

Despite efforts expended to develop artificial OBCs, model studies show that the ideal way to minimise the problem is to use as large a domain as possible. This can be seen as a further reason to opt for a nested approach, with a cheap outer grid of maximum possible extent. Both Bunpapong *et al.* (1985) and Blain *et al.* (1994) consider the storm surge problem for tropical cyclones in the Gulf of Mexico. Blain *et al.* used three grids of increasing size. The smallest covered a region with an extent of 175 km, corresponding to the local *SLOSH* model grid

(Jelesnianski *et al.* 1992). The second encompassed the entire Gulf, while the third extended into the Caribbean and the eastern US shelf. The results support those of Bunpapong *et al.* (1985), who showed the importance of the natural modes of oscillation of the Gulf to the storm surge response. Minor differences were found between results for the two larger grids, both of which produce significantly higher coastal water levels than for the *SLOSH* grid. Jarvinen and Lawrence (1985) also comment that the extent of the *SLOSH* grid is far too limited for use in operational modelling.

6.4.5 Overland Flooding and Drying

The 'standard' coastal boundary condition used in long wave models is that of no flow at the coastline, i.e., the component of transport normal to the coastline equals zero. Thus, this boundary condition essentially approximates the coast by a vertical cliff of unlimited height, against which the free surface water level, η, can rise and fall. Quite apart from the fact that all models can only approximate the position of the coastline (e.g., that corresponding to MSL), the topography there often changes gradually, not abruptly. In addition, many coastal regions are bordered by low-lying land: tidal flats such as those adjacent to parts of Cleveland Bay; large stretches of coastal plains close to sea level, such as those bordering the Gulf of Carpentaria; and inter-tidal lagoons and embayments. All may be subject to inundation at times of high astronomical tides or during a storm surge.

Thus, an important component of many coastal hydrodynamic models is the existence of modules to compute the extent of such incursions of seawater. These are often labelled wetting/drying or flooding algorithms. Such schemes will necessarily include a database of on-shore topography, at least for regions deemed flood-prone. The model must then compute the progress of the water across such areas – both the position of the wet/dry interface, and the depth of water in all 'wet' computational cells. This is *not* a simple problem. Indeed, the fact that various schemes are still being proposed in the recent modelling literature, is a strong indication that flooding and drying is not a closed issue.

Flooding and drying – modelling approaches

Two immediate and separate formulations suggest themselves for flooding and drying. The more natural one is to compute the position of the interface, which is tracked adaptively by a grid that changes over time. With this approach, grid cells can move or be added at the wet/dry interface at each time step. Computationally, this is a most demanding problem, as it requires continual regridding. In fact, even strong protagonists of finite element schemes (which in principle can be regridded to closely follow the evolving coastline) avoid this method; such are the computational difficulties and prohibitive CPU overheads. The second scheme operates with a fixed grid, in which all points can be either wet or dry at any timestep; in fact, this disjunction will usually only arise over a small fraction of the grid. In theory, a grid cell adjacent to a wet cell in which water has risen in the previous timestep to a level above its own base level, can become wet during the next timestep. In practice, this transition causes quite severe numerical problems.

What is commonly seen is a type of shock wave effect, due to the fact that cells flood and become instantaneously active (wet) – or else passive (dry) during the retreat of a flood. Numerically, this situation is often characterised by noisy solutions near the coastline, and a tendency for such models to become catastrophically unstable. One of the difficulties is that, under such conditions, the dynamics change markedly: from a long wave in which pressure

gradient and inertial terms are in approximate balance and friction is weak, to a very shallow water situation in which bottom friction provides the dominant balance for pressure forces. This was recognised by LeBlond (1978). He showed that in such situations, for 1D flow in a channel, the dynamics change from a wave equation with two characteristics, to a nonlinear diffusion equation with a single characteristic. Under 2D flow conditions, such problems are naturally far more complicated, especially when the advective terms are applied.

Despite this, most modellers have proceeded to treat the wetting and drying problem in a basically conventional fashion, using a standard long wave model, and employing various additional methods to prevent drastic temporal changes from occurring near the interface. Early work of this type included that by Leendertse (1970), and Flather and Heaps (1975). Later modifications, in which the equations for the wetted grid cells were modified to buffer the impacts of the encroaching interface, include Flather and Hubbert (1990). Other approaches to the problem include the use of weir formulae (Reid and Bodine, 1968; Sobey *et al.* 1982), and barriers along the boundaries of grid cells that can be added or removed to alter the progress of the flood wave. None can really be said to have "solved" the problem.

More recently, Hubbert and McInnes (1999), who employ explicit numerics in their storm surge model, report a scheme which seeks to limit the rate of flooding and drying of active grid cells. Under their methodology, an attempt is made to compute an appropriate approach or retreat velocity of the flood wave front over a number of timesteps in adjacent (wet) grid cells. They use this technique to reduce the noise generated by the continual switching of grid cells from active to passive, and vice versa. By comparison of the results against those from a rigid coastline model, Hubbert and McInnes claim that their scheme "ensures realistic and smoothly varying results". They concluded that fixed coastline models could lead to a significant over-estimation of the magnitude of the maximum surge at the coast. However, lack of detailed inundation data (a general problem with such assessments) allowed them to perform only a qualitative analysis of their flooding algorithm. At best they could say that the area of land inundated in the model was similar to that observed. No measurements of inundation water heights or water speeds were available to make any detailed calibrations of the model.

Flather (1994) has developed a novel approach to the flooding problem for the very extensive Bangladesh delta region, a region often hit by storm surges, with devastating losses of life and property. This extended earlier work by Flather and Hubbert (1990). The region is traversed by numerous river channels of a variety of sizes. In order to incorporate both the inundation of land and flow in river channels, Flather developed a hybrid 1D/2D system, within the overall context of a 2D model, using a variety of partial area and width factors. This attempt to represent sub-grid-scale effects is in some senses similar to the JCU reef parameterisation scheme (Bode *et al.*, 1997). The procedure appeared to be effective numerically. However, again there were no essentially no detailed data to allow adequate comparisons with reality. A linked 1D/2D approach is also utilised by a number of commercially available river floodplain models, such as those by Delft Hydraulics and the Danish Hydraulic Institute, and good verification against recorded terrestrial flood events is claimed.

Ip *et al.* (1998) adopt a significantly different approach, and revert to the friction-pressure gradient balance, initially demonstrated by LeBlond (1978) for flow in shallow tidal rivers. They combine this with a porous sublayer in cells that can become wet, in order to smooth the potentially troublesome temporal variations in water level. Their method seems to offer considerable promise (in part at least because it operates under the correct dynamical regime).

However, this approach would require considerable further development if it were to be proposed for an operational storm surge model. In the work they report, Ip *et al.* (1998) limit themselves to very near coastal situations, such as modelling the flooding of inter-tidal areas. For successful implementation in a storm surge model, their scheme would have to be interfaced across a transition zone to the main deepwater region of the model, where long wave dynamics apply.

In order to avoid instability in the switching between flooding and drying, the flood/drying scheme in *MMUSURGE* maintains a finite water depth (set to a very small value) in all cells where flooding is possible. In effect, there is no "drying" of cells. Although this avoids the instability problem, in an implicit model (such as *MMUSURGE*), the development of a flooding scheme is complicated by the significantly longer timesteps that are commonly used in implicit models. The highly nonlinear nature of the overland flooding process means that implicit models should have time steps that give Courant numbers number close to one in regions of overland flooding. However, time steps have already been reduced in order to resolve the forcing of a tropical cyclone. For example, with Δt = 900 s, Δs = 925 m, the Courant number is less than about 3 for water depths indicative of the flood front over dry ground (less than a about 1 m). Further, the value of $L/\Delta s$ remains above the threshold figure of 20 in equation (6.16) for a storm with a time scale of around 3 hours. Both of these should ensure that the numerical scheme satisfactorily describes the dynamical situation (Bode and Mason, 1994).

There are additional aspects of the storm surge flooding problem that require consideration. For example, very shallow flow of water over the land affects the determination of (i) bottom friction, and (ii) wind stress on water. Bottom friction will be enhanced by vegetation, housing and other roughness elements, far larger in physical extent than the few cm usually assumed for flow over the sea floor – with the exception of the GBR. Wind stress applied to the water surface, over what is nominally land, would tend to be reduced because of trees and other obstacles. On the other hand, certain situations would allow the application of a large surface stress to extensive regions of very shallow water (see below). At present, *MMUSURGE* uses a spatially constant value of bottom roughness. Thus the increased roughness of flooded areas, which are very different from the ocean floor, is not well represented. A spatial varying value of roughness can be simply incorporated into the calculation scheme. This is recommended if modelling of overland flooding is to be an important component of future projects.

Two separate cases apply to the overland flooding problem for Queensland. The first is the situation in the Gulf of Carpenteria, where the flood wave must move long distances over relatively featureless terrain. The second is low-lying populated areas (on the scale of a single suburb). Here the flood wave does not travel large distances, but must negotiate a very complicated flood path around obstacles, such as curbs, walls and houses. The first requires moderately accurate terrain information and adjustable bottom friction coefficients over the flooded area. The accuracy and obtainability of this data is the main problem. The second requires very fine scale descriptions of structures and needs much finer grid resolution. This very fine resolution is clearly impractical for the present purpose of modelling storm surge for the entire coast of Queensland. The alternative is to include sub-grid scale algorithms, in much the same way as MMUSURGE does for reef features (Bode *et al.*, 1997). Thus, these small-scale features are accounted for with a much larger spatial step size. This is clearly the only way the overland flooding can be modelled for anything but a very small region (a suburb or smaller). It is important to realise that these small-scale features may change (new

road, wall, or growth of vegetation) or even dynamically during a storm (i.e. erosion of dunes or change in channel).

A very important consideration in overland flooding is the need to know the *total water level*, which means that the simultaneous modelling of surge and tide is necessary. This adds considerably to the cost of modelling over that of the open coast where a superposition of tide and surge (perhaps with some adjustment) is possible.

In summary, while overland flooding is not important in many areas it is clearly an important issue in some locations. However, there remain significant difficulties in providing reliable flooding schemes, as well as accommodating their computational overheads.

6.5 Recent Developments

Accurate forecasting of storm surge is critically dependent on the quality of many model inputs and parameters. Especially important among these are: meteorological forcing and the parameterisation of air-sea interaction; open boundary conditions; bottom friction and bathymetry. Errors in any of these may lead to a marked deterioration in numerical results. Recent developments in a number of areas of ocean modelling have opened possibilities for distinct improvements in storm surge model predictions. Most of these are in their infancy as evidenced by the recent dates of the references cited. For the present, we focus here on developments in coupled surge-wave models. Another area of innovation covered by Bode and Hardy (1997) is the use of inverse methods, notably for data assimilation, a field of study that is currently undergoing rapid evolution in theoretical meteorology and oceanography.

6.5.1 Surge-Wave Interactions

At the time of the Heaps (1983) review, nonlinear surge-tide interactions were being incorporated in SSM. The chief agent of interaction there is bottom friction. It is equally recognised that specifying surface stress as a function of only the wind speed, underestimates the vital role that surface wind waves play in the transfer of momentum at the air-sea interface, particularly under the complex action of tropical cyclone wind fields. This interaction has been ignored in the past, and storm surge and waves have usually been studied and modelled in isolation. In this section we consider the effects of waves on sustained water levels. These interactions occur through at least three mechanisms – radiation stress, enhanced bottom stress, and enhanced surface wind stress. The last mechanism is the major focus of this section.

It is well known (Longuet-Higgins and Stewart, 1964) that waves cause a flow of momentum, and a spatial gradient in this momentum flux will force surface gradients and currents. This "radiation stress" is the mechanism for wave setup (refer Chapter 8). Radiation stress has been included in numerical surge and current models (e.g., Hubertz 1984), but usually only for calculating nearshore currents. However, Mastenbroek *et al.* (1993) – hereafter MBJ – include radiation stress forcing in a coupled surge and wave model of the North Sea. Every three hours an average radiation stress is calculated, based on output of a directional-spectral wave model, and the gradient of radiation stress is subtracted from the wind stress in the storm surge model's momentum equation. Mastenbroek *et al.* (1993) found that the contribution of radiation stress was negligible, compared with wind stress.

As discussed above, bottom friction depends nonlinearly on the contributions to the bottom current from surge, tidal, and wave components of the motion. Waves can be expected to have an increasing contribution with decreasing water depth. Therefore the wave contribution could be important for storm surge modelling over shallow shelves. We are not aware of storm surge models that directly include the effects of wave orbital velocities in bottom friction calculations. Wu and Flather (1992) and Wu *et al.* (1994) indicate that coupled wave and surge models have been used to provide enhanced bottom stress for surge calculations, but specific details of the implementation of their solution schemes were not given.

The transfer of momentum from the wind across the air-sea interface and into the water column is the main driving force for storm surge. Thus, assuming the wind field is known, the single most important parameter in a storm surge model is the surface drag coefficient. Some momentum is transferred directly into currents and the storm surge, but much enters indirectly by first being transferred from the wind into waves. Unfortunately, our understanding of momentum and energy transfer at the air-sea interface is incomplete. The main complication is the fact that the interface changes in both space and time. The interface moves, not only with a unidirectional motion (current) but also with an orbital motion (waves). The waves themselves constitute the roughness elements. They not only move relative to the interface, but their size and speed are also functions of time, as well of wind speed, direction, fetch, and water depth. In short, the BLs in both air and water are dynamically coupled through a moving and changing interface. The result is that the physics of these interactions is complex and poorly understood.

A logarithmic wind profile is usually assumed for neutral stratification, with Charnock's (1955) postulated expression (6.13) for the roughness length, z_0. From field measurements it became apparent, however, that the Charnock parameter α was not constant, but depended on at least the water depth and wave age, with smaller values of α for older or deepwater waves ($\alpha \approx 0.011$, e.g., Smith 1980, 1988) and larger values for younger or shallow water waves ($\alpha \approx 0.018$, e.g., Wu 1980, 1982) – see also Table 6.1. Further analyses of field data (e.g., Donelan 1982, Geernaert *et al.* 1986, Smith *et al.* 1992) have led to the hypothesis that z_0 is a function of wave age, usually specified as c_p / u_* (the ratio of wave celerity of the peak frequency to friction velocity). Thus, field data indicate that nondimensional roughness is not equal to a constant, but is a function of wave age. That is,

$$z_* = \frac{g z_0}{u_*^2} = f\left(\frac{c_p}{u_*}\right). \tag{6.23}$$

Heuristically, as waves grow, two interrelated processes affect the wave field's aerodynamic roughness. Firstly, the spectral peak progressively moves to lower frequencies, where the wave celerity approaches and then, at maturity, overtakes the wind speed. As the difference between wave celerity and wind speed decreases, the waves diminish in effectiveness as roughness elements. Secondly, spectra of fetch limited (younger) seas are characterised by an overshoot of energy, above that in mature waves, in the region of the peak frequency (refer also Chapter 7). Thus, the primary waves of the wave field are steeper for fetch limited waves than for fully developed waves. These factors combine to make younger waves aerodynamically rougher than mature waves.

Donelan (1992) found that z_0 depends quadratically on wind speed and approximately inversely on wave age, if z_0 and c_p are non-dimensionalised by *rms* wave height and U_{10}

respectively. This agrees with the findings of Maat *et al.* (1991) and Smith *et al.* (1992), namely that

$$z_* = \frac{g z_0}{u_*^2} = \frac{\mu}{c_p / u_*}, \tag{6.24}$$

where μ is a constant.

Johnson and Vested (1992) present an overview of published work into the effect of waves on surface shear stress. They propose a 'hybrid model' for the calculation of z_0, which uses expressions from Kitaigorodskii and Volkov (1965) and Kitaigorodskii (1973) for younger waves ($c_p/u_* < 10$), with an expression from Donelan (1990) for older waves ($c_p/u_* > 10$). This results in

$$z_0 = \begin{cases} \alpha_1 \sigma_{\text{hf}} 1.84 \left(\dfrac{u_*}{c_p} \right) & , \dfrac{c_p}{u_*} \geq 10 \\ \alpha_2 \sigma_{\text{hf}} \exp\left(-\kappa \dfrac{c_p}{u_*} \right) & , \dfrac{c_p}{u_*} < 10 \end{cases} \tag{6.25}$$

where α_1 and α_2 are calibration coefficients, and σ_{hf}^2 is the variance of the sea surface in the high frequency portion of the wave spectrum. High frequency is defined here as $k > 1.5\ k_p$, where k_p is the wavenumber of the spectral peak. The calibration coefficients are determined so as to agree with Smith and Banke (1975) under their deepwater wave conditions ($\alpha_1 = 1.17$ and $\alpha_2 = 0.31$). The result is a drag coefficient that is a function of wave age, wave height, and water depth. Johnson and Vested (1992) find that this formulation matches well with published data sets over the full range of wave ages.

Belcher *et al.* (1994) and Harris *et al.* (1996) provide analytical and numerical models that couple the air and water BLs. They argue an aerodynamically rough flow cannot be assumed. In fact, the flow is often smooth and thus a function of Reynolds number. The dependence of the flow on this additional parameter would help explain the scatter found when field measurements of roughness length or drag coefficient are plotted solely against wave age.

Mastenbroek *et al.* (1993) describe an ambitious attempt to incorporate the effect of waves on the drag coefficient. Instead of parameterising dimensionless roughness by wave age, they use the theory of Janssen (1991) which assumes that, close to the surface, waves contribute separately to the surface shear stress, so that $\boldsymbol{\tau}_s = \boldsymbol{\tau}_t + \boldsymbol{\tau}_w$, where $\boldsymbol{\tau}_t$ is turbulent shearing stress and $\boldsymbol{\tau}_w$ is the wave-induced stress. This wave-induced stress alters the BL in the air close to the surface, so that the velocity profile takes on a modified logarithmic form,

$$U_z = \frac{u_*}{\kappa} \ln\left(\frac{z + z_e - z_0}{z_e} \right). \tag{6.26}$$

The 'effective roughness', z_e, and the roughness length, z_0, are calculated as

$$z_e = \frac{z_0}{\sqrt{1-\tau_w/\tau_s}} \qquad \text{and} \qquad z_0 = \frac{\alpha' u_*^2}{g} \ , \tag{6.27}$$

where α' is tuned (α' = 0.01) so that $z_e = \alpha' u_*^2 / g$ for a fully developed sea. Thus, roughness is enhanced above z_0 if the wave-induced shear stress is a significant portion of the total shear stress. From conservation of momentum considerations, the wave-induced stress is assumed equal to the momentum flux from the wind into the waves, which is calculated by

$$\boldsymbol{\tau}_w = \frac{\rho_w}{2\pi} \int_0^{\infty} \mathrm{d}\omega \int_0^{2\pi} \omega S_{\mathrm{in}}(\omega,\theta) \frac{\mathbf{k}}{k} \, \mathrm{d}\theta \ . \tag{6.28}$$

where S_{in} is the wind source term from the accompanying wave model (refer Chapter 7), ω is the angular frequency of a wave component and θ its direction. Here, **k** and k are the vector wave number and its magnitude. The final result of the method of MBJ is the shear velocity u_*, from which the drag coefficient can be determined via $C_{10} = u_*^2 / U_{10}^2$. For the formulation of Janssen (1991), S_{in} is a function of u_* and z_e. Therefore, in MBJ, the equations form an implicit set. The surge and wave models are dynamically coupled, as the friction velocity and apparent roughness both determine, and are determined by, the waves. Mastenbroek *et al.* (1993) report that inclusion of the wave-dependent drag coefficient significantly increases the surge, and modelling using the wave-induced drag matches field measurements much better than that using the Smith and Banke (1975) drag coefficient. They do state, however, that a simple increase in the drag coefficient, above that of Smith and Banke, gives much the same improvement in results as the full surge-wave calculations.

Clearly, the understanding of the physics of momentum transfer across the air-sea interface is still developing. The introduction of swell and the possibility of wind and waves at oblique or even opposing directions add more complexity. We are a long way from a complete understanding of the processes involved with the interaction of winds and waves, especially during a tropical cyclone, in which rapid changes occur in both wind and wave conditions.

Despite this apparent lack of full understanding, numerical models that avoid including any wave-surge interactions have been able to hindcast tropical cyclone surges and also currents with acceptable accuracy. While attempts to improve the modelling of momentum transfer across the air-sea interface are to be applauded, the effect of these efforts must be kept in perspective. Difficulties in field measurement and lack of data for severe wind speeds have hampered the determination of the functional characteristics of the drag coefficient. Donelan (1992) estimates that the *rms* error in the estimation of C_{10} from field data is about 20%, and this translates into a range of values of z_0 that is greater than the natural variability.

6.6 Conclusions and Recommendations

Numerical storm surge models are based on governing equations that attempt to describe fundamental laws of nature. Although some empiricism exists in the formulation of the equations, the most important processes have been shown to be well represented. These equations are solved using well proven numerical techniques that have undergone a development process of several decades. In short, numerical surge models have proved themselves capable of accurately predicting surges under the dual complexity of cyclonic forcing and nearshore bathymetry.

The following points contain a brief discussion and recommendations on the main issues raised in this chapter.

(i) **2D or 3D models**

The difference in predicted water levels between 2D and 3D modelling is considered likely to be minor in most cases and the cost of 3D modelling is considerably higher.

2D modelling is adequate and 3D modelling is deemed impractical for the determination of water levels for a large ensemble of storms for the whole coast of Queensland.

(ii) **Effect of tide on surge**

Storm surge is inversely related to total water depth so that storm surge levels (not necessarily total water level or *storm tide* level) would be higher if the storm strikes at low tide rather than at high tide. Simultaneous surge and tide modelling is considered impractical for the determination of water levels for a large ensemble of storms for the whole coast of Queensland. Furthermore, the linear addition of surge and tide will tend to produce a slightly conservative result.

The linear addition of surge and tide is recommended for the production of surge statistics. For real-time forecasting purposes, combined surge-tide modelling is possible and should be considered. Combined modelling is essential for inland flooding (see below).

(iii) **Surface stress**

A number of surface stress formulations exist and this remains an area of continuing research. However, the existing methods provide somewhat similar results.

The surface stress formulation of Wu (1982) is recommended.

(iv) **Finite difference or finite element**

The vast majority of numerical models for storm surge use the finite difference technique and it has proven its worth in many projects in many locations throughout the world.

Finite difference modelling is recommended.

(v) **Explicit or implicit solution techniques**

Explicit models require less computing time per time step, but implicit models can have significantly longer time steps. Especially for model domains that contain deeper water, implicit models offer a distinct advantage. Furthermore, it can be difficult to choose economical time steps for modelling a large ensemble of storms with an explicit model while also insuring that the Courant condition is not violated. Thus, simulations that become unstable need to be rerun, whereas an implicit model might use the same time step for all situations and remain stable.

Use of implicit models is recommended.

(vi) Open boundaries and nested grids

Open boundaries can be difficult to model, because information on hydrodynamic forces outside of the model domain may not be available. The best solution is to place any open boundaries as far as possible from the area of interest and to include as much of the forcing directly within the model domain. This creates a conflict between the extent of the region to be modelled and the resolution needed to define the process of interest in the study area. It is not considered practical to do both in one grid.

Open boundaries should be removed far from the region of interest by using a nested grid system.

(vii) Space and time resolution

Model spatial and temporal scales must be able to resolve the tropical cyclone wind field, as well as bathymetric and topographic features.

A spatial resolution of 1.5 minutes of arc (≈ 2800 m) will resolve tropical cyclone wind fields. For regions of special interest (i.e. population centres), a further nested grid with a resolution of 0.3 minutes (≈ 555 m) is recommended. This should ensure important coastal geometry is resolved. The time step would nominally be 15 min for both grids, with consideration of a smaller time step for very small and very fast moving storms.

(viii) Overland flooding

Overland flooding will not be important for all coastal locations in Queensland but for some areas, it may be of critical importance.

An assessment of the importance of inland flooding should be undertaken for each model domain.

1. *If inland flooding is deemed not important then a fixed coastal boundary may be used.*
2. *If inland flooding is deemed important then one of the following conditions exists:*
   - *(a) If the floodable area is small and close to the coast so that the flood wave can be assumed to propagate across the floodable area without significant loss of elevation, then flood levels can be set equal to coastal water levels. This will produce a slightly conservative estimate of inland flood levels.*
   - *(b) If the floodable area is larger or farther from the coast so that loss in water elevation is expected then a flood/drying scheme such as in MMUSURGE will be adequate if the consequences of flooding are not severe.*
   - *(c) If floodable area is large, the path from the open coast is complicated and/or the consequences of flooding are severe then sub-grid scale features should be incorporated. This may require specification of linked 1D/2D flow paths to adequately represent very complex situations.*

The definitions of "small" and "close" in the above are difficult to quantify with precision. They depend on the flood path and the duration of the peak storm surge.

(ix) **Wave-surge interaction**

Short wave effects at both the free surface (roughness) and bottom (orbital velocity) can have an effect on storm surge generation. However, modelling the effect of wind waves on surge is impractical for the determination of water levels for a large ensemble of storms for the whole coast of Queensland. In any case, the corrections resulting from the inclusion of wave-induced surface drag or bottom friction in surge calculations would be relatively small. Any such corrections are likely to be smaller than the uncertainty that is usually inherent in the magnitude and direction of the applied wind forcing. The direct impact of wind waves on total water level, i.e. setup and runup, is however significant and is discussed in Chapter 8.

Inclusion of wave-surge interaction is not necessary for accurate storm surge modelling.

6.7 References

Abbott, M.B., and Basco, D.R. (1989) Computational fluid dynamics: an introduction for engineers, *Harlow Longman*, 425 pp.

ASCE Task Force of the Committee on Hydromechanics of the Hydraulics Division (1963) Friction factors in open channels. *Journal of the Hydraulic Division*, ASCE, 89, 97–143.

ASCE Task Committee on Turbulence Models in Hydraulic Computations (1988) Turbulence modelling of surface water flow and transport: Parts I–V. *Journal of Hydraulic Engineering*, ASCE, 114, 970–1073.

Belcher, S.E., Harris, J.A., and Street, R.L. (1994) Linear dynamics of wind waves in coupled turbulent air-water flow. Part 1. Theory. *Journal of Fluid Mechanics*, 271, 119–151.

Bentsen, M., Evensen, G., Drange, H. and Jenkins, A.D. (1999) Coordinate transformation on a sphere using conformal mapping. *Monthly Weather Review*, 127, 2733–2740.

Blain, C.A., Westerink, J.J., and Luettich, R.A., Jr. (1994) The influence of domain size on the response characteristics of a hurricane storm surge model. *Journal of Geophysical Research*, 99, 18467–18479.

Blumberg, A.F., and Mellor, G.L. (1987) A description of a three-dimensional coastal ocean circulation model. In Three-Dimensional Coastal Ocean Models, N.S. Heaps, Ed., *American Geophysical Union*, pp. 1–16.

Bode, L., and Smith, R.K. (1975) A parameterisation of the boundary layer of a tropical cyclone. *Boundary-Layer Meteorology*, 8, 3–19.

Bode, L., and Sobey, R.J. (1983) The open boundary problem for wind-driven circulations. Proceedings, 8th Australasian Fluid Mechanics Conference, *IEAust*, Newcastle, pp. 4A.1–4A.4.

Bode, L., and Sobey, R.J. (1984) Initial transients in long wave computations. *Journal of Hydraulic Engineering*., ASCE, 110, 1371–1397.

Bode, L. and Mason, L.B. (1992) Numerical modelling of tidal currents in the southern Great Barrier Reef. Marine Modelling Unit, Dept of Civil and Systems Engineering, *James Cook University of North Queensland*. (Prepared for The Department of Transport and Communications through the Victorian Institute of Marine Science)

Bode, L., and Mason, L.B. (1994) Application of an implicit hydrodynamic model over a range of spatial scales. Proceedings, 6th Computational Techniques and Applications Conference (CTAC93), D. Stewart, H. Gardner and D. Singleton, Eds., *World Scientific*, Singapore, 112–121.

Bode, L., and Hardy, T.A. (1997) Progress and recent developments in storm surge modelling. *Journal of Hydraulic Engineering*, ASCE, 123, 315–331.

Bode, L., Mason, L.B. and Middleton, J.H. (1997) Reef parameterisation schemes for long wave models. *Progress in Oceanography*, **40**, 285–324.

Bunpapong, M., Reid, R.O., and Whitaker, R.E. (1985) An investigation of hurricane-induced forerunner surge in the Gulf of Mexico. Technical Report CERC-85-5, *Coastal Engineering Research Center*, Vicksburg, Miss., 201 pp.

Chalikov, D. (1993) Comments on 'Wave-induced stress and the drag of air flow over sea waves' and 'Quasi-linear theory of wind-wave generation applied to wave forecasting'. *Journal of Physical Oceanography*, 23, 1597–1604.

Chan, J.C.L. and Williams, R.T. (1987) Analytical and numerical studies of the beta-effect in tropical cyclone motion. Part I: Zero mean flow. *Journal of the Atmospheric Sciences*, 44, 1257–1265.

Chapman, D.C. (1985) Numerical treatment of cross-shelf open boundaries in a barotropic coastal ocean model. *Journal of Physical Oceanography*, 15, 1060–1075.

Charnock, H. (1955) Wind stress on a water surface. *Quarterly Journal of the Royal Meteorological Society*, 81, 639–640.

Cooper, C., and Pearce, B. (1972) Numerical simulations of hurricane-generated currents. *Journal of Physical Oceanography*, 12, 1071–1091.

De Vries, J.W. (1991) The implementation of the WAQUA/CSM-16 model for real time storm surge forecasting. *KNMI Technical Report*, TR-131, 36 pp.

De Vries, J.W., Breton, M., de Mulder, T., Krestenitis, Y., Ozer, J., Proctor, R., Ruddick, K., Salomon, J.-C., and Voorrips, A. (1994) A comparison of 2D storm surge models applied to three shallow European seas. *Environmental Software* (in press).

Donelan, M.A. (1982) The dependence of the aerodynamic drag coefficient on wave parameters. Proceedings, *First International Conference on Meteorology and Air-sea Interaction of the Coastal Zone*, The Hague, 381–387.

Donelan, M.A. (1990) Air-sea interaction. In The Sea, *Ocean Engineering Science*, Volume 9, 239–292.

Donelan, M.A. (1992) The mechanical coupling between air and sea – an evolution of ideas and observations. In Strategies for Future Climate Research, M. Latif, Ed., *Max-Planck Institut fur Meteorologie*, 77–94.

Donelan, M.A., Dobson, F.W., Smith, S.D., and Anderson, R.J. (1993) On the dependence of sea surface roughness on wave development. *Journal of Physical Oceanography*, 23, 2143–2149.

Fandry, C.B., and Steedman, R.K. (1994) Modelling the dynamics of the transient, barotropic response of continental shelf waters to tropical cyclones. *Continental Shelf Research* (in press).

Flather, R.A. (1981) Storm-surge prediction using numerical models. In Monsoon Dynamics, J. Lighthill and R.P. Pearce, Eds, Joint IUTAM/IUGG International Symposium on Monsoon Dynamics, 1977, Delhi, India. *Cambridge University Press*, 659–687.

Flather, R.A. (1994) A storm surge prediction model for the northern Bay of Bengal with application to the cyclone disaster in April 1991. *Jnl of Physical Oceanography*, 24, 172–190.

Flather, R.A., and Heaps, N.S. (1975) Tidal computations for Morecambe Bay. *Geophysical Journal of the Royal Astronomical Society*, 42, 489–517.

Flather, R.A., and Hubbert, K.P. (1990) Tide and surge models for shallow water – Morecambe Bay revisited. In *Modelling Marine Systems*, A.M. Davies, Ed., CRC Press, 135–166.

Flather, R.A., Proctor, R., and Wolf, J. (1991) Oceanographic forecast models. In Computer Modelling in the Environ. Sciences, D.G. Farmer and M.J. Rycroft, Eds., *Oxford*, 15–30.

Foreman, M.G.G. (1984) A two-dimensional dispersion analysis of selected methods for solving the linearized shallow water equations. *Jnl of Computational Physics*, 56, 287–323.

Forristall, G.Z. (1974) Three-dimensional structure of storm-generated currents. *Journal of Geophysical Research*, 79, 2721–2729.

Garratt, J.R. (1977) Review of drag coefficients over oceans and continents. *Monthly Weather Review*, 105, 915–929.

Geernaernt, G.L., Katsaros, K.B., and Richter, K. (1986) Variation of the drag coefficient and its dependence on sea state. *Journal of Geophysical Research*, 91, 7667–7679.

Gerritsen, H., de Vries, H., and Philippart, M. (1995) The Dutch continental shelf model. In Quantitative Skill Assessment for Coastal Ocean Models, A.M. Davies and D.R. Lynch, Eds., Coastal and Estuarine Studies, Vol. 47, *American Geophysical Union* 425-467.

Gill, A.E. (1982) Atmospheric-ocean dynamics, *Academic Press*, 662 pp.

Haltiner, G.J., and Williams, R.T. (1980) Numerical Prediction and Dynamic Meteorology, 2nd edition, *Wiley*, 477 pp.

Hansen, W. (1956) Theorie zur errechnung des wasserstandes und der stroungen in randmeeren nebst anwendungen. *Tellus*, 8, 287–300.

Hardy, T.A., McConochie, J. and Mason, L.B. (2000) A wave model for the Great Barrier Reef. *Ocean Engineering* (in press).

Harper, B.A., Mason, L.B., and Bode, L. (1993) Tropical cyclone Orson – a severe test for modelling. Proc. 11th Aust. Conf. Coastal Ocean Engrg., *IEAust*, Townsville, 59–64.

Harris, D.L. (1982) The prediction of hurricane storm surges: a state-of-the-art survey. Report No. 49, Florida Sea Grant College, *University of Florida*.

Harris, J.A., Belcher, S.E., and Street, R.L. (1996) Linear dynamics of wind waves in coupled turbulent air-water flow. Part 2. Numerical model. *Journal of Fluid Mechanics*.

Heaps, N.S. (1983) Storm surges, 1967–1982. *Geophysical Journal of the Royal Astronomical Society*, 74, 331–376.

Heaps, N.S., Ed. (1987) Three-dimensional coastal ocean models, *American Geophysical Union*, 208 pp.

Hearn, C.J., and Holloway, P.E. (1990) A three-dimensional barotropic model of the response of the Australian North West Shelf to tropical cyclones. *Journal of Physical Oceanography*, 20, 60–80.

Henry, R.F., and Walters, R.A. (1993) Geometrically based, automatic generator for irregular triangular networks. *Intnl Journal for Numerical Methods in Engineering*, 9, 555–566.

Holland, G.J. (1980) An analytical model of the wind and pressure profiles in hurricanes. *Monthly Weather Review*, 108, 1212–1218.

Hubbert, G.D., Holland, G.J., Leslie, L.M., and Manton, M.J. (1991) A real time system for forecasting tropical cyclone storm surges. *Weather Forecasting*, 6, 86–97.

Hubbert, G.D. and McInnes, K.L. (1999) A storm surge inundation model for coastal planning and impact studies. *Journal of Coastal Research*, 15, 168–185.

Hubertz, J.M. (1984) Modelling of nearshore wave driven currents. Proc. 19th Int. Conf. Coastal Engineering, *ASCE*, Houston, 2208–2219.

Ip, J.T.C., Lynch, D.R. and Friedrichs, C.T. (1998) Simulation of estuarine flooding and dewatering with application to Great Bay, New Hampshire. *Estuarine Coastal and Shelf Science*, 47, 119–141.

Janssen, P.A.E.M. (1991) Quasi-linear theory of wind-wave generation applied to wave forecasting. *Journal of Physical Oceanography*, 21, 1631–1642.

Jarvinen, B.R., and Lawrence, M.B. (1985) An evaluation of the Slosh storm-surge model. *Bulletin of the American Meteorological Society*, 66, 1408–1411.

Jelesnianski, C.P. (1965) A numerical calculation of storm tides induced by a tropical storm impinging on a continental shelf. *Monthly Weather Review*, 93, 343–358.

Jelesnianski, C.P. (1970) Bottom stress time-history in linearized equations of motion for storm surges. *Monthly Weather Review*, 98, 462–478.

Jelesnianski, C.P., Chen, J., and Shaffer, W.A. (1992) SLOSH: Sea, Lake and Overland Surges from Hurricanes. *NOAA Technical Report*, NWS 48.

Johns, B., Dube, S.K., Mohanty, U.C., and Sinha, P.C. (1981) Numerical simulation of the surge generated by the 1977 Andhra cyclone. *Quarterly Journal of the Royal Meteorological Society*, 107, 919–934.

Johnson, H.K. and Vested, H.J. (1992) Effects of water waves on wind shear stress for current modelling. *Journal of Atmospheric and Oceanic Technology*, 9, 850–861.

Kitaigorodskii, S.A. (1973) The physics of air-sea interaction, *Israel Program for Scientific Translations*, 237 pp.

Kitaigorodskii, S.A., and Volkov, Y.A. (1965) On the roughness parameter of the sea surface and the calculation of momentum flux in the lower layer of the atmosphere. Izv. *Atmos. Ocean Phys.*, 1, 973–978.

Kurihara, Y., Bender, M.A., Tuleya, R.E. and Ross, R.J. (1995) Improvements in the GFDL hurricane prediction system. *Monthly Weather Review*, 125, 2791–2801.

Large, W.G., and Pond, S. (1981) Open ocean momentum flux measurements in moderate to strong winds. *Journal of Physical Oceanography*, 11, 324–336.

LeBlond, P.H. (1978) On tidal propagation in shallow rivers. *Journal of Geophysical Research*, 83, 4717–4721.

Leendertse, J.J. (1967) Aspects of a computational model for long period water-wave propagation. *Rand Corporation*, RM-5294-PR.

Leendertse, J.J. (1970) A water-quality simulation model for well-mixed estuaries and coastal seas: principles of computation. RM-6230-RC, *Rand Corp.*, Santa Monica, Calif.

Longuet-Higgins, M.S. and Stewart, R.W. (1964) Radiation stresses in water waves; a physical discussion, with applications. *Deep-Sea Research*, 11, 529–562.

Lynch, D.R., and Gray, W.G. (1979) A wave equation model for finite element tidal computations. *Computers and Fluids*, 7, 207–228.

Maat, N., Kraan, C., and Oost, W.A. (1991) The roughness of wind waves. *Boundary-Layer Meteorology*, 54, 89–103.

Martinsen, E.A., and Engedahl, H. (1987) Implementation and testing of a lateral boundary scheme as an open boundary condition in a barotropic ocean model. *Coastal Engineering*, 11, 603–627.

Mastenbroek, C. Burgers, G., and Janssen, P.A.E.M. (1993) The dynamical coupling of a wave model and a storm surge model through the atmospheric boundary layer. *Journal of Physical Oceanography*, 23, 1856–1866.

Mesinger, F. and Arakawa, A. (1976) Numerical methods used in atmospheric models. GARP Publication Series, No. 17, Vol. 1, *WMO/ICSU Joint Organising Committee*, 64 pp.

Murty, T.S. (1984) Storm surges: meteorological ocean tides, Canadian Bulletin of Fisheries and Aquatic Sciences, No. 212, *Department of Fisheries and Oceans*, Canada, 897 pp.

Murty, T.S., Flather, R.A., and Henry, R.F. (1986) The storm surge problem in the Bay of Bengal. *Progress in Oceanography*, 16, 195–233.

Myers, V.A. (1957) Maximum hurricane winds. *Bulletin of the American Meteorological Society*, 38, 227–228.

Orlanski, I. (1976) A simple boundary condition for unbounded hyperbolic flows. *Journal of Computational Physics*, 21, 251–269.

Powell, M.D. (1980) Evaluations of diagnostic marine boundary-layer models applied to hurricanes. *Monthly Weather Review*, 108, 757–766.

Prandle, D., and Wolf, J. (1978) The interaction of surge and tide in the North Sea and River Thames. *Geophysical Journal of the Royal Astronomical Society*, 55, 203–216.

Pratt, I. (1993) Operation of the Storm Tide Warning Service. Proceedings of the MAFF Conference of River and Coastal Engineers, *University of Loughborough*, UK, 22 pp.

Price, J.F., Sanford, T.B., and Forristall, G.Z. (1994) Forced stage response to a moving hurricane. *Journal of Physical Oceanography*, 24, 233–260.

Proctor, R., and Flather, R.A. (1983) Routine storm surge forecasting using numerical models: procedures and computer programs for use on the CDC 205E at the British Meteorological Office. *Institute of Oceanographic Sciences*, Report No. 167, 171 pp.

Proctor, R., and Wolf, J. (1990) An investigation of the storm surge of February 1, 1983 using numerical models. In *Modelling Marine Systems*, A.M. Davies, Ed., CRC Press, 43–72.

Pugh, D.T., (1987) Tides, surges and mean sea level, *Wiley*, 472 pp.

Reid, R.O. (1957) Modification of the quadratic bottom-stress law for turbulent channel flow in the presence of surface wind-stress. Technical Memorandum No. 93, U.*S. Army Corps of Engineers*, 33 pp.

Reid, R.O. (1975) Comments on 'Three-dimensional structure of storm-generated currents' by G.Z. Forristall. *Journal of Geophysical Research*, 80, 1184–1185.

Reid, R.O. (1990) Water level changes – tides and storm surges. In Handbook of Coastal and Ocean Engineering, J.B. Herbich, Ed., *Gulf Publishing*, Houston, 533–590.

Reid, R.O., and Bodine, B.R. (1968) Numerical model for storm surges in Galveston Bay. *Journal of the Waterways and Harbors Division*, ASCE, 94, 33–57.

Reid, R.O., Vastano, A.C., Whitaker, R.E., and Wanstrath, J.J. (1977) Experiments in storm surge simulation. In The Sea: Ideas and Observations on Progress in the Study of the Seas, Vol. 6 – Marine Modelling, E.D. Goldberg *et al.*, Eds., *Wiley*, 145–168.

Schwerdt, R.W., Ho, F.P., and Watkins, R.P. (1979) Meteorological criteria for standard project hurricane and probable maximum hurricane windfields, Gulf and east coast of the United States. *NOAA Technical Report*, NWS-23, 317 pp.

Shea, D.J., and Gray, W.M. (1973) The hurricane's inner core region . I. Symmetric and asymmetric structure. *Journal of the Atmospheric Sciences*, 30, 1544–1563.

Slordal, L.H., Martinsen, E.A., and Blumberg, A.F. (1994) Modelling the response of an idealized coastal ocean to a traveling storm and to flow over bottom topography. *Journal of Physical Oceanography*, 24, 1689–1705.

Smith, S.D. (1980) Wind stress and heat flux over the ocean in gale force winds. *Journal of Physical Oceanography*, 10, 709–726.

Smith, S.D. (1988) Coefficients for sea surface wind stress, heat flux, and wind profiles as a function of wind speed and temperature. *Journal of Geophysical Research*, 93, 15467–15472.

Smith, S.D., and Banke, E.G. (1975) Variation of the sea surface drag coefficient with wind speed. *Quarterly Journal of the Royal Meteorological Society*, 101, 665–673.

Smith, S.D., Anderson, R.J., Oost, W.A., Kraan, C., Maat, N., DeCosmo, J., Katsaros, K.B., Davidson, K.L., Bumke, K., Hasse, L., and Chadwick, H.M. (1992) The HEXOS results. *Boundary-Layer Meteorology*, 60, 109–142.

Smith, W.H.F. (1993) On the accuracy of digital bathymetric data. *Journal of Geophysical Research*, 98, 9591–9603.

Sobey, R.J., Harper, B.A., and Stark, K.P. (1977) Numerical simulation of tropical cyclone storm surge. Department of Civil & Systems Engineering, *James Cook University*, Australia, Research Bulletin No. CS14, 186 pp. + figs.

Sobey, R.J., Harper, B.A., and Mitchell, G.M. (1982) Numerical modelling of tropical cyclone storm surge. *Civil Engineering Transactions*, I.E.Aust., 24, 151–161. (See also Proc 17th International Conf Coastal Eng, ASCE, Sydney, 1980, 725-745).

Stark, K.P., Bode, L. and Mason, L.B. (1985) Simulation of tides and storm surges in the Great Barrier Reef Region. Proc 19th Intl Conf Coastal Eng, *ASCE*, Houston, USA, 226–242.

Tang, Y., and Grimshaw, R.H.J. (1995) A modal analysis of the coastally trapped waves generated by tropical cyclones. *Journal of Physical Oceanography*, 25, 1577-1598.

Tang, Y., and Grimshaw, R.H.J. (1996) Radiation boundary conditions in barotropic coastal ocean numerical models, *J. Comput. Phys.*

Taylor, C. and Davis, J. (1975) Tidal and long wave propagation – a finite element approach. *Computers and Fluids*, 3, 125–148.

Thacker, W.C. (1978) Comparison of finite-element and finite-difference schemes. Part II: Two-dimensional gravity wave motion. *Journal of Physical Oceanography*, 8, 680–689.

Verboom, G.K., de Rondo, J.G., and van Dijk, R.P. (1992) A fine grid tidal flow and storm surge model of the North Sea. *Continental Shelf Research*, 12, 213–233.

Vested, H.J., Jensen, H.R., Petersen, H.M., Jorgensen, A.-M., and Machenhauer, B. (1992) An operational hydrographic warning system for the North Sea and the Danish Belts. *Continental Shelf Research*, 12, 65–81.

Vested, H.J., Nielsen, J.W., Jensen, H.R., and Kristensen, K.B. (1994) Skill assessment of an operational hydrodynamic forecast system for the North Sea and Danish Belts. In Quantitative Skill Assessment for Coastal Ocean Models, A.M. Davies and D.R. Lynch, Eds., Coastal and Estuarine Studies, Vol. 47, *American Geophysical Union* 373-396.

Welander, P. (1961) Numerical prediction of storm surges. *Advs in Geophysics*, 8, 315–379.

Westerink, J.J., and Gray, W.G. (1991) Progress in surface water modelling. *Reviews of Geophysics*, 29, Supplement, 210–217.

Wilders, P., van Stijn, Th.L., Stelling, G.S., and Fokkema, G.A. (1988) A fully implicit splitting method for accurate tidal computations. *International Journal for Numerical Methods in Engineering*, 26, 2707–2721.

Wu, J. (1980) Wind-stress coefficients over sea surface near neutral conditions: a revisit. *Journal of Physical Oceanography*, 10, 727–740.

Wu, J. (1982) Wind stress coefficients over sea surface from sea breeze to hurricane. *Journal of Geophysical Research*, 87, 9704–9706.

Wu, X., and Flather, R.A. (1992) Hindcasting waves using a coupled wave-tide-surge model. In Third International Workshop on Wave Hindcasting and Forecasting, *Environment Canada*, 159–170.

Wu, X., Flather, R.A., and Wolf, J. (1994) A third generation wave model of European continental shelf seas with depth and current refraction due to tides and surges and its validation using Geosat and buoy measurements. *Proudman Oceanographic Laboratory*, UK, Report No. 33, 48 pp.

7. Numerical Modelling of Tropical Cyclone Wind Waves

7.1 Introduction

The prediction of ocean waves within coastal regions, as a result of the forcing provided by a tropical cyclone is a complex process. The wind field of the tropical cyclone is composed of a tight vortex which results in very high wind speeds and a direction vector which changes rapidly as a function of distance. These features require the use of a numerical model that has a relatively comprehensive description of wind wave generation physics. In coastal regions, the finite water depth and the range of additional physical mechanisms, which can influence the wave field, further increase complexity. Figure 7.1 shows some of these processes in a diagrammatic form, aspects of which are referred to in later sections.

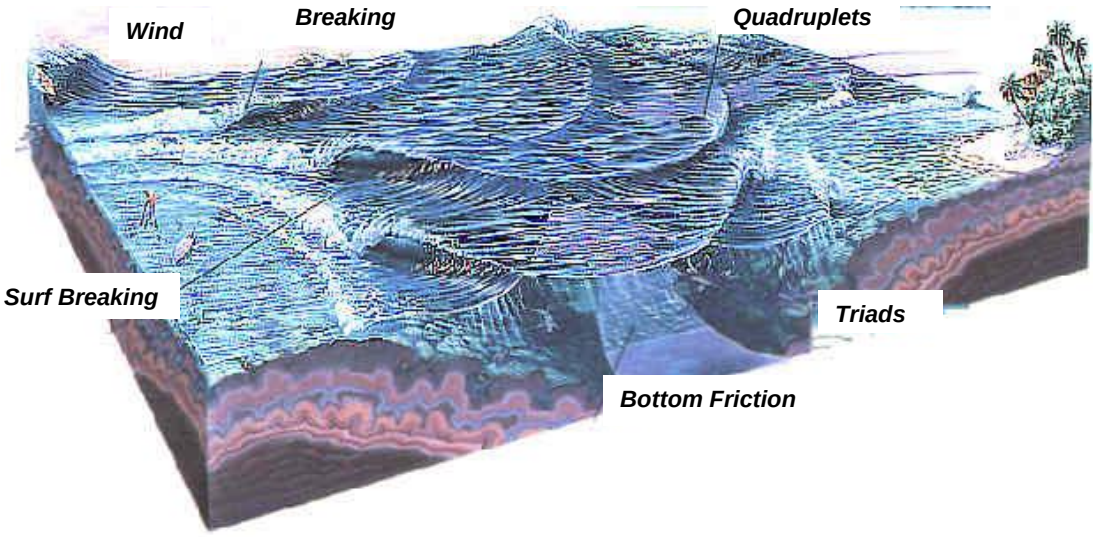

Figure 7.1 A diagrammatic representation of wind wave generation and propagation in the coastal region, with a number of the important physical processes shown [Holthuijsen *pers. comm.*].

No numerical model can represent all of the complex physical processes completely. The aim of wind wave modelling is, however, to use a model which represents the critical first order processes adequately and hence can reliably produce acceptable results at reasonable cost. The following sections critically review the various models that have been applied in such situations. In all cases, increased sophistication is achieved at the penalty of increased computational expense.

7.2 The Physics of Wind-Wave Evolution

7.2.1 Governing Equations

The aim of numerical wave modelling is to predict the evolution of the directional wave spectrum, $F(f,\theta)$, as a function of time, t and position x,y, where f is the frequency and θ is the direction of propagation of the spectral wave component. Young (1999) (amongst others) has shown that the evolution of the spectrum can be described by

$$\frac{d}{dt}\left(CC_gF\right) = CC_gS_{tot} \tag{7.1}$$

where C is the phase speed of the waves and C_g is the group velocity. The parameter S_{tot} represents a source terms which accounts for all physical processes which add or remove energy from the particular spectral component. Energy is advected along wave rays, and (7.1) holds along these wave rays, which are defined by

$$\begin{aligned}
\frac{dx}{dt} &= C_g\cos\theta \\
\frac{dy}{dt} &= C_g\sin\theta \\
\frac{d\theta}{dt} &= \frac{C_g}{C}\left[\sin\theta\frac{\partial C}{\partial x} - \cos\theta\frac{\partial C}{\partial y}\right]
\end{aligned} \tag{7.2}$$

Solution of (7.2) defines the wave rays along which (7.1) holds. Substitution of (7.2) into (7.1) yields

$$\begin{aligned}
&\frac{\partial}{\partial t}\left(CC_gF\right) + C_g\cos\theta\frac{\partial}{\partial x}\left(CC_gF\right) + C_g\sin\theta\frac{\partial}{\partial y}\left(CC_gF\right) + \\
&\frac{C_g}{C}\left[\sin\theta\frac{\partial C}{\partial x} - \cos\theta\frac{\partial C}{\partial y}\right]\frac{\partial}{\partial\theta}\left(CC_gF\right) = CC_gS_{tot}
\end{aligned} \tag{7.3}$$

Equation (7.3) is applicable in finite water depth, d. In deep water, the wave rays defined by (7.2) become (a) straight lines, assuming the earth is flat, or (b) great circles, assuming a spherical earth. In this case, (7.3) can be simplified to

$$\frac{\partial F}{\partial t} + \mathbf{C_g}\cdot\nabla F = S_{tot} \tag{7.4}$$

where $\mathbf{C_g}$ is the group velocity vector (having magnitude and direction). Solution of Equation (7.3) or (7.4) yields the directional wave spectrum $F(f,\theta)$ as a function of position and time.

7.2.2 Source Terms

The source term S_{tot} represents all physical processes that transfer energy to, from or within the spectrum. Consistent with the linear superposition assumption inherent in the spectral representation, it can be represented as the summation of a number of independent processes (Hasselmann, 1969; Hasselmann *et al.*, 1973), namely

$$S_{tot} = S_{in} + S_{nl} + S_{ds} + S_b + \cdots \tag{7.5}$$

where

$S_{in} \equiv$ atmospheric input from the wind

$S_{nl} \equiv$ nonlinear interactions between spectral components

$S_{ds} \equiv$ dissipation due to "white-capping"

$S_b \equiv$ dissipation due to interaction with the bottom

The four processes listed above are not exhaustive and there are undoubtedly many other factors that influence the evolution of waves. Knowledge in this area is far from complete. The processes listed above do, however, appear to account for the major fluxes of energy to the spectrum. The first three are all important in deep water, whilst interactions with the bottom are clearly only applicable in finite depth water. A detailed discussion of the functional forms for each of these source terms can be found in Young (1999).

7.3 Numerical Modelling of Waves

7.3.1 Introduction

A comprehensive model that incorporates our full understanding of wind wave physics and is applicable in all situations would be prohibitively expensive. Instead, a variety of models have been proposed for applications in specific situations. In order to select the most appropriate model requires an understanding of the relative importance of the various physical processes active in each domain. Such a classification has been presented by Battjes (1994), a modified form of which appears in Table 7.1. The table divides wave prediction into four physical domains:

- *Deep Oceans* - where bottom influences can be neglected.
- *Shelf Seas* - area between the deep oceans and the shoaling zone.
- *Shoaling Zone* - the area where shoaling becomes important.
- *Harbours* - taken to represent areas where there is an interaction between the waves and any structure (e.g. breakwater, oil platform, island, reef, etc.).

Table 7.1 The relative importance of various physical mechanisms in different domains.

Physical Process	Deep Oceans	Shelf Seas	Shoaling Zone	Harbours
Diffraction	⊗	⊗	°	∗
Depth refract./shoaling	⊗	●	∗	●
Current refraction	⊗	°	●	⊗
4 wave interactions	∗	∗	°	⊗
3 wave interactions	⊗	°	●	°
Atmospheric input	∗	∗	°	⊗
White-capping	∗	∗	°	⊗
Depth breaking	⊗	°	∗	⊗
Bottom friction	⊗	∗	●	⊗

⊗ - negligible; ° - minor importance; ● - significant; ∗ - dominant [after Battjes (1994)].

Models can be divided into two general classes: *phase resolving models*, which predict both the amplitude and phase of individual waves and *phase averaging models* which predict average quantities such as the spectrum or its integral properties (H_s the significant wave height, f_p the spectral peak frequency, etc.). Should phase averaged properties vary rapidly

(order of a few wavelengths) then it will generally be necessary to use a phase resolving model. Conversely, should the wave properties vary slowly, on a scale of many wavelengths, then phase averaging models should be adopted.

Neither of the two general classes is superior, their domains of application often do not overlap. Nevertheless, Battjes (1994) concludes that: *"Phase resolving models are computationally so much more demanding (per unit area of computational domain) that they should be used only where they are strictly needed"*. Of the processes considered in Table 7.1 only diffraction and 3 wave nonlinear interactions require phase resolving models. Hence, the domain of application of phase resolving models is generally confined to wave-structure interactions (harbours etc.) and the nearshore zone, where 3 wave interactions become important. Even around coastal islands and reefs there is little evidence that diffraction is important. Recent spectral models have also included 3 wave interactions in an approximate form (Eldeberky and Battjes, 1995). In the context of tropical cyclone wave prediction, even in the coastal environment, spectral (phase averaging) models have been shown to produce reliable results and the remainder of this review will be limited to this type of model.

7.3.2 Source Term Representation

The sophistication with which the source term S_{tot} has been represented has largely paralleled the increasing understanding of the physical processes responsible for wind-wave evolution and the exponential increase in available computational resources. Models are typically classed as first, second or third generation. These classifications are briefly described in Table 7.2.

Table 7.2 Definition of model classes based on the representation of the source terms.

	S_{in}	S_{nl}	S_{ds}
First Generation	• Based on growth rate measurements • Large in magnitude		• Saturation limit
Second Generation	• Based on flux measurements • Smaller than 1st Generation	• Parametric form • Limited flexibility	• Saturation limit, as in 1st Generation
Third Generation	• Based on flux measurements • Stress coupled to sea state	• Approximate form of Boltzman integral	• Explicit form

Each of these classes of model is discussed in the following sections.

7.3.3 First Generation Models

The first attempt to develop a wave prediction model based on a numerical solution to (7.4) was made by Gelci *et al.* (1957). This model pre-dated the development of the theory of quadruplet nonlinear interactions by Hasselmann (1962) and the source term was considered to be the sum of atmospheric input and white-cap dissipation.

$$S_{tot}^{(1)} = S_{in}^{(1)} + S_{ds}^{(1)} \qquad (7.6)$$

Models of this type are termed *first generation*, as indicated by the superscripts in (7.6). A number of other first generation models were later based on this same source term description

(Pierson *et al.*, 1966; Inoue, 1967; Isozaki and Uji, 1973; Cardone *et al.*, 1975; Cavaleri and Rizzoli, 1981; Chen and Wang, 1983). The atmospheric input term, $S_{in}^{(1)}$ in these models was generally represented as the sum of a linear (Phillips) term and an exponential (Miles) term. The exponential growth rate terms were based on direct measurements of wave growth such as those of Snyder and Cox, (1966). Atmospheric input terms obtained in this manner implicitly included the effects of other processes such as quadruplet interactions and overestimated the magnitude of the actual contribution due to atmospheric input alone.

The dissipation term, $S_{ds}^{(1)}$ was represented as an "on/off" limiter, which prevented the spectrum exceeding a pre-defined *saturation limit* (Phillips, 1958). Thus, the high frequency regions of the spectrum (saturation range) were forced to conform to this spectral form. This first generation spectral balance is shown diagrammatically in Figure 7.2.

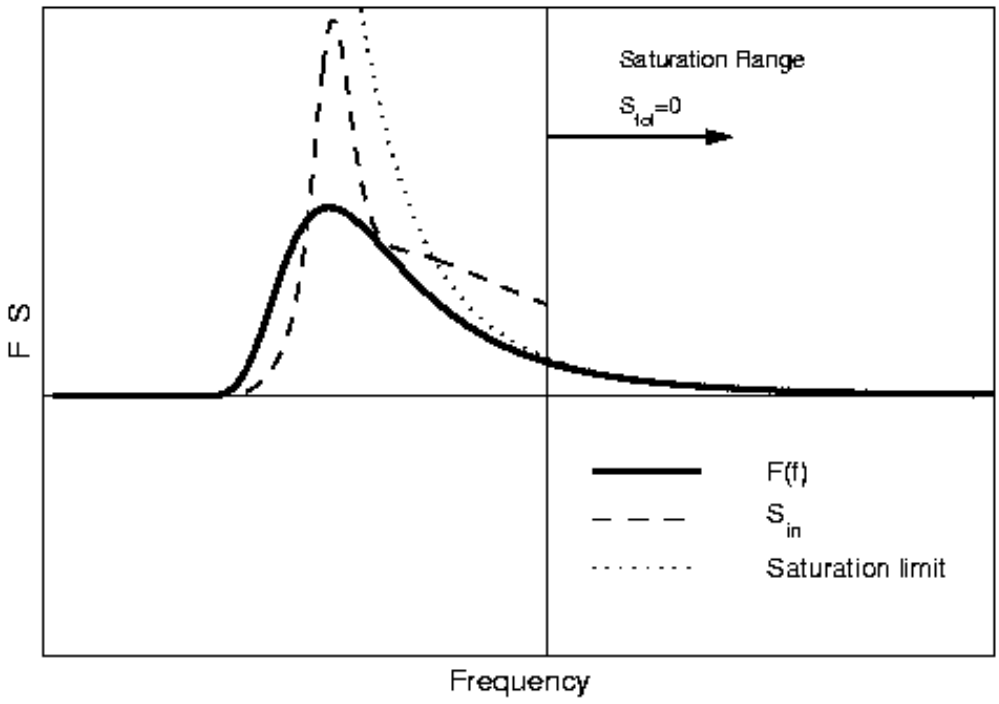

Figure 7.2 The source term balance for first generation wave models.

Note that S_{in} is larger than in later generation models and that the spectral balance at high frequencies is controlled by the imposition of a saturation limit on the spectrum.

First generation models were applied successfully for many applications. However, models tended to produce reliable results only for the geographic regions or meteorological systems for which they were developed. When applied to other cases, they often required re-calibration. In addition, they were incapable of predicting many aspects of spectral evolution such as the existence of the "overshoot effect" observed by Barnett and Wilkerson (1967) at frequencies immediately above the spectral peak frequency. Such models also performed poorly in complex meteorological situations, such as the rapidly turning winds in tropical cyclones. A systematic study of these limitations and a comparison between models was undertaken as part of the SWAMP study (SWAMP Group, 1985).

7.3.4 Second Generation Models

The JONSWAP study (Hasselmann *et al.*, 1973) clearly showed the central role played by quadruplet nonlinear interactions in the source term balance. Hence, it became clear that this term must be included within operational models. A major impediment to the inclusion of S_{nl}, was the significant computational time required for its evaluation. In order to overcome this problem a class of wave models which utilized approximations to this term developed (Barnett, 1968; Ewing, 1971; Golding, 1983; Allender *et al.*, 1985, Greenwood *et al.*, 1985; Sobey and Young, 1986; Young, 1988a). This class of model, the source term balance of which is shown in (7.7) become known as *second generation models*.

$$S_{tot}^{(2)} = S_{in}^{(2)} + S_{nl}^{(2)} + S_{ds}^{(2)} \qquad (7.7)$$

In contrast to first generation models, the atmospheric input term, $S_{in}^{(2)}$ was based on direct measurements of the normal stress exerted on the water surface (Snyder *et al.*, 1981). Hence, this term was significantly smaller than in first generation models. Also, many of the second generation models neglected the linear or Phillips term, as it was very small in comparison to the Miles exponential mechanism. The linear mechanism does, however, play a role in the initial growth of the spectrum from a calm sea. This initial "trigger" for growth was included in these models by defining the initial conditions for the model as some small, but finite, spectral energy.

The dissipation term $S_{ds}^{(2)}$ was included as a saturation limit to the spectrum. As the results of JONSWAP showed that this level varied with the wave age, a number of models included variable levels for this saturation spectrum.

The significant advancement with this class of model was the inclusion of a parametric representation for the quadruplet nonlinear interaction term, $S_{nl}^{(2)}$. A number of representations were implemented. In almost all cases these approximate forms represented the model spectrum in terms of a small number (3 to 5) of parameters. The JONSWAP spectral parameters were a common choice (Barnett, 1968; Ewing, 1971; Young, 1988a). As S_{nl} could be pre-computed for spectra with a range of these standard parameters, model values of $S_{nl}^{(2)}$ could then be determined based on the model spectral parameters. Naturally, problems occurred when the model spectrum did not conform to any of those for which S_{nl} had been precomputed. A further sub-class of models, termed *hybrid models*, took this process one step further and predicted the evolution of the parameters rather than the discrete values of the two-dimensional directional spectrum. Notable examples of these hybrid models are GONO (Sanders, 1976) and HYPA (Gunther *et al.*, 1979).

A diagrammatic representation of the source terms in second generation models is shown in Figure 7.3. In contrast to first generation models [Figure 7.2], it is clear that the inclusion of the nonlinear term has resulted in a reduction in the magnitude of the atmospheric input.

The inclusion of the parametric representations for S_{nl} generally resulted in an enhanced modelling capability. Even in demanding situations such as tropical cyclone wind fields, second generation models were able to produce reasonable results (Young, 1988a). Despite this, the relatively simple formulation for the nonlinear source term represented a significant short-coming of these models.

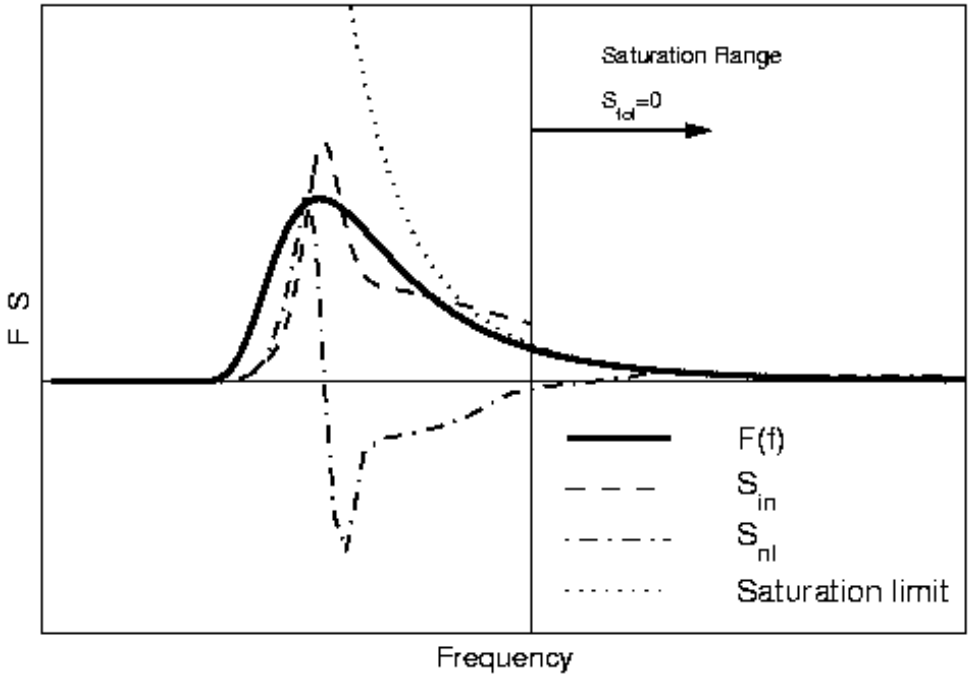

Figure 7.3 The source term balance for second generation wave models.

Note that S_{in} is smaller than in first generation models [see Figure 7.2].

7.3.5 Third Generation Models

By the middle 1980s a multitude of 1st and 2nd generation models were operational. Many of these were used for commercial purposes and numerous claims were made about the benefits of one model as opposed to another. In order to compare the physics of the various models and to assess their strengths and weaknesses a major international intercomparison study was initiated - the *Sea Wave Modeling Project, SWAMP*, (SWAMP Group, 1985). Rather than compare models against field data, this study utilized a series of idealized test cases, designed to highlight specific aspects of model physics. One of the significant findings of the study was: *"All present second-generation models suffer from limitations in the parameterization of the nonlinear energy transfer, S_{nl}"*. The directional wave spectrum $F(f,\theta)$ is typically represented by discrete values. In order to define the two-dimensional frequency-direction space, of order 100 points are required (typical implementations use about 300 values). The parameterizations for $S_{nl}^{(2)}$ typically use a maximum of 5 parameters. The mismatch is obvious: How can the evolution of a spectrum with hundreds of degrees of freedom be described by a source term defined by only a handful of parameters?

The solution to these short-comings was, however, a significant problem and the first steps to a solution were made in the spring of 1984 when Klaus Hasselmann invited wave researchers to Hamburg to discuss the possibility of a joint endeavour. The WAM (WAve Modelling) Group was formed. The aim of the group was to develop a *third generation* model, free from many of the assumptions that constrained earlier generation models. This significant international collaboration resulted in the WAM Model (WAMDI, 1988). Variants of this basic model were also developed by Tolman (1991) (WAVEWATCH) and more recently by Booij *et al.* (1996) (SWAN).

The source term balance in third generation models is essentially the same as in second generation models, that is

$$S_{tot}^{(3)} = S_{in}^{(3)} + S_{nl}^{(3)} + S_{ds}^{(3)} \qquad (7.8)$$

The details of the source terms are, however, significantly different to second generation models. The early versions of the WAM model utilized the Snyder *et al.* (1981) form of S_{in} as in second generation models. Later versions, however, incorporated the coupled air water drag model of Janssen (1991). In principal, a third generation model should have a full solution to the nonlinear quadruplet interaction term. In practice, however, this is still not computationally feasible in a two-dimensional model. Third generation models utilize the discrete interaction approximation (DIA) to the term (Hasselmann *et al.*, 1985). Although the DIA is still an approximation to S_{nl}, it is very different in its formulation to the simple parametric forms used in second generation models. The DIA retains the basic physics of the nonlinear interaction process, but considers a very small sub-set of all the possible interactions. In contrast to second generation parameterizations for S_{nl}, which have only a few degrees of freedom, the DIA has as many degrees of freedom as there are values in the discretely specified directional spectrum, $F(f,\theta)$.

As both the input and nonlinear terms of second generation models had significantly fewer degrees of freedom than the spectrum, the only way that stable spectral evolution could be achieved was by imposing the saturation limit at high frequencies. This is not necessary with third generation models and explicit forms for the still poorly understood white-cap dissipation term, S_{ds}, can be utilized. The general form used has been that of Komen *et al.* (1984).

The form of the source terms utilized in third generation models is shown in Figure 7.4. The significant difference compared to second generation models is that no artificially defined saturation limit is required to maintain a spectral balance at high frequencies. The spectrum is allowed to evolve without constraint until, at high frequencies a balance is achieved where $S_{tot}^{(3)} = 0$.

7.4 Computational Aspects

In addition to defining the source terms there are a number of computational aspects which need to be considered in the development of any numerical model. These include the advection scheme to be used, the specification of the computational grid and the initial and boundary conditions. Many of these aspects are common to the solution of advective transport equations found in related areas of computational physics and the model designer can draw extensively from this literature. There are, however, some unique problems associated with wave prediction which require specific attention. The vast bulk of the international wave modelling effort has been concentrated on the specification of the source terms. In comparison, the numerical aspects have received minimal attention.

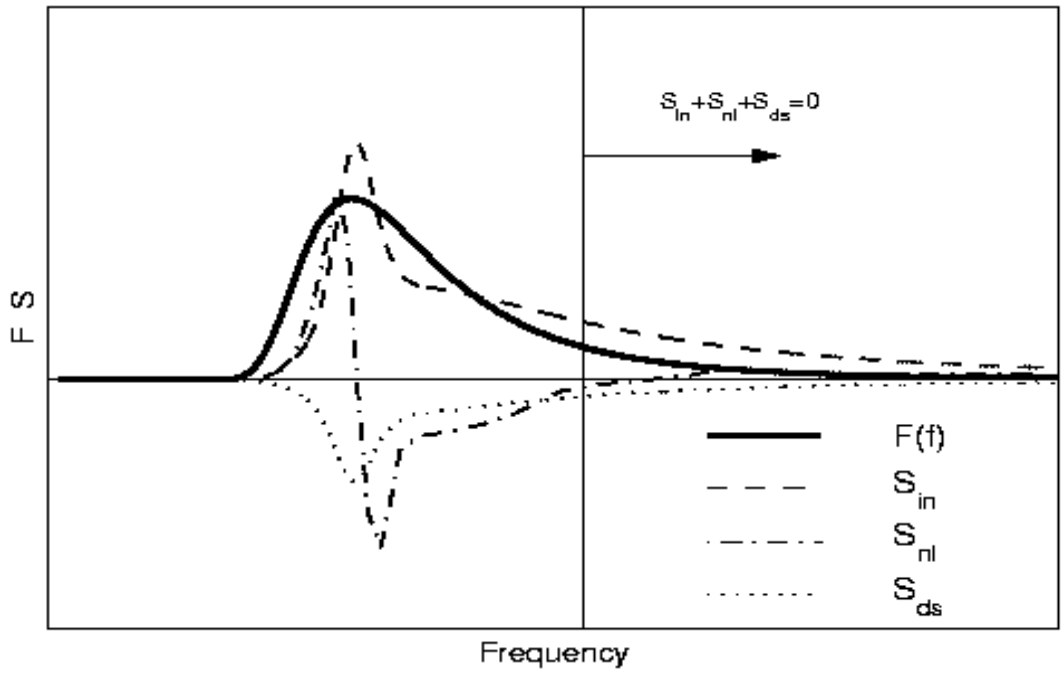

Figure 7.4 The source term balance for third generation wave models.

Note that at high frequencies a balance is achieved between the source terms, such that, $S_{tot}^{(3)} = 0$**.**

7.4.1 Advection of Energy

The second term on the left-hand side of (7.4) represents the advection of wave spectral energy at the group velocity, C_g. The advection of energy is more clearly seen when the transport equation is written in its characteristic form. Equation (7.3) is the finite depth form of (7.4). The set of characteristic equations, (7.2) define wave rays along which the wave action CC_gF is advected. In the absence of forcing (i.e. $S_{tot} = 0$), the wave action will be conserved along these rays. In deep water the rays become straight lines (or great circles if a spherical co-ordinate system is used) and due to the invariance of the group and phase velocities, the quantity conserved along the rays becomes the energy density, F. In finite depth situations or in the presence of spatially variable currents, the rays become bent, reflecting the effects of depth or current refraction.

The directional wave spectrum $F(f,\theta)$ is typically represented by a series of discrete frequency and direction bins. Thus, each of these bins will have some finite size (in frequency-direction space), $\Delta f - \Delta\theta$ as shown in Figure 7.5.

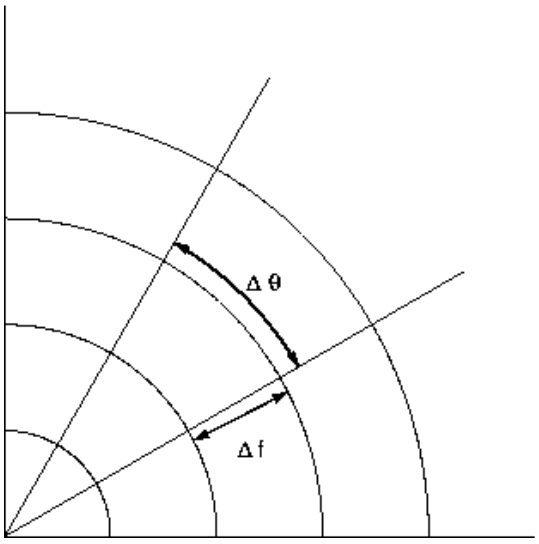

Figure 7.5 The directional wave spectrum.

$F(f,\theta)$ is typically represented within wave models as a series of discrete computational bins, each of size $\Delta f - \Delta\theta$.

A numerical scheme is required which can advect these discrete bins of energy at their respective group velocities. There are essentially four methods that have been used: finite differences, finite elements, full ray methods and piecewise ray methods. The vast majority of models have adopted finite difference techniques, WAM (WAMDI, 1988) being a good example. Finite elements have been less commonly used, although they possess some advantages in terms of fitting the grid to irregular coastlines.

Full ray methods construct rays which propagate throughout the complete grid. Equation (7.4) is then integrated numerically along these rays. This process decouples the rays, thus making it difficult to use source terms requiring coupling across spectral components (i.e. S_{nl}). Thus, full ray methods have generally not been used for second and third generation models. Piecewise ray methods trace all wave ray components from each computational point backward for one time step. The energy at each terminating ray point is then determined by interpolation amongst surrounding computational points. Although the method has a number of advantages, including being unconditionally stable, it has not been commonly used (Young, 1988a).

Whichever technique is used, the goal is the same: to advect the energy with minimal numerical distortion. Convective transport equations are well known for the problems associated with numerical dispersion. This is generally overcome by resort to higher order schemes. In the field of wave modelling, however, some special problems exist. As indicated above, the desire is to advect the bin of energy which has finite size $\Delta f - \Delta\theta$. As shown in Figure 7.6, because of the finite size of the bin some natural dispersion will occur. As the bin represents wave components with frequencies in the range, $f_0 \pm \Delta f / 2$, there will be a range of advection velocities for these components. The energy contained within the bin will naturally disperse, progressively being spread over an ever-increasing spatial extent as it propagates.

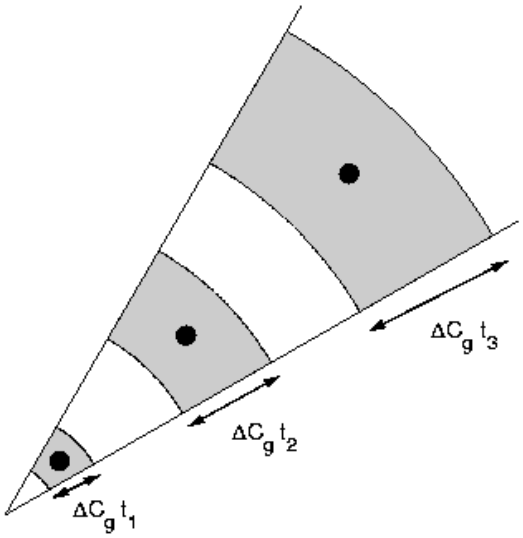

Figure 7.6 The natural dispersion of the bin of energy as it is advected.

Due to the finite range of group velocities and propagation directions contained within the bin, the spatial extent of the bin will increase with time. The single dots at the centre of the bin show the result of the use of a propagation scheme that has no numerical dispersion.

As shown in Figure 7.6, spatial extent of the bin of energy increases linearly with time. A consistent numerical propagation scheme should reproduce these linear dispersion rates. Figure 7.6 also shows the spatial distribution resulting from a propagation scheme with no dispersion. The energy will be concentrated at a single point at the centre of the continually enlarging bin of energy. The resulting "spotty" distribution of energy has been termed the *garden sprinkler effect*. Booij and Holthuijsen (1987) have shown that the required linear spreading rates may be achieved by introducing a variable diffusion coefficient proportional to the age of the bin of energy. To date, this concept has not been tested in the context of a full model.

As a result of the garden sprinkler effect, use of higher order propagation schemes will not necessarily improve results. To date, operational models have generally used relatively low order propagation schemes in the hope that the numerically dispersion inherent in such schemes is not too dissimilar to the required natural dispersion. As an example, the WAM model uses a first order upwinding scheme. In justification for this choice Janssen *et al.* (1994) take the pragmatic stance: *"... we have chosen the first order upwinding scheme because it is the simplest scheme to implement (requiring less computer time and memory) and because in practice it gives reasonable results"*. Higher order schemes have, however, been reported to yield improved results: Tolman (1992) - second order and Bender, (1996) - third order.

It is clear from the discussion above that relatively little effort has been devoted to the propagation algorithms used in present-day wave prediction models. Although it is claimed that present day models, such as WAM, predict swell propagation to a reasonable level of precision, other influences may also be active. The white-cap dissipation terms in third generation models have been "tuned" to ensure growth rates of wind sea and decay rates of

swell agree with measurements. Hence, the apparently acceptable results may be a result of this artificial tuning. It is reasonable to conclude that further research into the development of appropriate propagation algorithms for use in wind-wave models is required.

7.4.2 Computational Grids

Equation 7.4 must be solved on a two-dimensional spatial grid. The precise details of this computational grid can have significant influence on the solution. The grid must be sufficiently fine to ensure that the spatial distribution of the wind field is adequately resolved. An often-conflicting requirement is that the extent of the model should remain computationally tractable. Often, conflicts of scale also occur. For instance, a goal may be to model the waves generated by an extreme tropical cyclone. Adequate resolution of the tight vortex wind field of a small-scale tropical cyclone may require a very fine resolution grid (e.g. $\Delta x < 5$ km). At the same time, swell generated in this intense wind region can propagate large distances. Thus the spatial extent of the grid may need to be large (e.g. 2,000 km). Similarly, an extremely fine resolution grid may be required to accurately define the bathymetry in a coastal area. The meteorological system which generated the swell entering this region may, however, have occurred many thousands of kilometres away.

These conflicts of scale are often accommodated by the use of nested grids, particularly for coastal applications. A relatively coarse grid is initially used to model the generation of distant waves. Any number of finer nested grids can then be successively embedded within this coarse grid. Each of these finer grids takes their respective boundary conditions from the coarser grid in which they are nested.

Numerical wave prediction models can be divided into two general classes: global scale models and regional models. Global models operate on spherical grids. A typical example is the global WAM model which runs operationally at many centres, the most long standing implementation being that at the European Centre for Medium Range Weather Forecasting (ECMWF). In its original implementation at ECMWF, WAM operated on a 3^0 grid with a time step of 20 minutes, the spectral grid being represented by 25 frequencies and 12 directions. In later versions of the model, the spatial resolution was increased to 1.5^0.

At the other extreme, regional models often operate on Cartesian grids with resolutions as fine as a few hundred metres. Although the resolution can be reduced further, some consideration of the rationale for such a grid is required. Phase averaging models assume that the spectrum is changing relatively slowly, compared with the wave length. Therefore, if it is expected that the wave field will change significantly over a length of order 10 wave lengths, than the validity of the phase averaged model is questionable.

In addition to the selection of appropriate spatial resolution, the time step also needs to be matched to the particular problem. In models that use explicit finite difference schemes, such as WAM, the upper bound on the time step Δt is specified by the requirements of numerical stability. The Courant limit requires $\Delta t < \Delta x / C_g$, where Δx is the spatial resolution. Hence, the energy is constrained to propagate, at most, one grid element during the time step. At first appearances this may seem an overly restrictive limitation and the use of implicit schemes may seen advantageous. Such schemes may remain numerically stable with larger time steps but they are not necessarily accurate. If the spatial scale has been chosen to resolve the bathymetry and wind forcing, the time step should be such that wave energy propagating

through the area can appropriately interact with the local source terms. Hence, the Courant limit seems an appropriate upper bound for the time step to ensure, not only numerical stability, but also accuracy of the numerical solution.

7.4.3 Initial and Boundary Conditions

Models that do not have a Phillips mechanism require some initial spectral energy level to initiate growth. This is usually achieved by the introduction of a "seed" spectrum which has very low energy. The model then goes through a "spin-up" period where a wind field is imposed whilst the waves gradually reach a realistic level. The exact details of the seed spectrum are not important. One of the characteristics of spectral wave models (especially third generation models) is that they quickly modify the sea state to be in equilibrium with the local forcing wind.

All models require the specification of boundary conditions. Land boundaries are typically taken as completely absorbing with all energy being dissipated. Unless a global model is used, open boundary conditions must also be imposed. A common choice in such circumstances is to impose radiation conditions, in which energy can leave the computational domain but none can enter. If such boundaries are used, it is necessary to ensure that the computational domain is sufficiently large to ensure the boundary conditions do not influence the wave field at the points of interest.

7.5 The Tropical Cyclone Wave Field

Our present understanding of the tropical cyclone wave field has been gained from a combination of in situ measurements (both non-directional and directional) at single points during the passage of tropical cyclones, remote sensing data and the application of numerical models. Naturally, the wave field is strongly related to the driving wind field, which is usually characterized by the velocity of forward movement, V_{fm}, the maximum wind velocity in the storm, $V_{\max}$ and the radius to maximum winds, R (e.g. refer Chapter 5).

Much of the tropical cyclone wave data collected using in situ instruments has been obtained for commercial purposes and consequently, only a small fraction is in the public domain. The first comprehensive attempt to collect data under tropical cyclone conditions was the Ocean Data Gathering Program (Shemdin, 1977). This program involved instruments on six offshore oil platforms in the Gulf of Mexico. These systems operated between 1968 and 1971, during which data were collected for four hurricanes, including Camille. The program has been described in detail by Ward (1974) and Hamilton and Ward (1974).

Since 1972, the US NOAA Data Buoy Office has deployed buoys at various locations around the US coast (NOAA Data Buoy Office, 1973). Tropical cyclone data from these buoys have been presented in a number of publications including Withee and Johnson (1975).

In addition to the US data set, a significant tropical cyclone wave database has been established by the offshore oil industry on the northwest coast of Australia. Data have been obtained from more than 25 tropical cyclones over a period in excess of 20 years (Harper *et al.*, 1993).

Although non-directional observations of tropical cyclone wave conditions are valuable, a more comprehensive understanding can be obtained from directional measurements. Directional spectral observations during the passage of tropical cyclones have been reported by Forristall *et al.* (1978) and Black (1979). Remotely sensed data using *Synthetic Aperture Radar* data have also provided insight into the directional properties of waves within tropical cyclones (Elachi *et al.*, 1977; King and Shemdin, 1978; Shemdin, 1980; Gonzalez *et al.*, 1982; McLeish and Ross, 1983; Beal *et al.*, 1986; Holt and Gonzalez, 1986).

Numerous models have been proposed for the prediction of waves within tropical cyclones. These range from the largely empirical (Bretschneider, 1959; Bretschneider, 1972; Ijima *et al.*, 1968; Ross, 1976; Young, 1988b) to those based on solution of the radiative transfer equation (Patterson, 1972; Bea, 1974; Uji, 1975; Cardone *et al.*, 1977; Young 1988a).

Based on knowledge of the tropical cyclone wind field and the composite database of wave observations, a qualitative description of the tropical cyclone wave field emerges. The wind field is asymmetric, with higher winds to the left (Southern Hemisphere) of the tropical cyclone centre. The wave field has an even greater degree of asymmetry due to the combined influence of the asymmetry of the wind field and the extended fetch that exists within a translating tropical cyclone. The wind vector in the intense wind region to the left of the storm centre (Southern Hemisphere) is approximately aligned with the direction of forward propagation. Hence, waves generated in this region tend to move forward with the tropical cyclone and therefore remain in high wind regions for an extended period of time [see Figure 7.7]. In contrast, waves generated on the low wind side of the storm (right side in Southern Hemisphere) propagate in the opposite direction to the tropical cyclone translation and rapidly move away from the high wind areas. Low frequency waves generated in the intense wind regions to the left of the storm centre will have group velocities which are typically greater than the velocity of forward movement of the storm, V_{fm}. Hence, these components will "out run" the storm and appear as swell ahead of the storm centre. This swell radiates out from the spatially localized generation area. Hence, the spectrum ahead of the storm often consists of locally generated wind sea together with swell radiating from the centre of the storm. The two wave systems often intersect at angles near 90^0. As they are significantly separated in both frequency and direction, they can co-exist without any significant non-linear interaction between the two systems.

The concept of an "extended fetch" which occurs due to the forward motion of the storm is also important in determining the wave height within a tropical cyclone. Not only is the wave height determined by the maximum wind speed, $V_{\max}$, but also by the period of time the waves remain within the intense wind region (Shemdin, 1977). As $V_{\max}$ increases, the period of the waves generated and hence the group velocity at which they propagate also increases. Consequently, V_{fm} must also increase for the most severe wave conditions to occur. Should the tropical cyclone move too slowly, the waves will "outrun" the tropical cyclone, whereas should the tropical cyclone move too rapidly, the waves will be left behind. Consequently, for a given value of $V_{\max}$, the wave height could be expected to increase with increasing V_{fm} until a maximum is reached. A further increase in V_{fm} will result in a decrease in wave height. Similarly, the spatial distribution of wave height (asymmetry) will also depend on both $V_{\max}$ and V_{fm}.

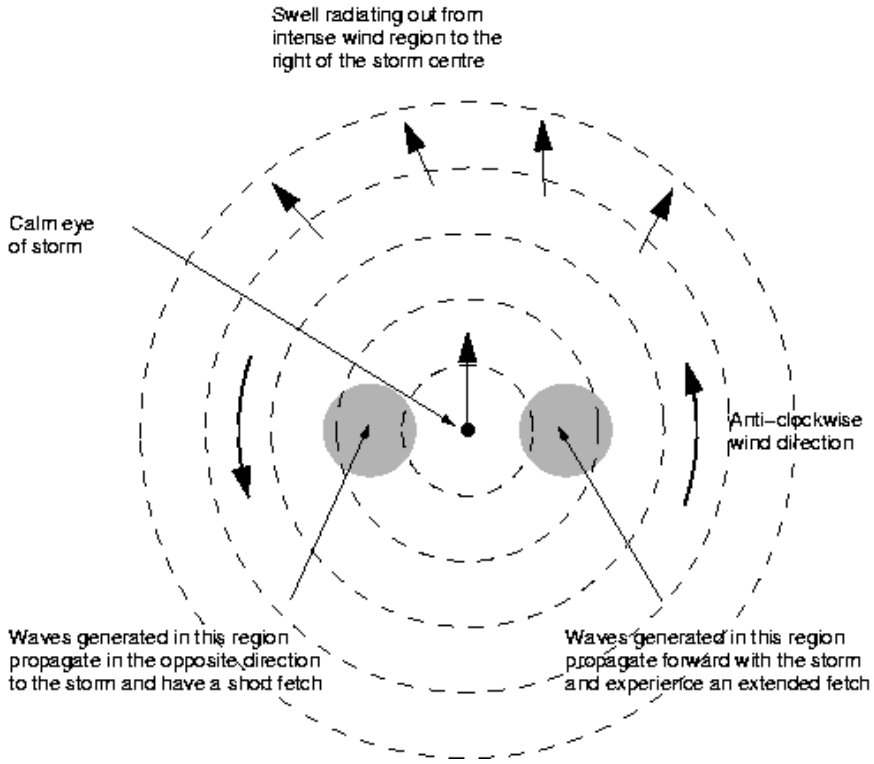

Figure 7.7 Schematic diagram showing the generation of waves within a translating hurricane (i.e northern hemisphere view).

The hurricane shown is translating "up the page" as shown by the arrow at the centre of the storm. The wave field is characterized by: (a) swell ahead of the storm, radiating out from the intense wind region to the right of the storm centre and (b) significant asymmetry caused by the higher winds and extended translating fetch to the right of the storm centre. Note that the system shown is for the Northern Hemisphere. For the Southern Hemisphere, the wave field will be the mirror image of that shown here.

An attempt to incorporate this qualitative understanding of the tropical cyclone wave field into a quantitative model was made by Young (1988b). Young (1988b) assumed that the JONSWAP (Hasselmann *et al.,* 1973) relationships, originally developed for fetch limited conditions, could also be applied in tropical cyclone wind fields with the specification of a suitable "equivalent fetch". Based on a synthetic database generated by a numerical model, the equivalent fetch was determined in terms of $V_{\max}$, V_{fm} and R. Although the model is empirical, it implicitly incorporates the intuitively consistent non-dimensional scaling of JONSWAP, together with the parameters observed to be important in determining the wave field within a tropical cyclone.

Given values of $V_{\max}$, V_{fm} and R, Young (1988b) found that an equivalent fetch F could be represented by the relationship:

$$F = \frac{x}{R'} = \psi\left[aV_{\max}^2 + bV_{\max}V_{fm} + cV_{fm}^2 + dV_{\max} + eV_{fm} + f\right] \quad (7.9)$$

where $a = -2.175\times10^{-3}, b = 1.506\times10^{-2}, c = -1.223\times10^{-1}, d = 2.190\times10^{-1}, e = 6.737\times10^{-1}$ and $f = 7.980\times10^{-1}$. The term ψ is a scaling factor which in the representation of Young (1988b) was taken as 1. The term R' can be found in terms of R as

$$R' = 22.5\times10^3 \log R - 70.8\times10^3 \quad (7.10)$$

In Equations (7.9) and (7.10) all terms are in standard S.I. units (i.e. $V_{\max}, V_{fm}$ - [m s^{-1}]; F, R, R' - [m]). The maximum significant wave height in the tropical cyclone, $H_s^{\max}$ can then be determined from a modified form of the JONSWAP (Hasselmann *et al.*, 1973) relationship

$$\frac{gH_s^{\max}}{V_{\max}^2} = 0.0016\left(\frac{gx}{V_{\max}^2}\right)^{0.5} \quad (7.11)$$

The spatial distributions of H_s are not obtainable directly in this case but have been determined from a series of numerical experiments. H_s can then be described in terms $H_s^{\max}$ using a series of diagrams for different values of $V_{\max}$ and V_{fm}.

Examples of the predicted spatial distribution of H_s are shown in Figure 7.8. The spatial scale is in terms of r/R' and the contours are of normalized significant wave height. In each case the wave field has been normalized such that the maximum value is 1. In all cases the maximum wind velocity in the storm, $V_{\max} = 40$ m s^{-1}. The velocity of forward movement gradually increases in each panel: (a) $V_{fm} = 2.5$ m s^{-1}, (b) $V_{fm} = 5.0$ m s^{-1}, (c) $V_{fm} = 7.5$ m s^{-1}, (d) $V_{fm} = 10.0$ m s^{-1}. The line of maximum winds $\theta_{\max}$ was chosen here as 70º (refer Chapter 5 for definitions). Note that all cases are shown for the Northern Hemisphere and Southern Hemisphere storms will the mirror images of those shown. For slow moving storms the spatial distribution is similar to the wind speed distribution. As V_{fm} increases the asymmetry of the wave field increases significantly as both the asymmetry of the wind field and the extended fetch to the right (Northern Hemisphere) of the storm increases in significance. For the largest values of V_{fm} the region of maximum waves moves from the right forward quadrant to the right rear quadrant. In these cases it is clear in the wave height distribution that the storm is propagating so quickly that it is "out running" the waves.

The accuracy of the results of the approach proposed by Young (1988b) is limited by the fact that a numerical model generated the synthetic database used. To assess the applicability of this approach Young and Burchell (1996) compared the results of the model with measurements of H_s obtained from overflights of tropical cyclones by the GEOSAT satellite altimeter. This satellite database was extensive, consisting of more than 100 tropical cyclones. Based on these data, Young and Burchell (1996) concluded that the model described by (7.9) contains a systematic bias and proposed that the scaling factor ψ should take the form:

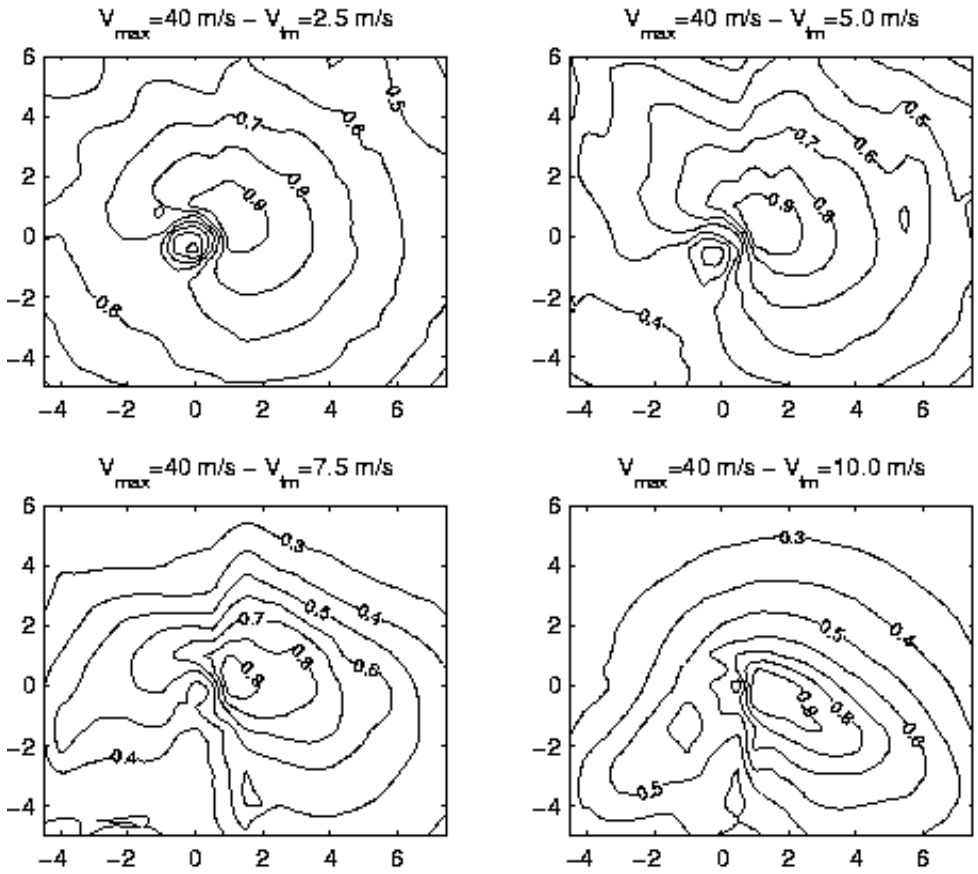

Figure 7.8 The wave height distribution as predicted by the numerical model results of Young (1988b).

$$\psi = 0.015V_{\max} + 0.0431V_{fm} + 1.30 \qquad (7.12)$$

where again $V_{\max}$ and V_{fm} have units of [m s^{-1}] and ψ is dimensionless. The resulting distribution of equivalent fetch x / R' obtained from (7.9) and (7.12) is shown in Figure 7.9.

The contours are of normalized equivalent fetch, x / R'. The figure was generated from (7.9) and (7.12). The surface takes the form of a ridge tilted towards the top right of the figure. Therefore, as storms become more intense (increase in $V_{\max}$) they must move increasingly more rapidly (larger values of V_{fm}) to generate the maximum possible waves for that intensity storm. Note that the relationships developed by Young and Burchell (1996) are not applicable outside the parameter range shown in this figure.

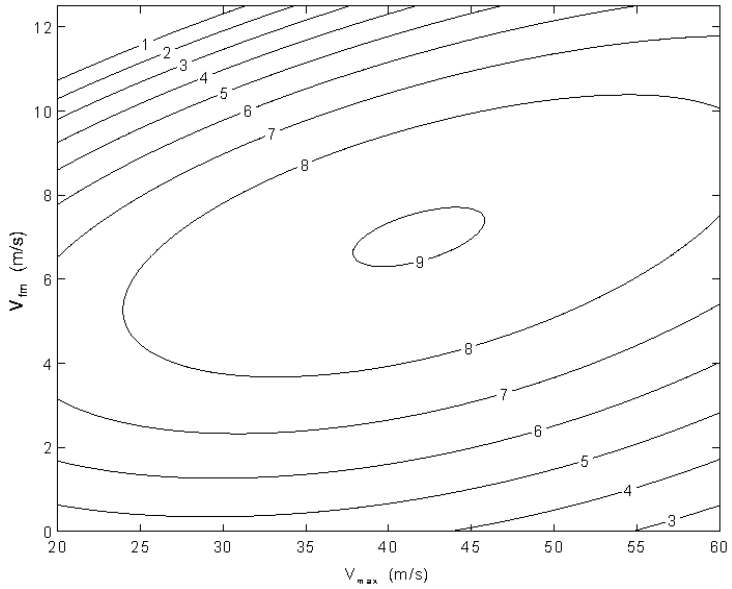

Figure 7.9 Contours of the equivalent fetch within a tropical cyclone. As proposed by Young and Burchell (1996).

7.6 Tropical Cyclone Wave Spectra

The vast majority of the studies discussed in Section 7.4 considered integral properties of the tropical cyclone wave field such as significant wave height and peak frequency. In many cases, information on the full spectrum is required. Significant data exists which describes the spectrum for fetch limited conditions. Based on the high frequency formulation of Phillips (1958), the JONSWAP experiment (Hasselmann *et al.*, 1973) found that the frequency spectrum of fetch-limited waves could be represented by the form

$$F(f) = \alpha g^2 (2\pi)^{-4} f^{-5} \exp\left[-\frac{5}{4}\left(\frac{f}{f_p}\right)^{-4}\right] \gamma^{\exp\left[\frac{-(f-f_p)^2}{2\sigma^2 f_p^2}\right]} \qquad (7.13)$$

where

$$\sigma = \begin{cases} \sigma_a & \text{for} \quad f \le f_p \\ \sigma_b & \text{for} \quad f > f_p \end{cases} \qquad (7.14)$$

and $F(f)$ is the energy spectrum and f is frequency. Equation 7.13 contains five parameters which define the spectral shape. The parameters f_p and α are scale parameters; f_p represents the frequency at the maximum of the spectrum and α corresponds to the Phillips proportionality "constant" (Phillips, 1958). The remaining three parameters define the shape of the spectrum: γ, the peak enhancement factor, is the ratio of the maximum spectral energy to the maximum of the corresponding Pierson-Moskowitz (Pierson and Moskowitz, 1964) spectrum with the same value of α and σ_a and σ_b define the left and right side widths respectively of the spectral peak region. The first term of (7.13) is the called the Pierson-

Moskowitz spectrum with the second term modifying the shape to make it more peaked. This enhancement is only significant for $f \approx f_p$. At large f / f_p the spectrum reverts to an f^{-5} decay as proposed by Phillips (1958).

An alternative formulation to (7.13), which has a high frequency region proportional to f^{-4} rather than f^{-5} has been proposed by Donelan *et al.* (1985)

$$F(f) = \beta g^2 (2\pi)^{-4} f_p^{-1} f^{-4} \exp\left[-\left(\frac{f}{f_p}\right)^{-4}\right] \gamma_d^{\exp\left[\frac{-(f-f_p)^2}{2\sigma^2 f_p^2}\right]} \qquad (7.15)$$

Note that β and γ_d have been used here to distinguish from α and γ in (7.13).

Studies that have considered detailed analysis of recorded wave spectra in tropical cyclones are far rarer than corresponding studies of integral properties. Whalen and Ochi (1978) investigated the spectra recorded during the passage of U.S. Hurricanes Camille, Celia, Edith and Eloise. As with a number of previous observations, they found that as the tropical cyclone approached the recording site, the spectra were initially bi-modal. As the tropical cyclone moved closer, the spectra became uni-modal. They attempted to model the spectra using both the JONSWAP form (Hasselmann *et al.,* 1973) and the 6 parameter form proposed by Ochi and Hubble (1976). The Ochi and Hubble (1976) spectral form can represent bi-modal spectra and consequently, it provided a better fit to the data than JONSWAP for such spectra. The JONSWAP spectrum, however, provided a good approximation to the data for the uni-modal spectra. They found that the data yielded mean JONSWAP parameters of $\gamma = 2.2$ and $\alpha = 0.023$. They also attempted to represent the parameters of the Ochi and Hubble (1976) spectrum in terms of the significant wave height, H_s. Although there appeared to be some dependence on H_s, there was significant scatter in the results. In view of the results of Shemdin (1980), Young (1988b) and Young and Burchell (1996), which clearly demonstrate that H_s is a function of the relative position of the tropical cyclone, the velocity of forward movement of the tropical cyclone, V_{fm} and the maximum wind speed within the tropical cyclone, $V_{\max}$, it seems unlikely that a bi-modal spectral form could be parameterized in terms of H_s, alone. The apparent dependence in the Whalen and Ochi (1978) data on H_s is most likely due to the very small number of tropical cyclones considered. Although there were four tropical cyclones in the total data base, the vast majority of the spectra were obtained from Hurricane Eloise.

Ochi and Chiu (1982) considered spectra recorded for U.S. Hurricane David. Again they confirmed that the JONSWAP form could model uni-modal spectra well and that the bi-modal spectra generated when the tropical cyclone was distant from the measurement site were well represented by the Ochi and Hubble (1976) form.

A detailed study of the properties of the one-dimensional spectrum, $F(f)$, under tropical cyclone conditions was presented by Young (1997). Young (1997) considered data recorded over a 16 year period off the north-west coast of Australia. Spectra obtained from 16 tropical cyclones were considered. The tropical cyclones had central pressures ranging from 905 hPa to 985 hPa. Hence, the data set was quite comprehensive. Young (1997) found that the spectra

were bi-modal when the storm centres were more than 8 times the radius to maximum winds, R, from the measurement site. Spectra recorded within $8R$ of the centre of the storm, however, appeared similar to fetch limited spectra. This occurred despite the fact that the wind fields were changing rapidly in direction and that the wave field consisted of a mix of locally generated waves and distant swell. Young (1997) concluded that the shape stabilizing effects of the nonlinear source term were sufficient to continually force the spectra back to the uni-modal form. As the swell and wind sea components became more separated in frequency and direction space (i.e. greater than $8R$ from the storm centre), the nonlinear coupling reduced in strength, and hence the spectra were bi-modal.

In order to assess whether the parametric spectral forms represented by JONSWAP (7.13) or Donelan *et al.* (1985) (7.14) may be suitable to model tropical cyclone spectra, Young (1997) examined the exponent n in the expression $F \propto f^n$.

Figure 7.10 shows a scatter plot of n as a function of the inverse wave age, U_{10}/C_p, where C_p is the phase speed of components at the spectral peak frequency. There is significant scatter in the data and no clear evidence that either of the proposed forms f^{-4} or f^{-5} is the preferred form for the high frequency region of the spectrum. The mean value is $n = -4.56$, indicating either spectral form could be applied to the data. Such a result is consistent with the variability of the exponent n reported by Liu (1989) for fetch limited spectra.

Also shown in Figure 7.10 is the demarcation between wind-sea and swell, $U_{10}/C_p = 0.83$ proposed by Donelan *et al.* (1985). Based on this limit, a significant proportion of the spectra of this data set would normally be characterized as swell (i.e. $U_{10}/C_p < 0.83$). Despite this, these spectra are still uni-modal.

7.6.1 JONSWAP Representation of Tropical Cyclone Spectra

As the spectral width parameter, σ, has little influence on the ultimate spectral form, and as previous fetch limited studies had found no systematic trend within the scatter of values, Young (1997) assumed a constant value of this parameter of $\sigma = 0.1$. Figures 7.11a and 7.11b shown the values of α and γ, respectively, for the JONSWAP form (7.13). Figure 7.11a also shows the JONSWAP (Hasselmann *et al.*, 1973) relationship for α expressed in terms of U_{10}/C_p :

$$\alpha = 0.008\left(\frac{U_{10}}{C_p}\right)^{0.73} \qquad (7.16)$$

Although there is significant scatter within the data, the values of α clearly increase with increasing U_{10}/C_p. The JONSWAP relationship (7.16), which was developed for fetch limited waves, is a remarkably good fit to the data. This is a clear demonstration of the shape stabilization provided by non-linear interactions. Even though the wind fields from which these spectra were obtained are spatially and temporarily variable, the spectra are remarkably similar to those obtained from idealized fetch limited situations.

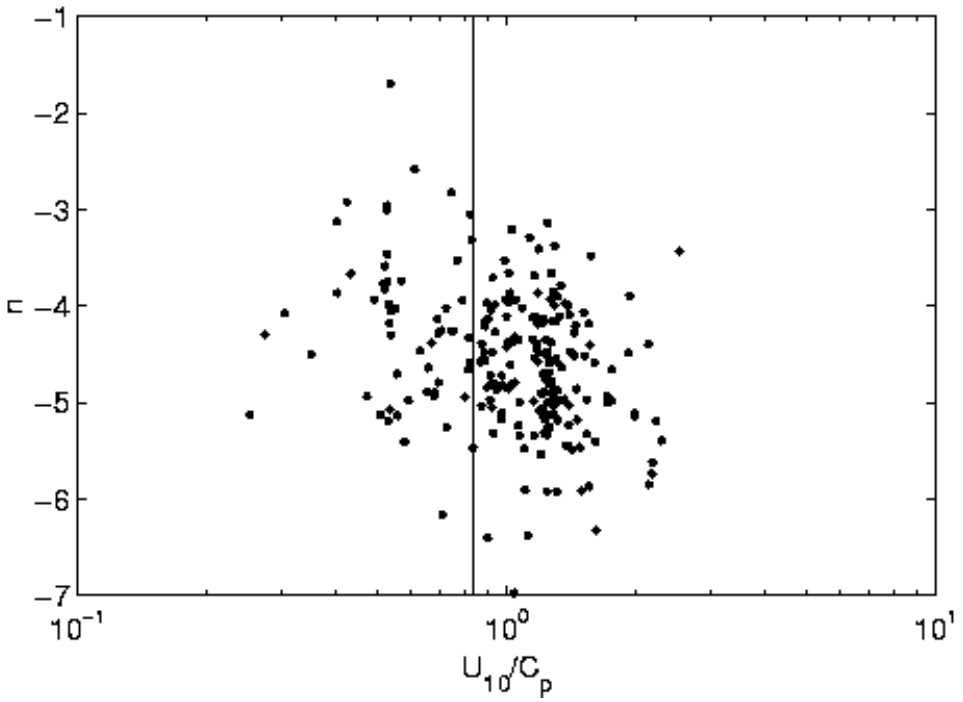

Figure 7.10 Values of the exponent in the relationship plotted as a function of the inverse wave age for the tropical cyclone data of Young (1997).

As the mean value of n is almost mid way between -4 and -5, Young (1997) concluded that either of the forms (7.13) or (7.14) could be used to represent the spectra. The parameters of these two formulations when applied to tropical cyclone wave spectra are discussed in Sections 7.6.1 and 7.6.2.

The same dependence between α and U_{10}/C_p continues for $U_{10}/C_p < 0.83$. This suggests that either the nonlinear interactions are capable of maintaining the spectral shape in the absence of active wind input or that components with $U_{10}/C_p < 0.83$ are still receiving such input. Naturally, the frequency components in the tail of the spectrum will still be propagating significantly slower than both the wind and the components at the spectral peak. Hence, they will still receive active atmospheric input even when $U_{10}/C_p < 0.83$. The fact that the components at the spectral peak can achieve such small values of inverse wave age occurs either since the local wind speed has decreased within the rapidly changing wind field vortex or that they have propagated to the measurement site from another location.

Figure 7.11b shows γ as a function of U_{10}/C_p. As with fetch limited results, there appears to be no systematic dependence on U_{10}/C_p. The mean value obtained from the data set is $\gamma = 1.9$, consistent with the value of $\gamma = 2.2$ obtained by Whalen and Ochi (1978) from their much smaller North American data set. The values of γ are consistently smaller than the mean JONSWAP value of $\gamma = 3.3$. Therefore, it appears that although much of the recorded energy has presumably propagated to the measurement stations from other locations as swell, it has been transformed locally by a combination of atmospheric input and nonlinear interactions into relatively broad wind-sea spectra.

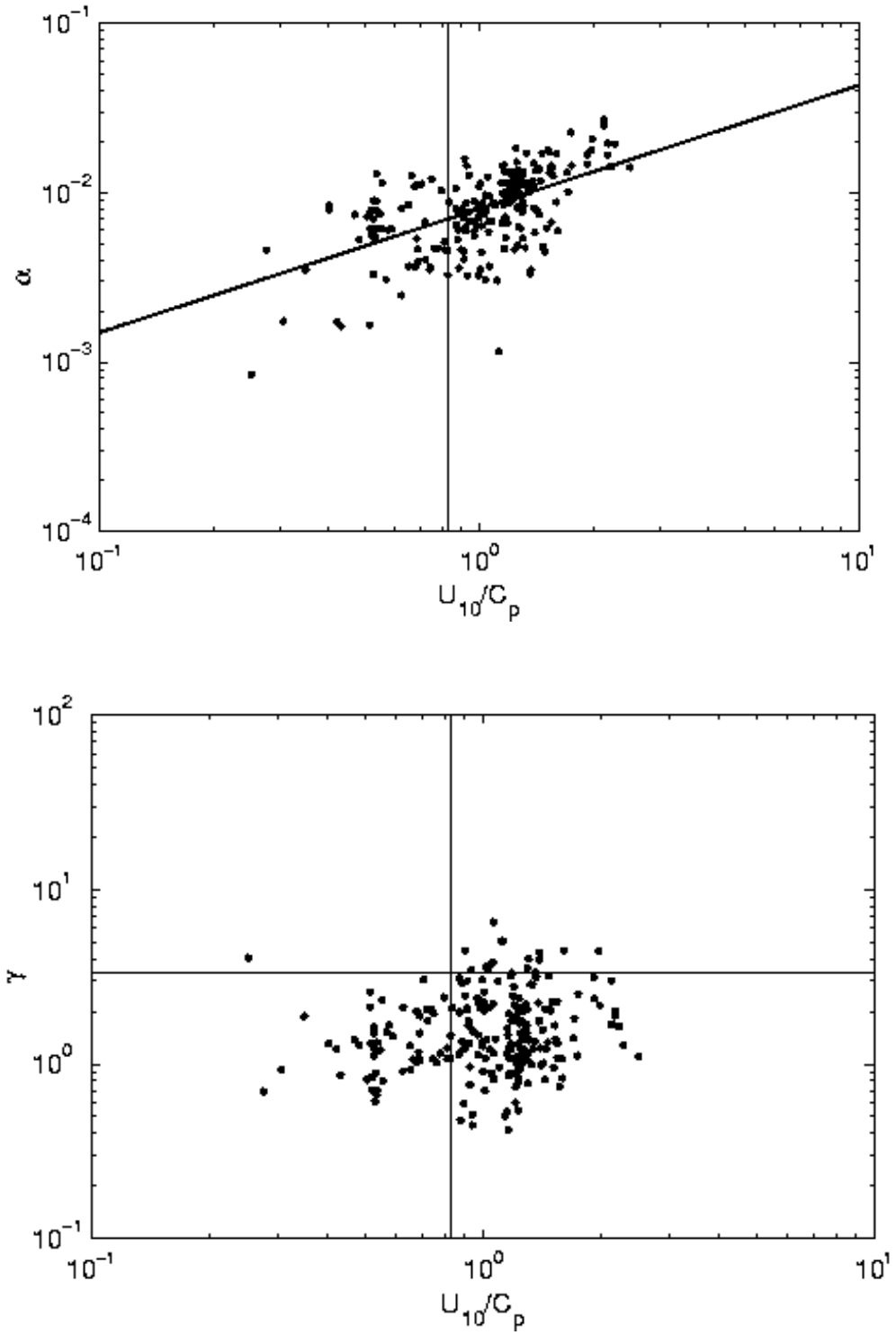

Figure 7.11 JONSWAP spectral parameters for tropical cyclone conditions.

(a) [top] Values of the parameter α as a function of the inverse wave age, U_{10}/C_p. The line through the data is the JONSWAP fetch limited relationship (7.16) and the vertical line is drawn at $U_{10}/C_p = 0.83$. (b) [bottom] Values of the parameter γ as a function of the inverse wave age U_{10}/C_p. The horizontal line represents the mean JONSWAP value, $\gamma = 3.3$ and the vertical line is drawn at $U_{10}/C_p = 0.83$.

7.6.2 Donelan *et al.* (1985) representation of Tropical Cyclone Spectra

Figures 7.12a and 7.12b show the parameters β and γ_d, respectively as functions of U_{10}/C_p, obtained for the Donelan *et al.* (1985) spectral form, Equation (7.15). The results are qualitatively similar to those shown in Figures 5.2 for the JONSWAP spectral form. Based on their fetch limited data, Donelan *et al.* (1985) proposed the following power law relationship between β and U_{10}/C_p.

$$\beta = 0.006\left(\frac{U_{10}}{C_p}\right)^{0.55} \tag{7.17}$$

Equation (7.17) is shown in Figure 7.12a together with the present data. The relationship represented by (7.17) is a remarkably good fit to the data, again indicating that the spectra are similar to fetch limited wind-sea spectra.

In contrast to JONSWAP (Hasselmann *et al.*, 1973), Donelan *et al.* (1985) found a dependence of γ_d on U_{10}/C_p. They proposed the following functional form

$$\gamma_d = \begin{cases} 1.7 & \text{for} \quad 0.83 < U_{10}/C_p < 1 \\ 1.7 + 6.0\log_{10}\left(U_{10}/C_p\right) & \text{for} \quad 1.00 < U_{10}/C_p < 5 \end{cases} \tag{7.18}$$

Equation (7.18) is shown in Figure 7.12b, together with the present data. There is significant scatter in the values of γ_d obtained from the tropical cyclone spectra and no clear trend is apparent within this scatter. Equation (7.18) is, however, consistent with the data set, indicating the peak enhancement of the present data is comparable to that observed for fetch limited spectra.

The parametric representations of the data for both the JONSWAP and Donelan *et al.* (1985) forms yield the same general conclusions. Despite the complex temporally and spatially variable wind fields of tropical cyclones, the spectra are remarkably similar to those measured under idealized fetch limited conditions. In addition, the spectra would generally be characterized as mature wind-sea. The vast majority of the data are for $U_{10}/C_p < 2$. Indeed, significant data are in the region, $U_{10}/C_p < 0.83$, which would normally be classified as swell. The functional dependence of the spectral parameters for these values with $U_{10}/C_p < 0.83$ is, however, consistent with the more highly forced data. Hence, the processes which force the spectra to conform to a parametric spectral form (such as nonlinear interactions), apparently remain active in the absence of significant wind input at the spectral peak frequency.

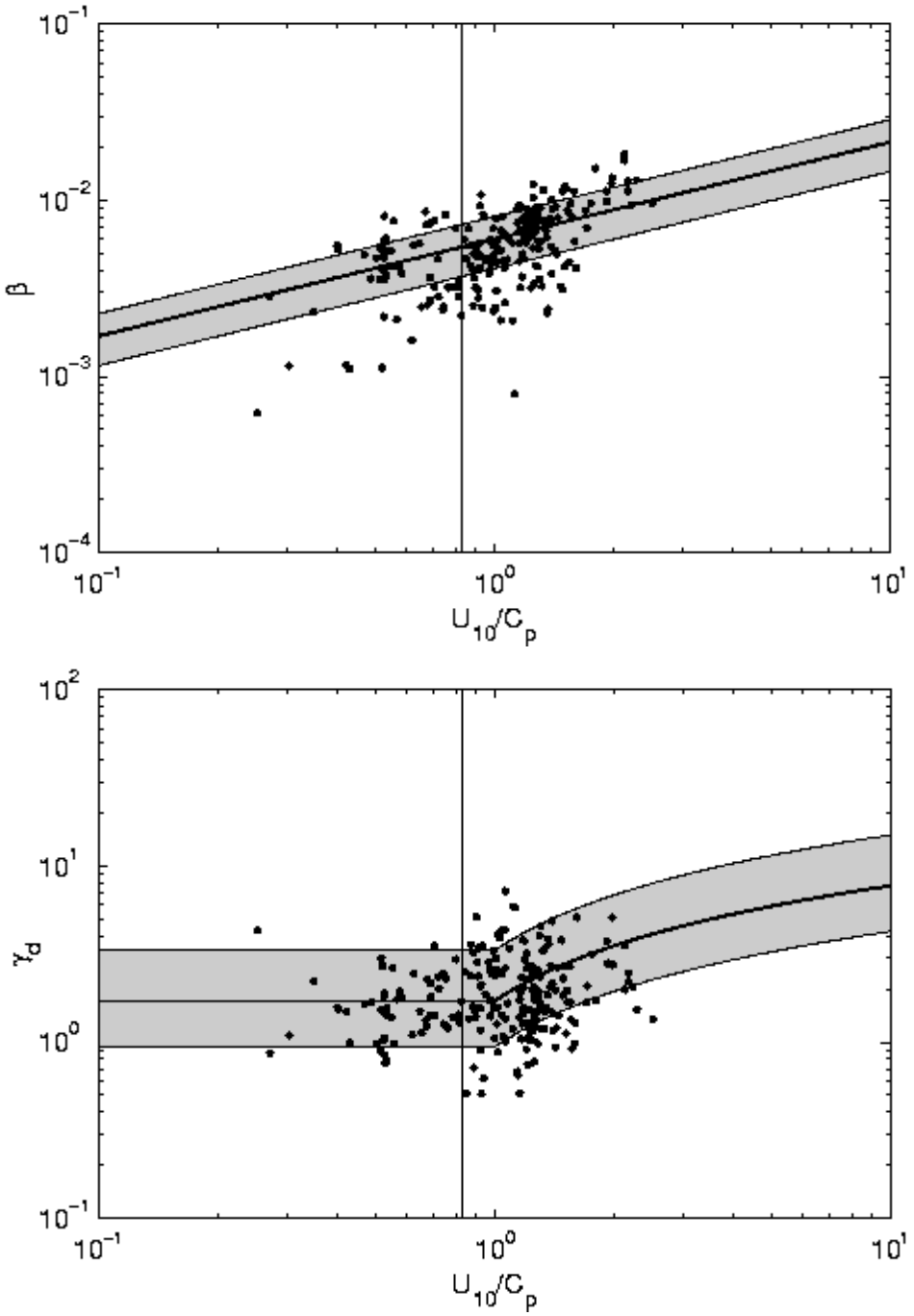

Figure 7.12 Donelan *et al.* (1985) spectral parameters for tropical cyclone conditions.

(a) [top] Values of the parameter β as a function of the inverse wave age, U_{10}/C_p. The line through the data is the Donelan *et al.* (1985) fetch limited relationship (7.17) and the vertical line is drawn at $U_{10}/C_p = 0.83$. The shaded region gives an estimate of the magnitude of the 95% confidence limits on the individual data points. (b) [bottom] Values of the parameter γ_d as a function of the inverse wave age, U_{10}/C_p. The line through the data is the Donelan *et al.* (1985) fetch limited relationship (7.18) and the vertical line is drawn at $U_{10}/C_p = 0.83$. The shaded region gives an estimate of the magnitude of the 95% confidence limits on the individual data points.

7.7 Conclusions and Recommendations

The present application poses a number of considerable challenges for numerical wave modelling. Tropical cyclone wind fields represent an intense wind vortex with the wind direction changing rapidly in space and time. The resulting wind seas are subjected to atmospheric input which also changes direction rapidly. This type of wind field is known to be a demanding test of model physics and generally requires the use of a sophisticated numerical model. In addition, coastal North Queensland is characterised by the presence of the Great Barrier Reef (GBR). The many reefs within the GBR, interspersed with narrow deep passages, will require very high resolution to adequately define the resulting bathymetry and potential for either local sheltering and/or wave transmission.

7.7.1 Choice of Model Physics

As described in Section 7.2, there are several choices of model physics which can be adopted. There are a number of examples of the successful use of 2nd Generation models under tropical cyclone conditions (Young, 1988a). Generally, however, the rapidly changing direction of the wind field within such storms represents a very demanding test of such models. The representation of S_{nl} in such models is generally based on the assumption that the spectrum conforms well to a standard JONSWAP form and that swell wind-sea interaction is not significant. As shown in Section 7.4, spectra near the centre of the storm are, indeed, similar to JONSWAP forms. This, however, is the result of the shape stabilization provided by S_{nl}. As one moves further away from the storm centre, a point is eventually reached where swell and wind-sea can co-exist. In order to model both of these features successfully, requires the use of a model with a sophisticated treatment of S_{nl}. These requirements mean that it is generally highly desirable to adopt a 3rd Generation model under tropical cyclone conditions. If interest is confined to the prediction of extreme conditions, as may occur near the centre of a landfalling tropical cyclone, a well tuned 2nd Generation model can produce acceptable results with considerably less computational expense. If this approach is adopted, it is important to select a model which has been extensively validated under extreme tropical cyclone conditions.

Waves generated by tropical cyclones can typically have periods as long as 13 seconds. Such waves will be modified by the typical water depths found on the continental shelf of Queensland. Hence the model adopted must be capable of representing depth dependent processes such as refraction and bottom friction. Although the water depth in the vicinity of coral reefs changes very rapidly (70 m to 0 m within 1 or 2 wavelengths), there is no observational evidence that diffraction is a significant mechanism in such areas. As a result, it is unlikely that time domain models are necessary in such situations.

The time-varying and directionally-changing nature of tropical cyclone forcing also prevents the practical application of commonly-used 2nd Generation coastal steady-state spectral wave models such as HISWA (Holthuijsen *et al.* 1989) and MIKE 20 (DHI 1991). These models can incorporate ambient current effects but the numerical solution methods limit wave propagation to within a narrow band relative to the orientation of the computational grid.

Based on the discussion above, there appears to be essentially three possible state-of-the-art model choices. These are WAM (Hasselmann *et al.*, 1988), WAVEWATCH III (Tolman, 1992) and SWAN (Booij *et al.*, 1996). SWAN has the most refined finite depth physics of the

three models and allows incorporation of the ambient current field, which could be significant in some storm tide situations. SWAN can also be used to estimate breaking wave setup (refer Chapter 8). SWAN is recommended for use in relatively small spatial domains (of the order of 50 km) and earlier versions have a highly dispersive propagation scheme. As such, it should not be applied unilaterally for modelling tropical cyclone conditions unless nested in combination with a larger scale deepwater model which can provide adequate open boundary information. WAVEWATCH III has been developed from WAM, although the physics within the model has been changed to some degree and a more refined propagation scheme has been added (second order compared to first order in WAM). WAVEWATCH III is, however, a deep water model only and the present version does not have bottom friction implemented within the model. As a result, it also would not be suitable for unilateral application within the Great Barrier Reef region. WAM, however, has the required 3rd Generation physics and is applicable within the transitional water depths of the Great Barrier Reef. A potential remaining drawback of WAM though is the relatively dispersive first order propagation scheme used in the original model. Because propagation distances for swell in the present situation are not great, this should not be a major problem. Adoption of a higher order scheme, as described by Hardy *et al.* (2000), would however improve model performance in this regard.

It is recommended that a 3rd Generation ocean wave model based on WAM (The WAMDI Group 1988*) be used for the modelling program. If possible, the propagation scheme should be updated, in a manner similar to that described by Hardy et al. (2000). For very fine scale modelling the SWAN model (Booij et al. 1996) could be further nested within WAM to provide optimal modelling in nearshore regions. If interest is confined to extreme conditions, near the centre of the tropical cyclone, a 2nd Generation model that has been extensively validated under tropical cyclone conditions may also yield acceptable results. Ideally, some comparative testing between a 3rd Generation model and any proposed 2nd Generation model would indicate the suitability or otherwise of adopting a 2nd Generation model.*

7.7.2 Grid Considerations

The modelling of tropical cyclones represents a conflict of scales. It is necessary to use a computational grid which is sufficiently large to encompass swell generated by the tropical cyclone when it is as far as 1000 km from the site of interest. At the same time, it is necessary to have a grid which is sufficiently fine to resolve the eye of the storm where the major wave generation regions are concentrated. The size of the eye varies, but may be as small as 20 km in diameter. In the present application, quite a fine grid will be required to adequately define the many reefs within the GBR and the complex coastal bathymetry.

The requirements listed above dictate the use of nested grids, with finer scale grids taking their boundary conditions from coarser, larger scale grids. Young and Hardy (1993) and Hardy *et al.* (2000) have adopted this approach for the modelling of tropical cyclones within the GBR. Both studies have utilized a series of three grids. Hardy *et al.* (2000) adopted grid sizes of 37 km, 7.5 km and 1.5 km, respectively for the three grids used. The largest grid encompassed most of the Coral Sea. In addition, they adopted a sub-grid scale treatment of dissipation (blockage) by the scattered reefs of the area.

It is recommended that a grid system comparable to that of Hardy et al. (2000) and consistent with other relevant scale parameters from Chapter 6 be adopted for any modelling in the GBR region.

A time step which is comparable with the spatial grid must also be adopted. If an explicit propagation scheme is adopted, the maximum time step is dictated by the Courant number (ie. energy can not propagate more than one grid square during the discrete time step). Implicit propagation scheme allow larger time steps, whilst maintaining stability. Although such schemes may be stable with the adoption of larger time steps, there will be a loss of accuracy. If a grid of a specified size is required to adequately resolve the bathymetry, a time step should be chosen such that $\Delta t < \Delta x / C_g$, where Δt and Δx are the model time and space steps, respectively. This is effectively the same limit dictated by the Courant number. It may be possible to relax this limit for the larger scale grid, where resolution of the coastal bathymetry is not critical.

It is recommended that for the finer scale (B and C) grids, where practical, the time step be chosen such that $\Delta t < \Delta x / C_g$.

7.7.3 Dissipation on Reefs

The scattered reefs of the GBR provide very effective dissipation of energy propagation through the region. Studies by Hardy and Young (1996) have shown, that even at high tide levels, considerable wave energy is dissipated by wave breaking and the high frictional resistance of the rough coral bottom. As a result, little energy is transmitted across individual reefs. As a result, Young and Hardy (1993) assumed that coral reefs acted effectively as land and dissipated all incident energy. This assumption produced acceptable results in their model studies. More recently, Hardy *et al.* (2000) have compared this assumption with a more involved method where sub-grid scale reef blockage is accounted for by the use of a directional porosity factor for each grid point. They reported improved results using this approach.

It appears that the assumption of complete blockage produces acceptable results, provided the grid size is sufficiently small. Should sufficient resources be available, the approach of Hardy et al. (2000) appears superior, both from a conceptual viewpoint and in terms of reported performance.

7.8 References

Allender, J.H., Barnett, T.P. and Lybanon, M. (1985) The DNS model: An improved spectral model for ocean wave prediction. In: 'Ocean wave modeling', SWAMP Group, *Plenum Press*, New York, 235-248.

Barnett, T.P. (1968) On the generation, dissipation and prediction of ocean wind waves. *J. Geophys. Res.*, 73, 513-529.

Barnett, T.P. and Wilkerson, J.C. (1967) On the generation of ocean wind waves as inferred by airborne radar measurements of fetch-limited spectra. *J. Marine Res.*, 25, 292-328.

Battjes, J.A. (1994) Shallow water wave modelling. Proc. *Int. Symp.: Waves -- Physical and Numerical Modelling*, Vancouver, 1-23.

Beal, R.C., Gerling, T.W., Irvine, D.E., Monaldo, F.M. and Tilley, D.G. (1986) Spatial variations of ocean wave directional spectra from the Seasat synthetic aperture radar. *J. Geophys. Res*., 91, 2433-2449.

Bea, R.G. (1974) Gulf of Mexico hurricane wave heights. *6th Offshore Technology Conf.*, Houston, OTC 2110.

Bender, L.C. (1996) Modification of the physics and numerics in a third-generation ocean wave model. *J. Atmos. Oceanic Tech*., 13, 726-750.

Black, J.L. (1979) Hurricane Eloise directional wave energy spectra. *11th Offshore Technology Conf*., Houston, OTC 3594.

Booij, N. and Holthuijsen, L.H. (1987) Propagation of ocean waves in discrete spectral wave models. *J. Comp. Phys*., 68, 307-326.

Booij, N., Holthuijsen, L.H. and Ris, R.C. (1996) The SWAN wave model for shallow water. Proc 25th Int. Conf. Coastal Eng., *ASCE*, Orlando, 668-676.

Bretschneider, C.L. (1959) Hurricane design - Wave practices. *Trans. ASCE*, 124, 39-62.

Bretschneider, C.L. (1972) A non-dimensional stationary hurricane wave model. *4th Offshore Technology Conf*., Houston, OTC 1517.

Cardone, V.J., Pierson, W.J. and Ward, E.G. (1975) Hindcasting the directional spectra of hurricane-generated waves. *J. Pet. Technol*., 261, 91-127.

Cardone, V.J., Ross, D.B. and Ahrens, M.R. (1977) An experiment in forecasting hurricane generated sea states. Proc. 11th Tech. Conf. on Hurricanes and Tropical Met., *AMS*, Miami.

Cavaleri, L. and Rizzoli, P.M. (1981) Wind wave prediction in shallow water: theory and application. *J. Geophys. Res*., 86, 10,961-10,973.

Chen, Y., and Wang, H. (1983) Numerical model of nonstationary shallow water wave spectral transformations. *J. Geophys. Res.*, 88, 9851-9863.

DHI (1991) MIKE 20 nearshore module - user's guide and reference manual, *Danish Hydraulic Institute.*

Donelan, M.A., Hamilton, J. and Hui, W.H. (1985) Directional spectra of wind-generated waves. *Philos. Trans. R. Soc. Lond*., A 315, 509-562.

Elachi, C., Thompson, T.W., and King, D.B. (1977) Observations of the ocean wave pattern under Hurricane Gloria with Synthetic Aperture Radar. *Science*, 198, 609-610.

Eldeberky, Y. and Battjes, J.A. (1995) Parameterization of triad interactions in wave energy models. *Coastal Dynamics '95*, Dally, W.R. and Zeidler, R.B. (eds), ASCE, 140-148.

Ewing, J.A. (1971) A numerical wave prediction method for the North Atlantic Ocean. *Dtsch. Hydrogh. Z*., 24, 241-261.

Forristall, G.Z., Ward, E.G., Cardone, V.J. and Borgmann, L.E. (1978) The directional spectra and kinematics of surface gravity waves in tropical storm Delia. *Jnl. Phys. Oceangr*., 8, 888-909.

Gelci, R., Cazale, J. and Vassal, J. (1957) Prevision de la houle. La methode des densites spectroangulaires. *Bull. Inform. Comite Central Oceanogr. D'Etude Cotes*, 9, 416-435.

Golding, B.W. (1983) A wave prediction system for real-time sea state forecasting. *Q. J. Roy. Meteorol. Soc*., 109, 393-416.

Gonzalez, F.I., Thompson, T.E., Brown, W.E. and Weissman, D.E. (1982) Seasat wind and wave observations of Northeast Pacific Hurricane Iva, August 13, 1978. *J. Geophys. Res*., 87, 3431-3438.

Greenwood, J.A., Cardone, V.J. and Lawson, L.M. (1985) Intercomparison test version of the SAIL wave model. In: 'Ocean wave modeling', SWAMP Group, *Plenum Press*, New York, 221-233.

Gunther, H., Rosenthal, W., Weare, T,J., Worthington, B.A., Hasselmann, K. and Ewing, J.A. (1979) A hybrid parametric wave prediction model. *J. Geophys. Res*., 84, 5727-5738.

Hamilton, R.C., and Ward, W.G. (1974) Ocean data gathering program - quality and reduction of data. *6th Offshore Technology Conf*., Houston, OTC 2108-A.

Hardy, T.A., Mason, L.B. and McConochie, J.D. (2000) A wave model for the Great Barrier Reef. *Ocean Engineering*, (in press).

Hardy, T.A. and Young, I.R. (1996) Field study of wave attenuation on an offshore coral reef. *J. Geophys. Res*., 101, 14,311-14,326.

Harper, B.A., Mason, L.B., and Bode, L. (1993) Tropical cyclone Orson - a severe test for modelling. Proc. 11th Aust. Conf. Coastal and Ocean Eng., *IEAust*, Townsville, 59-64.

Hasselmann, K. (1962) On the non-linear energy transfer in a gravity-wave spectrum, Part 1. General Theory. *J. Fluid Mech*., 12, 481-500.

Hasselmann, K. (1969) Weak-interaction theory of ocean waves. *Basic Developments in Fluid Mech.*, 2, 117-182.

Hasselmann, K. *et al.* (1973) Measurements of wind-wave growth and swell decay during the Joint North Sea Wave Project (JONSWAP). Suppl. A, 8, 12, 95pp.

Hasselmann, S. and Hasselmann, K. (1985) The wave model EXACT-NL. In 'Ocean wave modelling' (The SWAMP Group), 249-251, New York, *Plenum Press*.

Holt, B., and Gonzalez, F.I. (1986) SIR-B Observations of dominant ocean waves near Hurricane Josephine. *J. Geophys. Res*., 91, 8595-8598.

Holthuijsen, L.H., Booij, N. and Herbers, T.H.C. (1989), A prediction model for stationary, short-crested waves in shallow water with ambient currents, *Coastal Engineering*, 13, pp 23-54.

Ijima, T., Soejima, T. and Matsuo, T. (1968) Ocean wave distribution in typhoon area. *Proc. Coastal Eng. in Japan*, 2, 29-42.

Inoue, T. (1967) On the growth of the spectrum of a wind generated sea according to a modified Miles-Phillips mechanism and its application to wave forecasting. Ph.D. dissertation, *New York Univ*., New York.

Isozaki, I. and Uji, T. (1973) Numerical prediction of ocean wind waves. 24, 207-231.

Janssen, P.A.E.M. (1991) Quasi-linear theory of wind-wave generation applied to wave forecasting. *J. Phys. Oceanogr*., 21, 1631-1642.

Janssen, P.A.E.M., Hasselmann, S., Hasselmann, K. and Komen, G.J. (1994) Numerical modelling of wave evolution. Part 4: Numerical scheme. In Dynamics and modelling of ocean waves, G.J. Komen *et al.* (eds.), *Cambridge Uni. Press*, 233-238.

King, D.B., and Shemdin, O.H. (1978) Radar observations of hurricane wave directions. 16th Int. Conf. on Coastal Eng., *ASCE*, Hamburg, 209-226.

Komen, G.J., Hasselmann, S. and Hasselmann, K. (1984) On the existence of a fully developed wind-sea spectrum. *J. Phys. Oceanogr*., 14, 1271-1285.

Liu, P.C. (1989) On the slope of the equilibrium range in the frequency spectrum of wind waves. *J. Geophys. Res*., 94, 5017-5023.

McLeish, W., and Ross, D.B. (1983) Imaging radar observations of directional properties of ocean waves. *J. Geophys. Res*., 88, 4407-4419.

NOAA Data Buoy Office (1973) Practical experience with buoys developed by the NOAA Data Buoy Office. *U.S. Dept. of Commerce*.

Ochi, M.K. and E.N. Hubble (1976) On six-parameter wave spectra. Proc. 15th Int. Conf. Coastal Eng., *ASCE*, 1, 301-328.

Ochi, M.K. and M.H. Chiu (1982) Nearshore wave spectra measured during Hurricane David. 18th Int. Conf. Coastal Eng., Cape Town, *ASCE, 77-86.*

Patterson, M.M. (1972) Hindcasting hurricane waves in the Gulf of Mexico. *Soc. Pet. Eng*., 321-328.

Phillips, O.M. (1958) The equilibrium range in the spectrum of wind-generated waves. *J. Fluid Mech*., 4, 426-434.

Pierson, W.J. and Moskowitz, L. (1964) A proposed spectral form for fully developed wind seas based on the similarity theory of S.A. Kitaigorodskii. *J. Geophys. Res.*, 69, 5181-5190.

Pierson, W.J., Tick, L.G. and Baer, L. (1966) Computer-based procedures for predicting global wave forecasts and wind field analyses capable of using wave data obtained by spacecraft. *6th Naval Hydrodynamics Symposium*, Washington.

Ross, D.B. (1976) A simplified model for forecasting hurricane generated waves. *Bull. A.M.S.*, 113.

Sanders, J. W. (1976) A growth-stage scaling model for the wind-driven sea. *Dtsch. Hydrogr. Z.*, 29, 136-161.

Shemdin, O.H. (1977) Hurricane waves, storm surge and currents: An assessment of the state of the art. *U.S. - South East Asia Symp. on Eng. for Natural Hazards Protection*, Manila.

Shemdin, O.H. (1980) Prediction of dominant wave properties ahead of hurricanes. *17th Int. Coastal Eng. Conf.*, ASCE, Sydney, 600-609.

Snyder, R.L. and Cox, C.S. (1966) A field study of the wind generation of ocean waves. *J. Marine Res.*, 24, 141-178.

Snyder, R.L., Dobson, F.W., Elliot, J.A. and Long, R.B. (1981) Array measurements of atmospheric pressure fluctuations above surface gravity waves. *J. Fluid Mech.*, 102, 1-59.

Sobey, R.J. and Young, I.R. (1986) Hurricane wind waves -- A discrete spectral model. *J. Waterways Port Costal Ocean Eng.*, ASCE, 112, 370-389.

SWAMP Group (1985) Ocean wave modeling. *Plenum Press*, New York, 256pp.

Tolman, H.L. (1991) A third-generation model for wind on slowly varying unsteady and inhomogeneous depths and currents. *J. Phys. Oceanogr.*, 21, 782-797.

Tolman, H.L. (1992) Effects of numerics on the physics in a third-generation wind-wave model. *J. Phys. Oceanogr.*, 22, 1095-1111.

Uji, T. (1975) Numerical estimation of the sea wave in a typhoon area. *Papers in Meteorology and Geophysics*, 26, 199-217.

The WAMDI Group (Hasselmann, S., Hasselmann, K., Bauer, E., Janssen, P.A.E.M., Komen, G.J., Bertotti, L., Lionello, P., Guillaume, A., Cardone, V.C., Greenwood, J.A., Reistad, M., Zambresky, L. and Ewing, J.A.) (1988) The WAM model -- a third generation ocean wave prediction model. *J. Phys. Oceanogr.*, 18, 1775-1810.

Ward, E.G. (1974) Ocean data gathering program - an overview. *6th Offshore Technology Conf.*, Houston, OTC 2108-B.

Whalen, J.E. and M.K. Ochi (1978) Variability of wave spectral shapes associated with hurricanes. *10th Offshore Tech. Conf.*, 1515-1522.

Withee, G.W., and Johnson, A. (1975) Data report: buoy observations during hurricane Eloise (September 19 to October 11, 1975). *Environmental Science Div., Data Buoy Office, NOAA*, U.S. Dept. of Commerce.

Young, I.R. (1988a) A shallow water spectral wave model. *J. Geophys. Res*., 93, 5113-5129.

Young, I.R. (1988b) A parametric hurricane wave prediction model. *J. Waterways Port Coastal Ocean Eng.,* ASCE, 114, 637-652.

Young, I.R. (1999) Wind generated ocean waves. *Elsevier Sciences Ltd*., 306pp.

Young, I.R. (1997) Observations of the spectra of hurricane generated waves. *Ocean Engineering*, 25, 261-276.

Young, I.R. and Burchell, G.P. (1996) Hurricane generated waves as observed by satellite. *Ocean Engineering*, 23, 761-776.

Young, I.R. and Hardy, T.A. (1993) Measurement and modelling of tropical cyclone waves in the Great Barrier Reef. *Coral Reefs*, 12, 2, 85-95.

8. Estimation of Wave Setup and Runup

8.1 Introduction

Two wind wave related concepts are relevant to coastal inundation during tropical cyclones - wave setup and wave runup. Wave setup is the local overheight of the mean water surface (MWS) above the offshore still water level (SWL) due to the effects of energy transfer during wave breaking in the surf zone. Setup has been a particular concern historically through its influence on flood levels around coastal rivers and lagoons, even without the extreme wave conditions likely to be found during tropical cyclones. While breaking wave setup is a MWS phenomenon, wave runup is the process through which the remaining energy of individual waves impacting at the shoreface can cause erosion and/or inundation at even higher elevations. These two wave-induced water level components are often confused and it is important to realize their different nature. In the following they are treated separately and it will be shown that it is perfectly possible to treat them separately in applications.

The generation of waves by tropical cyclones has been discussed in Chapter 7 in terms of the 2-dimensional numerical modelling of discrete wave energy spectra, $E(f)$ or $E(f,\theta)$, from which it is possible to also directly estimate breaking wave setup (e.g. the SWAN model; Booij *et al.* (1996)). To assist understanding of the dominant processes, the present development decouples the generation and propagation aspects and treats the nearshore physics directly.

8.2 Waves in the Surf Zone

The following simplified treatment of surf zone processes and the resulting potential setup and runup is formulated in terms of wave height statistics and a single incident wave period.

The root-mean-square wave height corresponding to a particular discrete wave energy spectrum E can be estimated based on the fact that the water level elevation $\eta_{rms} = H/\sqrt{8}$ for a sine wave of height H and that η_{rms} is also the square root of the area under the energy spectrum, i.e. $\eta_{rms} = \sqrt{M_o}$ where $M_o = \int_1^n \int_0^{2\pi} E(f,\theta)\, \partial\theta\, \partial f$. This leads to

$$H_{rms} = \sqrt{8M_o} \tag{8.1}$$

The corresponding significant wave height H_s, defined as the average of the largest 1/3 of the waves is, under the assumption of a Rayleigh distribution for the wave heights $\sqrt{2}H_{rms}$, i.e.,

$$H_s = 4\sqrt{M_o} \tag{8.2}$$

The wave period used in most of the experimental work which forms the background for the following theoretical treatment, is the peak period T_p of the wave energy spectrum. Typically this would be measured, for example, by a nearshore waverider buoy, usually in water depths greater than 15 to 20 m.

Hence, in numerical modelling situations, the H_s and T_p value at the inshore limit of the wave generation model at each site of interest should be used as input into the wave setup and runup

analyses which follow. At the level of spatial resolutions discussed in earlier Chapters, this will also typically describe the nearshore wave conditions between 300 and 1500 m offshore.

8.2.1 The Surf Similarity Parameter

The extent to which the wave energy is dissipated by breaking as opposed to being reflected back off shore is determined by the *Iribarren Number* or the surf similarity parameter ξ_o based on the deep water wave parameters (L_o, H_o) and the slope of the beach face tan β_f.

$$\xi_o = \tan\beta\sqrt{L_o / H_o} \tag{8.3}$$

Waves will be predominantly reflected if ξ_o>4. For smaller ξ_o most of the energy will be dissipated through breaking.

8.2.2 Breaker Types

The surf similarity parameter also determines the breaking type. There are four main breaker types examples of which are shown in Figure 8.1. The approximate ranges of $\xi_b = \tan\beta\sqrt{L_o / H_b}$ for which they occur on a straight slope are given in Table 8.1 below.

Table 8.1 Surf similarity parameter ranges.

Surf similarity parameter range	Breaker type
$4 < \xi_b$	Little or no breaking
$2 < \xi_b < 4$	Surging or collapsing breakers
$0.4 < \xi_b < 2$	Plunging breakers
$\xi_b < 0.4$	Spilling breakers

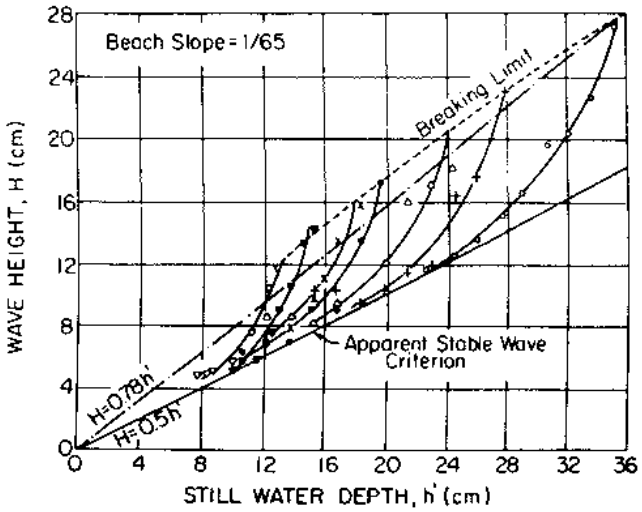

Figure 8.1 The wave breaking phenomenon.

Measured heights of waves with different deep water parameters after breaking on a straight slope. After Dally *et al.* (1985) based on data from Horikawa and Kuo (1966).

8.2.3 Breaker Heights

The limiting wave height to depth ratio for waves that propagate with constant form on a horizontal bed is theoretically limited to about 0.833. However, waves that are approaching breaking on a slope may reach $H/h = \gamma$-values in excess of unity in the process. The maximum wave height and the maximum H/h may happen shortly before the wave actually breaks, i.e., before part of the wave front becomes vertical and turns over.

8.2.4 Wave Height to Water Depth Ratio after Breaking

The wave height to depth ratio usually declines rather rapidly in the initial stages of breaking, see Figure 8.3. On a straight slope, an equilibrium condition with constant γ may be eventually reached. The equilibrium γ-value is a decreasing function of the bed slope tending towards 0.55 for $\beta \to 0$, *cf* Nelson (1997). In an equilibrium region where $H/h=\gamma$ is constant, the energy dissipation must relate in a special way to the beach slope. For example, assuming that the energy flux in the breaking waves is analogous to that in a linear shallow water wave

$$E_f = C_\beta \rho g H^2 \sqrt{gh} = C_\beta \rho g^{3/2} \gamma^2 h^{5/2} \tag{8.4}$$

where C_β is a slope dependent constant of the order 1/8. Then, the rate of energy dissipation must be

$$D_E = -\frac{dE_f}{dx} = -\frac{5}{2} C_\beta \rho g^{3/2} \gamma^2 h^{3/2} \frac{dh}{dx} = \frac{5}{2} C_\beta \rho g^{3/2} \gamma^2 h^{3/2} \tan\beta \tag{8.5}$$

On natural beaches the bottom slope usually varies throughout the surf zone and may become considerably steeper close to the shore. In the inner surf zone the breakers may then not be able to dissipate the energy at the rate given by (8.3). When that happens, the breaking waves become bores with practically vertical fronts. The height of the front of a bore can be many times the water depth into which it is propagating, see Figure 8.2. When the breaking wave has become a bore, H/h is no longer constant. It will usually increase until the bore collapses as it encounters zero depth.

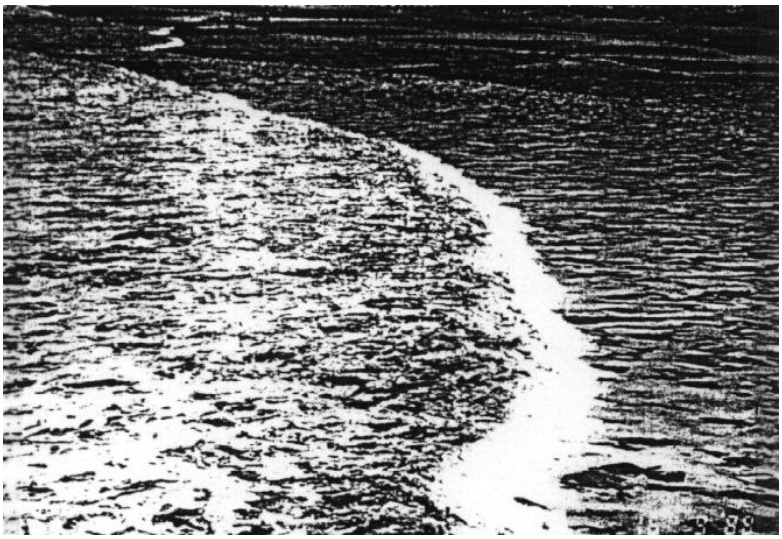

Figure 8.2 A surf zone bore carrying large amounts of suspended sand.

8.2.5 Surf Beat

Natural waves tend to be "groupy"; i.e. a wave record usually consists of groups of large waves with intervals of smaller wave heights in between. This variation in wave height can drive a corresponding variation in wave setup in general and in the shoreline setup in particular.

These oscillations are called surf beat. The period of surf beats is usually 100 to 300 seconds corresponding to the typical period of the offshore wave groups. The surface elevation amplitude of surf beat is (in contrast to the wind waves) greatest at the shoreline where it may exceed one metre during storms. See Figure 8.3.

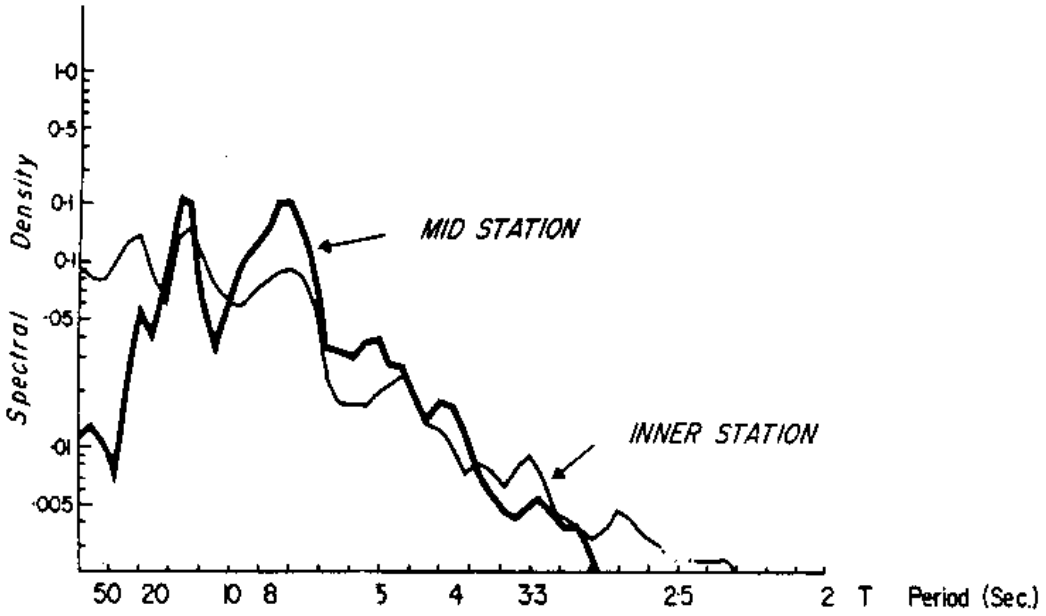

Figure 8.3 An example of surf beat.

The low frequency part of the spectrum, which represents the surf beat increases towards the shore while the high frequency part corresponding to wind wave frequencies decays. This indicates that the surf beat has the nature of standing non-breaking waves against the shoreline.

8.3 The Shape of the Surf Zone Mean Water Surface

8.3.1 Terminology and Definitions

The instantaneous surface elevations are denoted $\eta(x,y,t)$ where x is shore-normal and y is shore parallel. They are measured from the still water level (SWL) or the still water surface. See Figure 8.4. The still water surface is the plane (on the scale considered), horizontal water surface that would exist in the absence of wind and waves. It moves up and down relative to the mean sea level (MSL) with the tide.

The still water depth D is measured from the local bed level to the SWS. The intersection between the SWS and the beach is the still water shoreline. The mean water level $\overline{\eta}(x,y)$ is the time average of $\eta(x,y,t)$ over a few minutes, i.e., the corresponding mean water surface

(MWS) does not move up and down with the wind waves but it does move with the tide. The total depth or just depth *h* is measured to the MWS. As indicated by Figure 8.4, the MWS may be slightly below the SWS off-shore due to wave set-down. In the surf zone it is above the SWS due to wave setup.

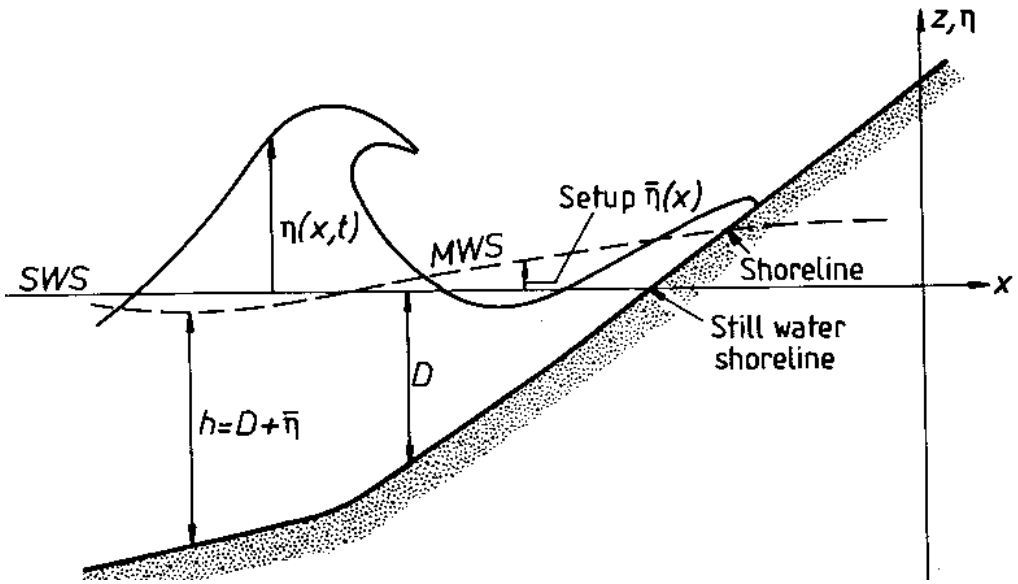

Figure 8.4 Definitions of surf zone levels and depths.

The deviations of the MWS from the plane SWS are due to wind and waves and can be quantified on the basis of Figure 8.5.

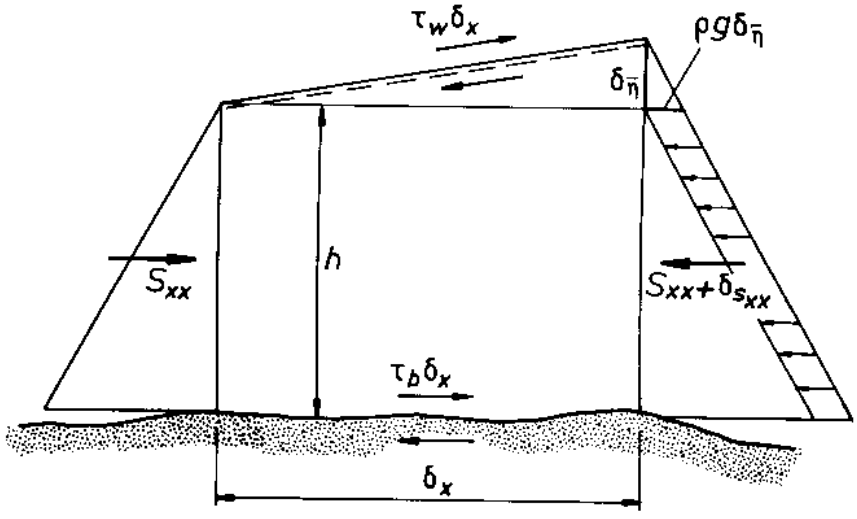

Figure 8.5 Time averaged, horizontal forces due to wind, waves and gravity acting on a surf zone control volume.

The static, shore-normal force balance on the control volume in Figure 8.5 gives

$$-\rho g \delta_{\bar{\eta}} h - \delta_{S_{xx}} + \tau_{wind}\delta_x - \tau_{bed}\delta_x = 0 \tag{8.6}$$

or

$$\frac{\partial \bar{\eta}}{\partial x} = -\frac{1}{\rho g h}\frac{\partial S_{xx}}{\partial x} + \frac{1}{\rho g h}(\tau_{wind} - \tau_{bed}) \tag{8.7}$$

8.3.2 Wave Setdown

Outside the surf zone, the wave radiation stress will increase towards the shore as indicated by the sine wave explicit approximation

$$S_{xx} = \frac{3}{16}\rho g H_o^2 \frac{1}{\sqrt{k_o h}}[1 + \frac{1}{18}k_o h\ ] \tag{8.8}$$

This formula is within 1% of linear wave theory for $k_o h < 0.94$.

Inserting this expression for the radiation stress into the slope equation (8.7), neglecting the shear stresses, and integrating with the boundary condition $\bar{\eta} \to 0$ for $k_o h \to \infty$, we get the following expression

$$\bar{\eta} = -\frac{1}{32}k_o H_o^2 (k_o h)^{-1.5}[1 - \frac{1}{6}k_o h\ ] \tag{8.9}$$

for the setdown, i.e. the lowering of the mean water level outside the surf zone. A setdown of this magnitude has often been measured in laboratory experiments with regular waves.

8.3.3 Wave Setup

Inside the surf zone the radiation stress (proportional to H^2 for sine waves) will decrease rapidly towards the shore due to wave breaking and therefore generate a positive MWS slope through Equation (8.7).

A simple model of the wave setup in the surf zone can be obtained by adopting the linear shallow water relation between radiation stress and wave height

$$S_{xx} = \frac{3}{16}\rho g H^2 \tag{8.10}$$

Neglecting the shear stress terms in (8.7) this leads to the slope

$$\frac{\partial \bar{\eta}}{\partial x} = -\frac{1}{h}\frac{3}{8}H\frac{\partial H}{\partial x} \tag{8.11}$$

In order to solve this and get the setup as function of *x* or *h*, it is further necessary to assume a relation between wave height and depth. If we assume a constant ratio $H/h \equiv \gamma$, we obtain

$$\frac{\partial \overline{\eta}}{\partial x} = -\frac{3}{8}\gamma^2 \frac{\partial h}{\partial x} \tag{8.12}$$

where we may insert $h = D + \overline{\eta}$ and get

$$\frac{\partial \overline{\eta}}{\partial x} = -\frac{3}{8}\gamma^2 \left(\frac{\partial D}{\partial x} + \frac{\partial \overline{\eta}}{\partial x}\right) \tag{8.13}$$

and hence

$$\frac{\partial \overline{\eta}}{\partial x} = -\frac{\frac{3}{8}\gamma^2}{1+\frac{3}{8}\gamma^2}\frac{\partial D}{\partial x} = \frac{\frac{3}{8}\gamma^2}{1+\frac{3}{8}\gamma^2}\tan\beta \tag{8.14}$$

where $\tan\beta = \frac{\partial D}{\partial x}$. That is, assuming linear shallow water wave theory and $\gamma \approx 0.5$ for the breaking waves we would expect a slope of the surf zone MWS of about .09 tanβ.

Seeking the setup as function of the total depth, we can solve Equation (8.12) with the boundary condition $\overline{\eta}(h_b) = \overline{\eta}_{\min}$ at the breakpoint and get

$$\overline{\eta}(h) = \overline{\eta}_{\min} + \frac{3}{8}\gamma^2 (h_b - h) \tag{8.15}$$

That is, according to the simple model based on regular waves, $S_{xx}(H)$ from linear wave theory and $H/h \equiv \gamma$, $\overline{\eta}$ varies linearly with *h*. The straight line in Figure 8.6 corresponds to Equation (8.15), i.e. regular waves, with $S_{xx}(H)$ from linear shallow water wave theory and for $H/h \equiv \gamma = 0.5$.

The deviation of the data from the straight line is mainly because the real waves are irregular and start to break at different depths. Hence, the gradual increase in $\frac{d\overline{\eta}}{dh}$ compared to the regular wave model.

The curved line in Figure 8.6 corresponds to the empirical formula

$$\overline{\eta} = \frac{0.4 H_{orms}}{1+10\frac{h}{H_{orms}}} \tag{8.16}$$

which provides a good fit to field data from a wide variety of beach morphologies.

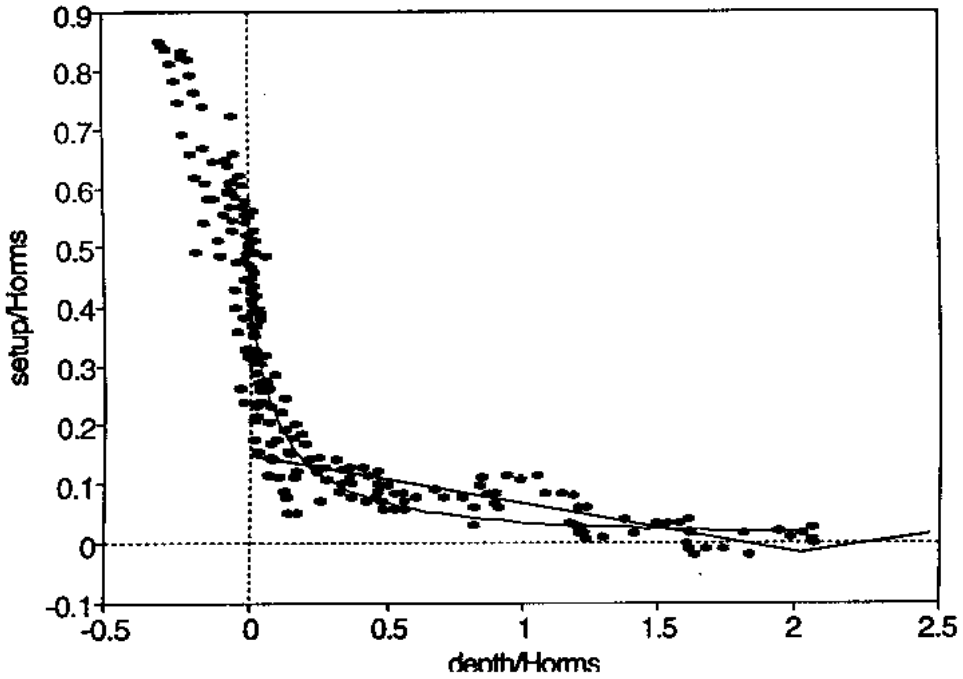

Figure 8.6 Setup profile in a natural surf zone.
Measurements from South Beach, Brunswick Heads 22/6/1989.

8.3.4 Shoreline Setup

The shoreline setup, i.e. the setup at h=0 is predicted by the simple setup model (8.15) to be

$$\overline{\eta}(0) = \overline{\eta}_{\min} + \frac{3}{8}\gamma^2 h_b = \overline{\eta}_{\min} + \frac{3}{8}\gamma H_b \tag{8.17}$$

This will however often be an underestimate of the actual shoreline setup under field conditions (at least if H_b is taken as $\sqrt{8}(\eta_{rms})_b$). The empirical curve (8.16) corresponds to

$$\text{Shoreline setup} = 0.4H_{\text{orms}} \tag{8.18}$$

A slightly more reliable estimate, *cf* Hanslow and Nielsen (1993), is

$$\text{Shoreline setup} = 0.048\sqrt{H_{orms}L_o} \tag{8.19}$$

Corresponding to

$$\overline{\eta}(h) = \frac{0.048\sqrt{H_{orms}L_o}}{1+10\dfrac{h}{H_{orms}}} \tag{8.20}$$

in analogy with (8.16).

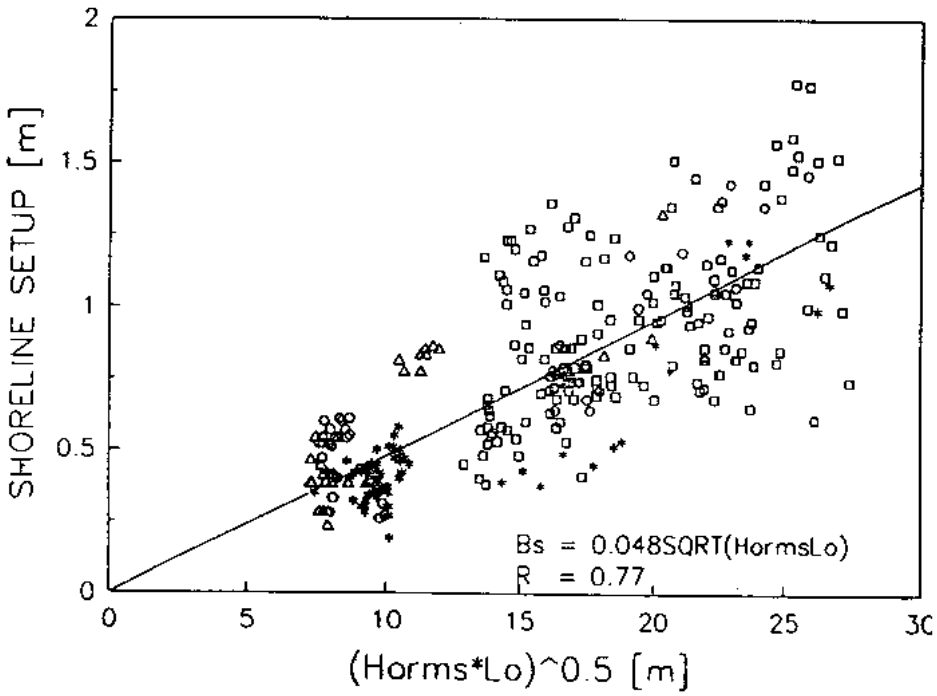

Figure 8.7 Observed shoreline setup on a wide variety of beaches.

After Hanslow and Nielsen (1993).

The straight line in Figure 8.7 corresponds to Equation (8.18). The data encompass almost the full morphology spectrum of sandy beaches in New South Wales with beach face slopes $tan\beta_f$ ranging from 0.03 to 0.12 during the experiments.

8.3.5 Wave Effects on River Tail-water Levels

In a river or lagoon entrance, where the waves eventually decay due to breaking and/or dissipation along breakwater walls, it has been expected that a wave-generated superelevation of the MWS would occur similar to the surf zone wave setup. Surprisingly however, measurements from the Brunswick River show the setup inside the river to be much smaller than expected. Indeed, the detailed waterlevel data of Nielsen *et al.* (1989) and Hanslow *et al.* (1996) show no measurable setup inside the river while the shoreline setup on the adjacent beach was over more than one metre. Figure 8.8 shows a manifestation of this waterlevel difference across the breakwater.

The same lack of wave generated effects on river entrance waterlevels is shown by the tidal anomaly versus wave height data in Figure 8.9.

The lack of correlation between wave height and tidal anomaly agrees with the detailed waterlevel measurements of Nielsen *et al.* (1989) and Hanslow *et al.* (1996). Both show that in a trained river like the Brunswick, waves (at least up to 4m H_s) generate no setup. The same will be true for the larger trained rivers like the Tweed and the Gold Coast Seaway. Recent research by Dunn *et al.* (1999) indicates that the lack of wave generated setup between breakwaters can be, at least partly, explained via transverse momentum fluxes which are

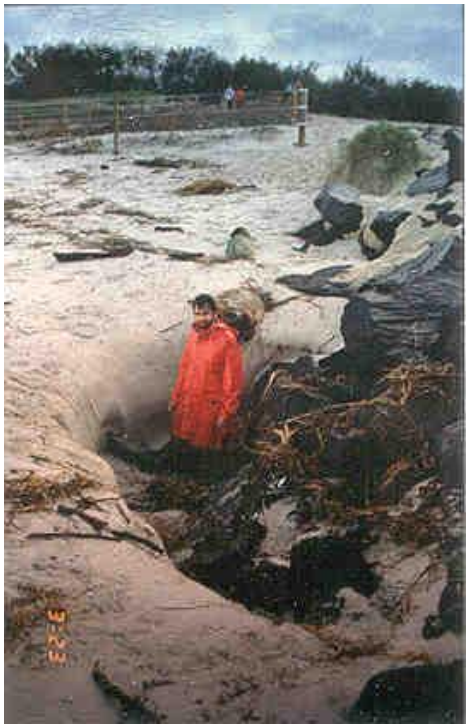

related to the curvature of the wave crests between absorbing breakwaters. Untrained or partly trained entrances like Noosa may show some wave setup but no detailed data is available.

Figure 8.8 Scour hole on the beach side of the southern Brunswick breakwater.

Created by water flowing from the swash zone on the beach through the breakwater and into the river.

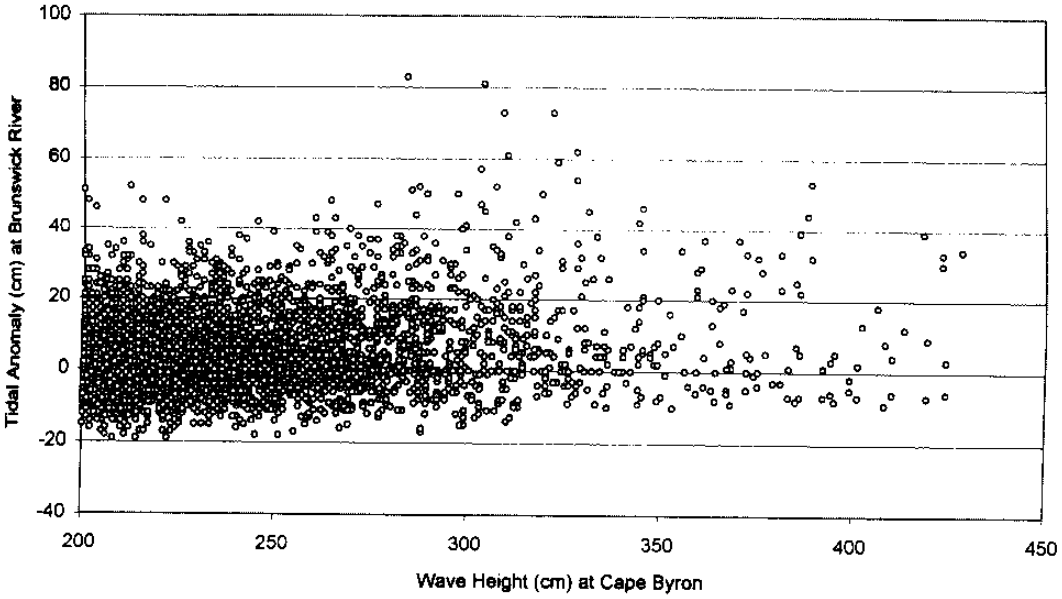

Figure 8.9 Tidal anomaly (measured tide minus predicted tide).

Brunswick River level versus offshore wave height at cape Byron. Data from the Manly Hydraulics Laboratory.

8.4 Swash and Runup Heights

8.4.1 Introduction

The water motion in the area where the beach face is alternately exposed and covered by water on the time scale of individual wind waves is called swash, *cf* Figure 8.10.

Figure 8.10 Bore collapsing at the beach face where it encounters zero depth and generating swash.

While the bed slope is usually variable through the surf zone the beach face is usually straight. Hence the slope $tan\beta_f$ of the beach face is well defined.

The swash is a highly asymmetrical motion where the depth and speed of the uprush is determined by the height and speed of the incoming bores while the backwash is driven by gravity. The sand onto which the swash is progressing may be saturated or unsaturated with water depending on the tidal phase and on the strengths of previous uprush events.

If the beach material is very coarse, the swash may also be asymmetrical with respect to volume. That is, the amount of water running back down the slope is less than what rushed up because a substantial part of the uprush volume has seeped into the slope.

On very flat beaches where breakers of constant form and dissipate energy fast enough (cf Equation 2.3) to maintain a constant H/h and hence, $H \to 0$ for $h \to 0$, there will be no swash at wind wave frequencies.

8.4.2 Runup heights for Regular Waves

When the incoming waves are regular having fixed height and period they will all run up to same height on the beach. In this case it makes sense to talk about *the* runup height *R*..

Experiments have shown that, when the waves are breaking, the runup height measured from the still water level is proportional to the wave height and to the surf similarity parameter

$$R = H\xi = H \tan\beta_F \sqrt{L_o / H} = \tan\beta_F \sqrt{HL_o} = \tan\beta_F \sqrt{H \frac{gT^2}{2\pi}} \quad (8.21)$$

In connection with this formula, we note, that the runup height depends more strongly on the wave period than on the height: $R \propto T\sqrt{H}$. This is why tsunami runup is so devastating compared to the runup of storm waves.

Equation (8.21) which is often called Hunt's formula is only valid for breaking waves with $\xi \leq 2$ corresponding to $R \leq 2H$ but this does cover the range of wind waves on most natural beaches.

8.4.3 Runup Heights for Irregular Waves

For natural waves with variable heights H_n the maximum heights R_n on the slope reached by the individual swash fronts will usually, like the offshore wave heights, follow a Rayleigh distribution:

$$P\{R_n > x\} = \exp[-(\frac{x}{L_R})^2] \quad (8.22)$$

where the vertical runup scale L_R depends mainly on the offshore wave parameters and the beach face slope as indicated by Figure 8.11.

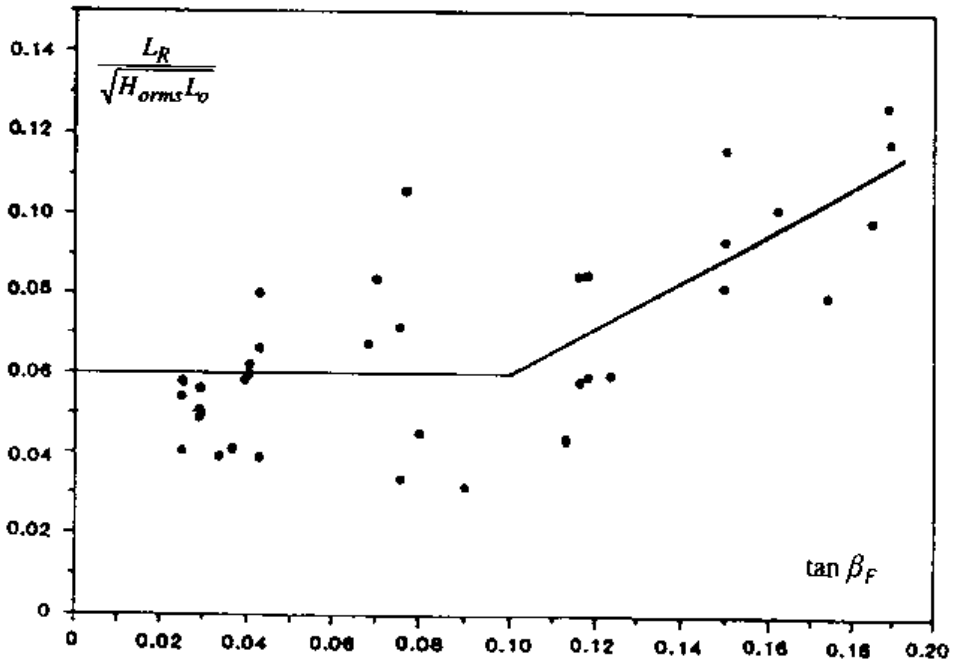

Figure 8.11 Relationship between the vertical scale LR in the Rayleigh runup distribution and the offshore wave parameters.

Data from Nielsen and Hanslow (1991).

For steep slopes L_R is approximately 0.6 times the runup height of the rms wave calculated from Equation (8.21), i.e.

$$L_R = 0.6 \tan\beta_F \sqrt{H_{orms} L_o} \qquad \text{for} \quad \tan\beta_F > 0.1 \tag{8.23}$$

for flatter slopes L_R is independent of β_F and approximately given by

$$L_R = 0.06 \sqrt{H_{orms} L_o} \qquad \text{for} \quad \tan\beta_F < 0.1 \tag{8.24}$$

According to the definition (8.22), the highest of N individual runup heights is, under the Rayleigh distribution, expected to be

$$E\{R_{\max}\} = L_R \sqrt{\ln N} \tag{8.25}$$

and the height (above the SWS) exceeded by just 1% of the runups is expected to be

$$E\{R_{1\%}\} = L_R \sqrt{\ln 100} = \sqrt{4.6} L_R \tag{8.26}$$

8.4.4 Extreme Runup Levels

The expected maximum runup level from N waves with a given L_R is according to (8.25) $L_R \sqrt{\ln N}$. This level has roughly a 50% probability of getting inundated (reached at least once) by these waves.

It is of interest to calculate the level Z which has a certain probability P of getting inundated during an event that contains N waves with a certain L_R. This can be done as follows

The probability of a given wave stopping below Z is $1 - \exp[-(\frac{Z}{L_R})^2]$. Consequently, the probability of all of the N waves stopping below Z is $\left\{1 - \exp[-(\frac{Z}{L_R})^2]\right\}^N$. Hence, the level Z_P that has probability P of being inundated is determined from

$$1 - P = \left\{1 - \exp[-(\frac{Z}{L_R})^2]\right\}^N \tag{8.27}$$

or

$$Z_P = L_R \sqrt{-\ln[1 - (1-P)^{1/N}]} \tag{8.28}$$

Example:

Extreme wave heights of 4.95m H_{orms} (7m H_s) typically occur for one or two hours per year along the east coast of Australia. The period varies, but T=11s is not atypical.. For beaches with moderate slopes ($tan\ \beta_f < 0.1$) this corresponds to L_R = 1.83m according to (8.24).

For a duration of one hour, the total number of waves is N = 3600/11 = 327.

This leads to an expected maximum runup level of $E\{R_{\max}\} = = L_R\sqrt{\ln N]}$ = 4.40m. The level which has 1% probability of getting inundated is $Z_{1\%} = L_R\sqrt{-\ln[1-.99^{1/327}]}$ = 5.99m.

8.5 Wave Setup on Coral Reefs

Coral reef environments present a specific set of physical characteristics which can often create very significant nearshore wave setup, raising the water levels on the reef-top, and driving reef-top current systems that may control lagoon flushing and sediment transport processes. In extreme situations, wave setup can be responsible for overtopping and flooding of low lying islands and, as mentioned in Chapter 2, is likely to be the largest component of storm tide at some offshore island sites. In particular, the combination of astronomical tide variation, storm surge and incident wave height and period present a very dynamic and sensitive wave setup environment.

Figure 8.12 presents a schematic view of a typical coral reef nearshore environment (Gourlay 1997), where:

Reef-face is the relatively steep seaward facing underwater slope of the reef;
Reef-top the skyward facing surface of the reef, usually submerged except at low tides;
Reef-rim the relatively flat seaward inclined surface between the reef-top and the reef-face;
Reef-edge the intersection between the reef-face and the reef-rim;
Reef-crest the highest part of the reef-rim or the intersection between the reef-rim and the reef-top;
Lagoon a body of water ponded on or enclosed by a reef or by a reef and a continental or island land mass.

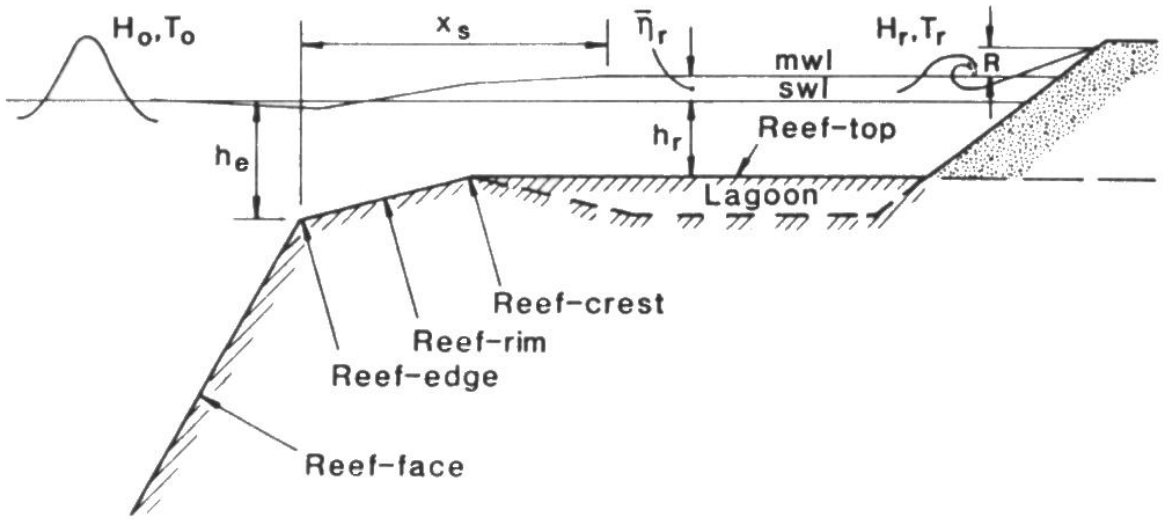

Figure 8.12 Coral reef wave setup definitions (after Gourlay 1997).

Clearly, reefs and reef platforms represent potentially very complex shorelines which, being living environments, have evolved at any specific location to be in equilibrium with the

incident wave and tide conditions. Even relatively small areas of reef platforms may display a myriad of channels, ridges and holes. Any estimate of wave setup must therefore be considered in a very generalised manner and applied with caution to specific locations. In particular, accurate information on reef-top water levels and slopes will be seen to be critical to any accurate assessment of reef setup.

Using an analysis combining wave energy flux and radiation stress concepts, Gourlay (1994b) derived the following equation for the wave setup $\overline{\eta}_r$ on a reef-top as a function of the offreef wave conditions H_o and T and the stillwater depth h_r on the reef top:

$$\overline{\eta}_r = \frac{3}{64\pi} K_p \frac{g^{1/2} H_o^2 T}{(\overline{\eta}_r + h_r)^{3/2}} \left[1 - K_r^2 - 4\pi K_R^2 \frac{1}{T} \sqrt{\frac{(\overline{\eta}_r + h_r)}{g}} \right] \tag{8.29}$$

where K_p is a reef profile factor (varies according to reef profile up to approximately 0.8)

K_R is the reflection coefficient (0 to 1)

K_r is the transmission coefficient (0 to 1)

and the term in **[...]** is subsequently referred to as the *transmission parameter* P_T .

Laboratory experiments (Gourlay 1996a) indicate that for steep reef-faces $K_R \le 0.3$, whereas for flatter slopes (Gourlay 1994) $K_R \le 0.1$. Hence wave reflection at most decreases the wave setup by about 10% and can be reasonably neglected.

The influence of wave transmission on wave setup however is a function of the relative submergence *S*, viz.

$$S = \frac{(\overline{\eta}_r + h_r)}{H_o} \tag{8.30}$$

and is also relatively small when S < 1. However it becomes increasingly significant as the submergence increases until, when S 〈 2.5, waves pass over the reef *without* breaking and hence without generating any setup (Gourlay 1996a).

To facilitate analysis, the transmission coefficient K_r $(\equiv H_r / H_o)$ can be expressed in terms of the reef-top wave height to depth ratio γ_r $(\equiv H_r / (\overline{\eta}_r + h_r))$. The resulting form of the transmission parameter P_T, neglecting K_R, is then:

$$P_T = \left[1 - 4\pi \gamma_r^2 \frac{1}{T} \sqrt{\frac{(\overline{\eta}_r + h_r)}{g}} \left(\frac{(\overline{\eta}_r + h_r)}{H_o} \right)^2 \right] \tag{8.31}$$

or

$$P_T = \left[1 - 4\pi \gamma_r^2 S^2 / D \right] \tag{8.32}$$

where D is the inverse of the relative depth of the reef-top waves, i.e.:

$$D = T\sqrt{\frac{g}{(\overline{\eta}_r + h_r)}} \tag{8.33}$$

On a horizontal or near-horizontal reef-top $\gamma_r \leq 0.55$ (Gourlay 1994; Nelson 1994), i.e. maximum wave heights never exceed 0.55 times the reef-top water depth $(\overline{\eta}_r + h_r)$. For regular waves with significant dissipation at the reef-edge, laboratory studies show $\gamma_r = 0.4$ (Gourlay 1994) and this value also has been found to apply for significant wave heights in the field (Hardy *et al.* 1991). Hence, when P_T is calculated with typical values of $\gamma_r = 0.4$ and $D = 12.5$, it can be simplified to the following form:

$$P_T = \left[1 - 0.16\, S^2\right] \tag{8.34}$$

thus correctly representing the observed condition that full transmission (and hence zero setup) occurs when S ⟨ 2.5. Alternatively, $P_T = 1$ when S=0 (or rather $K_R = 0$ and $K_r = 0$), and the maximum reef-top wave setup is estimated from Equation 8.29 as:

$$\overline{\eta}_{r\max} = \frac{3}{64\pi} K_p \frac{g^{1/2} H_o^2 T}{(\overline{\eta}_r + h_r)^{3/2}} \tag{8.35}$$

with typically achievable maximum setup values in the range 0.25 to 0.80 m even for average swell conditions at many exposed coral atolls, and potentially increasing above 3 m in extreme wave conditions, being modulated significantly by the tide and/or incident storm surge levels.

The reef profile factor K_p depends upon the roughness, permeability and shape of the reef. Gourlay (1996b) provides a range of K_p values derived from laboratory studies that increase with increasing profile slope tan α. For waves breaking at the reef-edge, the reef-face slope determines the value of K_p, whereas for waves breaking on a seaward sloping reef-rim, the reef-rim slope determines K_p. In the latter case it was found (Gourlay 1997) that an average water depth h_a determined over the reef-rim surf zone, was more appropriate than the reef-top water depth h_r for calculating the wave setup and use of a modified K_p' is recommended. Both relationships with respect to tan α are presented in Figure 8.13.

Hence, two situations are possible:

(a) Wave breaking occurs at the reef-edge:
- tan α is taken as the reef-face slope (i.e. into deepwater)
- S is calculated using either h_r for a horizontal reef-top or the average depth h_a over the reef-rim (assuming that the surf zone x_S extends over the full width of the reef-rim).
- the appropriate reef profile factor is K_p taken from Figure 8.13.

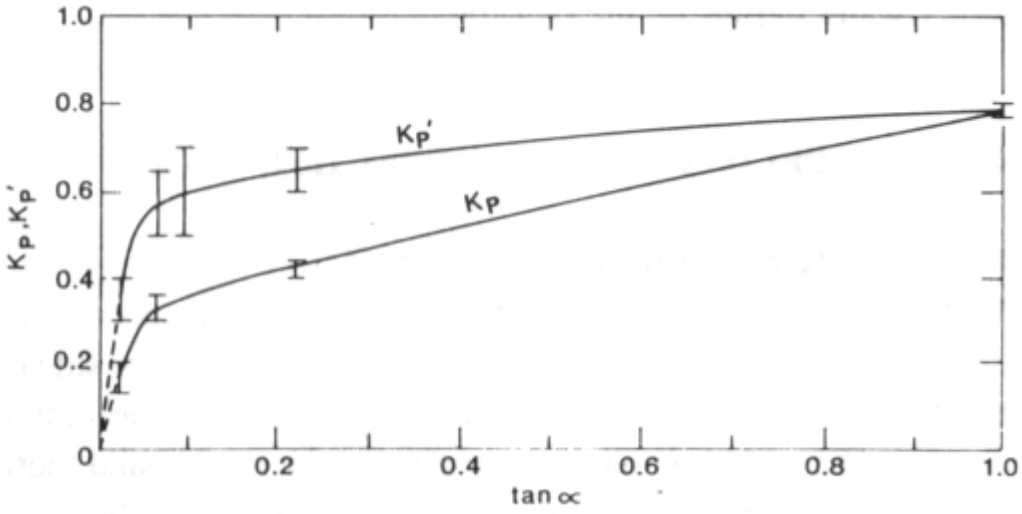

Figure 8.13 K_p and K_p' as a function of tan α (after Gourlay 1997).

(b) Wave breaking occurs at the reef-rim:

- the breakpoint should be calculated (i.e. the breaker depth related to the reef-rim slope)
- S is calculated using the average depth h_{ba} on the reef-rim between the breakpoint and the reef-crest (or for tan $\alpha > 0.1$, between the inner and outer surf zones)
- the appropriate reef profile factor is K_p' taken from Figure 8.13.

In the latter situation, the breakpoint depth ($d = d_b$) can be estimated as proposed by Gourlay (1992), ignoring possible wave-setdown, viz:

$$\frac{d_b}{H_o} = 0.259 \left[\tan^2 \alpha \left(\frac{H_o}{L_o} \right) \right]^{-0.17} \tag{8.36}$$

Furthermore, calculation of h_a or h_{ab} implies knowledge of the surf zone width x_S which can be estimated by the following equation from Gourlay (1994):

$$x_S = \left(2 + 1.1 \frac{H_o}{h_e} \right) T \sqrt{g\, h_e} \tag{8.37}$$

where h_e is the reef-edge depth.

Finally, irregular waves may be considered in an analogous manner, substituting the offreef wave parameters as follows, e.g.

$$H_o = H_{0rms} \equiv \frac{H_{os}}{\sqrt{2}} \tag{8.38}$$

where H_{os} is the offreef significant wave height, and

$$T_o = T_{0p} \tag{8.39}$$

where T_{op} is the peak spectral wave period, yielding a maximum reef-top setup value from Equation 8.35 of:

$$\overline{\eta}_{r\max} = 0.023\, K_p\, \frac{H_{os}^2\, T_{op}}{(\overline{\eta}_r + h_r)^{3/2}} \tag{8.40}$$

This maximum condition also assumes that wave crests approach normal to the reef profile and that H_{oS} is a measure of the shore-normal wave energy. This will not always be the case since the reefs are often surrounded by very deep water and refraction generally will be limited. Accordingly, in specific situations, the direction of wave approach relative to the orientation of the reef-shore should also be considered and, given the overall level of approximations involved, a simple transference is preferred, e.g.

$$H_{oS(\theta=0)} = H_{oS(\theta=\vartheta_o)}\, \cos\theta_o \tag{8.41}$$

where υ_o is the angle between the offshore deepwater wave energy and the shore-normal reef profile.

Depending on the reef-top characteristics, it may also be necessary to consider the possibility of surf beat oscillation, re-formed waves and bores in the lagoon and additional beach setup and runup. Gourlay (1997) provides further advice on such matters.

8.6 Conclusions and Recommendations

An introduction to the physics of nearshore wave behaviour in respect of wave setup and runup characteristics has been provided. Analytical formula are presented which will allow transfer of nearshore spectral wave model parameters to inshore environments and permit estimates of mean water level superelevation due to wave breaking. Advice on calculating wave runup of irregular waves is also included to assist in estimating berm erosion and overtopping and the special needs of coral reefs, atolls and cays is discussed.

It is concluded that breaking wave setup is a significant potential contributor to storm tide on the open coast and especially on low-lying offshore islands. Although the essential physics of wave setup is well understood, more research is required into the role of nearshore wind stress and the development of non-linear interactions between surge and setup during extreme inundation episodes. Where open coast wave setup estimates are available directly from a spectral wave model (e.g. SWAN) and the spatial resolution is sufficient, there may be advantages in using such estimates directly, especially if the nearshore environment is complex. In many open coast situations however, the simple analytical methods described here can be applied on a point specific basis using appropriate incident wave parameters taken from the inshore limit of a spectral model. Very sudden depth transitions, such as those characterising coral reefs, must always be treated separately in accordance with the guidance of Section 8.5.

*It is recommended that (a) analytical methods be applied to the estimation of wave setup using nearshore spectral wave model output parameters and that this be applied at a fine scale resolution (e.g. **C** grid minimum, refer Chapter 11) and (b) that further research be initiated into the nearshore physics of extreme inundation episodes so as to provide better guidance for the likely significant community impacts.*

8.7 References

Booij, N., Holthuijsen, L.H. and Ris, R.C. (1996) The SWAN wave model for shallow water. Proc 25th Int. Conf. Coastal Eng., *ASCE*, Orlando, 668-676.

Dunn S.L., Nielsen P. and Madsen P.A.(1999) Wave setup in jettied river entrances. Coasts and Ports '99: Proc 14th Australasian Coastal and Ocean Engineering Conference, Perth, WA, April 14-16, *IEAust*, 193-198.

Gourlay M.R. (1992) Wave set-up, wave run-up and beach water table: Interaction between surf zone hydraulics and groundwater hydraulics. *Coastal Engineering*, 17, 93-144.

Gourlay M.R. (1994) Wave transformation on a coral reef. *Coastal Engineering*, 23,17-42.

Gourlay M.R. (1996a) Wave setup on coral reefs. 1. Set-up and wave-generated flow on an idealised two dimensional horizontal reef. *Coastal Engineering*, 27,161-193.

Gourlay M.R. (1996b) Wave setup on coral reefs. 1. Set-up on reefs with various profiles. *Coastal Engineering*, 28, 17-55.

Gourlay M.R. (1997) Wave setup on coral reefs: some practical applications. Proc. 13th Australasian Conf Coastal and Ocean Engin., *IEAust*, Christchurch, Sep, 959-964.

Hanslow D.J. and Nielsen P. (1993) Shoreline setup on natural beaches. *J Coastal Res, Special Issue 15*, 1-10.

Hanslow D.J., Nielsen P. and Hibbert K. (1996) Wave setup at river entrances. Proc 25th Int Conf Coastal Eng, Orlando, September 1996, *ASCE*, 2244-2257.

Hardy T.A., Young I.R., Nelson R.C. and Gourlay M.R. (1991) Wave attenuation on an offshore coral reef. Proc. 22nd Intl Conf Coastal Engin., Delft, 1990, *ASCE*, New York, Vol 1, 330-344.

Nelson R.C. (1994) Depth limited design wave heights in very flat regions. *Coastal Engineering*, 23, 43-59.

Nielsen, P (1989) Measurements of wave setup and the watertable in beaches. Proc 9th Australasian Conf Coastal and Ocean Eng, Adelaide, *IEAust*, 275-279.

Nielsen P. and Hanslow D.J. (1991) Wave runup distributions on natural beaches. *J Coastal Res*, Vol 7, No 4, pp 1139-1152.

9. Storm Tide Statistics

9.1 Introduction

The expected long-term spatial and temporal variability of storm tide threats along a coastline can only be described statistically. *Storm tide statistics* then express the potential magnitude and duration of specific weather events in a mathematical context which accounts for the likelihood of experiencing storms which locally exceed certain intensity thresholds, combined with the presence of the astronomical tide. This requires measures of the natural variability of climate as well as the potential additional effects of Greenhouse-induced long-term climate change.

Knowledge of storm tide statistics is essential for sustainable economic development in the coastal zone and their potential application covers a diverse range of planning and investigation needs, viz

Community vulnerability and emergency planning:
- Inundation mapping
- Risk assessment of community housing and infrastructure
- Disaster cost estimation and design of insurance products
- Evacuation planning (onshore and offshore)

Tourism and environmental values:
- Protection of natural coastal systems (dunes, coastal lakes and wetlands etc)
- Extreme weather impacts on the Great Barrier Reef
- World heritage custodianship best practice
- Establishment of development control (buffer) zones

Coastal management, port infrastructure design and maintenance:
- Long term coastal erosion and accretion studies
- Beach nourishment programs
- Design criteria for fixed and floating structures, e.g. bridges, jetties, wharfs, breakwaters, revetments, pontoons, moorings
- Navigation needs, e.g. inlet and channel stability
- Harbour operations, e.g. port closure planning, dredging strategies
- Artificial waterways, e.g. canal estates
- Aquaculture

This section discusses a range of methodologies which are available for computing storm tide statistics, including requirements to take into account climate change, sea level rise, and decadal variability in cyclones. Recommendations are made as to the most appropriate technical options in the Queensland context and in regard to the overall aims of the present project.

9.2 The Historical Context

The threat of inundation and potential for loss of life from storm tide disasters was already evident from our earliest historical experience, much of which was chronicled by

Whittingham (1958, 1959, 1968) and Holthouse (1971) in regard to the famous 1899 Bathurst Bay and other significant events. Awareness of and interest in the ability to make predictions about the variation in storm surge characteristics around the Australian coast began in the late 1960s. This was supported by the advances in the USA where similar storm tide threats were being experienced along the rapidly developing Gulf of Mexico and Atlantic coastlines. This awareness had been fuelled by the significant outcomes in regard to meteorology and climatology of hurricanes from the US National Hurricane Research Project (Graham and Nunn 1959). The Shore Protection Manual (CERC 1966) provided basic design advice which was soon updated and extended by the work of many researchers such as Bretschneider (1967), Jelesnianski (1965, 1972). Nickerson (1971) formalised a manual estimation method for storm surges based on results from the Jelesnianski numerical modelling.

In the Australian context, tropical cyclone *Althea* in 1971 at Townsville provided a degree of urgency in understanding these phenomena and Stark (1972) provided a valuable primer for many subsequent studies. Initial work by the Bureau of Meteorology (Trajer 1973) adopted the Nickerson nomogram technique for the Southern Hemisphere and it has remained a useful operational tool to the present time (Callaghan 2000). This research was continued by Dexter (1975) who was among the first to consider statistical methods for estimating the potential variability of surge magnitudes and Nelson (1975) provided one of the earliest compendiums of historical surge data. Meanwhile Hopley and Harvey (1976) undertook extensive tidal data analyses and provided an Australia-wide perspective that provided some potential insight into the regional variability, together with Silvester and Mitchell (1977) who utilised a simplified modelling approach. None of the above studies, though, was sufficiently sophisticated to enable estimation of true *storm tide statistics*, i.e. the consideration of the very significant influence of the astronomical tide on the total mean water level.

From the mid-1970s onwards studies increasingly addressed the astronomical tide problem and began to provide predictions for a range of locations in Queensland. The techniques increased in complexity as access to computing facilities expanded and simulation-based approaches became more tractable. Table 9.1 provides a brief overview of progress over the past 25 years, taken predominantly from the recent review by Harper (1999a), while the actual methodologies are discussed in detail in subsequent sections. The main client organisation during this time was the Beach Protection Authority of Queensland (now a part of the Environmental Protection Agency) with a specific interest in the long-term behaviour of the coastal system. Other clients have included specific Local Government Authorities or private infrastructure developers requiring design information.

Some of the earlier studies (b) and (c) utilised analytical treatments of the "conditional probability" of combinations of water levels due to storm surge and the astronomical tide. In this case, the deterministic storm surge estimates were derived from the simplified nomogram technique of Nickerson (1971). The simulation techniques based on site-specific numerical hydrodynamic modelling, such as those indicated above as "Monte Carlo" approaches, were developing at that time (e.g. Russell 1971) and offered greater accuracy with fewer assumptions than the approximate analytical approaches. The reliance on simplified nomogram techniques became supplanted by the development of Australia's first generalised numerical hydrodynamic model of storm surges developed in the late 1970s by James Cook University (Sobey *et al.*, 1977; Harper *et al.* 1977). This model provided the means to construct site-specific "nomograms" for the Queensland coast based on a range of modelled "design" storms.

Table 9.1 Previous storm tide statistics studies in Queensland.

Study	Year	Location	Author	Method
a	1976	Yeppoon	Stark	Monte Carlo
b	1976	Mackay	Irish	Conditional Probability
c	1976	Yeppoon	Irish	Conditional Probability
d	1977	Townsville	Harper and Stark	Monte Carlo
e	1979	Cairns	Stark	Monte Carlo
f		Brisbane	McMonagle	Monte Carlo
g		Weipa	Sobey *et al.*	Monte Carlo
h	1980	Gladstone	McMonagle	Monte Carlo
i	1981	Hay Point	Harper	Monte Carlo
		Mackay	"	"
j	1985	Cooktown	Harper	Monte Carlo
		Mourilyan	"	"
		Lucinda	"	"
		Townsville	"	"
		Bowen	"	"
		Mackay	"	"
		Yeppoon	"	"
		Surfers Paradise	"	"
k	1985	Hervey Bay	Treloar	Monte Carlo
l	1987	Cairns	Hardy *et al.*	Joint Probability
m	1987	Palm Cove	Hardy *et al.*	Joint Probability
n	1992	Mulgrave Shire	Mason *et al.*	Joint Probability
o	1993	Cairns	Hardy and Mason	Joint Probability
p	1995	Cardwell	McMonagle	Monte Carlo
q	2000	Cairns	McInnes *et al.*	Monte Carlo

Of the studies in Table 9.1, Study (j) remains the most complete investigation to date and may be combined with Studies (i) and (p), which use the exact same methodology based on Harper and McMonagle (1985). Study (g) is also very similar. All of these rely on the deterministic modelling provided by Harper *et al.* (1977). The remaining "Monte Carlo" studies (k and q) essentially apply a similar methodology but are based on later deterministic storm surge modelling results. The so-called "Joint Probability" studies (l) to (o) represented extended deterministic surge modelling, in some cases combined with spectral wave modelling, undertaken later by Hardy and Mason at James Cook University.

Of the above, only Studies (i) and (l) to (o) explicitly utilised deterministic wave modelling and included a contribution by wave setup to the total storm tide. The remaining studies generally provided advice only in regard to wave setup. Furthermore, Study (i) is the only instance where the joint probability of water level and wave height was also explicitly addressed.

The "greyed" locations in Table 9.1 indicate those studies that have been extensively utilised and might be regarded as the current reference points. The essential differences between each

of these simulation approaches, as well as some alternative simulation methods, are discussed in the following section.

Figure 9.1 below summarises existing storm tide statistics for a selection of Queensland locations (from Harper 1999a). This is a typical example of how the results from a storm tide statistics analysis might be presented. At each location that has been studied, the vertical bar indicates the range of water levels corresponding to particular return period probability ranges. In this case the water level is given as being relative to the local Highest Astronomical Tide (HAT), meaning that any level above zero will indicate salt water occurring above the highest expected tide level. For any given location, the higher the return period transition point, the higher the storm tide risk, e.g. Townsville is the highest, followed by Yeppoon, Cairns, Mackay and Brisbane. The actual impact of such storm tide levels will then be dependent upon the vulnerability of the community at each location to those levels.

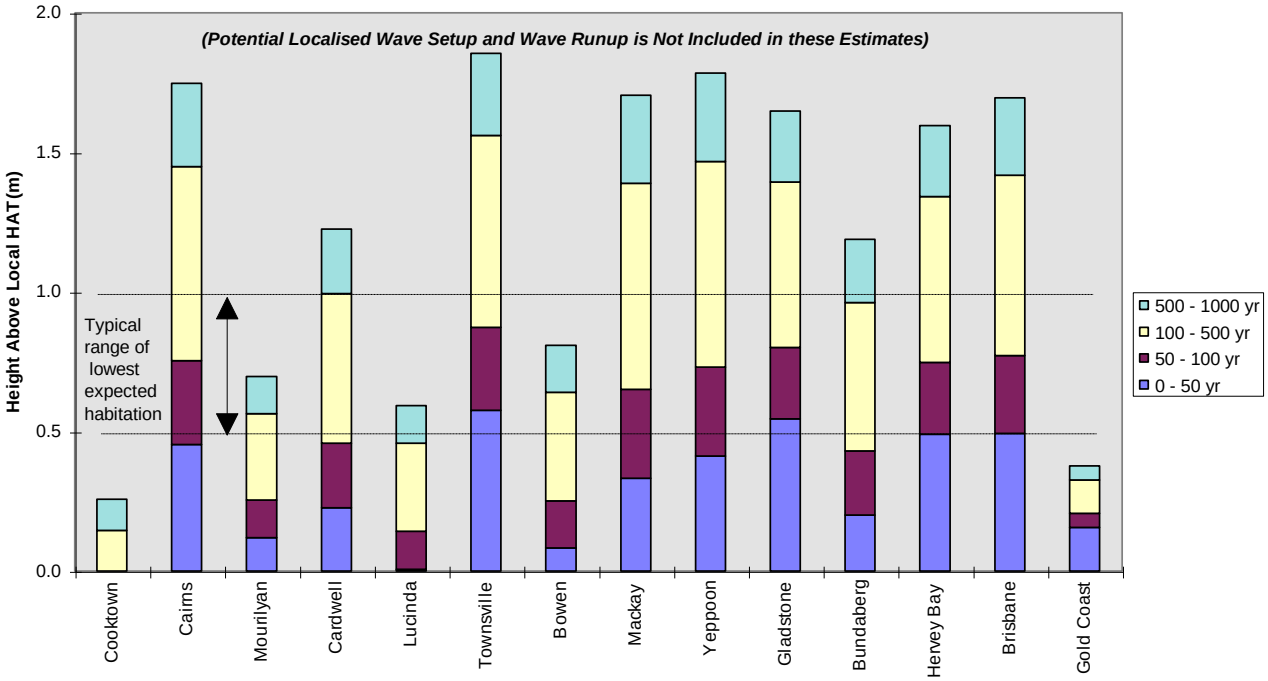

Figure 9.1 Some existing storm tide statistics for selected Queensland locations

(after Harper 1999a)

9.3 The Need for Revision and Update

Harper (1999a) presents a detailed case for a comprehensive update of the storm tide statistics for Queensland, of which the major points only are re-stated here.

(a) Incomplete Spatial Coverage

The extent of existing coverage is not complete, even for some highly populated regions, e.g.

- Sunshine Coast
- Whitsunday Islands
- Bundaberg - Gladstone
- Moreton Bay (incomplete)
- Cooktown

- Gulf of Carpentaria
- Torres Strait

(b) Differences in Basic Methodology

The techniques and models for undertaking storm surge analyses have developed since the mid 1970s with improved models of the tropical cyclone wind field now available, which will create slightly different surge responses for the same set of parameters. Numerical hydrodynamic models of surge have also progressed during this period with improved boundary conditions and allowance for overland flow where justified. Three dimensional modelling may now also be applied where necessary. Access to increased computational power also allows finer scale representation of coastal forms, wider parameter ranges, greater numbers of scenarios, modelling over longer periods and potential for inclusion of simultaneous tide, wave and current effects.

(c) Increased and Better Cyclone Data

The earliest statistical studies were limited by the climatological record of the time with the majority dependant on Lourensz (1981). However, following work by Holland (1981) it is now generally acknowledged that cyclone data in the Australian region can only be regarded as reasonably reliable since 1959/60 when the first satellite surveillance commenced. The ability to revise older cyclone data and more easily examine measured wind and pressure data has enabled the historical track details to be enhanced in some cases.

(d) Climate Change Scenarios

Only two of the existing studies have considered allowance for Greenhouse-induced climate scenarios and none consider inter-decadal variability. All of the other existing studies assume a static mean sea level based on present climate conditions. The impact of the changing statistical data set and scenarios of climate change or sea level rise could only be assessed by reworking present water level predictions.

(e) Increased Measured Data on Storm Tides

Over time an increasing number of significant storm tide events have been measured which provide opportunities for better model calibration and to provide insight into the potential interactions between surge, tides and waves.

(f) Wave Setup, Runup and Inundation

The existing studies covered large sections of coast and, commensurate with the scale of the storm surge itself, did not address fine scale details at any of the coastal sites. These include the local effect of wave setup, runup and overland flooding - all of which can have significant counter disaster ramifications. Few of the existing studies included explicit ocean wave modelling in the estimation of wave-induced setup and only one considered overland flooding.

(g) Non-Cyclonic Storm Tide Influences

Significant non-cyclonic weather events, such as monsoonal surges or deep extra-tropical systems, are capable of producing smaller but often more prolonged increases in coastal water levels. These may be responsible for more frequent episodes where the elevation of water levels reaches or just exceeds HAT. Longer duration is a critical factor for beach erosion and because of their potential linkage to episodes of heavy rain, such events are more likely to be associated with flooding. The Surfers Paradise storm tide predictions (Harper 1985) are the only case that presently includes some allowance for these effects.

9.4 The Prediction Problem

Traditional methods for estimating the probability of occurrence of extreme weather events (e.g. floods, winds, waves) are normally based on the statistical analysis of data. In many situations involving environmental processes, however, the data available for such analysis is typically incomplete, unrepresentative, often scant and, at worst, non-existent. For example, the estimation of extreme tropical cyclone wind speeds based only on recorded data is often inadequate for use in specialist engineering design (Harper 1999b). Firstly, the period of reliable data record at many sites is still relatively short (rarely exceeding 50 years) and the spatial separation of individual data sites is large. Secondly, the range of potential cyclone intensities can be high, their occurrence is typically very low and their area of influence relatively small. Even where reliable recorded data is available, extrapolation to long return periods (low probability levels) is problematical and retention of an associated parameter such as direction or persistence to any level of accuracy is difficult. Also, the statistical wind record itself does not contain explicit guidance on questions such as climate change, and is not directly suitable for other design considerations such as the determination of extreme wave heights and storm surge. Knowledge of the meteorological *system* and its applicable time and space scales then becomes of paramount importance rather than the isolated analysis of specific, and sometimes inadequate, site-specific records of its incidence. This is not to say that the data record should be ignored, but rather used as a valuable independent measure of the success of other indirect methods.

In the storm tide context, the astronomical tide component is quite precisely known at many locations because of its periodic gravity forcing on the planetary scale. Tidal prediction to an accuracy similar to the normal ability to measure it (sub-millimetre) requires harmonic analysis of a period of about 19 years of measured data. Such analyses have already been completed, except for some notable exceptions in the more remote regions of Australia, and they underpin the routine prediction of tides on a daily basis. By contrast, meteorologically forced deviations from the planetary motions occur daily and generate water-level anomalies on both regional and local time and space scales, but these variations are specifically removed by the tidal analysis procedures. Examples include the daily synoptic variation in atmospheric pressure due to solar heating, coastally trapped edge-waves and the like. The storm surge is simply the most dramatic manifestation of these meteorologically forced ocean water level events. However, its rarity means that the measurement record at any single coastal site yields insufficient instances to enable the use of traditional data extrapolation techniques. This situation is unlikely to change until many hundreds of years of data becomes available, by which time data stationarity assumptions will likely be violated due to the longer term impact of climate change, whether anthropogenic or natural. In spite of this, some researchers regard the historical record *is* adequate for such purposes in some special cases which can draw on stable antiquity data (Van Gelder 1996). In theory, paleo-climate analyses can also assist in

such assessments but the base data is often much filtered by the geological record and is best utilised as a general trend comparison rather than a site-specific quantitative prediction.

9.5 Estimation of Risks Without Long-Term Measured Data

Alternatives to the analysis of measured data for storm surge estimation are discussed here in the historical context of their development, allied with the parallel development needs for estimating design wind and wave conditions.

9.5.1 The "Design Storm" Approach

These basic data inadequacies have been recognised for a long time and led to philosophical considerations in the 1960s that considered so-called *indirect* methods of estimation of the parameters of interest. The first of these became known as the "design storm" approach. The *probable maximum hurricane* (US Weather Bureau 1968) is an upper-limit example of such a philosophy, which arose as a useful technique for establishing some type of regional benchmark. Typically, a "design storm" intensity would be based on an initial statistical assessment of the probability of such an occurrence within the area of interest, using nominal scales of storm influence. For example, Coleman (1972) provided the relevant climatology in the Australian context, from which an extreme value analysis of intensity could be constructed for a coastal region. Such a storm would then be *a priori* aligned along the most unfavourable track relative to the site of interest to provide a "worst case" scenario for a given storm intensity. This approach provides a potentially very conservative estimate of the associated return period of the winds, waves or storm surge being experienced at a specific point because the joint probability of intensity and proximity to site is not considered.

9.5.2 The "Hindcast" Approach

As computer modelling became more readily available through the 1970s, the "design storm" was replaced by the "hindcast" technique. This would involve selecting a number of extreme events from the record that would have been likely to have affected the site in question, but were not captured by a recording system at the time. Modelling of these events using historical track information then yielded a synthetic time series data set which, with sufficient samples, was amenable to traditional statistical extreme value extrapolation techniques. Such an approach was advocated by Dexter (1975) in response to the limitations of the design storm approach. This technique is reasonable for peak wind, wave and storm surge prediction when an adequate historical track record is available but fails in cases where the record is sparse, and the resulting predictions can be very site and data sensitive. Storm *tide* however remains additionally complicated by the simultaneous occurrence of the astronomical tide, which cannot be usefully incorporated directly into the hindcast technique and remains as a necessary analysis add-on. Dexter *et al.* (1977) provides a review of some Australian progress at this time, noting that the hybrid method of Irish (1977) offered a rational basis for estimating the influence of tidal variability. This involved analytically combining the frequency distribution for storm surge, estimated from a hindcast perspective, with the frequency distribution of the predicted tide at the location of interest. Unfortunately a number of time and space scale assumptions are needed in such an analysis which detract from its utility compared with the methods to be adopted later. The hindcast approach continued to be developed, most notably for the estimation of design wave conditions in deep water (e.g. Ward *et al.* 1979; Wyland and Thornton 1991) where water level variation can be ignored.

9.5.3 Simulation Techniques

At about the same time, simulation techniques came to be developed in an attempt to overcome the deficiencies of the other indirect methods. Their attraction lay in an ability to represent the processes at work rather than just the outcomes and, specifically, the capacity to correctly consider joint probability. This shifted focus away from the strict mathematical art of statistical extrapolation of site-specific scalar data towards a closer look at the possible underlying environmental mechanisms. Simulation techniques offer not only the best way of estimating extreme wind speed climates but the only reasonable way of doing so out to the long return periods (in excess of 2000 years) increasingly being demanded by today's risk managers. Three variants are discussed at this point - Monte Carlo, Joint Probability and Empirical Simulation.

The basic approaches in each case are as follows:

(a) Monte Carlo Methods (MCM) typically construct a complete artificial time history of storm tide events (surge + tide + setup) which are based on a discretely (i.e. individually) sampled storm climatology. Normally, each major climate parameter is assumed independent of any others (e.g. p_0, R, V_{fm} etc). In theory, the statistical interpretation can be reserved until the end of the generation phase where probability of exceedance is the typical outcome. In practice, the statistical analysis is performed in parallel with the generation and provides the criteria for acceptance of convergence of the outcome at a return period of interest. The method relies on the use of simplified (computationally efficient) parametric models for storm tide because of the very large number of realisations required. It does however allow considerable freedom in parameter selection and scenario development.

(b) Joint Probability Methods (JPM) are a logical improvement over the design storm approach whereby the technique seeks to apply detailed storm tide modelling to a specific site but only for a discrete range of storm conditions. To do this efficiently it needs to adopt a restricted storm climatology. Unlike the MCM, a complete time history of storm tide events does not need to be generated but rather a series of discrete episodes are assembled (e.g. $p_0=p_1$; $R=r_1$; $V_{fm}=v_1$ etc) whose individual probability of occurrence is assignable. The overall probability of water level exceedance can then be derived by combining the probabilities of each of the episodes when the individual storm tide responses are known. In essence the parameterisation is applied to the climatology rather than the storm tide calculation. The intention with JPM is to avoid redundancy in the storm generation phase because only the one realisation of a set of storm parameters needs to be modelled to generate the storm tide. The probability quantum of each storm tide episode can also be adjusted under scenario testing without necessarily reworking the detailed storm tide analyses. Random tide phasing must still be introduced separately in the analysis to obtain the total water level statistics.

(c) Empirical Simulation Techniques (EST) seek to bypass the traditional parameterisation of the climatology through a holistic assessment of the historical storm lifecycle data set. Spatial and temporal analysis of the climatology is undertaken to develop what is essentially an extended hindcast data set of storms. This is intended to retain "natural" characteristics of the data set such as curved paths and to preserve the dominant joint probabilities of various parameters. Essentially the effort with EST is put into the climatology and thereafter is similar to JPM in that detailed storm tide modelling is applied to each event. A quoted advantage of the method is that it is non-parametric but this can be a disadvantage where scenario development for climate change is concerned.

The development of each of these techniques is now followed to explain their advantages in more detail and gauge their level of application and acceptance.

9.5.3.1 Discrete Monte Carlo Methods

One of the earliest proponents of this technique was Russell (1971) whose novel assessment of hurricane impacts along the Texas Gulf coast commenced in the late 1960s. His technique was based on a climatology analysis followed by a discrete Monte Carlo simulation of hurricane lifecycles (track, intensity size etc) at a nominal timescale, coupled with the Graham and Nunn (1959) hurricane windfield model. The method generates synthetic time histories of the parameter of interest based on the assumptions embodied in the climatological analysis and through random sampling of various storm input distributions. After accumulation of a sufficiently long synthetic data record, traditional statistical analysis is then applied, often in a much-simplified framework of interpolation rather than extrapolation. His basic approach was subsequently repeated and further developed in a wide range of environmental studies. Australia was one of the first major applications of the method, with Martin (1974) applying it to the estimation of wind gust speeds. This was later refined and extended by Gomes and Vickery (1976) in a landmark study largely responsible for present design wind criteria throughout Australia. Similarly, Batts *et al.* (1980) produced the first simulation-based estimate of design wind speeds across the United States. This was partly refined by Georgiou *et al.* (1983) and Georgiou (1985) using updated windfield models, and more recently by Twisdale *et al.* (1992, 1993) and Vickery and Twisdale (1994, 1995ab). Although the analyses have become more sophisticated and been able to gradually take advantage of better data and meteorology, the relatively simple Monte Carlo simulation method of Russell (1971) underpins these approaches. In the more recent Australian context Harper (1996ab, 1999) extended the basic technique to provide fine-scale wind variability for metropolitan regions for application to insurance loss assessment studies. Harper (1999b) appears to be the only example of the use of measured wind data to provide independent verification of a MCM.

Extension of Russell's simulation approach to the allied areas of wave and surge prediction also occurred over this period, although such works relied on having a further model which would translate winds into the new response parameter of interest. This is further complicated to some extent by the inertial aspect of wave growth and storm surge generation, which is not present in the case of wind prediction. Stark (1976) was the first to develop a simple but seemingly effective Monte Carlo model that allowed the time history of a randomly-generated storm surge to be linearly combined with the astronomical tide. The statistics of the peak combined water level were then retained for analysis. His model - SATURN (*Surge And Tide Using Random Numbers*) - relied on a parametric storm surge model derived from a limited set of numerical hydrodynamic simulations for the area of interest. McMonagle (1979, 1980) then extended the basic Stark technique, which was later formalised by Harper and McMonagle (1985) into the original SATSIM model (*Surge and Tide SIMulation*) and applied extensively along the Queensland coast (Harper 1985). The climatology at this time was provided by Lourensz (1977, 1981) but later supplanted by the availability of the Bureau of Meteorology cyclone track database in digital format. More recently, Harper *et al.* (1989) extended the same technique to simultaneously generate statistics of extreme winds, waves, currents and surges for offshore oil and gas platform developments. The scalability of the technique allowed full retention of directional information for all parameters of interest (including multi-component 3D currents) and enabled rational joint probability return period estimation of design parameters out to 10,000 years.

9.5.3.2 Joint Probability Methods (JPM)

Development of this technique is normally attributed to Myers (1970), who devised the method specifically for considering storm tide along the US Atlantic coast. The aim of the method was to overcome some of the limitations of the design storm approach in allowing for the many variables that can affect the total water level at a coastal site. Essentially the technique also relies on an assumed climatology but a *priori* allocates probability space to particular parameter sets such as storm intensity, speed, radius etc. Then a (preferably limited) number of numerical hydrodynamic model simulations are undertaken to determine the water level response for that combination of parameters. This is done initially without consideration of the astronomical tide. When all storm-induced water level responses are known, the probability spaces assigned to the water level combinations can be used to construct a frequency of total water level exceedance for the site, combined with random phasing of the tidal signal.

This method suits situations where detailed hydrodynamic modelling is preferred to simpler parametric surge modelling of the type needed for the stochastically-intensive MCM, which generates a time history for each and every discrete event. Typically though with the JPM, use of computationally intensive numerical hydrodynamic model still needs to be limited and the results extended by further interpolation to cover the parameter range of interest. Execution of the analysis beyond that point, however, is typically more efficient than the MCM.

Further application of this approach was undertaken by NOAA (Ho *et al.*, 1976) and the US Army Corps of Engineers (Prater *et al.* 1985). It was subsequently applied in Australia by Hardy *et al.* (1987ab, 1993) and Mason (1992) for the Cairns region.

9.5.3.3 Empirical Simulation Techniques (EST)

This is a later development attributed to Borgman *et al.* (1992), applied by Scheffner *et al.* (1996) and Scheffner and Borgman (1996). The claimed advantages are to overcome the need to make specific assumptions about parameter independence, which are implicit in the JPM and to a lesser extent in the MCM. Consequently, the number of simulations is reduced because certain combinations are directly deemed inadmissible. The method essentially develops a temporal and spatial model of storm inputs and responses for a specific locality based on the actual historical dataset, which implicitly incorporates the joint relationships between parameters. This statistical model is then used to derive a much larger self-consistent dataset from which frequency relationships are developed.

In the Australian context, James and Mason (1999) have adopted aspects of the EST climatology technique only in generating a synthetic tropical cyclone database to be used for spectral wave modelling throughout the Great Barrier Reef region. They have developed an auto-regressive technique which utilises the existing historical database sample. A synthetic climatology is then developed and extended based on the historical dataset which provides a seamless along-coast variation in risk. The synthetic database is not constrained to simplified straightline track approximations for each storm, which is typical of those used in the MCM and JPM approaches, but rather permits specification of meandering tracks and varying intensities. These latter attributes are potentially important in order to generate representative variations in directional wind fetch conditions that lead to the development of tropical cyclone waves in a complex reef environment. However, extensive numerical hydrodynamic modelling is still required to assemble the synthetic time history of storm impacts (wind, wave and surge).

Similar techniques involving the spatial modelling of extremes (e.g. Casson and Coles 1998; 2000) may lead to even more sophisticated techniques which can be applied to the storm tide prediction problem.

9.6 Essential Elements for Statistical Storm Tide Prediction

The aim of any storm tide statistics methodology is to provide a rational basis for estimating the frequency of exceedance of storm tide levels at specific locations, so as to account for the various known interactions of astronomical tide, storm surge and wave setup. For the present discussion a "simulation" approach in some form is the subject of consideration. In addition, wave runup is not considered a component of the total storm tide because it depends directly on the immediate surface features (beach, cliff, wall etc). Within some philosophical context, all methodologies attempt to allow for the spatial and temporal variation that exists in each of those components and all require generation of synthetic storm events.

The principal issues involved are discussed below.

9.6.1 Representation of the Storm Climatology

This addresses the essential statistical variability of the problem, whereby storm tide events are the direct consequence of instances of severe storm events in the ocean or nearshore environment. A statistical description of the tropical cyclone climatology is therefore required which ideally includes *spatially and temporally varying* information regarding, for example:

- Frequency of occurrence (average, inter-annual, inter-decadal, long-term trends)
- Intensity (central pressure and windfield peakedness)
- Size (radius to maximum winds, radius to gales)
- Track (lifetime speed and direction of the notional centre)

In reality there may be known or suspected inter-relationships between any or all such information. A modelling process is then invoked to represent and preserve the more significant aspects whist enabling simplification of the problem. A common approach used is to establish a statistical *control volume;* within which homogeneity and stationarity of the sample data are assumed to apply, but from which a workable sample size can be extracted. Inevitably, this is a compromise between these two constraints. Based on the data sample it is then possible to propose statistical descriptions to various orders of approximation which appear to best represent the observed variability. This involves basic correlation testing as well as climatological reasoning. Typically, the sample is then stratified into particular classes of storms, often based on track characteristics, e.g. moving parallel to the coast, crossing the coast etc. One of the most common approaches is to consider a "length of coast" as one representation of the control volume, e.g. Russell (1971). In the Queensland context, Harper (1985) applied a coast length of 5º and an offshore extent of 2.5º, while Harper (1999b) takes a nominal 500 km radius from the point of interest.

The control volume approach is a robust concept which yields a number of individual statistical distributions which can be variously investigated to determine overall model sensitivities, to explore different scenarios and to permit calibration. This dimensional freedom however also presents challenges since approximations and assumptions must be made. The approach also introduces a discretisation of the sample on a spatial and, by virtue of the storm movement, a temporal basis. This is not always desirable where large sections of coast are being considered and a seamless variation in statistical behaviour is desirable. In this

case, more holistic techniques such as Casson and Coles (2000) or James and Mason (1999) may offer important advantages. Whatever the method though, it is important to justify the assumptions and seek verification of the results. While each method is essentially self-calibrating by virtue of the data reduction process, there is no similar assurance that the long-term (extreme) characteristics will emerge in a satisfactory context. Harper (1999b) advocates the use of comparisons with long-term coastal wind records in Australia to demonstrate at least the order of magnitude accuracy of any climatological model description. This requires matching the climatology model with a windfield model of choice.

The climatology should also be capable of representing the potential impact of long-term enhanced Greenhouse "climate change", i.e. increases in:

- Maximum potential intensity (MPI)
- Frequency of occurrence

and ideally incorporate "normal" climatic variability, i.e.:

- Annual
- Interannual (e.g. ENSO)
- Inter-decadal (e.g. IPO) variability

These influences need to be specified as time-varying modifications to the normally assumed stationary statistical process. The former can be based on a monotonic function consistent with the latest IPCC scenarios, whereas the latter require a quasi-periodic variability representative of the observed timescales which will reduce to the time-averaged case.

9.6.2 Representation of the Deterministic Forcing and Ocean Response

This provides the link between the severe storm event and the resulting ocean or nearshore response to that event. This is typically considered a deterministic link in the modelling process. Given the developing knowledge in matters such as tropical cyclone structure, the atmospheric boundary layer, surface stress transfer and the like (refer earlier Chapters) this might more correctly be assigned a degree of uncertainty

Relevant issues at this stage include:

- The choice of tropical cyclone wind and pressure model
- The choice of storm surge prediction model
- The choice of extreme wave prediction model
- Consideration of localised wave setup, runup and inundation
- Resolution, accuracy and coverage
- Consistency with the climatological assumptions

All of these issues must consider the balance between accuracy of prediction and numerical utility, otherwise the solution can quickly become intractable. Even with current advances in computational speed, compromises are needed to achieve results on practical timeframes. Choice of model resolution (space and time) is an important element, as well as domain size - the extent of the region within which results might be regarded as valid.

Because of the potential computational burden, *parametric* models are often preferred. These are typically analytical approximations to the problem as opposed to numerical solutions

based on primitive Newtonian equations. There are, for example, many tropical cyclone windfield models that are parametric and traditionally coupled with primitive equation models for storm surge and wave generation. More complex windfield models are available (e.g. Shapiro 1983) and have been variously applied, but often their increased computational needs dictate compromise in some other aspect of the overall analysis, such as the need to reduce the number of specific trials. Models that are even more complex are now emerging (e.g. Kepert and Wang 2000) whose application at least in the short term will probably need to be limited to the improvement of parametric models such as discussed in Chapter 5.

The need to consider the impact of extreme waves in the storm tide context adds additional layers of complexity over storm surge, relating to the fact that *inter alia* (refer Chapter 7):

(a) wave energy is a vector quantity requiring knowledge of direction (compared with the long wave storm surge magnitude);

(b) wave energy is frequency (or wavelength) dependent;

(c) multiple parameter representations and statistical descriptions are required;

(d) the spatial resolution required is often greater than for storm surge alone at all scales because of fetch requirements and shallow water refraction;

(e) the modelling computational and storage needs are then often an order of magnitude greater than for storm surge.

While the above issues determine the incident wave conditions at the shore, it remains to transfer the wave energy into wave setup which, as per the recommendations in Chapter 8, would ideally be analytically based to avoid the numerical complexities and relatively more simple to accommodate.

Additionally, localised wave runup and inundation will present significant data needs as well as modelling problems. Few if any Queensland localities would presently possess nearshore elevation data which would be sufficient to enable a detailed analysis. The time and cost to acquire such information must be considered in the process of aspiring to greater predictive accuracy.

9.6.3 Representation of the Combined Storm Tide Event

This aspect considers how the various components are combined and how the resulting information about the total event that can then be statistically interpreted. A simple technique might limit the predictive output to a series of point frequency estimates of, say, total water level at a particular site. A more comprehensive treatment might retain time history information in either discrete form (every case modelled) or a parametric (reduced data) format. Ideally, the time history of each component (tide, surge, wave, setup etc) would be retained in a manner that might allow re-interpretation as technology develops or client needs change. In ultimate configuration this would extend to include gridded fields of nearshore current components, in the case of storm surge, and various directional wave parameters (H_s, H_{max}, T_p, T_z, θ_{mean}, spectral shape etc) or even directional energy spectra $E(f,\theta)$ in the case of waves. This will prompt compromise in terms of data storage and recovery requirements, the expected utility of access to such data, and the cost of having to regenerate the data sets if later required.

Long-term climate change influence on mean sea level should also be considered, for example, Hardy *et al.* (1987ab) proposed modifying the encounter probability to allow for the IPCC water level scenarios to be incorporated into the prediction. On this basis, the probability that a particular elevation may be flooded would not be stationary but increase with time, for example, on a yearly basis. Other climatological factors such as potential increases in frequency or intensity could be best derived from the statistics if complete synthetic time histories are retained. Selective re-sampling and analysis would then yield estimates of the contribution from, and variation in, all such factors over time.

9.7 Conclusions and Recommendations

All storm tide statistics methodologies involve simplification of the complex natural processes to reduce the problem to one which can be reasonably solved at an acceptable level of accuracy. Ideally, the choice of model at each stage of the analysis must be self-consistent. A simulation approach is preferred over any design storm, hindcast or combined probability techniques. Regarding simulation methods (MCM, JPM, EST) there are two aspects:

(i) The approach for representing the storm climatology is a major differentiator. The EST utilises "natural" track parameters, whereas the JPM relies on a simplified description and the MCM can easily adopt either, depending on the skill of its parametric storm tide model, but has traditionally adopted a simplified description.

(ii) The storm surge response is handled either by parametric means (MCM) or by direct primitive equation modelling (EST, JPM).

Because of the above, there are potential advantages and disadvantages which can be associated with each method, which are considered in Table 9.2 below.

Table 9.2 Summary of the simulation methods.

	Climatology		Deterministic Storm Surge Waves and Wave Setup		Storm Tide Statistics	
Method	Advantage	Disadvantage	Advantage	Disadvantage	Advantage	Disadvantage
MCM	*Large parameter set*	*Assumptions required*	*Simple, fast with parametric*	*Potentially lesser accuracy*	*Complete time history*	*Large data set generated*
EST	*Natural tracks etc*	*Lack of parameters*	*Accuracy*	*High computation*	*Very site specific*	*Non-adjustable*
JPM	*Simplified description*	*Limited to a chosen subset*	*Accuracy*	*High computation*	*Adjustable after the event*	*Controlled by assumptions*

The lack of parameter control in the EST approach is seen as a significant drawback in the context of needing to undertake sensitivity testing and climate change scenarios. However, it is recommended that any MCM or JPM method should be based on a seamless climatology to enable application across the entire State.

If a parametric storm tide model is available, it is recommended that the Monte Carlo Method (MCM) be adopted as the most suitable technique for establishing storm tide statistics. This method provides the greatest opportunity for inclusion of a wide range of parameter

sensitivities, including interseasonal, interdecadal and climate change impacts. Alternatively, if a parametric model is not available, the Joint Probability Method (JPM) is favoured.

Finally, the adopted technique should automatically yield error or confidence limits in respect of the predictions. This can be done by accumulation of variance, analysis of variance (e.g. Twisdale *et al.* 1993) or use of sampling techniques such as the "bootstrap" (Prater *et al.* 1985; Hardy and Mason 1993).

9.8 References

Allen M.A. and Callaghan J. (2000) Extreme wave conditions for the south east Queensland coastal region. Environment Technical Report 32, *Environmental Protection Agency*, Qld.

Borgman L.E., Miller M.C., Butler H.L. and Reinhard R.D. (1992) Empirical simulation of future hurricane storm histories as a tool in engineering and economic analysis. Proc. Conf. Civil Engineering in the Oceans V, *ASCE*, 42-45.

Bretschneider C.L. (1967) Storm Surges. *Advances in Hydroscience*, 4, 341-414.

Casson E. and Coles S.G. (1998) Extreme hurricane wind speeds: estimation, extrapolation and spatial smoothing. *Jnl Wind Engin and Industrial Aerodynamics*, 74-76, 131-140.

Casson E. and Coles S.G. (2000) Spatial simulation of hurricane Events. *Applied Statistics* (to appear).

CERC (1966) Shore protection planning and design. Technical Report No. 4, US Army Corps of Engineers, Coastal Engineering Research Centre. 3rd Ed, *US Dept of the Army*.

Coleman F. (1972) Frequencies, tracks and intensities of tropical cyclones in the Australian region, 1909 - 1969. Bureau of Meteorology, *Meteorological Summary*. July.

Dexter P.E. (1975) Computing extreme value statistics for cyclone generated surges. Proc 2nd Aust Conf Coastal and Ocean Engin, *IEAust*. Apr. pp 200-206.

Dexter P.E., Trajer F.L. and Gordon B. (1977) Design cyclones and design surges. Proc. Hydrology Symposium, *IEAus*t, Brisbane, June.

Georgiou P.N., Davenport A.G. and Vickery P.J. (1983) Design wind speeds in regions dominated by tropical cyclones. *Jnl Wind Engineering and Industrial Aerodynamics*, 13, 139-152.

Georgiou P.N. (1985) Design wind speeds in tropical-cyclone prone areas. PhD Thesis. *The University of Western Ontario*, London, Sept.

Gomes L., and Vickery, B.J. (1976) On the prediction of tropical cyclone gust speeds along the Northern Australian Coast. Dept. of Civil Engineering, *Univ. Sydney*, Australia, Research Report No. R278, 1976.

Hardy T.A., Mason L.B., Young I.R., bin Mat H. and Stark K.P. (1987a) Frequency of cyclone induced water levels including the effect of mean sea level rise : Trinity Point. Dept

of Civil and Systems Engin, *James Cook University*. Prep for Macdonald Wagner Consulting Engineers. Oct.

Hardy T.A., Mason L.B., Young I.R., bin Mat H. and Stark K.P. (1987b) Frequency of cyclone induced water levels including the effect of mean sea level rise : Palm Cove. Dept of Civil and Systems Engin, *James Cook University*. Prep for Macdonald Wagner Consulting Engineers. Oct.

Hardy T.A. and Mason L.B. (1993) Frequency of cyclone induced water levels: Cairns Casino site. Dept of Civil and Systems Engin, *James Cook University*. Prep for Concrete Constructions Qld. Sep.

Harper B.A. Sobey R.J. and Stark K.P. (1977) Numerical simulation of tropical cyclone storm surge along the Queensland coast - Parts I to X. Dept Civil and Systems Engin., *James Cook University*, Nov.

Harper B.A. and Stark K.P. (1977) Probabilities of water levels at Townsville resulting from the combined effects of cyclone storm surge, tide and waves. Dept of Civil and Systems Engin., *James Cook University*, Dec.

Harper B.A. (1983) Half Tide tug harbour extreme water level study. Report prepared by *Blain Bremner and Williams Pty Ltd* for DBCT-UDC Joint Venture. Sept.

Harper B.A. and McMonagle C.J. (1985) Storm tide statistics - methodology. Report prepared by *Blain Bremner and Williams Pty Ltd* for the Beach Protection Authority Queensland, Jan.

Harper B.A. (1985) Storm tide statistics - Parts 1 to 8. Reports prepared by *Blain Bremner and Williams Pty Ltd* for the Beach Protection Authority Queensland, Jan.

Harper B.A. (1996a) Risk modelling of cyclone losses, Proc IEAust Annual Engin Conf, *IEAust*, Darwin, Ap, 53-88.

Harper B.A. (1996b) The application of numerical modelling in natural disaster risk management. Proc Conf on Natural Disaster Reduction NDR'96, *Institution of Engineers Australia*, Gold Coast, Sep, 107-114, ISBN 0 85825 662 2.

Harper B.A. (1999a) Storm tide threat in Queensland: history, prediction and relative risks. *Dept of Environment and Heritage*, Conservation Tech Rep No. 10, RE 208, ISSN 1037-4701, Jan (2nd ed.).

Harper B.A. (1999b) Numerical modelling of extreme tropical cyclone winds. APSWE Special Edition, *Journal of Wind Engineering and Industrial Aerodynamics*, 83, 35 - 47.

Ho F.P., Tracy R.J, Myers V. and Foat N.S. (1976) Storm tide frequency analysis for the open coast of Virginia, Maryland and Delaware. *NOAA Technical Memorandum* NWS HYDRO-32, Silver Spring.

Holland G.J. (1981) On the quality of the Australian tropical cyclone data base. *Aust Met Mag*, Vol 29 No 4. Dec.

Holthouse H. (1971) Cyclone. *Rigby*.

Irish J.L. (1976a) Report on storm tide levels for Pioneer River model study committee. Report prepared by *Cameron McNamara and Partners*. March.

Irish J.L. (1976b) Storm surge and flooding at Farnborough Beach. Report prepared by *Cameron McNamara and Partners* for Iwasaki Sangyo Co (Australia) Pty Ltd, March.

Irish J.L. (1977) Surge and storm tide frequency estimation for coastal locations subject to cyclones. Proc 3rd Aust Conf Coastal and Ocean Engin. *IEAust*. Apr.

James M. and Mason L. (1999) Generation of a synthetic tropical cyclone database. Proc. 14th Australasian Conf. Coastal and Ocean Engineering, *IEAust*, Perth, Apr, 407-412.

Jelesnianski C.P. (1965) A numerical calculation of storm tides induced by a tropical storm impinging on a continental shelf. *Monthly Weather Review*, 93, 343-358.

Jelesnianski C.P. (1972) SPLASH - special program to list amplitudes of surges from hurricanes - I landfall storms. *NOAA Technical Memorandum* NWS TDL-46.

Kepert J. and Wang Y. (2000) The dynamics of boundary layer jets within the tropical cyclone core - Part II: nonlinear enhancement. *Jnl Atmospheric Sciences* (to appear).

Lourensz R.S. (1977) Tropical cyclones in the Australian region July 1909 to June 1975. *Bureau of Meteorology*.

Lourensz R.S. (1981) Tropical cyclones in the Australian region July 1909 to June 1980. *Bureau of Meteorology*. Oct.

McMonagle C.J. (1979) Storm surge and tide investigations for new Brisbane Airport. Report prepared by *Blain Bremner and Williams Pty Ltd* for Commonwealth Dept Housing and Construction. Feb.

McMonagle C.J. (1980) Extreme water levels Gladstone and The Narrows. Report prep by *Blain Bremner and Williams Pty Ltd* for Coordinator General's Dept, Queensland. Nov.

McMonagle C.J. (1995a) Numerical simulation of storm surge along the Queensland coast - Part XI Cardwell Region. Report prepared by Rust PPK Pty Ltd for *The Beach Protection Authority Queensland*. Nov.

McMonagle C.J. (1995b) Storm tide statistics Cardwell region. Report prepared by Rust PPK Pty Ltd for *The Beach Protection Authority Queensland*, Oct.

Martin G.S. (1974) Probability distributions for hurricane wind gust speeds on the Australian coast. Proc. Conf. Applications of Probability Theory to Structural Design, *IEAust*, Melbourne, Australia, 1974, 55-56.

Mason L.B., Hardy T.A. and Bode L. (1992) Frequency of cyclone induced water levels - Marlin coast. Dept of Civil and Systems Engin, *James Cook University*. Prepared for Mulgrave Shire Council.

Nelson R.C. (1975) Tropical cyclone storm surges in Australia 1880 to 1970. Proc 2nd Aust Conf Coastal and Ocean Engin., *IEAust*.

Nickerson J.W. (1971) Storm surge forecasting. *Navy Weather Research Facility*, Tech Report 10-71.

Prater M.D., Hardy T.A., Butler H.L. and Borgman L.E. (1985) Estimating error of coastal stage frequency curves. Proc. 19th Intl. Conf. Coastal Engineering, *ASCE*, 162-172.

Russell, L.R. (1971) Probability distributions for hurricane effects. *Jnl. Waterways, Harbors and Coastal Eng. Div.*, ASCE., Paper 7886, February 1971.

Scheffner N.W., Borgman L.E. and Mark D.J. (1996) Empirical simulation technique based storm surge frequency analysis. *Jnl Waterways, Port, Coastal and Ocean Eng.*, ASCE, 122, 2, 93-101.

Scheffner N.W. and Borgman L.E. (1996) The empirical simulation technique - a bootstrap-based life cycle approach to frequency analysis. Proc Stochastic Hydraulics'96. In: Tickle, Goulter, Xu, Wasimi and Bouchart (eds), 1996, *Balkema*, Rotterdam, ISBN 90 5410 817 7, 389-394.

Shapiro L.J. 91983) The asymmetric boundary layer flow under a translating hurricane. *Jnl. Atmospheric Science*, AMS, 40(8), 1994-1998.

Silvester R. and Mitchell H.L. (1977) Storm surges around Australian coastlines. Proc 3rd Aust Conf Coastal and Ocean Engin. *IEAust*. Melb. Apr.

Sobey R.J., Harper B.A. and Stark K.P. (1977) Numerical simulation of tropical cyclone storm surge along the Queensland coast. Research Bulletin CS14. Dept Civil and Systems Engin. *James Cook University*, May.

Sobey R.J., Mitchell G.M. and Adil T.S. (1979) Trinity Inlet storm surge study. Report prepared by Dept Civil and Systems Engin *James Cook University* for Commonwealth Dept Housing and Construction.

Sobey R.J., Stark K.P. and Adil T.S. (1979) Weipa Peninsula extreme water level study. Report prepared by Dept of Civil and Systems Engin *James Cook University* for Comalco Limited. Aug.

Stark K.P. (Ed.) (1972) Cyclone Althea - Part II storm surge and coastal effects. *James Cook University*. Oct.

Stark K.P. (1976) Rosslyn Bay boat harbour surge investigation. Report prepared by Dept of Civil and Systems Engin *James Cook University*.

Stark K.P. (1979) Cairns storm surge plus tide levels. Report prepared by Dept of Civil and Systems Engin *James Cook University* for Cairns City Council. Dec.

Trajer F.L. (1973) A manual storm surge forecasting scheme for the Australian tropics. 1st Aust Conf Coastal Engin, *IEAust*, Sydney, May, 215-220.

Treloar D.G. (1985) Storm tide statistics - Hervey Bay region. Report prepared by *Lawson and Treloar Pty Ltd* for The Beach Protection Authority Queensland. Aug.

Twisdale L.A. and Vickery P.J. (1992) Predictive methods for hurricane winds in the United States - final report, SBIR Grant ISI 916035, *National Science Foundation*, Washington, DC, Sept.

Twisdale L.A., Vickery P.J. and Hardy M.B. (1993) Uncertainties in the prediction of hurricane windspeeds. Proc. Symp. Hurricanes of 1992, *ASCE*, Miami, Dec, ISBN 0-7844-0046-6, 706-715.

US Weather Bureau (1968) Meteorological characteristics of the Probable Maximum Hurricane, Atlantic and Gulf Coasts of the United States. *Dept. of Commerce*, Silver Spring, Md., Memo HUR 7-79 (unpublished).

Van Gelder P.H.A.J.M. (1996) A new statistical model for extreme water levels along the Dutch coast. Proc Stochastic Hydraulics'96. In: Tickle, Goulter, Xu, Wasimi and Bouchart (eds), 1996, *Balkema*, Rotterdam, ISBN 90 5410 817 7, 243-249.

Vickery P.J. and Twisdale L.A. (1994) Hurricane windspeeds at inland locations. Proc Structures Congress, *ASCE*, Apr.

Vickery P.J. and Twisdale L.A. (1995a) Prediction of hurricane wind speeds in the United States. *J. Struct. Engin*., 121(11), ASCE, 1691-1699.

Vickery P.J. and Twisdale L.A. (1995b) Wind-field and filling models for hurricane wind speed prediction. *J. Struct. Engin*., ASCE, 121(11), 1700-1709.

Ward E.G., Borgman L.E. and Cardone V.J. (1979) Statistics of hurricane waves in the Gulf of Mexico. *Jnl Petroleum Engineering*, 31, 5, 632-642.

Whittingham H.E. (1958) The Bathurst Bay hurricane and associated storm surge. *Aust. Met. Mag*., 23, Dec.

Whittingham H.E. (1959) Storm surges along the Queensland coast. *Aust Met. Mag*., 27, 40-41.

Whittingham H.E. (1968) The "Douglas Mawson" tropical cyclone of 1923. In Tropical Cyclones in the Northern Australian Regions for 1964-1965 Season, Appendix 1. *Meteorological Summary*. Bureau of Meteorology. Feb.

Wyland R.M. and Thornton E.B. (1991) Extremal wave statistics using three hindcasts. *Jnl Waterways, Port, Coastal and Ocean Engineering*, ASCE, 117,1, 60-74

10. Storm Surge Model Validation and Sensitivity Testing

The James Cook University storm surge model MMUSURGE is validated here against a number of historical Queensland cyclones to demonstrate its ability to accurately reproduce known events, to show the sensitivity of the model to a range of parameters and also to highlight areas of uncertainty in the storm surge prediction process.

10.1 Selection of Hindcast Storms

A number of historical storms were considered as candidates for hindcast and ranked on the basis of (i) availability of measured wind and surge data and (ii) their demonstration value as examples of significant historical storms affecting coastal communities. The hindcast storms chosen for comparison, together with the basis for selection, are summarised in Table 10.1.

Table 10.1 Hindcast storm set.

Storm	Date	Location	Peak Storm Tide (m AHD)	Storm Data	Surge Data	Basis for Selection
1918	21-Jan-1918	Mackay	5.5	poor	fair	Category 4 storm in a large tidal range environment with reef.
Althea	24-Dec-1971	Townsville	2.9	fair	good	A mature Category 3 storm in a mixed shelf and reef environment.
Ted	19-Dec-1976	Albert River	6*	fair	fair	A large Gulf of Carpentaria storm surge event with extensive overland flooding.
Steve	27-Feb-2000	Cairns	1.0	good	good	A small, relatively weak storm in a narrow shelf and extensive reef environment.

* estimated

All available storm-related data was sourced, together with any measured or reported water level information. The process of assembling the various data sets and the comparisons between measured and modelled data is discussed in detail in the following sections.

10.2 Details of the Numerical Storm Surge Modelling

A series of existing MMUSURGE numerical model grid domains were used for the hindcast experiments; the parameters of which are presented in Table 10.2 below. All but one of the grids are orientated to North. Mackay was modelled as a single 1 nmile resolution grid; Townsville in 3 stages (5 nmile, 1 nmile and 0.25 nmile); Cairns in 3 stages (5 nmile, 1 nmile, 0.1 nmile) with a Gulf of Carpentaria large scale (5 nmile) grid combined with a finer scale 0.5 nmile for the southern coastline. Figure 10.1 presents the Coral Sea grid and the finer east coast grids, which are further detailed in Figures 10.2 to 10.4. The Gulf of Carpentaria grids are shown in Figure 10.5.

The bathymetry for each grid has been derived from a mixture of ETOPO5, AUS series hydrographic charts, bathymetric series charts and, in some small areas, specific survey data. The Gulf bathymetry is the least accurate, especially the coastal salt marsh regions which are

based on GTOPO30. A model timestep of 900 s was adopted in all base cases but varied in some sensitivity testing.

Table 10.2 Hindcast model domains.

Storm	Grids Used	Base Timestep	Extent		Spatial Resolution		Extent	
		Δt	x	y	Δs		East	North
		s			nmile	km	km	km
1918	Mackay	900	301	301	1	1.85	558	558
Althea	Coral Sea	900	157	223	5	9.27	1455	2066
	Townsville	900	241	181	1	1.85	447	335
	Cleveland Bay	900	107	76	0.2	0.37	40	28
Ted	Gulf of Carpentaria	900	169	175	5	9.27	1566	1621
	Karumba	900	281	181	0.5	0.93	260	168
Steve	Coral Sea	900	157	223	5	9.27	1455	2066
	Cairns	900	181	331	1	1.85	335	613
	Trinity Bay	900	81	81	0.2	0.37	30	30

The standard open sea boundary condition used is the inverse barometer effect, applied to the boundary of the coarsest grid in each simulation. Where applied, astronomical tides are introduced as a water height variation along the deep open sea boundaries, by a tidal prediction subroutine which uses amplitudes and phases of tidal constituents supplied to the model at specific points. These are then interpolated to neighbouring boundary points. Secondary constituent effects generated by the nonlinear interaction of the major tidal constituents are then automatically generated by the model. The tidal data applied is summarised in Table 10.3 below. Only the Mackay tidal calibration was deemed sufficiently accurate to enable prediction of absolute water levels of the combined storm surge and tide, these constituents being based on an extensive investigation into tides in the region (Bode and Mason 1992). At the other locations, the basic effect of the surge-tide interaction can be determined but the absolute tidal levels are only within about 0.2 m of the predicted values at the coastal stations. Significantly more tidal calibration work would be required to improve the tide performance in the other grids.

Table 10.3 Tidal boundary information.

Tidal Boundary Grid	Constituents Used	Assessed Quality
Mackay	Q_1, O_1, P_1, K_1, $2N_2$, μ_2, N_2, υ_2, M_2, S_2, K_2	Very good
Townsville	O_1, K_1, N_2, M_2, S_2	Fair
Gulf of Carpentaria	O_1, K_1, N_2, M_2, S_2	Fair
Cairns	O_1, K_1, N_2, M_2, S_2	Fair

All hindcasts have used a common sea bed roughness height z_0=0.001 m (giving a roughness length ≈ 0.027 m) and $C_d=(v_k/(z_1/z_0))^2$, where v_k is Von Karman's constant and z_1 is half the water depth in the 2D model.

The model was run in 2D (depth-integrated) mode for all hindcasts. Limited 3D simulations were undertaken of cyclone *Althea*, where 5 sigma levels were run in conjunction with a turbulence closure model which calculates turbulent kinetic energy and turbulent length scales. These are then used to determine the vertical eddy viscosity parameters for the momentum model.

The following matrix summarises the range of sensitivity tests undertaken in conjunction with the hindcast experiments.

Table 10.4 Model sensitivity tests undertaken.

	Region:	**Mackay**	**Townsville**	**Gulf**	**Cairns**
	Storm:	***1918***	***Althea***	***Ted***	***Steve***
Sensitivity Test	**Case**				
Resolution (nmile)	5		X	X	X
	1	X	X		X
	0.5			X	
	0.2		X		X
Timestep (s)	300		X		
	900	X	X	X	X
	1800		X		
Dimension	2D	X	X	X	X
	3D		X		
Tide	Tide Only	X	X	X	X
	With Tide	X	X	X	X
	No Tide	X	X	X	X
Wetting	Dry	X	X	X	X
	Wet			X	
Reef	Reef	X	X		X
	No Reef	X	X	X	
Nonlinear Advection	Yes	X	X	X	X
	No		X		

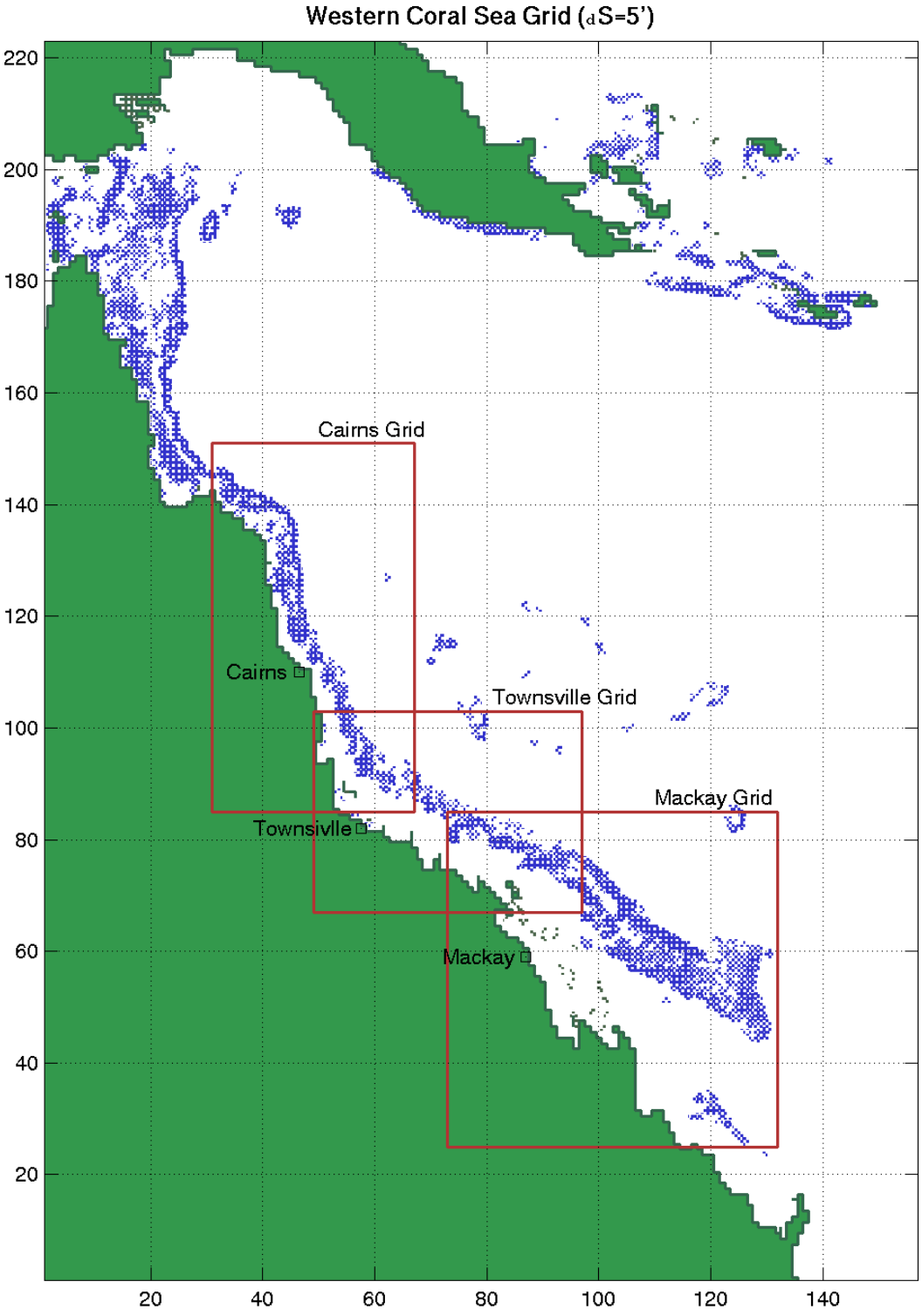

Figure 10.1 Overview of Coral Sea hindcast grids.

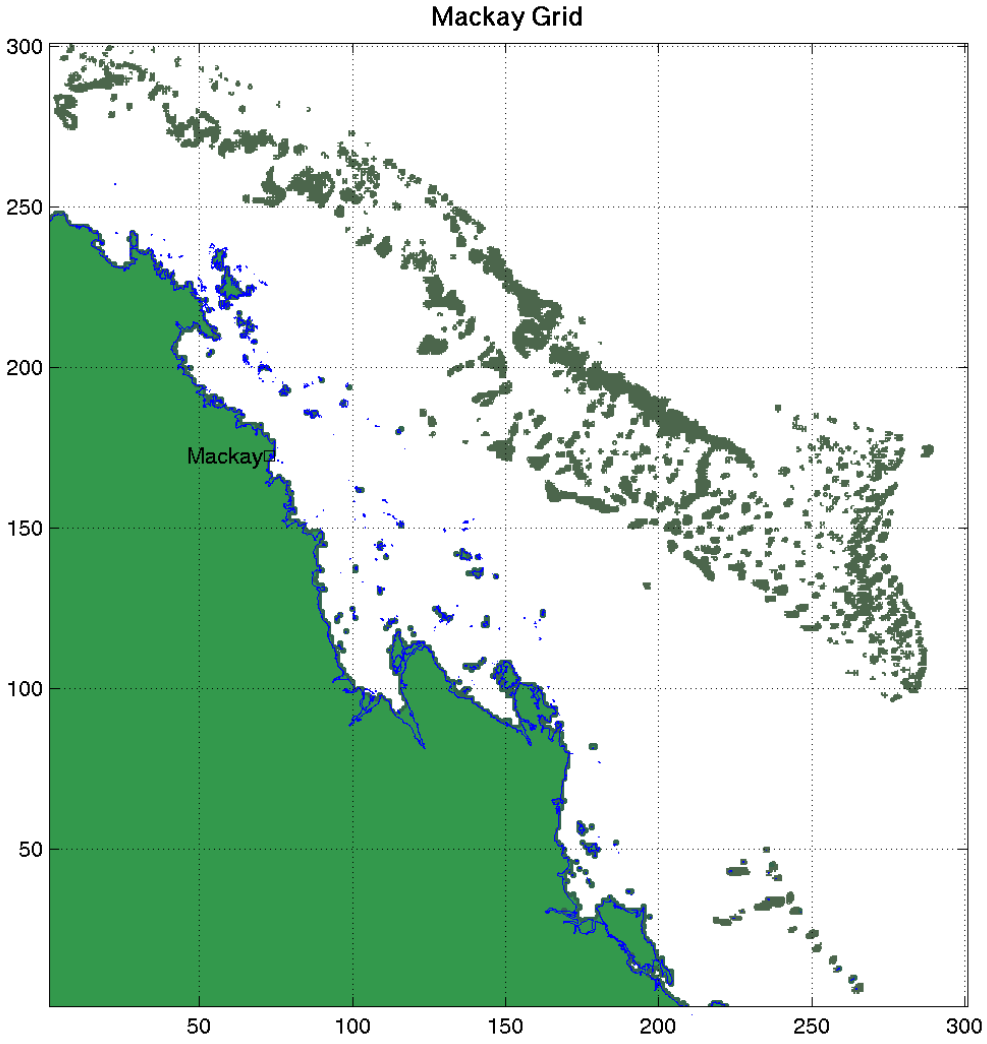

Figure 10.2 Mackay hindcast grid.

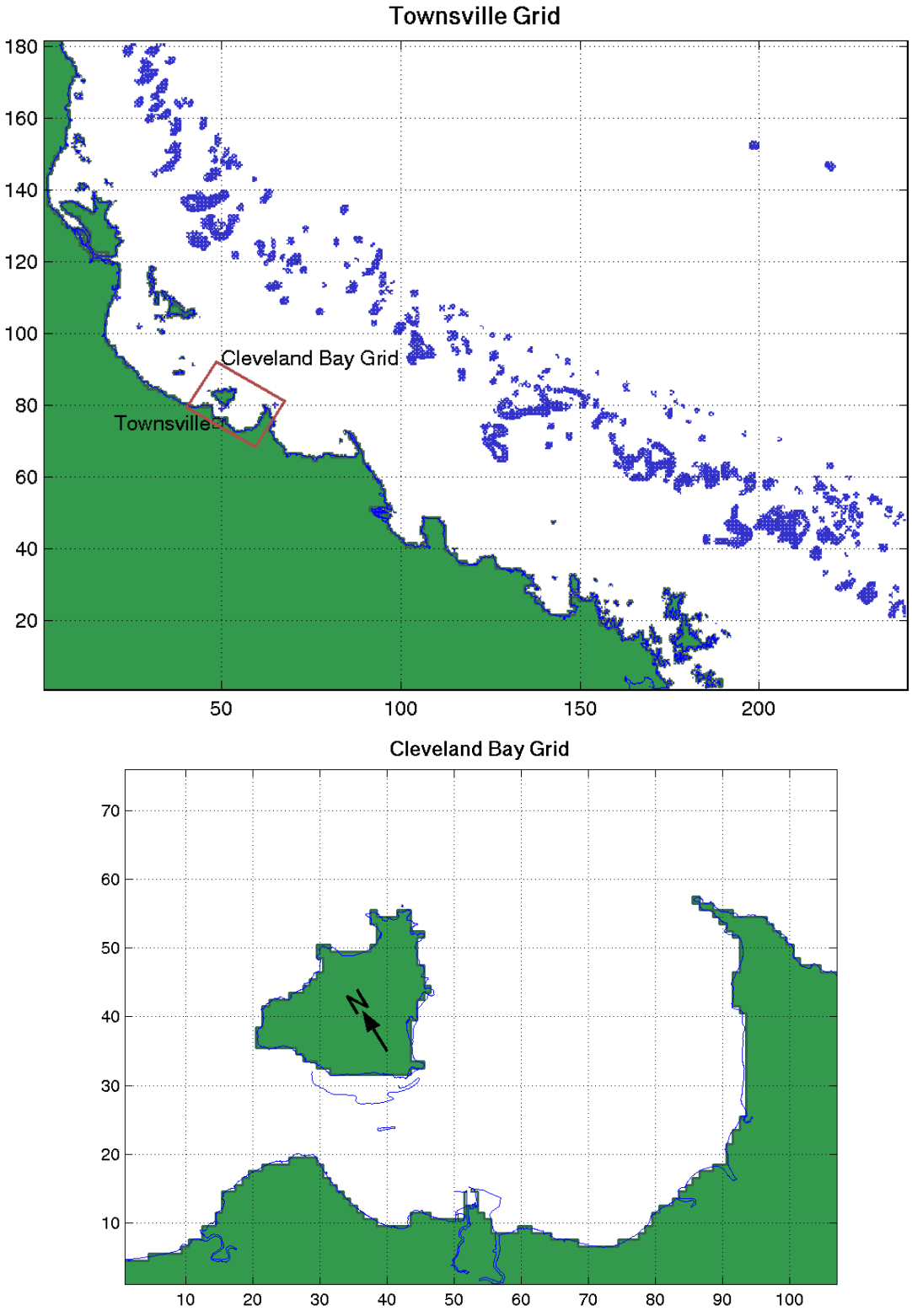

Figure 10.3 Townsville hindcast grids.

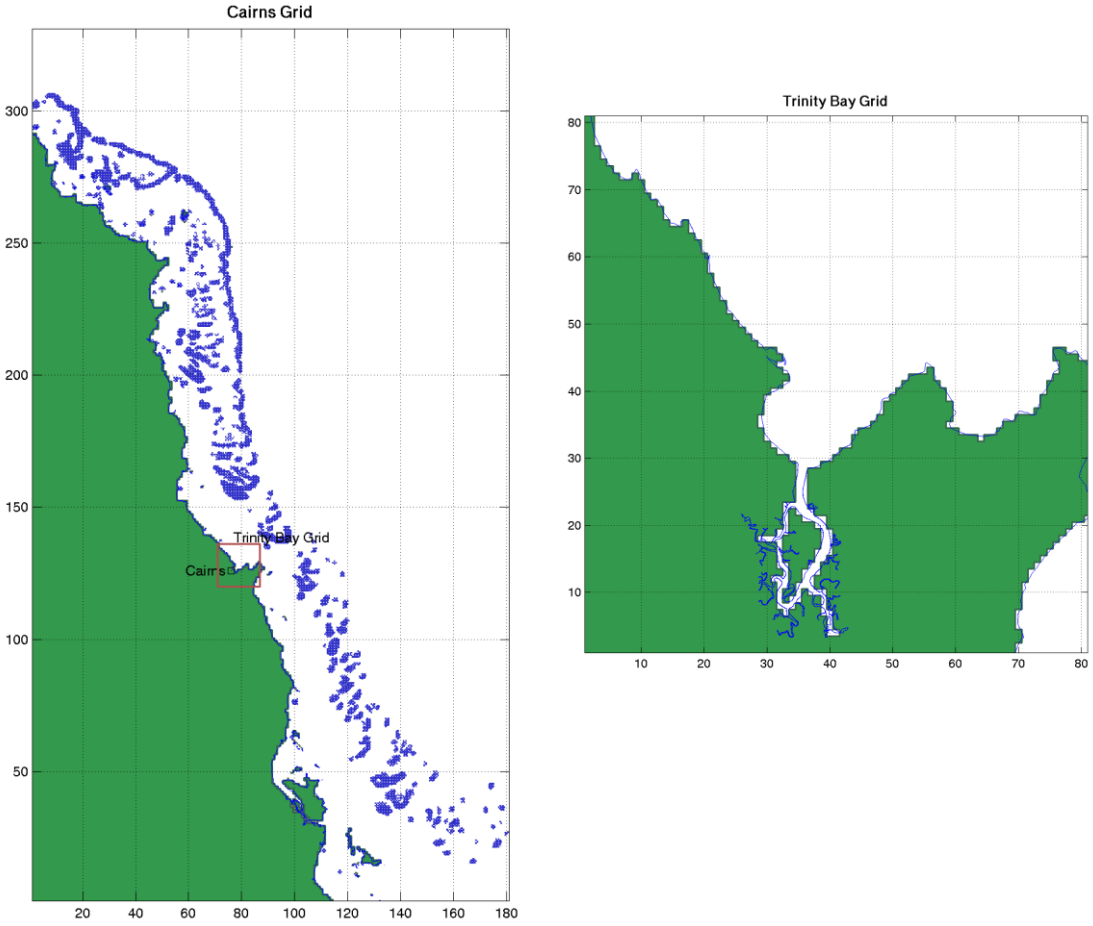

Figure 10.4 Cairns hindcast grids.

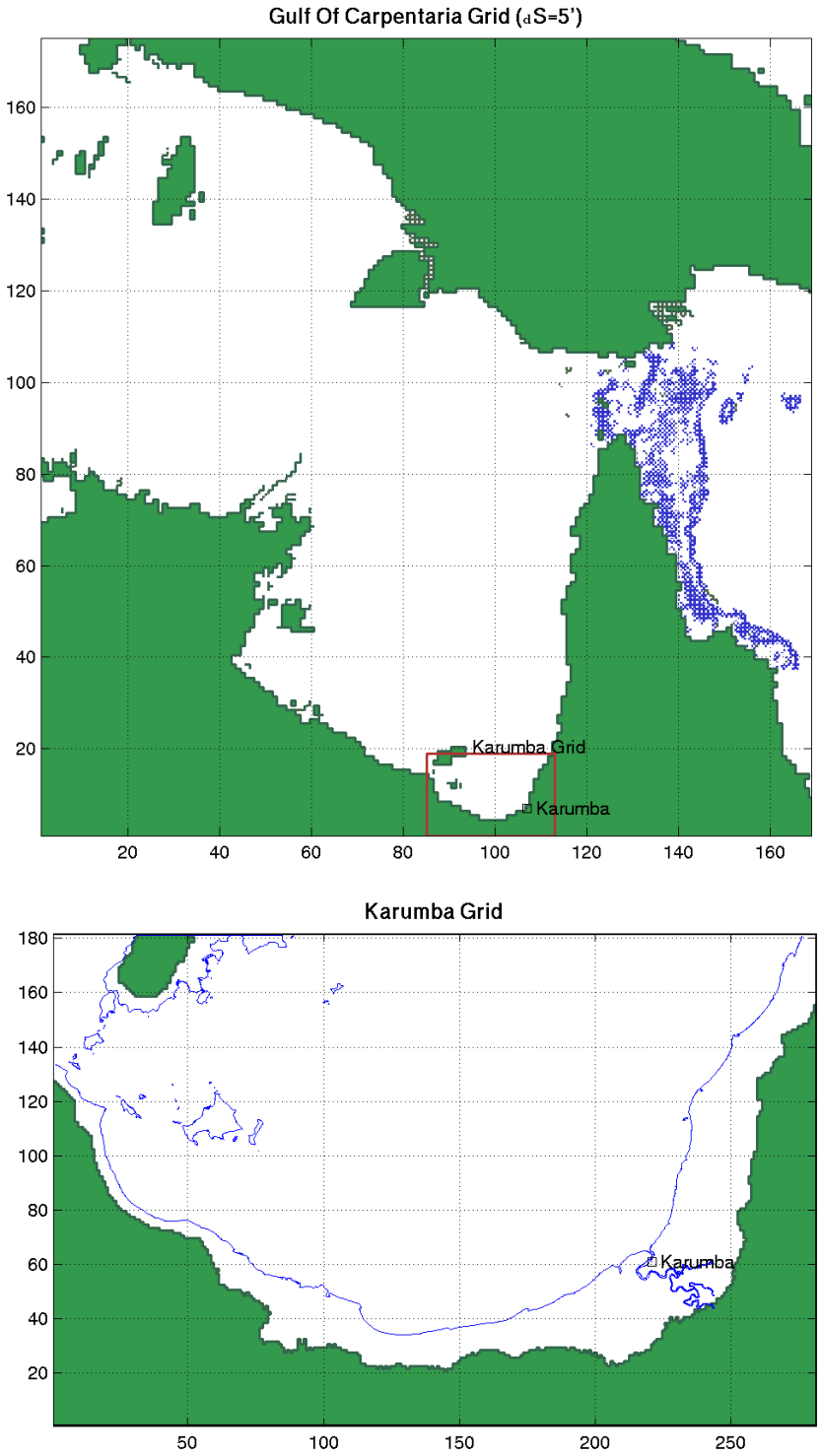

Figure 10.5 Gulf of Carpentaria hindcast grids.

10.3 The January 1918 Cyclone at Mackay

This event remains one of the most significant examples of the inundation of an Australian community by an extreme storm tide. However, due to the lack of widespread instrumentation of winds and water levels at that time, many specific details about the track and intensity of the storm and the actual water levels attained remain clouded. It is certain that a very intense cyclone crossed the coast to the north of Mackay on the morning of Monday 21st January 1918. A storm surge inundated the town and nearby beaches at about the same time. As a result of the heavy rain, the river subsequently again flooded the town on the following day. The following reconstruction of the event is based on information gained from only a few key sources but taken together these facts form a compelling and likely scenario of events. A detailed account in Bath (1957) attributed to the Harbour Master states that 14 bodies had been recovered by the 23rd January, with three vessels sunk, another three ashore and all wharves collapsed. The *Daily Mercury* of 28th January reported 20 deaths at that time and Visher and Hodge (1925) records that 30 lives were lost in total.

10.3.1 Available Tropical Cyclone Data

The National Climate Centre official track for this event is scant, essentially based on that of Lourensz (1981) which is probably derived from Bath (1957), at least in part. However, the NCC and Lourensz tracks share an error in the time of landfall which incorrectly has the storm making landfall on the 20th rather than the 21st (EST). This error was also noted by Gourlay and Hacker (1986) who point to the extensive account of events in the Mackay *Daily Mercury* newspaper report of 26th January. The earliest official assessment of the meteorology appears to be that by Bath (1957), who quotes extensively from the log of the Lightkeeper of Flat Top Island, a Captain G. F. Long. The Lightkeeper noted some pressure values and estimated wind speed variously throughout the storm whilst endeavouring to provide shelter to his family. Bath also provides the Post Office barograph and mentions reports by the Postmaster and a private observer - Mr T. *(sic)* Croker (refer later). The Daily Mercury (1918) also mentions a number of observations of atmospheric pressure made by a Mr P. Armati during the passage of the cyclone and some regional pressures are available from the Brisbane *Courier Mail* (Callaghan 2000). No direct wind speed measurements are available for the event but there are a number of pressure data as well as some observations of wind directional changes. Although the Daily Mercury (1918) contains extensive accounts of damage and personal hardships throughout the region, no eyewitnesses speak of experiencing the absolute calm of the eye. However, the later special historical feature (Daily Mercury 1993) does refer to the community experiencing a lull between 7 am and 8 am. It is considered possible that this comment has been "loosely inferred" from an eyewitness account elsewhere in the same issue by a Mr Andrew Fordyce and that the town did not experience a true eye effect. Mr Fordyce was at the Richmond Mill Plantation at the time, which was about 8 km NNW of the town. During the course of this investigation, a letter from the Croker family was provided which described a calm of about half an hour at Eimeo. Bath also reports that T. (*sic*) Croker reported a "sudden lull and the wind soon came from the north". His pressure measurement of 27.54"Hg (932.6 hPa) at about 0730 EST 21/1 (2230 UTC 20/1) is accepted by Bath as the lowest reading made during the event. Another measurement of 27.55"Hg is reported in the Daily Mercury (1993) as being due to the Harbour Master Captain Greenfield but this may simply be repeating the Croker value.

10.3.2 Available Storm Tide Data

There was no automatic tide recording system in operation at Mackay in 1918 and, although a number of tide boards were probably in existence along the river port area, all would have been inundated during the event. This is confirmed by Parkinson *et al.* (1950) which mentions that a visual marker system was first made available in 1928 near Flat Top Island and an automatic recording system at the Outer Harbour in 1939. Some timing and relative water level elevation data during the storm tide can be inferred from the Lightkeeper's account in Bath and from the *Daily Mercury* reports. The newspaper details the experiences of a number of individuals who were impacted by the storm tide both within the town and along the nearby coast. Some personal statements were also made available from survivors of the event that had been obtained during earlier historical investigations into flooding in the Pioneer River (Gourlay, *pers. comm.*). Based on all of the reports it is clear that the storm tide reached upriver to approximately the position of the Customs House located on the riverbank at the corner of Sydney St and River St (formerly North St). This is also the position of the Forgan Bridge. The most definitive peak water level value is first mentioned in a State Government report to Parliament (Harbours and Rivers Department 1918). The report states that the sea surface "*slowly rose for about an hour, reaching a height of 7 feet 9 inches above highest spring-tide level; it remained stationary at that height for about 10 minutes, and slowly fell again*". Besides the above, there is no specific detail provided of the event. Parkinson *et al.* (1950) is the next available reference - which states that sea water rose "*approximately 8ft above high water level*", thus according with the earlier value. However, neither reference allows recovery of a specific level without knowledge of the actual tide datum being referenced. Although the Parkinson report focuses particularly on river flooding it does include a map (Plan No. 14) which indicates the extent of seawater inundation during the 1918 event. This is reproduced in Figure 10.6 courtesy of AGSO (Granger, *pers. comm.*) where the original map has been digitised and the locations of known deaths due to drowning have been marked by AGSO.

This inundation line is shown as being slightly above the 17 ft ground contour on State Datum in the vicinity of the Customs House. Converting 17 ft to AHD yields a level of 5.35 m, which has been variously quoted as the actual peak level for the event. Unfortunately Parkinson does not quote a specific level and no description of exactly how the map levels were obtained is provided. It can only be assumed that all of the *Daily Mercury* reports were available and that the Harbour and Rivers Department level was used in some way. Indeed, the *Daily Mercury* and other eyewitness reports are certainly broadly consistent with this map. Work by Gourlay and Hacker (1986) however, is able to shed some light on the likely "*highest spring-tide level*" datum quoted by Harbour and Rivers, whereby a *Standard High Water Level (SHWL)* was used on charts from 1886 to 1930. This level, peculiar to Mackay, is now known to be 3.14 m AHD. Adding the 7 feet 9 inches to this level yields 5.50 m AHD (or 5.33 m on the old State Datum, being 17.5 ft). Accordingly, it is determined that 5.5 m AHD should be regarded as the highest inundation level due to the storm tide. This puts much reliance on the admittedly brief but vivid description given in the Harbour and Rivers report. However, it also acknowledges that this was reported and published in the actual year of the event and stated with some certainty by a technical source charged with the maintenance and navigation of the port. It is also likely that the closeness of the peak level to the Customs House benchmark probably greatly assisted in the recovery of such a level during the confusion of the disaster. For example, the consequent river flood two days later reached a slightly higher level (Gourlay and Hacker 1986), thus obliterating the storm tide debris lines.

The map by Parkinson remains as probably the most comprehensive record of the inundation by the storm tide but should be taken with an official peak level of 5.50 m AHD.

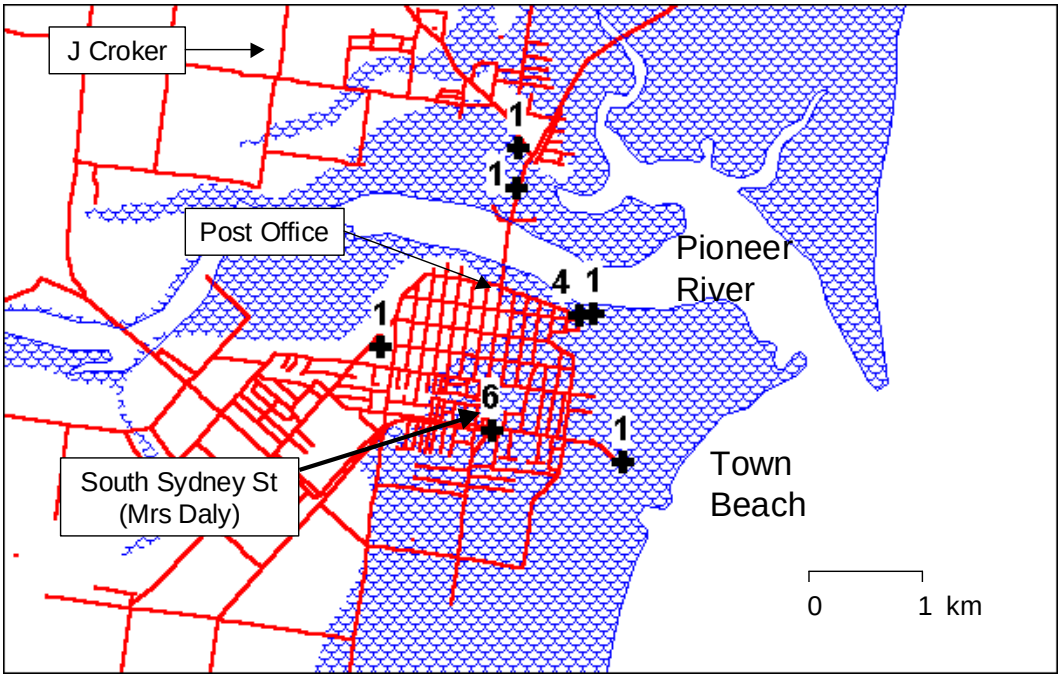

Figure 10.6 Extent of inundation due to the storm tide during *Mackay 1918*

(after Parkinson 1950, and AGSO 2000)

It should be noted that the Queensland Regional Office of the Bureau of Meteorology has in its archive a hand-drawn facsimile of the water level trace during the event together with the predicted tide. Clearly no such record existed and it is concluded that this was created to provide an illustration at some time to match the quoted 5.35 m peak level (possibly by Herbert Wittingham).

Taking all of the above into consideration, Figure 10.7 summarises the available data in regard to the magnitude and timing of the 1918 storm tide at Mackay. The predicted high tide on the morning of 21st January was 1.98 m AHD at 0630 EST (Broadbent 2000). The peak level of 5.5 m is shown nominally occurring at 7 am EST (2100 UTC) which is consistent with eyewitness accounts from the Daily Mercury (1918, 1993) where it was variously reported that the surge arrived quickly (in the town) at about 5 am (1900 UTC) and subsided about 9 am (2300 UTC). This may be assumed the approximate period where the water levels exceeded HAT, at which point some properties would have experienced initial flooding. The 7 am peak timing is also consistent with the Harbour and Rivers report of "*slowly rising over an hour*" if taken relative to exceeding HAT. Another report, apparently closer to the beach, tells of a "wall of water" at approximately 5 am (1900 UTC). Either way, the peak storm tide level apparently occurred close to the time of peak predicted tide, yielding a storm surge plus wave setup component of approximately 3.5 m. Eyewitness reports also described large waves ("rollers") within the town with heights of the order of 2.5 m to 3 m. Certainly this would have been possible in some areas since the depth of inundation above HAT was about 2 m. A number of houses were displaced from their piers and either destroyed or floated some distance from their property and the wave related debris was significant. Interestingly,

eyewitness accounts south of the town centre reported a general movement of water northwards i.e. towards the river. This would be in the direction of the wind but might also suggest that the river levels were lower at that time.

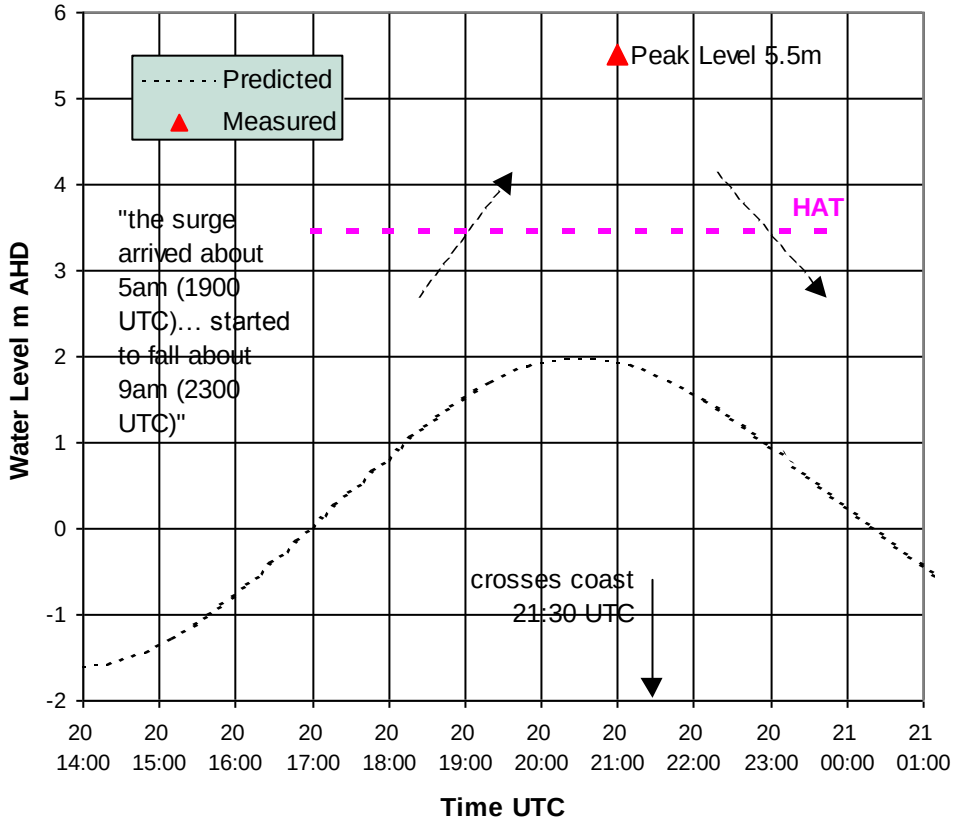

Figure 10.7 Established storm tide information for *Mackay 1918*.

The following account by 89 year old Ethel Daly was taken in 1987 by the Mackay Disaster District Control Group (copy of statement supplied by M.R.Gourlay). Her story as a 21 yr old is typical of many such stories by those who witnessed the event but is especially valuable in terms of the actual impact of the storm tide:

"At the time of the cyclone I was living in South-Sydney Street with friends [approx 1.8 km from the coast and 1.3 km from the river at a ground level of about 3.8 m AHD]. *I was about 5'4" in height* [1.6m]. *The house I was living in was a timber home on four (4) foot* [1.2 m] *blocks made of timber...(with a timber floor). The house was square in shape, divided down the centre by a hallway. A small verandah faced the front of the house on the left hand side. The kitchen was situated at the back left hand side of the house. The back wall was made of iron* [the eastern wall, closest to the sea]. *We called the kitchen and the harness room area the 'Skillion'. The external timber of the home had been cut in the sawmill. The house had an iron roof. I don't know how old the house was but it was in good condition. It was a good and strong house. There were houses on either side of us, but no houses behind. There were houses on the other side of the street* [to the west].

The storm started on the Saturday, with wind and rain. There were very high winds. It rained continuously, and we got 12" in 12 hours. It rained and blew all Saturday and Sunday, but no flood water came into our house. At no time did we go to bed. We were too frightened to go to bed.

At about 1am on Monday morning, the next door neighbours, Mrs Dwyer and three children, came knocking at our door. Their house had collapsed under the force of the wind and the rain. At that point in time there was no major flooding. We made them comfortable and gave them some dry clothes. I made a cup of tea on a primus.

A large piece of timber was blown through the window in the harness room. Bob was holding a cushion from the sulky up against the window trying to stop the rain from coming in.

At about 6.30am on Monday morning I had just finished putting the primus away, and called Bob to come in to us. He came in, and we were all in the dining room.

At that point in time, the back of the house collapsed. The noise sounded like a bomb going off. The entire back wall and the roof had fallen in. Straight away salt water was all around us and inside the house. The collapsed skillion effectively blocked the water from coming in, and water could only come in quickly through the front of the house.

Within seconds the salt water was up to my shoulders in the house. I went straight to the front of the house to try to throw some furniture back into the front door to stop all the furniture from going out through the front door. I was standing near the front door (and) *wedged myself against the door to stop from being washed outside the house. I looked around and saw Mr Lemberg's house collapse and be washed away. Mr and Mrs Harry Kenny's house on the left of our house was washed off the blocks and across the road. The house spun around and landed on Mr McIvor's fence across the road. Mr and Mrs Kenny were still in the house at the time. The Kenny's had to swim from their house to the steps of the McIvor's house.*

The Potter's house was washed off its high blocks. It was spun around and ended up facing the other way towards Juliet Street. I actually saw this occur from the front door.

As I was looking out the door I could see big rollers, just like the open ocean. The waves were about 8 or 9 feet high [2.6 m; local depth estimated as about 2 m at the time] *and were just like the surf at the beach. If I had been out in the street the waves would have been over my head. I was a competent swimmer in those days, but I believe that I could not have swum across the street.*

Inside our house two women and four children sat on the tables, and Bob and I stood in the water for the next five and half hours. In this time the water was all salt water. It took five and a half hours for the water to drop below the floorboards. We then went across the road to Mr Mincher's house and they looked after us. As we walked across the road the water was up to my waist [0.8 m].

The back of our house faced east towards Town Beach. The houses that were washed off their blocks were washed away from the Town Beach direction. There were no houses directly behind us which could have stopped some of the force of the wave. The rollers which I saw were going up Sydney Street in the direction of the river. Mattresses, animals, birds, all sorts of things, were floating up Sydney Street also towards the river."

10.3.3 Reconstruction of the Event

The following describes the methodology adopted in developing a consistent description of the storm parameters. It relies on the available data combined with theoretical spatial and temporal variations in wind and pressure as predicted by an analytical model (Harper and Holland 1999), detailed in Appendix C. The model was systematically adjusted for reasonable values of the key parameters such as track, central pressure and radius to maximum winds. The available information was then compared with the model output to determine the validity of the various assumptions. Consistent with experience from cyclone *Althea* (refer Section 10.4), a windfield asymmetry based on a υ_{max} of 115º was subsequently found to represent the best fit to wind and storm surge results.

10.3.3.1 Synoptic Situation

As reported by Bath (1957), significant Coral Sea activity was noted about 18th January. Figure 10.8 presents Bath's MSL charts for the region for the 20th and 21st, showing the extensive low-pressure development. Ambient surrounding pressure is indicated as approximately 29.75"Hg or 1007 hPa (the summer average) and this value has been used in the present assessment.

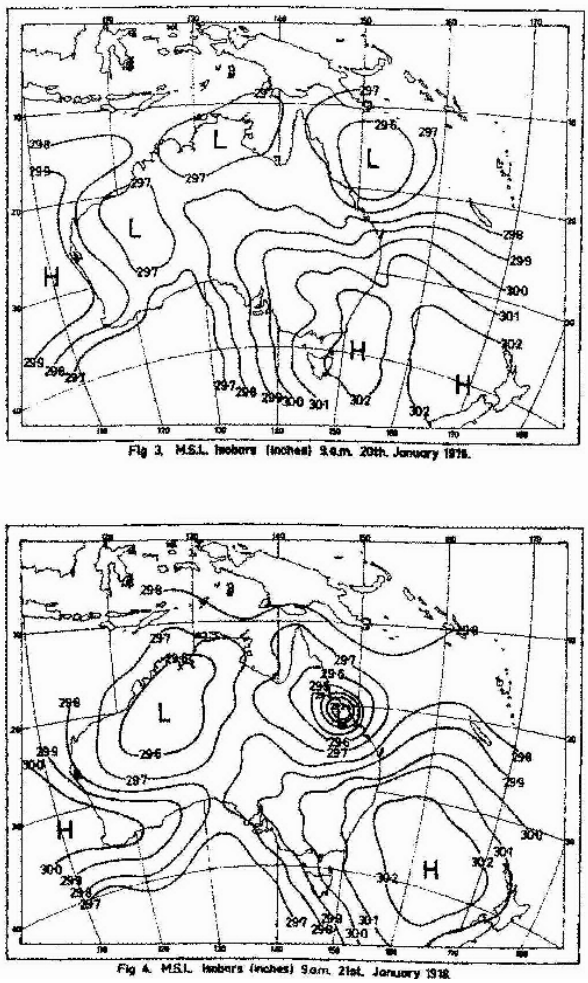

Figure 10.8 *Mackay 1918* synoptic development (after Bath 1957).

Besides the cyclone itself, the synoptic situation included a ridge to the south formed by the interaction with a high pressure in the Tasman Sea. The lifetime track of the storm from Bath (Figure 10.9) shows it crossed the coast near Mackay but continued far westward for several days before emerging across the NSW coast almost one week later.

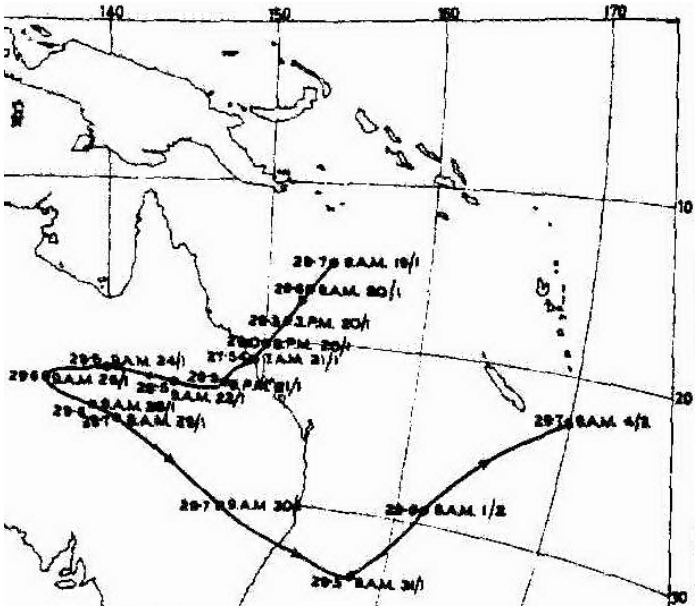

Figure 10.9 *Mackay 1918* storm track (after Bath 1957).

10.3.3.2 Intensity

The Post Office barograph, as given in Bath (1957; *Fig 7*), has been manually digitised on an hourly basis and is reproduced here as Figure 10.10, annotated with other nearby individual pressure values cited in the Daily Mercury (1918). A single reading is attributed to the Harbour Master Captain Greenfield but no timing is available (Daily Mercury 1993). This figure highlights a number of potential inconsistencies between the data that might be attributable not only to the valid spatial separation of the readings but also to the accuracy of pressure and timing values. The latter was undoubtedly somewhat nominal in the circumstances. Firstly, at around 2200 EST (1200 UTC) there is significant variance between Flat Top and Armati on the one hand, and the Post Office and Croker on the other. Of more particular concern though is that all barometers, with the apparent exception of Croker (27.54"Hg) and Greenfield (27.55"Hg), were unfortunately limited to a minimum pressure of 28"Hg (948.2 hPa). The Post Office reached this value shortly before 0600 EST (2000 UTC) and remained there for about 1 h, hence not recording the minimum pressure. Meanwhile, the pressure at Flat Top island was also noted to have bottomed at 0600 EST (2000 UTC) while Armati noted the same value at 0730 (2130 UTC).

In regard to spatial variability, Flat Top Island is located approximately 6.5 km ESE of the Post Office. It is noted from an advertisement in the *Daily Mercury* that a P. Armati was a "chemist and optician" and his plight in regard to the storm surge is mentioned in the eyewitness accounts therein. It is assumed that his pressure measurements were made within the town. The reading attributed to Greenfield (Daily Mercury 1993) was not cited by Bath

and is not mentioned elsewhere in the extensive descriptions which feature the Harbour Master and his actions and responsibilities. It is also likely that the Harbour Master's Office and/or residence was located near the Government Wharf, which was badly inundated and unlikely to have been the source of a barometer measurement. It is therefore considered possible that Greenfield, if correctly quoted, may have simply repeated the Croker value. Meanwhile, Bath notes that the Croker residence was located "3 miles from Mackay on the north side of the river". In an attempt to better locate this position, descendants of the Croker family were located by telephone, namely Mr P. Croker of Caloundra and Mr R. Croker of Bucasia, who are grandsons of Mr James Croker - an early dairy farmer in the region. His home ("Bona Vista") was situated on the top of a hill overlooking the Gooseponds area, in a suburb now known as Mount Pleasant and is about 3 km NW of the Post Office. Bath, who refers to a "T" rather than a "J" Croker, makes no mention of the need to adjust Croker's pressure values for height. The hill was approximately 50 m high (confirmed by K. Granger using AGSO elevation data) and would therefore have an offset of about 5 hPa relative to MSL. Given this significant elevation offset and the generally high level of awareness of such matters at the time, it is thought that the reported values are almost certainly MSL adjusted (Callaghan 2000). The lowest reading by Croker of 932.6 hPa must therefore be regarded as at least indicative for the event. However, because a full calm was not reported by Croker, the central pressure was clearly something less than this value and a nominal value of 930 hPa has been adopted for hindcast purposes.

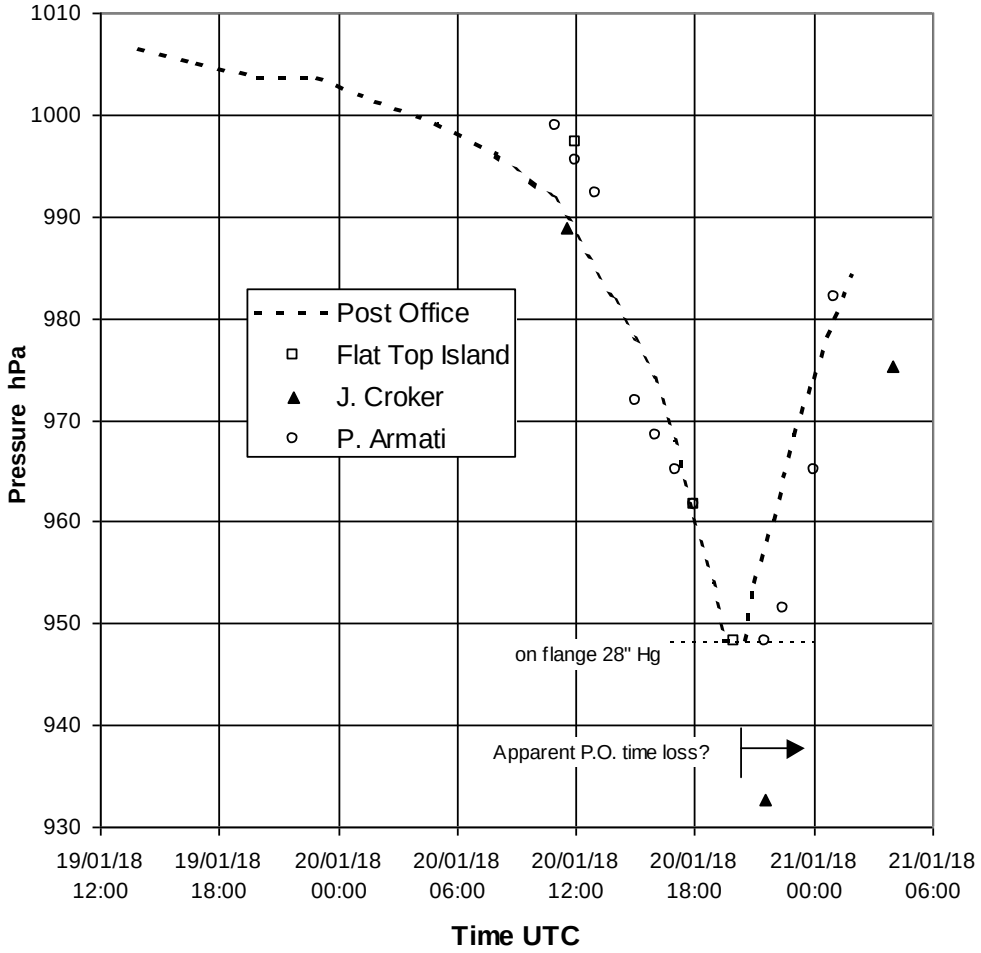

Figure 10.10 Collective pressure observations during *Mackay 1918*.

10.3.3.3 Timing

The likely timing of the passage of the storm was addressed next. Besides the gross error in the NCC track, no detail was available between a 2300 UTC fix of the storm on the (as corrected) 19th and the first overland fix 1 day later. Davidson *et al.* (1993) corrected the timing error and put the position at 0000 UTC 20/1 near 18.3ºS 152ºE with a constant track and speed to the coast, with the next position approx 30km inland at 21ºS 149ºE exactly 24 h later at 0000UTC 21/1. Taking a combination of the Davidson *et al.* and NCC starting points gave a nominal 0000 UTC 20/1 fix at 18.5ºS 152ºE, which is slightly to the south of Bath's track. The timing of the close approach was then assessed based on a combination of the pressure readings from the various sites and also the observed changes in wind direction at Flat Top Island and by Croker (when noting a "sudden lull"). The Davidson *et al.* inland fix was then brought forward 1.5 h to apply at 2230 UTC on the previous day rather than 0000 UTC.

The Post Office barograph timing was discounted because the pen settled on the instrument flange shortly before 0600 EST (2000 UTC) and there is an apparent timing error on the rising trace when compared with the 0730 EST (2330 UTC) Flat Top reading and also Armati's manual observations. It is considered possible (Callaghan 2000) that the instrument rotation was actually slowed by the pen resting on the flange and resulted in an apparent time gain on the rising trace, leading to the perception that the minimum pressure occurred earlier than at the other sites.

10.3.3.4 Distance

Clearly, the storm passed quite close to Mackay and on the northern side. Mr Peter Croker of Caloundra was able to quote from a letter written by his mother-to-be who was with a party staying at the Eimeo Hotel and, as reported in the Daily Mercury (1918), walked to "Bona Vista" later that day. In her letter, she described a calm of about half an hour at Eimeo. The Daily Mercury (1993) report by Fordyce indicates his experiencing a full calm at Richmond Mill Plantation that ended around 9 or 10 am, but no duration was given. Some guidance is also provided by noting that there were no other reports in the Daily Mercury (1918) of experiencing an eye from any of the other isolated small coastal settlements such as Slade Point or Blacks Beach. Moreover, these sites reported experiencing significant surge effects, suggesting a coastal crossing somewhere still further to the north, but apparently not as far as Seaforth, where another party of eyewitnesses not reporting a calm were situated. As a result of various sensitivity tests, a nominal +0.1 deg latitude shift was made to the Davidson *et al.* (1993) initial land fix. This resulted in a closest approach to the Mackay Post Office of 23 km at 2100 UTC 20/1, essentially being the time of landfall near Sand Bay, a sparsely settled area which is about 10 km west (and slightly north) of Shoal Pt. The full passage of the calm would have been about 1 h, making the Eimeo report consistent with being towards the southern edge of the eyewall and the Croker "sudden lull" consistent with clipping the southern edge only. On this basis, the model predicts that Seaforth might have experienced a similar lull to Eimeo and Richmond Mill Plantation may have had a longer lull because of the reduced inland winds, but not necessarily a complete calm. This is slightly at odds with the Richmond Mill account of a full calm which was apparently long enough to permit having breakfast, but the local wooded terrain may have contributes to lower wind speeds. Why some of the more inland communities such as Hatton did not report experiencing a calm still remains a mystery, but reports may have been suppressed by the sheer level of devastation suffered and a public lack of understanding of the structure of tropical cyclones.

10.3.3.5 Phasing

As noted earlier, little guidance was available in regard to the storm track as it approached the coast. Initial trials using a single offshore fix and a single onshore fix provided consistency amongst the various pressure measurement sites only at the time of closest approach. At other times, difficulties were experienced in matching the shape of the pressure trace, especially in matching the initial depression and then also the rapid descent to the minimum. One of the main difficulties appeared to be that the simple 2-point track placed the storm centre too far offshore about 12 h before landfall. Based on trial and error, an intermediate fix was then devised which placed the centre at 20°S 150.2°E at 1100 UTC on 20/1, still on a straightline approach but approximately 3.5 h earlier than the 2-point fix track. This provided a better fit to the early stages and provided greater scope for a steeper pressure profile near the eye.

10.3.3.6 Radius to Maximum Winds and Wind Profile Peakedness

The Holland analytical wind and pressure model uses a radius to maximum wind (R) and a wind profile peakedness parameter (B) to spatially vary wind speed, direction and pressure at any point relative to a storm centre. Based on the foregoing assessment of peak intensity, timing and closest approach, various combinations of R and B (or rather B_0, refer Appendix C) were systematically trialed and comparisons were made with the data. These changes were not made in isolation but rather integrally with the foregoing assessments and, based on this approach, an R of 40 km and a B_0 of 7.4 (B of 1.6) were selected as a reasonable compromise between peak error and bias error amongst the various sites, allowing for the "bottoming out" of several readings. This produced a relatively steep wind profile that is generally consistent with the visually observed winds at Flat Top Island.

10.3.3.7 Final Track Parameters

Table 10.5 summarises the final storm parameters, while Figure 10.11 shows the track and predicted wind and pressure field as the storm made landfall. Note that there is little benefit in assuming the storm was changing its central pressure or its radius on approach to shore and there is no supporting information either way. Given the extent of the synoptic feature it is likely that the storm was relatively mature during this phase. Maintaining the pressure after landfall is less supportable but is retained here on the basis that emphasis is on the prediction of the storm surge. Many reports also suggest that the highest winds were experienced from the north and north-east, i.e after landfall. With θ_{max} of 115º the analytical model does lend support to these observations, although the increased winds may equally have been caused by coastal convergence effects. Alternatively, this observation may have in part been due to a sudden increase in damage as a result of the wind direction having changed - it is likely that many buildings had "strain hardened" against the earlier wind direction but then were attacked from the other quadrant.

Table 10.5 Adopted hindcast parameters for the January 1918 cyclone.

Track Fix			Speed	Bearing	Central Pressure	Radius	Peakedness
Time	Lat	Long	V_{fm}	θ_{fm}	p_0	R	B_0
UTC	°	°	m s^{-1}	°	hPa	km	
20/01/1918 00:00	18.0	152.5	6.4	228	930	40	7.4
20/01/1918 11:00	20.0	152.2	4.4	228	930	40	7.4
20/01/1918 22:30	21.1	148.9	8.1	228	930	40	7.4
22/01/1918 00:00	22.8	142.0	8.1	255	930	40	7.4

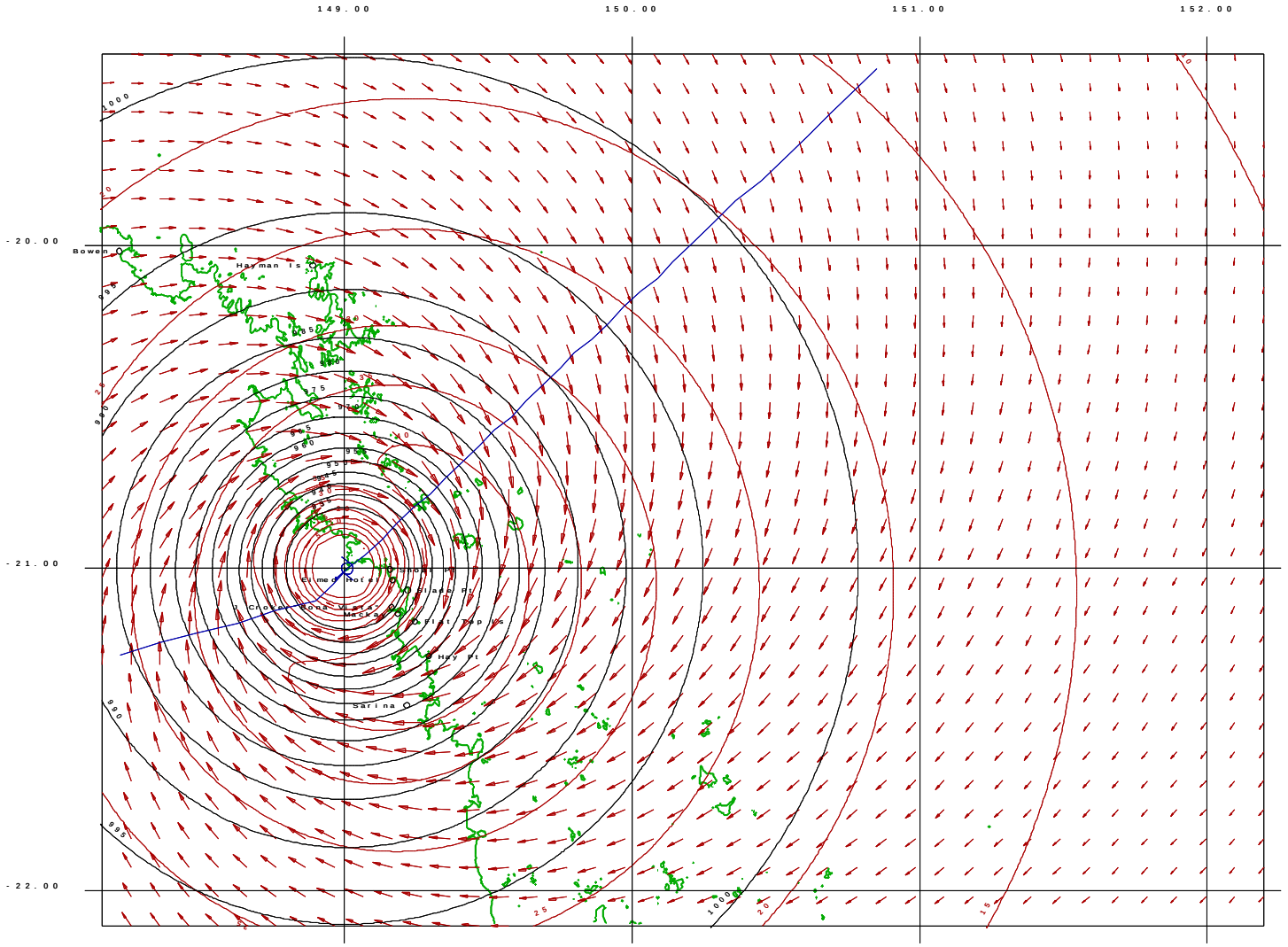

Figure 10.11 Reconstructed cyclone track and wind and pressure fields at landfall for *Mackay 1918*.

10.3.4 Model and Data Comparisons

Figure 10.12 presents the comparison between the observed pressure values and the modelled pressure variation at the various locations as a function of time. The observer positions are listed in Table 10.6 below.

Table 10.6 Observer locations during *Mackay 1918*.

Location	Lat	Long
	o	o
Mackay P.O.	-21.14122	149.18408
Flat Top Island	-21.16395	149.24556
J. Croker	-21.12056	149.16434
P. Armati	-21.14122	149.18408

The key reference pressure is the 0730 EST value of 932.6 hPa reported by Croker during a "sudden lull" around 0730 EST. However, good model agreement can be seen on the falling pressure trace at Flat Top Island and the rising trace for Armati. The Post Office trace appears to lead the model result on the downward trace, followed by the apparent "time loss" indicated by the narrowness of the measured trace near minimum pressure relative to the modelled trace and Armati. The relatively low pressure reported by Croker at 1400 EST in the afternoon remains inconsistent with any other locations and may be a typographical error in Bath (1957).

Figure 10.13 next compares estimated mean wind speed and direction at Flat Top Island and Croker locations against the model result. Firstly, the wind values at Flat Top are visual only and merely approximate values based on gale force (17 m s^{-1}) and hurricane force (34 m s^{-1}) as reported by the Lightkeeper. Values shown in excess of hurricane force here are nominal only, in response to the reports indicating "even greater" etc. Nevertheless, allowing for some overestimation by the Lightkeeper in response to the gustiness of the wind, the model comparison is quite reasonable. Likewise, the wind direction comparison is quite good. The same results for the Croker location are without the benefit of wind estimates except for the reported lull at time of minimum pressure. The model indeed indicates some eyewall effects at this time, which is consistent with Croker's note. Likewise, the directional change reported by Croker is well represented by the model. Also shown on this figure is the modelled wind at the location of the Eimeo Hotel where an extended lull of about half an hour was reported.

The 0900 EST 21/1 pressure value of 987.8 hPa from Bowen, some 160 km to the north of Mackay is overpredicted in this assessment, which concentrates on the inner vortex shape. Pressures at Rockhampton also show the effects of a ridge extending along the coast, which would have strengthened the SE winds ahead of and probably during the cyclone's approach to the coast. For wave prediction purposes, it would be advisable to try to match these two remote pressure values but for storm surge purposes, the nearer sites are preferred.

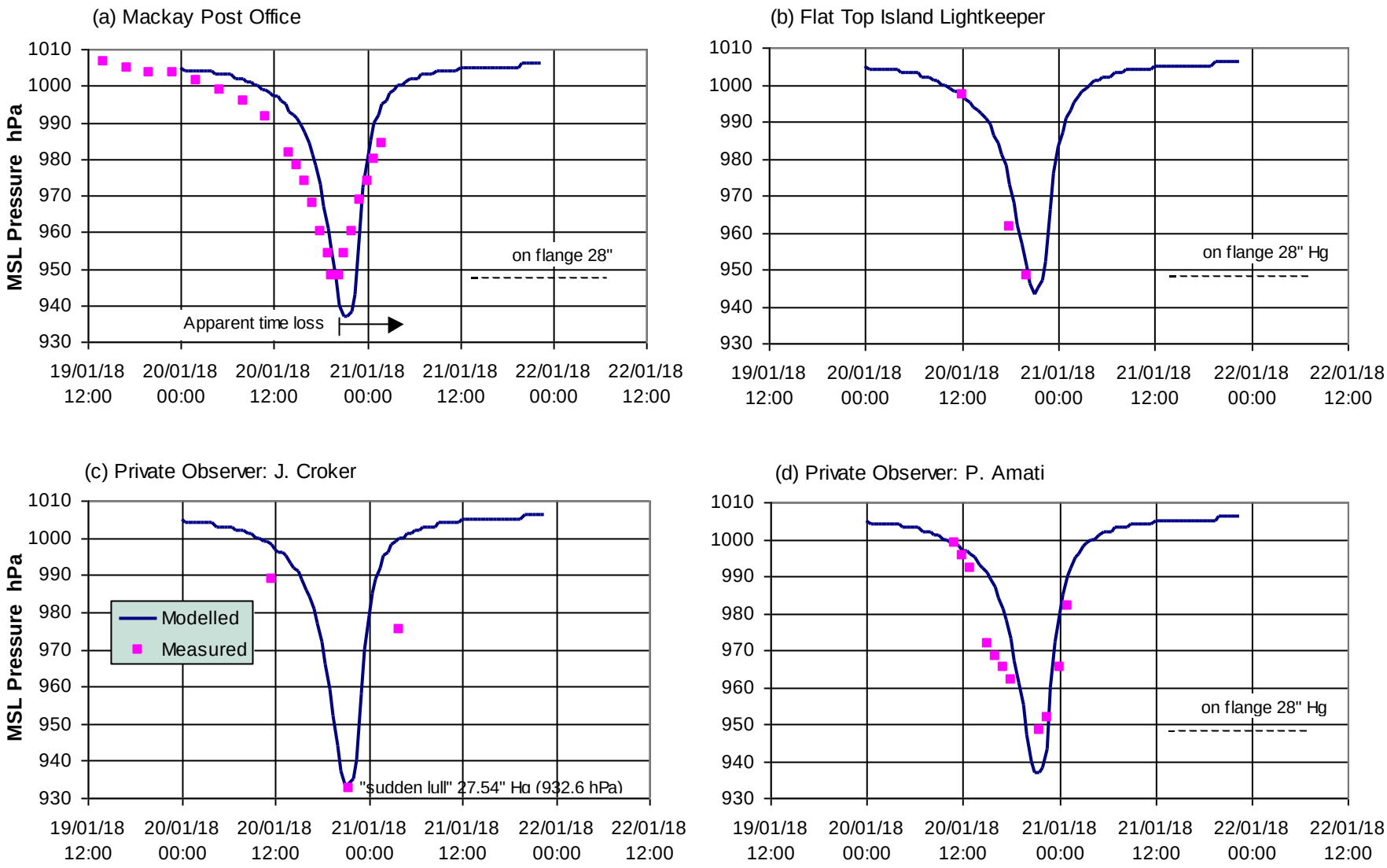

Figure 10.12 Comparison of modelled and measured pressures for *Mackay 1918*.

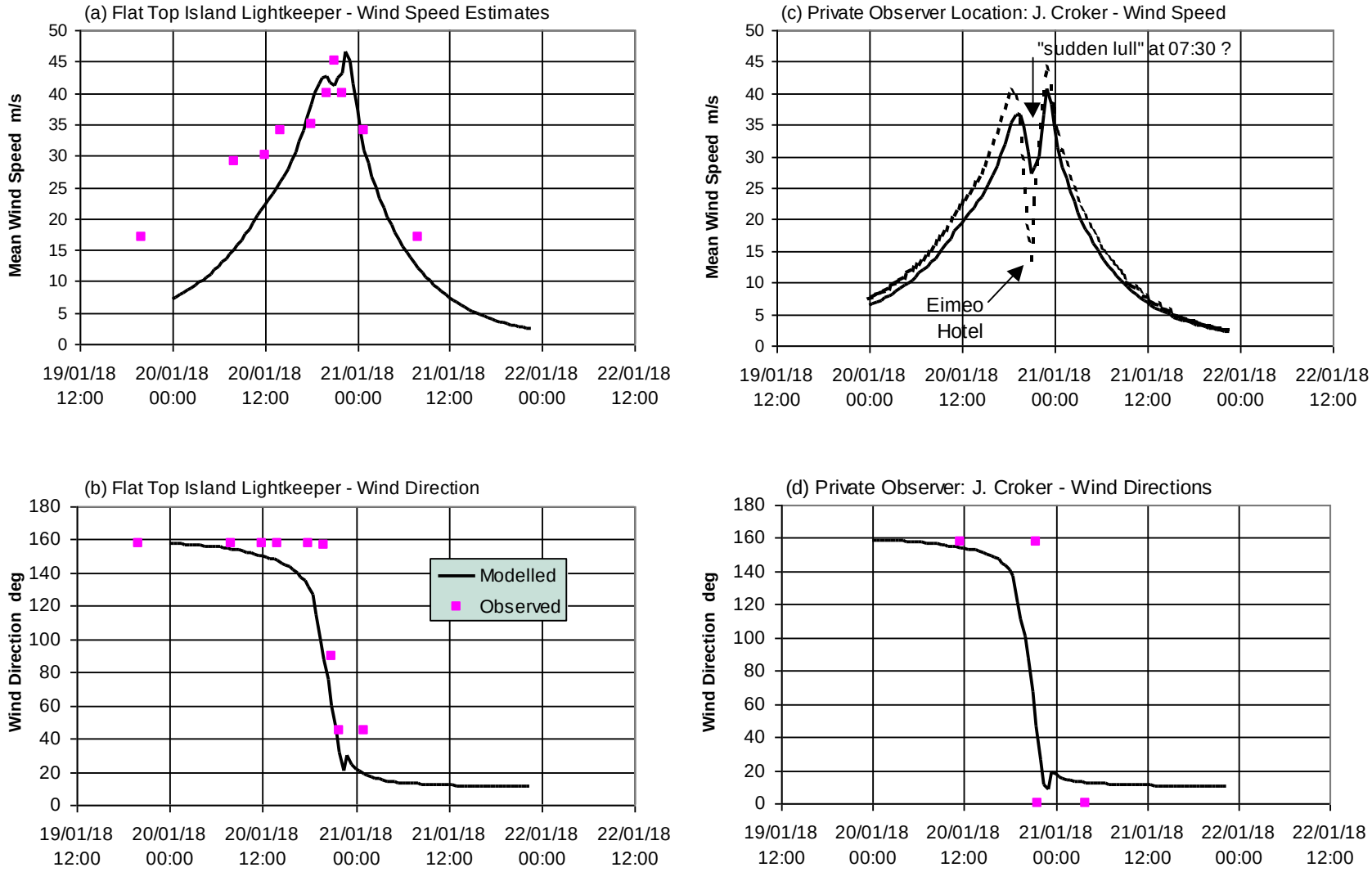

Figure 10.13 Comparison of wind speeds and directions for *Mackay 1918*.

10.3.5 Implications for Storm Surge Modelling

The 1918 cyclone at Mackay was clearly a quite large storm, the estimated radius of 40 km being on the high side relative to more recent events. It is also likely that it was undergoing a series of eyewall replacements such that the radius was shrinking towards landfall and that some coastal convergence effects also impacted the region. The central pressure may also have been slightly lower than 930 hPa but time was not available in the present investigation to pursue any more potentially viable sets of parameters.

In Figure 10.14 below, the modelled envelope of maximum winds shows the extreme band of onshore winds that would have acted to produce the extreme storm tide along the coast. The wind direction coincided with the open SSE fetch south of the Swain Reefs to also allow generation of extreme waves, thus adding to the storm tide level along the open coast.

The effect of the ridge to the south of Mackay may have also added to the surge potential on the day with at least 5 hPa additional gradient over that supplied by the vortex alone between Mackay and Rockhampton.

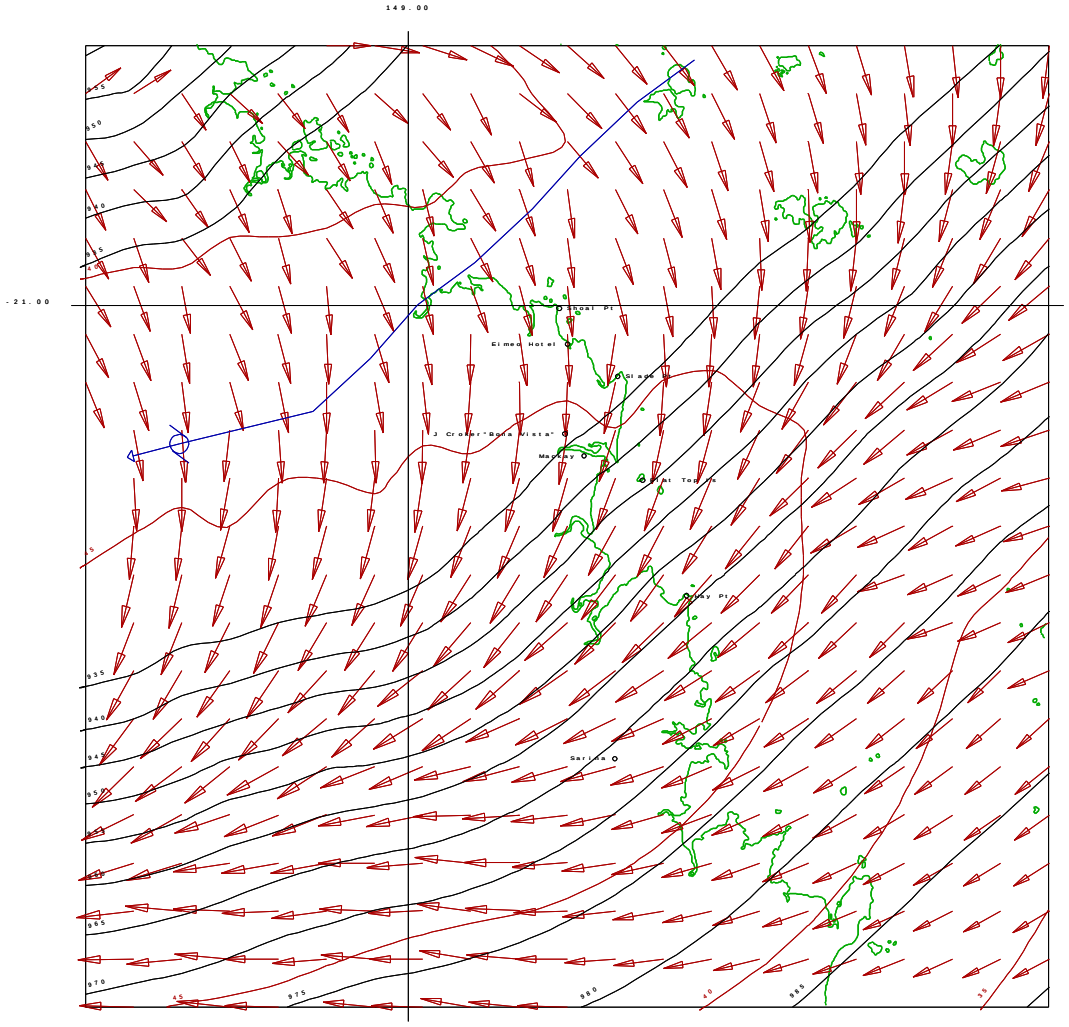

Figure 10.14 Modelled envelope of maximum winds and minimum pressure for *Mackay 1918*.

No wave modelling has been undertaken for the present investigation, but representative values are available from Harper (1983) - the spectral wave model study for the Half Tide Tug Harbour near Hay Point, south of Mackay. In that investigation a selection of model cyclones was considered and two cases of landfall near Mackay are relevant: 925 hPa on a W track and a 950 hPa on a SW track. Considering the 1918 event as a 930 hPa storm on a SW track, an indicative nearshore (< 5 km, 12 m depth) wave condition would be 7 m H_s with 8.5 s T_p. Applying Equation (8.19) then provides an order of magnitude estimate for shoreline setup of about 1 m at Far Beach.

Given that the peak water level reached at the town was 5.5 m AHD on a nominal 2 m AHD tide, and neglecting any other possible losses, the surge-only component could be as low as 2.5 m AHD at Far Beach, giving a SWL of about 4.5 m AHD. However, the extent to which wave setup in the river might have existed relative to Town Beach remains problematical because the river mouth at the time was a mixture of natural sand bars and some training walls designed to maintain a channel for navigation. It is also possible that there were overland flow losses from the sea to the town centre, justifying perhaps a nominal reduction over that distance. Accordingly, a storm surge component closer to 3 m (yielding 5 m AHD SWL) might be indicated, to which wave setup of at least 0.5 m is to be added.

10.3.6 Tidal Modelling

As mentioned previously, extensive tidal modelling has previously been undertaken for this complex tidal region by James Cook University and 11 tidal constituents are used on the open boundaries. Figure 10.15 below shows the comparison between the predicted tide[3] (Broadbent 2000) at Mackay Outer Harbour and the modelled tide. On the day of the storm tide the peak is particularly well matched, although the model tends to underpredict the low water levels. The modelled high tide of 2.01 m is 0.5 h ahead of the predicted maximum value of 1.98 m.

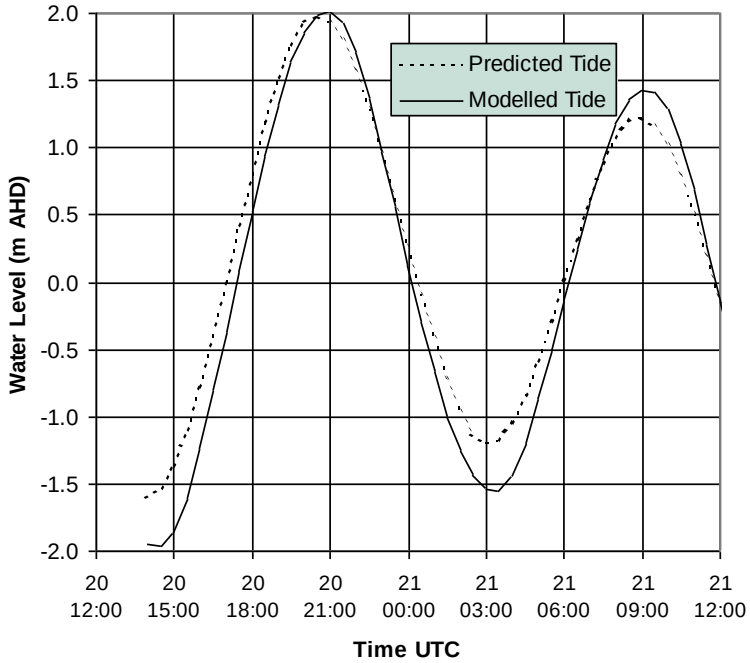

Figure 10.15 Comparison of modelled and predicted tide during *Mackay 1918*.

[3] It is also possible that the supplied predicted tide is subject to some error (J. Broadbent, *pers comm*)

10.3.7 Storm Surge Modelling

The model was first tested without tide effects. To illustrate the role of the open sea boundaries, Figure 10.16 shows surge levels 14 h before landfall when the cyclone is still in deep water and surge levels everywhere are dominated by the inverse barometer effect. The lack of significant distortion of the contour lines near the open boundaries suggests that the inverse barometer effect also dominates the surge in deep water (note this is not a nested grid). Therefore, the outer grid in a simulation sequence of nested grids should have open boundaries in deep water wherever possible. This "no tide" simulation yielded a peak storm surge at Far Beach of 3.72 m at 2000UTC 20/1, with 3.38 m near the Pioneer River mouth.

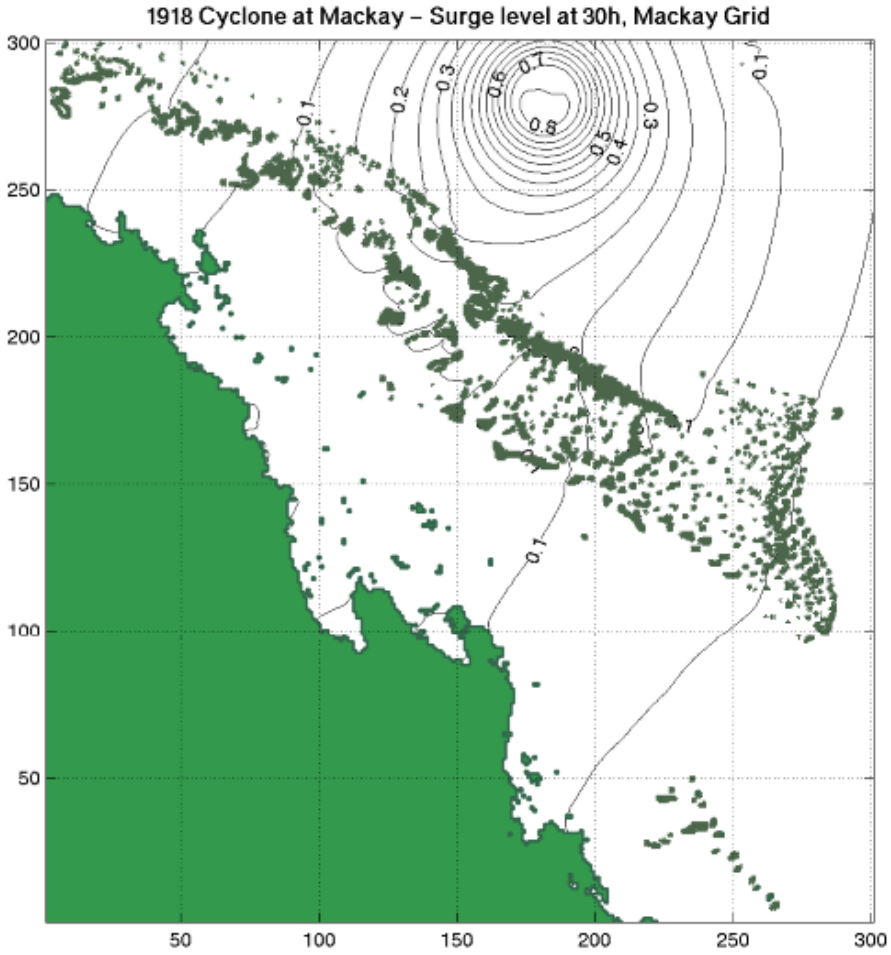

Figure 10.16 Water levels prior to storm landfall (no tide case) for *Mackay 1918*.

Figure 10.17 shows the situation when the tide is included and the storm is close to landfall. The highest modelled water level is now 5.28 m AHD at Far Beach at 2030 UTC 20/1. This agrees well with the maximum estimated water level of 5.5 m. Near the mouth of the Pioneer River the peak water level is slightly lower at 4.97 m. No overland flooding has been used in these simulations, due to a lack of data within the time available, but its inclusion would likely reduce the peak coastal water levels slightly, depending on the area of land flooded at these water levels.

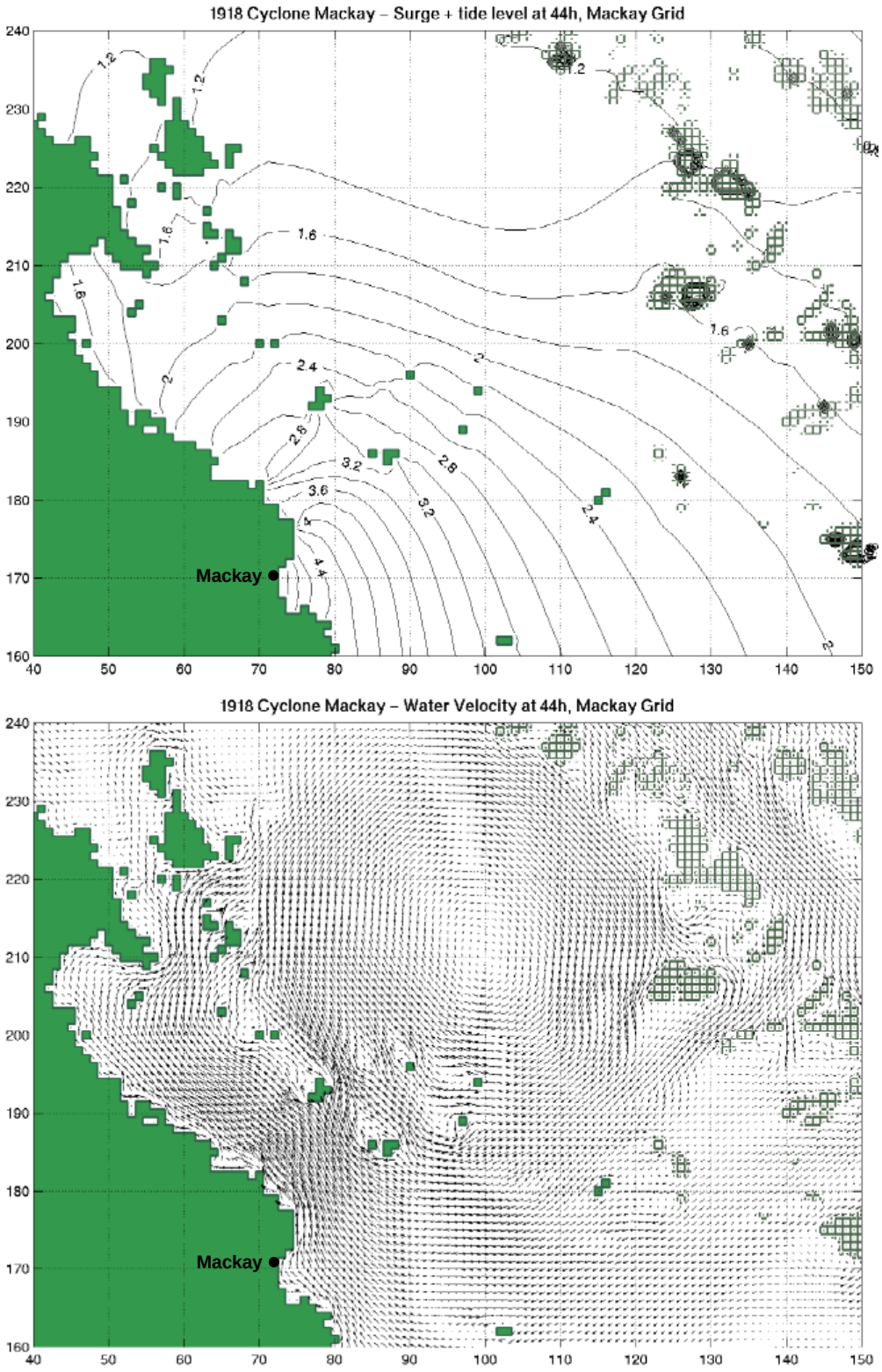

Figure 10.17 Storm tide elevations and velocities at landfall (tide included) for *Mackay 1918*.

The maximum storm *surge* in this case (i.e. total water level - tide) at Far Beach is 3.29 m, 0.43 m below the surge without the tide (a 12% reduction) due to the nonlinear interaction of the surge and tide. Because the tide level was rising as the storm approached the coast, the surface wind stress effect was slightly less in the deepening coastal waters. If the cyclone had arrived at low tide, the *surge* component may have increased but the total storm tide level would have been much reduced.

The results of the simulations are summarised in Figure 10.18, comparing the modelled levels with the estimated value of inundation in the town and the reported timing of the onset of flooding (i.e. levels above HAT). Considering the poor storm data available, the agreement is very satisfactory and is consistent with a potential wave setup component of at least 0.5 m needed to reach the 5.5 m AHD town level. Also of interest is the model prediction that water levels to the south are slightly higher than to the north, supporting the eyewitness accounts that the surge first entered the town from the south-east and then flowed northwards towards the river.

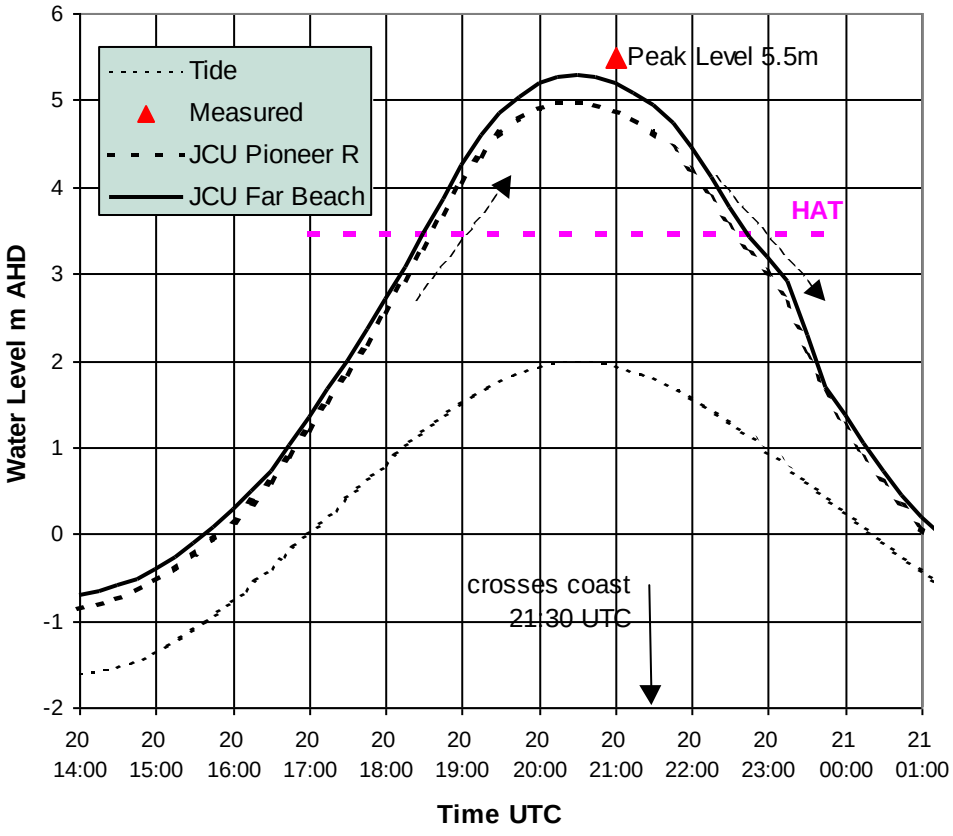

Figure 10.18 Time history comparisons of modelled and measured water levels for the *Mackay 1918* cyclone.

A further model test was then undertaken to determine the effect of the Great Barrier Reef on the predicted storm tide levels at Mackay and the results are summarised in Figure 10.19. Firstly, the difference between the surge magnitudes alone, with and without the reef present, show a small reduction of only 0.1 m (this adds the modelled surge at MSL to the predicted tide). Hence, the surge is mainly generated inside the reef on the relatively broad continental shelf that extends to the south east. However, if the tide is also modelled but without the reef

present, the total water level is about 0.4 m lower because the tide is significantly affected by the presence of the reef in this area.

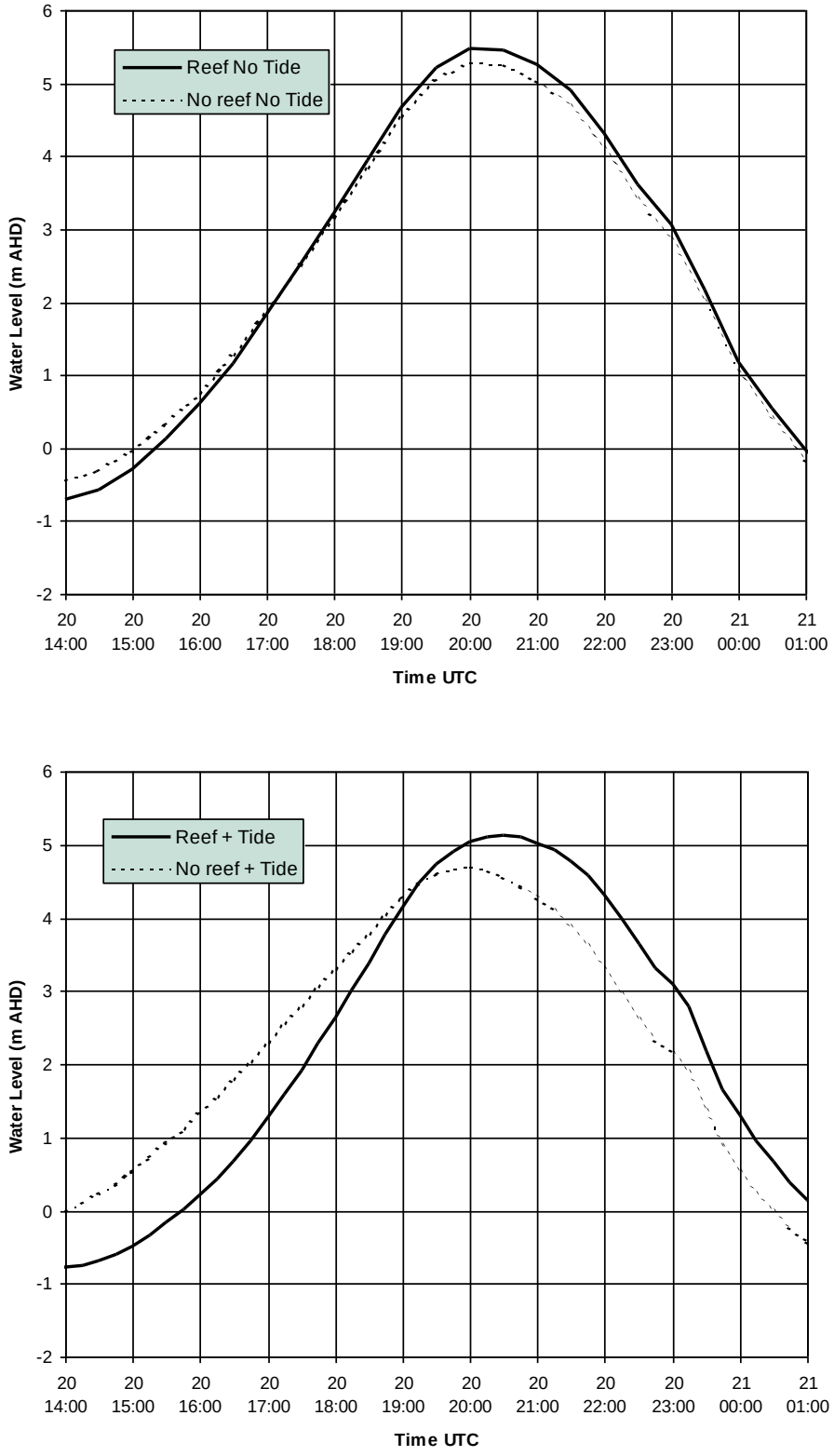

Figure 10.19 Influence of the Great Barrier Reef on *Mackay 1918.*

10.3.8 References

AGSO (2000) Community risk in Mackay - a multi-hazard risk assessment. *Australian Geological Survey Organisation*, Cities Project, ISBN 0 642 398623 (CD-ROM).

Broadbent G.J. (2000) Personal communication. *Queensland Department of Transport*.

Callaghan J. (2000) Personal communication. *Bureau of Meteorology*, Queensland Regional Office.

Croker P. (2000) Personal communication. *Letter by Phyllis MacArthur*, March 1st 1918.

Davidson, J.T., Hubbert, G.D., Woodcock, F., Bergin, M. and Morison, R. (1993) Modelling storm surge in the Mackay Region. Proc 11th Aust Conf Coastal and Ocean Engin. *IEAust*. Aug.

Bath A.T. (1957) The Mackay cyclone of 21 January, 1918. *Aust Met Mag*, 19, Dec 1957, 46-59.

Gourlay M.R. and Hacker J.L.F. (1986) Pioneer River estuary sedimentation studies. Dept of Civil Engin, *The University of Queensland*.

Gourlay M.R. (2000) Personal communication. *The University of Queensland*.

Harbours and Rivers Department (1918) Report from the engineer for harbours and rivers for the year ended 30th June, 1918. *Govt of Queensland*, C.A.58-1918.

Harper B.A. (1983) Half Tide tug harbour - tropical cyclone spectral wave modelling study. Report prepared by *Blain Bremner and Williams Pty Ltd* for the DBCT-UDC Joint Venture, Sep.

Harper B.A. and Holland G.J. (1999) An updated parametric model of the tropical cyclone. Proc. 23rd Conf. Hurricanes and Tropical Meteorology, *AMS*, Dallas, Texas, 10-15 Jan.

Lourensz, R.S. (1981) Tropical cyclones in the Australian Region July 1909 to June 1980. *Bureau of Meteorology*. Oct.

Daily Mercury (1918) *Monday January 28th 1918.*

Daily Mercury (1993) *1918 The big blow.* Special Feature. Wednesday January 27th 1993.

Parkinson C.E., Fison E.C., Leach R.A. and Wilmoth G.R. (1950) Flooding in the Pioneer River and its effect on the Mackay City area. Report of Committee of Enquiry to the *Co-ordinator General of Public Works*, Brisbane.

Visher S.S. and Hodge D. (1925) Australian hurricanes and related storms. *Bureau of Meteorology*, Feb, 54pp

10.4 Tropical Cyclone Althea December 1971 at Townsville

Tropical Cyclone *Althea* crossed the coast of Halifax Bay on the morning of 24th December 1971, the centre passing within 33 km north of the City of Townsville. *Althea* remains as one of the more significant tropical cyclones to affect a Queensland population centre, with a peak wind gust measured at the airport of 55 m s^{-1} (106 kn). Approximately 15% of all houses suffered at least a significant level of damage and some 2.5% of these were uninhabitable (Trollope 1972) resulting in an estimated $130M insurance loss in current values. It caused a significant storm surge of 2.9 m at Townsville (Stark 1972) which fortunately occurred shortly after a low tide and total water levels were only slightly above HAT. However, saltwater entered properties at Rowes Bay and Pallarenda. Debris levels closer to the landfall position near Toolakea indicated a possible peak surge in the vicinity of 3.6 m. Tidal readings are available from the Port of Townsville as well as a number of regional coastal centres.

10.4.1 Available Data

10.4.1.1 Storm Parameters

The National Climate Centre (NCC) official track for this event was obtained and compared with other references, notably BoM (1972, 1975) and Callaghan (1996). The cyclone was tracked by satellite during its early stages, revealing an eye of varying quality over the period 21/2307 UTC to 23/2254 UTC (overland). Radar images delineating the eye were available from Mt Stuart at Townsville from 23/0434 UTC to 24/0107 UTC. These showed a generally steady path towards the coast but with some short term digressions, which became more variable near the coast and at landfall, where the speed of translation seemed to increase. A variation in eye diameter between 5 km and 16 km was also noted from the radar. Satellite analysis, combined with AWS data from Lihou Reef, indicated the storm may have reached maturity around 22/1500 UTC with a central pressure of 950 hPa. The conclusion at the time was that *Althea* might have subsequently fallen short of its full potential. Reports of calm periods lasting 20 to 30 min from a number of small coastal communities near landfall suggested an eye diameter between 8 to 12 km.

A synoptic view of the cyclone over the three days prior to landfall is given in Figure 10.20 (after Callaghan 2000).

With the benefit of increased knowledge of eyewall replacement cycles, Callaghan (1996) revisited the radar data. He explained the apparent wide variation in eye diameter as being due to the presence of a double eyewall effect and showed that both the inner and outer storm eyes were shrinking as it neared the coast, as shown in Figure 10.21. The apparent short term shifts in position were then attributable to "wobble" of the inner eye feature to some extent. The original BoM (1972, 1975) intensity assessments at landfall (952 hPa) were nominally based on extrapolating the 971.5 hPa reading at Townsville, and assumed that the maximum winds occurred over the city with a radius to maximum winds of 38 km. On the basis of the shrinking eye, Callaghan (1996) questions whether higher winds may have been experienced closer to the position of the estimated peak surge.

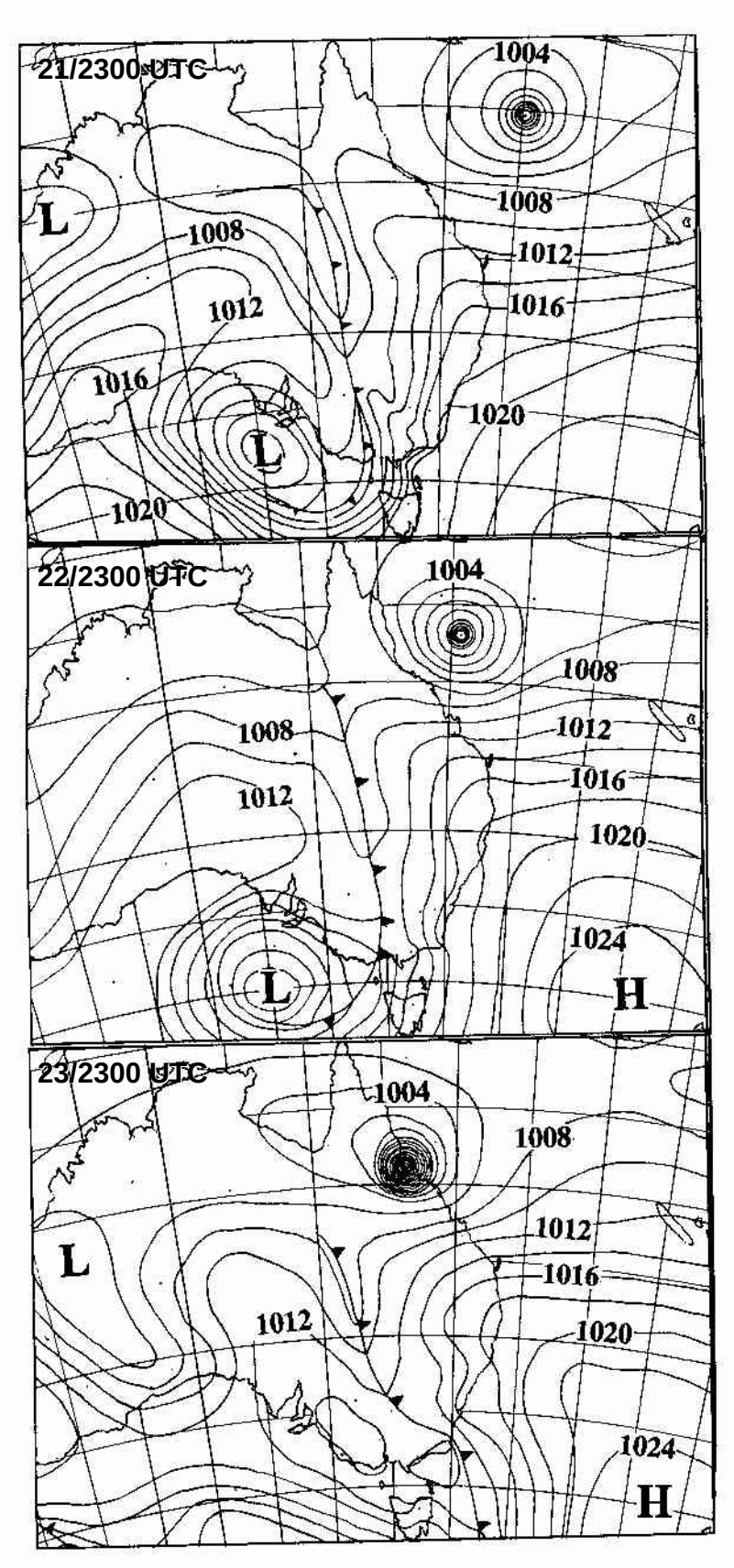

Figure 10.20 Synoptic situation for *Althea* (after Callaghan 2000)

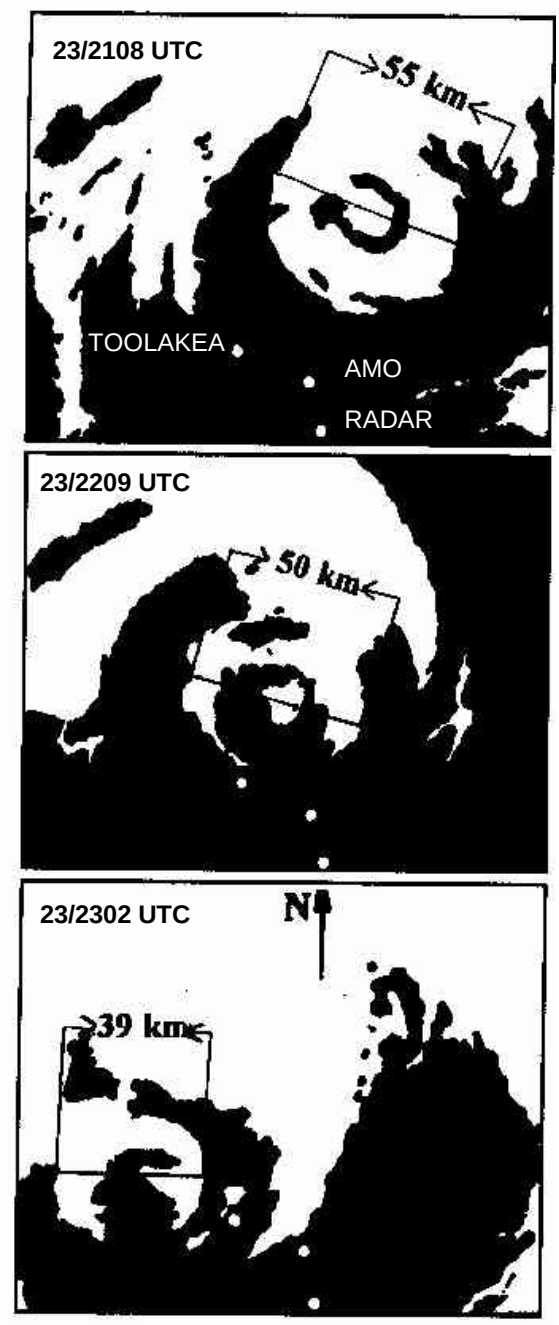

Figure 10.21 Radar images of *Althea* (after Callaghan 1996).

The barograph and Dines anemograph records from Townsville Airport are reproduced in Figure 10.22, taken from BoM (1972).

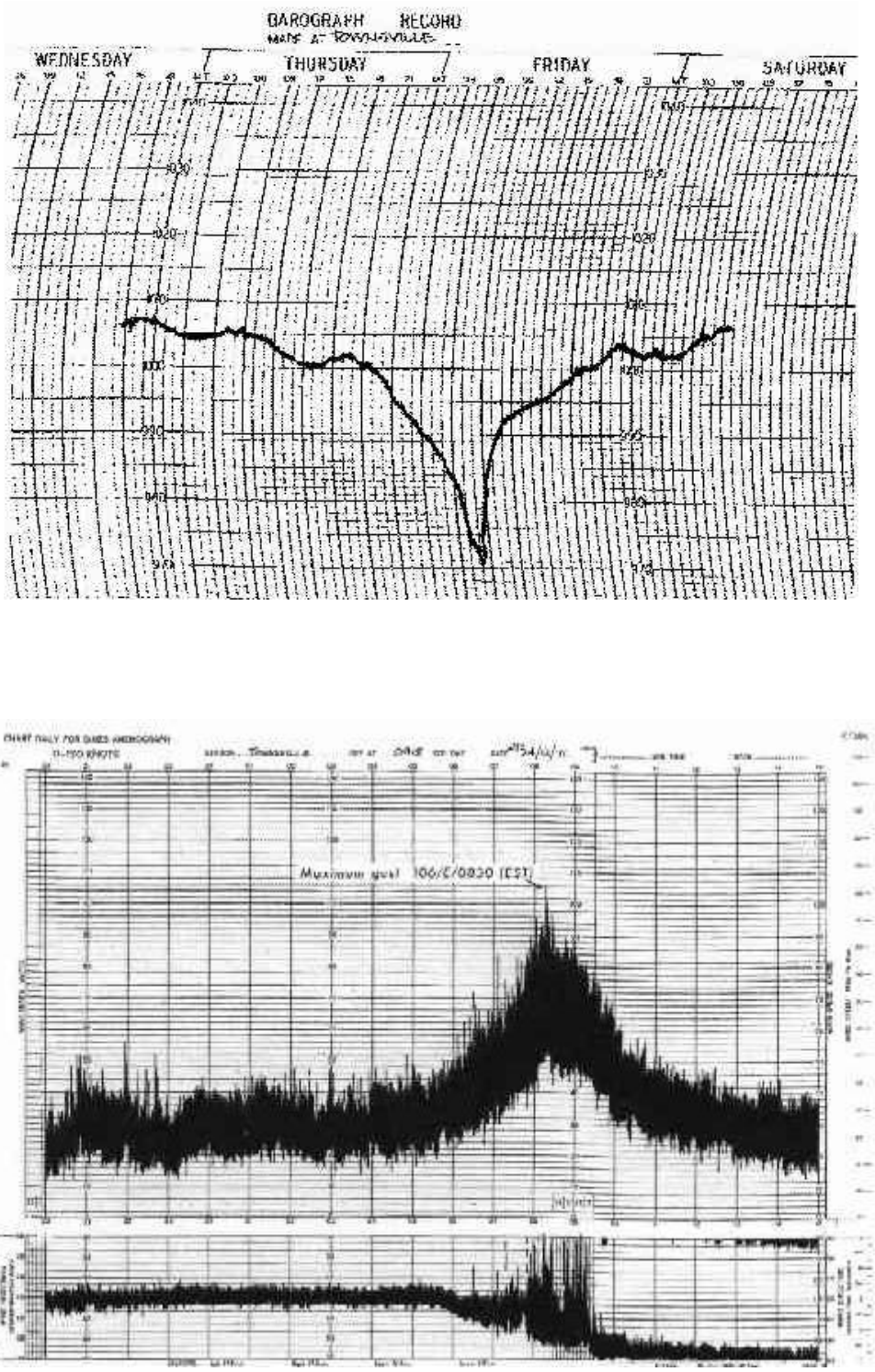

Figure 10.22 Barograph (top) and anemograph (bottom) from Townsville Airport.

10.4.1.2 Storm Surge

The impact of the *Althea* storm surge extended over an extensive period of coastline, being at least 0.5 m above predicted tide between Cairns, 290 km to the north and Mackay, 320 km to the south. Chart recording tide gauges at a number of sites provided accurate water level values and these were able to be augmented with estimates from a beach debris survey undertaken between Ingham and Ayr (Stark 1972).

BoM (1975) also reports some debris estimates from a Townsville Harbour Board report by E.M. Shepherd which clearly includes wave setup and runup influences. Table 10.7 below summarises these values, with positive landfall distances indicating southwards of the track. The Tobruk Pool reading* is reputedly "stillwater" inside the kiosk, presumably represented by a watermark. If accurate, this represents a possible 2 m wave setup and runup component at this point, which is quite close to the harbour tide gauge. At North Ward, Shepherd reported another debris level estimate of 5.84 m AHD as the limit of storm tide influence.

Table 10.7 Summary of estimated peak storm surge amplitude for *Althea*.

Location	Distance from Landfall	Level Reference	Surge Amplitude
	km		m
Cairns	-240	gauge	0.5
Mourilyan	-155	gauge	0.8
Lucinda	-50	gauge	0.9
Balgal	-18	debris	1.8 ?
Toolakea	19	debris	> 3.6 ?
Saunders Beach	26	debris	> 3.1 ?
Black River	30	debris	2.7 - 3.1 ?
Tobruk Pool	46.5	mark*	4.9*
Townsville	47	gauge	2.9
Cungulla	88	debris	2.1 ?
Alva Beach	132	debris	1.8 ?
Beach Mount Beach	147	debris	< 1.8
Bowen	227	gauge	1.0
Mackay	385	gauge	0.9

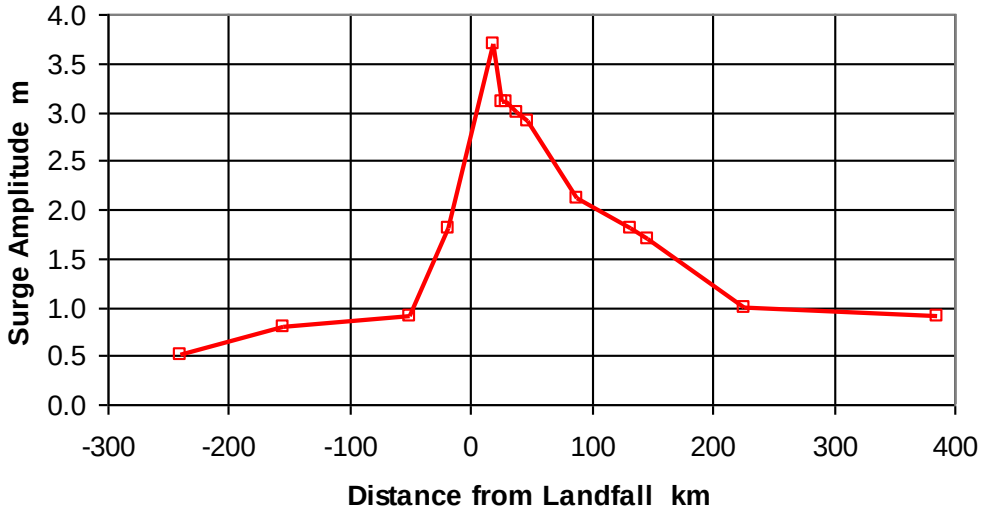

Figure 10.23 Alongshore variation in estimated peak storm surge amplitude for *Althea*.

Only the Townsville Harbour gauge can be considered a reliable "stillwater" surge amplitude because of its location within the harbour at the entrance to Ross Creek. The tide stilling basin filters the effects of any waves present and wave setup is not expected to occur inside the harbour due to its diffractive qualities, e.g. Dunn *et al.* (2000). The remaining values derived from debris heights remain indicative only for purposes of comparison with a model prediction because of the difficulty in not only estimating local RLs but also the influence of wave setup and runup on debris lines. All these levels are summarised on Figure 10.23.

Figures 10.24 and 10.25 show the tide gauge records from Townsville and Bowen, overplotted with the predicted tide and the resulting surge amplitude component. The storm tide at the Townsville gauge peaked at 2.53 m AHD, with a surge magnitude of 2.9 m.

10.4.2 Reconstruction of the Event

The following describes the result of a trial and error comparison between the available data and the predicted spatial and temporal variations in wind and pressure as predicted by an analytical model (Harper and Holland 1999), detailed in Appendix C. The model was systematically adjusted for reasonable values of the key parameters such as track, central pressure, windfield peakedness and radius to maximum winds. The available data from Townsville and a number AWS locations were then compared with the model output to determine the validity of the various assumptions. This was initially done objectively without reference to the effect of the reconstructed windfield on the generated storm surge. However, subsequent storm surge modelling identified a significant sensitivity to the assumed windfield asymmetry, namely θ_{max}, which was originally chosen as 65° based on currently accepted theory (refer Chapter 5). The final windfield calibration has adopted a "left rear" wind maxima of 115° and differences from the 65° assumption (left front) are indicated. The "left rear" assumption not only significantly improves the wind speed calibration at the majority of sites but also the storm surge result. Whilst this change might be due to a better representation of the outer windfield asymmetry it also significantly improves the wind speed comparison with sites closer to the storm centre.

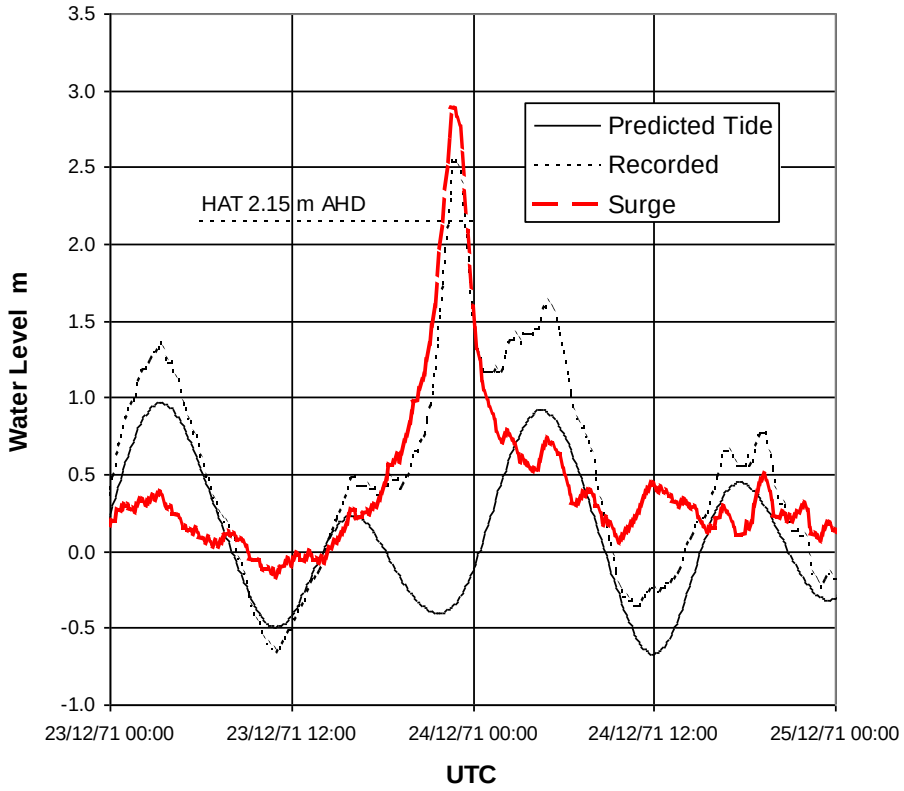

Figure 10.24 Tidal record at Townsville harbour during *Althea*.

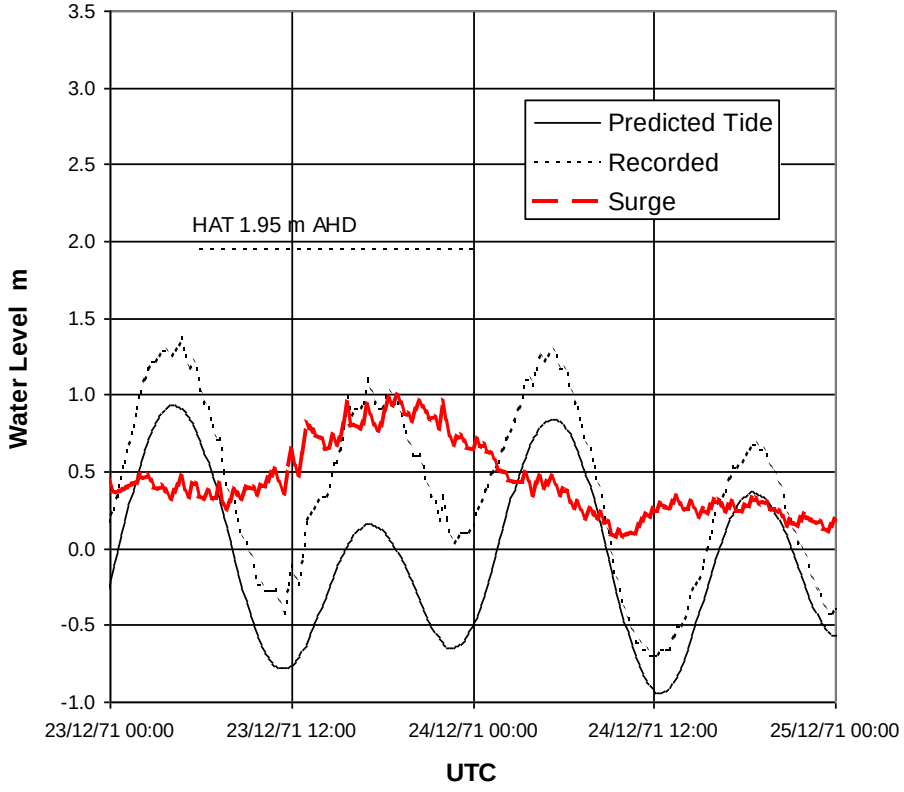

Figure 10.25 Tidal record at Bowen harbour during *Althea*.

The NCC track was first augmented to better represent the nearshore approach path based on the radar positions from BoM (1975), which were then temporally smoothed to suit a 0.1º spatial locator resolution. The outer radar diameters after Callaghan (1996) were also adopted, allowing a nominal +5 km from the edge of the eyewall reflectivity region outwards to the radius of maximum winds. This offset is broadly consistent with data from *Oliver*, which is reported in Callaghan (1996), and with data during Hurricane *Andrew* from Powell and Houston (1996). An earlier radar eye from BoM (1971) was also used, providing the following guidance in Table 10.8 for nearshore radius to maximum winds.

Table 10.8 Indicative radius to maximum winds for *Althea*.

Time	Radar Outer Eye Radius	Indicative Radius to Maximum Winds
UTC	km	km
23/1500	30	35
23/2108	27.5	33
23/2209	25	30
23/2302	19.5	25

In spite of the above, numerous tests showed that a nominal 30 km radius resulted in little variation in the predicted winds at Townsville from about 2100 UTC onwards. Accordingly, 30 km was adopted for the final track and it proved difficult to conclude that winds may have been higher between the city and the landfall point. This is because of the relatively flat windfield peakedness of 7.0 that was indicated by the model fitting procedure against the various wind and pressure records. Notwithstanding this conclusion, the eyewall replacement is not represented by the simplified parametric model so that a narrow region of higher winds may still have existed. Such a feature's impact on storm surge levels over the whole region would likely be small but may have contributed to some localised effects.

10.4.2.1 Final Track Parameters

Table 10.9 summarises the final storm parameters chosen, while Figure 10.26 shows the track and predicted wind and pressure field as the storm made landfall. An ambient pressure of 1007 hPa was chosen based on pre-cursor barograph readings. Minimum central pressure at landfall has been maintained as a nominal 950 hPa. Radius of maximum wind values following landfall (i.e. post 23rd) are here nominal only, the track recurving over land and emerging north of Brisbane several days later.

Table 10.9 Adopted hindcast parameters for tropical cyclone *Althea*.

Track Fix			Speed	Bearing	Central Pressure	Radius	Peakedness
Time	Lat	Long	V_{fm}	θ_{fm}	p_0	R	B_0
UTC	°	°	m s^{-1}	°	hPa	km	
19-Dec-1971 23:00	-10.9	159.0	3.3	218	999	100	7.0
20-Dec-1971 05:00	-11.4	158.6	3.0	211	998	100	7.0
20-Dec-1971 11:00	-11.9	158.3	3.3	218	998	100	7.0
20-Dec-1971 17:00	-12.4	157.9	3.7	213	997	100	7.0
20-Dec-1971 23:00	-13.0	157.5	3.6	224	996	100	7.0
21-Dec-1971 05:00	-13.5	157.0	4.0	219	994	100	7.0
21-Dec-1971 11:00	-14.1	156.5	4.7	229	991	100	7.0
21-Dec-1971 17:00	-14.7	155.8	5.4	228	986	79	7.0
21-Dec-1971 23:00	-15.4	155.0	5.8	238	980	61	7.0
22-Dec-1971 05:00	-16.0	154.0	6.7	243	973	49	7.0
22-Dec-1971 11:00	-16.6	152.8	6.1	255	962	37	7.0
22-Dec-1971 17:00	-16.9	151.6	5.5	259	950	30	7.0
22-Dec-1971 23:00	-17.1	150.5	5.9	235	950	30	7.0
23-Dec-1971 04:00	-17.7	149.7	5.9	235	950	30	7.0
23-Dec-1971 08:00	-17.9	149.0	5.3	253	950	30	7.0
23-Dec-1971 14:00	-18.2	148.1	5.4	259	950	30	7.0
23-Dec-1971 16:00	-18.2	147.6	4.4	242	950	30	7.0
23-Dec-1971 19:00	-18.4	147.2	6.8	205	950	30	7.0
23-Dec-1971 21:00	-18.8	147.0	8.5	224	950	30	7.0
23-Dec-1971 21:30	-18.9	146.9	11.7	253	950	30	7.0
23-Dec-1971 23:20	-19.1	146.2	8.2	258	950	30	7.0
24-Dec-1971 01:10	-19.2	145.7	6.0	224	950	30	7.0
24-Dec-1971 05:00	-19.9	145.4	2.8	223	988	30	7.0
24-Dec-1971 11:00	-20.3	145.0	4.9	264	990	30	7.0
24-Dec-1971 17:00	-20.4	144.0	4.9	258	990	30	7.0
24-Dec-1971 23:00	-20.6	143.0	2.9	209	995	30	7.0
25-Dec-1971 05:00	-21.1	142.7	4.1	180	997	30	7.0
25-Dec-1971 11:00	-21.9	142.7	5.2	175	998	30	7.0
25-Dec-1971 17:00	-22.9	142.8	7.2	148	998	30	7.0
25-Dec-1971 23:00	-24.1	143.6	7.8	122	998	30	7.0
26-Dec-1971 05:00	-24.9	145.0	6.2	115	996	30	7.0
26-Dec-1971 11:00	-25.4	146.2	5.4	107	997	30	7.0
26-Dec-1971 17:00	-25.7	147.3	6.1	95	995	30	7.0
26-Dec-1971 23:00	-25.8	148.6	9.3	87	997	30	7.0
27-Dec-1971 05:00	-25.7	150.6	9.8	90	992	30	7.0
27-Dec-1971 11:00	-25.7	152.7	5.6	85	992	30	7.0
27-Dec-1971 17:00	-25.6	153.9	3.2	61	984	30	7.0
27-Dec-1971 23:00	-25.3	154.5	5.2	79	978	30	7.0
28-Dec-1971 05:00	-25.1	155.6	7.0	86	982	30	7.0
28-Dec-1971 11:00	-25.0	157.1	8.6	100	984	30	7.0
28-Dec-1971 17:00	-25.3	158.9	10.0	111	986	30	7.0
28-Dec-1971 23:00	-26.0	160.9	11.4	133	990	30	7.0
29-Dec-1971 05:00	-27.5	162.7	11.9	150	990	30	7.0
29-Dec-1971 11:00	-29.5	164.0	12.7	166	991	30	7.0
29-Dec-1971 17:00	-31.9	164.7	14.9	180	990	30	7.0
29-Dec-1971 23:00	-34.8	164.7	14.9	180	990	30	7.0

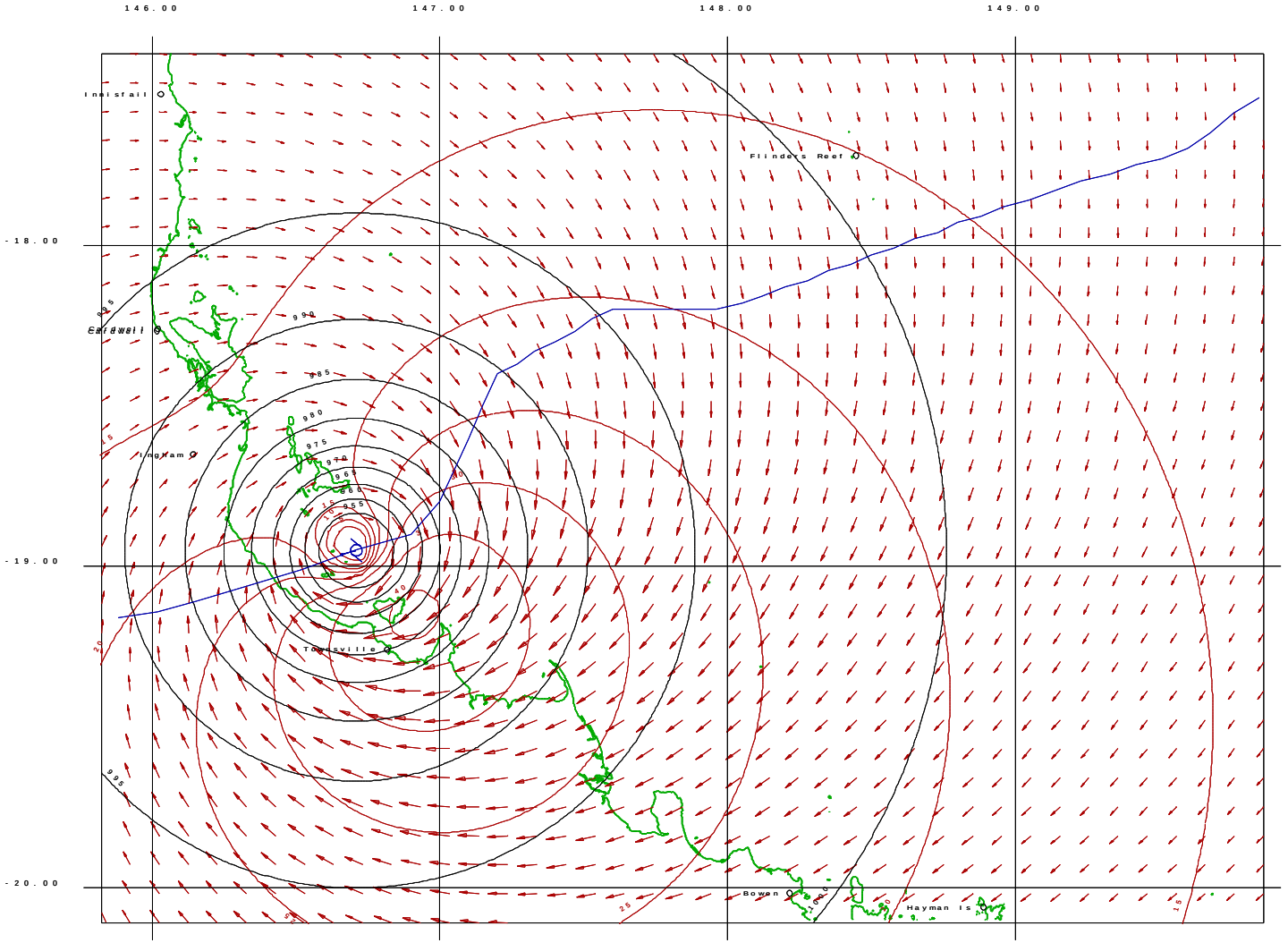

Figure 10.26 Reconstructed cyclone track and wind and pressure fields near landfall for *Althea*.

10.4.2.2 Comparison of Measured and Modelled Storm Parameters

These are considered in the order of storm passage. The first comparison shown is with Lihou Reef AWS 3 hourly data, which was supplied from the NCC database. Closest approach was 32 km to the north of the AWS at about 22/1500 UTC. The data is sparse but shows a very good agreement with the model for both pressure and wind speed and direction (Figure 10.27). The 65° winds appear to be leading slightly in phase whereas the 115°, although slightly high, are in better phase after the peak.

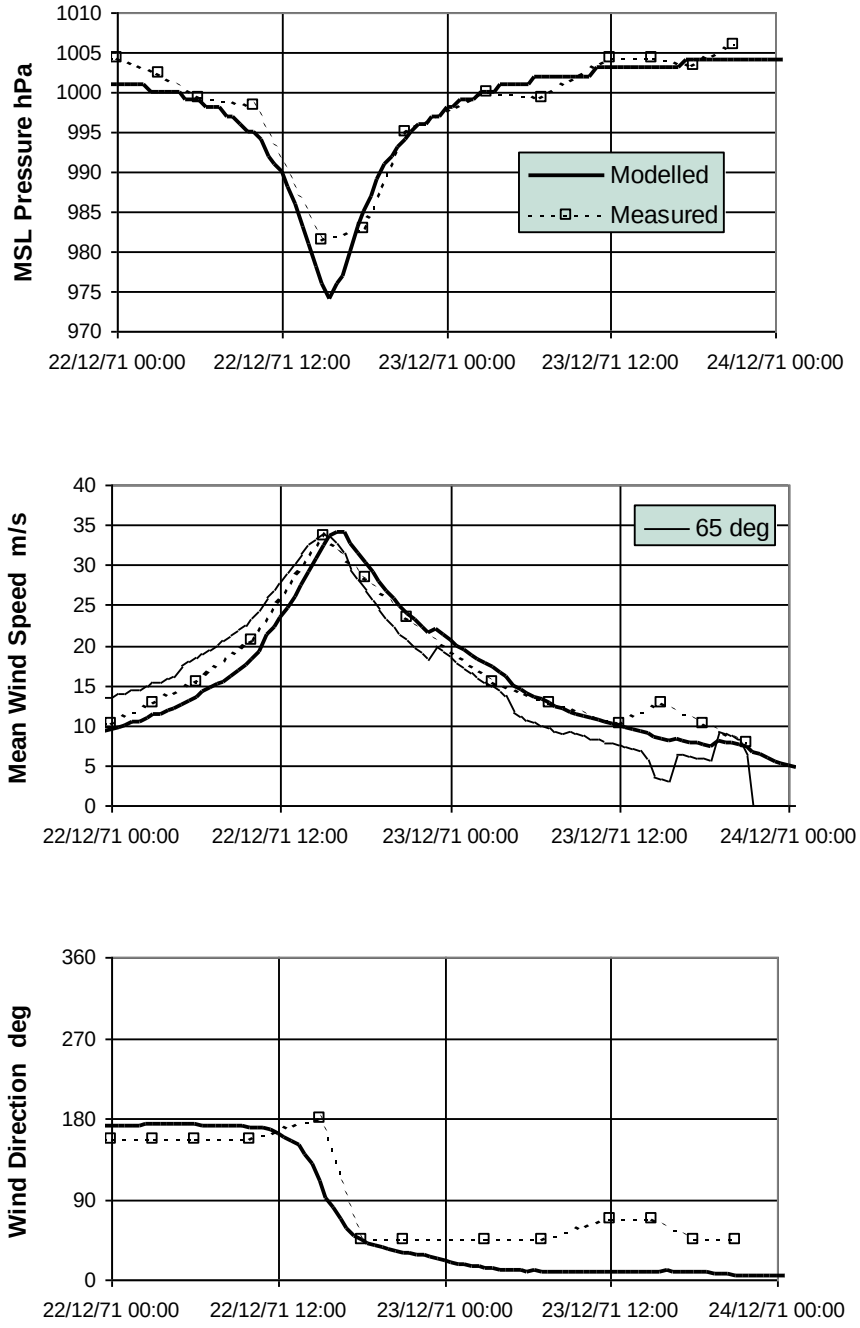

Figure 10.27 Modelled and measured pressures and winds at Lihou Reef for *Althea*.

Figure 10.28 shows the comparison with Willis Island AWS, where closest storm approach was about 102 km to the SSE near 23/0000. The model pressure and the 65° winds are leading the measured values by about 5 to 6 hours, whereas the adopted 115° winds are slightly leading also but again match the post-peak measured winds more accurately.

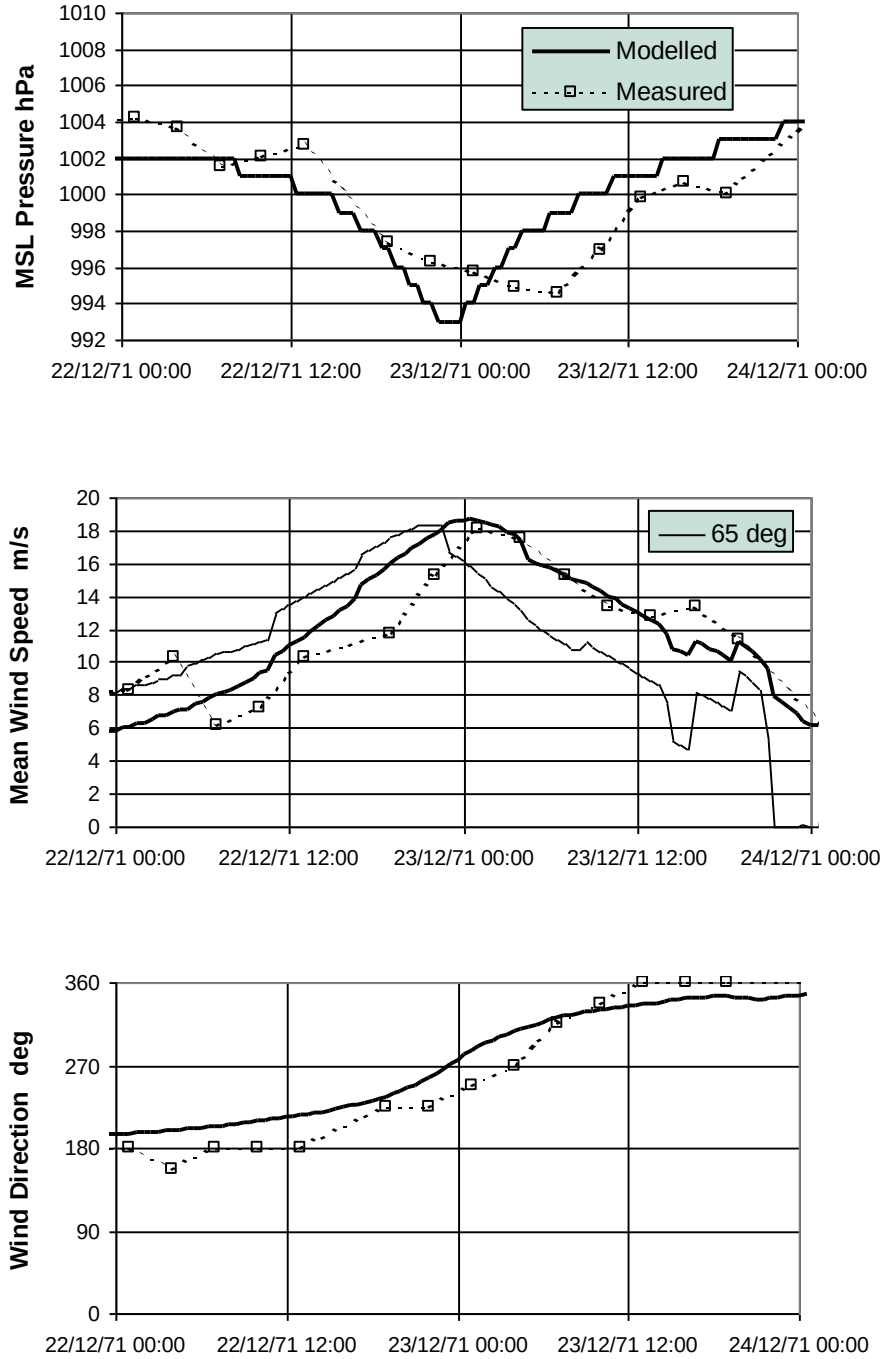

Figure 10.28 Modelled and measured pressures and winds at Willis Island for *Althea*.

Figure 10.29 shows the comparison with Flinders Reef AWS, where closest approach of 35 km to the SSE occurred near 23/1100 UTC, placing the site close to the eyewall. Again, the comparisons are very good although there is a hint of the eye in the data. While the 115° model does not perform as well as the 65º prior to the peak it is again better after the peak.

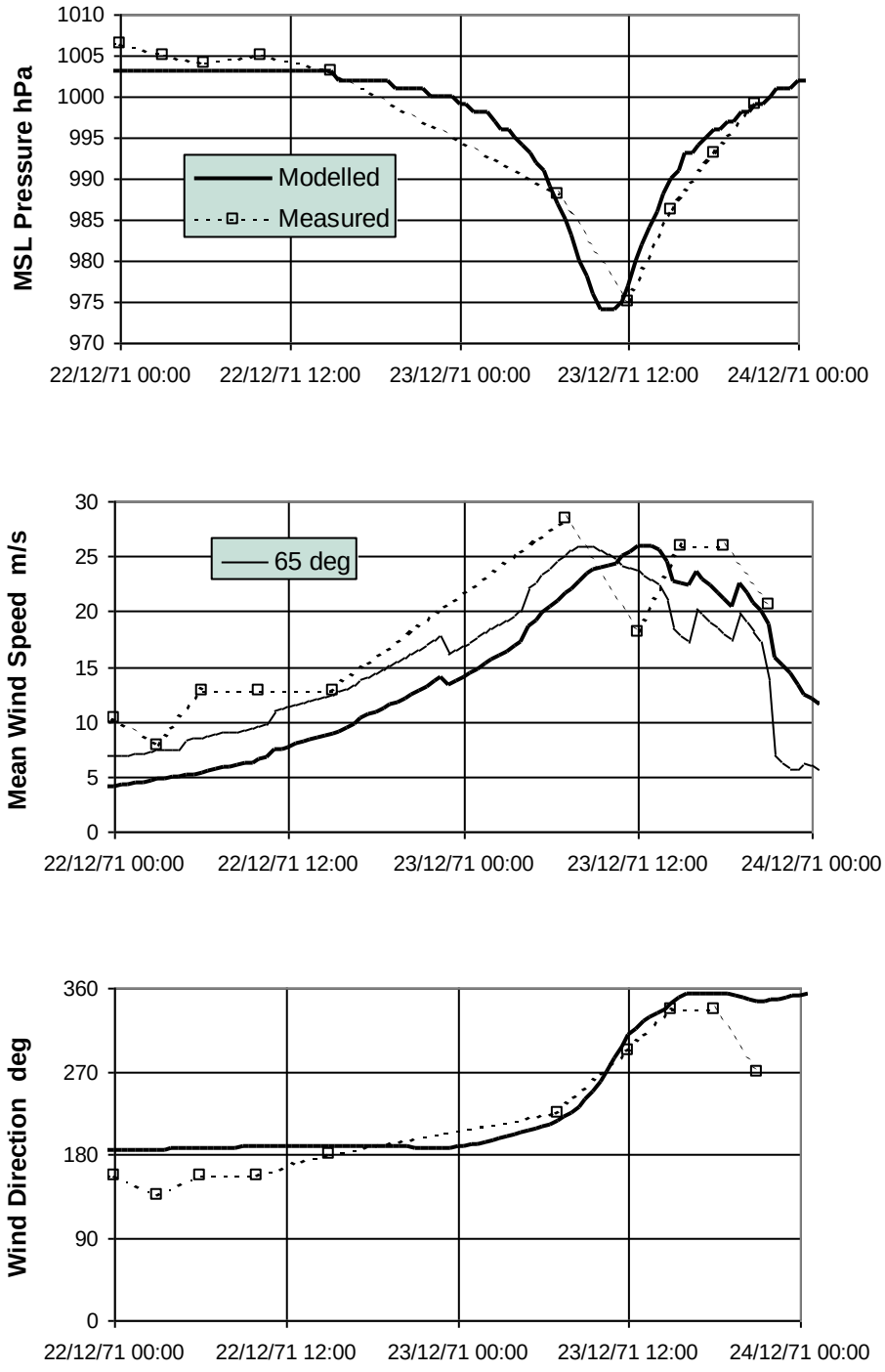

Figure 10.29 Modelled and measured pressures and winds at Flinders Reef for *Althea*.

The next comparison is with the Townsville Airport (AMO) barograph and Dines anemograph, both of which were hand-digitised for this study within several hours of the peaks in preference to using the NCC data sets. This involved digitising the upper and lower non-gust region of the anemograph trace and finding the midpoint estimate to represent the average 10-minute windspeed. In addition, two barograph records were located, the slightly higher minimum pressure chart presumably from the Post office. The Townsville AMO is in flat open terrain about 2 km from the coast with good exposure north of east. However, as shown in Figure 10.30, Castle Hill (300 m) is located about 3 km to the E and the shape of the coastline to the south dictates that SE winds will be predominantly overland. Accordingly, the

model predicted wind speed is adjusted slightly downwards here (Terrain Category 2.5 AS1170.2 1989) to represent the increased roughness due to the predominant SE wind direction during the storm approach. This adjustment does not consider direct influences from Castle Hill which, based on the recorded wind directions in Figure 10.22 at least, appears to have been significant during the strong easterly winds. [J. Ginger *pers. comm.* from James Cook University Cyclone Testing station advises preliminary wind tunnel tests indicate little or no reduction in wind speed is likely at the AMO site due to Castle Hill effects.]

Figure 10.30 Location of the Townsville AMO instrumentation.

Figure 10.31 shows the modelled and measured pressures and winds are very well predicted by the adopted 115° model. With 65° winds though, the comparison with the measured speeds during the SE approach flow is quite poor and the model is distinctly leading the measured peak by about half an hour. It was originally thought possible that the use of Daylight Saving Time (DST) had contaminated some of the data in this regard but no obvious timing errors could be found. The only alternative seems to be that the maximum winds were indeed located further to the rear of the storm rather than the front. The adopted 115° model has a peak speed error of only -1.1% and a bias (across the half-magnitude width) of only 4.4%. Peak errors for the 115° model at the other sites were less than 3.5%, except for Flinders Reef with its close encounter with the eyewall.

While gust speeds are not shown, the model also predicts a peak gust of around 52 m s^{-1} at the AMO, compared with the 55 m s^{-1} from the anemograph. A structural analysis of failed signage, principally road signs, by James Cook University (Trollope 1972) found that signs near the airport probably failed at about 47 m s^{-1} which is logically consistent with the recorded peak speed. However, a sign near Picnic Bay School on Magnetic Island was deemed to have failed at about 59 m s^{-1}. The modelled peak gust at that location is 58 m s^{-1}, assuming Picnic Bay is an open ocean site.

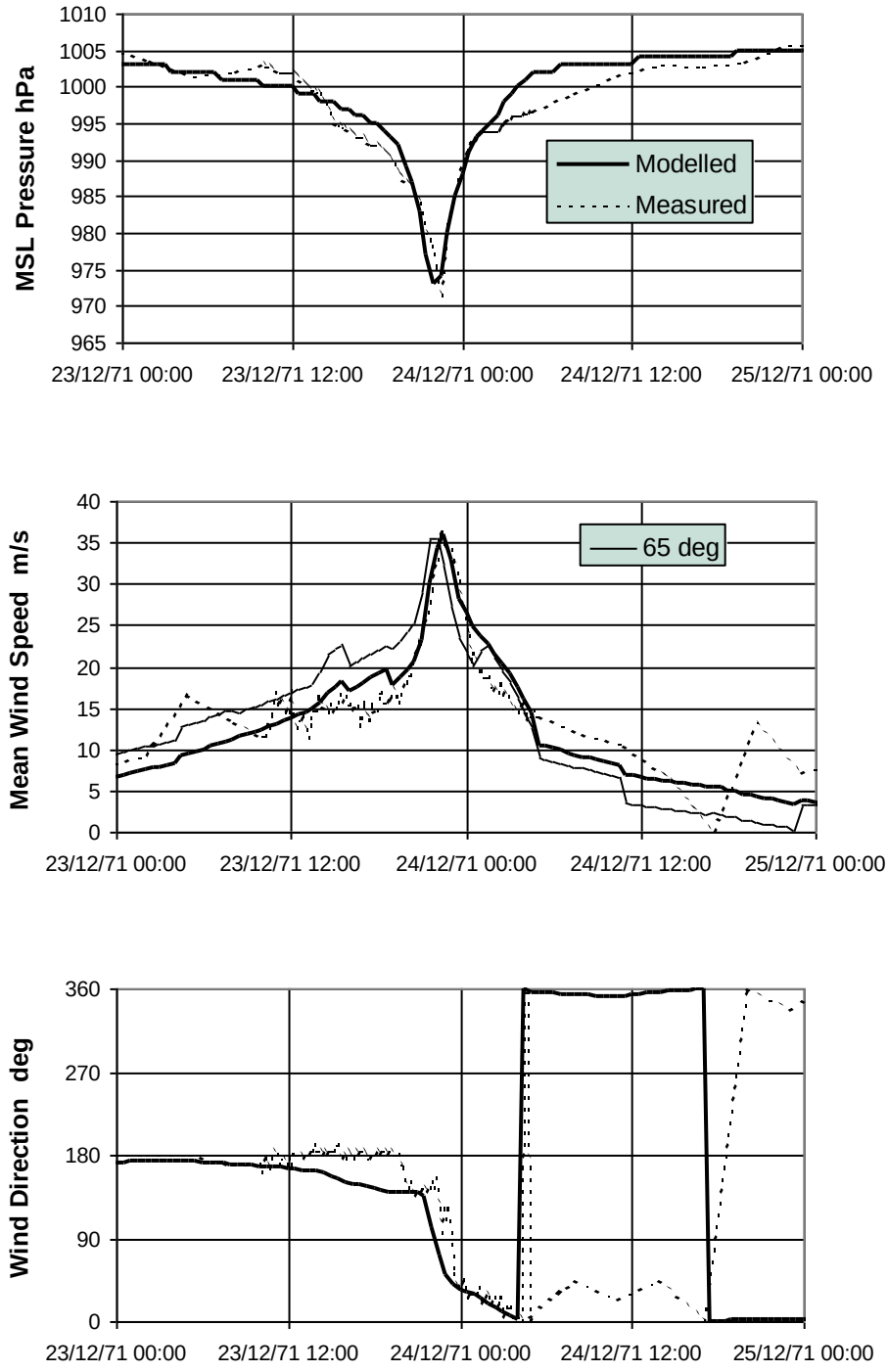

Figure 10.31 Modelled and measured pressures and winds at Townsville AMO for *Althea*.

The final comparison with instrumented pressure and wind is at Cardwell, some 140 km to the north and shielded to some extent by Hinchinbrook Island. Here the model appears to underestimate the recorded pressure but is reasonable in matching the wind magnitude (Figure 10.32). The adopted 115° model again is a much better result. The model also assumes Cardwell is Terrain Category 2 situation rather than an open ocean site.

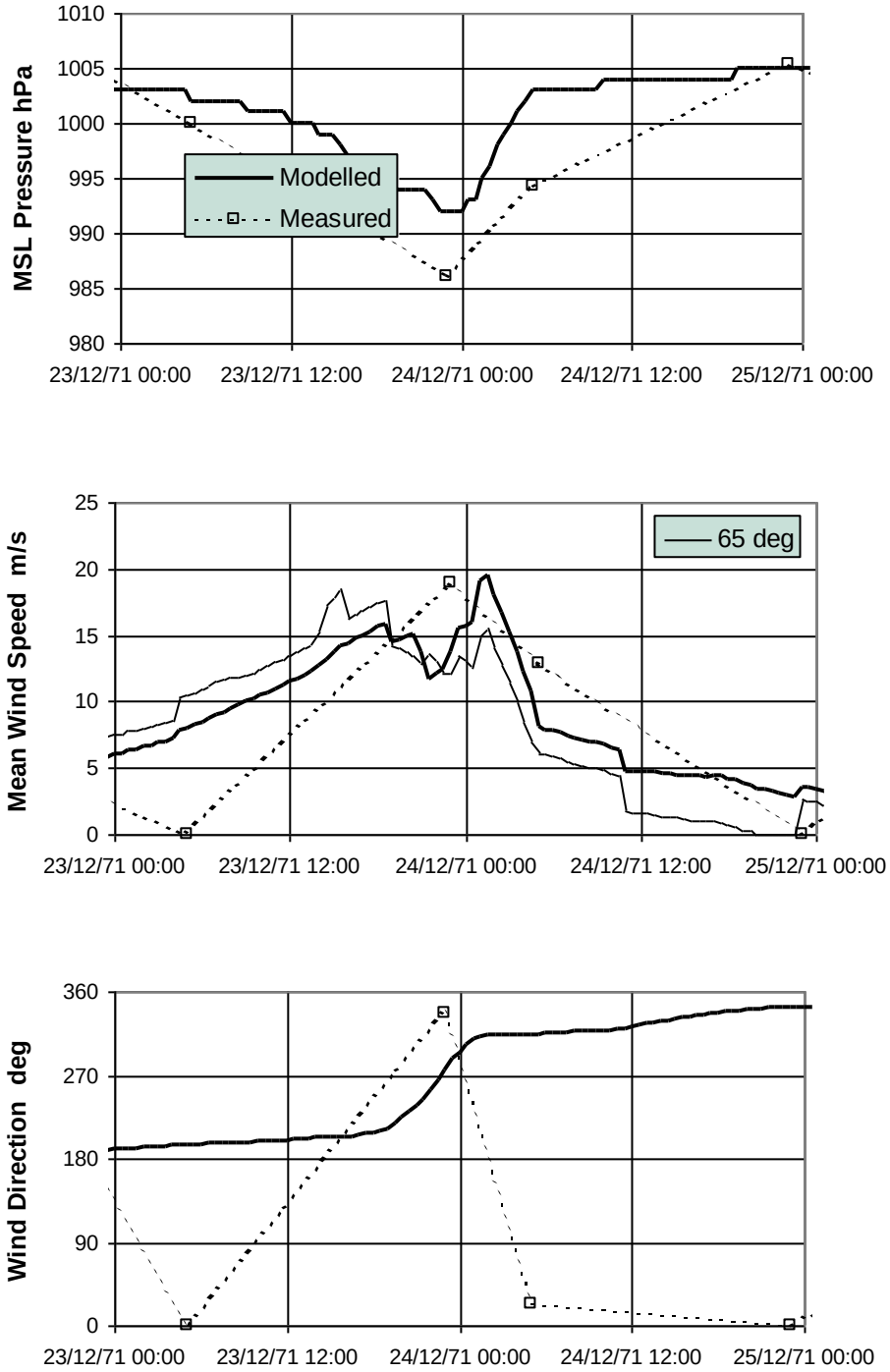

Figure 10.32 Modelled and measured pressures and winds at Cardwell for *Althea.*

10.4.3 Implications for Storm Surge Modelling

While there remain some minor inconsistencies between the modelled and measured wind and pressure data, the parametric model with 115° maximum winds generally performs extremely well. Some of these differences are in part due to errors in track, intensity and scale as well as the smoothing of those values within the model. Also, the "shrinking eye" undoubtedly created some localised variability as the storm neared the coast, which is currently beyond the capability of parametric models.

In Figure 10.33 below, the modelled envelope of maximum winds shows the extreme band of onshore winds that would have acted to produce this notable storm tide along the coast.

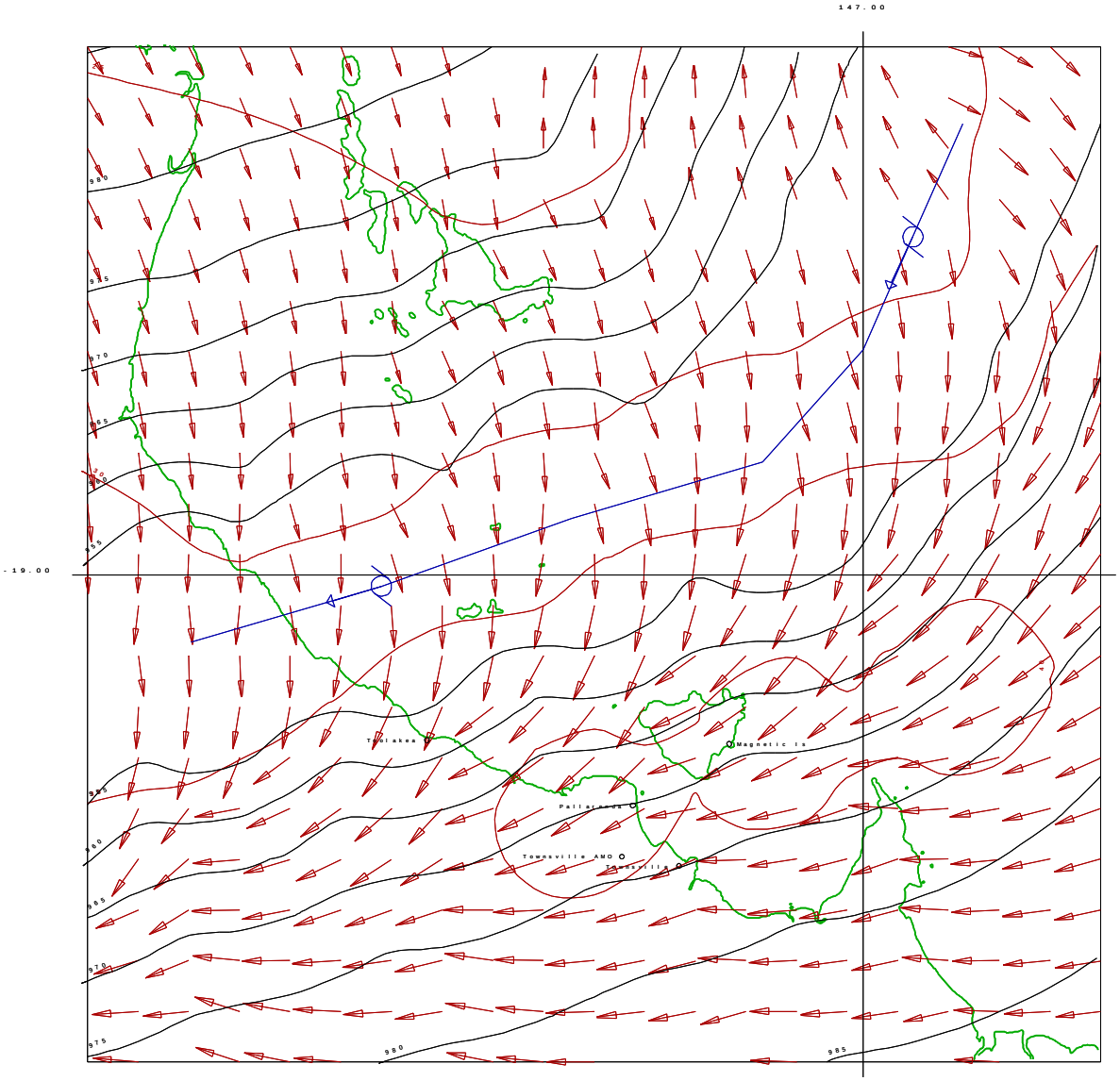

Figure 10.33 Modelled envelope of maximum winds and minimum pressure for *Althea*.

10.4.4 Tidal Modelling

Only five tidal constituents were available, but the modelled result is quite good as shown in Figure 10.34. The modelled tide is only about 0.05 m lower than the predicted low tide at 2130 UTC 23/12, close to the time of the peak surge. The following high tide is less accurate, being underpredicted by about 0.15 m.

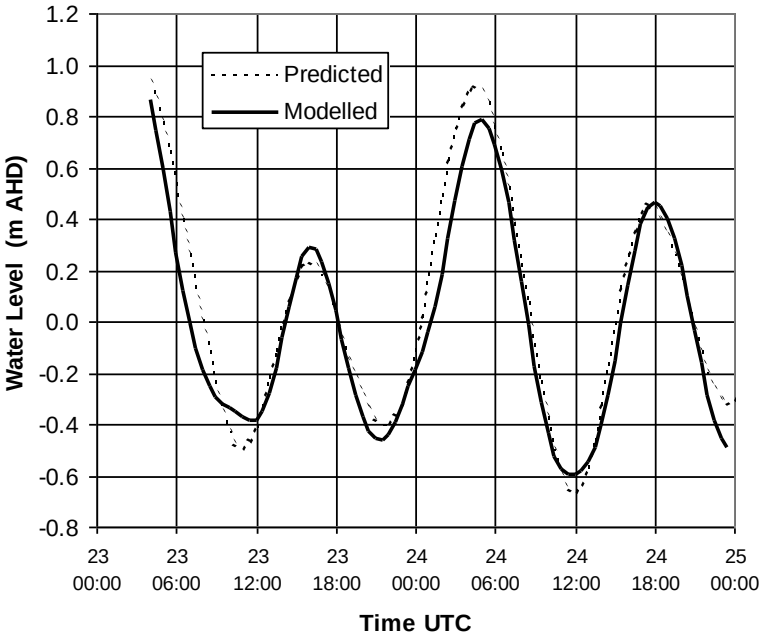

Figure 10.34 Comparison of modelled and predicted tide at Townsville Harbour.

10.4.5 Storm Surge Modelling

A large number of individual tests were undertaken on the *Althea* storm tide event. As discussed earlier, initial tests showed that the preferred windfield asymmetry assumption of a 65° or "front quadrant" θ_{max} proved insufficient in matching the recorded surge magnitude and was less successful in matching the recorded winds. Figure 10.35 presents the comparison between the front and rear quadrant wind assumptions on the modelled surge for the Townsville and Cleveland Bay grid domains. In the coarser Townsville grid, the surge is underpredicted by almost 24% and by 15% in the finer scale Cleveland Bay grid. This is a very significant sensitivity to a single parameter and accordingly the rear quadrant 115° winds were retained.

Firstly, based on the standard 2D model, Figure 10.36 illustrates the surge-only build-up some 6 h before the storm makes landfall on the 1 nmile Townsville grid. At this time, the inverted barometer effect is clearly visible near the storm centre, beyond the continental shelf. At the coast, some water level increases are concentrated south of Cape Cleveland and Cape Bowling Green. The shelf flow pattern indicates that a considerable northwards flow has already been initiated and strong currents are predicted on the outer edge of the Great Barrier Reef. In Figure 10.37, the nearshore water levels and flows within the 0.2 nmile Cleveland

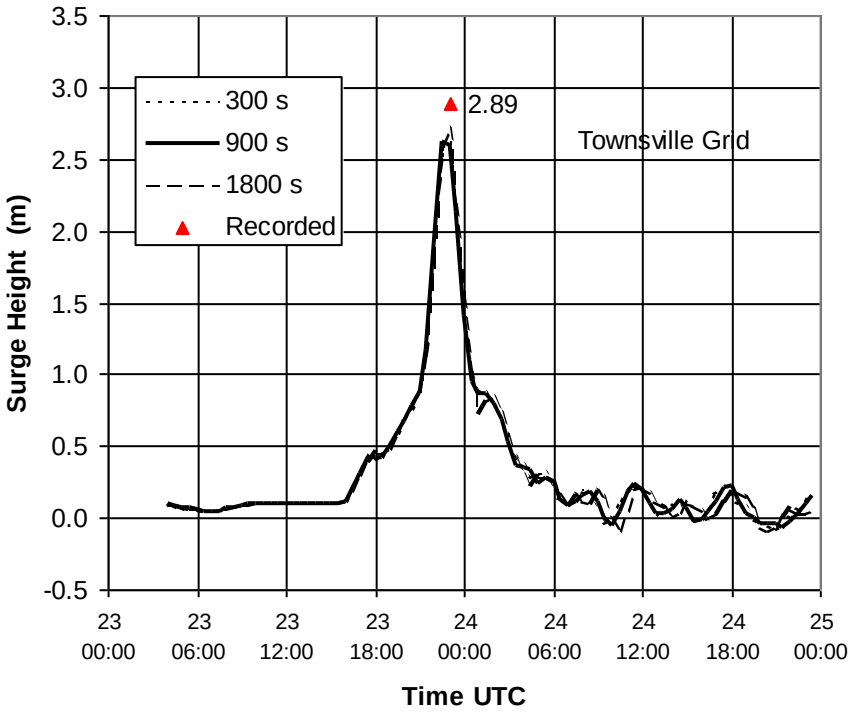

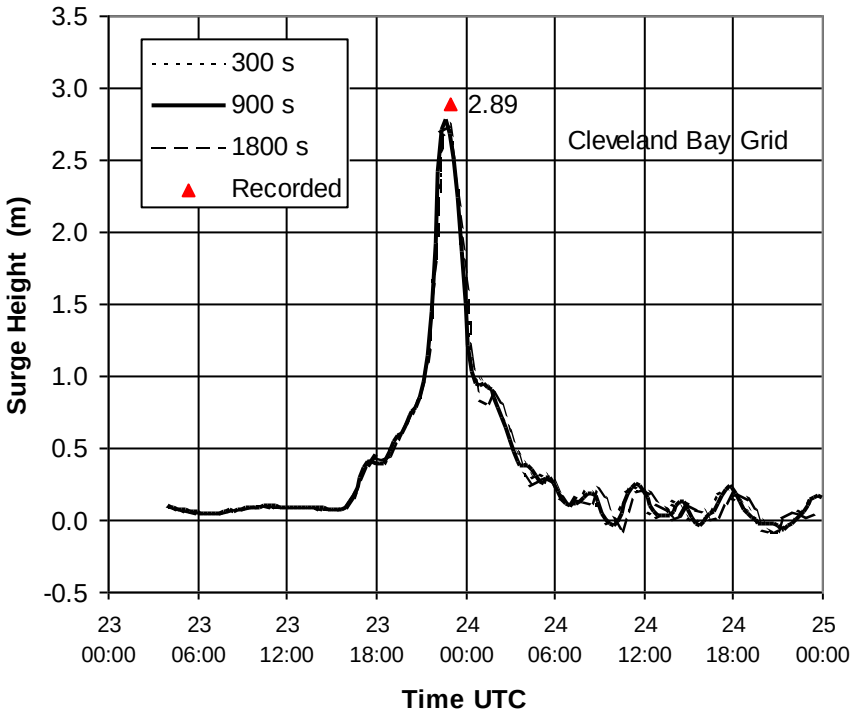

Figure 10.35 Effect of windfield asymmetry on surge response.

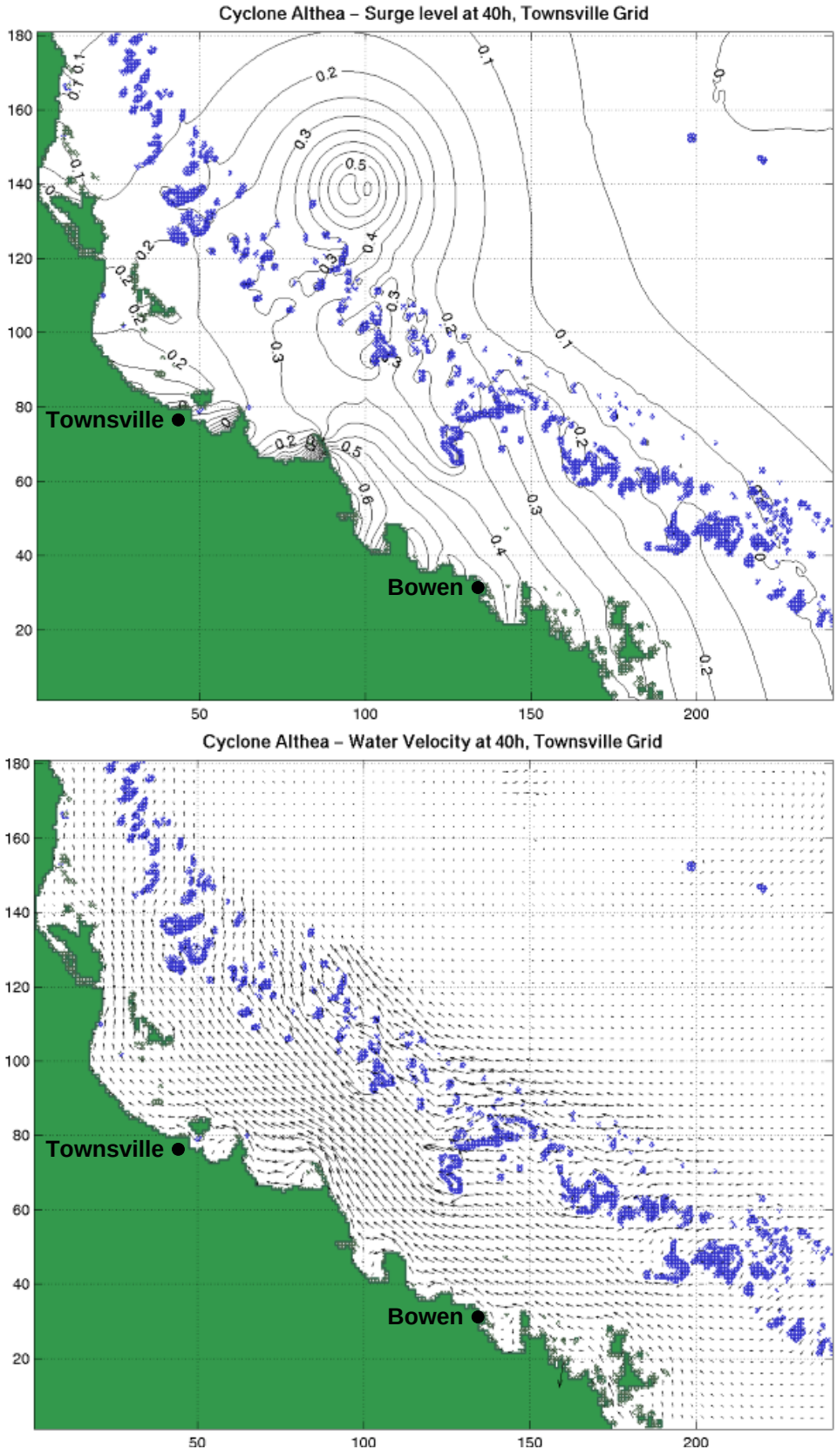

Figure 10.36 Modelled surge-only response of *Althea* 6 h before landfall.

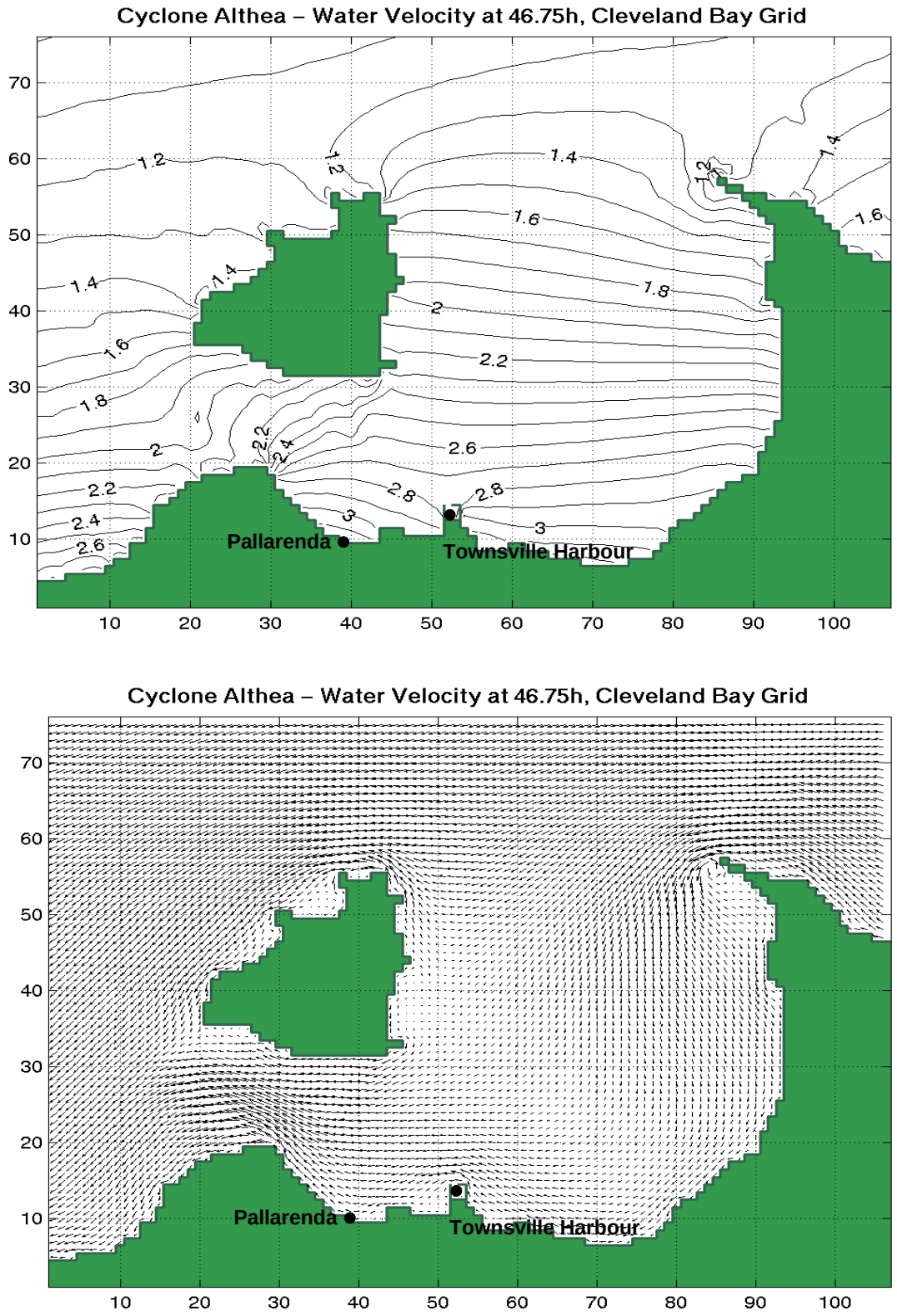

Figure 10.37 Nearshore surge-only response of *Althea* near time of landfall.

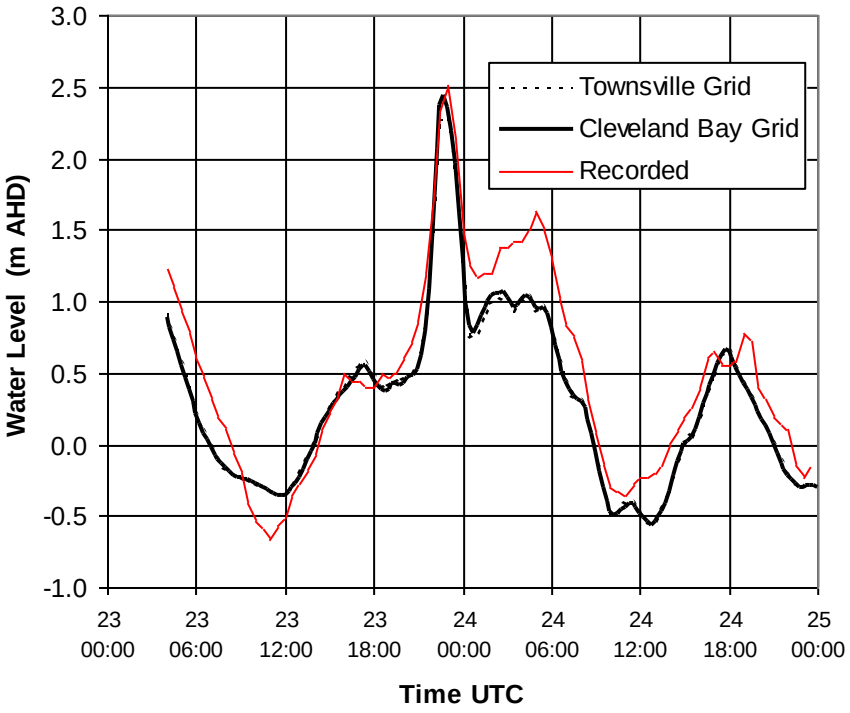

Figure 10.38 Measured and modelled storm tide at Townsville Harbour.

Bay grid are shown. Greatest build-up is indicated near Pallarenda, with strong currents between Magnetic Island and the shore.

Next, the combined modelling of surge and tide is given in Figure 10.38, which compares the time history of measured and modelled water levels at Townsville Harbour. Here the tide gauge record is compared with the modelled result using both the Townsville grid and the Cleveland Bay grid. It can be seen that there is very close agreement between all three curves at the peak water level (within 0.1 m) although the modelled results lead the recorded levels slightly. Considering that the tide is not modelled exactly, this is an excellent result. Away from the peak level the agreement is less satisfactory with the modelled result generally underpredicting the recorded levels, although this is again exacerbated by the error in the modelled tide.

The next example compares the storm tide prediction between the standard 2D and a 3D version of the model. The only significant role of 3D physics in this case is to permit return flow near the seabed when the strong surface flow is towards shore. This results in a small net increase of bed friction towards shore for the 3D case, creating slightly higher coastal water levels. In the case shown in Figure 10.39 for the Cleveland Bay grid, the increase is only 0.1 m at the peak.

The final example of the predicted storm tide levels is given in Figure 10.40 for the site of Bowen, 170 km to the south-east, which experienced a peak surge of about 1.2 m. Again, the tide prediction is not particularly accurate but the model closely predicts the storm tide level on the day of the peak at Townsville.

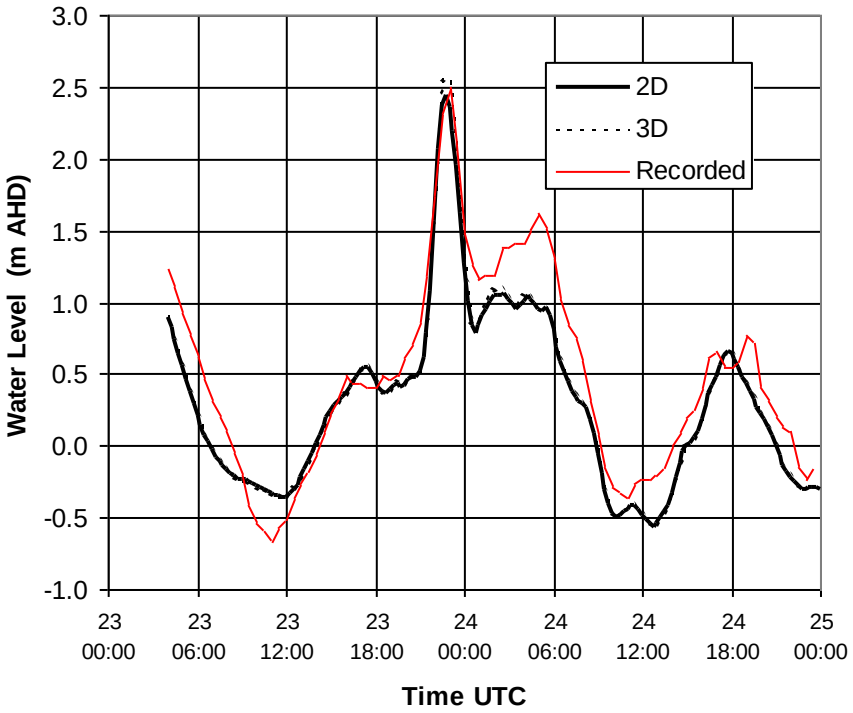

Figure 10.39 2D versus 3D model prediction for *Althea*.

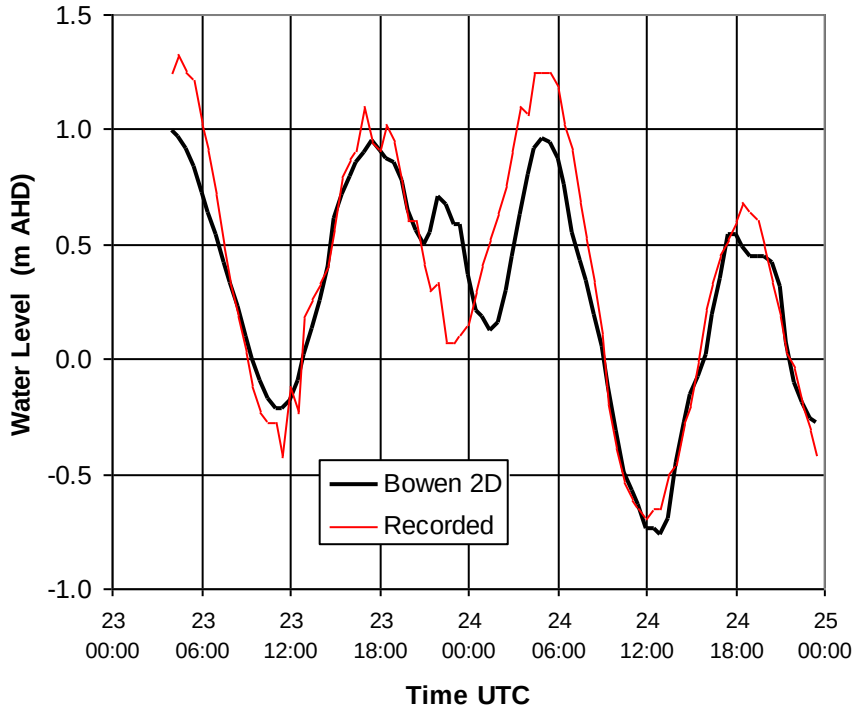

Figure 10.40 Measured and modelled storm tide levels at Bowen for *Althea*.

Given that the tide is not being especially well modelled in these cases, attention is now focussed on the accuracy in predicting the surge component alone (i.e. measured - predicted tide). The first example in Figure 10.41 shows the comparison with and without tide included for the Cleveland Bay grid and using the standard 2D model. In this example, it can be seen that much of the discrepancy in reproducing the combined storm tide level was in fact due to the error in the tidal prediction. Here the measured and modelled values are very closely matched prior to and during the peak, with some trailing wake effects evident after the storm passes which are slightly less accurately represented by the model. The difference between the storm surge component, with and without tide included in the model, is also shown. While this was seen as a significant factor in the case of the 1918 Mackay cyclone, it is clearly a very minor effect in the Townsville region and can safely be neglected.

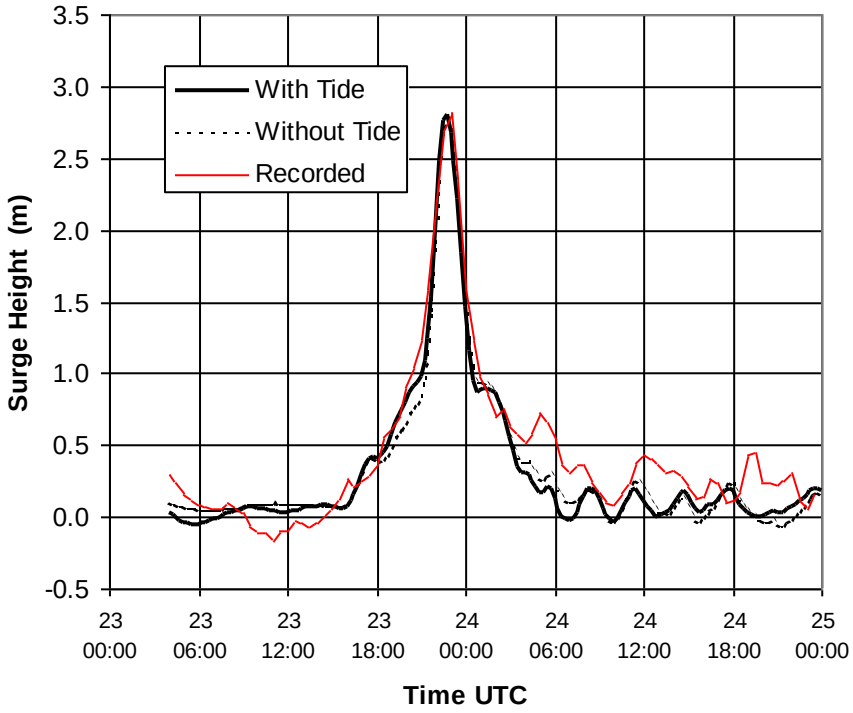

Figure 10.41 Measured and modelled surge component at Townsville Harbour for *Althea*.

The effect of grid resolution on the modelled storm surge result is illustrated next in Figure 10.42, where the results from each of the three nested grids for the same nominal Townsville Harbour location are superimposed. In this case, the measured water level is removed for clarity, replaced by the single peak recorded value alone for reference. For the 2D Cleveland Bay grid the modelled surge in the port compares well with the measured surge of 2.82 m whereas the large scale Coral Sea grid overpredicts the measured surge by about 0.5 m. This is likely due to the poorer local representation of the bathymetry and coast. By contrast, the intermediate Townsville grid slightly underpredicts the measured value by about 0.2 m.

Next, Figure 10.43 shows the effect of timestep resolution on the predicted water level. For the Cleveland Bay grid, it can be seen that the results are relatively insensitive to the timestep used. A characteristic of the model is that it attenuates the shortest period waves the most strongly. Therefore as timestep increases, some information is lost from the shortest period waves and the effect becomes apparent in the detail of the time history water level traces. In this case, a timestep of 1800 s is near the temporal resolution limit for this cyclone.

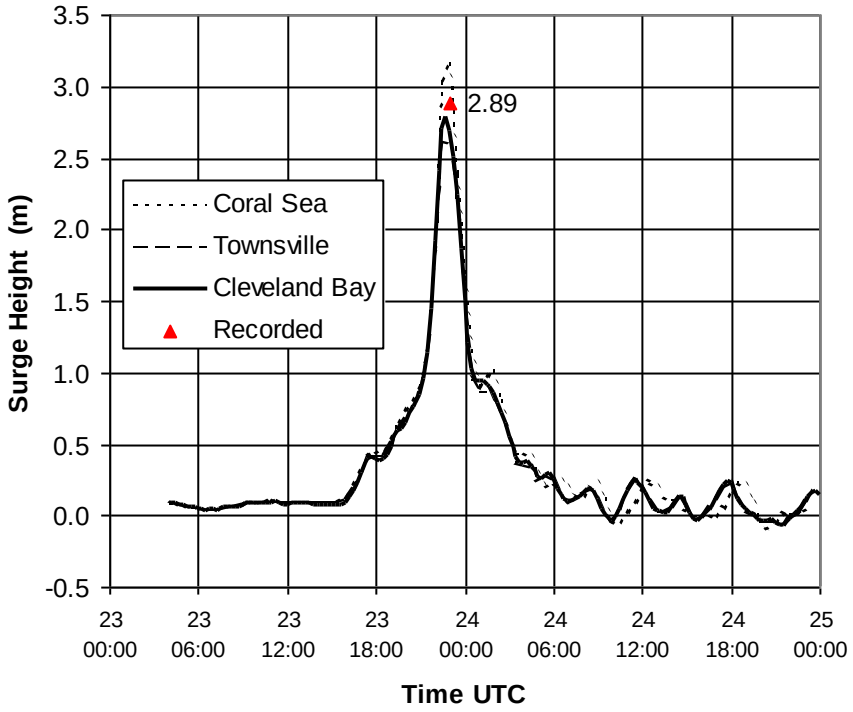

Figure 10.42 Influence of grid resolution on accuracy for *Althea*.

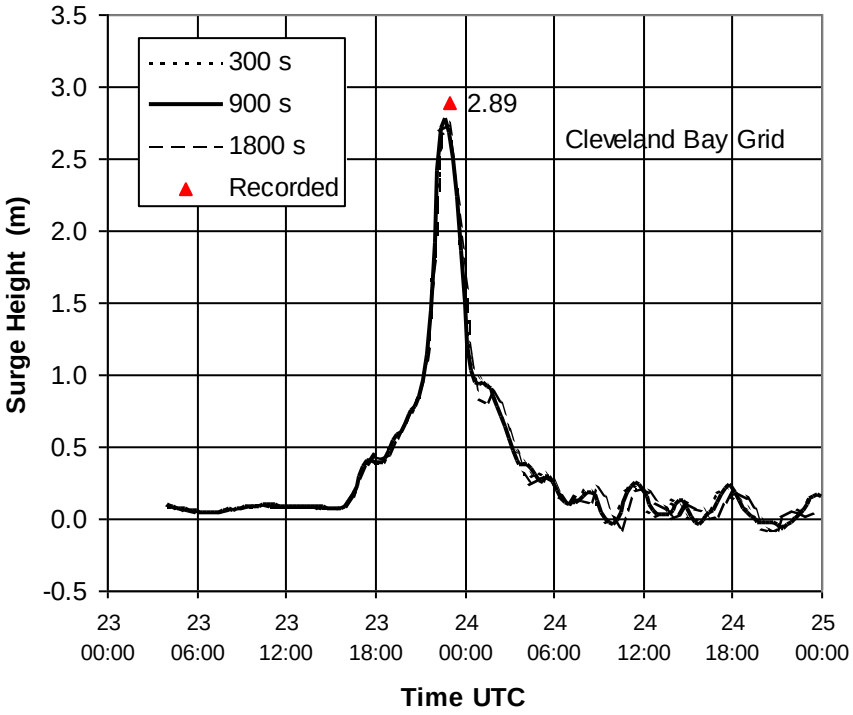

Figure 10.43 Influence of time step on accuracy for *Althea*.

As a guide, $T/\Delta t$ should be >= 20 (see Chapter 6), but the model can produce adequate results for $T/\Delta t$ near or slightly below 10. During the 12 hours before landfall $T/\Delta t$ ranges from approximately 6 to 15 for the 1800 s timestep case.

A sensitivity test was also carried out to determine the influence of the Great Barrier Reef on predicted storm tide at Townsville. The model reef boundaries were removed and *Althea* re-modelled, yielding almost no difference in the predicted peak storm surge at the harbour gauge. This result is consistent with Sobey and Harper (1977) who concluded that the continental shelf at Townsville was sufficiently wide that the reef had essentially no impact, at least for a storm track such as *Althea*. For tracks that are more southerly there may be an increased reef shielding effect.

An additional test was performed to gauge the influence of including the non-linear advection calculation in the model solution scheme (refer Appendix D). In this case, an additional test was run without non-linear advection and the results were essentially identical to the full non-linear case but with a 15% saving in computation time.

Finally, comparison between the final peak modelled values (Townsville and Cleveland Bay grids) and the estimated and/or measured peak storm surge magnitudes is shown in Figure 10.44. In this case, the debris line estimates from Figure 10.23 has been adjusted downward by 0.5 m as a nominal allowance for wave setup and is shown with a 60.5 m error bar. The triangles represent the recorded levels at tide gauges. The solid line is the model result and indicates the peak surge magnitude was near Pallarenda at a level of 3.2 m. At Toolakea Beach, the location of the peak debris level of 3.6 m, the model predicts a 2.4 m surge. This is much lower than the observed debris line, even after wave setup and runup are considered. It suggests that *Althea* may have had a second wind maximum near Toolakea with significantly stronger winds than those predicted by the current single vortex model.

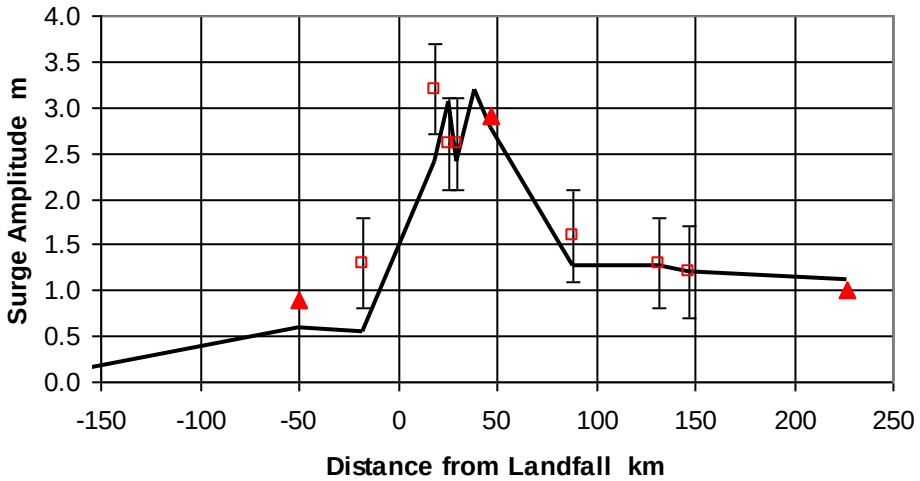

Figure 10.44 Comparison of modelled and measured alongshore surge profile for *Althea*.

10.4.6 References

BoM (1972) Report by Director of Meteorology on cyclone Althea. Bureau of Meteorology, Dept of Science, *AGPS*, Canberra, July.

BoM (1975) Tropical cyclones in the northern Australian regions. Meteorological Summary, Bureau of Meteorology, Dept of Science, *AGPS*, Canberra.

Broadbent G.J. (2000) Personal communication. *Queensland Department of Transport*.

Callaghan J. (1996) Tropical cyclones - analyses of the destructive wind zone. Proc. Conf. On Natural Disaster Reduction NDR 96, *IEAust*, Surfers Paradise, 29 Sept to 2 Oct, ISBN 0 85825 662 2, 341-345.

Callaghan J. (2000) Personal communication. *Bureau of Meteorology*, Queensland Regional Office.

Dunn S.L., Nielsen P., Madsen P.A. and Evans P. (2000) Wave diffraction and setup in jettied river entrances. Proc. 27th Intl. Conf. Coastal Engin., *IEAust*, 16 - 21st July, Sydney, ISBN 085825 722X.

Sobey R.J. and Harper B.A. (1977) Tropical cyclone surge penetration across the Great Barrier Reef, Proc 3rd Aust Conf Coastal and Ocean Eng, *IEAust*, Melbourne 1977, pp 58-63.

Harper B.A. and Holland G.J. (1999) An updated parametric model of the tropical cyclone. Proc. 23rd Conf. Hurricanes and Tropical Meteorology, *AMS*, Dallas, Texas, 10-15 Jan.

Powell M.D. and Houston S.H. (1996) Hurricane Andrew's landfall in South Florida. Part II: Surface wind fields and potential real-time applications. *Weather and Forecasting*, 11 (3), 329-349.

Stark K.P. (*Ed.*) (1972) Cyclone *Althea* part II - storm surges and coastal effects. *James Cook University of North Queensland*, October.

Trollope D.H. (*Ed.)* (1972a) Cyclone *Althea* part I -buildings. *James Cook University of North Queensland*, March.

10.5 Tropical Cyclone Ted December 1976 at Burketown

Tropical Cyclone *Ted* passed just westwards of Mornington Island and crossed the southern Gulf of Carpentaria coast on the afternoon of 19th December 1976, later passing directly over the town of Burketown. It caused a very significant storm surge which in parts extended 20 km inland and up as far as the town itself, which is 40 km upstream of the Albert River mouth. Reports from nearby cattle stations confirmed extensive inundation of the low-lying coastal flats immediately to the east (Callaghan 2000). The nearest tidal readings were unfortunately at Karumba, some 140 km to the east, although a single water level estimate from Mornington Island is available. Karumba was also close to being inundated, the peak levels reaching within about 1 m of the local ground levels.

10.5.1 Available Data

10.5.1.1 Storm Parameters

The National Climate Centre (NCC) official track for this event was obtained and considered together with track modifications proposed by Callaghan south from Mornington Island which were used in an earlier storm surge assessment by Victory and Davis (1996). Bureau hardcopy records were also made available which included barographs at Mornington Island and Burketown, and observer notes with some estimated wind speeds and directions. Observer reports were also available from a number of cattle stations near Burketown, some of which reported passage of a calm and Augustus Downs provided a detailed pressure history. An anemograph from Port McArthur some 300 km to the NW was also considered. The limited electronic data available from NCC records were insufficient for the present purposes and accordingly most of the data was hand-digitised from the hardcopy records.

The cyclone was tracked by satellite during its early stages, as reported in an internal Bureau report, which details an eye diameter of 25 nmile visible through a series of NOAA5 orbits from 17/1041 UTC to 18/1136 UTC (refer Figure 10.45). After 18/2349 UTC it was reported that the eye was becoming obscured by cellular cloud and the storm appeared to be broadening and weakening. This was at the time it was approaching Mornington Island and probably near the point of significant interaction between the outer circulation and the southwestern corner of the mainland. In spite of this intensity change assessment (i.e. weakening) the official pressure record shows a deepening system with the minimum pressure maintained as a nominal 950 hPa, based on the Burketown reading in the eye some 10 h later and 30 km overland.

In hindsight therefore, the storm may well have been considerably more intense than the nominal 960 hPa from the official track during the early period of the 18th UTC when the eye was very clear. Although the images are not ideal, Callaghan (2000) advises that a Dvorak visible intensity estimate suggests that 930 hPa or even less may have been possible at that time. This would be consistent with the subsequent signs of weakening and the higher pressures at Mornington Island and Burketown. A synoptic view of the cyclone at landfall after Callaghan (2000) is given in Figure 10.46.

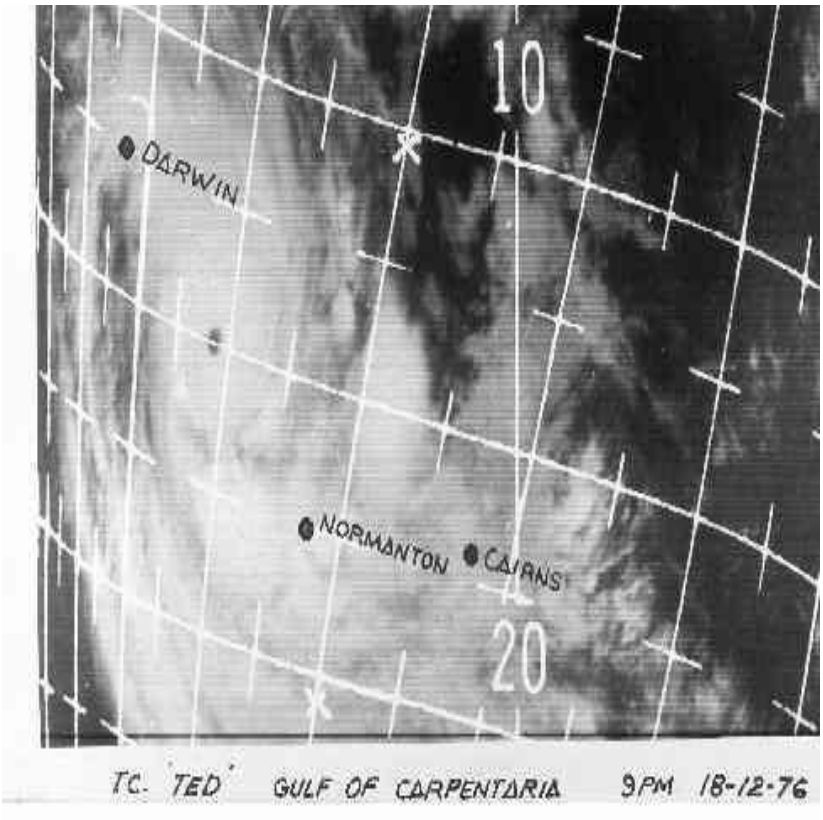

Figure 10.45 Satellite image of *Ted* (BoM photo)

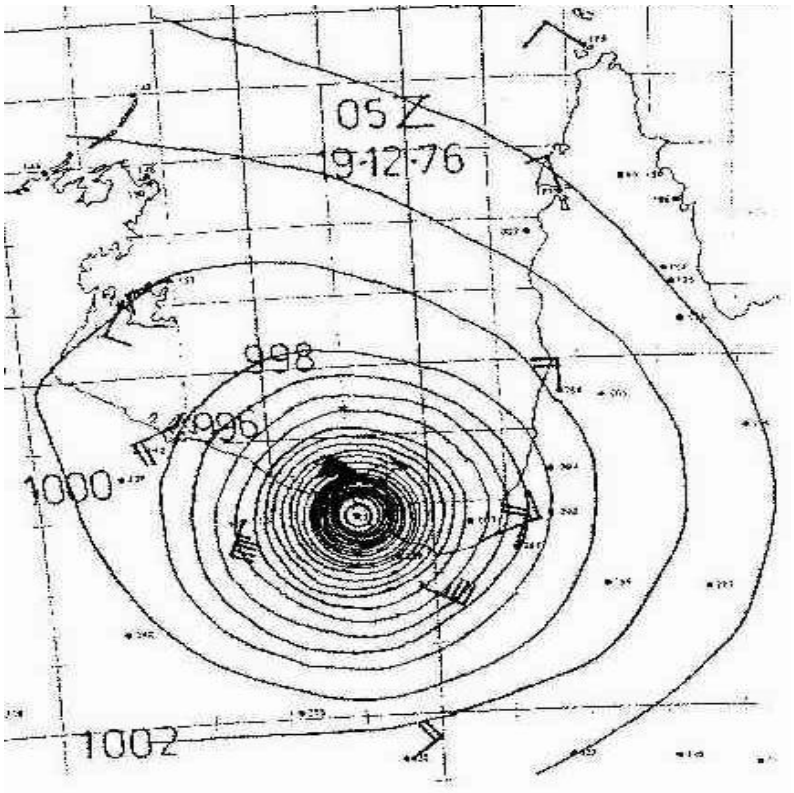

Figure 10.46 *Ted* synoptic situation (after Callaghan 2000).

10.5.1.2 Storm Surge

The only water level readings nearest to the cyclone landfall were taken at Karumba by a CSIRO research team and reported variously in Bureau internal reports as well as a Department of Harbours and Marine file note (H. Macdonald). These have been reconstructed together with the predicted tide supplied by Department of Transport (J. Broadbent) in the following Figure 10.47. The resulting inferred surge response is therefore of the order of 2 m for a period of almost 12 h and it is possible that the actual peak surge at Karumba occurred prior to the start of the monitoring period. The surge response also appears unusually flat and possibly shows signs of a later wave peak towards the end of the record although these values have been taken from handwritten annotations to the Harbours and Marine report. It is not known if the water level was recorded automatically or was manually noted. The peak water level recorded was 3.62 m AHD at 19/0900 UTC, approximately 1 h after the eye passed over Burketown 130 km to the west. This was approximately 1 m above HAT at Karumba (about 1 m below ground level) and clearly was associated with extensive flooding of the low-lying coastal lands between Karumba and the Albert River to the west.

The cyclone also impacted Mornington Island around 19/0200 UTC and caused disruption to its water supply, which is taken from the coastal aquifer. A report on the damage by engineers from Cardno and Davies Consulting Engineers was supplied, which details the elevation to which salt water was detected at the pump station. The level reported therein of 2.57 m AHD was later adjusted by the Harbours and Marine report slightly downwards after consideration of MSL references and a level of 2.29 m AHD established. The extent to which this figure might include wave setup and wave runup is unknown.

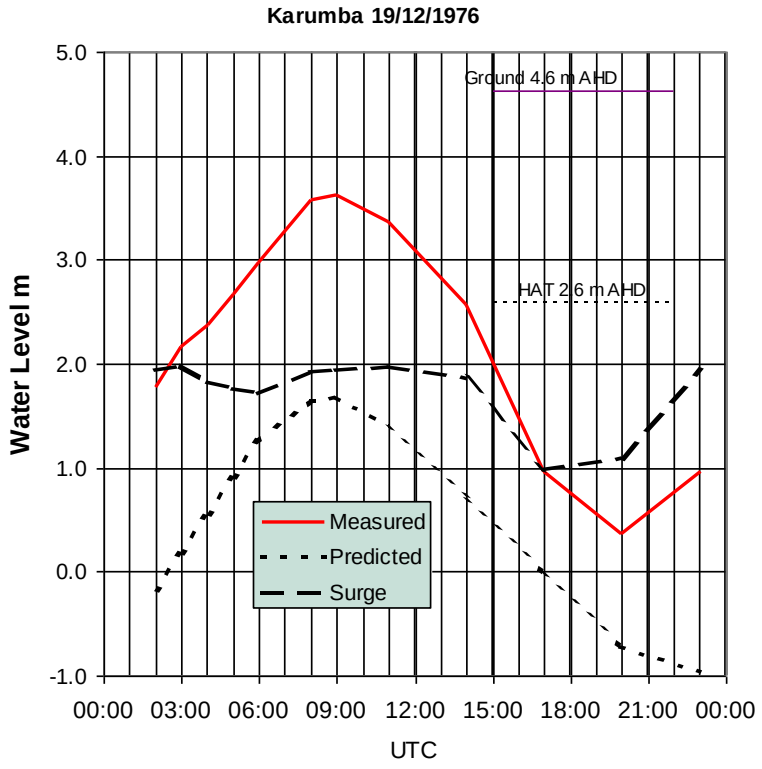

Figure 10.47 Tidal record from CSIRO observers at Karumba during *Ted*.

The very significant storm surge clearly flooded an extensive region of the low lying coastal plains and reached Burketown some 40 km upstream from the mouth of the Albert River.

However, no flooding of property in Burketown was reported and no actual water levels are available. Earlier numerical modelling by Victory and Davis (1996) attempted to represent the overland flow paths from the coast to Burketown and indicated that an attenuation of about 3 m in surge height was possible between the coast and the town. Their predicted open coast peak water level was 6 m AHD, giving a town level of about 3 m AHD. This is close to the level of the Burketown road crossing west of the town, which itself has a ground level of about 5.4 m. Their model also predicted a peak of 3.2 m AHD at the Truganinni Wharf some 7 km downstream that could be consistent with the damage suffered there. The Bureau observer in Burketown noted that water levels "came higher than any known flood".

10.5.2 Reconstruction of the Event

The following describes the result of a trial and error comparison between the available data and the predicted spatial and temporal variations in wind and pressure as predicted by an analytical model (Harper and Holland 1999), detailed in Appendix C. The model was systematically adjusted for reasonable values of the key parameters such as track, central pressure and radius to maximum winds. The available data from Burketown, Mornington Island and Augustus Downs were then compared with the model output to determine the validity of the various assumptions. Consistent with experience from cyclone *Althea* (refer Section 10.4), a windfield asymmetry based on a υ_{max} of 115º was applied.

The modified NCC track after Callaghan (2000) was utilised first and radius to maximum wind (R) and wind field peakedness parameters (B_0) were determined for Burketown and Mornington Island. The storm centre was mapped by Callaghan directly over Burketown and then based on whether or not a calm was experienced by the observers at various cattle stations to the south. The present analysis suggested that the true storm centre may have passed slightly more to the east of Burketown, thus aligning the period of calm more with the minimum pressure, as reported by the observer. The modelled calm duration was also slightly more consistent with the observed duration in the shifted configuration. South of Burketown a number of small track shifts, mainly to the east, were made to try to improve the model comparison at Augustus Downs and still be consistent with the other station reports. This was less successful and required the storm to increase its forward speed quite substantially over a short period, reaching speeds in excess of 8 m s^{-1}. No significant changes to the estimated central pressure were made.

10.5.2.1 Final Track Parameters

Table 10.10 summarises the final storm parameters chosen, while Figure 10.48 shows the track and predicted wind and pressure field as the storm made landfall. Radius values prior to close approach at Mornington Island were based on the satellite estimates of eye diameter where available and are nominal before that time. At around the time of landfall, model optimisation indicated a B_0 value of 7.1 and a radius of maximum winds around 50 km was appropriate. An ambient pressure of 1006 hPa was chosen based on pre-cursor barograph readings.

Table 10.10 Adopted hindcast parameters for tropical cyclone *Ted*.

Track Fix			Speed	Bearing	Central Pressure	Radius	Peakedness
Time	Lat	Long	V_{fm}	θ_{fm}	p_0	R	B_0
UTC	°	°	m s^{-1}	°	hPa	km	
15-Dec-1976 23:00	-12.6	140.5	2.1	256	1005	100	7.1
16-Dec-1976 05:00	-12.7	140.1	2.1	256	1001	100	7.1
16-Dec-1976 11:00	-12.8	139.7	2.1	256	997	100	7.1
16-Dec-1976 17:00	-12.9	139.3	1.6	251	994	100	7.1
16-Dec-1976 23:00	-13.0	139.0	1.0	270	990	100	7.1
17-Dec-1976 05:00	-13.0	138.8	1.1	243	982	82	7.1
17-Dec-1976 11:00	-13.1	138.6	1.0	270	974	64	7.1
17-Dec-1976 17:00	-13.1	138.4	1.6	251	969	46	7.1
17-Dec-1976 23:00	-13.2	138.1	3.7	213	964	28	7.1
18-Dec-1976 02:00	-13.5	137.9	3.7	213	963	28	7.1
18-Dec-1976 05:00	-13.8	137.7	4.2	166	962	28	7.1
18-Dec-1976 08:00	-14.2	137.8	5.2	169	961	28	7.1
18-Dec-1976 11:00	-14.7	137.9	4.1	151	960	28	7.1
18-Dec-1976 17:00	-15.4	138.3	4.1	151	955	35	7.1
18-Dec-1976 23:00	-16.1	138.7	6.0	162	950	42	7.1
19-Dec-1976 02:15	-16.7	138.9	6.0	161	950	45	7.1
19-Dec-1976 05:00	-17.2	139.1	4.1	136	950	48	7.1
19-Dec-1976 10:15	-17.7	139.6	4.5	136	948	54	7.1
19-Dec-1976 13:45	-18.1	140.0	6.8	144	955	55	7.1
19-Dec-1976 15:00	-18.4	140.2	8.1	105	965	55	7.1
19-Dec-1976 16:30	-18.5	140.6	8.5	136	970	55	7.1
19-Dec-1976 18:00	-18.8	140.9	6.8	205	970	55	7.1
19-Dec-1976 20:00	-19.2	140.7	3.2	162	980	55	7.1
19-Dec-1976 23:00	-19.5	140.8	1.5	180	985	55	7.1
19-Dec-1976 23:30	-19.5	140.8	1.5	180	985	55	7.1
20-Dec-1976 05:00	-19.8	140.8	1.5	180	988	55	7.1
20-Dec-1976 11:00	-20.1	140.8	1.5	180	992	55	7.1
20-Dec-1976 17:00	-20.4	140.8	1.5	180	996	55	7.1
20-Dec-1976 23:00	-20.7	140.8	1.5	180	1000	55	7.1

10.5.2.2 Comparison of Measured and Modelled Storm Parameters

The Burketown Post Office barograph was digitised and pressures adjusted to match the annotated chart time-check pressures. [Callaghan (2000) notes that it was routine procedure to set the barograph approximately +10 hPa relative to the actual pressure during summer to provide a safety factor against "bottoming out" at the 950 hPa chart limit in the event of a close cyclone.] The minimum MSL pressure recorded at Burketown on this basis was 948.6 hPa and, based on the observer notes, occurred during a calm which lasted 1.5 h. No wind speed or direction data is available. The digitised pressure trace together with the optimised model fit is reproduced here as Figure 10.49 indicating a peak mean wind of about 30 m s^{-1}.

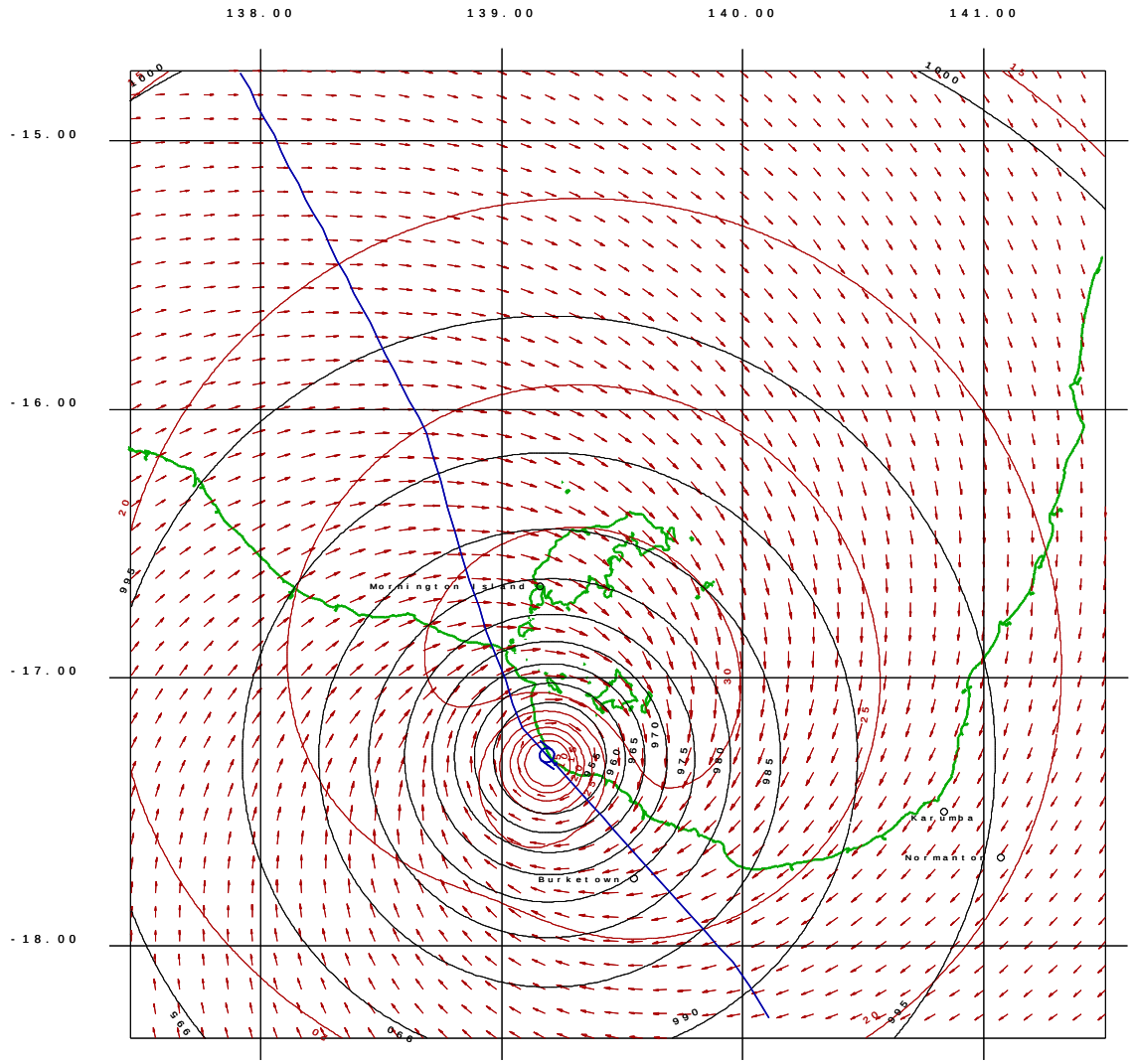

Figure 10.48 Reconstructed cyclone track and wind and pressure fields at landfall for *Ted*.

The Mornington Island barograph was similarly digitised and the wind direction estimates have been used in the measured and modelled comparison in Figure 10.50. Although wind estimates were made by the observer it is not clear whether mean or gust speeds were being reported at various times and as a result these values have been discarded for the present comparison. The model indicates mean winds of about 35 m s^{-1} and is close to matching the barograph minimum of 957 hPa at 19/0230 UTC. The observed wind direction changes are quite well matched and the model is consistent with no calm being experienced at Mornington Island.

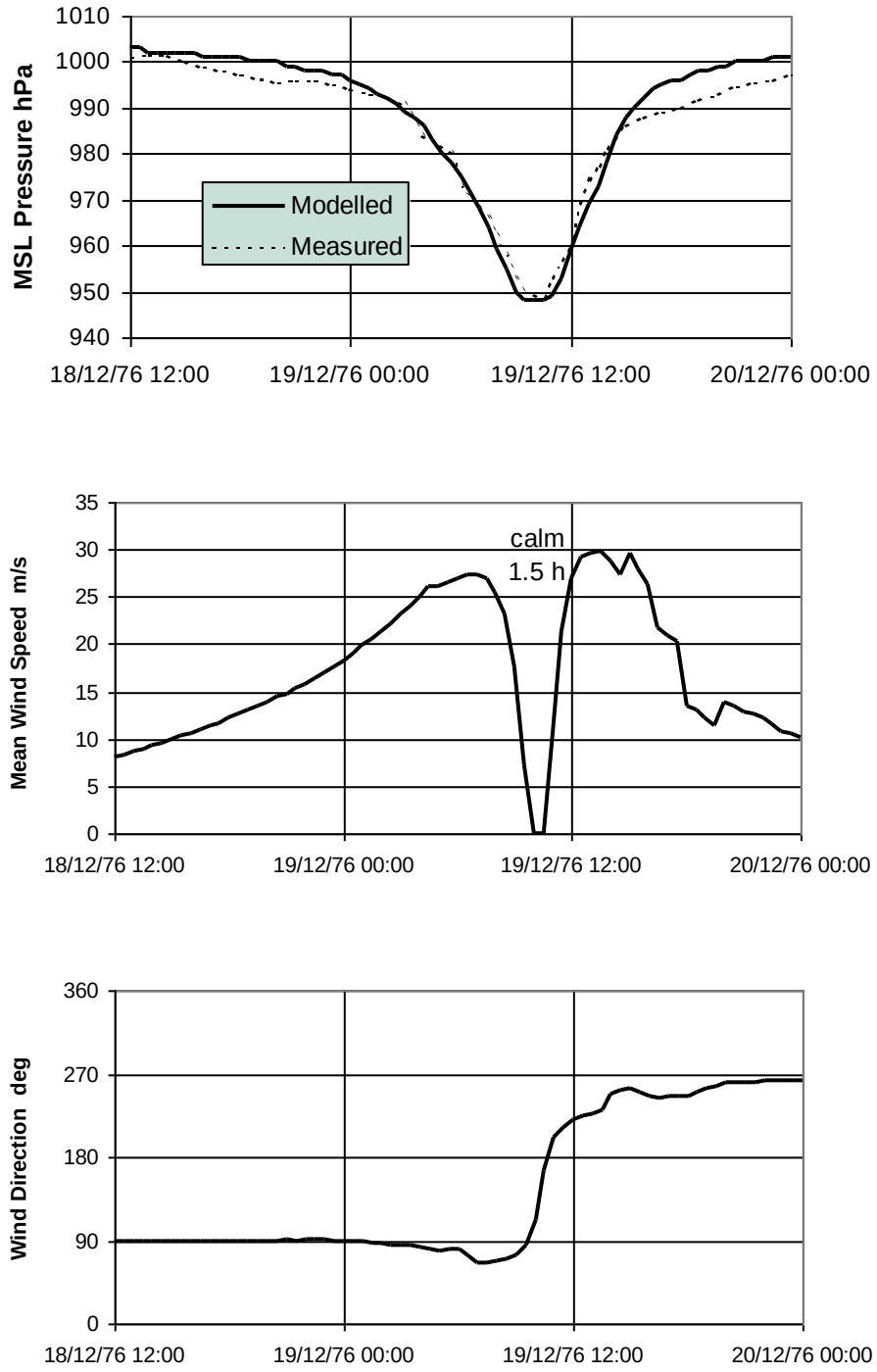

Figure 10.49 Modelled and measured pressures and winds at Burketown for *Ted*.

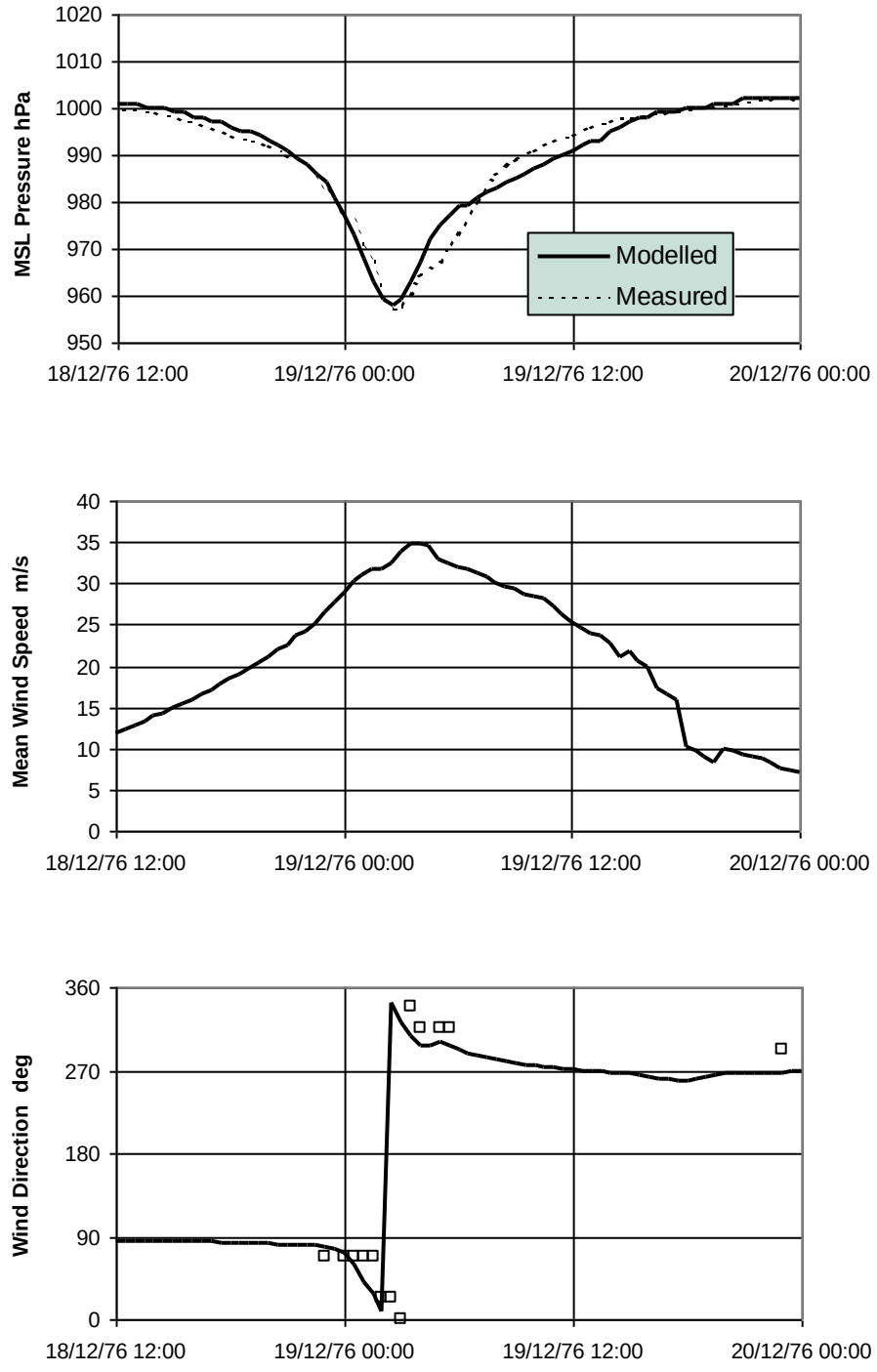

Figure 10.50 Modelled and measured pressures and winds at Mornington Island for *Ted*.

A number of pressure readings were also reported from Augustus Downs station, approximately 100 km south of Burketown. Values were taken hourly with a minimum of 973.4 hPa at 19/1600 UTC. Wind speed estimates were again discounted but direction changes are indicated in the comparison in Figure 10.51.

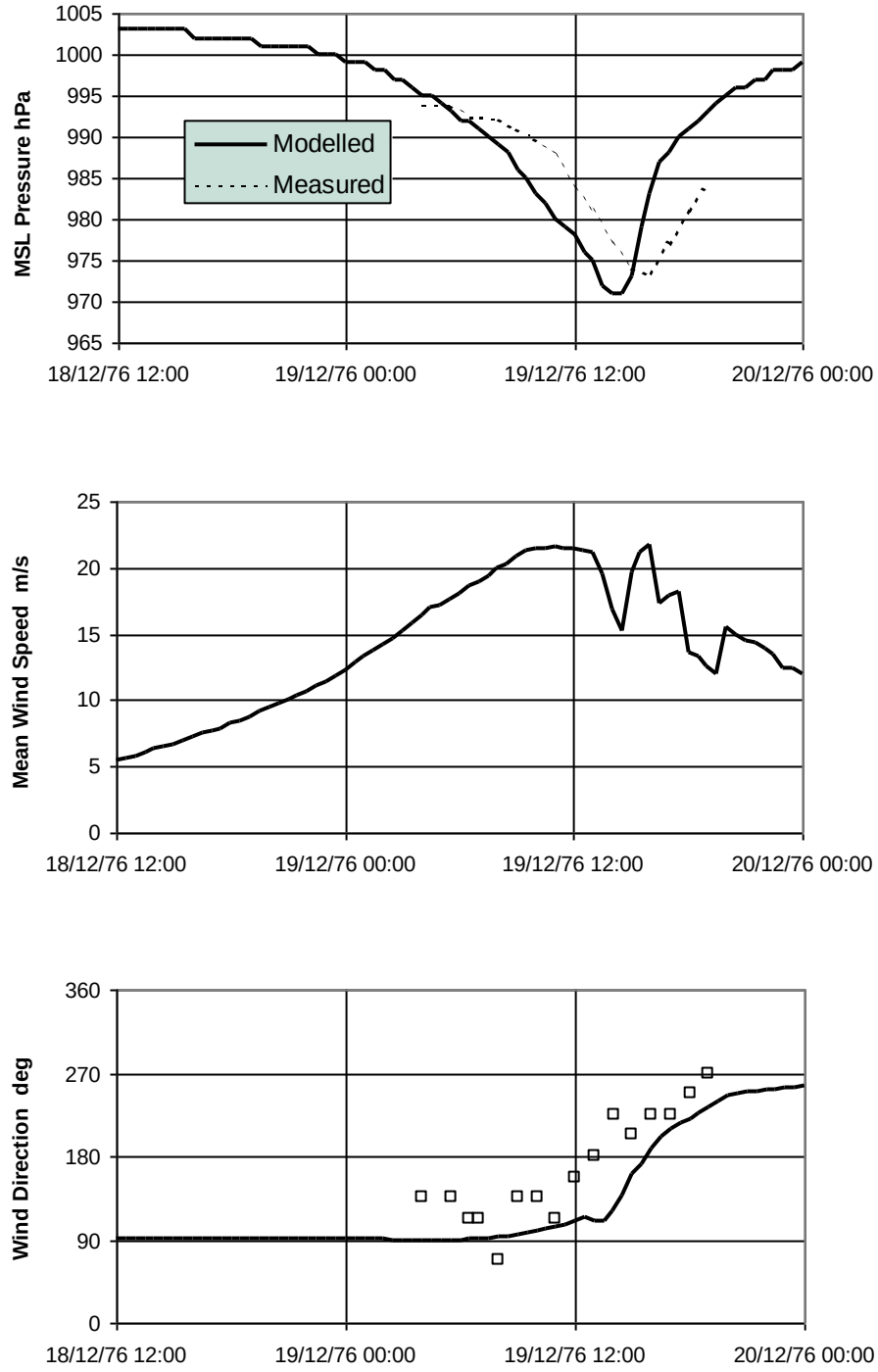

Figure 10.51 Modelled and measured pressures and winds at Augustus Downs for *Ted*.

The model slightly overestimates the recorded pressure but leads the time of the minimum by about 2 h while lagging the change in wind direction by a similar amount. Great difficulty was encountered trying to match these timings and the reasons remain unknown. Finally, Figure 10.52 presents modelled winds and pressures at Karumba but no data is available for comparison.

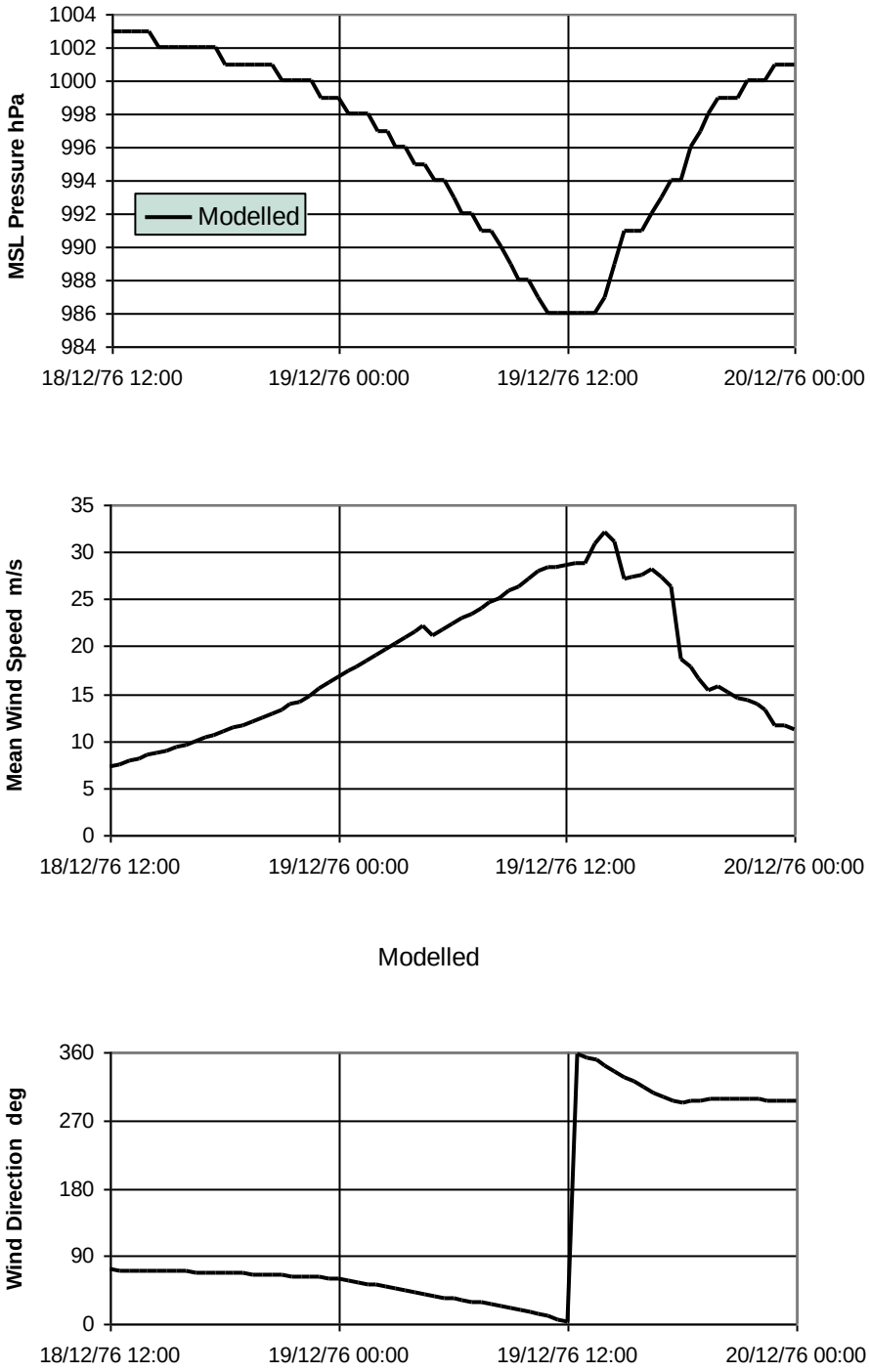

Figure 10.52 Modelled pressures and winds at Karumba for *Ted*.

10.5.3 Implications for Storm Surge Modelling

The intensity of cyclone *Ted* before its close approach to Mornington Island remains unknown, but the model optimisation is at least consistent with the observed broadening of the eye at that time, producing a relatively large scale storm circulation as a result. The quality of recorded water levels and an absence of objective wind data leave a relatively large margin of error in predicting the peak surge.

In Figure 10.53 below, the modelled envelope of maximum winds shows the extreme band of onshore winds that would have acted to produce an extreme storm tide along the coast.

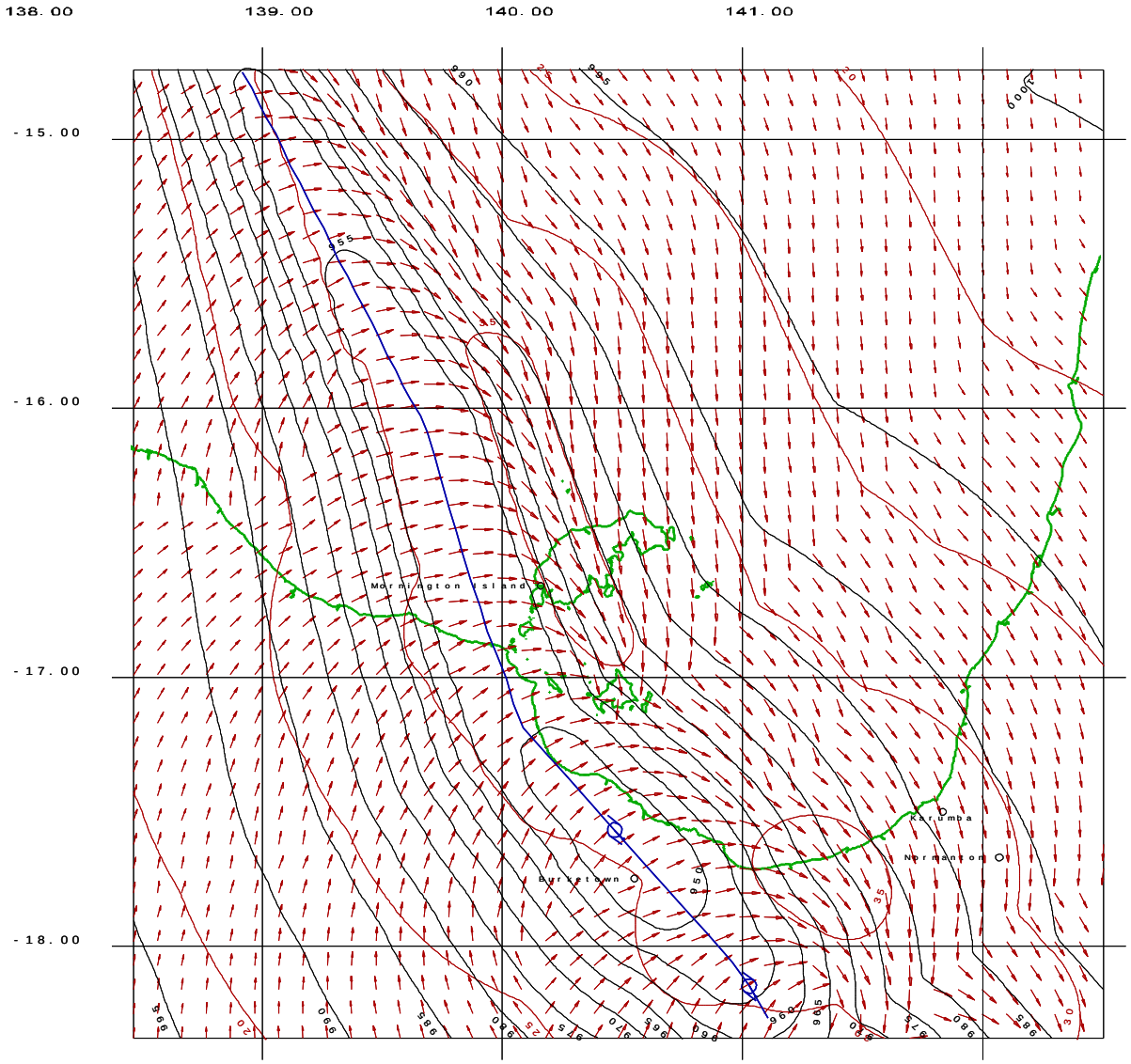

Figure 10.53 Modelled envelope of maximum winds and minimum pressure for *Ted*.

10.5.4 Tidal Modelling

The Arafura Sea and Gulf of Carpentaria is a unique part of the world oceans. The area is semi-enclosed and covers many hundreds of thousands of square kilometres of ocean that is less than 70 m deep. It is one of the world's largest sinks of tidal energy due to bottom friction. The region has both large diurnal and semi-diurnal tides. Semi-diurnal tides are dominant in the northern parts of the region while diurnal tides are relatively large in the southern part of the gulf. Non-tidally induced water height variations are also significant in this region. Oceanic water level fluctuations and wind stress are the major contributors to these variations. Both these mechanisms have a strong seasonal signal, and significant changes in water level (e.g. 0.3 - 1 m) have been observed over short periods with changing wind conditions. The coastal areas of the southern and southeastern part of the gulf are also usual. This part of the coast contains large areas of tidal flats which in places extend some tens of kilometres inland. As a result there are many hundreds of square kilometres of land potentially susceptible to storm surge inundation.

Because of the regional complexity, the hindcast modelling of *Ted* has been undertaken using an existing outer grid (5 nmile) that completely covers the Gulf of Carpentaria and the shallower parts of the Arafura Sea. A second smaller grid with a resolution of 0.5 nmile was especially generated for the area southeast of Mornington Island but does have known errors both in bathymetry and land elevation. Land elevations were taken from the GTOPO30 global database and individual grid points from this database were adjusted so that the minimum elevation was 2.5 m above AHD. This gives only a very approximate representation of the floodable land in the region.

Tidal boundary conditions were then applied to the Gulf of Carpentaria grid using only the five constituents available. These are not sufficient for accurately reproducing the tide at Karumba or Mornington Island. At the time of *Ted's* landfall the modelled high tide at Karumba was 0.5 m below predicted (refer Figure 10.54). At Mornington Island however, the model gives reasonable agreement at high tide but underpredicts the low tide (Figure 10.55).

A significant amount of work is indicated to improve the representation of the Gulf of Carpentaria region and to properly calibrate a tidal model. The present study has only been able to draw upon readily available sources of information.

10.5.5 Storm Surge Modelling

Because of the poor tide representation, the surge-only response without any tidal input is discussed initially. Discussion on water levels over flooded land is deferred to the tide-included case, although the levels are somewhat in error, because the extent of flooding critically depends on an absolute water level.

An overall view of the Gulf of Carpentaria modelled response to *Ted* is shown in Figure 10.56, approximately at the time of passage over Burketown. The largest surge build-up is indicated in the region between Karumba and Burketown, which is consistent with the experience of the various landowners.

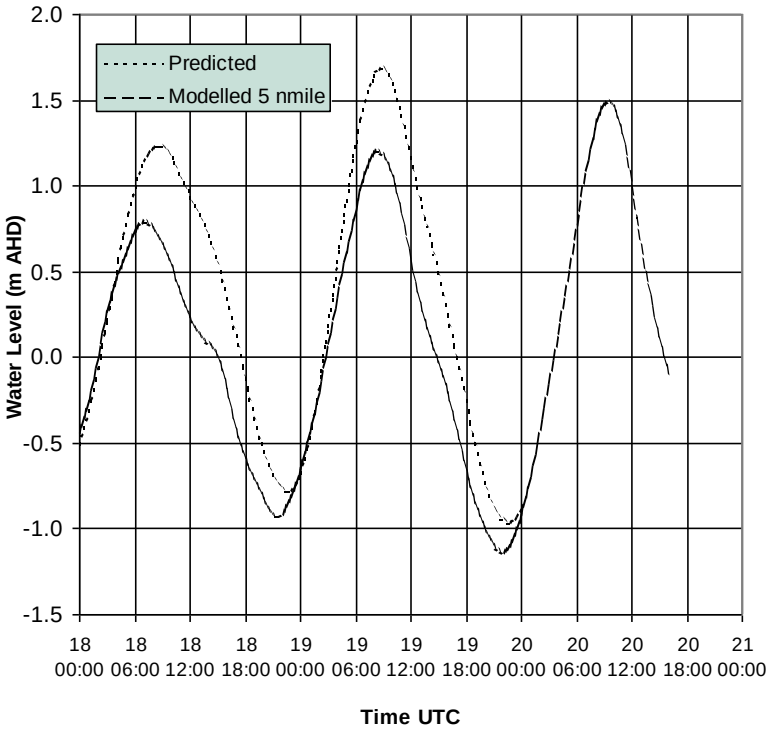

Figure 10.54 Modelled and measured tides at Karumba for *Ted*.

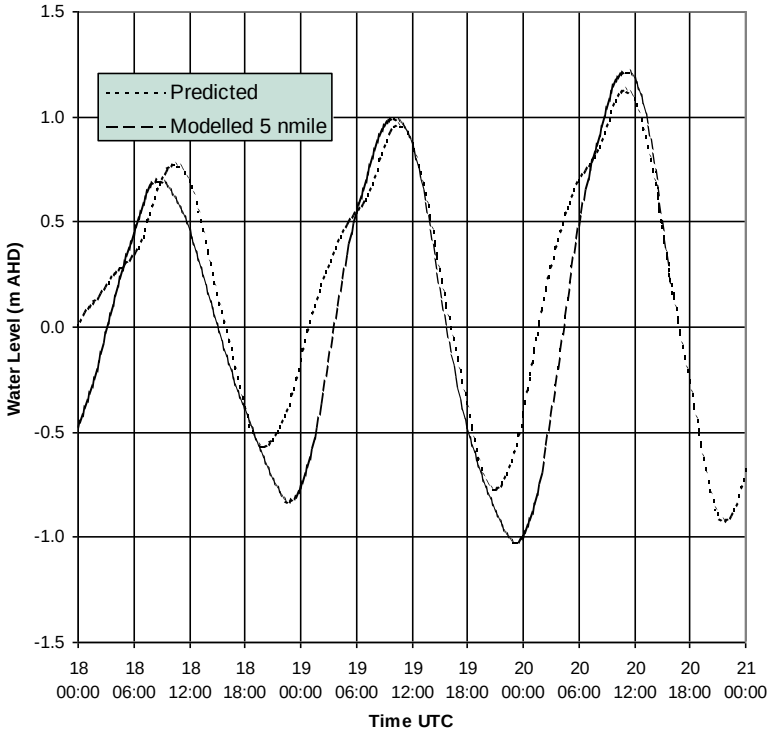

Figure 10.55 Measured and modelled tides at Mornington Island for *Ted*.

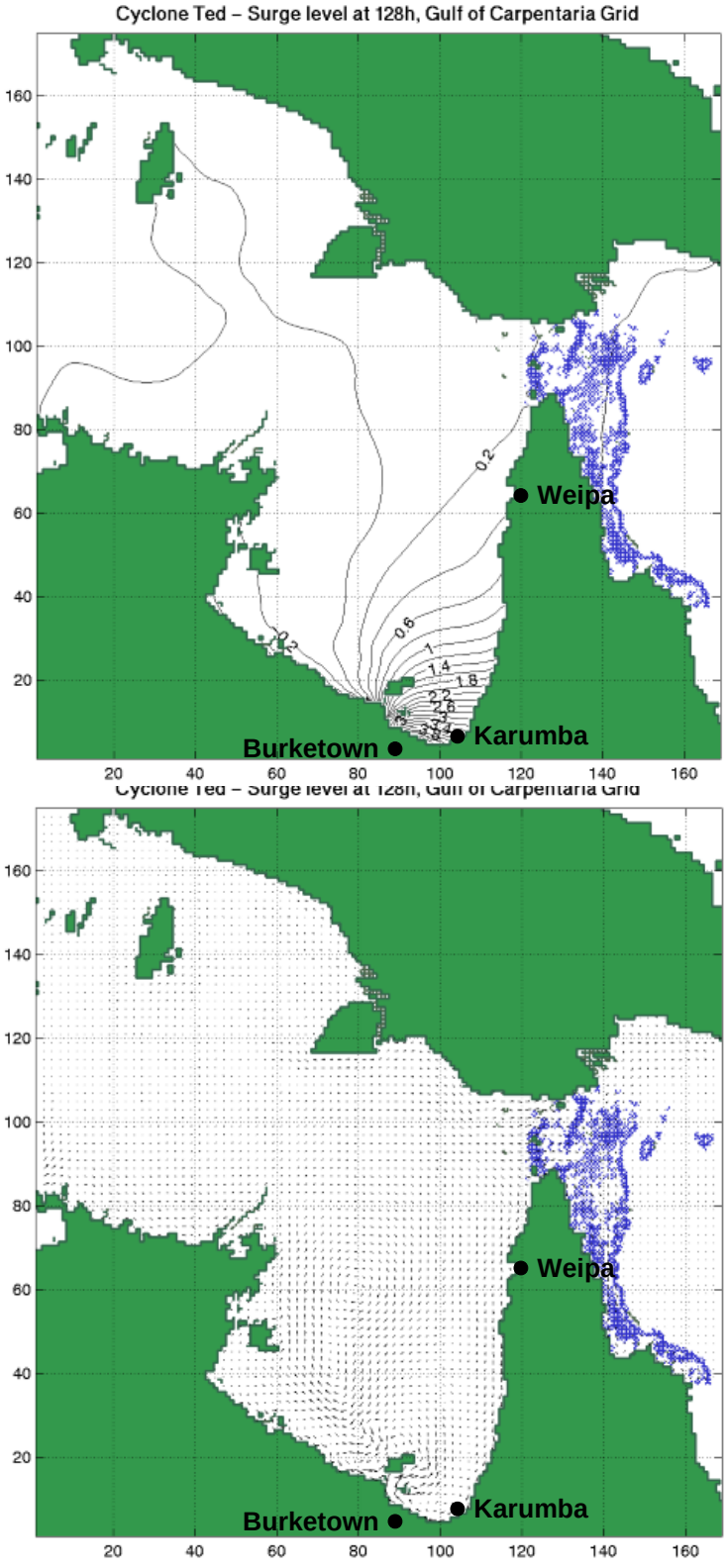

Figure 10.56 Storm surge response of *Ted* without tide.

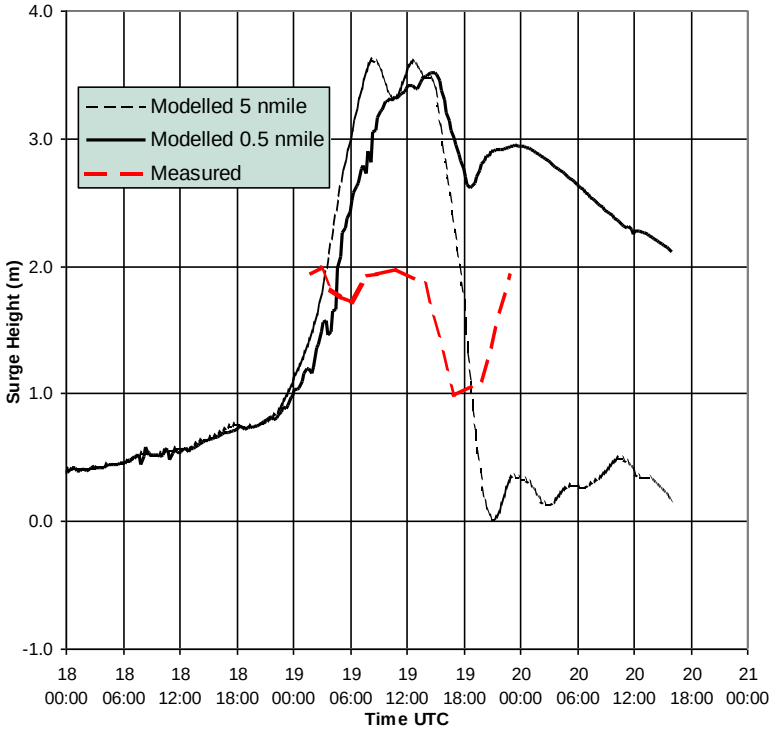

Figure 10.57 Measured and modelled surge height at Karumba for *Ted*.

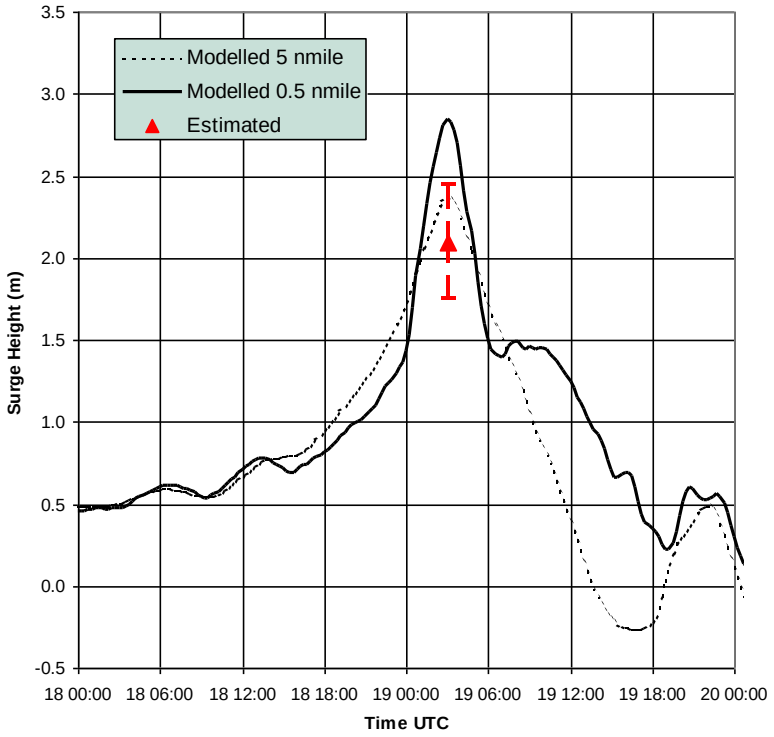

Figure 10.58 Measured and modelled surge height at Mornington Island for *Ted*.

The measured surge component at Karumba was approximately 2 m and was sustained at that level for almost 12 h. Although the models show elevated water levels for up to 12 h they significantly overestimate the surge, giving values of 3.62 and 3.57 m at the mouth of the Norman river, as shown in Figure 10.57. At Mornington Island the surge component is not really known but an estimate can be made based on the expected tide level at the time and the measured debris line at 2.29 m AHD. This yields a surge (+ setup) component somewhere between 1.75 m and 2.45 m, i.e. a mean of 2.1 m. As shown in Figure 10.58, the model seems to better predict the surge on the outer 5 nmile grid, which gives a surge of 2.37 m. However the finer 0.5 nmile grid overpredicted the likely water level range significantly (2.85 m). This overprediction is thought to be due to the rather poor detail of the bathymetry in this region of the model. At the mouth of the Albert River, the 1 nmile model predicted 4.43 m versus the 0.5 nmile 4.71 m - very significant storm surge by any standard.

Considering now the influence of the tide level on the absolute water level, this can be expected to result in a highly nonlinear response to the surge and tide combination. Figure 10.59 compares the modelled and measured total water levels at Karumba, where the highest recorded water level was 3.6 m AHD. For this case, the models predict water levels of 4.36 (outer) and 4.33 m (fine) at the mouth of the Norman River. This is reduced to 4 m at Karumba in the finer model, which attempts to resolve parts of the Norman River where Karumba is situated. Even allowing for our poor representation of the tide, this shows a large nonlinear effect associated with overland flooding. The impact was clearly very significant because the recorded levels are about 0.5 m lower, thus sparing the town from what may have been a very hazardous situation.

At Mornington Island (Figure 10.60), the modelled peak water level is 2.16 m on the outer grid, which is close to the estimated peak of 2.29 m, while the finer grid overpredicts by about 0.5 m. At the mouth of the Albert River, the models predict peak levels of 4.95 and 5.23 m AHD.

It is therefore considered likely that the accuracy with which the model predicts water levels at Karumba may be largely dependent on how well overland flooding is represented. For example, the second modelled peak in Figures 10.57 and 10.59 is due to the return flow of waters from the river system. The data shows a much smaller effect, thus indicating that the crude model representation is not resolving the complex channels, which would attenuate such a return flow. Due to a lack of data, the present model simply assumes large coastal areas in the southern Gulf are approximately at an elevation of 2.5 m AHD. To improve the model will therefore require a much better description of land elevations, and possibly overland friction and overland wind stress. The present model assumes a constant surface roughness and over-water wind stresses on water that has moved onto land.

One interesting result from the present model is that over the flooded lands to the west of Karumba peak surge levels could continue to increase inland from the coast. In Figure 10.61, the overland flooding is contrasted between the time of the peak level at Karumba to a time 10 h later. The surge peak increases from 4.62 m at the coast to 6.1 m approximately 20 km inland while the coastal surge has almost reduced to zero. This major ingress is in the general location of Magowra Station southwest of Normanton, which reported "tidal water came inland approximately 30 km".

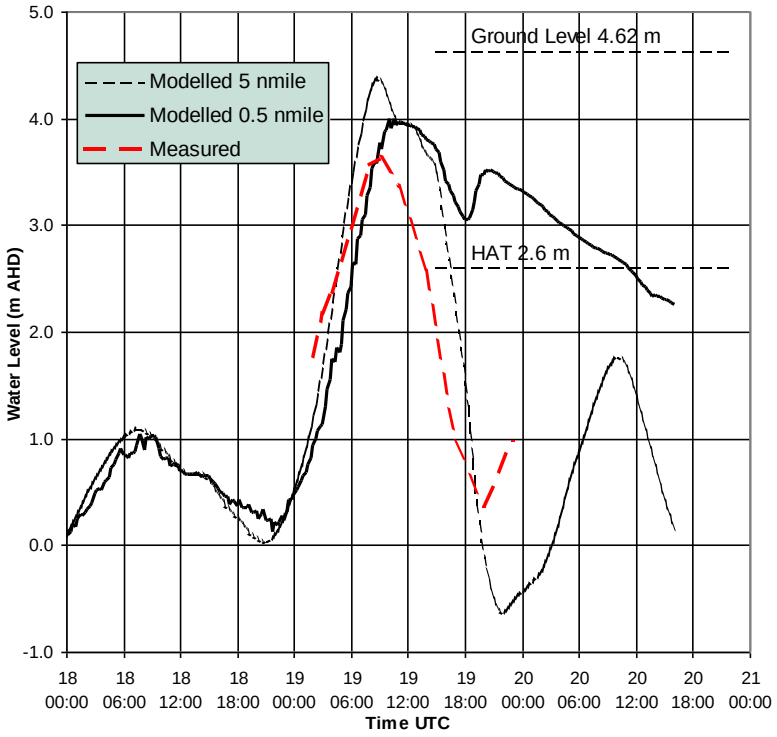

Figure 10.59 Measured and modelled absolute water levels at Karumba for *Ted*.

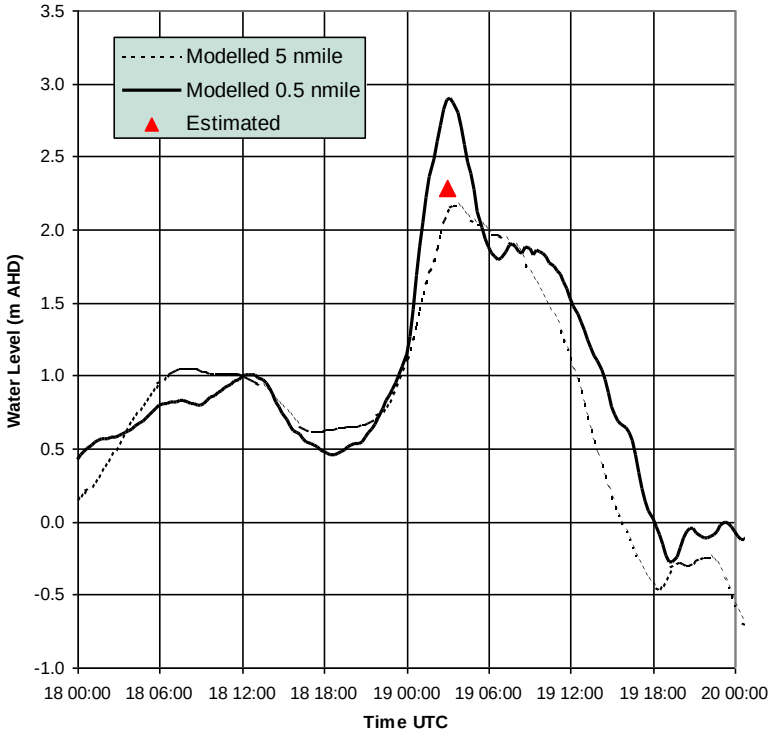

Figure 10.60 Measured and modelled absolute water levels at Mornington Island *Ted*.

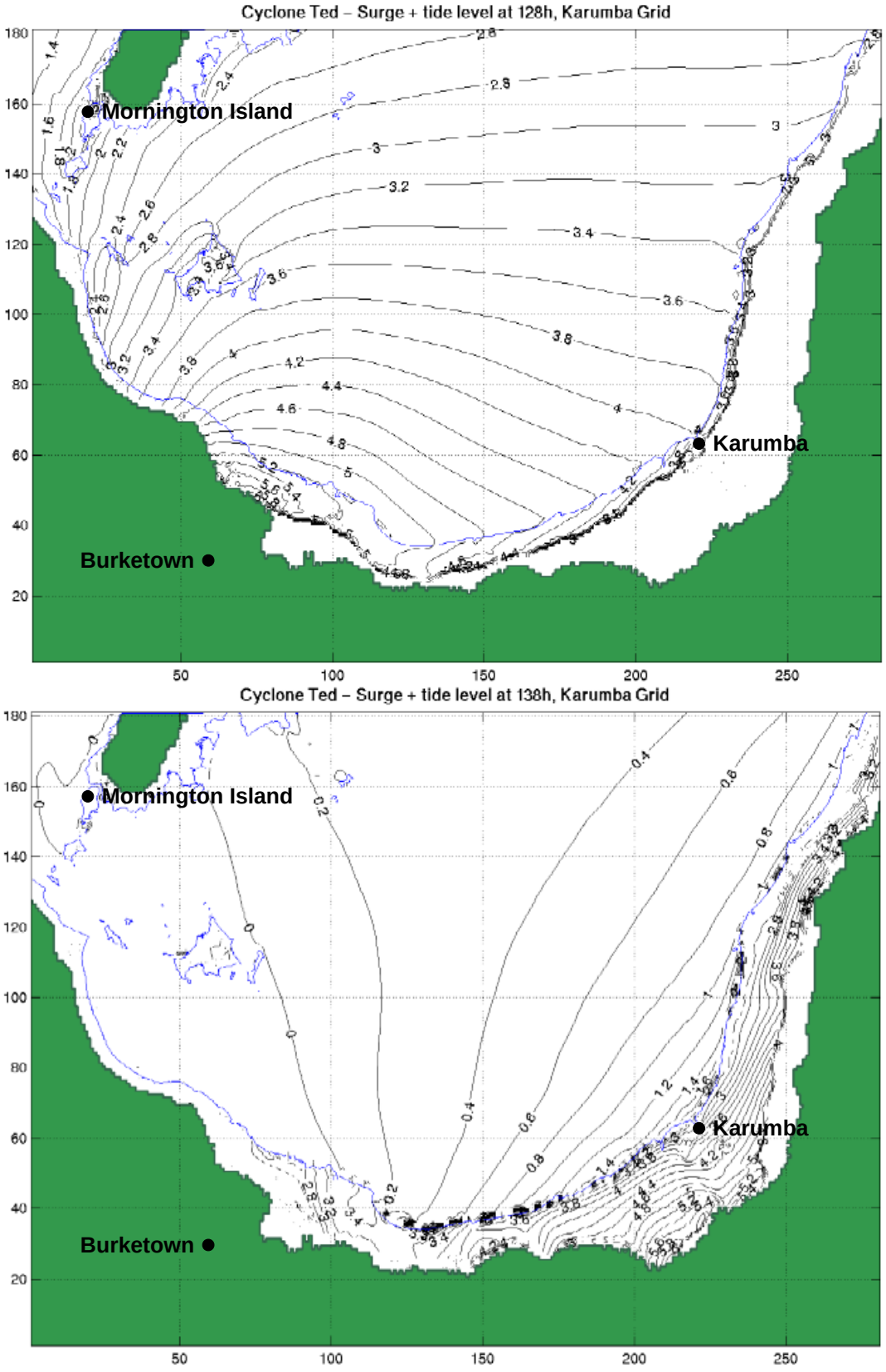

Figure 10.61 Example of overland flooding peaks for *Ted* increasing after peak storm tide.

10.5.6 References

Bureau of Meteorology (1976) Report on storm tide forecasts for cyclone "Ted" 19.12.76. *Unpublished*.

Broadbent G.J. (2000) Personal communication. *Queensland Department of Transport*.

Callaghan J. (2000) Personal communication. *Bureau of Meteorology*, Queensland Regional Office.

Department of Harbours and Marine (1976) Cyclone "Ted" report on storm surge. Intra-Departmental Memorandum by H.V.Macdonald. *Unpublished*.

Department of Harbours and Marine (1977) Storm surge Mornington Island 19/12/76: report from Cardno and Davies 907 B8. Intra-Departmental Memorandum by D. Wolter. *Unpublished*.

Harper B.A. and Holland G.J. (1999) An updated parametric model of the tropical cyclone. Proc. 23rd Conf. Hurricanes and Tropical Meteorology, *AMS*, Dallas, Texas, 10-15 Jan.

Victory S.J. and Davis B.D. (1996) Tropical cyclone “Ted” storm tide elevations re-examined. Dept of Environment and Heritage, Queensland. *Unpublished*.

10.6 Tropical Cyclone Steve February 2000 at Cairns

Tropical Cyclone *Steve* crossed the coast near Yorkeys Knob, 14 km north of Cairns in the early evening of 27th February about 7 pm EST. The cyclone formed from a complex low-pressure system imbedded in a monsoon trough but rapid intensification occurred only as the system approached quite close to the coast. Consequently it presented a difficult forecasting problem and only attained tropical cyclone status and was named barely 12 h before making landfall. By landfall it was deemed to have reached Category 2 strength, producing mean winds of 30 m s^{-1} at Cairns Airport and caused widespread but generally low level damage to trees and powerlines. It was a very small storm at landfall with an eye diameter of the order of 20 km. As it moved inland it caused major flooding, especially at Mareeba. A storm surge of approximately 1 m was recorded at Cairns Harbour.

Steve continued across Cape York and re-intensified briefly in the Gulf of Carpentaria, then crossed the Northern Territory and northwestern Western Australia to emerge near Broome and track down the West Australian coastline as variously a Category 1 or 2 storm. It recurved near Shark Bay and finally lost its circulation on 11th March, south of Esperance in the Great Australian Bight. *Steve* was notable for its longevity and its significant flooding impacts across three States. For North Queensland it represented a class of unpredictable mid-intensity cyclones whose storm tide impacts are quite difficult to estimate.

10.6.1 Available Data

Meteorological data for *Steve* was provided directly by the Severe Weather Section of the Queensland Regional Office of the Bureau of Meteorology. Storm tide information was provided by the Maritime Section of Queensland Transport.

10.6.1.1 Storm Parameters

The official track for this event during the initial period affecting the North Queensland coast was obtained from the Queensland Regional Office. Wind and pressure data was available from a number of offshore AWS and coastal stations.

A synoptic view of the cyclone during the two days prior to landfall is given in Figure 10.62 (after Callaghan 2000). The system became organised and, between 26/1200 UTC and 27/000 UTC, underwent a period of rapid intensification while the centre contracted. The general circulation was highly asymmetric with maximum winds to the SE and, as it moved onshore and intensified, was followed by an E to NE wind surge. The centre tracked between Flinders Reef and Willis Island, passed over Holmes Reef and very close to Green Island before coming ashore at Yorkeys Knob.

The visible satellite image in Figure 10.63 taken a few hours before landfall shows a partly obscured eye in the midst of heavy convection to the east, suggesting the system was still trying to fully organise. The later Cairns radar image at 27/0850 UTC in Figure 10.64 clearly shows the eye, with a diameter of about 22 km, located between Green Island and the coast.

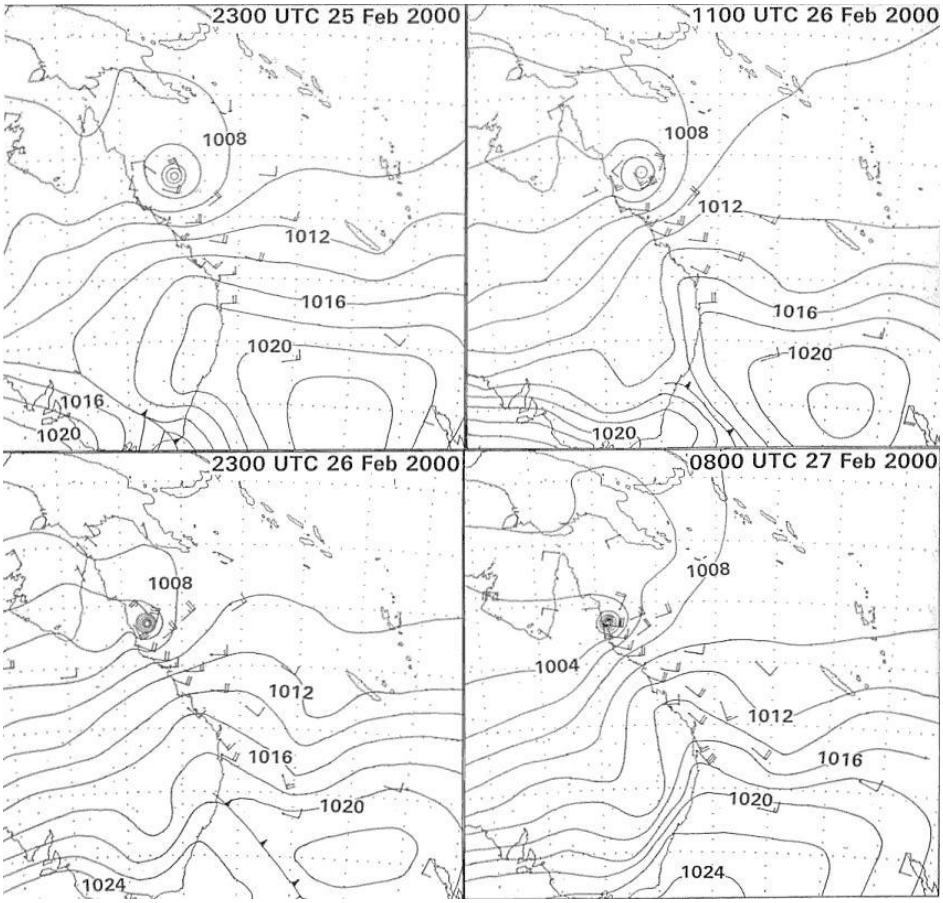

Figure 10.62 Synoptic situation for *Steve* (after Callaghan 2000)

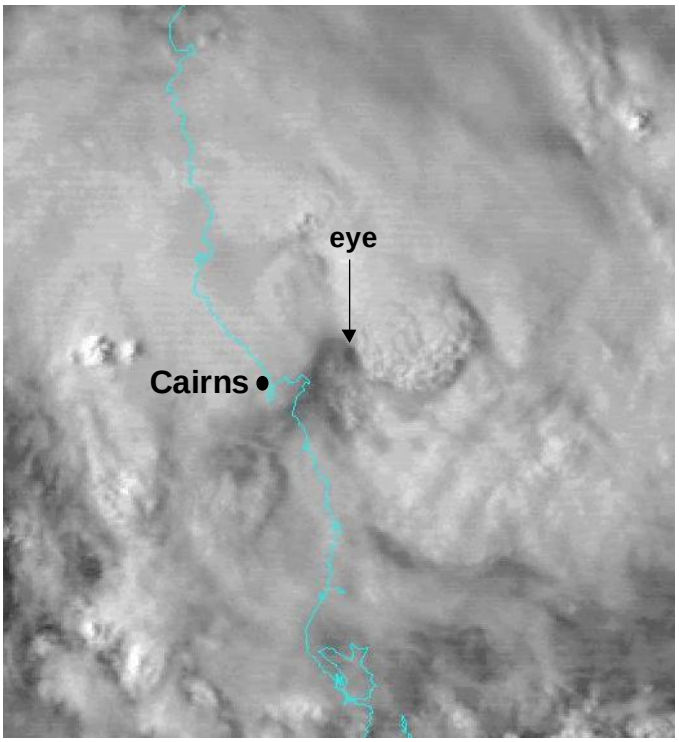

Figure 10.63 GMS 5 satellite image of *Steve* a few hours before landfall.

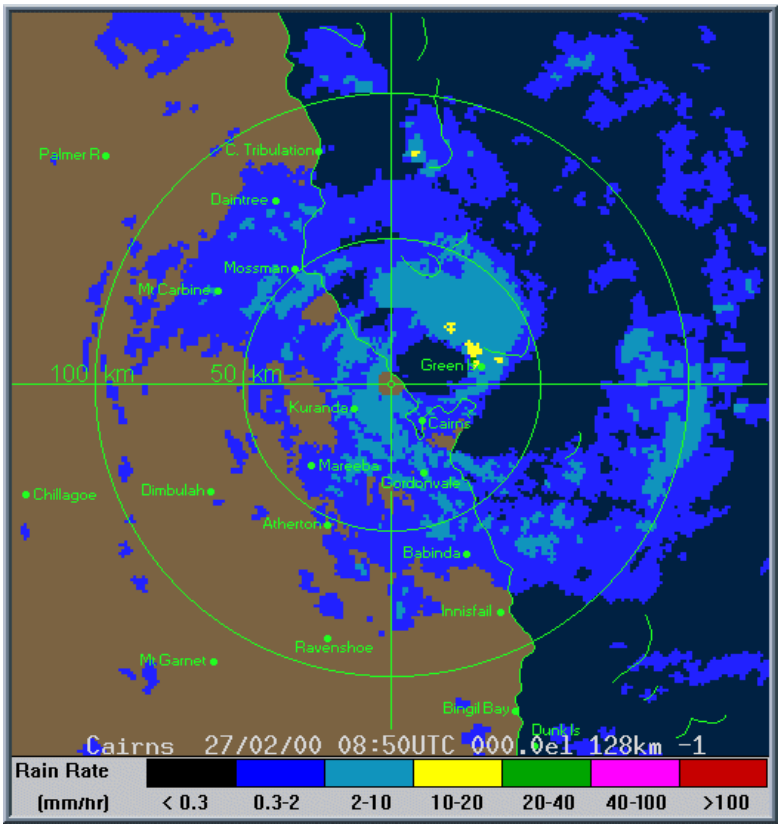

Figure 10.64 Radar image of *Steve* near landfall.

The anemograph record from Cairns Airport is given in Figure 10.65, registering a peak 10 minute wind of 30 m s^{-1} at +10 m. At Green Island, which experienced the edge of the eye, peak mean winds reached 34 m s^{-1} but at the anemometer height which is 40 m.

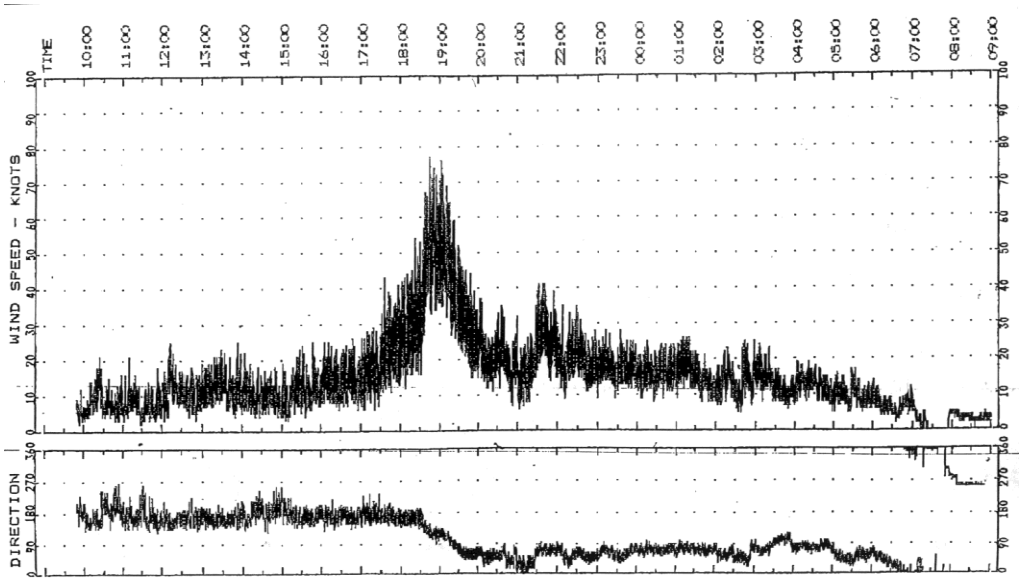

Figure 10.65 Anemograph from Cairns Airport during *Steve*.

10.6.1.2 Storm Surge

The storm surge from *Steve* was relatively small but the unpredictability of the storm and its rapid intensification near the coast is of interest in being able to reproduce its effects. A selection of regional storm surge magnitudes is given in Table 10.11.

Table 10.11 Summary of measured storm surge magnitudes for *Steve*.

Location	Distance from Landfall	Surge Magnitude
	km	m
Mossman	55	0.51
Port Douglas	46	0.43
Cairns	-14	1.00
Mourilyan	95	0.45
Clump Point	125	0.41

Figure 10.66 shows the tide gauge record from Cairns overplotted with the predicted tide and the resulting surge magnitude component. In the lead-up to the event, coastal water levels were already about 0.2 m higher than predicted, possibly because of the influence of the monsoon trough and the developing low offshore. Interest here is in the sudden onset of the surge between 0830 and 0900 UTC, as the cyclone centre passed about 15 km to the north. Prior to this time, the surge was apparently blocked by Cape Grafton. If the cyclone landfall had been about 12 h later, the total water level may have just exceeded HAT and caused some local flooding.

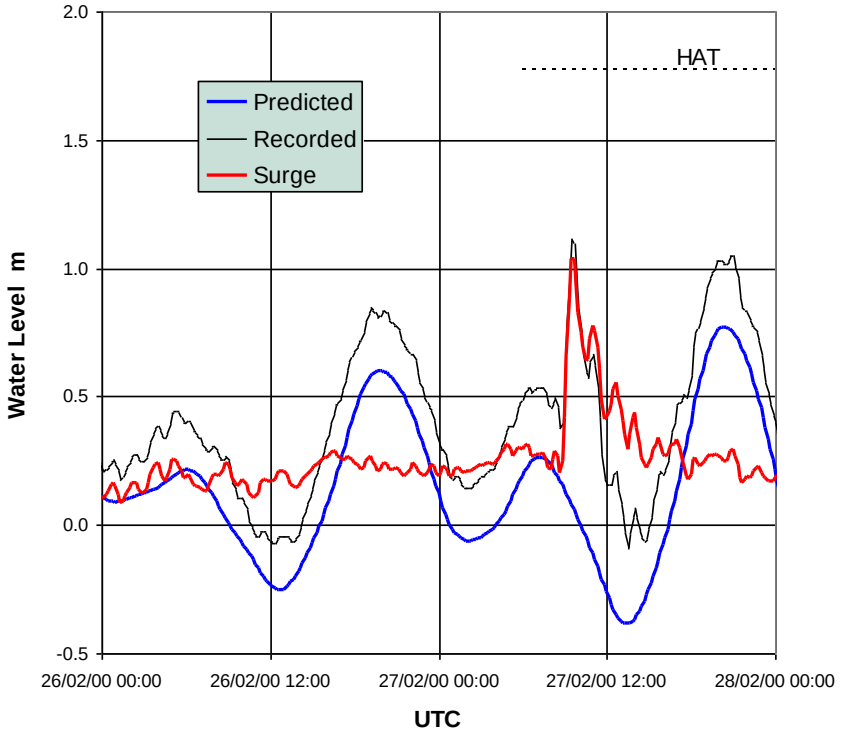

Figure 10.66 Tidal record at Cairns harbour during *Steve*.

10.6.2 Reconstruction of the Event

The following describes the result of a trial and error comparison between the available data and the predicted spatial and temporal variations in wind and pressure as predicted by an analytical model (Harper and Holland 1999), detailed in Appendix C. The model was systematically adjusted for reasonable values of the key parameters such as windfield peakedness and radius to maximum winds. The available data from Cairns and Green Island as well as a number of AWS locations were then compared with the model output to determine the validity of the various assumptions. Consistent with experience from cyclone *Althea* (refer Section 10.4), a windfield asymmetry based on a υ_{max} of 115º was applied.

Initially, emphasis was placed on the relatively close approaches of the storm to Green Island and Cairns Airport, since it was then at its most intense. From the official track it was determined that the centre passed less than 5 km north of the Green Island AWS at 27/0800 and registered a minimum pressure of 984.6 hPa. The site also experienced a lull in the winds on the edge of the eyewall. However, the official central pressure at that time was below 980 hPa, partway between the 0600 980 hPa and 0900 975 hPa fixes. From radar data, the eye diameter was about 30 km and shrinking fast, suggesting a radius to maximum winds of the order of 20 km and placing the AWS close to central pressure. Also, the recorded winds at Green Island AWS are measured at 40 m above ground on a transmission tower and adjustment to +10 m on a logarithmic basis yields a 0.78 height reduction factor and a peak mean wind of only 26 m s^{-1}. Considering all these factors, it seemed more consistent to adopt a central pressure of 984 hPa at this time and an additional 27/0800 fix was added to the track.

The close approach to Cairns Airport was considered next. In this case the peak measured winds were 30 m s^{-1} at 27/0850, which also seemed slightly inconsistent with the 975 hPa central pressure at landfall and the distance of about 10 km, given that the radar data indicated the radius to maximum winds was probably also around 10 km at this time. Accordingly, raising the landfall pressure to 980 hPa provided a more consistent parameter set.

Finally, attention was focussed on the offshore AWS readings to determine appropriate parameters earlier in the storm development. From the synoptic charts it was clear that the system had developed from a fairly broad low and then contracted during the period of rapid intensification, leaving the inner vortex but with an outer region still strengthening from the SE to NE. A variation in radius to maximum winds was then determined by inspection of the synoptic charts combined with model experimentation. Using the official central pressures, the following values of radius (Table 10.12) were found to give reasonable wind speed and direction matches with a number of AWS locations at least prior to the passage of the centre. After that time the vortex model alone was not capable of representing the easterly surge effects.

Table 10.12 Adopted radius to maximum winds for *Steve*.

Time	Radius to Maximum Winds *R*	Time	Radius to Maximum Winds *R*
UTC	km	UTC	km
25/0000	200	27/0000	50
26/0000	100	27/0800	20
26/1800	100	27/0900	10

10.6.2.1 Final Track Parameters

Table 10.13 summarises the final storm parameters chosen, while Figure 10.67 shows the track and predicted wind and pressure field as the storm made landfall. An ambient pressure of 1007 hPa was chosen based on pre-cursor barograph readings. Minimum central pressure at landfall has been adjusted upwards by 5 hPa from the official 975 hPa to 980 hPa and an additional fix added to match the Green Island AWS pressure of 984 hPa. Windfield peakedness B_0 was set at 7.4 throughout.

Table 10.13 Adopted hindcast parameters for tropical cyclone *Steve*.

Track Fix			Speed	Bearing	Central Pressure	Radius	Peakedness
Time	Lat	Long	V_{fm}	θ_{fm}	p_0	R	B_0
UTC	°	°	m s^{-1}	°	hPa	km	
25-Feb-00 00:00:00	-17.2	153.0	5.8	302.0	1003	200	7.4
25-Feb-00 06:00:00	-16.6	152.0	4.2	291.3	1001	175	7.4
25-Feb-00 12:00:00	-16.3	151.2	3.8	246.0	1003	150	7.4
25-Feb-00 18:00:00	-16.6	150.5	5.4	270.0	1000	125	7.4
26-Feb-00 00:00:00	-16.6	149.4	2.0	284.6	1001	100	7.4
26-Feb-00 06:00:00	-16.5	149.0	3.0	279.8	1001	100	7.4
26-Feb-00 12:00:00	-16.4	148.4	4.0	262.6	1000	100	7.4
26-Feb-00 18:00:00	-16.5	147.6	3.0	270.0	996	100	7.4
27-Feb-00 00:00:00	-16.5	147.0	3.5	261.6	988	50	7.4
27-Feb-00 06:00:00	-16.6	146.3	4.7	250.9	985	28	7.4
27-Feb-00 08:00:00	-16.7	146.0	6.7	242.5	984	20	7.4
27-Feb-00 09:00:00	-16.8	145.8	7.9	270.0	980	10	7.4
27-Feb-00 12:00:00	-16.8	145.0	5.8	238.0	990	23	7.4
27-Feb-00 15:00:00	-17.1	144.5	10.1	258.2	995	37	7.4
27-Feb-00 18:00:00	-17.3	143.5	4.6	256.9	999	50	7.4
28-Feb-00 00:00:00	-17.5	142.6	5.4	270.0	1002	100	7.4
28-Feb-00 06:00:00	-17.5	141.5	5.8	290.8	1002	100	7.4
28-Feb-00 12:00:00	-17.1	140.4	4.4	297.5	995	100	7.4
28-Feb-00 18:00:00	-16.7	139.6	2.7	292.6	992	100	7.4
29-Feb-00 00:00:00	-16.5	139.1	3.3	297.5	988	100	7.4
29-Feb-00 06:00:00	-16.2	138.5	3.3	117.4	988	100	7.4
29-Feb-00 12:00:00	-16.5	139.1	3.3	117.5	988	100	7.4

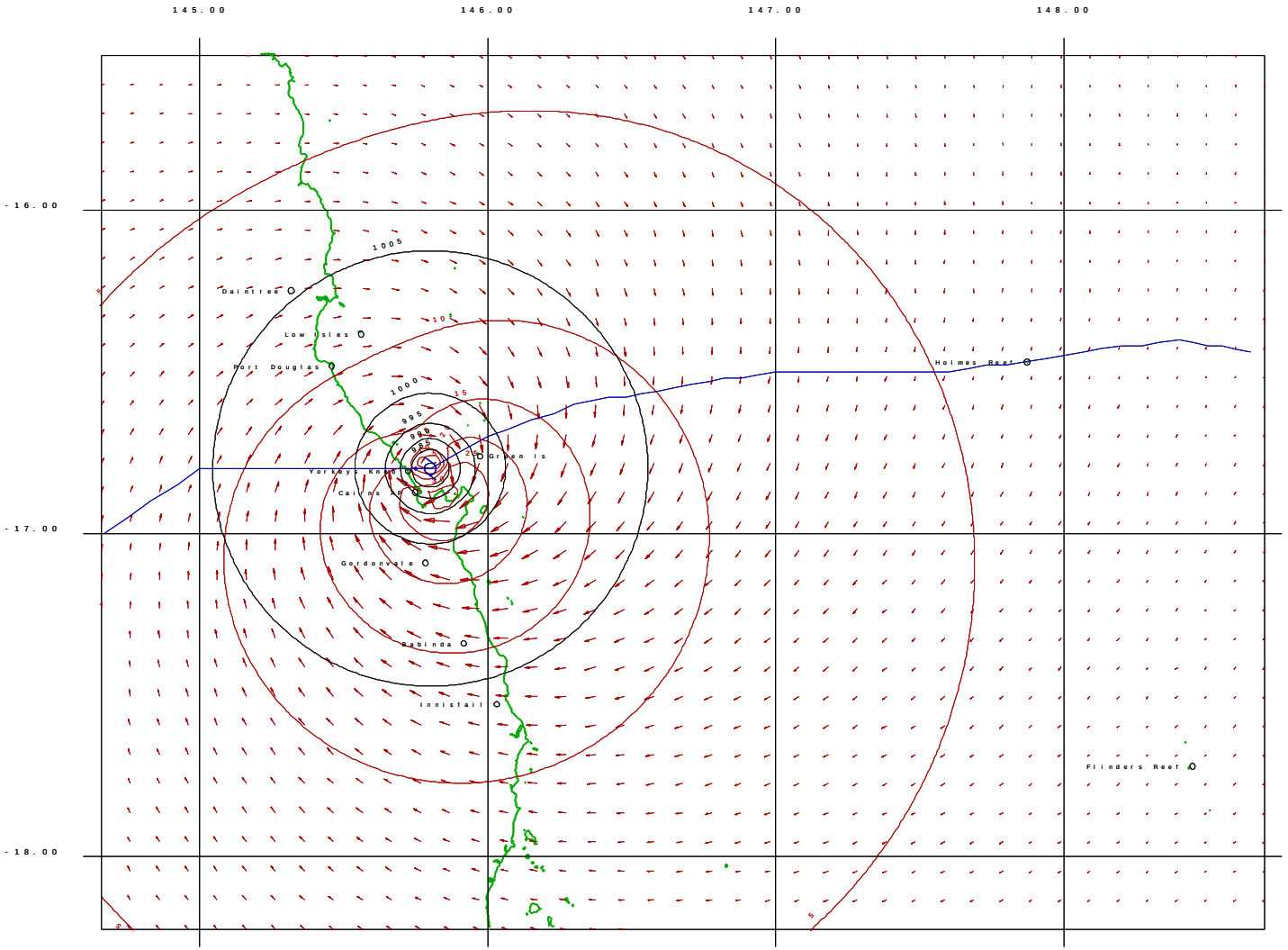

Figure 10.67 Reconstructed Steve track and wind and pressure fields near landfall.

10.6.2.2 Comparison of Measured and Modelled Storm Parameters

These are considered in the order of storm passage and the first comparison shown is with Flinders Reef AWS 3 hourly data supplied from the NCC database. Closest approach was 145 km to the north of the AWS at about 26/1000 UTC. The data is sparse but shows a reasonable agreement with the model in Figure 10.68 for both pressure and wind speed and direction at the time of closest approach. Afterwards, the model tends to overestimate the pressure drop and underestimate the winds as the northeasterly surge follows the vortex. Differences due to wind asymmetry assumptions are minor. Comparisons with Willis Island AWS earlier in the development of the low-pressure system are quite poor.

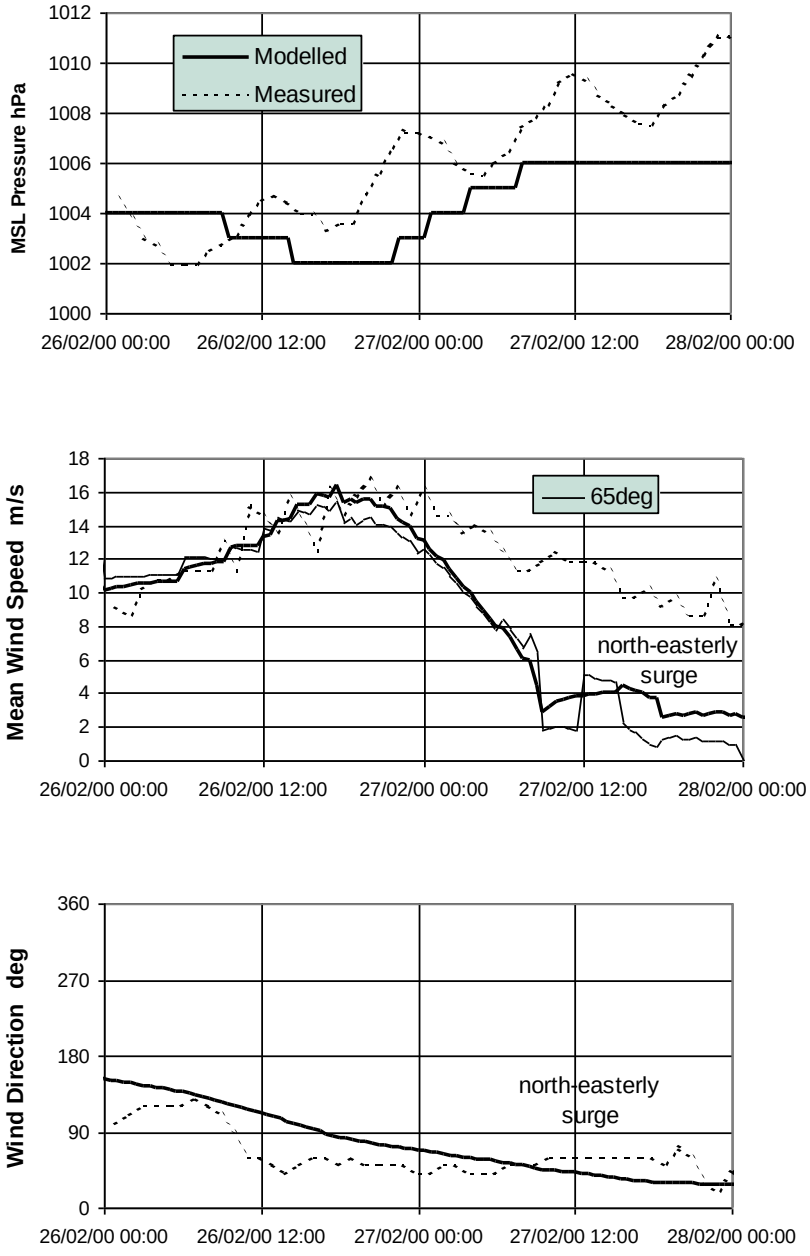

Figure 10.68 Modelled and measured pressures and winds at Flinders Reef for *Steve*.

Figure 10.69 shows the comparison with Holmes Reef AWS, which the developing storm centre passed directly over at 26/1600. The modelled pressure and winds are lagging the measured values by about 2 hours in this case and overestimating the pressure difference, but the 115º model is closer to the recorded wind speed. The easterly surge is quite prominent at this location.

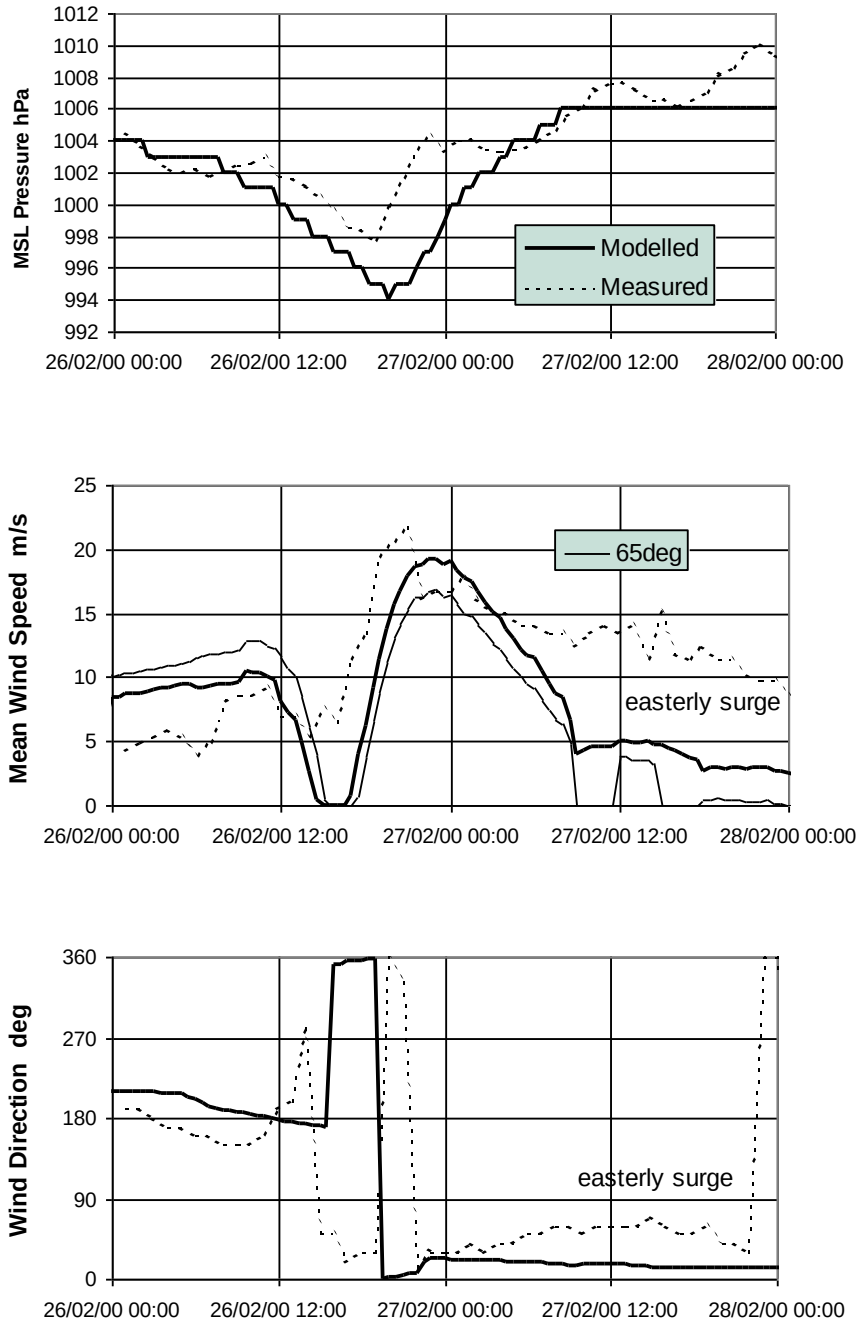

Figure 10.69 Modelled and measured pressures and winds at Holmes Reef for *Steve*.

Figure 10.70 shows the comparison with Bougainville Reef AWS, where closest approach of 110 km to the S occurred near 26/2300 UTC. Again, the comparisons are only fair although the wind speed and direction are representative near the time of closest approach. The 115º model is better overall.

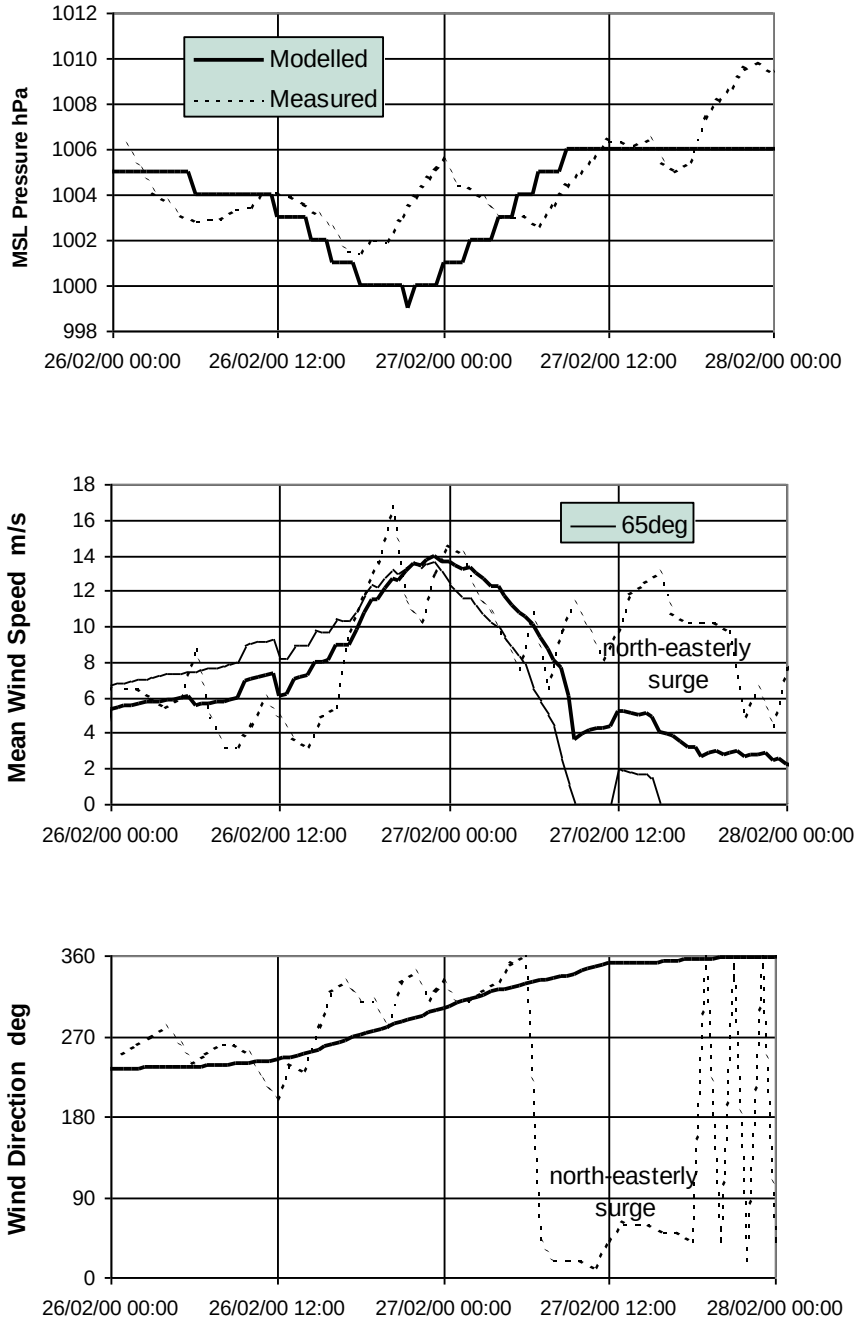

Figure 10.70 Modelled and measured pressures and winds at Bougainville Reef for *Steve*.

The next comparison is with the Green Island AWS, which as previously mentioned has the wind sensor at +40 m on a transmission tower about 25 m clear of the island canopy. Assuming open sea roughness and the logarithmic boundary layer approximation, this implies a reduction to +10 m of 0.78, which has been applied in this figure. Firstly, the modelled and measured pressure variation in Figure 10.71 are seen to be very good. The modelled wind speed shows a gradual increase in winds in response to the increasing intensity whereas the measured winds stay low until the direction veers to the SE. Then the measured winds experience the edge of the eye wall, which is also depicted by the 115º model but not the 65º model, the latter showing only a small dip in speed. Both model winds overestimate the

measured speed during the storm approach, the 65º case being the worst. It is conjectured that the southerly wind at Green Island may actually be shielded by the mainland features such as Cape Grafton. After the centre passes, the 115º model better matches the measured wind speeds but neither matches the direction, which remained easterly rather than turning northerly as predicted by the model.

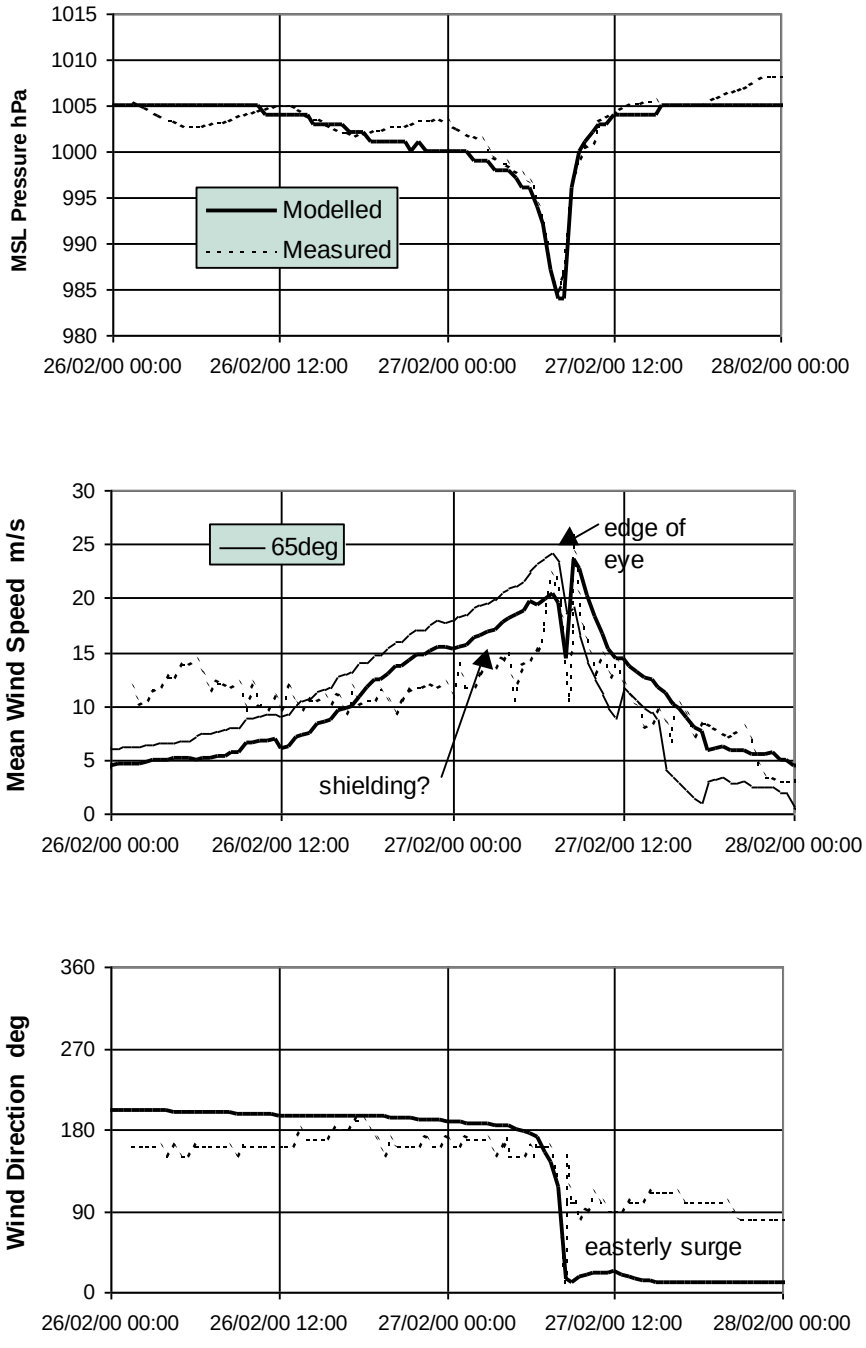

Figure 10.71 Modelled and measured pressures and winds at Green Island for *Steve*.

The final comparison is with the Cairns Airport AWS, shown in Figure 10.72. Again, the modelled pressure is very good, together with the peak wind and the change in direction near the peak. Prior to the peak however, the model significantly overestimates the local wind and this is also thought to be due to shielding of the southerly winds by Cape Grafton. As shown

in Figure 10.73, the airport is located close to the Whitfield Range and about 7 km north of the coastal ranges (800m elevation) which extend east forming Cape Grafton. As the winds turn easterly and become free of the mainland interference, both wind models show reasonable agreement at the measured peak.

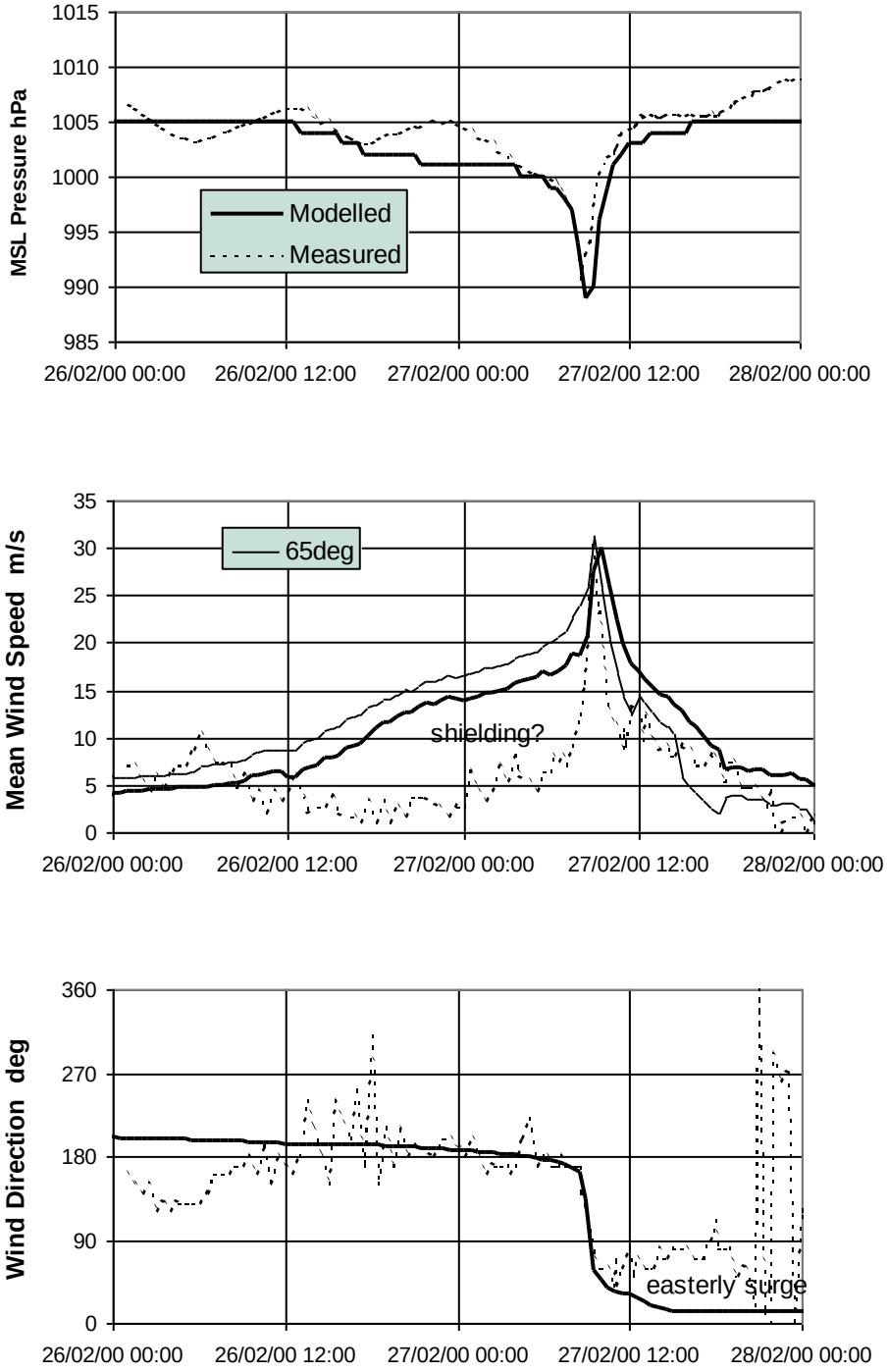

Figure 10.72 Modelled and measured pressures and winds at Cairns Airport for *Steve.*

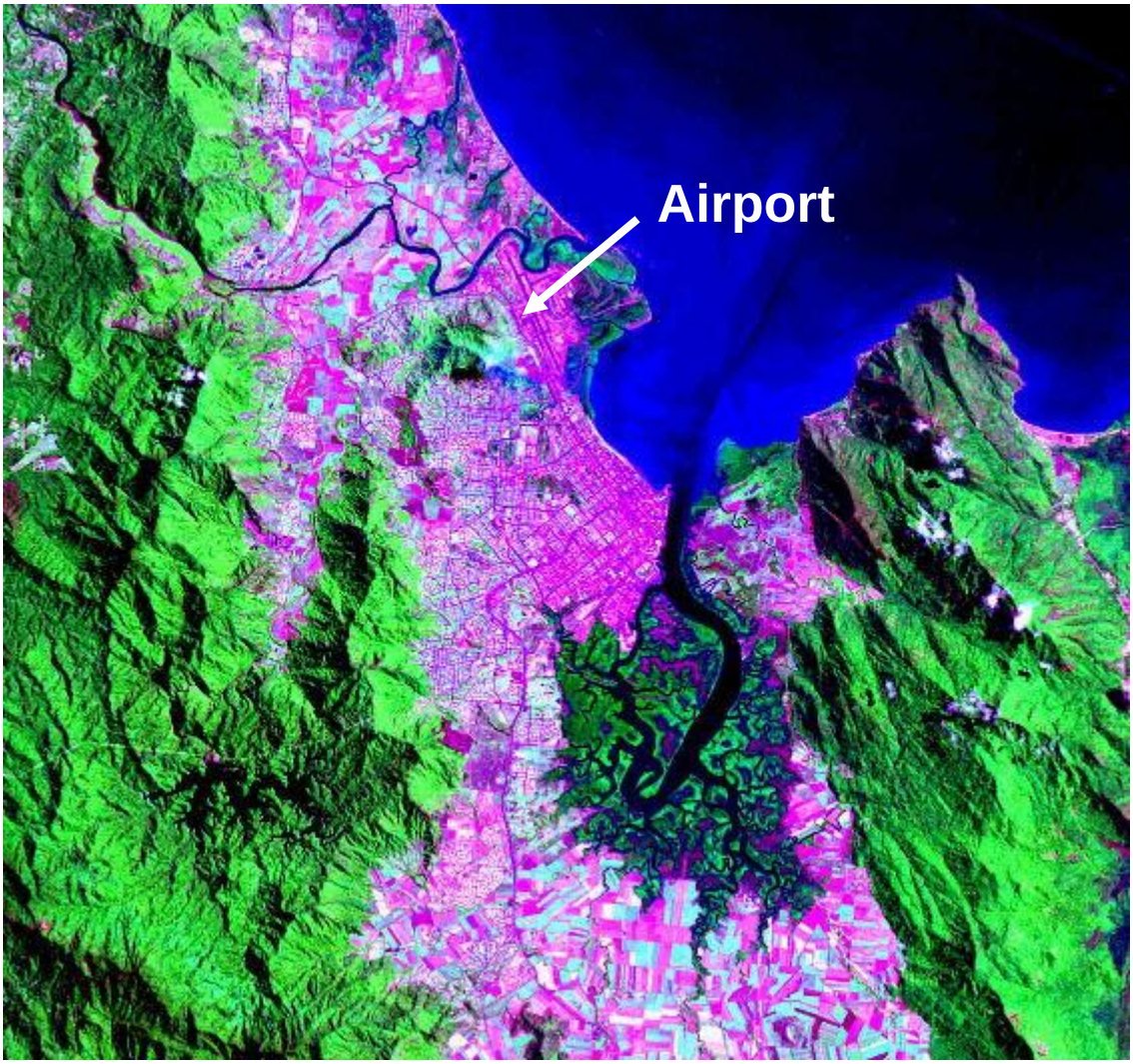

Figure 10.73 Location of the Cairns Airport instrumentation.

10.6.3 Implications for Storm Surge Modelling

While there remains some difficulty in the model representing the measured wind and pressure data offshore after the centre passes, the model appears adequate for the stronger winds. In general, the 115º wind model performs better than the 65º although the differences are less compelling than, for example, with *Althea*, and the present storm was far from mature. The omission of the easterly wind surge effect may affect the broader scale representation of the surge but is not expected to influence the peak value appreciably in this case. The overprediction of southerly winds during the approach to Green Island and Cairns is also not likely to cause significant error in the surge calculation since the shielding is essentially a near-coast affect.

In Figure 10.74 below, the modelled envelope of maximum winds shows the band of strong onshore winds which intersect the coast near Cape Grafton and would have acted to produce the small storm tide registered in Cairns Harbour.

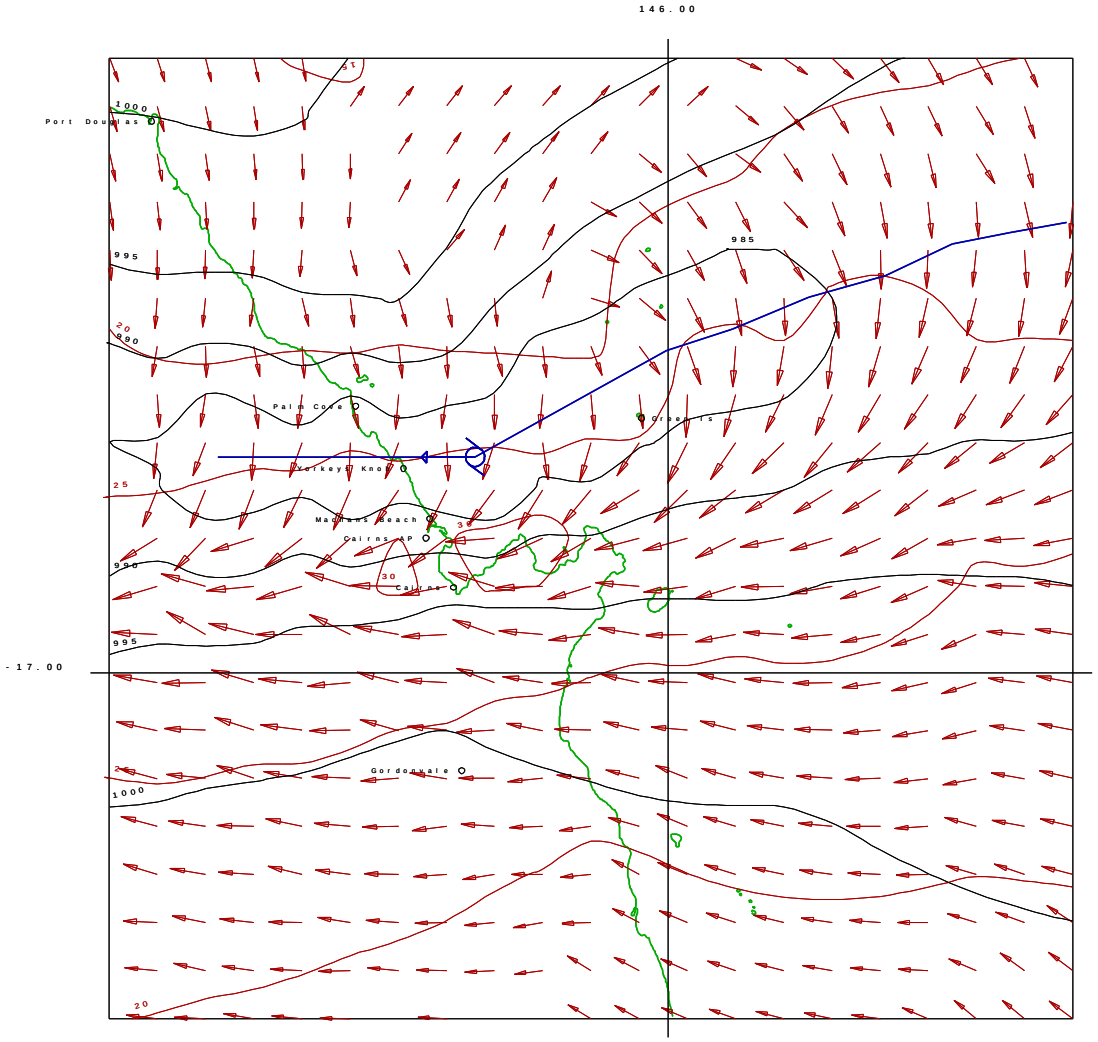

Figure 10.74 Modelled envelope of *Steve* maximum winds and minimum pressure.

10.6.4 Tidal Modelling

The hindcast of cyclone Steve was performed on a three grid system with cyclonic forcing on all grids but with tidal forcing introduced on the second grid (Cairns grid) using five constituents. The modelled tide is not sufficiently accurate to allow comparisons between measured and modelled absolute water levels but does assist in the interpretation of any surge-tide interaction. At the time of landfall, for example, there is a difference of approximately 0.2 m between the modelled and predicted tide at Cairns harbour.

Figure 10.75 presents the results of the tidal modelling at Cairns Harbour on the day of cyclone *Steve.* While the highest tides are reasonable well matched by both the outer and fine scale grids, the lower high water is consistently underpredicted. *Steve* crossed the coast shortly after the lower high water peak on the 27th.

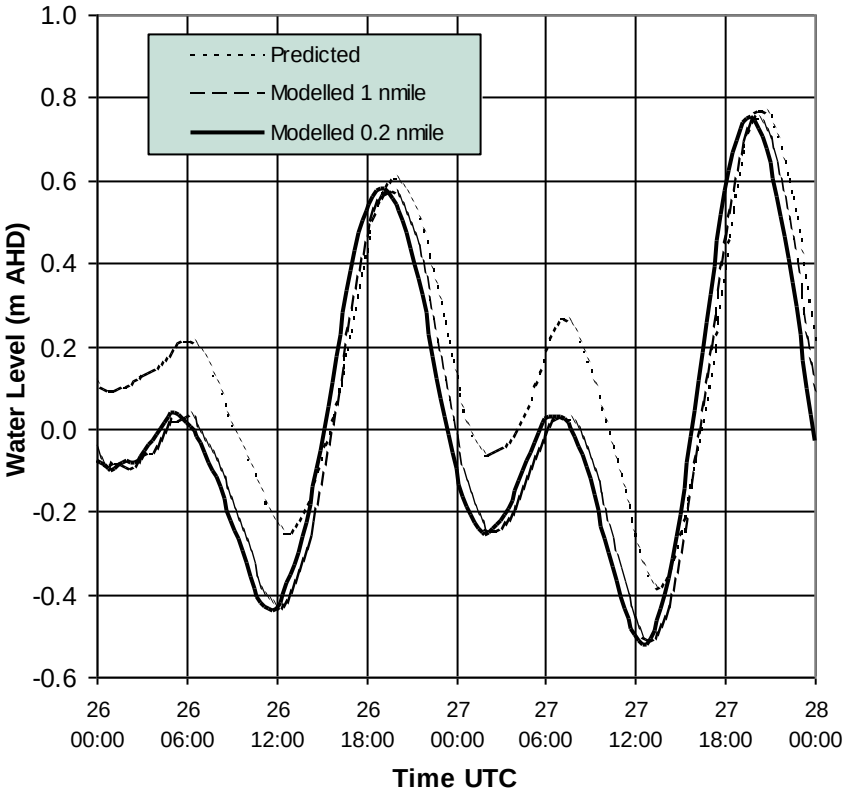

Figure 10.75 Modelled and predicted tides at Cairns Harbour for *Steve*.

10.6.5 Storm Surge Modelling

Firstly, Figure 10.76 shows the storm surge pattern some 8 h before landfall when *Steve* is located in deepwater beyond the Great Barrier Reef. The inverted barometer effect is clearly evident in the deeper water and there is some nearshore setup of water levels south from Mourilyan and especially towards the Palm Island group. Figure 10.77 presents the equivalent view of the induced circulation that is already well established on the shelf south from Cairns.

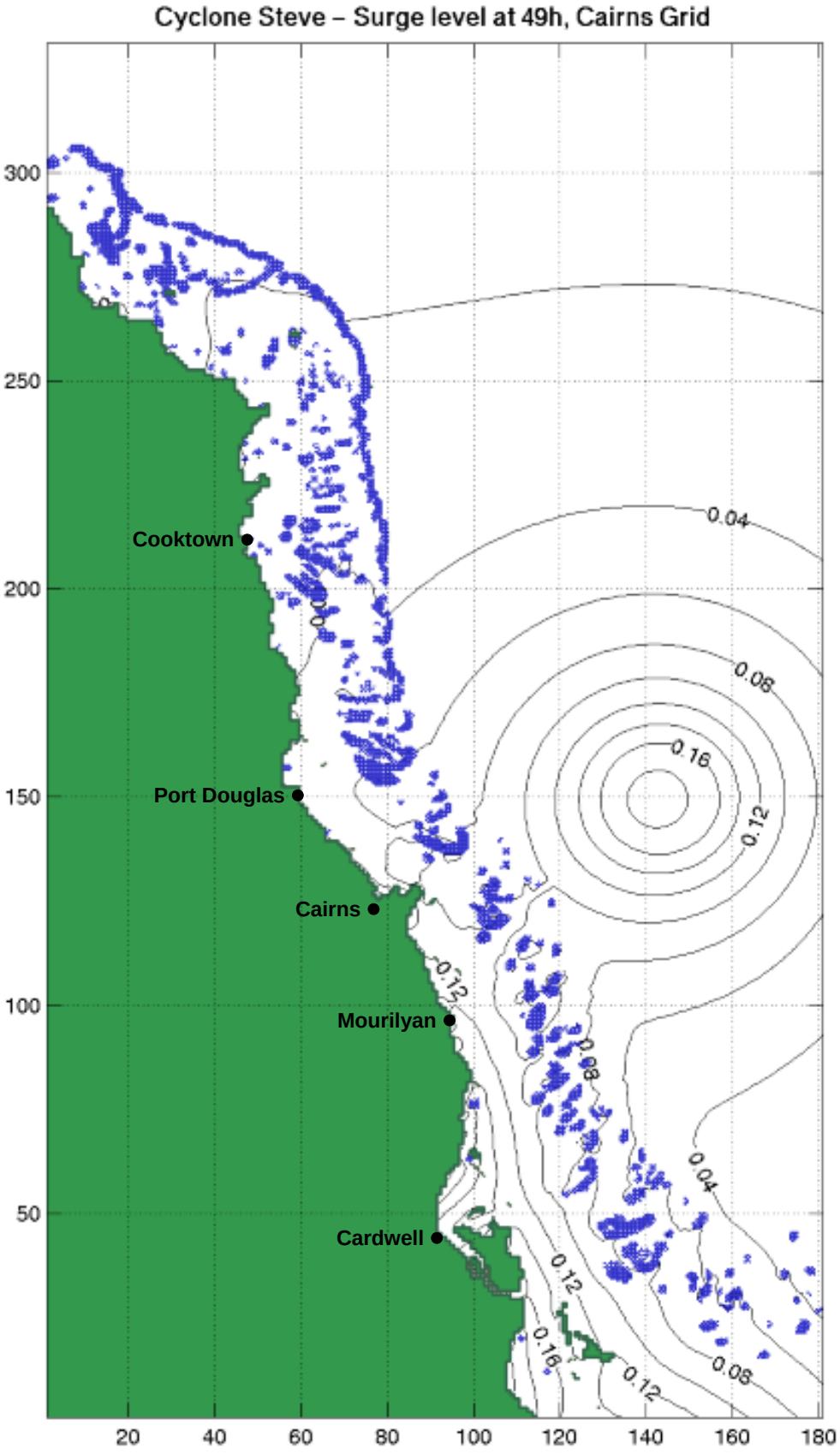

Figure 10.76 *Steve* modelled storm surge levels 8 h before landfall.

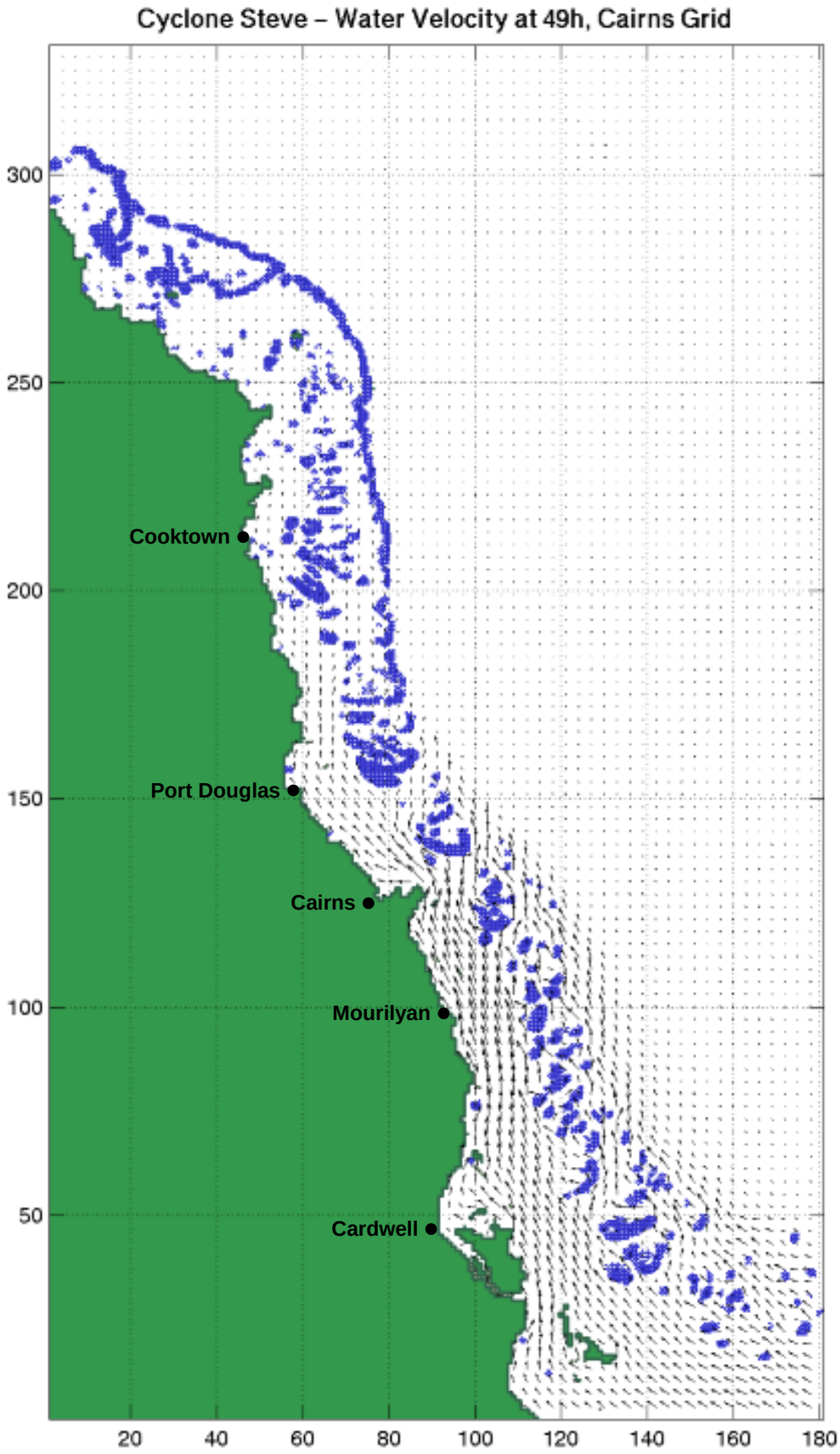

Figure 10.77 *Steve* modelled storm surge circulation 8 h before landfall.

A comparison of the measured and modelled surge components (without tide) is given in Figure 10.78. The measured surge component at the Cairns Harbour tide gauge shows a pre-existing level of about 0.2 m and then a sharp rise to a peak of 1.04 m. The model does not reproduce the initial small rise in level but the fine scale (0.2 nmile) grid result peaks at 1.01 m. The absence of the initial small increase in level prior to the peak is probably because of the difficulty in matching the wind field prior to landfall, whereas the vortex winds are better represented.

The outer (1 nmile) grid overpredicts the peak surge by about 30%, giving a value of 1.32 m. The overprediction is thought to be due to the fact that the outer grid does not resolve the extensive Trinity Inlet backwater, whose channel widths are of the order of 200 - 500 m. The extra volume available to the finer grid allows the (relatively small) propagating surge wave in this case to be more readily assimilated and hence the resulting water level is locally lower.

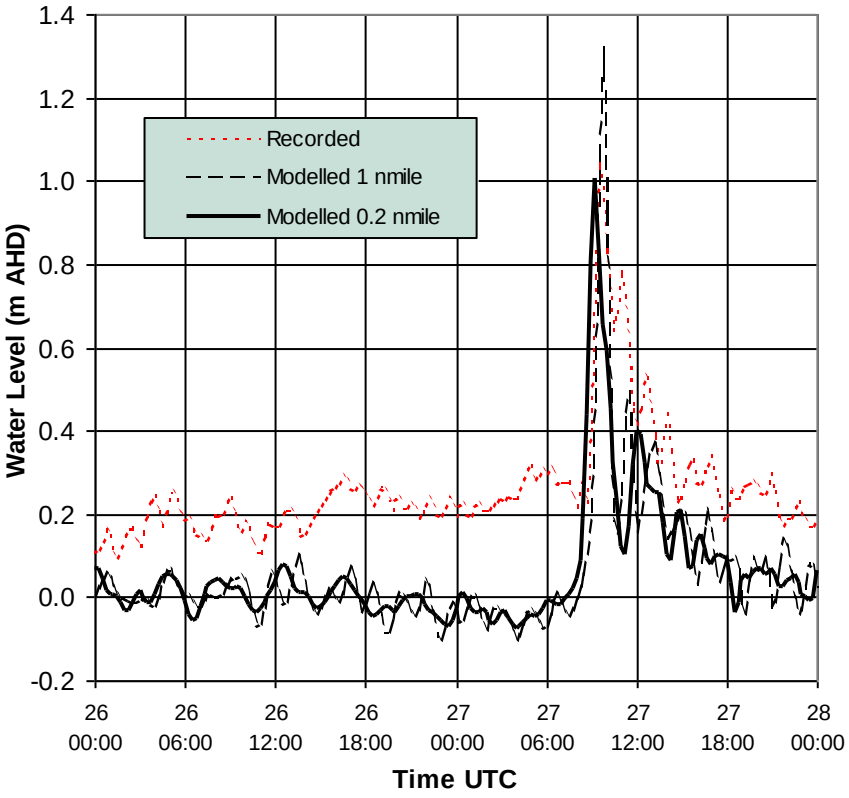

Figure 10.78 Modelled and measured storm surge at Cairns Harbour for *Steve*.

Steve was a reasonably fast moving storm (7.9 m s^{-1}) at landfall and had a small radius of about 10 km. This has produced a storm surge with a very narrow peak (in time), which is represented by only 3 or 4 model timestep points. In this case the model value of $T/\Delta t$ (refer Chapter 6) at the time of landfall is quite small (approximately 6) and a better representation of the peak might be achieved with the smaller timestep of 300 s. This would increase $T/\Delta t$ to about 18, which is close to the recommended value.

The fine scale grid output is shown in Figure 10.79 and 10.80 for water level and flow velocities at the time of cyclone landfall. The peak surge can be seen to be concentrated along the Cairns Esplanade area and there is considerable flow up through the mangrove reaches of Trinity Inlet and around Admiralty Island.

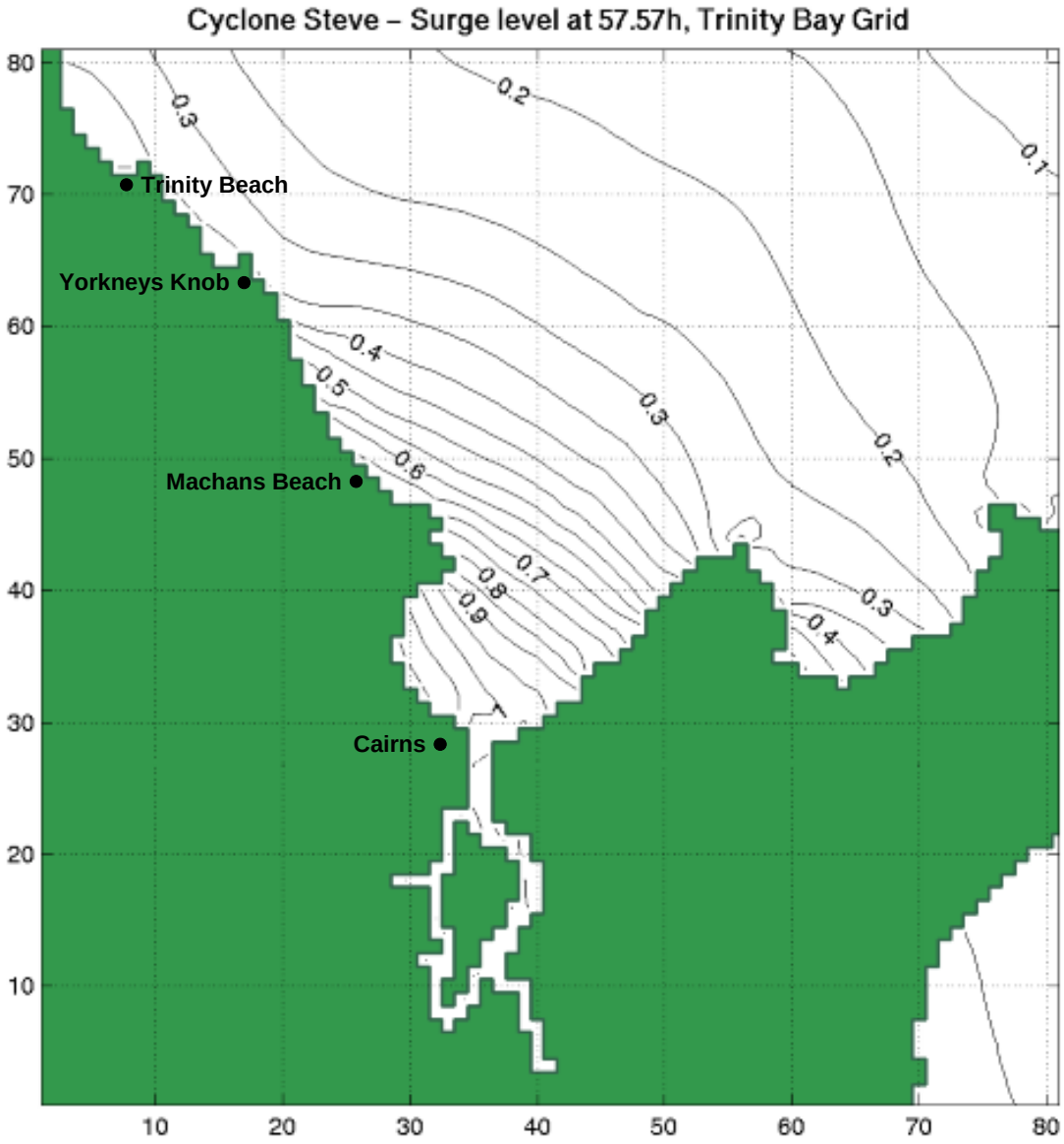

Figure 10.79 Storm surge levels in Trinity Inlet near the time of cyclone *Steve* landfall.

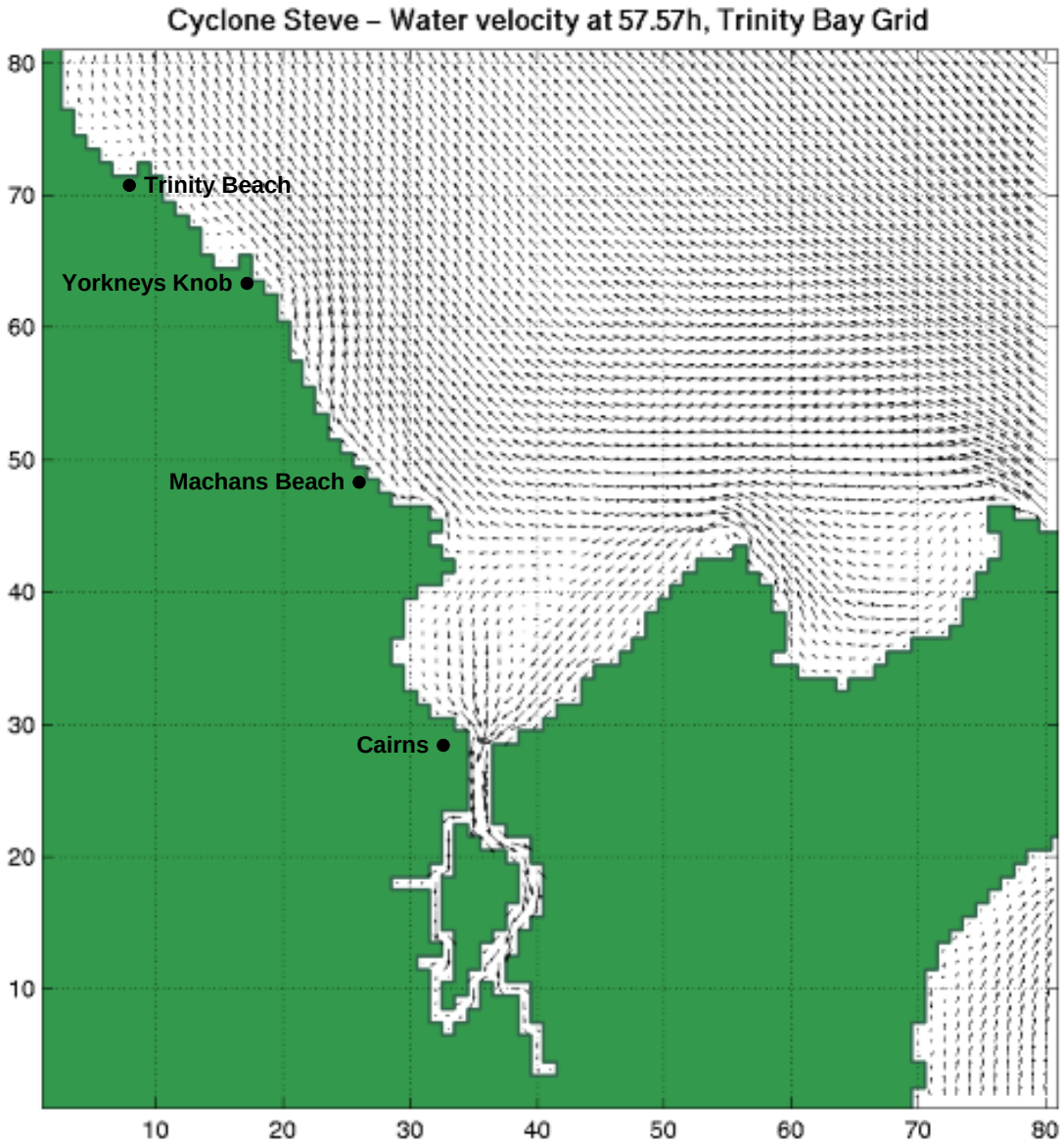

Figure 10.80 Storm surge velocity in Trinity Inlet near the time of cyclone *Steve* landfall.

Finally, Figure 10.81 shows the comparison between the measured and modelled total water level at Cairns Harbour. The peak surge actually occurred when the predicted tide was very close to MSL and results in a total water level (1.12 m) which is very close to the surge component alone (1.04 m). However, the modelled tide was about 0.2 m lower than predicted at this time such that the fine grid modelled level is lower than measured. Coincidentally, the coarse grid result, which overpredicted the surge component, is now very close to the measured total water level.

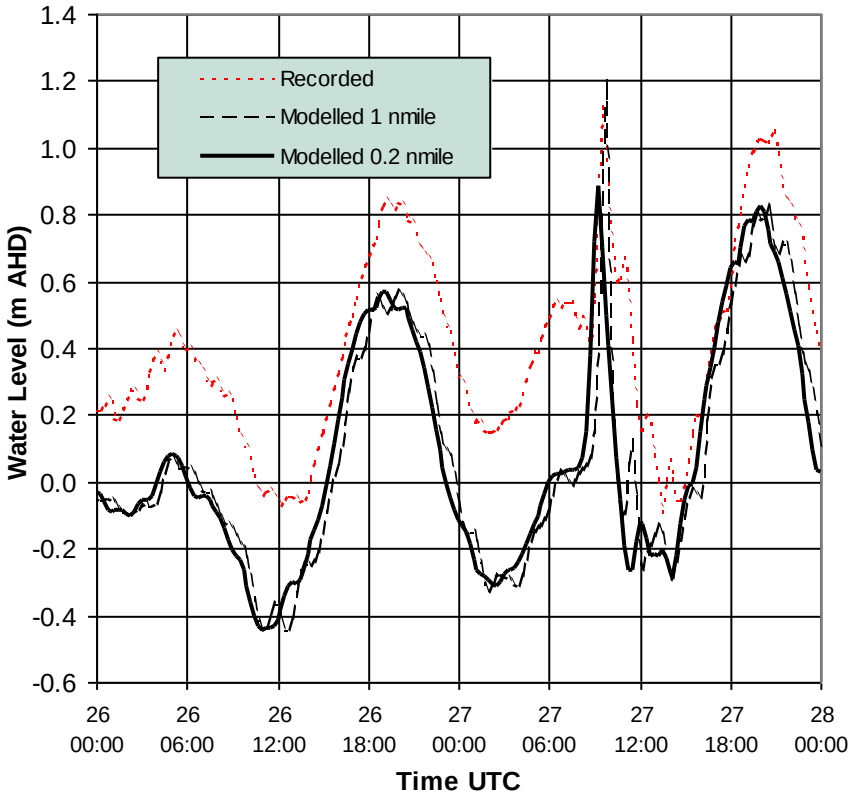

Figure 10.81 Measured and modelled total water level at Cairns Harbour during *Steve*.

10.6.6 References

Broadbent G.J. (2000) Personal communication. *Queensland Department of Transport*.

Callaghan J. (2000) Personal communication. *Bureau of Meteorology*, Queensland Regional Office.

Harper B.A. and Holland G.J. (1999) An updated parametric model of the tropical cyclone. Proc. 23rd Conf. Hurricanes and Tropical Meteorology, *AMS*, Dallas, Texas, 10-15 Jan.

10.7 Summary and Conclusions

Four historical tropical cyclones were selected on the basis of their general characteristics, impacts and relevance to forecasting storm tides in Queensland. The paucity of important data for many of these storms has meant that a considerable amount of effort was required to assemble a reasonably accurate reconstruction of each event. The accuracy and coverage of both measured winds and water levels has varied significantly between each storm case, making the process of comparison with modelled winds and water levels somewhat difficult. Also, the degree to which some of the historical water level estimates were affected by wave setup remains unknown.

The hindcast exercise was designed to be as objective as possible; the wind field and water level data were independently assembled by Systems Engineering Australia Pty Ltd and then passed to the James Cook University Marine Modelling Unit for storm surge modelling and comparison. The initial storms tested were *Mackay 1918* and *Althea* and in both cases the initial modelling results indicated that the recorded and/or estimated surge levels would be underpredicted, even though the best possible wind and pressure field data had been assembled. The degree of underprediction varied but was typically of the order of 15% or 0.5 m and prompted a series of sensitivity tests to determine the most likely source of error. Since existing versions of the storm surge model had utilised rear quadrant maximum winds (θ_{max} = 115°), this was one of the tests conducted, and immediately showed a significant improvement in the results for both storms compared with the original front quadrant result (θ_{max} = 65°). The modified wind fields were then compared against the anemometer data for *Althea* and checked for consistency against the sparse *Mackay 1918* data. While the *Mackay* results remain inconclusive due to a lack of data, the *Althea* anemometer comparisons are deemed significantly better with the revised rear quadrant winds. Accordingly, the improved storm surge results with the rear quadrant winds are accepted here as the more representative for those storms. Accordingly, the other storms were similarly modelled, with *Ted* also lacking corroborative data but *Steve* being marginally improved by the rear quadrant wind field. While it is acknowledged that this is a meagre sample from which to draw definite conclusions, time does not permit a more exhaustive analysis in this context.

Table 10.14 summarises the results of the four storm validations by comparing peak measured and modelled storm surge and also storm tide levels at those locations with the most accurate water level data. Shaded parts of the table indicate situations where the best available data is still only an estimate. Considering each storm individually:

Mackay 1918

This has required a significant effort in forensic meteorology, which has achieved admirable success and shows the potential strengths of both parametric wind field models and storm surge models for situations where storms are relatively intense. The only normally reliable information on the storm intensity, the Post Office barograph, proved suspect in this case and had to be augmented with a variety of other estimates and public reports of the passage of the eye and/or turning winds. No measured wind data at all was available. Establishing the maximum water level in the town also required significant research but it is believed that the level of 5.5 m AHD should now be regarded as the definitive impact for this event. Because the level is some distance from the coast and inundation effects were not modelled due to lack of data, there still

remains doubt as to the exact open coast storm surge level and the contribution from wave setup. However, the predicted open coast surge plus tide level is only 0.4 m (averaged) below the town level, with the expectation of at least a 0.5 m wave setup component. The timing of the surge also agrees well with eyewitness accounts and the alongshore gradient of surge level is consistent with the reported flooding pattern. The model also indicates non-linear surge and tide interaction plays some part in the Mackay region, with a difference of 0.43 m (12%) in the surge component between landfall at MSL compared with the actual high tide levels. The Great Barrier Reef has also been shown to be quite important in this region when modelling combined storm surge and tide because of its indirect effect in controlling the tidal response. The direct influence on surge magnitude though has been shown to be small.

Table 10.14 Summary of storm surge model hindcast accuracy.

		Peak Storm Surge								Peak Storm Tide						
		Measured		Modelled			Error			Measured		Modelled		Error		
Cyclone	Location	Ht m	Time	Grid km	Ht m	Time	Ht m	%	Time	Elev m AHD	Time	Elev m AHD	Time	Elev m	%	Time
Mackay 1918	City	3.50	21:00	1.85	3.38	20:00	-0.12	-3.4	-01:00	5.50	21:00	4.97	20:30	-0.53	-9.6	-00:30
	Far Bch				3.72		0.22	6.3				5.28		-0.22	-4.1	
	(Av.)				3.55		0.05	1.4				5.12		-0.38	-6.8	
Althea	T'ville	2.89	22:40	9.27	3.27	22:45	0.38	13.1	+00:05	2.53	22:40					
				1.85	2.70	22:45	-0.19	-6.6	+00:05			2.36	22:45	-0.17	-6.9	+00:05
				0.37	2.78	22:45	-0.11	-3.8	+00:05			2.44	22:45	-0.09	-3.7	+00:05
				3D	2.96	22:45	0.07	2.4	+00:05							
	Bowen	0.94	17:00	9.27	0.50	16:30	-0.44	-46.8	-00:30	1.10	17:00					
				1.85	0.66	17:30	-0.28	-29.8	+00:30			0.95	17:30	-0.15	-13.6	+00:30
Ted	Karumba	1.97	11:00	9.27	3.62	08:30	1.65	83.8	-02:30	3.62	09:00	4.36	08:45	0.74	20.4	-00:15
				0.93	3.31	10:15	1.34	68.0	-00:45			4.00	10:00	0.38	10.5	+01:00
	Morning. I.	2.10	03:00	9.27	2.37	03:30	0.27	12.9	+00:30	2.29	03:00	2.16	03:30	-0.13	-5.7	+00:30
				0.93	2.85	03:00	0.75	35.7	00:00			2.89	03:15	0.60	26.2	+00:15
Steve	Cairns	1.04	09:30	1.85	1.32	09:45	0.28	26.9	+00:15	1.12	09:30	1.20	09:45	0.08	7.1	+00:15
				0.37	1.01	09:45	-0.03	-2.9	+00:15			0.89	09:45	-0.23	-20.5	+00:15

Shading indicates estimates only

Althea

Although *Althea* has considerably more data, the present study uncovered the need for further assessment of the storm path towards landfall and the effect of the apparent eyewall replacement cycles during that time remains largely unknown. However, the reconstructed wind and pressure fields (assuming 115° θ_{max}) are deemed reasonably accurate with peak wind speeds within 3.5% and bias within 5% for the majority of anemometers available. The resulting storm surge levels are seen to be of comparable accuracy to the wind speeds, translating to less than 0.2 m error in magnitude of surge and height of storm tide at the Townsville tide gauge. There remains the possibility that wave setup and runup contributed significantly to the reported debris levels at other nearby locations. There may also have been higher levels than modelled at locations closer to the storm track due to the complex eye structure. The *Althea* test case has also shown that the Great Barrier Reef has a minor effect on storm surge generation in this area and that 3D modelling offers little advantage over 2D.

Ted

This storm also presented significant challenges due to the lack of reliable wind and water level data. The track was reconstructed based on a reassessment of all available reports of pressures and winds, although the latter proved unreliable at Mornington Island. The intensity of this storm appears likely to have been greater than official figures prior to its approach to Mornington Island. While the model significantly overpredicted (170%) the surge at the only available recording location of Weipa, the overall result at Mornington Island and Burketown is consistent with eyewitness accounts. The most significant problem in this case is the lack of accurate bathymetry and, because of the low-lying land, the extent of overland flooding which is possible. The present exercise has served to demonstrate the MMUSURGE model's capabilities but falls short of an accurate hindcast due to a lack of detailed data. In addition, the available tidal information for the Gulf is only approximate and hence the actual storm tide levels are not well predicted. Because inundation depends on total water level, and non-linear interactions are likely to be large, it is not possible to improve this result within the present study timeframe.

Steve

While this is a modern event with the benefit of many AWS locations, it is still a difficult storm to characterise and model because of its continuing development during the approach to landfall. Its relatively low intensity has proved the sensitivity of the model to even small impacts and shown its ability to resolve the complex nearshore flows on the narrow reef-fringed continental shelf. The focused storm surge at Cairns has also demonstrated the importance of grid resolution in some situations. In particular, the 1.85 km grid overpredicts the storm surge by almost 0.3 m (27%) because it fails to adequately resolve the Trinity Inlet and its storage capacity. For a larger surge, this might not be quite as important since the additional storage will be a smaller proportion of the surge.

Notwithstanding some of the difficulties discussed above, it is concluded that the James Cook University storm surge model MMUSURGE is capable of accurately representing storm surge magnitudes (<5%) and timing (<15 min) along the Queensland coast, when:

1. The wind and pressure fields can be determined with reasonable certainty, and

2. The bathymetry of the coastal areas is reasonably accurate.

Furthermore, for areas which have well-calibrated tidal boundaries,

3. The model is capable of accurately representing total surge plus tide levels to AHD.

Based on this assessment, and consistent with the recommendations of Chapter 6, it is concluded that accurate nearshore storm tide modelling can be achieved in 2D mode, without non-linear advection, provided that spatial resolutions can correctly resolve the local features (in the range 2 km to 0.5 km) and at timesteps of the order of 900 s (15 min). The Great Barrier Reef parameterisation should be retained to ensure accurate tidal modelling wherever possible and to maintain correct storm surge magnitude and timing.

11. System Design Considerations for Storm Tide Prediction

The study scope requires consideration of the two inter-related approaches to the storm tide problem:

1. Tactical - A storm tide warning capability
2. Strategic - A storm tide planning capability

Both capabilities are essential for ensuring minimisation of community impacts from storm tide and each need to be consistently applied and updated with the latest knowledge. Accordingly, there are many aspects of the storm tide problem which are shared by each requirement, namely

- Knowledge of cyclone climatology, structure and behaviour
- Ability to model wind and pressure fields
- Ability to model ocean responses of waves and storm surge
- Ability to make predictions in regard to storm tide
- Overall accuracy of the prediction

However, needs differ significantly in the following areas:

1. Warnings:

   The immediate sensitivity to parameter changes is critical.
   In essence, the warning problem has no specific requirement to be aware of the statistical likelihood of any individual storm tide event, except in regard to choosing representative parameter ranges in its various scenario considerations. The accuracy of a prediction for a given set of parameters and the ability to consider uncertainty in those parameter values within a specific time period is the essential requirement. The critical need is for timely and accurate information for decision making by Government, industry and the general public leading to the minimisation of impact from a specific event.

2. Planning:

   The probability of a specific storm tide level is critical.
   The planning problem, by nature of its extended time scale, needs information for decision making which can be interpreted statistically, leading to an assessment of both relative and absolute levels of risks. Such information can then be used in cost/benefit assessment of planning criteria and for justification of the need for ongoing data collection, research and investigation. The critical need is for a comprehensive consideration of the magnitude and frequency of storm tide events which includes potential climatic variability (e.g. inter-decadal) and long term climate change (e.g. Greenhouse). The aim of the planning activity is to minimise the impact from all such events by reducing the community vulnerability in an affordable and practical manner.

Because of these philosophical differences between the warning and planning regimes, differences in the methodologies to achieve their goals also arise. The following sections discuss these differences and examine opportunities that could be taken to achieve a common outcome of mutual benefit.

11.1 Storm Tide Warning - the MEOW Approach

The MEOW (*Maximum Envelope of Waters)* technique identifies a methodology first outlined by Jarvinen and Lawrence (1985) as a valuable tool for hurricane storm tide warning purposes and has been operational within the US Weather Service for many years. The aim of the method is to provide an estimate of the maximum sea level that might occur anywhere within the warning zone during the period of the forecast threat.

The basic MEOW technique was evaluated by the BMRC and subsequently recommended by Sanderson *et al.* (1995) for application in Australia. It is noted that the current US approach (refer Appendix E) places less emphasis on the MEOW being used as an approximation to a real-time numerical model than the presently envisaged operation (i.e. Sanderson *et al.*). In the US context the MEOW is used almost entirely for evacuation planning and therefore may be significantly simplified. The method outlined below is therefore something of an extension of the original US concept, moving it from a largely static decision making tool towards a more dynamic environment.

The following discussion is designed to provide a philosophical overview of the technique as proposed by Sanderson *et al.*, while Appendix E reviews the technique currently used in the US and its potential deficiencies for Australian conditions. Subsequently, Chapter 12 discusses operational issues and develops a functional specification for a MEOW-based forecast system, which is further detailed in Appendix G.

11.1.1 The Envisaged BMRC Procedure

The generalised MEOW technique is a straightforward combination of (i) pre-computed detailed output from a numerical storm surge modelling system, (ii) the predicted real-time tide level and (iii) a series of storm forecast scenarios. Figure 11.1 summarises the basic approach as envisaged by Sanderson *et al.* (1995).

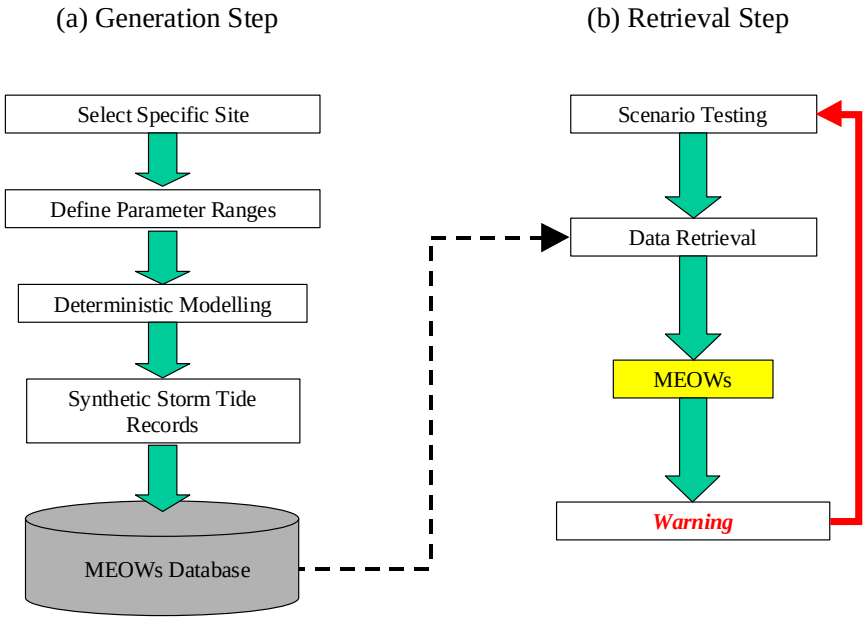

Figure 11.1 The MEOW warning technique.

The MEOW is site-specific in that it draws upon a series of pre-computed storm surge responses which (ideally) cover a wide range of possible storm parameters, including the distance between the storm centre and the warning location, and the angle of the track to the coast etc. During the *data generation step*, a large number of deterministic storm surge model simulations are performed to "map" the storm tide response for an area. Historically, a primitive equation model (e.g. SLOSH, BMRC or MMUSURGE etc) is used for this purpose although, as discussed later, simpler parametric storm tide models could also be used if their accuracy is comparable. The generation step is schematised in Figure 11.2, indicating that a large number of individual simulations are undertaken to ensure coverage of the expected parameter space. To simplify the problem and reduce the permutations, typically straight-line storm tracks are adopted with storms having constant parameters. The simulations are also normally performed at a constant sea level (typically mean sea level), without regard for specific tide conditions. Some empirical adjustments can be added to allow for those regions having significant non-linear surge-tide interaction. The result is then a site-specific database of the expected storm surge response, from a wide variety of tropical cyclones, which can be progressively extended and expanded to cover whole regions of coastline. The "traditional" MEOW approach above does not explicitly consider the wave setup component, now known to be significant in some cases. Accordingly, a complementary set of wave model simulations is needed to add this capability or, again, empirical or parametric add-ons are required to provide the wave-setup estimate.

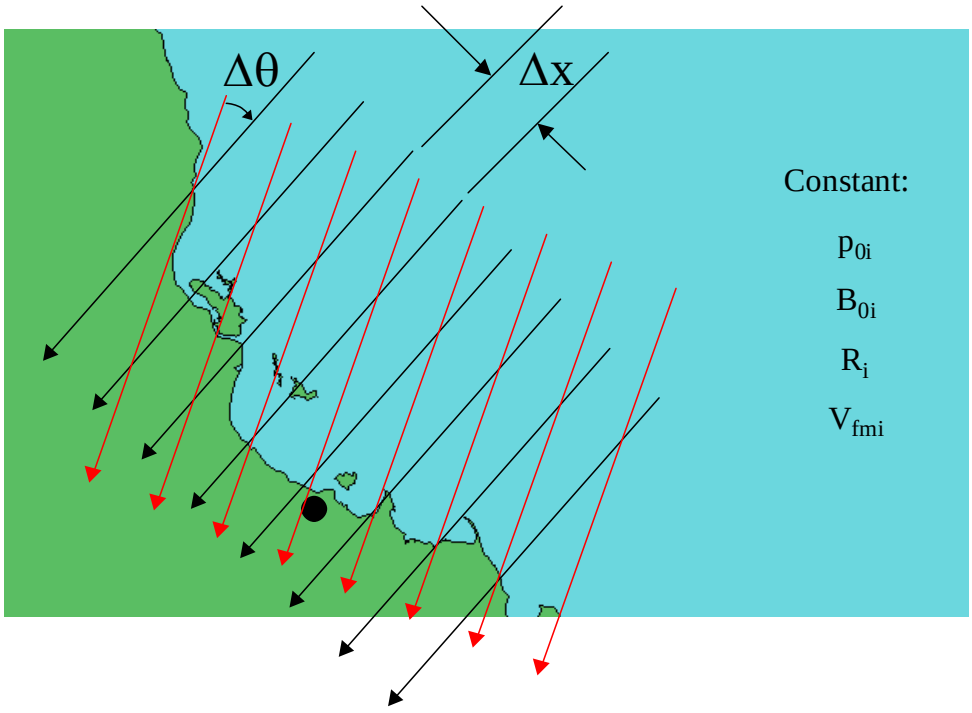

Figure 11.2 The MEOW storm surge generation step.

In the MEOW *data retrieval step*, the context is real-time and a predicted tide is available for a specific location. This is then combined with a storm parameter scenario based on the current forecast and the MEOW database is accessed to retrieve and/or interpolate the most applicable pre-computed array of storm surge levels to match that scenario. The time-varying storm surge record is then combined with the predicted tide[4] to produce a storm tide record and, ideally, includes the predicted wave-setup component. Importantly, at this point, the aim

[4] Section 12 details how this step is different in detail from the original Sanderson *et al.* (1995) approach.

is to provide a *maximum envelope* of water levels that will incorporate the degree of uncertainty of the forecast parameters. Therefore, the technique is to generate not one but a variety of potential storm tide outcomes. This is done by a simple perturbation of the forecast parameters on the basis of some type of uncertainty model, which may simply represent the mean and standard deviation, for example, of the historical forecast performance of the relevant storm parameter. The requisite number of scenario results is then extracted from the pre-computed database and the maximum of all the results, together with the forecast timing, becomes the basic warning output from the MEOW technique. Clearly, a statistical description of that envelope can also be provided for specific customer needs.

11.1.2 Conclusions

The MEOW technique appears to satisfy many of the basic requirements for an effective warning system. The approach is simple, easily understood and communicated, and can be adapted over time depending on the operating needs of the forecasting organisation and the community client requirements. Its principal drawback, in traditional form, is the potential need for a large number of simulations during the *generation step* and the consequent data storage and recovery overheads associated with maintaining the system.

When the method was first devised in the late-1970s, its principal advantage was in overcoming the computational burden of numerical modelling in a real-time context, whereas present computer capabilities are significantly greater. However, the basic technique can be directly updated to incorporate either a parametric model data source or a real-time model data source without relying on the generation phase and its extensive database. This would be more consistent with the increasing trend towards use of real-time numerical regional weather models, which could provide the boundary conditions of surrounding ambient winds and pressures for the storm surge model vortex and also link directly to track forecasting tools.

11.2 Storm Tide Planning - Statistical Approaches

A variety of methods for attributing probability of exceedance to storm tide levels were reviewed in Chapter 9. The three somewhat similar estimation methods of *Monte Carlo (MCM), Joint Probability (JPM)* and *Empirical Simulation (EST)* were discussed and a recommendation formed which favoured use of either *MCM* or *JPM*, depending on the availability of a parametric storm tide model, i.e.

(i) The *MCM* is generally limited to the use of parametric storm tide models because of its many degrees of freedom, which provide advantages for the types of sensitivity testing required in the present project.

(ii) The *JPM* restricts the range of parameter pairings and assigns probability space estimates for later reconstruction, thus permitting increased use of primitive equation modelling, but without the full freedom of the *MCM* approach.

The end result in each case, as depicted in Figure 11.3, is a statistical database of storm tide estimates, each built upon a different set of assumptions, yielding long-term probabilities of exceedance of storm tide levels (i.e surge plus tide plus wave setup). The preferred technique is then the one which delivers the greatest accuracy within a practical timeframe and which provides sufficient parameter dynamic range to test sensitivity to factors such as climate change.

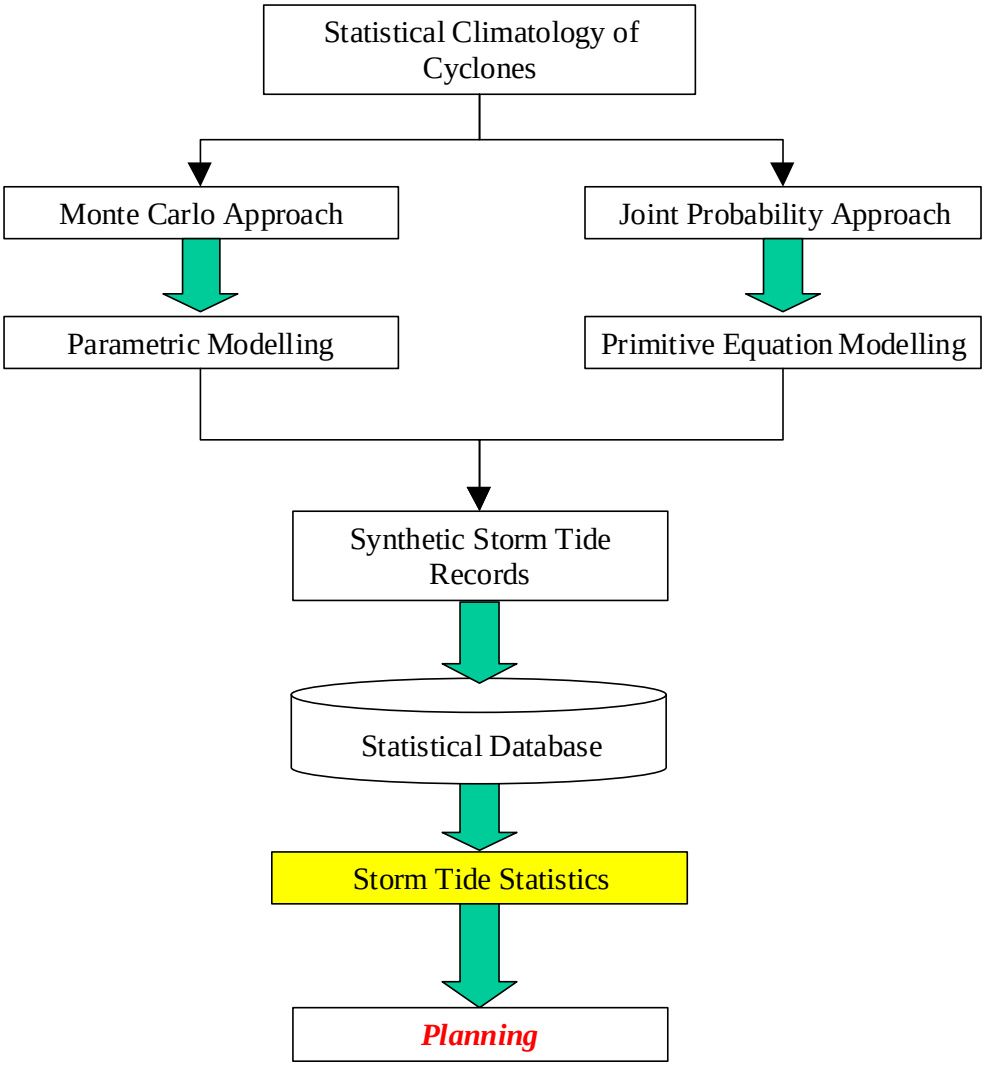

Figure 11.3 Recommended options for statistical storm tide estimation.

The accuracy of storm tide statistics developed using any of the above methods will benefit greatly from a "seamless" tropical cyclone climatology description of the type discussed in Chapter 9. This should be regarded as an essential pre-requisite for conducting a major storm tide statistics investigation. Such a climatology description will also be valuable for the sensible selection of parameter ranges for any MEOW investigation and can be utilised in real-time forecasting uncertainty analysis (refer Chapter 12). The climatology description should include a comprehensive assessment of maximum potential intensity (MPI) as well as inter-seasonal variability (SOI, IPO) and impacts of potential long term climate change (enhanced-Greenhouse).

Implicit in the use of the term "storm tide" is that storm surge, tide and *wave setup* will be included. Wave setup calculations ideally require estimates of local wave heights and periods at resolutions of the order of 500 m, which can only be provided by numerical wave modelling in a manner consistent with that undertaken for storm surge. This will yield information that can be used directly to provide estimates of extreme wave heights and their

associated parameters such as period, direction and persistence. The numerical demands of wave modelling are also potentially much greater than that for storm surge alone. If wave action during overland flooding episodes is also to be assessed, nearshore model resolutions will need to be reduced further to the order of 100 m and likely incorporate analytical approximations to wave transformation such as bore formation.

It is clear that the estimation of storm tide statistics for the entire Queensland coast, at an accuracy which will lead to localised or community inundation detail, will require considerable numerical effort. If undertaken in a staged systematic manner, however, this need not be prohibitive and the results will be equally valuable for the storm tide *warning* process.

11.3 A Suggested Hybrid Approach

From the above development, it can be seen that there are many shared issues in regard to the desirable capabilities of warning (tactical) and planning (strategic) tools. By combining some of the above concepts a hybrid approach is suggested, which should deliver the relevant accuracy and economies at each stage of the warning and planning processes whilst having a common predictive basis. The overall expected advantage of a combined approach would be to minimise the number of computationally expensive primitive equation model simulations (storm surge and waves) relative to any MEOW and storm tide analyses being undertaken independently.

The suggested key to merging these common aims is to develop *parametric* models to describe the regional storm surge and wave response characteristics. In this sense, a parametric (empirical or *black box*) model is any analytical device that can accurately describe a system response when given a set of parameter inputs. A well-constructed parametric model is one that represents a distillation of otherwise complex knowledge in a concise and efficient framework. The wind and pressure model of Appendix C is an example of a very successful parametric model of the complex behaviour of tropical cyclones; the wind stress formulations discussed in Chapter 6 are likewise simple parametric models. In the present context, parametric models of storm surge and waves would be constructed *based on* the results of a series of primitive equation storm surge and spectral wave model results.

As discussed in Chapter 9, simple parametric storm tide models (storm + tide only) have already been used extensively in establishing storm tide statistics for the Queensland coast, e.g. Harper and McMonagle (1985). Their apparent utility, even based on limited underlying numerical modelling, is due to the largely linear relationship between storm intensity and peak surge height at many coastal locations. This results in a similarity behaviour that allows scaling of the surge response. Harper (1983) extended this concept to include extreme waves and wave setup by combining with limited spectral wave modelling and the results compare favourably with recent statistical analyses of long-term wave data (M. Allen, EPA, *pers. comm.*). Recently updated analyses of the storm tide risk at the Gold coast (GCCC 1999) are also very similar to values developed initially by Harper and McMonagle (1985). Examples of the application of this *circa* 1985 parametric model to *Althea* and the *1918 Mackay* cyclone are given in Figures 11.4 and 11.5 respectively, derived from studies described in Harper (1996) and labelled here as MIRAM. This simple model is based on interpolation of numerical model results between only three storm intensities at each of three approach directions, with a forward speed adjustment factor based on Nickerson

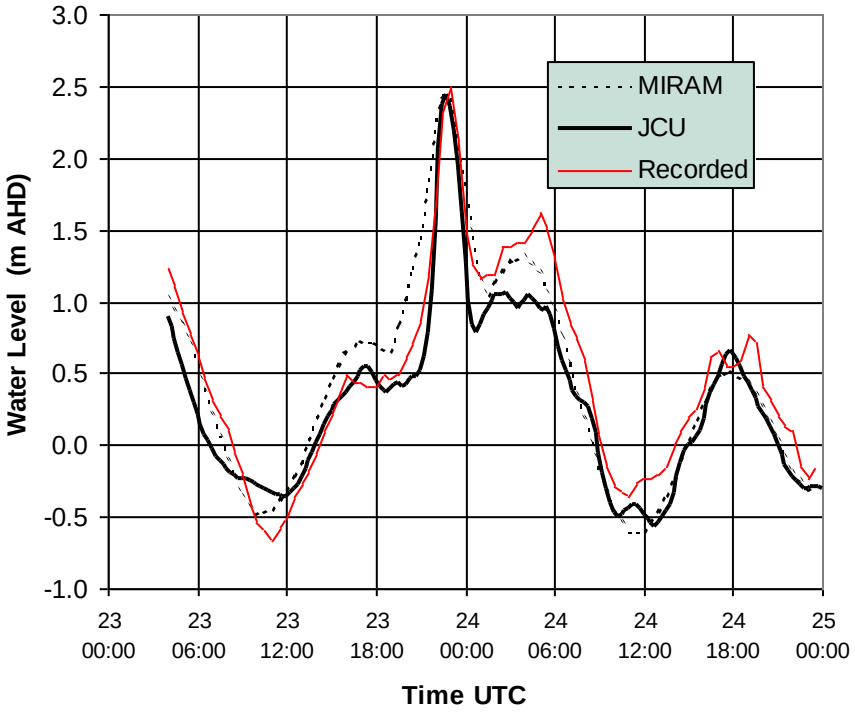

Figure 11.4 MIRAM parametric storm tide model prediction for *Althea.*

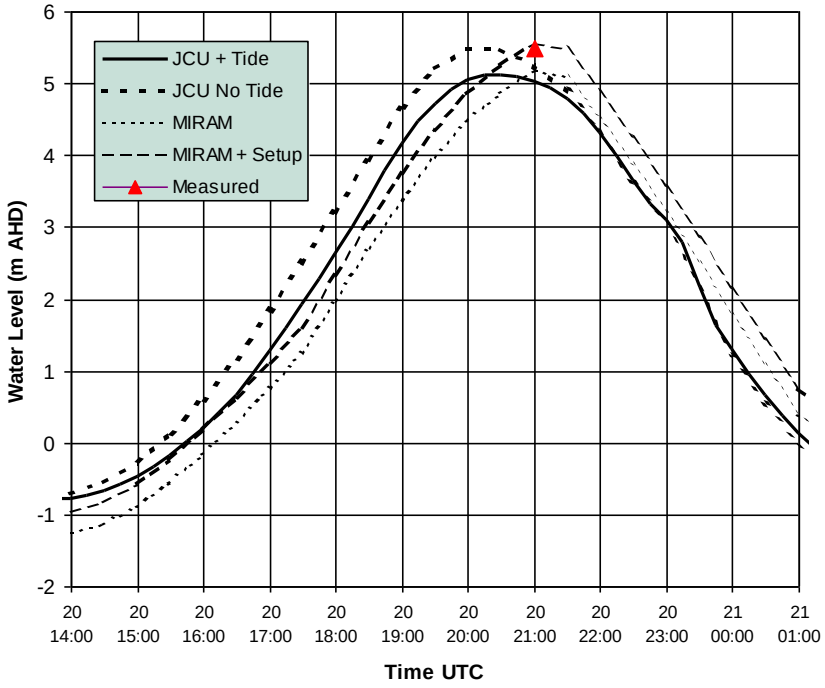

Figure 11.5 MIRAM parametric model prediction for the 1918 *Mackay.*

(1971) and a constant *B* and *R*. The model also incorporates a basic wave setup predictor which is proportional to storm central pressure. Hence, a simple parametric model based on only nine numerical simulations is capable of producing a storm tide estimate of notionally similar accuracy to the present primitive equation result for these two storms.

It is argued that a more sophisticated parametric model could now be developed with the advantages of improved and more efficient primitive equation models. For example, the spatial resolution of the original numerical modelling was limited to 5 n mile (9.25 km). The above parametric model is presently limited to prediction of coastal storm tide levels only but can simultaneously represent a number of coastal locations with varying tidal characteristics and local storm surge and wave height amplification factors. Importantly, the model provides the estimated time history of water levels for phase interaction with the tide. If a velocity field is required or a full spatial description of the water level field is needed, a primitive equation model result is essential. Given that the parametric model must be developed from a set of primitive equation model simulations, such detailed datasets will remain available for subsequent application in any allied areas.

Taking all of the above into consideration, Figure 11.6 provides an overview of a possible way forward, consisting of three basic elements:

1. The first element relates to establishment of a comprehensive statistical climatology of tropical cyclones. Next follows the large scale deterministic modelling of discrete parameter selections from that climatology using primitive equation models for surge and waves. These results would form an extensive synthetic storm tide (surge and wave) database for specific regions. Based on that database, a series of regional parametric storm tide models would then be developed. The parametric models will then be applied in association with the statistical aspects of the climatology to generate synthetic storm tide records, leading directly to the establishment of storm tide statistics for *planning* purposes.

2. Under the second element, the same parametric (surge and wave) models would be used within the Bureau AIFS forecasting environment as a simple MEOW *preparedness* tool, designed for rapid real-time scenario testing having a high availability and a low likelihood of failure. The climatology would be used for forecast uncertainty analysis.

3. The third element would interface the deterministic storm surge and wave models used previously to the Bureau TCLAPS atmospheric model and associated tropical cyclone track forecasting tools. The numerical surge and wave models would then make use of the best wind and pressure information in an integrated environment and could incorporate tidal modelling, thus avoiding the surge-tide interaction issue in the warning context. A limited set of MEOW scenarios would then be undertaken in real-time, again guided by the established climatology. While this approach is already technically feasible (refer Table 11.3 later), it will become more so in the coming years as computer memory and computational speeds continue to increase.

This hybrid approach has the capacity to integrate both warning and planning needs in a consistent and mutually beneficial staged development. The parametric models could be

developed on a regional basis using a MEOW-like approach to ensure the full parameter space is explored. As completed, the parametric models become available for both MEOW forecasting and storm tide statistics planning. The numerical modelling results would remain as a base resource for whatever purpose might be envisaged in the future. The real-time forecasting capability can be further developed in parallel and make use of the fine scale bathymetry and climatology data that will arise from the regional studies. Chapter 12 discusses, for example, how the AIFS environment could be designed to be independent of the actual data source used in constructing MEOW warnings.

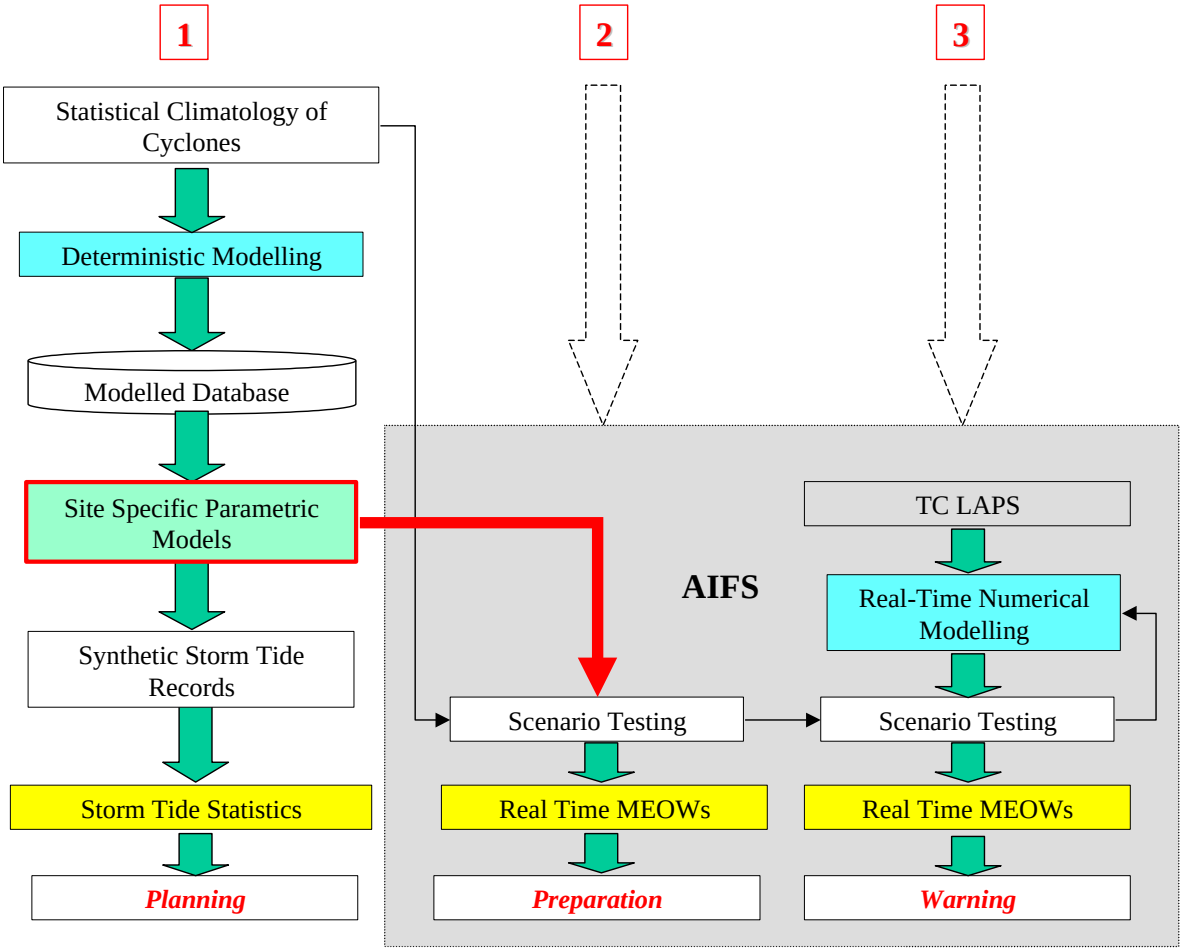

Figure 11.6 A suggested hybrid approach to the storm tide prediction problem.

11.4 Storm Surge Model Domains for the Queensland Coast

Regardless as to which approach is used, it remains necessary to develop a number of storm surge model domains for the Queensland coast under workscope items A-2 and B-1 (refer Appendix A), to suit the MMUSURGE model. These domains lead to the development of estimates of computation time and storage requirements for various MEOW and/or parametric model generation options using MMUSURGE.

11.4.1 Selection Rationale

The selection of modelling domains has considered (a) the need to ensure that the large-scale forcing of storm tide (surge and waves) will be represented and that (b) the ability to model at very fine scales in specific community areas will be optimised for future nearshore wave and wave setup models. This presents a conflict of scales and resolution such that a nested series of model domains is required, as recommended in Chapters 6 and 7 in regard to both storm tide and spectral wave modelling. To provide guidance in the selection of appropriate domain sizes and resolutions, Table 11.1 presents a summary assessment of scale criteria relevant to the storm tide prediction problem that were developed earlier. Here some typical values of the principal parameters are again assumed, i.e. Δs is the model domain spatial resolution (minutes-of-arc or km); Δt is the time resolution (s); R is radius to maximum winds (30 km); V_{fm} is the maximum forward speed (10 m s^{-1}); d is depth (m). Desirable bathymetry accuracy and likely sources of depth data are also indicated. The table identifies the principal ocean environment scales (ocean, coastal, bay and beach) and, with regard to a selection of relevant scale parameters, suggests typical criteria for each situation. This highlights the need for some relaxation of certain criteria to satisfy the conflict of scales. A system of 4 nested transitions is suggested (**A**, **B**, **C**, **D**), with the **A** grid representing the largest extent and lowest resolution; the **D** grid representing the smallest extent and the highest resolution, and with a nesting ratio of 5 between successive grids.

Table 11.1 Scale considerations in model domain selection.

Scale Consideration	Criterion for Each Environment				*Selected Resolutions (' arc)*			
	Ocean	Coastal	Bay	Beach	*7.5*	*1.5*	*0.3*	*0.06*
					A Grid	B Grid	C Grid	D Grid
Coastal features resolution (nominal) Δs	Δs < 15km	Δs < 5 km	Δs < 1 km	Δs < 0.2km	13.9 km	2.8 km	0.56 km	0.11 km
Windfield resolution $\Delta s \le R/4$	$\Delta s \le R/3$	$\Delta s \le R/4$	$\Delta s \le R/5$	$\Delta s \le R/5$	10 km	7 km	6 km	6 km
Wavelength resolution $\Delta s \le 4R/20$	$\Delta s < 0.4R$	$\Delta s < 0.2R$	$\Delta s < 0.1R$	n/a	12 km	6 km	3 km	n/a
Waveperiod resolution $\Delta t \le 4R/(20V_{fm})$	$\Delta t < 0.8\ R/V_{fm}$	$\Delta t < 0.4\ R/V_{fm}$	$\Delta t < 0.2\ R/V_{fm}$	n/a	2400 s	1200 s	600 s	n/a
Along-shore spatial response (nominal) Y	50 R	10 -15 R	2 R	n/a	1500 km	450 km	50 km	n/a
Cross-shore spatial response (nominal) X	10 R	5 R	1 R	n/a	300 km	150 km	30 km	n/a
Deepwater boundary (nominal)	d > 500 m	d > 50 m	d > 20 m	d > 10 m	(location specific)			
Bathymetry accuracy (nominal)	d < 10 m	d < 5 m	d < 2 m	d < 1 m	ETOPO5 5′	AUS charts	AGSO 15″	survey

11.4.2 Model Domain Specification

Figure 11.7 and Table 11.2 present the recommended domain selection, which is based on broadly satisfying the above scale arguments, allowing for significant population centres and ensuring generous overlap. Appendix F details the domain origins and other geometric

properties needed to specify their properties to the model's spherical coordinate system (described in Appendix D).

Only **A** and **B** domains are defined here because of the readily available bathymetry set, which is limited to ETOPO5 (5′ arc) in deep water, augmented by the AUS hydrographic chart and bathymetric series in shelf and nearshore regions. AGSO 30″ data was also considered in this regard but in discussions with AGSO personnel it was not considered greatly superior to the data already available to the Marine Modelling Unit derived from the other sources. Higher resolution data (e.g. AGSO's planned 15″ arc dataset) would be required for **C** grids[5], while **D** grids would demand local survey data. It is considered that such fine scale grids need to be developed in the context of undertaking detailed regional studies. While parts of the grid generation can be automated, there remains a significant amount of manual intervention required to ensure the grid depths are commensurably accurate with the spatial resolution and that the actual coastline is properly preserved. The availability of some **C** grid data domains for Townsville and Cairns, which were used for the present hindcast activity, is due to earlier research studies conducted by the Marine Modelling Unit. That data would be available to assist in compatible **C** and/or **D** grid construction for those regions.

Table 11.2 Selected MEOW model domain parameters.

Grid No.	Location	Timestep	Resolution		Extent		Dimension (km)	
		s	' arc	km	Alongshore	Offshore	Alongshore	Offshore
A0	Queensland Coast	1800	7.5	13.9	201	57	2780	778
A1	Southern Queensland	1800	7.5	13.9	101	57	1390	778
A2	Central Queensland	1800	7.5	13.9	101	57	1390	778
A3	Northern Queensland	1800	7.5	13.9	101	57	1390	778
A4	Gulf of Carpentaria	1800	7.5	13.9	105	117	1966	1612
B1	Brisbane	900	1.5	2.8	161	65	448	179
B2	Hervey Bay - Gladstone	900	1.5	2.8	153	61	426	168
B3	Mackay	900	1.5	2.8	161	125	448	347
B4	Whitsunday	900	1.5	2.8	201	101	560	280
B5	Townsville	900	1.5	2.8	161	65	448	179
B6	Cairns	900	1.5	2.8	177	45	493	123
B7	Cooktown	900	1.5	2.8	161	73	448	202
B8	Lockhart River	900	1.5	2.8	149	65	414	179
B9	Torres Strait	900	1.5	2.8	131	141	364	392
B10	Weipa	900	1.5	2.8	161	41	448	112
B11	Karumba	900	1.5	2.8	169	49	470	134
B12	Mornington Island	900	1.5	2.8	161	57	448	157

[5] Testing of *Althea* using the recommended **A2** and **B5** grids here shows only a 3% overprediction relative to the recorded water levels as detailed in Section 10.

Five **A** grid domains have been selected to provide well-conditioned boundary data to each of the **B** grids. The first **A** grid (**A0**) covers the whole of the Queensland coast and is expected to be applicable for situations where there is considerable synoptic scale forcing in addition to the vortex (e.g. high pressure ridging etc). Grids **A1**, **A2** and **A3** are sub-grids of **A0** with 50% overlap, which to be used with the nearest **B** grid. Grid **A4** covers the Gulf of Carpentaria, which is an area with extensive shallow water regions and complex tides, where synoptic-scale forcing is known to be important. It is expected that every **B** grid simulation will obtain boundary data from the most appropriate adjacent **A** grid. It should be noted that the extent of potential **C** grids should ideally be decided before conducting **B** grid simulations so that the boundary data can be retained.

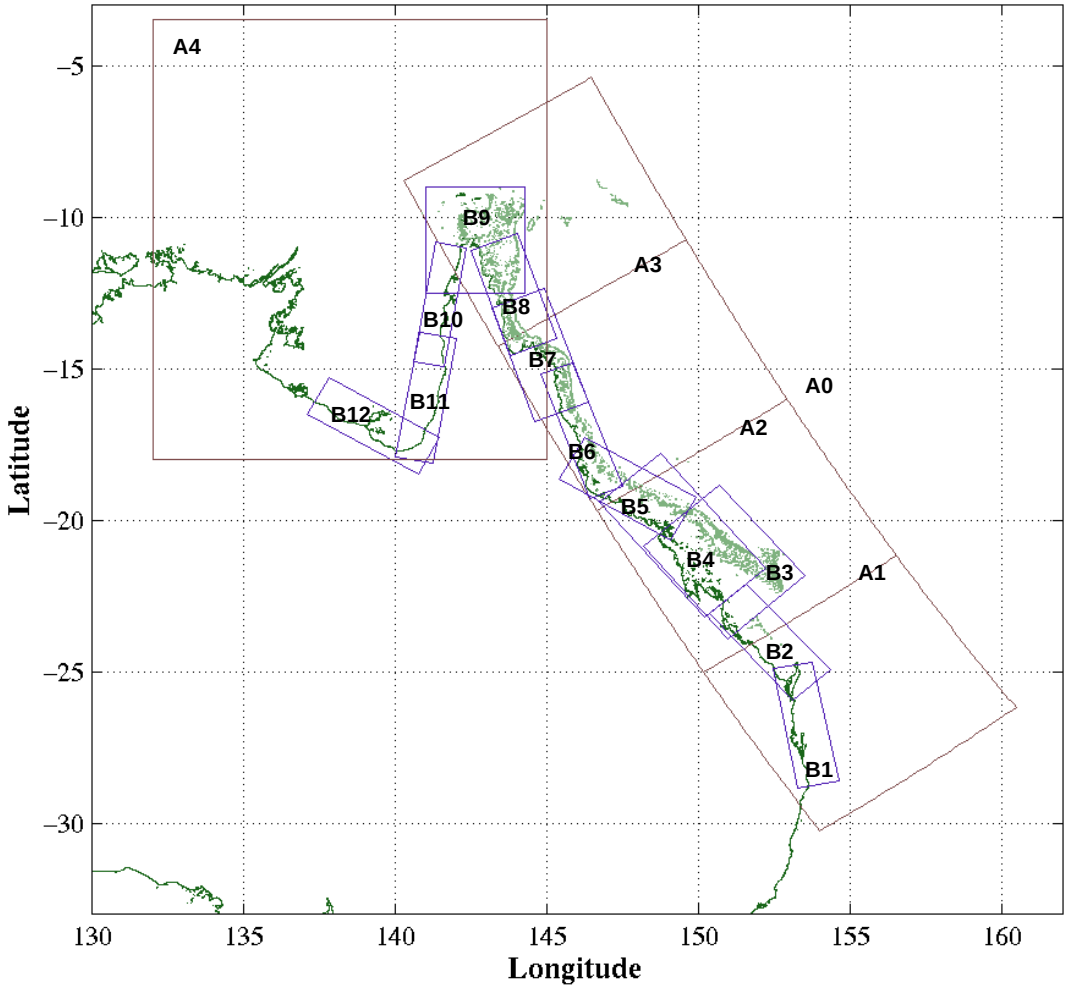

Figure 11.7 Storm surge model A and B domains for the Queensland coast.

11.5 Estimating Model Simulation Times and Storage Requirements

This section addresses workscope item A-4 in regard to estimating the computational requirements and database needs of the MMUSURGE model (Mason and McConochie 2001) as a function of selected model domain and length of simulation. This is then extended to

consider the implementation of some specific MEOW data generation steps utilising Bureau of Meteorology computing resources within the Queensland Regional Office.

11.5.1 Model Requirements

The MMUSURGE storm surge model is implemented in FORTRAN 90 and its computational speed is somewhat dependent on the specific architecture of the machine being used (instruction set, caching, pipelining etc) in addition to the base CPU clock speed. Its memory requirements may also be slightly non-linear relative to domain size because of the implicit matrix solution of the hydrodynamic equations. It is also likely to be sensitive to the operating system being used (e.g. UNIX™, LINUX™ or Windows™ NT/2000). The model has been developed and run successfully to date on a variety of UNIX™-based machines at James Cook University.

Under Part B-1 of the current workscope MMUSURGE has been ported to the CIRRUS1 workstation at the Queensland Regional Office of the Bureau of Meteorology in Brisbane, which has the following configuration:

IBM 43P Model 150
PowerPC™ 604e 375MHz
512 MB RAM
2 x 9.1GB disk
AIX™ 4.3.3 operating system (a UNIX™ variant)
XLF90 FORTRAN 90[6]

Benchmark testing has shown that the above machine[7] has comparable performance to any Intel™ Celeron™ level personal computer of similar clock speed and that only modest RAM (e.g. 64 MB) and disk storage (e.g. 1 GB) is needed to successfully execute the MMUSURGE model. Based on discussions with Queensland Regional Office computing staff, a number of machines of this capacity could be utilised wholly or partly within Regional Office. It may even be possible to install joint operating systems (LINUX™/Windows™) on machines that are only lightly loaded, without inconveniencing normal operations. Data archiving requirements will need to be separately addressed.

Assuming CIRRUS1 is utilised, Table 11.3 presents actual CPU time (min) and disk storage (MB) required as a function of storm duration for each of the A and **B** grids. The disk storage calculation assumes all model output parameters (H,U,V) at all grid points are output in binary at every timestep (e.g. 30 min for **A** grid; 15 min for **B** grid), together with 10 time history locations. Allowance is also made for the **A**-**B** grid boundary transition file. Note that each **B** grid simulation must have a corresponding **A** grid simulation as well and the total under "Option (i)" in Table 11.3 allows for this fact. For example, to process a single 24 h storm scenario in each of the 12 **B** grid domains would require 105 h CPU time and generate 206 MB of disk output on CIRRUS1.

Table 11.3 "Option (i)" represents the "base case" whereby the full model capability is utilised and full output is retained. To reduce computational overheads for open coast MEOWs it is

[6] An ANSI compliant FORTRAN 90 compiler is required to generate an executable version of the model and MATLAB™ is required to access the graphical output capabilities.
[7] Latest Compaq Alpha™, Intel Pentium III™ and AMD Athlon™ processors would likely exceed the computational speed of CIRRUS1 by a factor of 2 or 3 or more.

recommended that the non-linear advection terms in the model momentum calculation be omitted. Their contribution to water levels is shown to be generally small (refer Section 10.7) and a saving of approximately 15% in simulation time is obtained as indicated by "Option (ii)". This recommendation is also consistent with that by Sanderson *et al.* (1995) in regard to the present BMRC model. In addition, as shown in "Scenario (iii) and (iv)" the output data may be drastically reduced if it is deemed necessary only to retain information either a short distance out to sea or just along the coast. Caution is advised however in limiting the data too severely given the high CPU cost in conducting the simulations and the potential value of full field data for other future purposes. Note that time and disk estimates for each "Option" in Table 11.3 are additive.

Based on the above domain-specific CPU and storage parameters it is possible to estimate the order-of-magnitude computational effort to undertake a range of MEOW modelling studies for the whole of the Queensland coast. "Option (iii)" with a 24 h storm duration is retained for further consideration in the analysis of Table 11.4.

Table 11.3 CPU and disk storage requirements for MMUSURGE on the CIRRUS1 workstation.

Grid No.	Location	CPU Minutes for Duration				Disk Storage MB for Duration			
		24 h	48 h	72 h	96 h	24 h	48 h	72 h	96 h
A1	Southern Queensland	1.5	3.0	4.5	6.0	3.3	6.5	9.8	13.0
A2	Central Queensland	1.9	3.8	5.6	7.5	3.3	6.5	9.8	13.0
A3	Northern Queensland	1.8	3.6	5.5	7.3	3.3	6.5	9.8	13.0
A4	Gulf of Carpentaria	2.2	4.5	6.7	9.0	5.8	11.7	17.5	23.4
B1	Brisbane	3.7	7.3	11.0	14.7	11.3	22.7	34.0	45.3
B2	Hervey Bay - Gladstone	3.5	7.0	10.4	13.9	10.3	20.5	30.8	41.1
B3	Mackay	13.9	27.8	41.7	55.6	22.1	44.2	66.4	88.5
B4	Whitsunday	13.7	27.5	41.2	55.0	22.3	44.6	66.9	89.3
B5	Townsville	6.7	13.4	20.1	26.8	11.5	23.0	34.5	46.0
B6	Cairns	5.9	11.7	17.6	23.4	8.8	17.5	26.3	35.0
B7	Cooktown	8.0	16.0	24.1	32.1	12.9	25.8	38.8	51.7
B8	Lockhart River	8.2	16.3	24.5	32.7	10.7	21.3	32.0	42.6
B9	Torres Strait	12.3	24.6	36.9	49.2	20.3	40.6	60.9	81.2
B10	Weipa	1.7	3.4	5.2	6.9	7.3	14.5	21.8	29.1
B11	Karumba	2.1	4.2	6.4	8.5	9.1	18.2	27.3	36.4
B12	Mornington Island	2.4	4.7	7.1	9.4	10.1	20.2	30.3	40.4
Possible Options									
(i) All grids (per storm)		105	210	315	419	**206**	**412**	**618**	**824**
(ii) Advection 0		89	178	267	356	**206**	**412**	**618**	**824**
(iii) Within 10 points of the coast		105	210	315	419	**16.2**	**32.4**	**48.6**	**64.8**
(iv) Coast data only		105	210	315	419	**1.6**	**3.2**	**4.9**	**6.5**

11.5.2 MEOW Parameter Selection

The number of MEOW storm simulations required is controlled by permutations of the number of point values selected to span the desirable range of model storm parameters. For illustration and discussion purposes, a number of scenarios are presented below and summarised in Table 11.4. The parameter ranges considered are { Δp , B , R , V_{fm} , θ_{fm} , X , θ_{max} } and each is specified in terms of a nominal *start* or lower bound, an *interval*, and an *end* or upper bound. The total number of simulations required to cover each parameter range is then indicated and the total permutations calculated, together with the estimated CPU time (weeks on CIRRUS1) and disk storage (GB assuming all data is retained). In each case it is assumed that "Option (iii)" from Table 11.3 is adopted, together with a storm duration of 24 h. Figure 11.8 summarises the resulting CPU and disk storage relationships graphically for each scenario.

The five scenarios presented here are:

1. "Ideal"

This is a simple discretisation of the tropical cyclone parameter space based on "ideal" scales of variation i.e. linearly spaced intervals covering the expected range at a nominal resolution. Only half the full along-shore grid extent is used here due to overlap. Whilst these chosen parameter ranges and resolutions are familiar in terms of known storm surge sensitivities, it is clear that such a MEOW selection is not practically achievable, probably even with supercomputer capability.

2. "Desirable"

Scenario 2 below assumes a coarser *X* resolution and a limited coverage of each MEOW grid, with nominal reductions in all the other parameters. In this case, the coastal crossings would be concentrated only at significant population areas. Further discussion on Scenario 2 is included later.

3. Current US practice

This is based on the information provided in FEMA *et al. (1999)*, as discussed in detail in Appendix E. This scenario is characterised by well defined directions and closely spaced tracks (which are varied according to direction etc) but considers only a single value for *R* and *B*. The target region considered is the northwest Gulf of Mexico.

4. BoM QRO

This refers to BoM (1999), a preliminary MEOW exercise conducted in Queensland Regional Office. This scenario has reduced directional and intensity resolution compared with the US practice but allows for variation in *R*. The target regions envisaged were Cairns, Townsville and Mackay.

5. BMRC

Refers to Sanderson *et al.* (1995), the BMRC review and recommendation report on implementing MEOW techniques in the Australian context. This has the coarsest directional and *X* resolution and was nominally considered to apply to the Mackay region.

It should be noted that only scenarios 1 and 2 here consider variation in *B*, which has been shown even within the present hindcast modelling to be an important storm surge parameter.

Table 11.4 Estimated run times and storage needs for example MEOW scenarios.

			"Option (iii)" and 24 h Duration									
			Scenario 1		Scenario 2		Scenario 3		Scenario 4		Scenario 5	
Storm			"ideal"		"desirable"		US Practice		BoM QRO		BMRC	
Parameter	Unit	Range	Values	Totals	Values	Totals	Values	Totals	Values	Totals	Values	Totals
Δp	hPa	Start	10	11	10	6	15	5	15	4	35	4
		Interval	10		20		20		25		25	
		End	110		110		95		90		110	
B		Start	1	7	1	3	1	1	1.5	1	1.5	1
		Interval	0.25		0.5		0		0		0	
		End	2.5		2		1		1.5		1.5	
R	km	Start	5	6	10	3	40	1	10	3	10	3
		Interval	10		25		0		25		25	
		End	55		60		40		60		60	
V_{fm}	m s^{-1}	Start	2.5	5	2	4	2.2	3	0	4	0	4
		Interval	2.5		2		4.5		5		5	
		End	12.5		8		11.2		15		15	
θ_{fm}	º	Start	0	17	0	9	0	17	0	5	0	4
		Interval	11.25		22.5		11.25		30		45	
		End	180		180		180		120		135	
X	km	Start	0	11	-100	9	-100	11	-500	11	-300	7
		Interval	20		25		20		100		100	
		End	200		100		100		500		300	
θ_{max}	º	Start	65	2	65	2	70	1	70	1	70	1
		Interval	50		50		0		0		0	
		End	115		115		70		70		70	
No. Runs			863940		34992		2805		2640		1344	
CPU time	wk		7639		309		25		23		12	
Disk Space	GB		13677		554		44		42		21	

Based on this small selection of possible scenarios it is clear that *a priori* determination of parameter ranges is a highly subjective matter and that regional coastal characteristics will and arguably should influence the final decision. However, if a standard template is required, Scenario 2 is suggested as a reasonable compromise when compared with the other alternatives. For example, considering each of the parameter ranges in order:

Δp A total of 6 values are suggested to ensure coverage at 20 hPa resolution from the Category 1 to Category 5 and/or MPI. This is the same resolution as US practice but with an expanded range for the weaker storms.

B It is deemed essential that some variability in *B* is included. As a minimum, three values would seem essential in order to cover the 1 to 2 *B* range. Extension to 2.5 is sacrificed on the basis that such storms might tend to be relatively small and hence less likely to be large generators of storm surge.

R This is a primary spatial scale of the tropical cyclone which will interact with the scale of principal coastal features such as the continental shelf width and major bays and capes etc. Limiting its range to only 3 values with a 25 km resolution is considered a minimum requirement.

V_{fm} A resolution of 2 m s^{-1} appears highly desirable in order to detect any regional sensitivity across the most common range of forward speeds. However, conjecture remains as to its influence at higher values and 8 m s^{-1} would seem a minimum in this regard. Arguably, some higher values should also be considered, perhaps substituting for one of the lower values in practice.

θ_{fm} A nominal 180º range is suggested at a 22.5º resolution. It is noted that this is half the resolution of US practice.

X A nominal 25 km resolution is selected, indicative of *R*, which must cover a 200 km range. It is noted US practice chooses to typically concentrate tracks near the target warning site at a resolution as low as 8 km.

θ_{max} Two nominal values are included consistent with the outcome of Section 10.7 and the BMRC review (Kepert 2000).

On the above basis, Scenario 2 is carried forward for further consideration. It represents about 12 times the computational effort of Scenario 3, but there are deemed to be significant drawbacks in applying the US practice to the Queensland context (refer Appendix E).

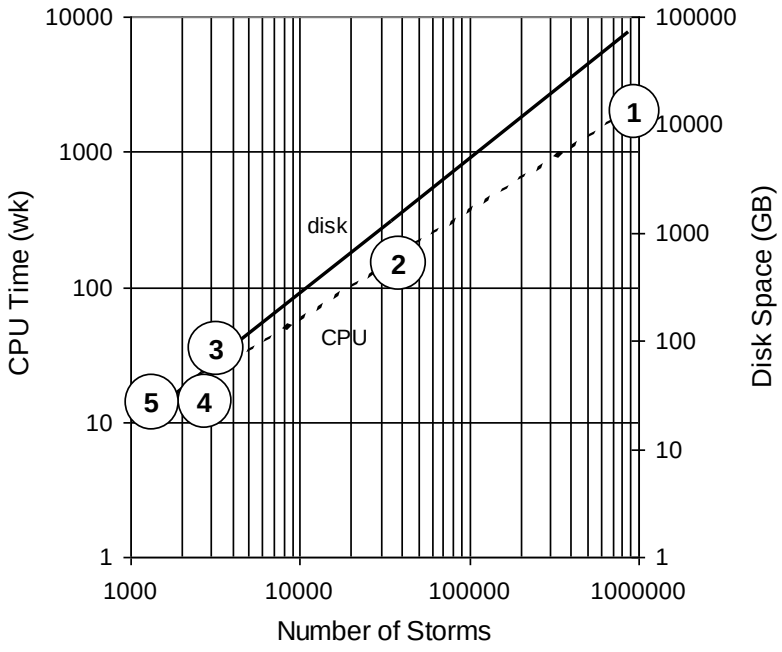

Figure 11.8 Summary MEOW resource requirements for 24 h "Option (iii)".

Scenario 2 yields approximately 6 years of CPU effort based on the standard machine and 554 GB. Assuming multiple machines are available (but not necessarily with a 100% duty cycle), Table 11.5 provides some estimates of elapsed times to complete Scenario 2. It can be seen that with (say) six machines available, the CPU effort could be reduced to less than 2 years. It is envisaged that the available machines would be accessible on a common network and be controlled by a series of automated scripts. These estimates assume full utilisation of each machine whereas there will be practical turn-around losses, general downtime and the like which may erode these figures. Appendix H addresses database issues and storage costs in respect of Scenario 2.

On this basis, Scenario 2 does not appear achievable unless significantly faster machines are made available, in which case it might be reduced to around 1 year's effort. If the θ_{max} requirement is removed by adopting a single value, the total time could reduce to around 6 months.

Table 11.5 Benefit of multiple CPUs for MEOW Scenario 2.

CPU Weeks	**% Availability**				
No. CPUs	**100**	**80**	**60**	**40**	**20**
1	*309*	*387*	*516*	*773*	*1547*
2	*155*	*193*	*258*	*387*	*773*
3	*103*	*129*	*172*	*258*	*516*
4	*77*	*97*	*129*	*193*	*387*
5	*62*	*77*	*103*	*155*	*309*
6	*52*	*64*	*86*	*129*	*258*
7	*44*	*55*	*74*	*110*	*221*
8	*39*	*48*	*64*	*97*	*193*
9	*34*	*43*	*57*	*86*	*172*
10	*31*	*39*	*52*	*77*	*155*

In practice, optimisation of the parameter range selection on a site-specific basis might provide further reductions. For example, alongshore resolution could be varied whereby the more critical regions of the coast are addressed first at perhaps a half-parameter resolution and then later completed to their full resolution, or all track directions might not be required for all grids etc. The operational system could be updated over time with the additional parameter results as required. However, choosing to optimise each set of runs will require a dedicated Bureau officer to make such decisions, document the outcomes and ensure that the system runs smoothly over an extended period of time.

It should be noted that the above refers to MEOWs calculated only for the **B** grid domains and then limited to 24 h duration. At this stage, it is not considered feasible to extend a traditional MEOW database approach to the **C** grid or finer scales. Likewise, the above makes no parameter allowance for synoptic scale influences in either the Gulf or east coast domains or wave and wave setup affects. It also assumes all simulations would be done at mean sea level, with any surge-tide interaction and wave-setup allowance to be empirically added during the forecast phase.

11.6 Conclusions and Recommendations

This section has examined the system design considerations for storm tide prediction, building on the individual recommendations from Chapters 3 through 9 and the outcomes from Chapter 10. The proposed MEOW technique for enabling conservative forecasts of storm tide in a *warning* environment was examined and compared with present US practice. The requirements in support of developing long-term storm tide statistics for *planning* environments was also considered, and found to have many elements in common with the forecasting environment. A hybrid approach was then suggested as a means of ensuring both requirements can be satisfied in an efficient and consistent way.

Consistent with the scope of work requirement, a series of model domains for conducting storm surge calculations along the entire Queensland coast were developed and estimates of MMUSURGE runtimes on the CIRRUS1 workstation were presented. Next, a number of traditional MEOW scenarios were proposed to enable coverage of the whole State in a consistent manner and the total computing resources (time and storage) were estimated.

It is concluded that a traditional MEOWs database approach relying on essentially *a priori* sets of permutations of parameters and using a primitive equation model, is not practical for addressing the needs of the whole Queensland coast, unless it is acceptable to stage the development and extend the analyses over many years. A very large computational effort would be required, not just for the **A** and **B** grid simulations, but for subsequent fine scale simulations which will ultimately be needed to provide more specific detail at sites of interest. Currently envisaged storm surge MEOW data sets alone will also not deliver wave setup estimates and separate wave modelling will be required which, if performed to the same format, would be prohibitively time consuming and generate extremely large data sets.

The recommended technique for delivering the most accurate warning of storm tides is real-time storm surge and wave prediction, fully integrated into Bureau of Meteorology operational systems. However, the computational requirements to achieve this are significant and this goal may take some further years of effort to complete. The alternative solution recommended for immediate warning requirements and for use as a preparedness tool, is a parametric storm tide model developed on the basis of a MEOWs approach, which when combined with detailed climatology descriptions, will have direct application also for enhanced Greenhouse climate change and storm tide statistics analyses. It is further recommended that such a parametric model be designed to be operationally equivalent to a MEOWs scenario environment whereby forecast perturbation analysis is based on expected trends and error bands.

It is recommended that the parametric models so developed then be applied in conjunction with a climatology description via a Monte Carlo Method (MCM) to provide estimates of long-term storm tide statistics for use in evacuation and land use planning, and the protection of environmental values. This approach should aim to provide statistics of (i) extreme storm surge magnitudes; (ii) extreme wave heights and periods; (iii) wave setup and (iv) combined storm tide levels. Furthermore, joint probability estimates of all parameters should also be developed.

If a MEOW data set approach is preferred over parametric models, it is recommended that storm tide statistics be developed using the Joint Probability Method (JPM). In this case,

relevant water level responses would be derived directly from a selection of MEOW data sets and their probability quantum allocated based on the climatology information.

It is envisaged that development of regional parametric storm tide models would initially parallel a MEOW data generation step strategy, but only as many surge and wave simulations as needed to obtain sufficient accuracy would be undertaken in each region. A relatively crude parameter set would be chosen first, then the initial model would be developed and tested using primitive equation modelling (storm surge and waves) to the **C** grid level. Full datasets could then be retained for possible future project uses. Further parameter selection would then be initiated if accuracy failed to meet defined criteria. This iterative design approach will automatically be sensitive to regional non-linearities and scale interactions such that some domains will require more complex models than others will. In addition, as a result of following this methodology, knowledge will be gained about the dynamics of storm tide behaviour in each region, which might otherwise become subsumed under the weight of data in a traditional MEOWs data generation step. At least an order of magnitude reduction in computational effort over the traditional MEOW would be the target outcome. Operationally, very low data requirements are expected, with the parametric models able to execute on any personal computer and be contained within a single CDROM.

It is further envisaged that a systematic model development process would be ideally investigated by undertaking an initial pilot study for a specific domain. This would provide the detailed methodology for application to other areas and allow the process to become routinely applied for the other domains. An ability to extend the methodology to other Australian regions in a timely manner is also seen as highly desirable. The parametric approach is also believed to be the only viable method for incorporating synoptic scale influences and the like, by significantly limiting the MEOW case studies that might normally have to be considered.

11.7 References

BoM (1999) The MAPINFO MEOWS (storm surge) gis display program. Prepared by A. Smallegange, *Bureau of Meteorology*, Queensland Regional Office, Jul, 10pp.

FEMA *et al.* (1999) Northwest Florida hurricane evacuation study. *Prep by FEMA, NOAA, State of Florida and US Army Corps of Engineers*, July.

GCCC (1999) 1999 Planning scheme – background study paper flooding review. Gold Coast City Council Planning Scheme, *Gold Coast City Council*.

Harper B.A. (1983) Half Tide Tug Harbour extreme water level study. Report prepared by *Blain Bremner and Williams Pty Ltd* for DBCT-UDC Joint Venture. Sept.

Harper B.A. and McMonagle C.J. (1985) Storm tide statistics - methodology. Report prepared by Blain Bremner and Williams Pty Ltd for the *Beach Protection Authority* Queensland, Jan.

Harper B.A. (1996) Risk modelling of cyclone losses, Proc IEAust Annual Engin Conf, *IEAust*, Darwin, Apr, 53-88.

Jarvinen B.R. and Lawrence M.B. (1985) An evaluation of the SLOSH storm-surge model. *Bull. Am. Met. Soc.*, 66(11),1408-1411.

Mason L.B. and McConochie J.D. (2001) MMUSURGE user's guide. School of Engineering, Marine Modelling Unit, *James Cook University*, Townsville.

Kepert J.D. (2000) Review of tropical cyclone surface windfield modelling. Prepared by *Bureau of Meteorology Research Centre* on behalf of Queensland Regional Office and at the request of Systems Engineering Australia Pty Ltd, Nov.

Nickerson J.W. (1971) Storm surge forecasting. *Navy Weather Research Facility*, Tech Report 10-71.

Sanderson B., Tang Y.M., Holland G., Grimshaw R. and Woodcock F. (1995) A tropical cyclone maximum envelope of waters (MEOW) technique. *Bureau of Meteorology*, BMRC Res. Rep. No. 51, Oct, 19pp.

12. Operational Considerations for a Storm Tide Forecast System

12.1 Background

Notwithstanding the actual method of computation of a MEOW storm tide warning, as discussed in the previous Chapter, it remains to propose an operational interface which will ensure that the forecast activity is carried out efficiently and effectively, with a very low probability of confusion or error. Additionally, it is essential that the resulting forecast warning information can be effectively transmitted physically and logically to the various layers of emergency management who are required to act on its advice.

Two examples of existing BoM MEOW-related systems were made available to the present study for background information, together with the comprehensive assessment by Sanderson *et al.* (1995) as to a methodology for undertaking MEOW warnings. In addition, preliminary design parameters for the planned tropical cyclone module of the *Australian Integrated Forecasting System (AIFS)* were made available (BoM 2000bcd).

These example systems and supporting material will be briefly evaluated for the purpose of identifying some potential *pros* and *cons* of various approaches, leading to a revised functional specification for a future comprehensive storm tide forecasting system.

12.1.1 NMOC Operational Storm Tide Model Interface

This implements the Sanderson *et al.* (1995) numerical storm surge model (the current "BMRC" model) for general Bureau usage through the Numerical Modelling Operations Centre. The operation of the system is described in BoM (2000a) and is a combination of database functionality (linking to bathymetry data sets and storm track parameter files), the BMRC numerical model itself and output and display routines. Additionally, a batch interface to the Bureau supercomputing system completes the functionality of the system. In software terms, the system utilises ORACLE™ and IDL™ database and graphical display capabilities respectively.

This not a MEOW system as such but an automated (GUI) means of operating the current BMRC storm surge model. Further development would be required to incorporate addition of tides and consideration of forecasting uncertainties and the like to generate ensemble results for a full MEOW, but in theory this process can be undertaken manually by forecasters.

While reasonably comprehensive in its present form, this style of system does not appear to be ideally suited to forecast needs. For example, it requires users to make decisions about the actual model domain to be used for the computation. Besides being an additional impost on the forecaster this is a decision best made by the model designers for (a) sound physical and numerical reasons and (b) for assured consistency and recoverability of results. Also, the output style offered by the graphical routines is not sufficiently clear and simple to be applied directly to warnings. In essence, the system allows a non-modeller to access and operate the model but it contains neither safeguards nor added value for the forecaster.

It is recommended that this style of storm surge model interface (regardless of the underlying hydrodynamic model used) be limited to the development and/or testing environment and not be made available generally for forecasting purposes.

12.1.2 Queensland Regional Office MEOW Display System

This is a MAPINFO™ application created by the Queensland Regional Office (BoM 1999) as a means of displaying the ensemble results from a numerical storm surge model (such as the BMRC model). It accesses a database of model results already undertaken for Cairns, Townsville and Mackay using an earlier version of the BMRC model. While it does provide a MEOW-style capability of interpolation between parameter values, it does not yet incorporate logic which would allow explicitly for forecast parameter uncertainty or the generation or inclusion of the astronomical tide and the effects of wave setup.

The system has a range of functionality but suffers lack of generality due to the limitations of the host software and operationally is relatively slow due to the need to access the large MEOW model data sets. It also stops short of actually being a forecast tool and its design is biased towards display of information rather than decision making based on that information. This observation reflects more the present stage of its development rather than its envisaged potential. Nevertheless, the concept is hampered by the lack of versatility of the GIS mapping software environment and the burden of large MEOW data sets.

12.1.3 Planned AIFS Tropical Cyclone Module

This is not yet an operational system, but rather a planned module extension of the AIFS environment due for completion in 2001 (BoM 2000bcd). In present specification it merely acknowledges that an existing AIFS storm surge modelling application interface is available (NMOC) but that a MEOW application (via the present study) is expected to be added at some future time.

This AIFS extension appears to represent an evolutionary development of the original AIFS environment (J. Kelly personal communication) and a move towards use of more OpenGL software systems with implicit Internet functionality (e.g. use of VisAD[8] Java applets etc). Accordingly it is assumed more proprietary display software such as MAPINFO™ and IDL™ will be progressively phased out.

Given that this system is presently under development, it is recommended that any operational MEOW application be designed for this environment. Accordingly, issues such as database operability, licencing, maintenance costs, hardware dependency etc (as required to be addressed in the scope of work; Appendix A) are best deferred to the custodians of the planned operating environment. In essence, this appears to presently favour use of ORACLE™ and VisAD environments.

Based on the information provided, there is no reason to expect that a suitable MEOW application could not be developed for this environment. Depending on the actual form of implementation (traditional MEOW, parametric or real-time model) efficiency requirements may dictate specific computational modules to be provided in, for example, C or FORTRAN source codes. Certainly, while a mapping capability is needed for interaction and display, survey accuracy in that role is not required and so traditional GIS software is neither essential nor necessarily desirable.

[8] VisAD is an open source Java component library created jointly by the University of Wisconsin-Madison; the National Centre for Atmospheric Research (UCAR) and the NCSA. The name VisAD is an acronym for "Visualization for Algorithm Development"; refer http://www.ssec.wisc.edu/~billh/visad.html#intro

The advantage of the AIFS module environment will be that the basic operational, display and reporting functionality will be already provided and the MEOW module design can focus on delivering specific high value-added storm tide forecast products.

12.1.4 Existing Sanderson *et al.* (1995) Methodology

The Sanderson *et al.* document presents a comprehensive summary of the traditional MEOW approach after Jarvinen and Lawrence (1985) with suggested application to the Mackay region of Queensland. It provides an overview of the philosophy and a formalised mathematical description of the basic technique, advocating simple linear interpolation methods provided the parameter space is shown to be adequate for the region in question. In general, these recommendations are endorsed; the suggested nominal parameter spaces being similar to those independently devised herein in Chapter 11. It is noted that concerns about the potential computational burden of the traditional approach are also raised and emphasis is placed on ensuring the regional response characteristics are investigated. In this regard, the approach is similar to that recommended here in regard to the staged development of a parametric model.

However, one essential departure from the overall technique outlined by Sanderson *et al.* is recommended here. This relates to the order in which the final MEOW is assembled. Whereas Sanderson *et al.* refers to undertaking forecast parameter uncertainty analysis to determine the maximum envelope of (surge) waters and subsequently adding the predicted tide, it remains important to retain the variability in the tide signal as well to ensure the total (storm tide) water level is detected. Importantly, the tide phase variability is subject to the forecast parameter error in track speed and direction.

The suggested use of standard deviation uncertainty estimates of forecast parameters by Sanderson *et al.* is also supported, but these could be additionally augmented by user-supplied probability distribution estimates, as detailed later, to provide event-specific judgement.

12.2 Functional Specification

12.2.1 Background

During the approach of a tropical cyclone towards the coast or other threatened location, interest centres on the immediate 12 h forecast position. The intensity and size of the storm is likely to be known with greater certainty than its immediate track (J. Callaghan, *pers comm*). Errors in the forecast track then not only spatially alter the target landfall position but can also significantly alter the timing of the landfall and accordingly the relative phase between the predicted astronomical tide and the storm surge. The MEOW forecast system needs to be focused towards this critical 12 h look-ahead period and provide succinct guidance in an efficient and easy to use software environment.

12.2.2 Scope

Provision of an accurate and convenient generalised software tool based on the Maximum Envelope of Waters (MEOW) technique for the forecasting of tropical cyclone storm tide events in Australian waters for emergency management purposes. Figure 12.1 provides a schematic overview of the intended system.

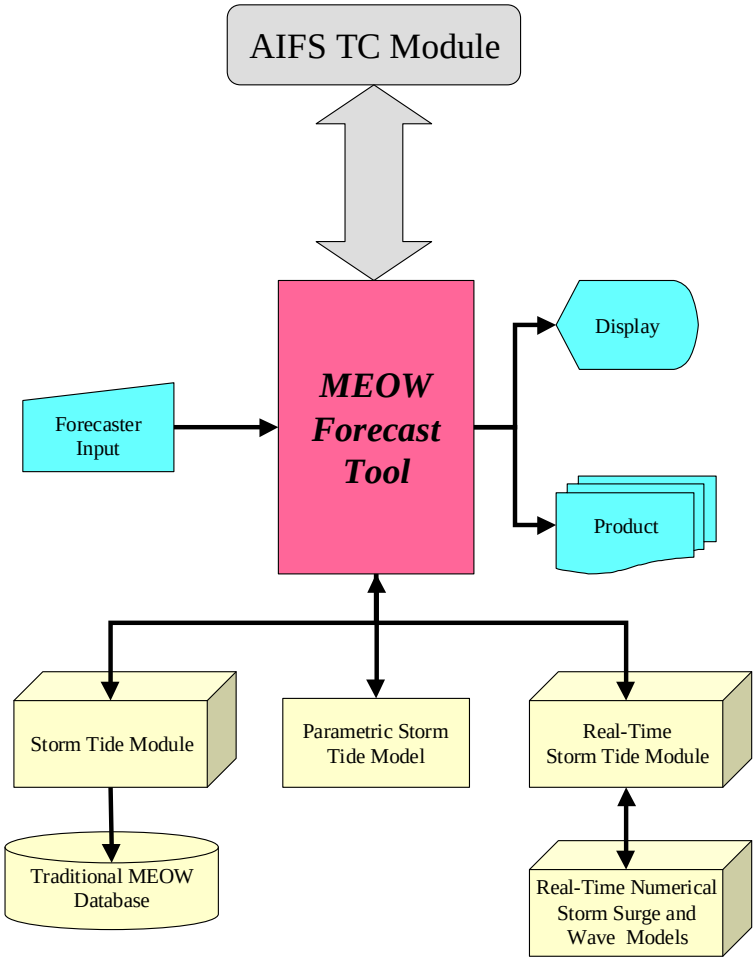

Figure 12.1 Schematic operation of a MEOW forecast tool.

12.2.3 Accuracy

The MEOW technique is designed to ensure a maximum forecast surge level is not exceeded but not to be so overly conservative as to produce false alarms or unnecessary evacuation.

The following target performance accuracy is suggested at this time:

Accuracy Measure	Underprediction	Overprediction
Elevation AHD	-0.25 m	+0.5 m
	-5%	+10%
	(whichever is the greater value)	
Timing of peak elevation	-0.5 h	+1.0 h

12.2.4 Functionality

- To be able to be applied to any Australian coastal location, inclusive of islands and barrier reef situations

- To operate as an integrated tool within the AIFS tropical cyclone module environment
- To be optimised for forecaster usage and forecast requirements
- To be simple and efficient in operation
- To calculate MEOWs in a manner which is independent of the preferred model data source (i.e. traditional, parametric or real-time)
- To provide probabilistic MEOW estimates
- To generate forecast products for distribution purposes
- To provide automatic audit trail and verification statistics

12.2.5 Input Requirements

A MEOW data source sub-system, being either or any of:
- a traditional MEOW database system combined with tide and forecast uncertainty utilities
- a parametric storm tide model incorporating tide and forecast uncertainty
- a real-time numerical storm surge model interfaced to TCLAPS with tide and forecast uncertainty utilities and a multiple simulation batching interface

An astronomical tide database comprising:
- Tidal constituents at all standard ports
- Tidal phase and range offsets at all secondary ports and/or coastal localities to be warned
- Tidal planes at all relevant sites, to include Australian Height Datum (AHD) offsets.

A geometric description of the coastline forming the warning zone, i.e.
- A series of straightline approximations in 2D spatial coordinates; or
- A matrix defining land/sea etc

Forecast tropical cyclone track parameters (default AIFS *working forecast track*), to include:
- minimum 24 h track duration
- surrounding ambient pressure p_n hPa
- pre-existing tidal anomaly[9] Δ m
- storm centre fixes as appropriate, comprising:
  - Time t dd/mm/yyyy hh:mm UTC
  - Latitude ϕ º (-ve Southern Hemisphere)
  - Longitude λ º
  - Central pressure p_0 hPa
  - Radius to maximum winds R km
  - Holland peakedness parameter B -
  - Forward speed asymmetry factor* δ -
  - Angle to maximum winds* θ_{max} º

  * Depending on the final wind field model characteristics.

Forecast track parameter uncertainty estimates, either of:
- Standard deviations of all parameters based on forecast verification studies

[9] This is the actual pre-existing tidal anomaly before the storm tide is computed, normally caused by larger scale persistent or previous weather systems. It may be positive or negative but will generally be less than 0.3 m in magnitude. This value will need to be obtained operationally from the relevant State authority, e.g. Queensland Transport - Maritime Section or EPA Environment and Technical Services.

- User-specified parameter uncertainty estimates as modified standard deviations or cumulative distribution functions (e.g. upper and lower quantiles to allow representation of skew etc)

12.2.6 Computational Requirements

The computational needs of the storm tide forecast module will vary depending on the MEOW data source being utilised but the essential aim is to produce an estimate of the highest storm tide level possible at the sites of interest, within the bounds of the parameters provided. Additionally, probabilistic information should also be presented based on the parameter uncertainty ranges.

The general approach is documented by Sanderson *et al.* (1995) in accord with the concept of Jarvinen and Lawrence (1985). The method is further extended here to retain elements of the probability of the error estimates (assuming parameter independence) and to ensure the correct tide phase is included when calculating the total storm tide level. Appendix G provides a concise summary of the MEOW technique whereas only the operational elements regarding parameter uncertainty ranges are detailed here.

The storm tide level at each site is constructed as the linear superposition of various time varying components, such that:

$$[\xi]_t = \{ \Delta + [\zeta]_t + [\eta]_t \} + [\psi]_t \qquad (12.1)$$

where Δ is the local tidal anomaly; $[\zeta]_t$ is the astronomical tide; $[\eta]_t$ is the storm surge, and $[\psi]_t$ is the wave setup. The maximum water level or MEOW is then of interest, together with the time of the maximum, e.g.

$$[\xi]_{t=tmax} = max\,([\xi]_t)_{\,t=t1,t2} \qquad (12.2)$$

The MEOW data source module must construct a time history forecast for each warning site formed by an *n*-dimensional parameter space, e.g. for the storm surge component

$$[\eta_i]_t = \boldsymbol{F}\,[\, p_{0i}, R_i, B_i, X_i, V_{fmi}, \theta_{fmi}, \ldots]_{\,t} \qquad (12.3)$$

where t is time, X is closest approach to site and i = 0,1,2,3,... indicates multiple parameter cases determined by expanding the specified forecast uncertainty bounds of each parameter (χ), viz

i	=	0 = expected or mean parameter value	$[\chi]$
		1 = upper bound parameter value; say	$[\chi + \varepsilon_i(\chi)]$
		2 = lower bound parameter value; say	$[\chi - \varepsilon_i(\chi)]$ etc

where $\varepsilon_i(\chi)$ is the parameter error value having cumulative non-exceedance probability $P_i(\chi)$.

An example would be, say, for the uncertainty in forecast central pressure to be assumed to be distributed normally about the mean and an estimate of the standard deviation alone used as the measure of parameter dispersion:

p_{0i}	i=0	940	expected pressure at landfall (hPa)
	i=1	945	based on one standard deviation upper bound → $[\varepsilon_1(p_{01}), P_1(p_{01})]$ of [5.0 , 0.8413]
	i=2	935	based on one standard deviation lower bound → $[\varepsilon_2(p_{02}), P_2(p_{02})]$ of [5.0 , 0.1587]

This can be extended to as many *i* values as deemed necessary in describing the probability of non-exceedance function for that parameter. In practice, it is unlikely that more than 2 or 3 probability limits per parameter would be chosen but it may be desirable to include skewness (unequal upper and lower intervals etc) depending on the particular forecast trends. If the information can be related to climatology then more detailed probability values could be used as the defaults.

While the uncertainty limits in central pressure, radius and peakedness would be specified directly, the track speed and direction uncertainty can be provided simply as alternate forecast track time and position fixes. The relevant uncertainty in direction and speed can then be directly obtained from the series of alternate fixes. This will also dictate the relative phasing of the storm surge (and setup) with the astronomical tide.

The final MEOW levels can then be expressed together with a probability of non-exceedance associated with the forecast or a MEOW response function can be produced as a function of probability of non-exceedance. Representing the probability function rather than a single value will enable appreciation of the sensitivity of the MEOW to the current forecast parameter space.

(a) Traditional MEOWS Database

The MEOW data source module in this case constructs a time history forecast for each warning site derived by linear interpolation from a series of pre-computed storm surge responses stored in a database formed by the n-dimensional parameter space e.g.

$$[\eta]_t = \boldsymbol{I}\ [\ p_0{}^p, R^r, B^b, X^x, V_{fm}{}^v, \theta_{fm}{}^\theta, \ldots\ ] \qquad (12.4)$$

where $\boldsymbol{I}$ is an interpolation operator within the n-dimensional parameter space defined by the range of discrete parameter values $\{p, r, b, x, v, \theta, \ldots\}$ obtained from a series of systematic numerical model results.

The extent to which estimates of localised wave setup can also be included in the traditional approach depends on whether corresponding n-dimensional wave parameters have also been devised or if a simplified parametric wave setup is invoked.

(b) Parametric Storm Tide Method

The MEOW data source module in this case constructs a forecast for each site derived directly from an analytic description for the *n*-dimensional parameter space. Otherwise, the procedure is identical to (a) in regard to the probability concepts.

Wave setup components are similarly provided, depending on the method of parameterisation.

(c) Real-Time Numerical Model(s)

The MEOW data source module in this case constructs a forecast for each site derived from a limited number of numerical hydrodynamic model simulations representing sensitivity tests of the *n*-dimensional parameter space. Otherwise, the procedure is identical to (a) in regard to the probability concepts. The number of simulations possible would be a function of the computing capacity and the time available to complete the forecast. Likely, a super-computing batching arrangement would be utilised, in essence similar to the existing NMOC arrangements.

In this case any non-linear tidal interactions can be incorporated directly (provided regional tide open boundary data is available) and the current composited surface wind and pressure field (e.g. TCLAPS) can be utilised for representation of the forcing. Wave setup could be provided from a simultaneous numerical wave model or provided as a parametric function.

12.2.7 Output Requirements

(a) Basic:
Forecast storm tide water elevation to AHD and an estimate of the probability of exceedance plus forecast timing of the peak level for all nominated coastal or other locations, together with associated tidal plane data (e.g. HAT).

(b) Text Based:
Unambiguous tabulation of *inter alia* :

- coastal location
- date and time
- forecast storm tide level and probability of non-exceedance
- predicted level relative to HAT
- predicted tide level
- predicted wave height and period
- predicted wave setup component

together with a record of all forecast assumptions (track parameters, uncertainties, tidal anomaly etc)

(c) Graphical:

- 2D (map) views of the spatial distribution of storm tide levels at selected forecast times (either full-field or coastal ribbon depending on the MEOW data source method) consisting of annotated and/or contoured water elevation to AHD together with the location of warning sites;
- As above, but ocean velocity vectors for guidance (depending on MEOW data source);
- Alongshore profile graphs showing the forecast variation (magnitude, slope etc) of storm tide levels at selected forecast times, annotated with the location of warning sites and predicted tide levels;
- Time history graphs of forecast storm tide levels at selected warning sites together with predicted tide variation, tidal planes and forecast wave height and setup components;
- Probabilistic MEOW summary showing storm tide versus probability of non-exceedance.

12.2.8 Forecast Products

A range of forecast products could be produced, tailored to suit the specific client groupings and their information needs. These might include replica output to that described above, derivative products stripped of extraneous detail to focus on a specific response role or be value-added products. Possible examples include:

- Simple summary tabulations of forecast locations, times and levels
- 2D map views of forecast alongshore storm tide levels at the time of peak forecast levels
- As above but with forecast times of storm force winds, overlaid traffic routes etc

12.2.9 Use Cases

The following are preliminary *Use Cases* provided to illustrate the basic envisaged operation of the forecast system. Further detailed *Use Cases* should be developed as necessary to fully describe the system. The following assumes a *working forecast track* is available which contains the additional storm parameters required for a storm tide forecast.

USE CASE 1	Specify forecast track uncertainty parameter ranges	
Trigger	Initial forecast or modified storm tide forecast	
Description	Step	Action
	1	Select forecast parameter of interest (e.g. track fix)
	2	Select method of error estimate (std dev, CDF ordinate pairs)
	3	Edit error estimates to match present expectations and limits
	4	Save current parameter settings

USE CASE 2	Produce storm tide forecast	
Trigger	Scheduled advice due, or Trial advice required	
Description	Step	Action
	1	Select preferred storm track file (default *working track*)
	2	Confirm or edit current parameter error estimates
	3	Calculate MEOW or initiate batch run
	4	Generate storm tide forecast output

USE CASE 3	Generate storm tide forecast output	
Trigger	Scheduled advice due, or Trial advice required	
Description	Step	Action
	1	Select type of output required (tabular, graphical etc)
	2	Select time (fix or range)
	3	Select warning site(s)
	4	Print or display results

12.2.10 Associated Tools

(a) An Operational Parametric Windfield Model

In the cases of non-real-time simulation of MEOWs, the specification of the forecast storm track parameters is likely to require additional guidance, especially in regard to consistent

pairing of *R* and *B* values, forward speed asymmetry and the like. A real-time parametric wind field model with linked access to AWS data would be highly beneficial in ensuring these parameters are wholly consistent. The model could also be used to provide direct quantitative assistance in the prediction of time of onset of gales and the extent of the warning zones etc. Such a facility would provide a base quantitative best-track documentation to enable future verification/hindcast studies of the storm tide forecasting system.

(b) An Astronomical Tide Generator

Notwithstanding the fact that the MEOW output is specified to also indicate the predicted tide levels, this could be a useful tool to produce simple graphs and tabulations of the predicted astronomical tide to supplement the more basic information available from published tide tables.

(c) CLIPER Model Improvements

The specification of track parameter uncertainty estimates could benefit from an updated and/or revised CLIPER statistical model to provide objective track guidance.

(d) Forecast Verification Tools

These could lead to direct estimates of forecast parameter uncertainties as a function of various prediction scenarios (e.g. rapidly deepening, shearing, trough interaction etc) which could be invoked as required.

12.3 Conclusions and Recommendations

A number of existing (interim) Bureau of Meteorology storm tide warning systems and/or proposals have been examined, together with present US practice. It is concluded that none of these approaches will deliver a reliable operational forecast system without significant modification or enhancement. Furthermore, it is concluded that the present US practice for constructing MEOW-based warnings would not be suitable for Queensland because of its neglect of tide magnitude and phasing issues.

A functional specification was developed which would include the necessary technical features of a MEOW warning system and provide a practical forecast environment integrated into the AIFS system. The functional specification was developed to be independent of the actual MEOW data source being used (i.e. traditional data set, parametric model or real-time model). Appendix G is further provided as a detailed technical description of constructing a MEOW warning.

It is recommended that a detailed MEOW-based storm tide forecast system design specification now be prepared which will preserve tidal phase and surge relationships, incorporate probabilistic parameter estimates and allow a selection of data source modules (i.e. traditional, parametric or real-time).

12.4 References

BoM (1999) The MAPINFO MEOWS (storm surge) gis display program. Prepared by A. Smallegange, *Bureau of Meteorology*, Queensland Regional Office, Jul, 10pp.

BoM (2000a) Storm surge system user guide. *Bureau of Meteorology,* NMOC, 6pp.

BoM (2000b) SPB/COSB Tropical cyclone module: project plan. http://www2.bom.gov.au/sect_info/tcmodule/project_goals/project_plan.htm, *Bureau of Meteorology,* Apr, 7pp.

BoM (2000c) SPB/COSB Tropical cyclone module: function requirements. http://www2.bom.gov.au/sect_info/tcmodule/project_goals/function-require.htm, *Bureau of Meteorology,* Mar, 7pp.

BoM (2000d) SPB/COSB Tropical cyclone module: use cases. http://www2.bom.gov.au/sect_info/tcmodule/project_goals/use_cases.htm, *Bureau of Meteorology,* Oct, 9pp.

Jarvinen, B.R., and Lawrence, M.B. (1985). An evaluation of the Slosh storm-surge model. *Bulletin of the American Meteorological Society*, 66, 1408–1411.

Sanderson B., Tang Y.M., Holland G., Grimshaw R. and Woodcock F. (1995) A tropical cyclone maximum envelope of waters (MEOW) technique. *Bureau of Meteorology*, BMRC Res. Rep. No. 51, Oct, 19pp.

13. Dissemination of Tropical Cyclone Storm Tide Hazard Information

13.1 General

It is critically important that the outcomes from hazard assessment studies, such as those envisaged under the present project plan, be effectively disseminated and communicated to the full range of stakeholders. The nature of the investigations is complex and the specific technical details may only be fully understood by particular specialist personnel, but the outcomes are universal and require careful product design to target those who need to know and act upon the various types of information which will become available.

Tropical cyclones have the potential to affect any part of the State of Queensland, either by wind, rain, flood or ocean hazards. In that context, the entire community is a stakeholder. Within the present narrower context of ocean hazards, the focus is more towards the coastal strip, but since this is where the majority of the population resides (85%), the potential audience is still very large and the impacts from tropical cyclones cross many social and jurisdictional boundaries. In the simplest context, Government and the Public are the principal stakeholders, but as is explored below, there are a number of important elements that need to be considered.

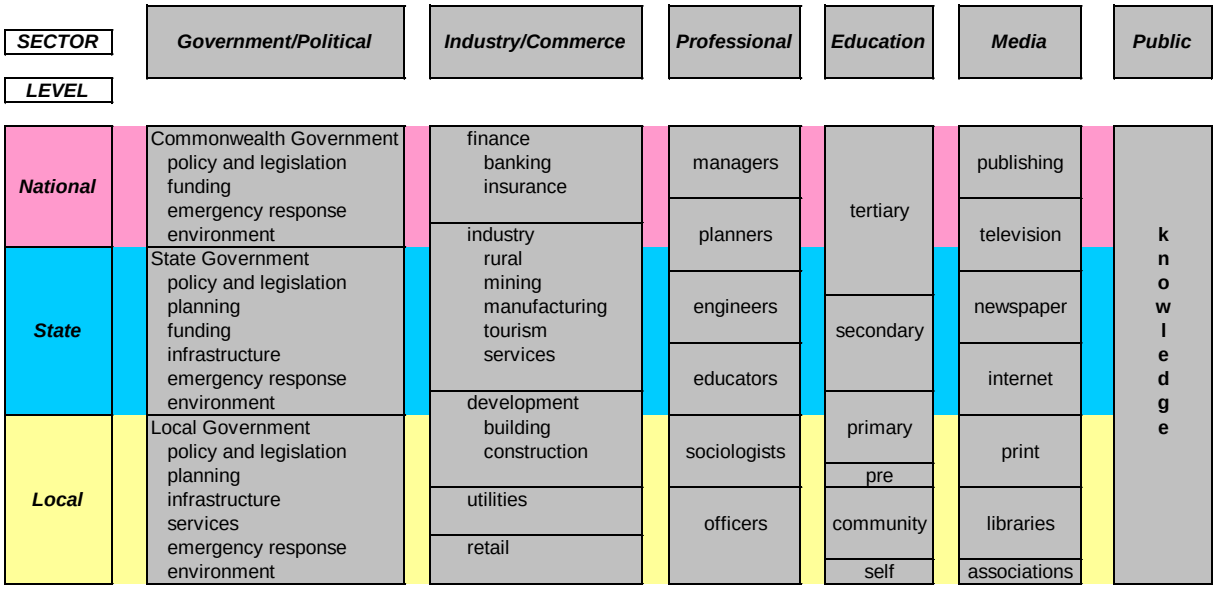

Figure 13.1 The potentially broad range of stakeholders of tropical cyclone storm tide hazard information.

Figure 13.1 outlines diagrammatically the potentially broad range of stakeholder groups, forming a matrix based on socio-geographic *LEVEL* (national, state and local) and occupational or society *SECTOR*. Clearly, *Government* becomes a prime stakeholder sector at all levels, but only for providing appropriate services to the other community sectors. Ultimately the *Public* sector becomes the recipient of the information and services that flow from the inter-related activities in each sector. Rather than dissect these relationships in a detailed way at this time, the following attempts to identify the *principal and key stakeholder* groups within this matrix, then suggests a variety of suitable information products and finally

proposes a match between each sector grouping and the information product type. It is expected that subsequent detailed product design would need to involve information and communication professionals as well as social scientists, working with the base information creators e.g. professional engineers and/or physical scientists.

13.2 Principal Stakeholder Groups

These are identified below in the general sectoral groupings from Figure 13.1 and provided here as an information resource to provide initial guidance to others for future design and dissemination of various information products.

13.2.1 Government/Political

Identified stakeholders here include, in alphabetical order by Departments:

(a) Commonwealth Government

- Department of Defence
  - Australian Army
  - Emergency Management Australia (EMA)
  - Royal Australian Navy (RAN)
- Department of Environment and Heritage
  - Bureau of Meteorology
    - Regional Offices
      - QTCCC
    - TCWCs
    - FWCs
    - NMOC
    - NCC
    - BMRC
  - Great Barrier Reef Marine Park Authority (GBRMPA)
  - Marine Group
    - Coastal and Marine Planning
    - Coasts and Clean Seas
    - Coastcare
    - Australian Coastal Atlas
  - Australian Greenhouse Office (AGO)
- Department of Industry, Science and Resources
  - Australian Geological Survey Organisation (AGSO)
    - Cities Project
  - Australian Institute of Marine Science (AIMS)
  - Commonwealth Scientific and Industrial Research Organisation (CSIRO)
    - Atmospheric Research
    - Marine research
  - Cooperative Research Centres
- Department of Transport and Regional Services
  - Australian Maritime Safety Authority (AMSA)
  - Australian Transport Safety Bureau (ATSB)
  - Local Government
  - Australia's Territories

(b) State Government (Queensland only)

- Department of Communication, Information, Local Government, Planning and Sport
  - Communication and Information
  - Board of Professional Engineers

- Building Codes
- Regional and Urban Planning

Education Queensland (EQ)
- Queensland School Curriculum Council (QSCC)

Department of Emergency Services (DES)
- Disaster Policy and Research
- State Emergency Service (SES)
- State Counter Disaster Organisation (SCDO)

Environmental Protection Agency (EPA)
- Beach Protection Authority
- Coasts and Waterways
- Environmental and Technical Services

Department of Main Roads (DMR)
- Strategic Policy and development
- Road System and Engineering

Department of Mines and Energy (DME)
- Energex
- Ergon Energy
- Powerlink

Department of Natural Resources and Mines (NRM)
- Resource Sciences and Knowledge
- Lands
- QSIIC/QSID

Department of Primary Industries (DPI)
- QCCA

Department of Public Works (DPW)

Queensland Transport (QT)
- Maritime
- Planning and Projects

Department of State Development (DSD)
- Regional Development
- Strategic Policy

Department of Tourism and Racing (DTR)
- Tourism Queensland

(c) Local Government (Queensland only)

There are 40 local government authorities with coastal boundaries in the State of Queensland.

13.2.2 Industry/Commerce

These include but may not be limited to (at all *levels*, Queensland specific):

Association of Consulting Engineers Australia (ACEA)
Association of Consulting Surveyors
Association of Marine Park Tourist Operators (AMPTO)
Australian Chamber of Shipping (ACS)
Australian Association of Ports and Marine Authorities (AAPMA)
Australian Local Government Association (ALGA)
Insurance Council of Australia (ICA)
Local Government Association of Queensland Inc (LGAQ)
Local Government Industry Training Advisory Body
Queensland Chamber of Commerce and Industry (QCCI)
Queensland Ports Association (QPA)
- Bundaberg Port Authority
- Cairns Port Authority
- Gladstone Port Authority
- Port of Brisbane Authority
- Ports Corporation Queensland
- Townsville Port Authority

Queensland Master Builders Association (QMBA)
Queensland Tourism and Hospitality Industry Training Council Inc
Real Estate Institute of Queensland (REIQ)
Standards Australia (SA)

13.2.3 Professional

These include but may not be limited to (at all *levels*, Queensland specific):

Australian Journalist's Association (AJA)
Australian Institute of Management (AIM)
Australian Institute of Petroleum (AIP)
Australian Insurance Institute (AII)
Eastern Dredging Association (EDA)
Institute of Actuaries of Australia (IAA)
Institute of Emergency Services (Qld)
Institute of Municipal Management (Qld Div)
Institute of Public Works Engineering Australia (Qld Div)
Institution of Engineers, Australia (IEAust)
    Queensland Division
        Water Panel
    National Committee on Coastal and Ocean Engineering (NCCOE)
Institution of Surveyors, Australia
Royal Australian Institute of Architects (RAIA)
Royal Australian Planning Institute (RAPI)

13.2.4 Education and Media

These include but may not be limited to (at all *levels*, Queensland specific):

Universities
    James Cook University
        Centre for Disaster Studies
        Cyclone Structural Testing Station
        Marine Modelling Unit
        Reef Research CRC
TAFEs
Secondary Schools
Primary and Pre-Schools
Community associations, interest groups and the like.
National, State and Local Libraries
Newspaper Proprietors
Television Networks

13.3 The Key Stakeholders and/or Key Methods of Information Delivery

Notwithstanding the above broad stakeholdings and interest groups, specific key agencies and organisations provide the information delivery mechanisms. In the main, with the exception of the Bureau of Meteorology and Emergency Management Australia, these are State or Local Government organisations. Their roles and responsibilities are briefly outlined below within the context of either long term preparedness or short term responsiveness roles or sometimes dual roles.

13.3.1 Bureau of Meteorology

The Bureau of Meteorology (BoM 2000) is the National Meteorological Service for Australia, established by an Act of the Commonwealth Parliament in 1906. Its responsibilities include:

- Provision of essential weather, climate and related environmental services to the Australian community;
- Custodianship of the official records of Australian weather and climate;
- Meeting Australia's international obligations under the Convention of the *World Meteorological Organization* and other multilateral treaty obligations to provide meteorological support for the safety of international shipping and aviation and the protection of the global atmosphere

Bureau services include:

- warnings of dangerous weather such as severe thunderstorms and tropical cyclones, and weather conditions leading to floods or bush fires;
- weather forecasts for the land areas and for the coasts and oceans around Australia;
- seasonal outlooks of Australia's climate;
- data and information services on the weather and climate of Australia and surrounding areas; and
- scientific advisory and consultancy services in meteorology, hydrology and oceanography.

In terms of local planning and information dissemination, the Queensland Regional Office (jointly with the *Department of Emergency Services*) organises and convenes the *Queensland Tropical Cyclone Coordination Committee (QTCCC)* which draws membership from a wide range of government and industry organisations. The QTCCC meets quarterly, its terms of reference being:

- To advise and receive input from government authorities and other organisations on the measures necessary to reduce the impacts of tropical cyclones and related storm tides in Queensland;
- To review cyclone experiences and consider the measures necessary to overcome deficiencies;
- To obtain advice and information, consider and make representations on any matter relevant to the good management of cyclone and storm tide threats in Queensland;
- To coordinate the continuing development of tropical cyclone and storm tide warning and response arrangements;
- To form special purpose working groups as necessary.

The QTCCC provides and annual report on its operations to the SCDO (see below) and the Director of Meteorology.

Storm tide warnings are issued by the Bureau of Meteorology in conjunction with the *State Counter Disaster Organization* (SCDO 2000) which interfaces with a number of key State Government organizations. The *Department of Emergency Services* provides the executive role for the SCDO and the *Beach Protection Authority* provides specialist advice and data in respect of wave and storm surge readings from its real-time network of waverider buoys and storm surge gauges. The issuing of storm tide warnings is also staged depending on the threat and the expected onset of high winds at the affected locations, which might impede potential evacuation to higher ground.

13.3.2 Emergency Management Australia (EMA)

EMA is the Federal agency responsible for reducing the impact of natural and human-caused disasters on the Australian community and the lead agency for coordinating Federal disaster response (EMA 2000). EMA reports to the Minister for Defence who has Government-wide responsibility for emergency and disaster matters. Its key responsibilities include:

- developing Commonwealth Government and national emergency management policies, plans and programs;
- through the *Australian Emergency Management Institute*, developing national emergency management education and training curriculum and programs. It also develops emergency management doctrine reflecting best practice in all facets of emergency management and fosters emergency management research;
- working closely with Commonwealth Government agencies, state and territory emergency management organisations, local government and the international community, particularly the island nations of the South Pacific;
- fostering and providing disaster awareness and education materials and campaigns in conjunction with state and territory organisation;
- supporting the development of Australia's civil defence capability;
- providing financial support to states and territories for the development of emergency capabilities through the *Commonwealth Government's State Support Package*.

13.3.3 Queensland Department of Communication, Information, Local Govt, Planning and Sport

Through **Regional and Urban Planning Services** (DCILGP 2000), the Department implements and manages best practice planning and development assessment systems, principally through the *Integrated Planning Act 1997 (IPA).* The system is designed to bring all relevant State and local government approvals into one common process called the *Integrated Development Assessment System (IDAS)*. This system focuses on achieving ecologically sustainable development in Queensland, through integrated planning that balances social, economic and environmental considerations. The Department maintains the legislative and regulatory framework for the conduct of planning and development. In partnership with key clients and stakeholders, it supports the preparation and implementation of regional planning strategies and provides an extensive range of essential planning information to meet client needs and help users of the planning system. On request, the Department also assists local governments and others to resolve land use and development issues.

13.3.4 Queensland Department of Emergency Services (DES)

The role of DES is to serve and support the Queensland community in preventing, planning for, responding to and recovering from emergencies and disasters (DES 2000).

Counter Disaster and Rescue Services is responsible for Queensland's disaster management arrangements, core staffing of the *State Counter Disaster Organisation (SCDO)* and the provision of emergency helicopter and chemical hazard advisory services. It is also joint convenor of the *Queensland Tropical Cyclone Coordination Committee (QTCCC)*, together with the *Bureau of Meteorology*.

Disaster management services include:

- Disaster policy development, planning and operational co-ordination;
- Disaster management advice, training and information;
- Disaster response and recovery;
- Strategic whole-of-Government disaster management policy, and support to the *Central Control Group (CCG),* State Counter Disaster Organisation;
- Liaison with Government Departments with functional and threat-specific disaster responsibilities, the Australian Defence Force and the Local Government Association of Queensland on disaster management issues;
- Disaster-related research projects.

State Emergency Service (SES) and Volunteer Marine Rescue (VMR) Operational Preparedness:

- Training support services and equipment support services to SES volunteers and *State Emergency Service Cadet Groups*;
- Provision of support to *Australian Volunteer Coast Guard (AVCG)* and *Volunteer Marine Rescue Association of Queensland (VMRAQ)* groups; *Surf Life Saving Queensland (SLSQ)* and *Royal Life Saving Society (RLSS)* beach patrols.

State Counter Disaster Organisation (SCDO):
The *SCDO* is an umbrella organisation that encompasses all agencies, groups and officers that make up the *Queensland Disaster Management System*. The *SCDO* is only activated during times of disaster and provides assistance to Queensland communities when local resources are unavailable or have become exhausted. *Local Government Counter Disaster Committees* coordinate the response to a disaster at the local level. If resources are not available locally to properly respond to the disaster, the Local Government can request additional resources from the *Disaster District*.

13.3.5 Queensland Environmental Protection Agency (EPA)

The EPA administers the key Queensland legislation of the *Environmental Protection Act 1994*, the *Nature Conservation Act 1992*, the *Marine Parks Act 1982*, the *Coastal Protection and Management Act 1995* and the *Queensland Heritage Act 1992* (EPA 2000a).

Divisional Roles:

Coasts and Waterways is responsible for coastal management and integrated planning for the coastal zone, including waterways and wetlands. This involves setting standards and policies, planning for protection and management of all aquatic, coastal, marine and wetland areas under Queensland jurisdiction. This function also supports the **Beach Protection Authority**, the statutory objective of which is to regulate and provide advice in respect of certain activities affecting the coast, to protect the amenity of the coast and to minimise damage to property from erosion or encroachment by tidal water. **Planning and Assessment** co-ordinates the implementation of *Integrated Planning Act (IPA)* requirements covering impact assessment, state-level impact assessment and strategic assessments associated with special projects. **Strategic Policy** is responsible for major environmental policy projects which involve whole-of-government co-ordination and intergovernmental negotiations, and for managing environmental policy processes that cross jurisdictional boundaries. It manages the development of Queensland's *Greenhouse Response Strategy* and related programs, including the *Queensland Greenhouse Inventory* and promotion of the *Greenhouse Challenge*

Program. **Legislation** develops applied policy for the EPA and co-ordinates development of environmental legislation, regulations and environmental protection policies. It also contains a *Local Government Group* to provide a key reference point for local governments in Queensland to liaise with the EPA on environmental issues. It is also responsible for managing a protocol agreement with the *Local Government Association of Queensland*, and implementing the EPA's Delegations and Authorisations Policy. **Economics** evaluates economic implications of environmental policy proposals and other factors which impact on the environment. **Environmental and Technical Services - Coastal Services** undertakes a range of State-wide monitoring and modelling functions as well as providing expert advice on coastal processes in so far as they relate to EPA policies and strategies.

The State Coastal Plan:

The EPA is currently developing the *State Coastal Plan* (EPA 2000b), which is to form a framework for considering coastal management outcomes, principles and policies when undertaking planning, assessing development applications and undertaking management decisions. The State Coastal Plan has the effect of a *State Planning Policy* under the *Integrated Planning Act 1997* and will be one of the matters that are coordinated and integrated into new LGA planning schemes during their preparation over the next few years. The *State Coastal Plan* will set a new standard for coastal management in Queensland and aims to promote consistency in the way coastal management is implemented by identifying in a single document the State's coastal management outcomes, principles and policies. Together with regional coastal management plans it will have the force of law under the *Coastal Act* and agencies and persons with responsibilities in the coastal zone that are governed by or linked to the *Coastal Act*, will need to have regard to the provisions of these plans. These include agencies and persons preparing plans, undertaking assessments and issuing approvals, and making management decisions.

The Coastal Protection Advisory Council:

Under the *Coastal Act*, the *Coastal Protection Advisory Council* advises the Minister for Environment directly on coastal management matters. These matters include the development and implementation of coastal plans and their relationship to other plans, areas within Queensland requiring special coastal management, research and other studies relating to the coastal zone, developing public awareness and consultation programs, and assistance that local government and other agencies may need in undertaking coastal management.

13.3.6 Queensland Local Government Authorities

There are 125 Local Government Authorities (LGAs) in Queensland which, under *The Local Government Act (1993),* are granted authority to enact Local Laws for the general well being and governance of the community. Within the present study context, LGAs undertake three important roles, namely:

Community Planning:

LGA planners are responsible for preparing planning schemes under the *Integrated Planning Act 1997* taking into account matters of State and regional interest such as the State Coastal Plan and Emergency Management Plans in assessing particular development applications. Such plans may incorporate risk mitigation measures and many LGAs are currently receiving

funding assistance directly from EMA and DES in this regard to understand and reduce their long-term risk to many natural hazards.

Infrastructure Provision:

LGA engineers are responsible for the adequate design of community infrastructure (roads, bridges, water supply and sewerage, ports and marinas, beaches, building approvals, certification etc). They need to be aware of special design provisions likely to be required to ensure tropical cyclone hazards are adequately considered. This will include specific issues in regard to risk mitigation plans.

Counter Disaster:

Many coastal LGAs already maintain storm tide impact and evacuation maps which address presently interpretations of the tropical cyclone threat to their communities. Under the Queensland Disaster Management System, *Local Government Counter Disaster Committees* coordinate the response to any disaster at the local level. If resources are not available locally to properly respond to the disaster, the Local Government can request additional resources from the Disaster District via the SCDO. The LGA emergency managers involved in (part-time) counter disaster measures are often drawn from engineering or planning divisions but may be completely separate staff members without access to the same information on tropical cyclone risks or without specific training in the interpretation of such information.

13.3.7 Industry Associations

A number of influential industry associations exist to service a wide range of needs for their member organisations. Tropical cyclone impacts and issues will figure in many aspects of their services, training and advice.

LGAs in Queensland are supported by the *Local Government Association of Queensland*, which provides a range of information and policy services and will be an important LGA conduit for tropical cyclone hazard information and education. Other major associations include the *Association of Consulting Engineers Australia*, *Queensland Ports Association (*formerly Harbour Board Association) and the *Queensland Master Builders Association*.

In operational terms, organisations such as the *Association of Marine Park Tourist Operators* may be valuable communicators of risk information to the tourism industry. Over the longer term, mitigation efforts may be strengthened by the support of the *Insurance Council of Australia*, and *Standards Australia* provides mechanisms by which design practice can be influenced by the various professional bodies.

13.3.8 Professional Bodies

Various professional bodies provide a range of information, networking and continuing education services to individual personnel with important roles in either long-term disaster preparedness or counter disaster response.

For example, LGA engineers and planners look to their professional bodies such as the *Institute of Public Works Engineering Australia* (previously the Local Government Engineers Association Queensland), the *Institution of Engineers, Australia (IEAust)* and the *Royal*

Australian Planning Institute for state of practice guidance. The *IEAust* has Local Branch representation at Gold Coast, Sunshine Coast, Wide Bay, Gladstone, Rockhampton, Townsville and Cairns where regular meetings are held. Emergency managers, for example, are additionally served by an *Institute of Emergency Services*.

Many of these professional bodies conduct education and training, annual conferences and the like or produce publications which form a valuable reference source for day to day professional practice and measures of acceptable peer conduct such as *duty of care*.

13.4 Potential Information Products

A variety of information products could be envisaged to deliver the relevant information, advice and guidance to the full range of stakeholders. However, this needs to be specifically targeted to each sector to maximise the information transfer value. Figure 13.2 presents an overview of the likely match between each sector (as identified in Figure 13.1) earlier) and a range of possible information products. It is suggested that different sectors will expect and seek information in different formats and levels of detail. As illustrated, there are at least 8 identifiable tiers of information that will require consideration for an effective information strategy.

13.4.1 Media Delivery Mechanisms

The *Internet* is expected to be an increasingly important media delivery mechanism because of its ease of access and ability to incorporate graphical and interactive tools. However, there will remain a significant requirement for traditional documentation and especially quality control and tracking procedures to ensure accurate information is always being provided to decision managers. Inclusion of essential aspects of knowledge into general school curricula should be pursued.

Final technical recommendations and procedures would ideally be enshrined into State legislation and Local Government Laws for ease of reference and enforcement.

13.4.2 Content

Within the above context, two basic information streams are also required:

- Warning and response
- Planning and mitigation

These information streams need to be mutually consistent and supportive to allow the information seeker to move freely between the two contexts. For example, local emergency managers should become familiar with the relative risks of inundation due to storm tide (predominantly a planning issue) when responding and reacting to actual warnings. Evacuation plans and the like should ensure that they are at least optimised to handle the more likely scenarios whilst incorporating contingency for the ultimate event. Conversely, those having planning and design responsibility should appreciate that the ultimate event is possible and consider the likely community impacts in that situation. Economics will play a part in each case and *decision-making tools* will be required to ensure consistency of approaches across organisations and regions.

Spatial and temporal variability and integrated storm tide risks need to be described at

- Local,
- Regional and
- State levels

and include the relative contributions of tide, surge and extreme waves. Graphical summaries with tabular backup are likely to have the greatest practical value provided that procedural material guides the decision-making processes. Liberal use of examples and situation scenarios would be an essential element. Interactive decision tools are seen as essential components of any information heirachy in the modern and emerging computing environment.

13.4.3 Associated Knowledge Needs

In addition to conveying the basic outcomes of a storm tide hazard investigation, there are many associated issues which ideally need to be included in a comprehensive information package. For example, the effective uptake of storm tide information will rely to some extent on allied knowledge and understanding. This could include, *inter alia*:

- Climatology of Tropical Cyclones
- Seasonal Variability (El Niño etc)
- Greenhouse Issues
- Risk Concepts, Identification, Management
- Warning Systems
- Accuracy of Predictions
- Research, Training and Education Needs

To some extent many of these topics are being addressed already in various ways but authorities are urged to ensure an holistic approach is maintained to ultimately raise the overall knowledge of the community and ensure penetration of information into the many and varied sectors of society.

13.5 Conclusions and Recommendations

A wide range of potential stakeholders in regard to storm tide warning, preparedness and planning has been identified, ranging from the Federal Government to individual members of the public. The roles of several of the more major organisations, mostly State and Local Government, have also been further detailed. A heirachy of information products is suggested to ensure the correct matching of ocean hazard information to stakeholder needs.

It is recommended that information products be jointly developed and designed by engineering/scientific advisers and professional information and communication personnel, including social scientists. It is also recommended that information products cover a variety of media and formats to be specifically targeted to a range of important government, industry, occupational, educational and public sector groups.

It is timely to consider recent salient US experience in respect of hurricane preparedness and response which highlights the challenges ahead for the Queensland community in ensuring all stakeholders are involved in the long term decision making processes. As Queensland

continues its rapid development it is likely that the State will approach the types of problems being experienced in the USA along the Gulf and Atlantic coasts which are subject to significant levels of hurricane attack.

The following is a precis of findings made at a recent multi-disciplinary forum organised by the American Meteorological Society and sponsored by The Weather Channel (AMS 2000):

> *The nation's hurricane policy has evolved so that it depends primarily on preparedness, prediction and evacuation and places only minimal reliance on land use strategies, structural engineering and building codes.*
>
> *Reliance on weather prediction and evacuation is increasingly strained by population and economic development in coastal areas; evacuation clearance times are increasing to the point where they exceed the lead-time of high-confidence forecasts; many people remain in high-risk areas while the road and shelter infrastructure becomes overloaded with people at much lower risk; local evacuation decisions are triggering mass population movements with severe traffic congestion and shelter shortages on a regional scale.*
>
> *Strains in existing procedures are forcing new response strategies for managers away from total reliance on comprehensive evacuations; shelter-in-place or refuge-of-last-resort solutions are being considered which reduce response times but carry higher risk and are yet to be fully studied and evaluated by the communities they serve.*
>
> *There is poor understanding and application of uncertainties in hurricane forecasts, risk assessments, population responses, infrastructure capacities and media coverage; future development of the preparedness, forecast, communications and response system must address the full range of uncertainties.*

13.6 References

AMS (2000) Policy issues in hurricane preparedness and response. Proc of The Weather Channel Forum, Developed by the Atmospheric Policy Program of the American Meteorological Society, *AMS*, Sept.

BoM (2000) Extracted from http://www.bom.gov.au, Nov.

DCILGP (2000) Extracted from http://www.dcilgp.qld.gov.au/index_planning.html, Nov.

DES (2000) Extracted from http://emergency.qld.gov.au, Nov.

EMA (2000) Extracted from http://www.ema.gov.au/1aboutema/ataglance.html, Nov.

EPA (2000a) Extracted from http://www.env.qld.gov.au/environment/about/structure, Nov.

EPA (2000b) Extracted from
http://www.env.qld.gov.au/environment/coast/management/welcome.html, Nov.

SCDO (2000) Storm tide warning-response system. Jointly issued by the *State Counter Disaster Organisation* and the *Bureau of Meteorology* (Qld).

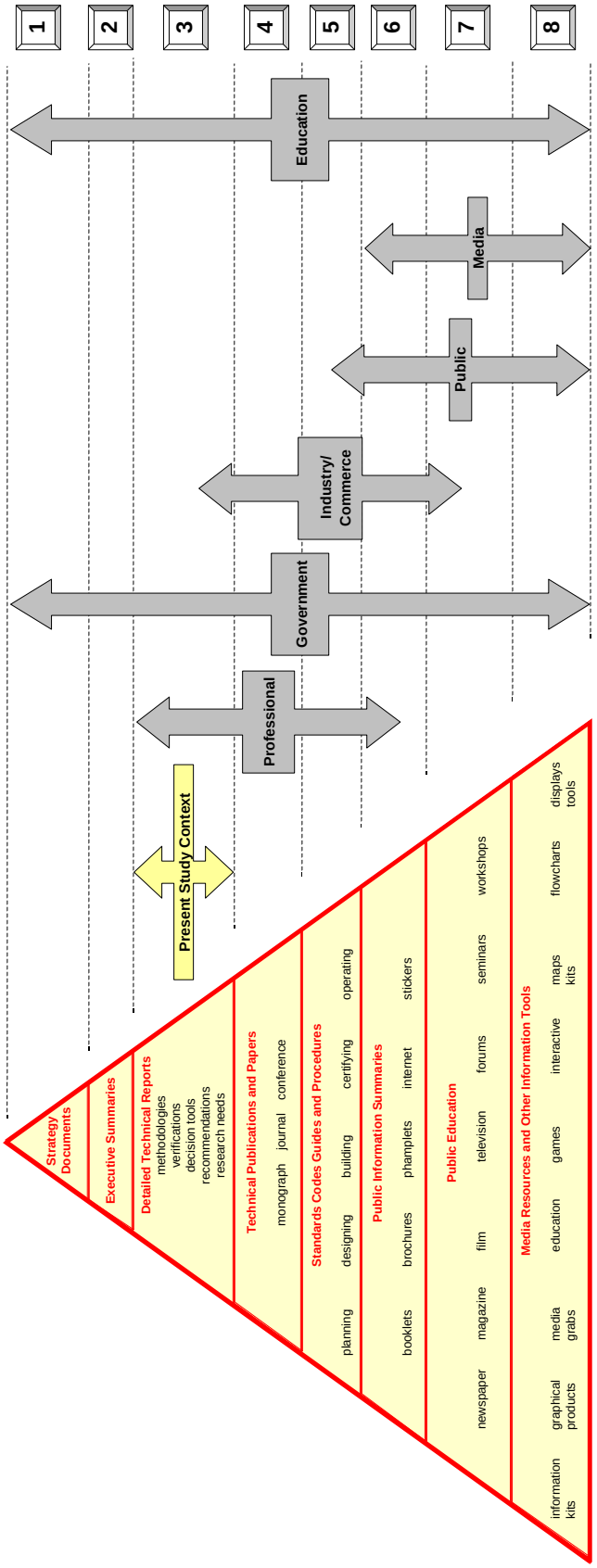

Figure 13.2 Suggested matchings between potential information products and various community sectors.

14. Summary Conclusions and Recommendations

This report presents the results of work undertaken in respect of the project scope for *Part A: Review of Project Technical Requirements*, sub-scopes A-1 to A6, detailed below (refer Appendix A for details of the project scope). Part B-1 of the project relates to the provision of a numerical modelling system for storm surge prediction and is separately documented in the form of a *User Guide* and other supporting information.

Each Chapter of this report contains specific conclusions and recommendations that should be referenced for further clarification and guidance. In respect of each Part A sub-scope, the following summary conclusions and ***10*** specific recommendations are made:

Scope: General

Chapter 2 introduces the concepts and definitions relevant to the assessment of ocean hazards from tropical cyclones in Queensland within the context of both existing climate and the potential for enhanced Greenhouse climate change.

Chapter 3 provides an overview of the known climatology of tropical cyclones in Queensland and considers issues of data quality and applicability for ocean hazard assessment. The potential influence of interseasonal (ENSO) and interdecadal (IPO) oscillations is considered.

1 *It is recommended that a comprehensive climatology study be undertaken which will provide a "seamless" statistical description of tropical cyclone variability across the State of Queensland (similar to that described in Chapter 9) to be used for long term estimates of storm tide and other impacts and also to provide guidance for real-time forecasting. Synoptic scale interactions with tropical cyclone vortices should also be considered, together with decay after landfall, recurvature and regeneration issues.*

Scope A-1: Assessment of Greenhouse climate change and sea level rise.

Chapter 4 provides a comprehensive assessment of the current state of knowledge of Greenhouse climate change and sea level rise. Special consideration is given to the possible impacts of changes in tropical cyclone characteristics in the Australian region relevant to the generation of storm surges, including the maximum potential intensities (MPIs) of tropical cyclones.

2 *It is recommended that the assessment of long-term storm tide risks to the Queensland coast should include allowance for the current estimates of enhanced Greenhouse sea level rise and a 10% to 20% potential increase in the MPI of tropical cyclones. Although no significant increase in frequency of occurrence or geographical coverage is anticipated, it is considered prudent to investigate the sensitivity of storm tide statistics to a 10% variation in these aspects of the climatology under an enhanced Greenhouse scenario.*

Scope A-2: Review the technical requirements for numerical modelling of cyclone storm surge.

Chapter 5 provides an overview of the development and current science of analytical models of the tropical cyclone wind and pressure field environment relevant to the generation of

cyclone storm surge and extreme waves. It is concluded that parametric models of the tropical cyclone surface forcing are generally robust but there are aspects still requiring research and development which may significantly impact the prediction of storm tide in Queensland. Chapter 10, for example, shows a high sensitivity to wind field asymmetry assumptions. Synoptic-scale interactions with the tropical cyclone vortex will also be important in some situations and Appendix D describes additional MMUSURGE capabilities in that regard.

3 *It is recommended that further sensitivity testing of the impact of the latest tropical cyclone boundary layer research (e.g. BMRC model) be undertaken by selective hindcasting and comparison with existing Australian wind data before committing to an extensive storm tide modelling project.*

Chapter 6 provides a comprehensive technical review of the state-of-the-art of numerical hydrodynamic modelling of tropical cyclone storm surge, which discusses the essential physics, necessary approximations, simplifications and numerical treatments. The development parallels the current status of the James Cook University Marine Modelling Unit storm surge model (MMUSURGE), the details of which are given in Appendix D.

Chapter 10 presents the results of an extensive investigation into the meteorology and ocean response of a number of significant historical tropical cyclone events in Queensland. Hindcasting of the storm tides has demonstrated the accuracy of the MMUSURGE model in a variety of coastal environments and over a range of tropical cyclone classes. A series of sensitivity tests has highlighted desirable parameter settings. It is concluded that the model performs accurately when wind and pressure data is also accurate and the domain bathymetry is reasonably well defined. Situations of extensive overland flooding, such as the Gulf of Carpentaria, are the most poorly represented in the model due to a lack of accurate data. More tidal analysis is also required to provide accurate real-time prediction of simultaneous surge and tide propagation for many areas of Queensland. These matters are not model limitations but simply reflect a lack of tidal data and inadequate bathymetry in many areas.

4 *It is concluded that the numerical storm surge model MMUSURGE is capable of accurately and efficiently modelling the generation and propagation of storm tide provided that wind and pressure data is also accurate and that the coastal representation and other parameters are consistent with the recommendations of Chapter 6. It is recommended that further model calibration with improved data be undertaken to (a) ensure improved representation of overland flooding - especially in the high-risk Gulf of Carpentaria region and (b) to undertake further tidal calibration work to provide real-time surge and tide modelling capability needed for inundation modelling.*

Chapter 9 provides a comprehensive overview of techniques for developing storm tide statistics and the various advantages and disadvantages of a number of methods. It is concluded that three simulation methods have similar potential but differ in their needs for the description of the climatology and the extent of primitive equation modelling required.

5 *It is recommended that the Monte Carlo Method (MCM) be adopted as the most suitable technique for establishing storm tide statistics, assuming a parametric storm tide model is available (refer recommendation 8). This method provides the greatest opportunity for inclusion of a wide range of parameter sensitivities, including interseasonal, interdecadal and climate change impacts. Alternatively, if a parametric model is not available, the Joint Probability Method (JPM) is favoured.*

Scope A-3: Review the technical requirements for numerical modelling of cyclone wind waves.

Chapter 7 provides a comprehensive overview of the status of numerical modelling of tropical cyclone wind waves. It is concluded that the WAM-derivative model (WAMGBR) is an example of a state-of-the-art spectral wave model suitable for this purpose. It is concluded that phase-resolving nearshore models are neither desirable nor necessary to obtain accurate nearshore wave estimates suitable for input into analytical coastal wave setup algorithms. Phase resolving (diffraction) modelling may still be desirable for specific infrastructure elements such as harbours or for estimating wave impact forces during inundation episodes.

6 *It is recommended that a 3rd Generation spectral wave model (e.g. such as WAMGBR) be adopted for numerical modelling of tropical cyclone generated wind waves in support of coastal storm tide prediction and planning requirements. It is further recommended that wave modelling be conducted in parallel with storm surge modelling, utilising the same model domains and resolutions where possible and that nearshore extreme wave estimates be included in any statistical estimates of coastal storm tide.*

Chapter 8 provides an introduction to the physics of nearshore wave behaviour in respect of wave setup and runup characteristics. Analytical formula are presented which will allow transfer of nearshore spectral wave model parameters to inshore environments and permit estimates of mean water level superelevation due to wave breaking. Advice on calculating wave runup of irregular waves is also included to assist in estimating berm erosion and overtopping and the special needs of coral reefs, atolls and cays is discussed. It is concluded that wave setup can be a significant contributor to storm tide on the open coast and especially on low-lying offshore islands. For better understanding of potentially extreme inundation episodes, research is still required into the physics of nearshore wind stress and the development of non-linear interactions between surge and setup.

7 *It is recommended that (a) analytical methods be applied to the estimation of wave setup using nearshore spectral wave model output parameters and that this be applied at a fine scale resolution (e.g. **C** grid minimum) and (b) that further research be initiated into the nearshore physics of extreme inundation episodes so as to provide better guidance for the likely significant community impacts.*

Scope A-4: Database design.

Chapter 11 addresses a number of system design issues in regard to the need to provide both a storm tide warning capability and a long-term planning tool. The traditional MEOW database approach is investigated as a means of achieving a warning capability and a number of different approaches are examined, including present US practice. Depending on the parameter ranges chosen it is demonstrated that there are considerable computational and data storage needs. Possible database requirements for one such option are presented in Appendix H based on a set of numerical modelling domains for the Queensland coast. The model domains are detailed in Appendix F, consisting of so-called **A** and **B** storm surge grids only at this time. Tidal boundary data for these grids will need to be developed if simultaneous surge and tide modelling is also required.

Chapter 11 also considers alternative means of satisfying the design outcomes of a MEOW forecast and warning system whilst also simultaneously satisfying the long-term planning requirements for predicting storm tide levels. A hybrid approach is developed which would be based on a series of regional parametric storm tide (surge and nearshore wave) models. This procedure differs from the traditional MEOWs approach only in the sense that the number of separate model simulations undertaken would be dependent on the developing accuracy of the parametric model when optimised for the characteristics of each region. The traditional MEOW approach is, by comparison, to normally generate a complete set of *a priori* ranges of track parameters and to store the results for future interpretation. The parametric model philosophy is to perform the interpretation (value adding) during the modelling phase and to condense the data into a simplified predictive format. A very simple parametric storm tide model has already been used extensively throughout Queensland for estimating statistical storm tide levels in this manner.

It is recommended that:
(a) the optimum long-term storm tide forecast and warning system would be based on real-time application of numerical storm surge and spectral wave models integrated into Bureau of Meteorology forecasting systems,
(b) a shorter-term implementation of a MEOW-style capability be based on development of parametric models for tide, storm surge and wave setup using a traditional MEOW strategy but limiting and focusing the range of model simulations required to match accuracy criteria, and
(c) the same parametric models be applied in storm tide statistics analyses.

8

Scope A-5: Review the technical requirements for an operational MEOWs system

Chapter 12 reviews a number of existing and proposed MEOW-based operational forecast systems and develops a functional specification for an AIFS module. Appendix G provides a concise technical description of how a MEOW forecast would be constructed in order to suit Australian conditions.

It is recommended that, based on Chapter 12 and Appendix G, a detailed MEOW-based storm tide forecast system design specification now be prepared which will preserve tidal phase and surge relationships, include extreme waves and wave setup, incorporate probabilistic parameter estimates and allow a selection of data source modules (i.e. traditional, parametric or real-time).

9

Scope A-6: Dissemination of results

Chapter 13 explores the wide range of potential stakeholders with interest in knowledge regarding storm tide hazards and identifies a range of potential information products which can be targeted towards different types of community needs.

It is recommended that:
(a) information products be jointly developed and designed by engineering/scientific advisers and professional information and communication personnel, including social scientists; and
(b) that information products cover a variety of media and formats to be specifically targeted to a range of important government, industry, occupational, educational and public sector groups.

10

APPENDICES

A Extract from the Scope of Work

B Summary Parameters of all Tropical Cyclones in Queensland since 1906/07

C Tropical Cyclone Wind and Pressure Model

D Technical Description of the James Cook University Storm Surge Model (MMUSURGE)

E Present US Practice for MEOW Storm Tide Warnings

F Details of Supplied MEOW Model A and B Domains

G Recommended MEOW Technique for Storm Tide Forecasting

H MEOW Database Requirements and Storage Costs

(This page intentionally left blank)

Appendix A Extract from the Scope of Work

**Invitation for Offers for the Provision of Consultancy Services for
Queensland Climate Change and Community Vulnerability to Tropical Cyclones Ocean Hazards Assessment - Stage 1**

1. BACKGROUND

1.1 Project Overview

The Bureau of Meteorology, in conjunction with a number of Queensland government agencies and with financial support from the Queensland Greenhouse Taskforce, is undertaking a project to assess the magnitude of the ocean threat from tropical cyclones in Queensland. This project is intended to update and extend the present understanding of the threat of storm tide inundation in Queensland on a state wide scale including the effects of storm wave conditions in selected areas, and estimates of potential Greenhouse impacts.

The Bureau is seeking a suitably qualified Consultant to undertake Stage 1 of the project which includes:

c) a review of technical requirements in order to further develop the project; and
d) completion of numerical simulations of tropical cyclone storm surge.

Storm surges are temporary increases in coastal water levels associated with severe weather systems such as tropical cyclones. A storm tide is the combined effect of a storm surge and the normal astronomical tide which may result in a short term increase of water levels above the high water mark and inundation of low lying coastal land. In exposed coastal areas the effects of the storm tide may be exacerbated by an additional wave set-up component and increased hazard caused by breaking waves.

Climate change predictions include a rise in sea level in the range of 15 to 95 cm, with a best estimate of the order of 50 cm, during the next century and an increase in tropical cyclone intensity of 10-20 %. Either of these factors could lead to higher levels of coastal inundation risk or erosion in tropical cyclone events. Recently, there has been increasing levels of growth in the population and assets in high risk coastal areas in Queensland. Loss of human life due to storm tide inundation remains low in Australia compared with some under developed countries. However, the potential for damage and economic loss is high and is increasing significantly. The risk to life is also substantial and places increasing pressure on warning systems and disaster avoidance plans in Queensland.

Since 1976 there has been a cyclical downturn in cyclone activity in Queensland, with no category 4 or 5 cyclones crossing the coast. It is unlikely that this situation will continue. In addition public awareness of the threat from tropical cyclone and storm tide activity is assessed to be inadequate.

The combination of increased population and assets, a community insufficiently prepared for category 4 or 5 cyclones in the current climate, and the contemporary climate change predictions, point to the need to better define the risk levels in Queensland from tropical cyclone winds, waves and storm surges. Improved understanding is required from a state-wide perspective down to local community levels.

The risk probabilities of coastal inundation by the sea caused by tropical cyclones are derived from the consideration of tropical cyclone storm surge, astronomical tide, and wave conditions. The only comprehensive storm surge studies covering all the major coastal centres in Queensland were completed in the late 1970's and did not include a consideration of storm wave conditions.

1.2 The Bureau of Meteorology

The Bureau of Meteorology is the national meteorological service for Australia. It was established by an Act of the Commonwealth Parliament in 1906 to provide essential meteorological services to all sectors of the community.

A key service provided by the Bureau is the provision of warnings of dangerous weather conditions including tropical cyclones. In accordance with present arrangements in Queensland, the Bureau of Meteorology is responsible for issuing warnings of storm tides to the public and the State Counter Disaster Organisation.

2. TERMS OF REFERENCE

2.1 Purpose of Overall Project

The overall project will be carried out in a number of stages. It seeks to prepare new storm surge and wave simulation data and to update the statistics of coastal inundation risk based on the present climate. A comprehensive description of extreme wave height statistics for a number of areas will also be developed. The project will investigate the effect of potential Greenhouse related changes in tropical cyclone characteristics and sea level rise and develop estimates of likely changes to coastal inundation risk and extreme wave statistics.

The Bureau of Meteorology's Research Centre (BMRC) has developed a numerical model methodology applicable to assessing storm surge water elevations from a full range of cyclone scenarios over extended coastal basins. The model is a numerically coupled ocean atmosphere model in which the reduced atmospheric pressures and extreme wind driven currents are simulated with a cyclone model moving over the bathymetry applicable to the region to estimate the storm surge. The model does not include simulation of storm waves.

The intensity and characteristics of tropical cyclones may be schematised and represented by a limited number of parameters. A full range of cyclone scenarios will be modelled for overlapping coastal basins for the entire Queensland coast. The water elevations at each point and on each time step for each model run will be stored in a large database. This will enable the retrieval of maximum water elevations at any point along the coast for like "families" of cyclones in order to determine the maximum envelopes of water (MEOWs) in a later stage of the project. The MEOWs will be used in an operational mode to assist in the preparation of storm tide warnings and in a planning mode to assess the effects of cyclone scenarios applicable to an area.

Overall the project, comprising a number of separate stages, will consist of the following elements:

- Review current knowledge and make technical recommendations for the overall project
- Appraise and adapt the BMRC storm surge model software for the purposes of this project

- Install the software on the Bureau of Meteorology's computer system in Brisbane with assistance from a Bureau of Meteorology scientist
- Complete storm surge modelling for the Queensland coast with assistance from a Bureau of Meteorology scientist
- Undertake modelling of storm wave parameters for selected areas on the Queensland coast.
- Develop software to compute and display storm surge maximum envelope of waters (MEOWs) for individual cyclone model runs and for families of cyclone model runs on a regional basis.
- Develop estimates of coastal inundation risk due to storm tide and extreme waves associated with tropical cyclones.
- Develop estimates of extreme wave statistics for key coastal locations.
- Develop Greenhouse scenario estimates of coastal inundation risk and extreme waves.

2.2 Scope of Stage 1 of the Project

The present Consultancy is limited to Stage 1 of the project only.

The study area comprises the entire Queensland coastal region from the Northern Territory border in the Gulf of Carpentaria to the New South Wales border at Coolangatta. Limited areas of the coast may be excluded from the scope of the project where it can be shown that the risk of tropical cyclone storm surge is sufficiently low.

2.3 Objectives

The objectives of Stage 1 of the project are to:

a) review technical requirements and provide recommendations for the overall project including future stages; and
b) prepare storm surge simulation data necessary for the later stages of the overall project.

2.4 Tasks

The following tasks are required for Stage 1 of the project:

Part A: REVIEW OF PROJECT TECHNICAL REQUIREMENTS

A-1. Assessment of Greenhouse climate change and sea level rise

The Consultant shall provide a written review and assessment of the current state of knowledge of Greenhouse climate change and sea level rise relevant to the completion of the overall project. The discussion should include a review of possible changes in tropical cyclone characteristics in the Australian region relevant to the generation of storm surges, including the maximum potential intensities (MPIs) of tropical cyclones.

A-2. Review the technical requirements for numerical modelling of tropical cyclone storm surge.

Storm surge simulation data are required for use in operational mode (MEOWs) and in planning mode (storm tide risk statistics). It should be noted that an existing body of work has been completed as part of a previous study as described by Sanderson et. al., given in Attachment 1. The Consultant is required to liaise with a nominated

investigator involved in the earlier work as necessary and critically review the existing storm surge simulations undertaken using the BMRC model. The Consultant shall provide recommendations for additional work to prepare the necessary storm surge simulation data required to meet the objectives of the project. The discussion should include, but would not be limited to:

a) methodologies for computing storm tide statistics, including requirements to take into account climate change, sea level rise, and decadal variability in cyclones
b) parameterisation of tropical cyclones including the range and discretisation of parameter values;
c) model bathymetry including coverage and spatial discretisation; and
d) time steps used in numerical simulations and model output datasets, particularly for the subsequent use in storm tide statistical analysis.

A-3 Review the technical requirements for numerical modelling of tropical cyclone wind waves

Wave simulation data are required for calculation of a wave set-up component for inclusion in the estimation of storm tide statistics and for estimation of extreme wave statistics related to tropical cyclones. The consultant is required to briefly review the "state of the art" in this field and provide recommendations on the production of wave simulation data required to meet the objectives of the project. The discussion should include, but would not be limited to:

a) parameterisation of tropical cyclones, particularly the discretisation of parameter values;
b) model bathymetry including coverage and spatial discretisation;
c) representative output wave parameters, particularly for wave direction;
d) verification of numerical simulations;
e) computation of wave set-up; and
f) the optimum model output locations to meet requirements from an economic and disaster prevention perspective.

A-4 Database Design

The production of storm surge and wave simulation data will result in the generation of large datasets. It is envisaged that the efficient storage and retrieval of these data will require a dedicated database system which will be established on the Bureau of Meteorology computer system. The Consultant is required to review the current BMRC storm surge data base design and provide recommendations and a draft specification for a suitable database design to accommodate simulation data generated by this project and potential future work. The discussion should include, but would not be limited to:

a) magnitude of data storage requirements;
b) data access rates, particularly retrieval times;
c) metadata;
d) database maintenance requirements;
e) order of costs including ongoing licence and maintenance charges; and
f) computer hardware dependence.

A-5 Review the technical requirements for an operational MEOWs system

A later stage of the project requires the development of an operational system to calculate and display the maximum envelope of waters (MEOWs) for individual tropical cyclone model runs, and selectable families of cyclones over a region. It is envisaged this system will be map based with a graphical user interface that enables non specialist staff to conveniently access and interpret the storm surge simulation data. Prototype access and display systems have been developed based on "Mapinfo" and "Arcview" systems. The Consultant is required to provide recommendations and a draft specification for development of the operational MEOWs system compatible with the Bureau of Meteorology's computer system, for use both within the Bureau and for external users. The discussion should include, but would not be limited to:

a) spatial and temporal interpolation techniques;
b) user input screens including default settings and override options;
c) output formats;
d) database interoperability;
e) order of costs including ongoing licence and maintenance charges; and
f) computer hardware dependence.

A-6 Dissemination of results

An important future stage of the overall project will be the communication of the study findings to stakeholder groups. Stakeholders include emergency management planners, engineers, local government authorities and the general public. It is likely that different communication strategies will be required for different groups. It is envisaged that the types of communication formats would include published material such as technical papers, reports, brochures and web pages and may involve a series of stakeholder meetings. In consultation with various staff available to the project, the Consultant is required to provide recommendations on suitable strategies for the cost-effective communication of the overall study findings to stakeholder groups. The discussion should include, but would not be limited to:

a) graphical representation of storm surge and wave simulation data summaries; and
b) presentation of storm tide risk and extreme wave statistics.

Part B: NUMERICAL MODELLING OF TROPICAL CYCLONE STORM SURGE

B-1 Establishment of the storm surge modelling system and database

The Consultant, in consultation and with assistance from the Bureau's Project Officer, is required to establish the storm surge modelling system and an associated database at the Bureau's Regional Office in Brisbane. The modelling system is to be based on the existing Bureau of Meteorology Research Centre (BMRC) model. This component of the work shall commence only after acceptance by the project manager of parts A-1 to A-4 inclusive and the establishment of a work plan agreed by the Consultant and the Project Manager.

Tasks include:

a) compilation and appropriate refinements of the modelling software (NOTE: substantial modifications to the software shall be made only by agreement with the Project Manager);
b) establish the bathymetry data files;

c) develop appropriate pre-processing and post-processing utilities including a batch processing facility, where required;
d) establish the database; and
e) appropriate testing.

Payment

Payment for this component of the work will be included in the fixed contract lump sum however where unforeseen work is required additional payment may be made according to an agreed hourly rate. The Consultant should factor in provision for some assistance from a Bureau scientist with knowledge of Bureau computer systems, and a scientist familiar with running the existing BMRC model during the set up stage.

B-2 Production of numerical simulation data

Undertake model runs for the production of the required storm surge simulation data. It is envisaged that some of this work will be undertaken by the Project Officer and other Bureau of Meteorology technical staff. The Consultant's role will be in the form of facilitation and technical direction, as requested by the Project Manager. Payment for this component of the work will be calculated according to an agreed hourly rate.

This component of the work shall commence only after completion of part B-1.

2.5 Outputs

Completion of Stage 1 of the project will result in three key outputs, as follows:

1. Report on Technical Requirements

The outcomes of Stage 1 of the project are to be documented as a written technical report. This would be initially in the form of a brief discussion paper summarising the findings of tasks A-1 to A-4 for early consideration by the project steering committee. The completed study report would include the following:

- review of the technical requirements of the overall project and recommendations as required by tasks A-1 to A-6
- documentation of the numerical model system development and production runs as required by tasks B-1 and B-2.

The report shall be initially supplied as a working draft (5 copies required) for review by the project steering committee. The project timeline should allow 15 working days for this review stage. A final draft (5 copies required) would then be prepared and submitted for approval. At the completion of the study, 15 bound copies of the final report shall be supplied along with an electronic copy, including figures (format to be compatible with WORDPERFECT and/or Microsoft WORD).

2. Establishment of the storm surge modelling system

The BMRC's storm surge modelling system and agreed modifications will be established at the Bureau of Meteorology's Queensland office in Brisbane (including the bathymetry data and associated utilities). The correct operation of the model will

be verified against appropriate test cases.

3. Model data

   The completion of Stage 1 of the project will result in a database of storm surge simulations covering the Queensland coastal area.

2.6 Existing Information and Project Resources

The existing information relating to Stage 1 of the project is outlined in the report by Sanderson et. al. The following items are available for perusal at the Bureau of Meteorology's Brisbane office:

- details of the Bureaus's computer system intended for use in this project
- copies of existing storm surge simulation data
- source code of the existing BMRC storm surge model and bathymetry data
- a prototype of an operational MEOWs system developed utilising "Mapinfo" software.

Consultants should contact the Project Officer to arrange a suitable time to view these items. A prototype of a basic MEOWs system utilising ArcView Internet Map Server software has been produced by a University group and may be further developed in connection with this project

2.7 Program of Major Events/Suggested Timetable

Any offer to carry out this study must include details of the timeframe within which progress may be assessed. It should include the timing for key milestones including the Stage 1 outputs. Suggested milestones are as follows:

1. Report on Technical Requirements
   a) discussion paper on the findings of tasks A-1 to A-4
   b) submission of draft report
2. Establishment of the storm surge modelling system
3. Complete storm surge simulation data modelling

The target date for completion of item 1 is within two months of establishment of the Consultancy.

Variation (dated 31 March 2000)

After lengthy investigation by the Bureau we have determined that there exists some operational problems with the existing Bureau storm surge model, as a consequence we are inviting all Tenderers to put forward an amended proposal for the consultancy services (as per above) that is we are inviting Tenderers to resubmit a variation to their proposal which will include a proven numerical storm surge model to be used in the Bureau's MEOW program and associated cost changes to the proposal.

It is envisaged that the total MEOW software suite including the Storm Surge model will be maintained by the Bureau and used for further public interest studies in the future. The variation to the proposal should include a full description of the attributes of the model including its verification along with any terms and conditions associated with the continued use of the model for future "public interest" style studies by the Bureau of Meteorology.

Appendix B Summary Parameters of all Tropical Cyclones in Queensland since 1906/07

		Start				Finish				Lifetime				At Maximum Intensity				
Seq.	Name	Date	Time	Lat	Long	Date	Time	Lat	Long	Dur	Path	Vfm	Theta	p0	Date	Time	Vfm	Theta
No.			hhmm	°S	°E		hhmm	°S	°E	h	km	m s^{-1}	°	hPa		hhmm	m s^{-1}	°
190601	614	17-Jan-1907	2300	13.0	146.5	26-Jan-1907	2300	29.0	140.0	216	2576	3.3	200	993	18-Jan-1907	2300	2.8	297
190701	613	06-Jan-1908	2300	13.0	140.0	10-Jan-1908	2300	21.0	156.0	96	2002	5.8	117	999	06-Jan-1908	2300	9.3	110
190702	612	11-Mar-1908	2300	18.0	150.2	13-Mar-1908	2300	26.5	150.5	48	983	5.7	178	992	12-Mar-1908	2300	4.8	158
190801	611	29-Jan-1909	2300	14.0	153.0	03-Feb-1909	2300	24.5	159.3	120	1358	3.1	150	990	02-Feb-1909	2300	4.9	144
190901	1	24-Jan-1910	2300	12.7	147.9	30-Jan-1910	2300	21.4	154.2	144	1727	3.3	145	988	25-Jan-1910	2300	2.9	211
191002	3	02-Jan-1911	2300	14.7	138.4	12-Jan-1911	0800	28.0	148.0	225	2028	2.5	145	965	02-Jan-1911	2300	1.3	151
191004	5	09-Feb-1911	2300	12.7	143.2	12-Feb-1911	2300	23.8	149.0	72	1484	5.7	153	988	10-Feb-1911	2000	9.7	162
191005	6	15-Mar-1911	2300	15.1	146.9	17-Mar-1911	2300	15.8	140.0	48	977	5.7	264	988	15-Mar-1911	2300	3.3	237
191006	7	20-Mar-1911	2300	13.8	149.1	26-Mar-1911	2300	21.6	157.0	144	1642	3.2	135	996	22-Mar-1911	2300	1.7	180
191101	8	05-Jan-1912	2300	19.6	155.1	08-Jan-1912	1100	26.6	161.0	60	1067	4.9	142	988	06-Jan-1912	2300	4.0	155
191105	12	04-Apr-1912	2300	13.0	147.3	06-Apr-1912	2300	18.2	149.0	48	756	4.4	162	977	04-Apr-1912	2300	4.9	203
191106	13	13-Apr-1912	2300	13.9	151.8	16-Apr-1912	2300	16.3	154.4	72	485	1.9	133	998	13-Apr-1912	2300	1.2	197
191201	14	06-Jan-1913	2300	24.6	144.0	08-Jan-1913	2300	21.0	156.2	48	1318	7.6	72	1000	06-Jan-1913	2300	9.1	80
191202	15	11-Jan-1913	2300	12.5	154.0	17-Jan-1913	2300	20.3	152.0	144	1083	2.1	193	990	14-Jan-1913	2300	1.3	196
191203	16	19-Jan-1913	2300	13.1	138.0	22-Jan-1913	2300	15.2	152.1	72	1541	5.9	98	990	19-Jan-1913	2300	3.5	94
191204	17	27-Jan-1913	2300	17.0	152.0	09-Feb-1913	2330	17.4	132.0	312	3782	3.4	268	985	30-Jan-1913	1100	3.2	270
191205	18	03-Apr-1913	2300	12.0	147.2	07-Apr-1913	2300	29.3	158.2	96	2244	6.5	149	985	03-Apr-1913	2300	9.9	154
191301	19	26-Dec-1913	2300	12.7	141.5	04-Jan-1914	2330	15.3	129.2	216	1421	1.8	257	988	26-Dec-1913	2300	0.5	315
191302	20	17-Feb-1914	2300	16.0	159.1	20-Feb-1914	2300	28.2	163.1	72	1819	7.0	163	996	17-Feb-1914	2300	8.0	210
191303	21	05-Mar-1914	2300	13.0	156.9	11-Mar-1914	2300	18.4	160.5	144	1531	3.0	147	988	08-Mar-1914	2300	1.4	170
191401	22	27-Dec-1914	2300	19.0	142.5	30-Dec-1914	2300	30.8	154.0	72	1747	6.7	138	994	27-Dec-1914	2300	0.3	154
191402	23	04-Feb-1915	2300	16.9	147.5	10-Feb-1915	2300	30.9	159.7	144	2091	4.0	141	986	08-Feb-1915	2300	4.5	146
191404	25	09-Mar-1915	2300	13.0	152.9	24-Mar-1915	2300	13.0	154.0	360	2659	2.1	90	986	09-Mar-1915	2300	2.1	236
191502	27	04-Jan-1916	2300	17.0	159.0	06-Jan-1916	2300	21.0	164.9	48	764	4.4	125	988	04-Jan-1916	2300	3.6	122
191504	29	08-Feb-1916	2300	17.4	157.4	11-Feb-1916	2300	29.4	161.3	72	1561	6.0	163	992	08-Feb-1916	2300	3.3	182
191505	30	17-Feb-1916	2300	11.9	147.9	19-Feb-1916	2300	11.8	145.9	48	218	1.3	272	992	17-Feb-1916	2300	1.4	270
191507	32	10-Apr-1916	2300	16.0	153.0	14-Apr-1916	2300	27.3	164.0	96	1884	5.5	137	988	12-Apr-1916	2300	6.9	130
191601	33	25-Dec-1916	2300	16.8	151.5	27-Dec-1916	2300	22.8	140.1	48	1378	8.0	240	988	25-Dec-1916	2300	6.8	247
191602	610	31-Dec-1916	2300	17.7	140.5	03-Jan-1917	2300	22.6	149.0	72	1047	4.0	121	992	31-Dec-1916	2300	7.1	126
191605	36	25-Mar-1917	2300	13.3	147.6	28-Mar-1917	2300	21.4	163.8	72	1952	7.5	117	1000	25-Mar-1917	2300	12.5	122
191701	38	12-Dec-1917	2300	17.8	163.0	17-Dec-1917	1700	20.9	165.0	114	3448	8.4	148	991	12-Dec-1917	2300	13.2	269
191703	40	20-Jan-1918	0000	18.5	152.0	22-Jan-1918	0000	22.8	142.0	48	1171	6.8	245	930	20-Jan-1918	0000	6.4	228
191705	42	10-Feb-1918	2300	16.6	164.0	12-Feb-1918	1800	22.7	165.0	43	833	5.4	171	970	11-Feb-1918	1300	2.9	197
191706	43	07-Mar-1918	2300	13.9	153.5	11-Mar-1918	2300	24.3	140.4	96	1958	5.7	230	926	07-Mar-1918	2300	6.9	243
191707	44	14-Mar-1918	2300	16.7	161.5	17-Mar-1918	1000	26.9	162.0	59	1305	6.1	177	985	16-Mar-1918	2300	7.1	134
191708	45	23-Mar-1918	2300	18.0	161.6	25-Mar-1918	1700	22.7	165.0	42	842	5.6	145	985	23-Mar-1918	2300	3.8	205
191801	46	01-Mar-1919	2300	20.7	154.6	04-Mar-1919	0800	29.1	153.5	57	1028	5.0	186	988	01-Mar-1919	2300	4.6	216
191901	48	01-Feb-1920	2300	15.2	150.7	03-Feb-1920	2300	19.9	140.0	48	1296	7.5	245	988	01-Feb-1920	2300	8.2	266
192001	52	16-Dec-1920	2300	10.6	146.5	24-Dec-1920	0100	23.0	124.0	170	3606	5.9	240	988	16-Dec-1920	2300	3.9	273
192002	53	07-Jan-1921	2300	12.8	138.3	11-Jan-1921	2330	16.6	131.9	96	1055	3.0	238	992	07-Jan-1921	2300	4.1	255

		Start				Finish				Lifetime				At Maximum Intensity				
Seq.	Name	Date	Time	Lat	Long	Date	Time	Lat	Long	Dur	Path	Vfm	Theta	p0	Date	Time	Vfm	Theta
No.			hhmm	°S	°E		hhmm	°S	°E	h	km	m s^{-1}	°	hPa		hhmm	m s^{-1}	°
192003	54	19-Jan-1921	2300	14.9	149.9	30-Jan-1921	2300	23.7	160.0	264	3023	3.2	132	990	28-Jan-1921	2300	2.6	146
192005	56	28-Mar-1921	2300	12.0	147.2	04-Apr-1921	2300	19.5	140.0	168	1314	2.2	222	982	31-Mar-1921	2300	4.4	235
192006	57	01-Apr-1921	2300	14.1	150.5	07-Apr-1921	2300	28.3	159.2	144	2136	4.1	150	982	01-Apr-1921	2300	2.2	192
192101	58	15-Jan-1922	2300	12.2	151.6	19-Jan-1922	2300	20.8	162.9	96	1603	4.6	128	971	19-Jan-1922	2300	4.6	101
192102	59	06-Feb-1922	2300	19.8	155.7	21-Feb-1922	2300	23.0	162.8	360	4119	3.2	115	971	06-Feb-1922	2300	0.4	136
192203	61	29-Jan-1923	0300	20.3	165.0	29-Jan-1923	2200	25.8	165.0	19	728	10.7	180	960	29-Jan-1923	1100	10.1	188
192204	62	21-Feb-1923	2300	11.0	150.9	26-Feb-1923	2300	28.2	161.6	120	2871	6.6	149	960	21-Feb-1923	2300	4.0	245
192208	65	20-Mar-1923	2300	12.0	146.0	31-Mar-1923	2330	15.0	133.7	264	2069	2.2	255	974	29-Mar-1923	2300	3.3	258
192209	66	10-Apr-1923	2300	21.2	156.1	14-Apr-1923	2300	26.2	164.2	96	1452	4.2	123	998	10-Apr-1923	2300	4.3	191
192210	67	25-Apr-1923	2300	22.3	153.1	28-Apr-1923	1300	32.0	157.2	62	1171	5.2	159	998	25-Apr-1923	2300	4.2	145
192301	68	17-Jan-1924	2300	19.9	157.3	22-Jan-1924	2300	29.7	160.1	120	1148	2.7	165	989	20-Jan-1924	2300	2.4	174
192403	71	24-Feb-1925	2300	18.2	152.1	27-Feb-1925	0500	16.7	140.4	54	1339	6.9	277	952	24-Feb-1925	2300	6.5	264
192404	72	18-Jun-1925	0500	20.1	152.1	22-Jun-1925	2300	32.6	162.7	114	2076	5.1	142	992	18-Jun-1925	0500	4.1	203
192503	74	06-Feb-1926	2300	15.0	151.2	12-Feb-1926	2300	18.2	153.3	144	1290	2.5	147	995	06-Feb-1926	2300	5.0	232
192504	607	21-Mar-1926	2300	16.4	129.1	25-Mar-1926	2300	37.0	165.5	96	4246	12.3	122	996	24-Mar-1926	2300	12.7	118
192505	75	15-May-1926	2300	22.0	154.2	19-May-1926	2300	32.7	162.8	96	1577	4.6	144	999	15-May-1926	2300	5.3	180
192602	77	05-Feb-1927	2300	15.1	152.9	11-Feb-1927	2300	16.0	140.7	144	1486	2.9	265	989	07-Feb-1927	2300	2.1	255
192606	81	29-Mar-1927	2300	14.6	153.1	02-Apr-1927	1800	32.0	158.0	91	2043	6.2	165	990	01-Apr-1927	1800	6.9	170
192701	82	28-Nov-1927	2300	22.5	157.1	30-Nov-1927	2300	31.1	160.2	48	1050	6.1	162	999	28-Nov-1927	2300	7.9	193
192703	84	12-Feb-1928	2300	24.9	155.2	14-Feb-1928	0500	28.0	151.0	30	603	5.6	230	992	12-Feb-1928	2300	4.7	195
192704	85	01-Mar-1928	2300	16.6	148.0	08-Mar-1928	2300	17.4	157.5	168	1433	2.4	95	992	01-Mar-1928	2300	2.2	337
192706	86	18-Apr-1928	2300	17.5	152.9	22-Apr-1928	2300	22.5	155.2	96	686	2.0	156	999	18-Apr-1928	2300	3.2	203
192803	88	10-Jan-1929	2300	19.7	153.8	14-Jan-1929	2300	24.0	155.6	96	679	2.0	158	992	12-Jan-1929	2300	1.1	146
192804	89	20-Jan-1929	2300	15.4	151.4	24-Jan-1929	2300	19.6	153.3	96	1103	3.2	156	992	20-Jan-1929	2300	5.0	240
192806	91	19-Feb-1929	2300	18.3	151.1	22-Feb-1929	2300	20.6	154.0	72	572	2.2	129	996	19-Feb-1929	2300	2.3	212
192807	92	23-Feb-1929	2300	14.4	152.9	02-Mar-1929	2300	32.6	160.8	168	3365	5.6	158	985	24-Feb-1929	2300	4.0	241
192808	93	25-Feb-1929	2300	16.4	144.1	28-Feb-1929	2330	15.2	131.5	72	1362	5.2	275	985	25-Feb-1929	2300	5.4	280
192809	94	13-Jun-1929	2300	18.0	153.8	16-Jun-1929	2300	26.6	158.0	72	1165	4.5	155	996	15-Jun-1929	2300	6.7	133
192901	95	03-Jan-1930	2300	13.9	149.1	08-Jan-1930	2030	16.9	132.9	117	1906	4.5	259	996	03-Jan-1930	2300	7.8	271
192902	96	18-Jan-1930	2300	14.9	152.8	22-Jan-1930	2300	18.8	140.2	96	1452	4.2	252	992	18-Jan-1930	2300	6.2	268
192903	97	27-Jan-1930	2300	16.9	150.2	31-Jan-1930	2300	23.8	156.7	96	1276	3.7	138	992	29-Jan-1930	2300	2.9	115
192905	99	01-Mar-1930	2300	13.7	149.8	04-Mar-1930	2300	17.8	156.8	72	1078	4.2	121	992	01-Mar-1930	2300	1.4	224
193003	102	29-Jan-1931	2330	14.8	137.0	07-Feb-1931	2300	23.1	158.8	215	3070	4.0	111	982	03-Feb-1931	2300	2.8	155
193101	104	16-Jan-1932	2300	13.9	140.6	20-Jan-1932	2300	19.0	150.0	96	1153	3.3	119	965	16-Jan-1932	2300	2.4	117
193201	106	06-Mar-1933	2300	22.4	154.7	10-Mar-1933	2300	26.0	162.8	96	1046	3.0	115	994	06-Mar-1933	2300	3.6	158
193202	107	09-Mar-1933	2300	15.1	152.6	16-Mar-1933	2300	31.9	164.9	168	2315	3.8	146	1002	09-Mar-1933	2300	3.6	197
193301	108	24-Dec-1933	2300	16.8	153.8	29-Dec-1933	2300	25.1	160.0	120	1553	3.6	145	990	24-Dec-1933	2300	1.3	239
193302	109	17-Jan-1934	2300	14.1	156.1	22-Jan-1934	2300	17.2	144.5	120	1332	3.1	254	984	19-Jan-1934	2300	1.5	220
193303	110	30-Jan-1934	2300	16.6	139.6	01-Feb-1934	2300	31.5	153.7	48	2236	12.9	139	985	30-Jan-1934	2300	14.2	130
193304	111	18-Feb-1934	2300	12.8	146.7	21-Feb-1934	2300	30.7	151.1	72	2066	8.0	167	985	18-Feb-1934	2300	8.3	188
193306	113	09-Mar-1934	2300	12.2	152.8	12-Mar-1934	2300	15.2	139.1	72	1619	6.2	257	968	11-Mar-1934	2300	7.6	279
193401	115	29-Aug-1934	2300	21.0	156.8	02-Sep-1934	2300	31.8	161.8	96	1501	4.3	157	999	31-Aug-1934	2300	3.7	140
193402	116	14-Jan-1935	2330	13.1	137.0	20-Jan-1935	2330	20.6	133.9	144	1123	2.2	201	994	18-Jan-1935	2330	3.4	220

		Start				Finish				Lifetime				At Maximum Intensity				
Seq.	Name	Date	Time	Lat	Long	Date	Time	Lat	Long	Dur	Path	Vfm	Theta	p0	Date	Time	Vfm	Theta
No.			hhmm	°S	°E		hhmm	°S	°E	h	km	m s^{-1}	°	hPa		hhmm	m s^{-1}	°
193406	120	24-May-1935	2300	15.1	154.1	26-May-1935	2300	29.6	159.6	48	1736	10.0	160	957	24-May-1935	2300	10.2	171
193501	121	06-Jul-1935	2300	17.6	151.2	09-Jul-1935	2300	24.5	162.9	72	1811	7.0	122	1002	06-Jul-1935	2300	6.0	199
193503	123	13-Feb-1936	2300	11.8	151.9	21-Feb-1936	2330	19.2	135.0	192	2124	3.1	245	966	13-Feb-1936	2300	3.6	246
193504	124	17-Mar-1936	2300	13.7	155.1	23-Mar-1936	2300	27.0	161.8	144	1986	3.8	154	992	17-Mar-1936	2300	3.6	215
193603	606	14-Feb-1937	2300	14.0	158.0	20-Feb-1937	2300	35.0	158.1	144	2625	5.1	179	980	16-Feb-1937	2300	3.3	144
193604	127	15-Feb-1937	2300	14.9	160.1	20-Feb-1937	1000	32.0	163.5	107	1984	5.2	169	980	16-Feb-1937	2300	4.6	152
193606	605	10-Mar-1937	2300	12.7	131.2	15-Mar-1937	2300	29.8	149.6	120	2797	6.5	134	996	12-Mar-1937	2300	5.1	125
193701	129	16-Jan-1938	2300	19.6	160.6	22-Jan-1938	1200	32.0	156.3	133	2123	4.4	197	992	18-Jan-1938	2300	1.7	233
193704	131	22-Mar-1938	2300	14.9	158.7	31-Mar-1938	2300	27.9	158.6	216	2359	3.0	180	992	24-Mar-1938	2300	2.8	242
193802	133	25-Jan-1939	2300	22.5	145.4	28-Jan-1939	2300	22.3	154.2	72	912	3.5	88	954	25-Jan-1939	2300	5.1	82
193804	135	02-Mar-1939	2300	23.3	156.3	05-Mar-1939	2300	29.8	153.5	72	787	3.0	201	993	04-Mar-1939	2300	4.4	195
193805	136	18-Mar-1939	2300	13.1	148.2	27-Mar-1939	2330	19.5	135.8	216	1585	2.0	241	993	18-Mar-1939	2300	2.5	245
193902	138	11-Feb-1940	2300	14.0	156.0	20-Feb-1940	2300	21.8	139.0	216	2007	2.6	244	965	17-Feb-1940	2300	2.4	234
193903	139	20-Feb-1940	2300	22.3	162.2	22-Feb-1940	2300	29.0	159.0	48	1107	6.4	203	990	20-Feb-1940	2300	6.9	251
193904	140	02-Mar-1940	2300	13.0	151.9	07-Mar-1940	2300	16.5	140.0	120	1346	3.1	253	1000	04-Mar-1940	2300	2.7	261
193905	141	14-Mar-1940	2300	17.0	158.0	17-Mar-1940	2300	22.6	149.0	72	1232	4.8	236	987	16-Mar-1940	2300	3.7	207
193906	142	21-Mar-1940	2300	14.0	152.0	29-Mar-1940	0100	20.9	122.1	170	3738	6.1	256	998	21-Mar-1940	2300	5.7	275
193907	143	30-Mar-1940	2300	13.0	155.0	07-Apr-1940	2300	19.9	144.4	192	1431	2.1	235	993	04-Apr-1940	2300	2.6	267
194002	145	01-Apr-1941	2300	12.6	150.2	04-Apr-1941	2300	20.8	151.0	72	1189	4.6	174	1002	02-Apr-1941	2300	7.6	174
194003	146	28-May-1941	2300	16.8	148.1	30-May-1941	2300	22.3	155.2	48	1859	10.8	129	997	29-May-1941	2300	9.4	258
194103	149	06-Feb-1942	2300	15.0	157.0	08-Feb-1942	2300	22.5	149.1	48	1183	6.8	225	999	07-Feb-1942	2300	9.4	228
194105	151	15-Feb-1942	2300	17.2	149.4	21-Feb-1942	2300	26.0	159.9	144	2466	4.8	131	996	17-Feb-1942	2300	4.6	129
194106	152	05-Mar-1942	2300	22.6	158.2	08-Mar-1942	2300	31.8	158.5	72	1226	4.7	178	996	06-Mar-1942	2300	5.6	203
194202	155	31-Dec-1942	2300	14.0	148.0	07-Jan-1943	0500	23.8	160.0	150	1712	3.2	130	970	03-Jan-1943	2300	3.9	125
194203	156	26-Jan-1943	2300	13.8	154.1	30-Jan-1943	2300	22.8	150.4	96	1254	3.6	201	990	28-Jan-1943	2300	9.4	192
194204	157	09-Feb-1943	2300	14.6	150.3	13-Feb-1943	2300	23.1	152.0	96	1265	3.7	169	996	10-Feb-1943	2300	2.8	172
194301	163	14-Dec-1943	2300	12.8	146.6	16-Dec-1943	2300	16.4	138.5	48	964	5.6	245	999	14-Dec-1943	2300	4.6	250
194304	165	05-Mar-1944	2300	17.0	153.0	09-Mar-1944	2300	27.0	159.0	96	1527	4.4	150	996	07-Mar-1944	2300	3.0	143
194305	166	24-Mar-1944	2300	15.0	153.0	28-Mar-1944	0800	19.6	146.1	81	910	3.1	235	993	25-Mar-1944	2300	2.7	220
194402	168	29-Jan-1945	2300	14.0	149.1	02-Feb-1945	2300	22.0	157.0	96	2053	5.9	136	996	30-Jan-1945	2300	4.8	229
194404	170	03-Mar-1945	2300	15.2	141.9	07-Mar-1945	2300	26.0	160.0	96	2289	6.6	122	997	04-Mar-1945	2300	9.3	134
194405	171	12-Mar-1945	2300	13.8	151.2	18-Mar-1945	2300	15.5	141.5	144	1097	2.1	259	994	15-Mar-1945	2300	1.6	246
194502	175	15-Jan-1946	2300	15.0	148.1	19-Jan-1946	2300	22.8	149.1	96	936	2.7	173	999	17-Jan-1946	2300	4.7	160
194504	177	06-Feb-1946	2300	12.7	150.4	11-Feb-1946	2330	15.8	136.3	120	1782	4.1	257	996	08-Feb-1946	2000	6.3	250
194506	179	27-Feb-1946	2300	14.1	152.8	07-Mar-1946	2300	26.9	162.0	192	2834	4.1	145	982	01-Mar-1946	2300	1.9	205
194508	181	19-Mar-1946	2300	16.0	161.2	25-Mar-1946	2300	31.0	156.0	144	2048	4.0	197	988	23-Mar-1946	2300	3.9	199
194509	182	31-Mar-1946	2300	15.0	155.0	04-Apr-1946	2300	30.0	158.7	96	1867	5.4	167	998	02-Apr-1946	2300	6.0	165
194602	184	29-Dec-1946	2300	16.1	147.9	03-Jan-1947	2300	24.8	162.0	120	1838	4.3	123	999	31-Dec-1946	2300	2.0	141
194603	185	19-Jan-1947	2300	14.0	159.9	23-Jan-1947	2300	28.7	150.9	96	1960	5.7	209	990	21-Jan-1947	2300	6.5	217
194604	186	01-Feb-1947	2300	12.6	146.9	12-Feb-1947	2300	27.0	152.8	264	2654	2.8	158	996	02-Feb-1947	2300	3.2	197
194606	604	13-Feb-1947	2300	25.0	154.5	14-Feb-1947	2300	23.0	153.6	24	239	2.8	337	1001	13-Feb-1947	2300	2.8	337
194610	603	02-Apr-1947	2300	23.3	155.2	03-Apr-1947	2300	23.3	157.4	24	225	2.6	90	1006	02-Apr-1947	2300	2.6	90
194702	192	06-Jan-1948	0500	10.4	141.5	07-Jan-1948	2300	15.5	147.0	42	876	5.8	133	989	06-Jan-1948	0500	7.9	106

		Start				Finish				Lifetime				At Maximum Intensity				
Seq.	Name	Date	Time	Lat	Long	Date	Time	Lat	Long	Dur	Path	Vfm	Theta	p0	Date	Time	Vfm	Theta
No.			hhmm	°S	°E		hhmm	°S	°E	h	km	m s^{-1}	°	hPa		hhmm	m s^{-1}	°
194703	193	10-Jan-1948	2300	15.0	140.0	15-Jan-1948	2300	24.0	161.0	120	2669	6.2	114	995	11-Jan-1948	2300	3.9	136
194705	195	19-Feb-1948	2330	12.8	134.3	24-Feb-1948	2330	23.1	134.0	120	1627	3.8	181	996	22-Feb-1948	2330	4.3	187
194707	197	19-Mar-1948	2300	10.7	156.1	25-Mar-1948	2300	28.0	161.0	144	2457	4.7	164	990	24-Mar-1948	2300	7.4	111
194709	199	29-Apr-1948	2300	22.8	153.1	01-May-1948	2300	24.9	150.0	48	419	2.4	233	1002	30-Apr-1948	2300	2.4	254
194803	201	08-Jan-1949	2300	13.6	142.0	12-Jan-1949	2300	23.5	162.0	96	2387	6.9	117	992	10-Jan-1949	2300	8.5	111
194805	203	07-Feb-1949	2300	14.0	152.0	16-Feb-1949	2300	30.2	163.8	216	4468	5.7	145	994	09-Feb-1949	2300	2.1	303
194807	205	25-Feb-1949	2300	14.0	156.0	02-Mar-1949	2300	23.1	149.1	120	1957	4.5	215	972	02-Mar-1949	0500	2.6	285
194901	207	12-Jan-1950	2300	14.0	146.9	16-Jan-1950	2300	22.3	152.5	96	1321	3.8	147	994	14-Jan-1950	0600	1.7	167
194902	208	13-Jan-1950	2300	16.0	139.0	18-Jan-1950	1100	28.0	150.0	108	1766	4.5	139	988	16-Jan-1950	2300	5.1	141
194904	210	22-Feb-1950	2300	15.6	153.3	27-Feb-1950	1100	24.6	151.5	108	1383	3.6	190	998	24-Feb-1950	2300	2.7	244
194906	212	04-Mar-1950	2300	13.0	146.4	11-Mar-1950	2300	22.9	144.1	168	3158	5.2	192	992	10-Mar-1950	2300	6.2	256
195002	602	08-Jan-1951	2300	16.2	140.0	23-Jan-1951	2300	21.9	143.0	360	3769	2.9	153	995	09-Jan-1951	2300	5.1	151
195003	214	18-Jan-1951	2300	16.4	139.7	22-Jan-1951	2300	19.1	140.3	96	367	1.1	168	995	20-Jan-1951	2300	2.0	180
195004	215	24-Jan-1951	2300	24.7	151.7	29-Jan-1951	2300	26.0	150.9	120	1173	2.7	209	999	25-Jan-1951	2300	2.2	31
195010	219	09-Mar-1951	2300	12.5	145.5	18-Mar-1951	2300	26.2	151.6	216	3287	4.2	157	996	16-Mar-1951	2300	6.5	239
195011	220	23-Mar-1951	2300	7.4	158.8	31-Mar-1951	2300	23.6	162.7	192	2591	3.7	166	994	31-Mar-1951	2300	7.9	133
195102	222	18-Jan-1952	2330	11.4	139.4	21-Jan-1952	2300	18.2	139.2	71	1075	4.2	181	994	19-Jan-1952	2300	2.8	185
195106	225	15-Apr-1952	2300	9.1	155.5	21-Apr-1952	2300	25.0	165.0	144	2577	5.0	150	940	18-Apr-1952	0800	1.8	153
195201	226	26-Oct-1952	2000	15.7	150.0	28-Oct-1952	2300	22.9	160.9	51	1498	8.2	124	998	26-Oct-1952	2000	11.4	170
195202	227	15-Dec-1952	1100	17.4	158.3	16-Dec-1952	2300	23.6	159.0	36	1205	9.3	173	998	16-Dec-1952	2300	12.2	110
195204	228	12-Jan-1953	2300	15.4	139.6	14-Jan-1953	2330	18.8	137.6	48	455	2.6	209	995	13-Jan-1953	2000	9.6	210
195206	229	19-Feb-1953	0500	17.4	158.7	22-Feb-1953	2300	26.0	157.0	90	1141	3.5	190	1002	19-Feb-1953	0500	5.2	211
195208	231	21-Mar-1953	2300	23.2	153.0	22-Mar-1953	2000	25.0	151.2	21	295	3.9	222	1004	21-Mar-1953	2300	4.5	250
195209	232	14-Apr-1953	2000	10.4	142.6	15-Apr-1953	2330	10.9	138.2	27	498	5	263	1003	14-Apr-1953	2000	12.7	241
195301	234	02-Jan-1954	2300	13.0	142.0	07-Jan-1954	2300	30.3	159.4	120	3180	7.4	136	996	03-Jan-1954	2300	9.1	119
195302	235	04-Feb-1954	2300	14.0	149.0	08-Feb-1954	1100	22.6	148.7	84	1046	3.5	181	990	07-Feb-1954	0800	1.1	212
195303	236	16-Feb-1954	0200	16.0	165.0	20-Feb-1954	2300	29.1	152.4	117	2190	5.2	221	980	19-Feb-1954	1100	2.4	222
195401	238	19-Dec-1954	2300	12.2	155.0	22-Dec-1954	1100	17.0	162.0	60	924	4.3	125	1000	22-Dec-1954	1100	5.6	117
195403	601	30-Dec-1954	2300	12.7	160.1	11-Jan-1955	2300	24.6	171.2	288	3158	3	138	1002	30-Dec-1954	2300	0.9	81
195407	600	01-Mar-1955	2300	17.9	169.0	18-Mar-1955	2300	23.5	138.6	408	5760	3.9	258	968	06-Mar-1955	2300	4.9	261
195408	244	21-Mar-1955	2300	11.0	164.0	05-Apr-1955	2300	30.0	157.6	360	5525	4.3	197	985	26-Mar-1955	2300	4.5	226
195502	599	06-Dec-1955	2300	20.4	166.5	16-Dec-1955	0500	38.0	166.0	222	4284	5.4	181	1001	10-Dec-1955	0500	4.8	254
195504	247	26-Dec-1955	0500	17.0	160.0	27-Dec-1955	1100	20.0	164.5	30	630	5.8	125	993	27-Dec-1955	0500	6.9	81
195505	248	15-Jan-1956	2300	15.0	140.0	27-Jan-1956	2300	29.9	160.2	288	4777	4.6	128	968	25-Jan-1956	2300	7.2	139
195510	630	06-Feb-1956	0500	15.0	149.5	12-Feb-1956	1100	46.2	166.5	150	4618	8.6	154	994	10-Feb-1956	1100	4.5	180
195511	629	14-Feb-1956	0500	14.0	146.5	18-Feb-1956	2300	32.5	151.2	114	2683	6.5	166	990	18-Feb-1956	0200	3.5	194
195513	AGNES	23-Feb-1956	0500	17.0	175.0	11-Mar-1956	2300	29.5	141.2	426	5676	3.7	248	961	06-Mar-1956	0500	5.7	309
195515	254	14-Mar-1956	2300	24.6	165.3	16-Mar-1956	2300	29.2	157.2	48	1076	6.2	237	998	16-Mar-1956	2300	4.7	171
195517	595	02-Apr-1956	1100	14.0	154.0	08-Apr-1956	1700	42.0	173.5	150	4414	8.2	148	998	04-Apr-1956	0500	9.1	115
195603	258	11-Nov-1956	1100	12.0	156.5	14-Nov-1956	0500	15.0	163.0	66	828	3.5	115	1002	11-Nov-1956	2300	4.3	135
195605	PRIMARY	18-Dec-1956	0500	15.0	134.5	21-Dec-1956	0800	18.0	141.3	75	881	3.3	114	982	21-Dec-1956	0500	4.4	117
195606	259	19-Dec-1956	1400	15.1	136.9	21-Dec-1956	2300	20.0	146.1	57	1169	5.7	119	982	21-Dec-1956	0500	6.7	117
195607	SECONDARY	21-Dec-1956	2000	26.3	153.5	23-Dec-1956	0500	22.3	156.0	33	2603	21.9	29	998	22-Dec-1956	0500	7.7	338

		Start				Finish				Lifetime				At Maximum Intensity				
Seq.	Name	Date	Time	Lat	Long	Date	Time	Lat	Long	Dur	Path	Vfm	Theta	p0	Date	Time	Vfm	Theta
No.			hhmm	°S	°E		hhmm	°S	°E	h	km	m s^{-1}	°	hPa		hhmm	m s^{-1}	°
195608	260	21-Dec-1956	2300	25.9	153.5	23-Dec-1956	1700	25.0	163.0	42	1402	9.3	84	998	21-Dec-1956	2300	4.0	348
195609	261	04-Jan-1957	2300	19.6	155.6	06-Jan-1957	0500	21.2	163.5	30	843	7.8	102	990	06-Jan-1957	0500	12.4	104
195610	642	08-Jan-1957	0500	16.5	132.8	12-Jan-1957	0300	21.5	167.5	94	3704	10.9	98	994	10-Jan-1957	0500	12.2	99
195611	262	10-Jan-1957	1700	21.0	151.0	11-Jan-1957	1700	21.3	164.0	24	1351	15.6	91	994	10-Jan-1957	1700	16.4	90
195612	643	15-Jan-1957	2300	11.3	161.5	22-Jan-1957	2300	25.2	160.6	168	1987	3.3	183	998	20-Jan-1957	1700	5.0	219
195615	264	31-Jan-1957	2300	12.2	140.2	19-Feb-1957	0500	32.0	152.0	438	5140	3.3	151	953	07-Feb-1957	2300	3.7	327
195619	266	04-Mar-1957	2330	12.6	128.3	10-Mar-1957	2300	17.7	140.8	143	1710	3.3	112	1003	09-Mar-1957	2330	3.5	83
195621	641	07-Apr-1957	0500	10.0	135.0	11-Apr-1957	2300	9.5	141.5	114	2160	5.3	85	1002	09-Apr-1957	1700	4.6	333
195704	634	11-Jan-1958	0500	11.0	137.0	16-Jan-1958	1700	16.0	121.0	132	2760	5.8	252	1004	12-Jan-1958	1100	5.2	190
195705	635	14-Jan-1958	1700	15.0	162.0	18-Jan-1958	2300	17.0	164.5	102	1554	4.2	129	1002	18-Jan-1958	0500	3.8	114
195708	639	12-Feb-1958	0500	13.0	139.0	24-Feb-1958	2300	17.6	158.6	306	4744	4.3	103	994	19-Feb-1958	1100	8.9	202
195711	636	11-Mar-1958	0500	12.6	174.5	19-Mar-1958	2300	18.6	155.4	210	4335	5.7	251	997	19-Mar-1958	0500	1.5	270
195713	272	31-Mar-1958	0500	17.4	151.0	02-Apr-1958	0500	20.3	146.2	48	639	3.7	237	968	01-Apr-1958	1100	3.5	253
195714	273	02-Apr-1958	0500	10.0	159.2	07-Apr-1958	1100	13.0	164.6	126	1527	3.4	119	999	05-Apr-1958	0500	1.5	90
195715	637	09-Apr-1958	0500	12.5	153.0	09-Apr-1958	2300	14.0	152.0	18	210	3.3	213	1000	09-Apr-1958	0500	2.6	180
195717	275	17-Apr-1958	2300	12.0	161.2	23-Apr-1958	2300	21.7	159.5	144	1765	3.4	189	998	22-Apr-1958	0500	4.4	117
195718	276	04-Jun-1958	0500	11.0	161.7	12-Jun-1958	1700	29.4	163.8	204	3110	4.2	173	988	06-Jun-1958	2300	4.6	180
195719	638	18-Jun-1958	2300	28.2	155.0	22-Jun-1958	1100	32.5	167.0	84	1842	6.1	112	1006	19-Jun-1958	1100	10.3	180
195804	278	04-Jan-1959	0500	14.1	124.1	22-Jan-1959	2300	21.4	159.2	450	7060	4.4	102	980	20-Jan-1959	0500	5.4	95
195805	279	16-Jan-1959	0500	14.0	165.2	21-Jan-1959	2300	28.5	149.8	138	2922	5.9	224	980	20-Jan-1959	1100	9.4	250
195808	280	11-Feb-1959	1100	17.2	157.4	17-Feb-1959	0500	24.4	149.1	138	2171	4.4	227	948	16-Feb-1959	0500	2.7	200
195810	282	06-Mar-1959	1700	11.5	164.7	12-Mar-1959	2300	19.5	164.7	150	2405	4.5	180	994	11-Mar-1959	2300	0.5	90
195901	285	19-Dec-1959	2300	6.0	156.5	27-Dec-1959	2300	18.2	165.3	192	1872	2.7	144	990	24-Dec-1959	1100	2.9	121
195902	286	24-Dec-1959	2300	12.5	133.2	31-Dec-1959	2300	17.5	164.0	168	3638	6	99	986	25-Dec-1959	2300	7.9	135
195904	288	27-Feb-1960	2300	16.7	155.3	03-Mar-1960	2300	28.7	158.3	120	1412	3.3	166	964	29-Feb-1960	1100	2.3	154
195905	649	03-Mar-1960	1100	13.5	154.5	09-Mar-1960	1100	18.7	146.5	144	1219	2.4	236	1000	04-Mar-1960	1700	3.6	224
195906	289	14-Mar-1960	2300	12.4	149.0	27-Mar-1960	1100	32.8	115.5	300	5443	5	236	998	20-Mar-1960	0500	2.1	284
195907	290	01-Apr-1960	2300	13.7	155.4	06-Apr-1960	1700	19.8	165.2	114	1274	3.1	122	995	05-Apr-1960	1700	2.6	112
196003	293	02-Jan-1961	2300	18.6	146.5	06-Jan-1961	2300	18.2	150.6	96	1561	4.5	84	993	05-Jan-1961	2300	3.2	322
196006	296	26-Jan-1961	2300	14.3	161.2	01-Feb-1961	2300	31.7	162.0	144	2171	4.2	177	998	28-Jan-1961	2300	3.7	195
196007	297	02-Feb-1961	2300	13.7	165.0	06-Feb-1961	1100	20.0	163.5	84	1120	3.7	192	990	06-Feb-1961	1100	6.0	139
196013	301	02-Mar-1961	0500	11.1	136.8	08-Mar-1961	1700	13.3	159.7	156	3688	6.6	95	988	02-Mar-1961	1700	8.0	108
196014	302	15-Mar-1961	0500	14.0	162.0	21-Mar-1961	0500	30.9	158.8	144	2536	4.9	189	986	21-Mar-1961	0500	10.9	189
196101	303	28-Nov-1961	2300	11.3	156.5	02-Dec-1961	2300	22.5	165.3	96	1556	4.5	142	978	01-Dec-1961	2300	5.7	143
196102	304	22-Dec-1961	1700	16.7	148.7	25-Dec-1961	1100	25.3	159.7	66	1522	6.4	129	1000	22-Dec-1961	2300	3.9	141
196107	309	16-Feb-1962	0500	12.9	136.9	19-Feb-1962	1100	14.1	142.5	78	655	2.3	102	997	18-Feb-1962	0500	2.5	90
196203	650	24-Dec-1962	0500	16.7	150.8	26-Dec-1962	2300	18.3	158.3	66	860	3.6	102	995	26-Dec-1962	0500	2.9	90
196204	PRIMARY	29-Dec-1962	2300	17.7	150.8	31-Dec-1962	2300	26.0	151.7	48	1263	7.3	174	978	31-Dec-1962	1700	6.0	270
196212	315	21-Jan-1963	2300	15.5	154.3	23-Jan-1963	2300	23.2	161.2	48	1136	6.6	139	1000	22-Jan-1963	2300	7.1	136
196215	317	03-Feb-1963	1700	16.0	151.5	06-Feb-1963	2300	32.0	161.3	78	2180	7.8	150	994	04-Feb-1963	2300	9.1	148
196218	320	15-Feb-1963	2300	15.0	159.0	19-Feb-1963	2300	31.8	167.0	96	2446	7.1	156	960	18-Feb-1963	1100	9.1	124
196220	322	01-Mar-1963	0500	14.2	159.0	02-Mar-1963	2300	19.8	166.4	42	1013	6.7	128	1003	01-Mar-1963	1700	5.8	121
196222	655	25-Mar-1963	0500	12.0	139.0	26-Mar-1963	1100	17.0	142.0	30	663	6.1	149	996	25-Mar-1963	0500	4.8	148

		Start				Finish				Lifetime				At Maximum Intensity				
Seq.	Name	Date	Time	Lat	Long	Date	Time	Lat	Long	Dur	Path	Vfm	Theta	p0	Date	Time	Vfm	Theta
No.			hhmm	°S	°E		hhmm	°S	°E	h	km	m s^{-1}	°	hPa		hhmm	m s^{-1}	°
196223	656	26-Mar-1963	1700	10.7	137.8	30-Mar-1963	1700	22.4	144.9	96	1673	4.8	149	998	27-Mar-1963	0500	7.3	124
196224	323	30-Mar-1963	2300	22.3	153.0	02-Apr-1963	0500	24.3	165.0	54	1294	6.7	100	996	01-Apr-1963	2300	8.7	76
196226	325	20-Apr-1963	2300	12.0	153.8	25-Apr-1963	2300	27.2	159.2	120	2395	5.5	161	996	22-Apr-1963	2300	8.9	167
196303	AUDREY	06-Jan-1964	2300	10.2	141.5	14-Jan-1964	0500	30.4	153.9	174	3472	5.5	149	983	10-Jan-1964	2300	3.6	223
196304	BERTHE	26-Jan-1964	2300	14.0	151.3	01-Feb-1964	2300	24.7	162.2	144	1886	3.6	136	992	28-Jan-1964	2300	4.9	114
196305	DORA64	27-Jan-1964	2300	9.2	131.0	07-Feb-1964	2300	18.0	139.7	264	2185	2.3	136	974	02-Feb-1964	2300	3.2	142
196309	GERT64	14-Mar-1964	0500	16.3	149.7	17-Mar-1964	2300	20.4	155.6	90	934	2.9	126	999	15-Mar-1964	0500	3.0	150
196311	HENRIETTA	31-Mar-1964	2300	16.2	164.1	04-Apr-1964	2300	27.0	165.0	96	1829	5.3	175	960	03-Apr-1964	2300	5.6	155
196402	FLOR64	30-Nov-1964	2300	10.7	134.5	08-Dec-1964	2300	20.0	152.8	192	2879	4.2	117	992	05-Dec-1964	1100	5.7	129
196406	UN6405	12-Jan-1965	0500	11.7	138.4	20-Jan-1965	2300	17.8	155.8	210	2073	2.7	109	996	13-Jan-1965	0500	3.0	90
196407	JUDY	25-Jan-1965	2300	11.6	133.0	05-Feb-1965	1700	31.5	164.5	258	5185	5.6	124	986	31-Jan-1965	2300	8.2	124
196510	CONNIE	23-Feb-1966	2300	13.8	149.0	01-Mar-1966	2300	24.1	164.7	144	2163	4.2	124	990	25-Feb-1966	1100	2.7	112
196601	ANGELA	13-Nov-1966	2300	8.6	161.1	18-Nov-1966	2300	15.0	160.7	120	1357	3.1	183	1000	15-Nov-1966	2300	3.4	243
196607	DINAH	22-Jan-1967	2300	12.7	163.8	31-Jan-1967	2300	35.2	161.5	216	3376	4.3	185	945	28-Jan-1967	2300	5.3	164
196608	BARBARA	17-Feb-1967	0500	13.1	163.5	21-Feb-1967	2300	28.8	152.6	114	2149	5.2	213	987	21-Feb-1967	1700	3.3	252
196610	DULCIE	13-Mar-1967	0200	15.0	156.5	17-Mar-1967	0800	28.0	163.0	102	1880	5.1	154	996	14-Mar-1967	0800	3.2	130
196611	ELAINE	13-Mar-1967	0500	14.7	149.3	19-Mar-1967	1700	32.0	164.0	156	3204	5.7	141	996	15-Mar-1967	0500	4.5	117
196612	CYNTHIA	13-Mar-1967	2300	14.9	137.9	19-Mar-1967	1100	15.9	137.1	132	1305	2.7	217	995	14-Mar-1967	1700	1.8	304
196613	GLENDA	26-Mar-1967	0500	12.5	155.3	05-Apr-1967	1100	31.7	159.3	246	3098	3.5	169	982	30-Mar-1967	2300	2.1	180
196701	ANNIE	10-Nov-1967	0500	5.9	164.3	16-Nov-1967	0500	20.7	167.0	144	3886	7.5	169	980	12-Nov-1967	2300	5.5	201
196702	UN6702	06-Dec-1967	0500	15.5	151.6	10-Dec-1967	1700	27.7	163.7	108	2820	7.3	137	996	08-Dec-1967	2300	5.5	138
196703	UN6703	09-Dec-1967	1700	24.9	154.5	12-Dec-1967	0500	21.9	156.4	60	1188	5.5	30	998	10-Dec-1967	0500	2.5	146
196706	BRENDA	13-Jan-1968	2300	12.9	165.6	18-Jan-1968	2300	21.5	167.0	120	1884	4.4	171	993	18-Jan-1968	0500	7.1	106
196711	DIXIE	25-Jan-1968	2300	14.3	138.5	27-Jan-1968	2300	17.9	139.3	48	483	2.8	167	986	27-Jan-1968	0500	5.3	163
196712	UN6712	02-Feb-1968	2300	14.5	139.7	05-Feb-1968	0500	16.0	134.9	54	596	3.1	252	1002	04-Feb-1968	0500	5.0	270
196714	UN6714	12-Feb-1968	2300	16.7	138.5	16-Feb-1968	1700	22.2	140.3	90	1095	3.4	162	996	15-Feb-1968	0500	5.8	165
196716	BONNIE	19-Feb-1968	2300	13.0	139.0	26-Feb-1968	2300	16.9	128.1	168	1326	2.2	249	1005	19-Feb-1968	2300	2.6	258
196718	UN6718	25-Feb-1968	0500	13.4	147.5	28-Feb-1968	2300	13.8	156.0	90	941	2.9	92	1005	28-Feb-1968	0500	3.0	90
196719	GISELLE	02-Apr-1968	2300	8.1	156.3	07-Apr-1968	0500	21.1	163.2	102	1920	5.2	152	980	07-Apr-1968	0500	6.6	149
196801	ADELE	22-Nov-1968	2300	9.2	153.1	28-Nov-1968	2300	20.0	154.0	144	1359	2.6	175	998	26-Nov-1968	2300	2.6	180
196807	BRIDGET	23-Jan-1969	2300	13.0	148.0	26-Jan-1969	2300	18.0	147.0	72	569	2.2	190	1002	25-Jan-1969	1100	2.1	193
196808	COLLEEN	27-Jan-1969	0500	7.5	161.3	04-Feb-1969	2300	32.0	163.7	210	3978	5.3	174	984	30-Jan-1969	1100	4.3	110
196811	IRENE	18-Feb-1969	2300	19.6	166.3	23-Feb-1969	2300	17.0	153.5	120	1462	3.4	282	989	20-Feb-1969	0500	2.9	280
196815	UN6815	08-Apr-1969	1100	11.3	156.0	15-Apr-1969	2300	22.1	158.0	180	1740	2.7	169	996	12-Apr-1969	2300	2.6	191
196816	UN6816	11-Apr-1969	1100	10.6	164.9	16-Apr-1969	1700	31.5	160.0	126	2694	5.9	192	996	16-Apr-1969	1100	4.0	129
196817	ESTHER	25-Apr-1969	2300	8.7	152.7	02-May-1969	1100	17.5	165.5	156	2577	4.6	125	992	30-Apr-1969	2300	6.7	117
196901	UN6901	14-Nov-1969	0200	20.1	154.0	15-Nov-1969	2000	32.4	152.5	42	1474	9.8	186	1004	15-Nov-1969	0200	9.6	163
196902	ADA	02-Jan-1970	2300	15.8	165.1	18-Jan-1970	1100	21.1	148.5	372	4109	3.1	251	962	17-Jan-1970	1700	1.8	212
196905	DAWN70	10-Feb-1970	0500	13.9	138.5	19-Feb-1970	0500	25.0	158.0	216	3886	5.0	121	990	11-Feb-1970	1700	10.9	103
196906	FLORENCE	10-Feb-1970	2300	14.1	154.5	12-Feb-1970	1700	15.6	160.0	42	654	4.3	105	990	12-Feb-1970	1100	9.9	92
196907	UN6907	01-Mar-1970	0500	13.6	147.0	04-Mar-1970	2300	16.7	153.1	90	838	2.6	117	1000	04-Mar-1970	0500	3.6	106
196908	CINDY	15-Mar-1970	2300	13.7	139.9	20-Mar-1970	2300	16.6	140.2	120	1215	2.8	174	999	19-Mar-1970	1700	2.1	75
196909	ISA	13-Apr-1970	2300	9.6	164.0	18-Apr-1970	2300	9.5	154.5	120	1325	3.1	270	1003	17-Apr-1970	2300	0.7	224

		Start				Finish				Lifetime				At Maximum Intensity				
Seq.	Name	Date	Time	Lat	Long	Date	Time	Lat	Long	Dur	Path	Vfm	Theta	p0	Date	Time	Vfm	Theta
No.			hhmm	°S	°E		hhmm	°S	°E	h	km	m s^{-1}	°	hPa		hhmm	m s^{-1}	°
197012	AGGIE	31-Jan-1971	2300	15.1	136.9	03-Feb-1971	2300	15.7	133.1	72	907	3.5	260	984	02-Feb-1971	1700	2.1	284
197014	DORA71	10-Feb-1971	1100	19.5	152.7	17-Feb-1971	1700	25.7	151.9	174	2491	4.0	186	990	11-Feb-1971	1100	8.1	124
197015	GERT71	10-Feb-1971	2300	16.9	149.5	16-Feb-1971	0500	17.5	144.5	126	1698	3.7	262	983	13-Feb-1971	1100	1.4	223
197016	IDA71	15-Feb-1971	2300	17.0	155.2	20-Feb-1971	2300	25.0	165.0	120	1805	4.2	131	980	17-Feb-1971	1100	2.9	57
197017	FIONA	16-Feb-1971	2300	16.0	140.8	28-Feb-1971	1100	20.8	161.8	276	4000	4.0	103	960	18-Feb-1971	2300	7.5	138
197020	LENA	13-Mar-1971	0500	12.4	154.8	19-Mar-1971	2300	24.0	167.8	162	2918	5.0	133	980	15-Mar-1971	0500	4.5	205
197105	ALTHEA	19-Dec-1971	2300	10.9	159.0	29-Dec-1971	2300	34.8	164.7	240	5450	6.3	167	950	22-Dec-1971	1700	5.5	259
197106	BRONW1	02-Jan-1972	2300	16.2	138.7	06-Jan-1972	2300	11.8	141.9	96	798	2.3	35	993	06-Jan-1972	0500	2.1	104
197107	CARLOTTA	04-Jan-1972	2300	9.5	151.8	21-Jan-1972	2300	29.8	173.7	408	6241	4.2	134	940	15-Jan-1972	1100	1.8	234
197108	BRONW2	07-Jan-1972	0500	13.7	141.5	11-Jan-1972	2300	25.1	142.6	114	1467	3.6	174	993	07-Jan-1972	0500	1.5	90
197109	WENDY	04-Feb-1972	0500	16.0	165.2	09-Feb-1972	1700	25.8	156.0	132	1777	3.7	221	949	05-Feb-1972	1100	5.3	227
197110	DAISY	05-Feb-1972	2300	14.9	150.0	13-Feb-1972	2300	27.4	158.1	192	2399	3.5	148	959	10-Feb-1972	1100	2.4	270
197116	EMILY	27-Mar-1972	2300	11.0	157.5	04-Apr-1972	0500	34.4	153.2	174	3052	4.9	189	942	30-Mar-1972	1700	4.4	199
197118	FAITH	10-Apr-1972	1700	11.0	139.5	24-Apr-1972	0500	9.6	139.5	324	3129	2.7	0	990	12-Apr-1972	0500	2.3	153
197119	GAIL	11-Apr-1972	0500	12.9	154.1	17-Apr-1972	2300	16.3	170.0	162	2007	3.4	102	945	13-Apr-1972	2300	5.0	136
197120	HANNAH	07-May-1972	2300	5.7	155.5	11-May-1972	1100	10.0	150.0	84	1182	3.9	231	970	10-May-1972	1100	3.1	180
197121	IDA72	29-May-1972	2300	5.0	156.4	03-Jun-1972	0500	22.0	168.0	102	2369	6.5	146	985	02-Jun-1972	0500	10.3	148
197205	ADELINE	27-Jan-1973	0600	14.0	138.1	29-Jan-1973	0000	16.2	137.5	42	252	1.7	194	970	28-Jan-1973	1800	1.6	197
197207	KIRSTY	24-Feb-1973	2300	14.6	157.4	01-Mar-1973	0500	34.3	160.6	102	2380	6.5	171	975	26-Feb-1973	2300	8.4	166
197208	LEAH	27-Feb-1973	0000	11.1	139.3	01-Mar-1973	0000	14.0	135.1	48	639	3.7	234	995	28-Feb-1973	0000	9.3	247
197209	MADGE	28-Feb-1973	1700	8.1	160.8	17-Mar-1973	2300	20.2	87.5	414	8260	5.5	260	985	05-Mar-1973	0500	6.1	295
197212	BELLA	20-Mar-1973	0000	8.9	130.9	25-Mar-1973	1800	16.3	136.2	138	1288	2.6	144	1002	25-Mar-1973	0600	2.1	193
197304	NATALIE	30-Nov-1973	2300	15.0	161.0	01-Dec-1973	2300	17.5	158.0	24	460	5.3	229	995	30-Nov-1973	2300	5.1	258
197306	UNA	14-Dec-1973	2300	13.9	156.8	19-Dec-1973	2300	23.7	148.3	120	1852	4.3	219	988	18-Dec-1973	1700	6.7	180
197310	VERA1	17-Jan-1974	2300	20.2	149.4	19-Jan-1974	1100	16.8	150.0	36	572	4.4	9	996	18-Jan-1974	1700	3.0	80
197311	VERA2	19-Jan-1974	1700	18.4	152.7	21-Jan-1974	1100	23.7	164.6	42	1378	9.1	115	986	20-Jan-1974	1700	10.6	125
197312	WANDA	20-Jan-1974	1400	17.7	148.8	25-Jan-1974	0800	27.3	149.9	114	1693	4.1	173	997	24-Jan-1974	0800	4.2	222
197313	PAM	03-Feb-1974	2300	19.9	163.1	06-Feb-1974	0500	29.9	157.8	54	1273	6.6	205	965	03-Feb-1974	2300	6.3	223
197314	YVONNE	08-Feb-1974	1100	18.3	152.6	11-Feb-1974	2300	16.6	139.8	84	1404	4.6	277	995	09-Feb-1974	2300	4.9	275
197316	ZOE	06-Mar-1974	0500	18.8	154.3	14-Mar-1974	0500	32.0	158.8	192	2007	2.9	162	968	08-Mar-1974	2300	0.7	223
197321	ALICE	21-Mar-1974	1100	22.6	154.3	22-Mar-1974	2300	29.7	161.1	36	1040	8.0	139	1010	21-Mar-1974	1100	10.0	145
197406	FLOR75	12-Jan-1975	2300	14.1	160.0	15-Jan-1975	2300	18.3	165.9	72	1344	5.2	126	988	14-Jan-1975	1700	3.5	98
197408	GLORIA	15-Jan-1975	2300	16.2	146.5	19-Jan-1975	2300	26.0	165.0	96	2246	6.5	119	976	17-Jan-1975	0500	4.6	109
197411	ALISON	06-Mar-1975	0500	17.6	164.9	06-Mar-1975	2300	19.5	165.0	18	582	9.0	177	990	06-Mar-1975	1700	11.1	123
197503	KIM	07-Dec-1975	2300	13.5	136.2	09-Dec-1975	2300	14.8	142.0	48	794	4.6	102	990	09-Dec-1975	0500	3.8	113
197506	DAVID	13-Jan-1976	2300	15.4	167.4	21-Jan-1976	2300	27.9	143.2	192	3281	4.7	241	961	19-Jan-1976	1100	6.8	261
197508	ALAN	29-Jan-1976	2300	12.5	162.0	09-Feb-1976	1100	25.9	138.9	252	4348	4.8	238	992	04-Feb-1976	0500	1.9	270
197509	BETH	13-Feb-1976	1700	16.5	149.9	22-Feb-1976	0500	24.9	151.3	204	3247	4.4	171	972	17-Feb-1976	2300	9.9	108
197511	COLIN	25-Feb-1976	1700	10.3	155.5	04-Mar-1976	1100	33.8	158.9	186	3111	4.6	172	954	29-Feb-1976	2300	6.7	171
197513	DAWN76	03-Mar-1976	2300	17.4	145.6	06-Mar-1976	1100	30.4	155.7	60	1837	8.5	144	988	05-Mar-1976	0500	9.4	135
197515	WATOREA	25-Apr-1976	1100	9.5	152.6	28-Apr-1976	2300	27.1	158.9	84	2604	8.6	161	970	26-Apr-1976	2300	4.7	219
197602	TED	15-Dec-1976	2300	12.6	140.5	20-Dec-1976	2300	20.7	140.8	120	1241	2.9	177	948	19-Dec-1976	1015	4.9	136
197604	JUNE	16-Jan-1977	2300	15.4	150.2	19-Jan-1977	1100	17.5	160.5	60	1277	5.9	101	994	17-Jan-1977	2300	6.6	76

		Start				Finish				Lifetime				At Maximum Intensity				
Seq.	Name	Date	Time	Lat	Long	Date	Time	Lat	Long	Dur	Path	Vfm	Theta	p0	Date	Time	Vfm	Theta
No.			hhmm	°S	°E		hhmm	°S	°E	h	km	m s^{-1}	°	hPa		hhmm	m s^{-1}	°
197605	KEITH	29-Jan-1977	2300	15.2	148.2	31-Jan-1977	2300	19.6	147.4	48	652	3.8	189	992	30-Jan-1977	1100	3.0	260
197606	LILY	08-Feb-1977	2300	15.8	148.0	11-Feb-1977	2300	15.0	150.2	72	273	1.1	69	996	11-Feb-1977	0500	0.0	90
197607	MILES	09-Feb-1977	1700	16.6	156.5	13-Feb-1977	0500	15.3	160.0	84	494	1.6	68	994	11-Feb-1977	1700	2.0	75
197608	NANC77	11-Feb-1977	2300	15.4	147.8	13-Feb-1977	0500	15.7	144.6	30	356	3.3	264	998	12-Feb-1977	0500	1.1	242
197611	OTTO(PRIMA	06-Mar-1977	1700	14.0	140.1	10-Mar-1977	0500	22.6	145.4	84	1806	6.0	149	984	07-Mar-1977	0500	5.6	117
197701	TOM	06-Nov-1977	2300	8.5	154.6	11-Nov-1977	2300	18.5	159.7	120	1793	4.2	153	990	09-Nov-1977	0500	4.6	102
197705	GWEN	24-Feb-1978	2300	11.2	136.3	27-Feb-1978	1100	17.0	144.0	60	1193	5.5	127	987	26-Feb-1978	1700	7.2	124
197709	HAL	06-Apr-1978	0500	12.2	138.1	11-Apr-1978	2300	21.0	154.0	138	2268	4.6	119	985	06-Apr-1978	1700	4.7	131
197801	PETER	29-Dec-1978	2300	12.7	137.7	03-Jan-1979	1100	15.3	145.3	108	1049	2.7	109	980	31-Dec-1978	0500	3.8	113
197802	GRETA	08-Jan-1979	1100	13.9	137.2	13-Jan-1979	0500	17.8	139.3	114	1807	4.4	152	986	09-Jan-1979	2300	6.0	90
197803	GORDON	08-Jan-1979	1700	19.6	162.6	11-Jan-1979	2300	20.6	148.5	78	1507	5.4	265	988	08-Jan-1979	1700	9.7	270
197804	ROSA	11-Feb-1979	2300	11.2	160.9	03-Mar-1979	1700	22.6	113.7	474	6773	4.0	255	965	25-Feb-1979	2300	4.3	248
197805	KERRY	12-Feb-1979	2300	8.1	170.1	04-Mar-1979	2300	21.5	150.7	480	5351	3.1	234	945	18-Feb-1979	2300	3.6	223
197809	STAN	06-Apr-1979	0500	11.1	150.1	15-Apr-1979	1700	13.2	152.8	228	3273	4.0	128	995	13-Apr-1979	1700	3.7	124
197904	PAUL	02-Jan-1980	2300	15.1	137.1	08-Jan-1980	1100	30.0	159.6	132	3041	6.4	125	989	07-Jan-1980	1700	11.2	141
197909	RUTH	11-Feb-1980	0500	19.7	151.2	19-Feb-1980	0500	21.1	153.4	192	2777	4.0	124	979	13-Feb-1980	1100	1.1	242
197912	SIMON	20-Feb-1980	0500	16.0	159.6	28-Feb-1980	1100	30.3	160.6	198	2663	3.7	176	960	25-Feb-1980	2300	1.5	109
197913	SINA	09-Mar-1980	0500	12.4	161.2	14-Mar-1980	2300	35.2	175.5	138	3115	6.3	150	981	12-Mar-1980	2300	10.2	139
197916	UN7916	27-Mar-1980	1700	14.3	138.7	31-Mar-1980	1100	10.5	133.2	90	864	2.7	305	999	28-Mar-1980	0500	2.6	11
198008	EDDIE	08-Feb-1981	1200	14.0	153.1	13-Feb-1981	0000	20.0	126.5	108	2997	7.7	256	981	11-Feb-1981	0600	8.0	258
198009	CLIFF	12-Feb-1981	0000	18.6	167.6	15-Feb-1981	0600	26.1	147.3	78	2388	8.5	248	978	13-Feb-1981	0000	10.2	220
198011	FREDA	24-Feb-1981	1800	14.4	140.6	07-Mar-1981	0000	24.0	165.1	246	3626	4.1	112	962	06-Mar-1981	0000	4.1	151
198103	AMELIA	30-Nov-1981	2300	16.0	139.0	06-Dec-1981	0500	14.2	121.5	126	2250	5.0	276	1002	01-Dec-1981	0500	6.1	295
198104	UN8104	19-Dec-1981	2300	11.7	140.3	22-Dec-1981	1100	11.4	125.0	60	1697	7.9	271	1004	19-Dec-1981	2300	7.6	262
198109	ABIGAIL	22-Jan-1982	0000	25.7	154.3	05-Feb-1982	0000	26.2	166.5	336	4577	3.8	92	947	03-Feb-1982	0000	4.2	166
198111	CORAL	04-Feb-1982	0500	13.5	140.5	06-Feb-1982	0500	14.8	132.8	48	891	5.2	260	996	04-Feb-1982	2300	5.5	264
198114	BERNIE	01-Apr-1982	0600	6.2	159.4	07-Apr-1982	0000	23.4	161.9	138	2180	4.4	171	945	06-Apr-1982	0000	5.0	144
198115	DOMINIC	05-Apr-1982	0000	11.5	139.6	14-Apr-1982	0600	15.4	144.5	222	2857	3.6	129	950	07-Apr-1982	1200	4.6	102
198117	CLAUDIA	14-May-1982	1800	13.9	156.4	17-May-1982	0000	12.2	162.5	54	718	3.7	74	992	16-May-1982	0000	3.2	71
198202	DES	14-Jan-1983	1200	16.3	146.9	23-Jan-1983	0000	13.5	157.0	204	2959	4.0	74	994	17-Jan-1983	1200	6.7	171
198203	ELINOR	10-Feb-1983	1800	10.6	158.0	03-Mar-1983	1800	21.8	149.9	504	4714	2.6	214	935	26-Feb-1983	0000	2.0	255
198304	FRITZ	09-Dec-1983	0600	14.4	147.8	13-Dec-1983	0000	15.7	151.2	90	784	2.4	111	992	12-Dec-1983	0600	1.5	270
198309	GRACE	11-Jan-1984	0000	18.5	148.5	20-Jan-1984	1200	23.4	163.0	228	2450	3.0	109	970	16-Jan-1984	0600	4.6	132
198313	HARVEY	03-Feb-1984	1800	14.7	152.3	09-Feb-1984	1800	22.0	163.4	144	1571	3.0	124	980	06-Feb-1984	1800	5.0	128
198315	INGRID	20-Feb-1984	1200	17.4	147.6	25-Feb-1984	1200	23.9	157.6	120	1968	4.6	124	975	23-Feb-1984	0000	7.7	105
198318	JIM	06-Mar-1984	0000	11.6	150.7	09-Mar-1984	0600	14.3	137.8	78	1494	5.3	257	976	09-Mar-1984	0600	6.7	242
198320	KATHY	16-Mar-1984	1800	12.0	148.5	24-Mar-1984	0000	18.2	134.0	174	1824	2.9	246	920	22-Mar-1984	1200	2.5	232
198321	LANCE	04-Apr-1984	0000	13.5	153.4	07-Apr-1984	1800	23.7	159.3	90	1761	5.4	151	992	05-Apr-1984	1200	1.5	180
198403	MONICA	26-Dec-1984	0000	14.5	148.5	28-Dec-1984	1200	21.5	160.0	60	1447	6.7	122	982	27-Dec-1984	1800	10.5	122
198404	NIGEL	14-Jan-1985	1200	16.5	150.3	16-Jan-1985	1800	16.0	159.0	54	933	4.8	86	996	16-Jan-1985	1800	7.4	86
198405	ODETTE	16-Jan-1985	1200	14.6	145.6	19-Jan-1985	1200	16.2	159.8	72	1555	6.0	96	930	19-Jan-1985	0600	6.5	85
198409	PIERRE	18-Feb-1985	0600	11.8	143.3	24-Feb-1985	0600	23.8	160.0	144	2492	4.8	126	986	21-Feb-1985	0000	9.8	153
198411	REBECCA	20-Feb-1985	0600	11.1	135.7	23-Feb-1985	1200	16.7	143.5	78	1268	4.5	126	994	22-Feb-1985	0000	4.8	122

		Start				Finish				Lifetime				At Maximum Intensity				
Seq.	Name	Date	Time	Lat	Long	Date	Time	Lat	Long	Dur	Path	Vfm	Theta	p0	Date	Time	Vfm	Theta
No.			hhmm	°S	°E		hhmm	°S	°E	h	km	m s^{-1}	°	hPa		hhmm	m s^{-1}	°
198414	SANDY	20-Mar-1985	1800	13.4	138.2	24-Mar-1985	1800	14.5	135.1	96	766	2.2	249	953	22-Mar-1985	1200	2.6	191
198415	TANYA	27-Mar-1985	0600	13.2	151.5	01-Apr-1985	1800	15.2	142.8	132	1082	2.3	256	982	30-Mar-1985	0600	2.6	281
198505	VERNON	21-Jan-1986	0000	16.5	139.5	24-Jan-1986	1800	24.0	160.0	90	2365	7.3	111	990	24-Jan-1986	0000	13.2	117
198506	WINIFRED	27-Jan-1986	0600	12.9	144.8	05-Feb-1986	1800	20.9	144.2	228	2009	2.4	184	957	01-Feb-1986	0700	4.5	260
198511	ALFRED	02-Mar-1986	1800	14.8	150.2	08-Mar-1986	0000	18.5	164.0	126	1628	3.6	105	992	07-Mar-1986	1800	10.6	112
198513	MANU	21-Apr-1986	0000	8.0	156.0	27-Apr-1986	0000	16.0	144.6	144	1584	3.1	234	970	24-Apr-1986	1200	3.4	242
198515	NAMU	16-May-1986	1800	7.0	163.9	22-May-1986	0000	18.4	165.4	126	2068	4.6	172	960	20-May-1986	1200	6.6	157
198602	IRMA	19-Jan-1987	0600	12.6	139.0	21-Jan-1987	0000	15.4	134.1	42	656	4.3	239	994	19-Jan-1987	1200	3.1	260
198604	JASON	05-Feb-1987	1800	12.0	142.8	14-Feb-1987	0000	21.1	139.4	198	2028	2.8	199	965	12-Feb-1987	1200	2.9	135
198607	BLANCH	21-May-1987	0600	10.1	166.8	27-May-1987	0000	19.9	157.0	138	1931	3.9	224	990	22-May-1987	1800	2.5	216
198701	AGI	08-Jan-1988	0000	15.0	157.0	14-Jan-1988	0600	19.5	162.0	150	2164	4.0	133	980	12-Jan-1988	1800	6.6	148
198704	CHARLIE	21-Feb-1988	0000	12.8	159.1	01-Mar-1988	1800	20.9	147.5	234	2085	2.5	233	972	29-Feb-1988	1200	1.1	154
198802	DELILAH	28-Dec-1988	1800	16.7	148.4	01-Jan-1989	1200	18.4	160.0	90	1671	5.2	98	988	01-Jan-1989	0600	10.0	101
198806	HARRY	13-Feb-1989	0600	19.7	160.3	17-Feb-1989	0600	20.9	160.4	96	927	2.7	175	925	14-Feb-1989	0000	2.0	284
198809	AIVU	01-Apr-1989	1200	12.1	152.0	05-Apr-1989	1200	22.0	142.2	96	1624	4.7	223	935	03-Apr-1989	0600	4.7	192
198811	MEENA	05-May-1989	0000	13.4	160.0	10-May-1989	0600	11.5	137.4	126	2640	5.8	274	990	06-May-1989	0600	5.7	315
198812	ERNIE	09-May-1989	1800	12.0	155.6	12-May-1989	1200	12.3	148.8	66	1217	5.1	267	998	11-May-1989	0000	8.6	270
198902	FELICITY	13-Dec-1989	0000	11.6	134.0	19-Dec-1989	1200	20.2	160.2	156	3366	6.0	108	975	15-Dec-1989	0600	5.6	117
198906	NANC90	28-Jan-1990	0600	18.3	156.0	04-Feb-1990	1200	34.5	155.0	174	4054	6.5	183	975	01-Feb-1990	0600	8.4	266
198907	GREG	01-Mar-1990	1800	11.9	137.9	03-Mar-1990	0000	12.1	139.8	30	225	2.1	96	992	03-Mar-1990	0000	1.8	124
198910	HILDA	04-Mar-1990	0000	18.8	153.2	07-Mar-1990	1800	26.0	165.0	90	1831	5.7	123	970	06-Mar-1990	0000	1.8	54
198912	IVOR	16-Mar-1990	0000	15.8	160.8	26-Mar-1990	1200	21.9	146.8	252	4075	4.5	245	965	19-Mar-1990	0000	5.0	264
199002	JOY	19-Dec-1990	0600	12.3	152.8	26-Dec-1990	0600	19.2	147.5	168	1327	2.2	216	940	23-Dec-1990	0000	1.0	180
199005	KELVIN	25-Feb-1991	0600	15.5	149.4	05-Mar-1991	1200	14.0	149.7	198	1666	2.3	10	980	26-Feb-1991	1800	2.5	307
199010	LISA	08-May-1991	0600	10.3	154.3	11-May-1991	0000	16.8	159.1	66	1026	4.3	144	975	10-May-1991	0600	4.9	114
199102	MARK	07-Jan-1992	1200	13.3	136.1	10-Jan-1992	1800	13.3	143.5	78	870	3.1	90	980	09-Jan-1992	1800	4.3	53
199103	BETSY	10-Jan-1992	1200	19.5	160.0	14-Jan-1992	0600	27.6	160.0	90	1178	3.6	180	950	10-Jan-1992	1200	5.0	258
199104	DAMAN	15-Feb-1992	0600	13.1	168.5	19-Feb-1992	1200	31.6	157.0	102	2634	7.2	209	965	17-Feb-1992	1800	8.8	215
199106	ESAU	26-Feb-1992	0600	15.5	167.3	04-Mar-1992	0000	19.8	165.3	162	1980	3.4	203	925	28-Feb-1992	1200	1.8	327
199108	FRAN	09-Mar-1992	0600	18.6	168.3	17-Mar-1992	1200	25.5	159.0	198	2872	4.0	231	950	11-Mar-1992	1800	2.5	258
199202	NINA	23-Dec-1992	0000	13.0	140.0	02-Jan-1993	1800	11.5	171.0	258	4000	4.3	87	960	31-Dec-1992	1800	7.7	57
199204	OLIVER	05-Feb-1993	0000	15.0	150.1	12-Feb-1993	1800	22.0	154.6	186	1549	2.3	148	945	07-Feb-1993	1200	2.1	223
199205	POLLY	25-Feb-1993	0000	16.0	158.0	02-Mar-1993	0000	24.3	165.5	120	1355	3.1	139	955	01-Mar-1993	0000	5.7	154
199206	ROGER	12-Mar-1993	0000	10.0	157.0	21-Mar-1993	0000	21.3	160.9	216	2737	3.5	161	975	15-Mar-1993	0000	1.5	180
199301	REWA	28-Dec-1993	0600	9.5	165.5	21-Jan-1994	1200	29.0	158.0	582	8958	4.3	200	920	02-Jan-1994	1200	4.8	162
199302	SADIE	29-Jan-1994	0600	12.3	137.8	31-Jan-1994	1200	20.1	142.5	54	1123	5.8	149	985	30-Jan-1994	1800	5.3	163
199303	THEODORE	23-Feb-1994	0600	10.5	154.6	27-Feb-1994	0300	22.7	168.1	93	2148	6.4	133	910	25-Feb-1994	0600	4.3	135
199401	VIOLET	03-Mar-1995	0600	16.0	152.5	08-Mar-1995	0000	29.2	155.1	114	2648	6.5	169	960	05-Mar-1995	1200	10.0	157
199402	WARREN	04-Mar-1995	0000	13.3	140.1	06-Mar-1995	0100	17.2	137.8	49	781	4.4	209	960	05-Mar-1995	1700	6.7	242
199403	AGNES	17-Apr-1995	0000	11.8	147.3	21-Apr-1995	0000	12.1	147.6	96	456	1.3	135	945	18-Apr-1995	1800	0.0	90
199501	BARRY	03-Jan-1996	0000	15.0	136.8	09-Jan-1996	0000	23.1	147.5	144	1641	3.2	128	950	05-Jan-1996	0700	4.3	136
199502	CELESTE	26-Jan-1996	1200	18.2	146.3	28-Jan-1996	0100	19.2	151.3	37	620	4.7	101	960	27-Jan-1996	0800	5.8	90
199503	DENNIS	15-Feb-1996	0000	11.8	140.3	18-Feb-1996	0600	15.6	151.0	78	1311	4.7	110	990	16-Feb-1996	1200	4.8	108

		Start				Finish				Lifetime				At Maximum Intensity				
Seq.	Name	Date	Time	Lat	Long	Date	Time	Lat	Long	Dur	Path	Vfm	Theta	p0	Date	Time	Vfm	Theta
No.			hhmm	°S	°E		hhmm	°S	°E	h	km	m s^{-1}	°	hPa		hhmm	m s^{-1}	°
199504	ETHEL	07-Mar-1996	1800	15.8	139.5	13-Mar-1996	0600	17.2	136.3	132	2285	4.8	245	980	09-Mar-1996	1800	6.1	80
199601	FERGUS	22-Dec-1996	2100	11.3	160.8	30-Dec-1996	1200	38.0	177.0	183	4735	7.2	151	975	25-Dec-1996	0000	8.1	82
199602	DRENA	02-Jan-1997	0000	10.0	172.0	09-Jan-1997	0600	29.1	168.3	174	3843	6.1	190	935	06-Jan-1997	0000	2.0	180
199603	GILLIAN	09-Feb-1997	0600	12.5	150.5	12-Feb-1997	1800	19.3	146.8	84	896	3.0	207	995	11-Feb-1997	0600	3.3	201
199604	HAROLD	16-Feb-1997	0600	13.6	157.8	22-Feb-1997	1200	33.4	166.8	150	2830	5.2	157	975	18-Feb-1997	1800	4.0	120
199605	ITA	23-Feb-1997	1200	15.1	148.3	24-Feb-1997	1800	20.0	146.6	30	640	5.9	198	994	24-Feb-1997	1200	5.3	219
199606	JUSTIN	06-Mar-1997	1800	17.0	153.5	23-Mar-1997	2300	19.2	147.3	413	3679	2.5	249	955	17-Mar-1997	1200	3.9	337
199701	NUTE	18-Nov-1997	0000	11.1	165.1	20-Nov-1997	1200	18.5	158.3	60	1151	5.3	221	975	19-Nov-1997	0600	4.3	233
199702	SID	24-Dec-1997	0600	13.5	130.8	28-Dec-1997	2100	16.2	137.1	111	1797	4.5	113	985	28-Dec-1997	0000	5.8	148
199703	KATRINA	02-Jan-1998	0000	15.0	152.0	29-Jan-1998	0000	17.2	149.6	648	6719	2.9	226	940	15-Jan-1998	1200	3.0	210
199704	LES	19-Jan-1998	0000	13.0	138.0	29-Jan-1998	1200	14.5	127.6	252	2847	3.1	261	982	24-Jan-1998	1200	4.8	251
199705	MAY	24-Feb-1998	1800	13.1	139.1	07-Mar-1998	0000	14.8	136.3	246	2271	2.6	238	990	26-Feb-1998	0600	5.9	150
199706	NATHAN	20-Mar-1998	1800	11.1	143.3	31-Mar-1998	0000	13.8	145.0	246	3498	4.0	148	990	21-Mar-1998	0600	1.5	90
199801	OLINDA	20-Jan-1999	0900	17.2	158.3	21-Jan-1999	1800	19.8	159.3	33	310	2.6	159	987	21-Jan-1999	1800	3.2	162
199802	PETE	21-Jan-1999	0000	15.0	149.0	23-Jan-1999	1800	22.7	159.8	66	1510	6.4	126	985	23-Jan-1999	0600	7.4	128
199803	RONA	09-Feb-1999	1100	15.1	146.8	12-Feb-1999	1100	15.8	145.0	72	876	3.4	248	970	11-Feb-1999	1200	5.0	275
199804	FRANK	16-Feb-1999	1200	21.5	150.1	18-Feb-1999	1200	20.2	159.8	48	1039	6.0	81	994	18-Feb-1999	0600	3.4	90
199901	STEVE	25-Feb-2000	0000	17.2	153.0	29-Feb-2000	1200	16.5	139.1	108	1704	4.4	273	980	27-Feb-2000	0900	7.9	270
199902	VAUGHAN	28-Mar-2000	2300	20.0	168.0	07-Apr-2000	0000	14.6	146.3	217	2839	3.6	284	975	05-Apr-2000	1800	4.0	262
199903	TESSI	31-Mar-2000	0000	14.8	156.2	03-Apr-2000	1200	17.5	143.5	84	1507	5.0	257	980	02-Apr-2000	2000	0.0	90

Appendix C Tropical Cyclone Wind and Pressure Model

The following provides an overview of the parametric tropical cyclone wind and pressure model adopted for this study, which is similar to Harper and Holland (1999). Further elaboration is provided here of specific formulations which have been developed over a number of years as a result of extensive wind, wave and current hindcasting, e.g. Harper *et al.* (1989, 1993) and Harper (1999).

C.1 Definitions and Background

A tropical cyclone (hurricane or typhoon) is defined as a non-frontal cyclonically rotating (clockwise in the Southern Hemisphere) low pressure system (below 1000 hPa) of tropical origin, in which 10 min mean wind speeds at +10 m MSL (V_m) exceed gale force (63 km h^{-1}, 34 kn, or 17.5 m s^{-1}). In view of the complex nature of tropical cyclones and their interaction with surrounding synoptic scale mechanisms, most empirical wind and pressure models (Lovell 1990) represent the surface wind field by considering the storm as a steady axisymmetric vortex which is stationary in a fluid at rest.

The vortex solution is based on the Eulerian equations of motion in a rotating frame of reference (Smith 1968). The analysis begins with a consideration of force balance at the geostrophic, or gradient, wind level above the influence of the planetary boundary layer. The gradient wind speed can be expressed as a function of storm pressure, size, air density and latitude. The gradient wind speed is then reduced to the surface reference level of +10 m MSL (mean sea level) by consideration of gross boundary layer effects, wind inflow (also due to frictional effects) and asymmetric effects due to storm forward motion or surrounding synoptic pressure gradients.

C.2 Radial Pressure Field

A primary assumption of almost all empirical tropical cyclone models is that the radial pressure field at gradient wind speed level can be expressed as:

$$p(r) = p_0 + (p_n - p_0)\, exp\, (-R/r) \qquad \text{(C.1)}$$

where r = radial distance from storm centre
$p(r)$ = pressure at r
p_0 = pressure at the storm centre (central pressure)
p_n = ambient surrounding pressure field
and R = radius to maximum winds

This exponential pressure profile was first proposed by Schloemer (1954). Holland (1980) noted deficiencies in the ability of Equation C.1 to represent many observed pressure profiles and that the Schloemer base-profiles resembled a family of rectangular hyperbolae, viz:

$$r^B\, ln\, [p/(\, p_n - p_0)] = A \qquad \text{(C.2)}$$

where A and B are storm-dependent scaling parameters.

This modification leads to the following radial pressure field, which forms the basis of the 'Holland' model:

$$p(r) = p_0 + (p_n - p_0) \exp(-A/r^B) \quad \text{(C.3)}$$

C.3 Gradient Wind Speed

The gradient level winds are derived by considering the balance between centrifugal and Coriolis forces acting outwards and the presence gradient force acting inwards, leading to the so-called gradient wind equation:

$$V_g^2(r)/r + f V_g = 1/\rho_a \; dp(r)/dr \quad \text{(C.4)}$$

where $V_g(r)$ = gradient level wind at distance r from the centre
ρ_a = air density
f = Coriolis parameter
= $2\omega \sin \phi$
and ω = radial rotational speed of the earth
ϕ = latitude

The pressure gradient term for the Holland model is:

$$dp(r)/dr = p / r \, (AB/r^B) \exp(-A/r^B) \quad \text{(C.5)}$$

and substituting into Equation C.4 gives

$$V_g(r) = -r f/2 + [(p_n - p_0)/\rho_a \, (AB/r^B) \exp(-A/r^B) + r^2 f^2/4]^{1/2} \quad \text{(C.6)}$$

The so-called cyclostrophic wind equation, which neglects the Coriolis components, is then

$$V_c(r) = [(p_n - p_0)/\rho_a \, (AB/r^B) \exp(-A/r^B)]^{1/2} \quad \text{(C.7)}$$

with $V_c(r)$ attaining its maximum value when $dV_c(r)/dr = 0$ which, after differentiating, is satisfied when

$$-A/r^B + 1 = 0$$

and since, by definition, $r = R$ when $V_c(r)$ is a maximum

$$R = A^{1/B}$$
or $$A = R^B \quad \text{(C.8)}$$

Back-substituting into the model equations yields:

$$p(r) = p_0 + (p_n - p_0) \exp(-R/r)^B \quad \text{(C.9)}$$

$$V_g(r) = -r f/2 + [(p_n - p_0)/\rho_a \, B(R/r)^B \exp(-R/r)^B + r^2 f^2/4]^{1/2} \quad \text{(C.10)}$$

which, for the particular case of B=1 the basic set of relationships reduces to the Schloemer model.

The influence of B is one of a 'peakedness' parameter which in the region of R causes an increase in pressure gradient as B increases and a corresponding increase in peak wind speed of $B^{½}$ near R and with lower wind speeds at increasing r. Holland (1980) uses conservation of angular momentum and a review of pressure gradient and R data to propose restricting the dynamic range of B as 1.0 to 2.5. Furthermore, based on the climatological work of Atkinson and Holliday (1977) and Dvorak (1975), Holland suggested 'standard' B values might be inferred of the form

$$B = 2.0 - (p_0 - 900)/160 \qquad \text{(C.11)}$$

making B a direct function of the storm intensity.

However, due to the inherent scatter in the climatological data it is reasonable to allow further variability whilst still maintaining the identified parameter trend, viz:

$$B = B_0 - p_0/160 \qquad \text{(C.12)}$$

where B_0 is the so-called intercept value of B.

C.4 Open Ocean Atmospheric Boundary Layer

Following Powell (1980), a gross simplification of the complex atmospheric boundary later is made by transferring gradient level wind speeds (V_g) to the +10 m MSL reference level (V_m) by way of a boundary layer coefficient (K_m) viz:

$$V_m = K_m V_g \qquad \text{(C.13)}$$

Additionally, variation with height above the ground is derived on the basis of a traditional roughness height and logarithmic deficit law approach whereby the near-surface boundary layer profile at any height z is a function of the surface roughness and the reference speed at +10 m MSL, ie:

$$V_m (z) = V_m (10) \ ln(z/z_0)/ln(10/z_0) \qquad \text{(C.14)}$$

which is terminated at a nominal gradient height z_g such that

$$V_m (z_g) = V_g = V_m (10) \ ln(z_g/z_0)/ln(10/z_0) \qquad \text{(C.15)}$$

hence

$$V_m (10) = V_g \ ln(10/z_0)/ln(z_g/10) \qquad \text{(C.16)}$$

$$K_m = ln (10/z_0)/ln(z_g/z_0) \qquad \text{(C.17)}$$

requiring a priori selection of z_0 and z_g which are both known to vary; the former as a function of wave height (wind speed and fetch) and the latter as a function of storm energetics.

North West Cape data sets presented by Wilson (1979) give a lower limit estimate of z_g as 60 m for the open ocean environment, yielding a typical z_0 of 0.3 m for wind speeds of the order of 30 m s^{-1}. Garratt (1977) provides a functional form for z_0 at lower wind speeds

(generally agreed to around 20 m s^{-1}) and nominal z_g values form Standards Australia (1989) allow the following representation of the variation of z_0 and z_g :

$$\ln(z_0) = 0.367\ V_m - 12 \qquad 0 < V_m < 30 \qquad \text{(C.18)}$$
$$\ln(z_0) = -1.204 \qquad V_m \geq 30$$

$$z_g = 228 - 5.6\ V_m \qquad 0 < V_m < 30 \qquad \text{(C.19)}$$
$$z_g = 60 \qquad V_m \geq 30$$

which, when combined into Equation C.17 and referenced to the V_g level, yield

$$K_m = 0.81 \qquad 0 < V_g < 6 \qquad \text{(C.20)}$$
$$K_m = 0.81 - 2.96 \times 10^{-3} (V_g - 6) \qquad 6 \leq V_g < 19.5$$
$$K_m = 0.77 - 4.31 \times 10^{-3} (V_g - 19.5) \qquad 19.5 \leq V_g < 45$$
$$K_m = 0.66 \qquad V_g \geq 45$$

The above speed-dependent formulation for K_m was devised in an attempt to try to improve wind speed calibrations from a number of tropical cyclones in Australia where measured wind, wave and current data was available. It embodies the observation that winds from more remote storms and/or winds on the "weak" side of storms were generally underpredicted using a constant K_m. This can also be interpreted as an attempt to devise a spatially varying K_m formulation, which has some similarity with, for example, the findings of Kepert and Wang (2000). For practical purposes in strong winds, this Equation C.20 yields a K_m of about 0.7, which is in the range observed by Powell (1980) and subsequently, for a number of US hurricanes. In Australia, McConochie *et al.* (1999) report favourable results using the above formulation on the east coast of Queensland.

C.5 Inflow Angle and Windfield Asymmetry

In addition to direct boundary layer attenuation, frictional effects cause the inflow of winds across the line of the isobars, towards the centre of the storm. This inflow (β) is typically of the order of 25º but decreases towards the storm centre, viz:

$$\beta = \begin{cases} (10\ (r/R) & 0 \leq r < R \\ (10 + 75\ (r/R\text{-}1) & R \leq r < 1.2\ R \\ (25 & r \geq 1.2\ R \end{cases} \qquad \text{(C.21)}$$

following Sobey *et al.* (1977).

The observed gross features of moving storms is accounted for by including an asymmetry effect which, on one side of the storm adds the forward speed of the storm centre (V_{fm}) and subtracts it from the other side, relative to an assumed line of maximum wind θ_{max}, ie

$$V_m (r,\theta) = K_m\ V_g\ (r) + V_{fm} \cos (\theta_{max} - \theta) \qquad \text{(C.22)}$$

Where θ_{max} is commonly taken to be in the range of either 65º to 70º (left forward quadrant for Southern Hemisphere) or as 115º (left rear quadrant for Southern Hemisphere) measured upwind from the line of V_{fm} to which θ is referenced.

Figure C.1 presents the geometry of the wind field model in detail, including consideration of north point references for θ_{fm} and V_b (the bearing of V_m).

C.6 References

Atkinson G.D. and Holliday C.R. (1977) Tropical cyclone minimum sea level pressure/maximum sustained wind relationship for the Western North Pacific. *Monthly Weather Review*, 105, 421-427.

Dvorak V.F. (1975) Tropical cyclone intensity analysis and forecasting from satellite imagery.
Monthly Weather Review, 103, 420-430.

Garratt J.R. (1977) Review of drag coefficients over oceans and continents.
Monthly Weather Review, 105, 915-929.

Harper B.A., Lovell, K.F., Chandler B.D. and Todd D.J. (1989) The derivation of environmental design criteria for Goodwyn 'A' Platform, Proc. 9th Aust Conf. Coastal and Ocean Engin., *Institution of Engineers Australia*, Adelaide, Dec.

Harper B.A., Mason L.B. and Bode L. (1993) Tropical cyclone Orson - a severe test for modelling, Proc. 11th Australian Conf. on Coastal and Ocean Engin., *Institution of Engineers Australia*, Townsville, Aug, 59-64.

Harper B.A. (1999) Numerical modelling of extreme tropical cyclone winds. APSWE Special Edition, *Journal of Wind Engineering and Industrial Aerodynamics*, 83, 35 - 47.

Harper B.A. and Holland G.J. (1999) An updated parametric model of the tropical cyclone. Proc. 23rd Conf. Hurricanes and Tropical Meteorology, *American Meteorological Society*, Dallas, Texas, 10-15 Jan.

Holland G.J (1980) An analytic model of the wind and pressure profiles in hurricanes. *Monthly Weather Review*, 108, 1212-1218.

Kepert J.D. and Wang Y. (2000) The dynamics of boundary layer jets within the tropical cyclone core. Part II: Nonlinear enhancement. To appear *Jnl Atmospheric Science*.

Lovell K.F. (1990) Review of empirical tropical cyclone wind and pressure models. MEngSt Thesis, Dept Civil Engineering, *University of Western Australia*.

McConochie J.D., Mason L.B. and Hardy T.A. (1999) A Coral Sea wind model intended for wave modelling. Proc. 14th Australasian Conf. Coastal and Ocean Enginering, *IEAust*, Perth, April, 413-418.

NOAA (1979) Meteorological criteria for standard project hurricane and probable maximum hurricane windfields, Gulf and East Coasts of the United States", NOAA Tech Rep NWS23, *US Dept of Commerce*, Sept.

Powell, M.D. (1980) Evaluations of diagnostic marine boundary-layer models applied to hurricanes. *Monthly Weather Review*, 108, 757-766.

Schloemer R.W. (1954) Analysis and synthesis of hurricane wind patterns over Lake Okeechobee, Florida. *US Weather Bureau*, March.

Smith R.K. (1968) The surface boundary layer of a hurricane. *Tellus*, 0, 473-484.

Sobey R.J., Harper B.A. and Stark K.P. (1977) Numerical simulation of tropical cyclone storm surge. Research Bulletin CS-14, Dept Civil and Systems Engineering, *James Cook University*, March.

Standards Australia (1989) AS 1170.2 - 1989 SAA loading code part 2: wind loads. 96 pp.

Wilson K.J. (1979) Wind observations from an instrumented tower during tropical cyclone Karen, 1977. 12th Tech Conf on Hurricanes and Tropical Meteorology, *American Meteorological Society*, New Orleans, April.

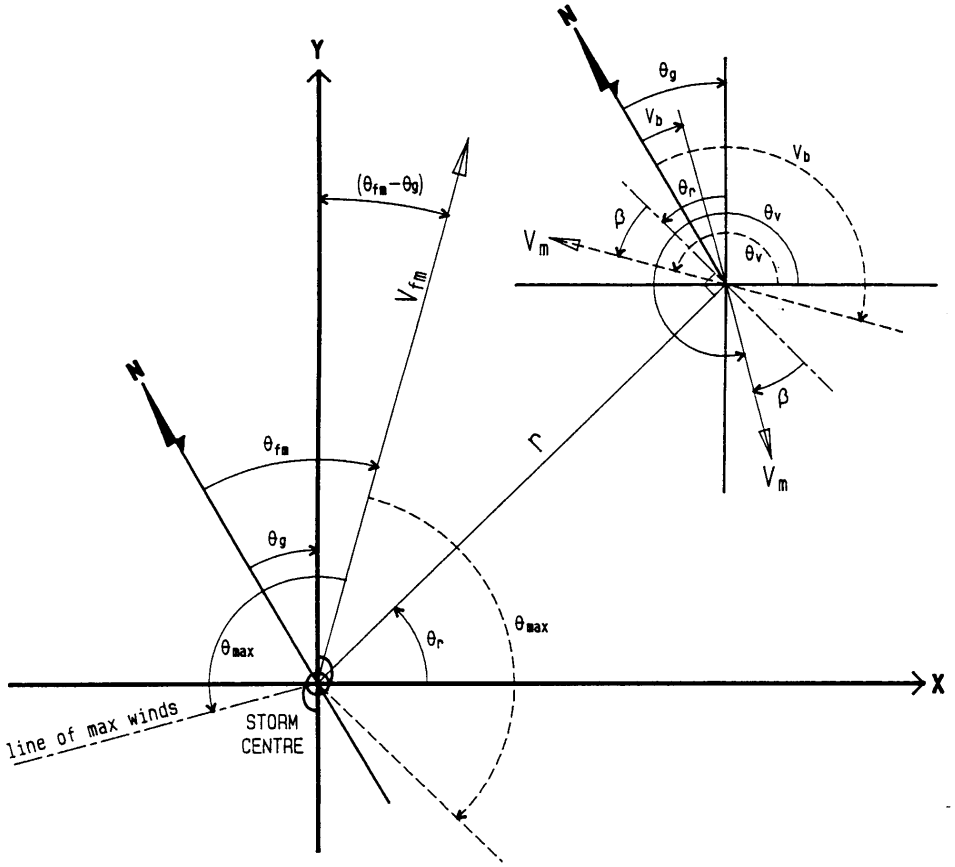

	SOUTHERN HEMISPHERE	NORTHERN HEMISPHERE
θ_{max}	+ 115	- 115
θ_v	$270 + \theta_r - \beta$	$90 + \theta_r + \beta$
V_b	$-\theta_r + \beta + \theta_g$	$180 - \theta_r - \beta + \theta_g$

TROPICAL CYCLONE MODEL
WIND FIELD GEOMETRY

Figure C.1

Appendix D Technical Description of the James Cook University Storm Surge Model (MMUSURGE)

D.1 Introduction

This appendix describes the basis of the 2D depth integrated hydrodynamic model (MMUSURGE) developed by the Marine Modelling Unit at the School of Engineering, James Cook University. The model is based on the depth integrated equations of motion using the usual assumption that the fluid is incompressible and homogeneous. It is formulated in a spherical coordinate system and includes all the basic momentum terms such as Coriolis, advection, horizontal diffusion, surface and bottom stress and the inverse barometer effect. Wind stress is parameterised through a quadratic drag law using the drag coefficient of Wu (1982). Bottom friction is also parameterised using a quadratic friction law with the drag coefficient coming from the assumption of a logarithmic profile. One unique aspect of this model is its ability to include the effects of sub-grid scale reef and barriers on water flow.

The model has a built-in tropical cyclone wind field model and a built-in uniform wind field model. The tropical cyclone wind field is based on that of Holland, consistent with Appendix C, with modifications that make it suitable for the Coral Sea region. The model is capable of producing output that includes water levels and velocities. The output can be in the form of time histories or full gridded output. The User Guide (Mason and McConochie 2001) provides specific detail of how to incorporate varying surface wind and pressure fields.

D.2 Equations of Motion

The equations of motion are the two-dimensional (2D) long wave equations, describing conservation of momentum and mass for a homogeneous fluid. In the present work, these equations are formulated in standard spherical polar coordinates, used in models over significant portions of the earth's surface.

By the use of the hydrostatic approximation, the equations become:

$$\alpha\frac{\partial U}{\partial t}+\frac{U}{D'}\frac{\partial U}{a\cos\phi\,\partial\lambda}+\frac{V}{D'}\frac{\partial U}{a\partial\phi}-\frac{UV}{aD'}\tan\phi$$
$$-\frac{U}{D'}\left[\alpha\frac{\partial\eta}{\partial t}+\frac{U}{D'}\frac{\partial D'}{a\cos\phi\,\partial\lambda}+\frac{V}{D'}\frac{\partial D'}{a\partial\phi}\right]-fV \qquad \text{(D.1)}$$
$$=-gD\frac{\partial(\eta-\eta_e+p_s/\rho)}{a\cos\phi\,\partial\lambda}+\frac{\tau_{s\lambda}}{\rho}-\beta\frac{\tau_{b\lambda}}{\rho}+A_m\nabla_h^2U,$$

$$\alpha\frac{\partial V}{\partial t}+\frac{U}{D'}\frac{\partial V}{a\cos\theta\,\partial\lambda}+\frac{V}{D'}\frac{\partial V}{a\partial\phi}-\frac{U^2}{aD'}\tan\phi$$
$$-\frac{V}{D'}\left[\alpha\frac{\partial\eta}{\partial t}+\frac{U}{D'}\frac{\partial D'}{a\cos\phi\,\partial\lambda}+\frac{V}{D'}\frac{\partial D'}{a\partial\phi}\right]+fU \qquad \text{(D.2)}$$
$$=-gD\frac{\partial(\eta-\eta_e+p_s/\rho)}{a\,\partial\phi}+\frac{\tau_{s\phi}}{\rho}-\beta\frac{\tau_{b\phi}}{\rho}+A_m\nabla_h^2V,$$

$$\frac{\partial\eta}{\partial t}+\frac{1}{a\cos\phi}\left[\frac{\partial U}{\partial\lambda}+\frac{\partial V\cos\phi}{\partial\phi}\right]=0. \qquad \text{(D.3)}$$

Here: λ is east longitude; ϕ is latitude; t is time; $D = \eta - h$ is total water depth; η is the surface elevation, relative to Mean Sea Level (MSL) datum; h is the bottom elevation; D' is

the minimum average or effective depth where sub-grid scale reef or barriers are included; the components of transport (U and V) are, defined by (U, V) = D(u, v), where $\bar{u}$ = (u, v) is depth averaged fluid velocity; f is the Coriolis parameter (equal to $2\Omega\sin\phi$, where Ω = 7.292 $\times$ 10^{-5} s^{-1} is the earth's angular velocity); a is the earth's radius; η_e is the equilibrium tide height; p_s is atmospheric pressure; ρ is the density of seawater; A_m is the horizontal eddy viscosity; and ∇_h^2 denotes the horizontal Laplacian operator.

At the water surface, wind stress ($\vec{\tau}_s$), when required, is modelled conventionally through the quadratic drag law,

$$\vec{\tau}_s = C_{10}\rho_a \left| \vec{W}_{10} \right| \vec{W}_{10}, \qquad \text{(D.4)}$$

where $\vec{W}_{10}$ is the wind at a standard anemometer height of 10 m, ρ_a is the density of air and C_{10} is the surface drag coefficient. The (dimensionless) drag coefficient is a function of the magnitude of the wind speed. The formula used in the present study is that of Wu (1982):

$$C_{10} = \left(0.8 + 0.065\left|\vec{W}_{10}\right|\right)\times 10^{-3}, \qquad \text{(D.5)}$$

where the magnitude of $\vec{W}_{10}$ is given in m s^{-1}. At the sea bed, the bottom shear stress (τ_b) is expressed in terms of the total near bottom transport Q = (U^2 + V^2)$^{0.5}$ and total water depth D, by the quadratic friction law:

$$\vec{\tau}_b = (\tau_{b\lambda,}\tau_{b\theta}) = \frac{\rho C_b |Q|}{D^2}(U,V) \qquad \text{(D.6)}$$

where C_b is a drag coefficient. For fully developed turbulent flow, the near bottom currents are very closely approximated by a logarithmic profile. From this relationship, it can be shown that the drag coefficient can then be expressed as:

$$C_b = \left[\frac{\kappa}{In(z_b / z_0)}\right]^2 \qquad \text{(D.7)}$$

where κ = 0.4 is the well known von Karman constant, z_b is the elevation of the lowest horizontal transports (U_b, V_b), and z_0 is the bottom roughness length. The physical or Nikuradse roughness is approximately equal to $30z_0$.

When no partial (sub-grid scale) barriers or reefs are defined, α=1and β=1, otherwise they are given by

$$\alpha = (1-b) + \frac{bw_3}{w_1^2} + \Phi(w_1) \qquad \text{(D.8)}$$

and

$$\beta = (1-b)\frac{b}{w_1^2} + 1.56w_1^{-0.56}\Phi(w_1). \qquad \text{(D.9)}$$

Here Φ, the end effects, is defined as

$$\Phi(w_1) = \frac{1}{\pi}\left[\left(1+\frac{1}{w_1}\right)\ln\frac{1+w_1}{1-w_1} + 2\ln\frac{1-w_1^2}{4w_1}\right] \qquad \text{(D.10)}$$

and the modified gap fractions are

$$w_1 = w + (1-w)R_t, w_3 = w + (1-w)\frac{R_t^2}{R_h}, R_h = \frac{D_{reef}}{D_{bed}}, R_t = \frac{C_{b_{reef}}}{C_{b_{bed}}}. \qquad \text{(D.11)}$$

The reef gap fraction, w, and reef width fraction, b, are related to the proportion of the grid space taken up by reefs or barriers.

D.3 Implicit Hydrodynamic Model

We present in this section a basic description of the two-dimensional, nonlinear hydrodynamic surge model, using an implicit form of time-stepping for finite difference (FD) schemes, as first described in Bode and Mason (1994).

D.3.1 Background

Despite advances in solution methods for very large sparse systems of linear equations that arise from the discretisation of partial differential equations, many two-dimensional (2D) hydrodynamic models continue to use explicit time-stepping. Ease of code generation is the main incentive to use explicit schemes. However, this is in spite of the well known but highly restrictive timestep constraint that is needed to ensure computational stability:

$$C = \frac{\Delta t\sqrt{2gH_{\max}}}{\Delta s} \le 1. \qquad \text{(D.12)}$$

Here, Δt and Δs are the temporal and spatial increments, g is gravitational acceleration, $D_{\max}$ is the maximum total water depth, and C is the so-called dimensionless Courant number. With continuing dramatic improvements in computer power and memory, models have been able to utilise much finer grids, thus allowing improved model realism. However, an immediate consequence is that extremely small values of Δt are demanded by the constraint (D.12). For example, in the case of a storm surge model that extends into deep water (e.g., $D_{\max}$ = 1000 m), a typical value of Δs = 3 km demands a Δt value of around 15″. Such values of Δt are several orders of magnitude less than the significant time scales of the storm surge phenomenon. This situation is exacerbated by higher spatial resolution, with the CPU cost of a 2D model increasing with $(\Delta s)^{-3}$.

The need for such restrictive timesteps in explicit models led to enhanced interest in implicit schemes, which can be shown by simple analysis to guarantee numerical stability, at least for linear regimes. The pioneering and influential work of Leendertse (1967), which employed the alternating direction implicit (ADI) method, was taken up by many modellers. Here, the 2D equations are separated into individual components in each of the two spatial directions x and y, say). Then, one such part (e.g., x) is made implicit over $\Delta t/2$, while the other remains explicit; this action is reversed in a second half-timestep. The advantage is that the 2D model essentially devolves into two coupled 1D implicit models. At the same time, the simultaneous equations that arise are generally only tridiagonal, so causing little CPU penalty for such methods. However, significant difficulties were shown to arise from use of the ADI method for more spatially complex model geometries, which may be expected to arise in near-coastal regions (Stelling *et al*., 1986).

These limitations of the ADI schemes can be overcome by using a fully implicit model, as is done here. Fully implicit models require the solution of the "full" 2D equations at each timestep. In reality, this undertaking is impossible because of the high degree of nonlinearity in the long wave equations, so that various stratagems, such as operator splitting, need to be invoked to make the computations feasible. However, implicit models still require the inversion of huge, multi-banded sparse matrices at each timestep, and the basic code is more complex, naturally, than that for explicit or ADI models. As a result, modellers have been slow to recognise the advantages of such schemes. Two noteworthy exceptions are Backhaus *et al*. (1983), which suffered by using the old-fashioned and slow relaxation (SOR) method, and Wilders *et al*. (1988), which has formed the basis for our own scheme. The advent of efficient computer packages such as NSPCG (Oppe *et al*., 1988), which employ various pre-

conditioned conjugate gradient schemes for the solution of large banded systems of equations, has now made implicit models much more feasible than in the past.

D.3.2 Model description

We illustrate the numerical model scheme with the full equations of motion used in the storm surge simulations, although for notational simplicity we employ the Cartesian form of these, rather than the spherical. The equations are:

$$\frac{\partial U}{\partial t}+\frac{\partial}{\partial x}\left(\frac{U^2}{D}\right)+\frac{\partial}{\partial y}\left(\frac{UV}{D}\right)-fV=-gD\frac{\partial(\eta)}{\partial x}+\frac{1}{\rho}\left[\tau_{sx}-\tau_{bx}\right], \qquad \text{(D.13)}$$

$$\frac{\partial V}{\partial t}+\frac{\partial}{\partial x}\left(\frac{UV}{D}\right)+\frac{\partial}{\partial y}\left(\frac{V^2}{D}\right)+fU=-gD\frac{\partial \eta}{\partial y}+\frac{1}{\rho}\left[\tau_{sy}-\tau_{by}\right], \qquad \text{(D.14)}$$

$$\frac{\partial \eta}{\partial t}+\frac{\partial U}{\partial x}+\frac{\partial V}{\partial y}=0. \qquad \text{(D.15)}$$

Notation is as follows: t is time; U and V are the components of horizontal transport or depth-integrated velocity; the water column extends from the sea surface at $z=\eta(x,y)$ to the sea floor at $z=-h(x,y)$, giving a total water depth of $D = h + \eta$; f is the Coriolis parameter, with $f\approx -4.8\times10^{-5}$ s^{-1} at the latitude of Townsville; $\boldsymbol{\tau}_s = (\tau_{sx},\tau_{sy})$ is surface stress due to the wind; $\boldsymbol{\tau}_b = (\tau_{bx},\tau_{by})$ is the seabed stress. We follow accepted 2D modelling practice and set

$$\frac{\tau_b}{\rho}=\frac{\lambda\left(U^2+V^2\right)^{1/2}}{D^2}(U,V), \qquad \text{(D.16)}$$

where ρ is the density of seawater (assumed constant), and λ is a weakly depth-dependent dimensionless drag coefficient -- typical values lie around 2.5×10^{-3} (Sobey *et al*., 1977). The basic geometric layout is depicted in the schematic below (Figure D.1).

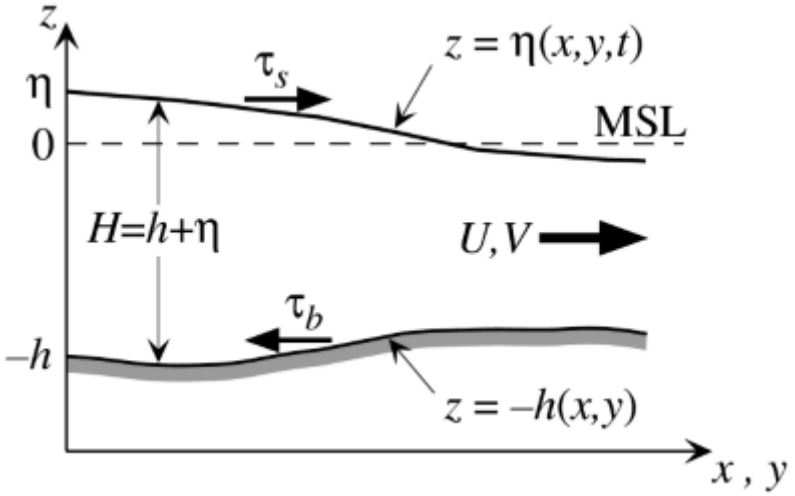

Figure D.1 Schematic layout of model geometry in cartesian coordinates (*x*,*y*,*z*). The water column of total depth D extends from the free surface, $z = \eta(x,y,t)$, to the sea floor, $z = -h(x,y)$. The vertical datum is depicted here as Mean Sea Level (MSL), $z = 0$. Also shown are the surface and bottom stresses, τ_s and τ_b, and the transport, $U = (U,V)$.

Our method is based on that described in Wilders *et al*. (1988), but with some significant modifications. Changes from the original 2D scheme of Wilders *et al*. (1988) include the use

of transport rather than velocity components as prognostic variables, and an implicit method for treating the Coriolis terms. The numerical FD scheme consists of a combination of explicit and implicit steps, which combine to produce trapezoidal or Crank-Nicolson time differencing. In the horizontal, the prognostic variables *U*, *V* and η are specified on a spatially staggered finite difference grid (the standard Arakawa `C' arrangement -- Mesinger and Arakawa (1976) – as shown in Figure D.2.

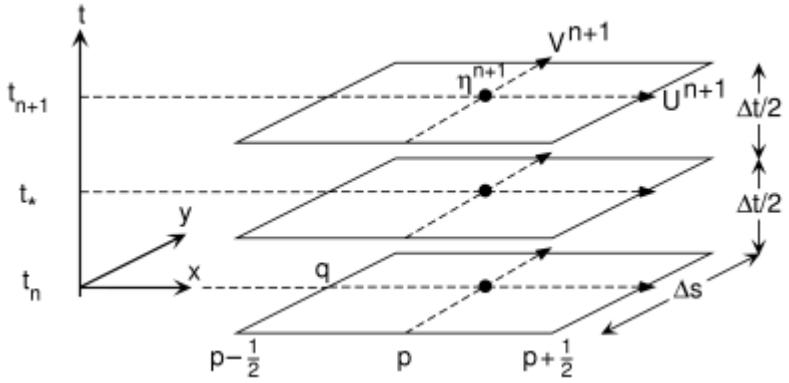

Figure D.2 Space-time distribution of *U*, *V* and η variables on the C-grid.

Use of a C-grid greatly simplifies coastal boundary conditions in coastal ocean modelling, although the Coriolis terms then require spatial averaging, which can cause complications with implicit models. A method that has been devised to overcome such problems on a staggered grid is described in brief below. We assume here a square spatial grid ($\Delta x = \Delta y = \Delta s$), although this restriction can be easily relaxed, and define variables on the discrete space-time grid in standard fashion,

$$\eta^n_{p,q} = \eta\left(x_p, y_q, t_n\right) = \eta\left(p\Delta s, q\Delta s, n\Delta t\right), \qquad \text{(D.17)}$$

and similarly for *U* and *V* at their corresponding positions. We use the flow chart of Figure D.3 to describe the implementation of the scheme, where we define an intermediate and temporary half-timestep, by $t^* = t_{n+1/2}$. The steps then proceed sequentially, as indicated on this diagram.

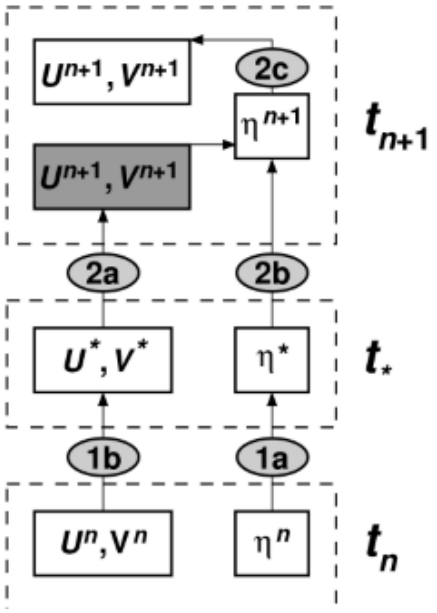

Figure D.3 Sequence of operations over one timestep for the split implicit FD scheme.

1a. Equation (D.16) is solved *explicitly* for $\eta^*_{p,q}$

$$\frac{\eta^*_{p,q}-\eta^n_{p,q}}{\Delta t/2}+\left[\left(U^n_{p+1/2,q}-U^n_{p-1/2,qp,q}\right)+\left(V^n_{p,q+1/2}-V^n_{p,q-1/2}\right)\right]=0. \qquad \text{(D.18)}$$

1b. Then, using the known fields of U^n, V^n, η^n and η^*, discretised versions of (D.14) and (D.15) are solved for (U^*,V^*). The Coriolis terms are formulated explicitly at this stage using standard 4-point averages; bottom friction is discretised in the standard semi-implicit manner (Bode and Hardy, 1997) to enhance stability; and the nonlinear advective terms are expressed implicitly, using a combination of centred and higher-order upwinding differences. If we omit the advective and wind stress terms, this step can be demonstrated for the *U*-momentum equation by the following equation:

$$\frac{U^*-U^n}{\Delta t/2}-f\left(\overline{V}^{xy}\right)^n=-g\left(\overline{D}^x\right)^*\frac{\eta^n_{p+1,q}-\eta^n_{p,q}}{\Delta s}-\frac{\lambda Q^n}{\left[\left(\overline{D}^x\right)^*\right]^2}U^* \qquad \text{(D.19)}$$

where evaluation at the spatial grid position (p+1/2,q) is implied and Q=(U^2 +V^2)$^{1/2}$. A similar equation for V^* follows from (D.15). If advective terms are omitted, this step is fully explicit; if included, these equations become implicit, but can be solved cheaply by NSPCG, usually in 1 or 2 iterations.

2a. The FD forms of (D.14) and (D.15) are rewritten at the next half-timestep, so as to solve *algebraically* for the (U^{n+1},V^{n+1}) fields. Bottom friction is again treated semi-implicitly; Coriolis terms are treated by the method described below.

2b. The expressions for (U^{n+1},V^{n+1}) are finally substituted into a backward-differenced form of (D.16), in which the divergence terms are computed at t^{n+1}, in order to make the method centred and thus second-order in time. This produces a discrete Helmholtz equation for η^{n+1}, which can be solved by NSPCG, the most computationally demanding part of the scheme. Usually around 10 iterations are sufficient to give convergence to 1 part in 10^5. The banded matrix contains 9 diagonals.

2c. The (U^{n+1},V^{n+1}) fields are found by simple back-substitution in the formula used in 2b.

Despite being based on the work of Wilders *et al*. (1988), the present scheme has involved a number of significant modifications:

- We use transport rather than velocity in the momentum equations. This has greatly simplified the key step in the implicit updating via the continuity equation η^* to η^{n+1}, which ensures mass conservation. This is now done by a single iterative process, rather than the two-step (inner-outer) method of Wilders *et al*. The nonlinearity that was previously present in the velocity-based continuity equation now reverts to the momentum equations, where it causes fewer difficulties.

- The bottom friction computations are time-centred. This raises the temporal accuracy of this term to second order, and leads to improved stability characteristics.

- Considerable numerical experimentation has been carried out to improve the formulation and resulting stability of the nonlinear advective terms.

- Coriolis terms were *not* included in the work of Wilders *et al*. They cause an inherent problem because of the time splitting factorisation. We have been able to devise a method that incorporates the Coriolis terms on the staggered C grid, yet still ensures the desired level of accuracy and stability, see
- D.3.3 Treatment of Coriolis terms .

D.3.3 Treatment of Coriolis terms

The need for spatial averaging of the Coriolis terms on a C-grid complicates the formulation of implicit schemes. Note also that explicit schemes are weakly unstable with a growth rate of order fΔt, although system friction is usually enough to control this potential problem. The fundamentals of our method can be demonstrated by using a reduced set of equations, the so-called 'rotational equations' (Mesinger and Arakawa, 1976). These equations are obtained by removing all but the temporal derivative and Coriolis terms from (D.14) and (D.15), which thus reduce to

$$\frac{\partial U}{\partial t} - fV = 0, \quad \text{and} \quad \frac{\partial V}{\partial t} + fU = 0. \tag{D.20}$$

By defining the complex transport $W = U+iV$, (D.21) becomes

$$\frac{\partial W}{\partial t} + ifW = 0, \tag{D.21}$$

with the simple solution

$$W(t) = W_0 \exp(-ift). \tag{D.22}$$

This represents inertial oscillations, with period $T_f = 2\pi/f$, or half a pendulum day.

On the Arakawa B-grid, for which the *U* and *V* locations coincide, no spatial averaging is required for the Coriolis terms. For this case, Gadd (1980) devised a strategy whereby the rotational equations can be written in what appears as an implicit Crank-Nicolson form. We discretise (D.21), as follows:

$$\frac{U^{n+1} - U^n}{\Delta t} - \frac{f}{2}\left(V^{n+1} + V^n\right) = 0, \tag{D.23}$$

$$\frac{V^{n+1} - V^n}{\Delta t} + \frac{f}{2}\left(U^{n+1} + U^n\right) = 0. \tag{D.24}$$

This system is neutrally stable, numerically, yet can be converted to a fully *explicit* form with matrix representation

$$\begin{bmatrix} 1 & -\phi \\ \phi & 1 \end{bmatrix}\begin{bmatrix} U^{n+1} \\ V^{n+1} \end{bmatrix} = \begin{bmatrix} 1 & \phi \\ -\phi & 1 \end{bmatrix}\begin{bmatrix} U^{n} \\ V^{n} \end{bmatrix}, \tag{D.25}$$

where $\phi = 2f\,\Delta t$. This 2×2 system can be solved directly for (U^{n+1}, V^{n+1}). Thus, although formulated implicitly (and hence stable), the FD equations (D.24 and D.25) can be expressed in an equivalent explicit form, thus avoiding the need for any matrix inversions.

On the C-grid, however, the need for spatial averaging of the Coriolis terms precludes the direct use of this approach. We need to recall that in Step 2a of the split scheme, algebraic expressions for (U^{n+1}, V^{n+1}) are required to obtain the Helmholtz equation for η^{n+1}. If the fact that the spatial positions of *U* and *V* do *not* coincide is temporarily ignored, no such problems arise: the solution of (D.26) can be used to obtain explicit expressions for (U^{n+1}, V^{n+1}). (Other terms in the momentum equations complicate the algebra but do not affect the overall methodology.) When the staggered nature of the grid is taken into account, some terms will not be defined at their pre-specified locations at Step 2b, and spatial averaging is *then* used,

where appropriate. This increases the bandwidth of the sparse matrix used to solve for η^{n+1} in Step 2b. Although no analysis is presented here, the method can be shown to be stable, and in fact slightly dissipative for high wave numbers – an additional advantage.

D.3.4 Reef parameterisation scheme

The fundamental problem in adapting long wave models to shelf-scale reefal areas is one of spatial resolution, as is apparent from consideration of the geometry that applies in the Great Barrier Reef (GBR). Relatively fine FD grids for continental shelf-scale models (e.g. Δs = 1 nmile), do not even remotely resolve major features: for example, the deep channels between reefs can be as narrow as 100 m. In much of the GBR, where the tidal range is large, considerable volumes of water can flow through these channels. Reef complexes, such as those found throughout the GBR, are basically sub-grid-scale (using almost any feasible spatial grid). The resulting resolution problems are so severe that a parameterised approach to the numerical modelling of long wave motions at the scale of the continental shelf is essential. These considerations apply equally for tidal, circulation or tropical cyclone storm surge modelling.

To overcome these problems, yet still make long wave modelling in the GBR a feasible and accurate proposition, an effective but relatively simple and accurate reef parameterisation scheme was devised by Bode *et al*. (1997). This was originally developed from an analytical, quasi-1D model of Huthnance (1985), the geometry for which is shown in Figure D.4. The solution includes terms that correspond to the 2D nature of the flow around the openings in inter-reef passages (so-called 'end effects').

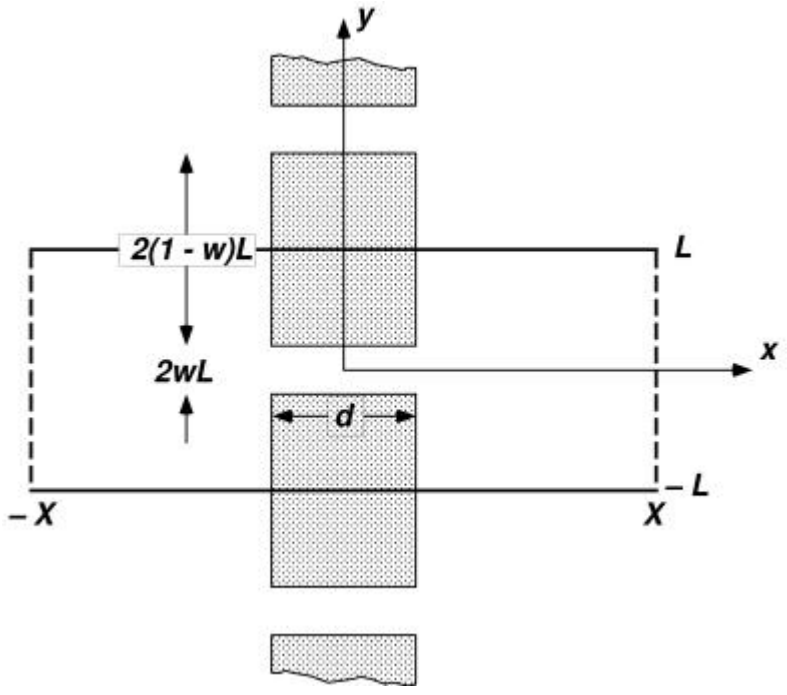

Figure D.4 Idealised reef geometry for *x*-directed flow, with 'gap fraction' denoted by *w*.

This simple model of Huthnance was extended to cover a wider range of problems, including flow over reef barriers, leading to impedance formulae with obvious electrical circuit analogies. Importantly, the scheme can be extended to treat the more realistic case of

quadratic bottom friction, thus including nonlinear frictional effects, associated with enhanced velocities through the narrow inter-reefal gaps. The formulation of the scheme is such that it can be incorporated relatively easily into time-dependent numerical models with quadratic bottom friction. As a simple summary, we consider the case which corresponds to flow occurring only through the gaps between (but not over) the reefs, under quadratic friction and no wind stress. The reduced 1D momentum equation for the flow through a complete FD square, corresponding to (D.14), can be shown (Bode *et al*., 1997) to reduce to

$$\alpha \frac{\partial U}{\partial t} = -gh_s \frac{\partial \eta}{\partial x} - \beta \frac{C_b |U|}{h_s^2} U. \qquad \text{(D.26)}$$

The derived reef parameters α and β are given in terms of the gap fraction *w* and the reef breadth fraction *b*, as shown in Figure D.5, as follows:

$$\alpha = (1-b) + \frac{b}{w} \quad \text{and} \quad \beta = (1-b) + \frac{b}{w^2}. \qquad \text{(D.27)}$$

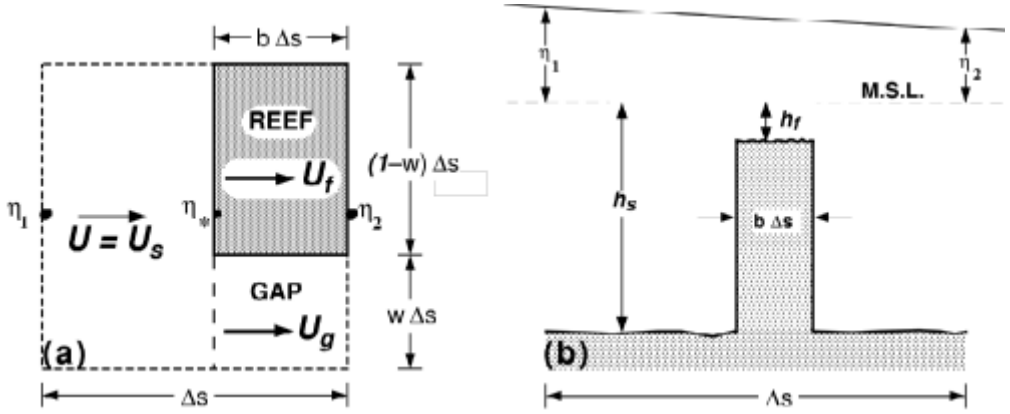

Figure D.5 Idealised reef geometry for FD grid. (a) Planform shows gap and reef breadth fractions, *w* and b. Transport U has contributions U_g and U_f from the gap and reef flat. (b) Cross-section, with shelf depth, h_s, reef flat depth, h_f, and surface elevations η_1 and η_2, shown in (a).

Bode *et al*. (1997) present modifications of (D.27) for the more general case where flow can also occur over reef flats. They give results for numerical tests of the parameterisation scheme, which demonstrate its accuracy by comparisons with high resolution, explicitly resolved, idealised reef geometries. They also applied the scheme to tidal modelling in the macro-tidal region of the Southern GBR, with extremely accurate results being found. Furthermore, this work shows the substantial influence of the GBR on the tidal response. The almost continuous reef matrix in certain sections leads to large local elevation gradients and velocities. Removal of the reefs from the model produces a completely different and erroneous response. This modelling also demonstrates that inclusion of momentum advection is generally required in such regions.

The form of the momentum equations given in Bode *et al*., (1997), is such that the reef parameterisation schemes can be incorporated almost unchanged in standard FD numerical long wave algorithms. For each momentum equation, the parameterisation schemes require the specification of just two geometric parameters, *w* and *b*, as in Figure D.5a. We determine these reef parameters automatically, an approach that is necessitated by the magnitude of the task. This automated procedure uses high resolution digitised reef outlines, overlaid on an ultra-fine mesh for each grid square, and inherently incorporates end effects.

Thus, the parameterised approach leads to equivalent analytical momentum equations, in which the coefficients of certain terms are modified by geometric factors (α and β) which depend only on *w* and *b*, and also account for end effects. For the general case, in which water can flow over reefs as well as through gaps, the parameterisation scheme is shown to give good agreement with the high-resolution overflow reef solutions, over a wide range of forcing frequencies, including the time scales encompassed by the passage of a tropical cyclone. The analytical solutions confirm the general conclusions in H85, that reef chains are largely transparent to long waves, but that this is *not* the case if reef coverage is particularly dense. Almost all flow occurs in the inter-reef channels, although it is shown that flow over reefs can cause subtle modifications to the dynamical response. The fact that the modified momentum equations, including those for quadratic friction, can be adapted immediately to standard numerical algorithms, simplifies considerably the task of model development in geometrically complex regions such as the GBR.

The numerical parameterisation scheme is applied to the M_2 tides of the Southern GBR region of Australia. This area, with its wide continental shelf and dense reef matrix, exhibits anomalous tidal behaviour (Middleton *et al*., 1984) and significantly amplified semidiurnal tides. Overall, the model is able to capture the unusual tidal characteristics of the region, and produces results that are in excellent quantitative agreement with data over the entire model domain.

Although only tides were considered explicitly in Bode *et al*. (1997), because these offered the best opportunity for model verification, the parameterised approach applies equally to the many other significant classes of low frequency motions in the GBR, notably tropical cyclone storm surge.

D.4 Overland flooding and drying

The “standard” coastal boundary condition used in long wave models is that of no flow at the coastline, i.e., the component of transport normal to the coastline equals zero. Thus, this boundary condition essentially approximates the coast by a vertical cliff of unlimited height, against which the free surface water level, η, can rise and fall. Quite apart from the fact that *all* models can only approximate the position of the coastline (e.g., that at M.S.L.), the topography there generally changes gradually, not abruptly. Further, many coastal regions are bordered by low-lying land: tidal flats such as those adjacent to parts of Cleveland Bay; large stretches of coastal plains close to sea level, such as those bordering the Gulf of Carpentaria; and inter-tidal lagoons and embayments. All may be subject to inundation at times of high astronomical tides or during a storm surge.

Thus, an important component of many coastal hydrodynamic models is the existence of modules to compute the extent of such incursions of sea water. These are often labelled wetting/drying or flooding algorithms. Such schemes will necessarily include a database of on-shore topography, at least for regions deemed flood-prone. The model must then compute the progress of the water across such areas -- both the position of the wet/dry interface, and the depth of water in all `wet' computational cells. This is *not* a simple problem. Indeed, the fact that various schemes are still being proposed in the recent modelling literature, is a strong indication that flooding and drying is not a closed issue.

D.4.1 Flooding algorithm for the JCU model

In our implicit model, the development of a flooding scheme is complicated by the significantly longer timesteps that are used, relative to those commonly employed for the explicit case. Any tendency for the formation of shocks and other problems, leading ultimately to model instability, will thus be amplified much more over this longer period of time. Nevertheless, we have been able to model flooding and drying with some success.

In our present scheme, we limit the minimum water depth in all cells to a small value, so that the implicit scheme has a finite water column to work with. However, the total water level is used nonlinearly in other parts of the momentum balance, e.g., for the pressure term. This means that there can be a tendency for the production of some very high gradients in water level, near wet/dry interface. This can then interact with the advective terms and cause model instability. It may also mean that the propagation speed of the wave front may be in error.

Overland flooding is undoubtedly an important issue for storm surge modelling, at least in some areas. However, there remain difficulties with reliable flooding schemes, as well as with the computational overheads that they incur. The simplest approach to the problem is that in which a fixed coastline model is used, and the computed surge relative to M.S.L. is compared against the levels of the adjacent land. In general, this will produce a "conservative" result, i.e., an over-estimation of the maximum surge level. Thus, we would recommend that *operational* surge modelling be conducted with the standard rigid coastline. However, in certain regions with very extensive areas of low-lying land, such as the Gulf of Carpentaria, the models may need to include flooding, at least for the purposes of sensitivity studies.

D.5 References

Backhaus, J.O. (1983) A semi-implicit scheme for the shallow water equations for application to shelf sea modelling. *Continental Shelf Research*, **2**, 243–254.

Bode, L. and Hardy, T.A. (1997) Progress and recent developments in storm surge modelling. *J. of Hydraulic Engineering*, ASCE, 123(4), April, 315-331.

Bode, L. and Mason, L.B. (1994) Application of an implicit hydrodynamic model over a range of spatial scales. Computational Techniques and Applications: CTAC93, D. Stewart, H. Gardner and D. Singleton, Eds., *World Scientific Press*, 112–121.

Bode, L. and Mason, L.B. (1995) Tidal modelling in Torres Strait and the Gulf of Papua. *Proceedings, Pacific Congress on Marine Science and Technology: PACON 94*, Townsville, O. Bellwood, H. Choat and N. Saxena, Eds., 55–65.

Bode, L., Mason, L.B. and Middleton, J.H. (1997) Reef parameterisation schemes for long wave models. *Progress in Oceanography*, **40**, 285–324.

Gadd, A.J. (1980) Two refinements of the split explicit integration scheme. *Quarterly Journal of the Royal Meteorological Society*, **106**, 215–220.

Huthnance, J.M. (1985) Flow across reefs or between islands, and effects on shelf-sea motion. *Continental Shelf Research*, **4**, 709--731.

Leendertse, J.J. (1967). Aspects of a computational model for long period water-wave propagation. *RM-5294-PR, Rand Corp*., Santa Monica, Calif.

Mason L.B. and McConochie J.D. (2001) MMUSURGE user's guide. School of Engineering, Marine Modelling Unit, *James Cook University*, Townsville.

Mesinger, F. and Arakawa, A. (1976) Numerical methods used in atmospheric models. GARP Publication Series, No. 17, Vol. 1, *WMO/ICSU Joint Organising Committee*, 64 pp.

Middleton, J.H., Buchwald, V.T. and Huthnance, J.H. (1984) The anomalous tides of Broad Sound. *Continental Shelf Research*, Vol. 3, 359-381.

Oppe, T.C., Joubert, W.D. and Kincaid, D.R. (1988) NSPCG user's guide. *University of Texas*, Austin, 82 pp.

Sobey, R.J., Harper, B.A. and Stark, K.P. (1977) Numerical simulation of tropical cyclone storm surge. Department of Civil and Systems Engineering, *James Cook University*, Research Bulletin CS14, 186 pp. + figs.

Stelling, G.S., Wiersma, A.K. and Willemse, J.B.T.M. (1986) Practical Aspects Of Accurate Tidal Computations. *Journal of Hydraulic Engineering*, ASCE, **112**, 802–817.

Wilders, P., van Stijn, Th.L., Stelling G.S., and Fokkema, G.A. (1988) A fully implicit splitting method for accurate tidal computations. *International Journal for Numerical Methods in Engineering*, **26**, 2707–2721.

Wu, J. (1982). Wind stress coefficients over sea surface from sea breeze to hurricane. *Journal of Geophysical Research*, 87, 9704–9706.

Appendix E Present US Practice for MEOW Storm Tide Warnings

E.1 Background

During the course of this study special efforts were made to determine the current status of US Weather Bureau MEOW storm tide warning practice and whether any changes to their systems were being considered. A note was received from Mr Brian Jarvinen, Chief of the Storm Surge Group at the National Hurricane Centre (NHC) in Miami, Florida. Brian confirmed that their MEOW approach commenced development in the mid-1970s and is still used by emergency managers to plan evacuations. Brian advised that there was no specific detailed technical report which described their current system fully, nor was there a document describing future plans. However, he confirmed that MEOW studies continue to be conducted under the auspices of FEMA on a regional community basis and a copy of a recent report (FEMA *et al.* 1999) was made available. During the last two hurricane seasons, the NHC has also been undertaking real-time storm tide simulations based on the operational forecast track and intensity. The real-time information is not currently being used for evacuation decision making.

E.2 Example Northwest Florida Study

The example report (FEMA *et al.* 1999) provides some insight into the US MEOW philosophy, although it is clearly designed to give an overview of the methodology for emergency managers and lacks any significant technical detail. In addition to the basic storm surge modelling aspect (which utilises the SLOSH model, e.g. Jelesnianski *et al.* 1992) the report also covers hazard and vulnerability analysis, community response to warning and evacuation instructions and transportation modelling. The region considered is the northwest Florida coastline south of Alabama and Georgia, consisting of eight counties. Two storm surge model domains are utilised, one targeting the western side (Pensacola) and the other the eastern side (Panama City).

Figure E.1 is taken from the report and indicates the set of discrete MEOW tracks adopted for the case of NNW moving storms in the Pensacola region. Also superimposed on the base figure is the outline of the SLOSH model grid used for these tracks and some indication of scale. Straightline tracks are generally used, except where climatology indicates persistent curvature (such as more westward-moving storms) and a "bent" track is used.

The model domains are based on a telescoping elliptical coordinate system which is designed to allow a varying gridsize from deeper offshore areas to the inland waterways. For the two grids utilised, offshore resolution varies between approximately 2.7 km to 1.8 km offshore, reducing to 500 m landward of the coast. The actual domain sizes are relatively small, being of the order of 150 km offshore and 225 km alongshore.

For each of the two separate domains, the simulation runs consisted of 5 intensities (Category 1 to 5); 3 forward speeds and 9 directions (@ 22.5º). Radius is fixed at 40 km (25 mile) and *B* variability is not acknowledged (nominal *B*=1?). The number of coast crossing positions (X) then varies depending on the direction, but averages 11 in total for each domain. Storm parameter fixes are specified 6 hourly with a total storm duration of 72 h. Table E.1 below summarises the resulting set of parameters, which yields close to 1500 runs for each domain. No wave setup is considered in the computation of the coastal water levels and the tide level

is set at a fixed "high tide" level (+0.23 m), together with a background tide anomaly (+ 0.38 m), i.e. a fixed level of MSL + 0.61 m. It is stated that allowance for overland storm decay and an increase in the value of *R* is included in the modelling process.

The maximum water levels from each of these simulations are then initially placed in directional MEOW classes as a function of speed and intensity (without regard to *X*), totaling 15 MEOWs for each direction, or a total of 135 for each domain. Following inspection, these results were further compressed by ignoring speed and direction, yielding only 5 results depending on storm category alone. These are termed MOMs (MEOWs of MEOWs).

Table E.1 Summary of Northwest Florida MEOW parameter set (per domain).

Parameter		Start	Interval	End	Total
Δp	cat	1	1	5	5
B	-		Not considered		-
R	km	40	0	40	1
V_{fm}	m s^{-1}	2.2	4.5	11.2	3
θ_{fm}	°	270	22.5	90	9
X	km	- 100	varies	+ 100	11 (av)
			No. of Runs		1485

E.3 Evaluation in an Australian Context

The US technique, as exemplified by FEMA *et al.* (1999), undertakes a large number of simulations at relatively closely spaced track positions, appearing to "target" the specific county in question. The track spacing is relative to that site with a "zero" track followed by ± 24 km (typically), then with further tracks at 8 km spacing on either side, finishing about ± 70 km. The rationale for this varying resolution is not clear, it appears to be permitting lower resolution about a region ± *R*/2 relative to the storm centreline. Since the actual centreline will vary, this does not appear superior to a fixed interval unless the alongshore coastal response is essentially constant. In the Queensland context, such an approach would probably need to be limited to the region bounded by the Sunshine Coast and Gold Coast or some parts of the Gulf of Carpentaria.

The use of a single *R* value may be justified by regional climatology but a minimum of two values in any circumstance would appear desirable. The choice of 40 km may be based on maintaining a conservative position, since larger *R* will generally produce a larger surge. The omission of peakedness (*B*) variation may also be based on the same philosophy, with a flatter wind profile tending to produce the larger surge. However, *B* does not appear to be included in the base windfield model (Houston *et al.* 1999) so this may the sole reason for its exclusion.

The choice of intensities appears reasonable, while the forward speeds are relatively high by Queensland standards (refer Chapter 3). The directional resolution appears generous in the context of a reasonably featureless coast. The use of the elliptical grid may provide some advantage in increasing resolution along the coast and the inland waterways but appears to result in arbitrary domain shape offshore, which may not always suit the location of open boundaries. Indeed, the domain extents given are relatively small (of order 3 *R*) and would be difficult to justify based on our experience. We accept that the testing carried out has satisfied the model developers in this case.

The US approach involves a number of major assumptions which would not be applicable in the Australian context. Foremost among these is the fixing of the tide level, which is justified in the case cited due to the very small tidal range. This permits using the maximum water levels from the model simulations without the need to consider phase relationships, i.e. the "storm surge" values are immediately considered as "storm tide" values. Also, wave setup is ignored, although the study report acknowledges it can be significant and, *anecdotally*, was possibly quite significant locally during Hurricane *Opal* in 1995. The extensive shallow offshore regions of the Gulf of Mexico (10 m contour at 4 km) will tend to afford some protection to wave setup due to frictional decay but this component should not be ignored generally in the Australian context.

The operational construction of the MEOW is also of interest, with the need to further devise MOMs suggesting pressure from emergency managers to provide further simplifications. Certainly, the level of resolution under which the MEOWs are constructed (1500 runs for about 130 km of coast) seems at odds with the final distillation into firstly 15 results for 9 directions and then only 5 results as a function of intensity. This approach would certainly ensure that the maximum possible level would be determined but appears to have unnecessarily neglected other useful information.

E.4 Conclusions

The methodology described in FEMA *et al.* (1999) embodies a number of significant assumptions which would not be applicable to Australian conditions. Also, it seems designed to produce "never to be exceeded" levels rather than the upper limit within a range of uncertainties, which is understood to be the intent of the present scope (Appendix A). Indeed the MOMs appear to be more suited philosophically to a planning environment, but come without the benefit of in-built statistical guidance. The adopted MEOW parameter ranges are also of interest, giving a relatively dense coverage in many respects. Applying a similar density to much of the Queensland coast (11.5 runs/km) could require many tens of thousands of simulations. Finally, the US approach would appear to lead towards over-warning, a perception clearly voiced at a recent discussion forum (AMS 2000) attended by a wide range of US interests. Over-warning brings considerable community cost and can also lead to complacency. With the present modelling capabilities available it would seem that a more reliable warning system could be devised, provided that emergency managers are able to react to a greater level of warning detail.

It is noted that the US study is nevertheless comprehensive in terms of its attention to community responses to warnings and evacuations and also the need for extensive transportation modelling. These are aspects which must equally be considered in the Australian context.

E.5 References

AMS (2000) Policy issues in hurricane preparedness and response. Proc of The Weather Channel Forum, Developed by the Atmospheric Policy Program of the American Meteorological Society, Sept.

FEMA *et al.* (1999) Northwest Florida hurricane evacuation study. *Prep by FEMA, NOAA, State of Florida and US Army Corps of Engineers*, July.

Houston, S.H., Shaffer, W.A., Powell, M.D. and Chen, J., 1999: Comparisons of HRD and SLOSH surface wind fields in hurricanes: Implications for storm surge modeling. *Weather and Forecasting*, 14, Oct, 671-686.

Jelesnianski C.P, Chen J. and Shaffer, W.A. (1992) "SLOSH" sea, lake and overland surges from hurricanes. NOAA tech Report, *Dept of Commerce*, NOAA.

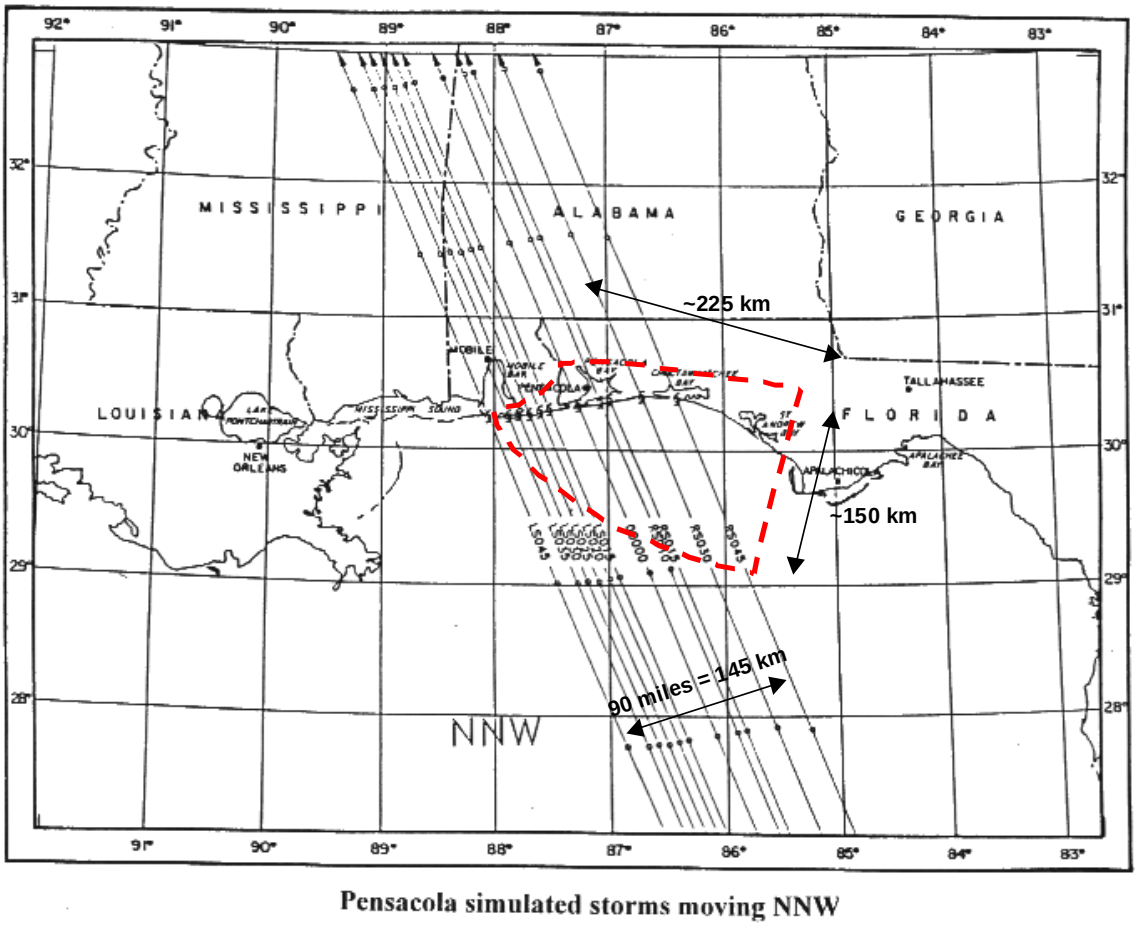

Figure E.1 Example MEOW tracks and model domain (from FEMA *et al.* 1999)

Appendix F Details of Supplied MEOW Model A and B Domains

							Spherical transform reference point				
Name	Grid	Grid Resolution ′ arc	Grid Size X	Grid Size Y	Transformed Longitude of Origin º	Transformed Latitude of Origin º	Longitude º	Latitude º	Transformed Longitude º	Transformed Latitude º	Rotation Angle º
Queensland Coast	A0	7.5	201	57	168	1.5	145	-20	180	0	-60
Southern Queensland Coast	A1	7.5	101	57	180.5	1.5	145	-20	180	0	-60
Central Queensland Coast	A2	7.5	101	57	174.25	1.5	145	-20	180	0	-60
Northern Queensland Coast	A3	7.5	101	57	168	1.5	145	-20	180	0	-60
Gulf of Carpentaria	A4	7.5	105	117	132	-18	0	0	0	0	0
Brisbane	B1	1.5	161	65	179	0.6	152	-26	180	0	-80
Hervey Bay - Gladstone	B2	1.5	153	61	183	0.3	148	-21	180	0	-50
Mackay	B3	1.5	161	125	180	0.2	148	-21	180	0	-50
Whitsunday	B4	1.5	201	101	178	0.1	148	-21	180	0	-50
Townsville	B5	1.5	161	65	178	0.4	147	-20	180	0	-30
Cairns	B6	1.5	177	45	180.6	1.1	143.5	-15	180	0	-70
Cooktown	B7	1.5	161	73	178	0.4	143.5	-15	180	0	-70
Lockhart River	B8	1.5	149	65	176	0.4	143.5	-15	180	0	-70
Torres Strait	B9	1.5	131	141	141	-12.5	0	0	0	0	0
Weipa	B10	1.5	161	41	179	0.2	142	-14	180	0	80
Karumba	B11	1.5	169	49	175.8	0	142	-14	180	0	80
Mornington Island	B12	1.5	161	57	179	0	138	-17	180	0	-30

Appendix G Recommended MEOW Technique for Storm Tide Forecasting

The following outlines the computational steps required to produce a MEOW forecast and addresses the variety of methods which can be used in satisfying the data needs. The development here aims to preserve as much as possible the essential phase relationships inherent in the storm tide interaction, avoiding any simplifications which would otherwise dilute or destroy these elements. In the Australian context this is deemed to be an essential feature of an accurate MEOW forecast system.

G.1 Objective

The *Maximum Envelope of Waters* (MEOW) technique was originally outlined by Jarvinen and Lawrence (1985) as a robust storm tide forecast tool. The objective of the technique is to obtain the maximum forecast water level in a coastal domain due to the close approach and/or landfall of a tropical cyclone. Given that there is always uncertainty in any set of forecast storm parameters, the MEOW represents the prudent approach, or a "least regrets" philosophy, to try to ensure the safe evacuation of affected communities should that be required. On the other hand, forecasts should not be overly conservative to the extent that false alarms are excessive and the community is exposed to unnecessary evacuation risks and disruption, ultimately leading to complacency.

G.2 Background

The basic method has been in use by the US Weather Bureau for many years based on numerical simulations of storm surge using the SLOSH hydrodynamic model (Jelesnianski *et al.* 1992). Guided by climatology, the SLOSH model is applied in a systematic manner to particular sections of coastline (e.g. FEMA *et al.* 1999), the various storm parameters are varied and the pre-computed storm surge results invoked during the forecasting process. Notwithstanding the basic philosophy, the actual technique can be implemented in a number of different ways and the US approach involves significant simplifications in some areas which would not be applicable in Australia. For example, the tidal range is relatively low in the Gulf of Mexico and accordingly the actual tide variation is merely approximated. Also, wave setup is excluded on the basis of the extensive shallow offshore regions. These latter approximations, together with further data reduction by the use of MOMS (MEOWS of MEOWS) may be the reason why there appears to be some present dissatisfaction with the US warning system, leading to the perception that it is overly conservative (AMS 2000).

Besides its philosophical context, the "traditional" MEOW's principal advantage has been in overcoming the computational burden of utilising a sophisticated numerical simulation model of storm surge in a real-time context. In the mid-1980s, for example, the computational overheads of real-time scenario testing of storm tide were prohibitive and a method which pre-computed these estimates was necessary. It also represented a considerable step forward relative to the manual nomogram technique based on the earlier SPLASH model (e.g. Nickerson 1971) not just in utility but also accuracy, since the nomogram methods relied on schematised rather than actual coastlines. The present study has also introduced the potential advantages of parametric methods as a way of reducing the data requirements of pre-computed MEOWs. Present computer capabilities are significantly greater now than when the method was introduced and fast approaching the capability to undertake multiple full scenario simulations. However, the MEOW philosophy remains as the important forecast element,

regardless of the data source being used. The following development therefore concentrates on the MEOW philosophy and comments where appropriate on differences in application depending on the various data sources which could be used.

G.3 Definitions

The following definitions set the scene for the development which follows. A generalised coastal site is considered where the resulting storm tide level over time will be a function of the relative phasing of each of the time-varying components of astronomical tide, imposed storm surge and wave setup.

The variation with time *t* of the normal astronomical tide (to AHD) at any coastal location is described by $[\zeta]_t$ which may be modified by a local tidal anomaly Δ due to background meteorological or other temporary influences not directly related to the incident storm tide. The storm surge is described by $[\eta]_t$ and the wave setup by $[\psi]_t$. The resulting storm tide level $[\xi]_t$ may then be considered (to first order accuracy) as the linear superposition of these various time varying components, such that:

$$[\xi]_t = \{ \Delta + [\zeta]_t + [\eta]_t \} + [\psi]_t \qquad \text{(G.1)}$$

is the time varying *storm tide level* for any coastal site. Here Δ is assumed constant for the duration of the storm tide event and is simply an offset to ensure the temporally local MWL is correctly matched. While there are some (generally) weak non-linearities in regard to overall water depth which influence both the tide and the storm surge these may be neglected initially. On the other hand, wave setup is a strong function of incident wave height, which is a function of water depth. To preserve this relationship, the following procedure ensures that wave setup is calculated only after the tide and surge components are known.

The maximum water level or MEOW is then of interest, together with the time of the maximum, e.g.

$$[\xi]_{t=tmax} = \max ([\xi]_t)_{t=t1,t2} \qquad \text{(G.2)}$$

The MEOW can then be similarly applied across multiple sites, typically along a coastline or even as a 2-dimensional field of elevations if required.

G.4 Basic Methodology

The requirements needed to satisfy Eq (G.1) are now taken in order.

Tidal Anomaly Δ

This is best obtained procedurally in real-time from the relevant State authority and based on actual monitoring of the tide at an appropriate open coast site during the immediate few days and/or hours. The difference between the predicted tide and the measured tide (the residual) over a finite period of record then provides the estimate of the tidal anomaly component. It may be negative or positive depending on the situation but will typically be less than 0.3 m. In the absence of real-time advice, pre-stored seasonal residuals derived from long term tidal analysis could be used as a base reference, assigned to the various *Standard Ports* (see below,

State authorities should be consulted to determine the extent to which seasonal anomalies are already included in the predicted tide and its published harmonic constituents).

Astronomical Tide $[\zeta]_t$

This can be computed from a suitable set of harmonic constituents for each site and/or the most appropriate *Standard Port* in the circumstances. All available constituents should be used, subject to the advice of the relevant State authority, and harmonic reconstitution carried out in an appropriate manner (e.g. Foreman 1977). Resulting levels must be referred to Australian Height Datum (AHD) and tidal plane information also recorded, especially Highest Astronomical Tide (HAT).

Tidal heights and planes at other sites should be based on published range and phase ratios relative to their *Standard Port* or interpolated appropriately as required to form a reference standard. Adjustment of heights and phases relative to the *Standard Port* should be done in accordance with advice from the relevant State authority.

Because the time of landfall and/or peak storm surge is not known *apriori* it remains to construct a vector of tide levels for each site spanning the period of interest (e.g. 24 h) which may then be combined with subsequent storm surge and wave setup time vectors. This can be done efficiently in real-time.

Storm Surge $[\eta]_t$

We now acknowledge that storm surge is a complex function $\mathbf{F}$ of the *nearshore*[10] incident tropical cyclone parameters combined (implicitly here) with the localised bathymetry of the coastal site under consideration.

$$[\eta]_t = \mathbf{F}\,[\, p_0, R, B, V_{fm}, \theta_{fm}, X, \ldots \,]_t \qquad \text{(G.3)}$$

where X represents the perpendicular distance of the storm centre from the site in question. For landfalling tracks X is taken as the perpendicular distance between the site and a straightline approximation of the track at the nominal "landfall" position. A positive X indicates the site is located on the LHS of the storm. The "landfall" position is the intersection of the straightline track and a line representing the coast, aligned at a bearing θ_L relative to north (refer Figure G.1 for details). For near-parallel-coast tracks X is the closest approach distance perpendicular to the straightline approximation to the track. The ellipses "..." indicates that the parameter dependence is likely subject to some variation, either due to developing knowledge of the best representation of these events, or due to local synoptic features and the like (e.g. associated ridging).

Initially, we consider the case of estimating $[\eta]_t$ on the basis of simply the "best track" information, which will vary depending upon the particular data source being utilised, as follows:

(a) Real-time numerical modelling
In this situation, a full scale hydrodynamic model (such as MMUSURGE) is invoked together with a representation of the site bathymetry, the tidal forcing and the surface wind and

[10] *Nearshore* is taken here to imply within 6 to 12 h of landfall or closest approach.

pressure field based on the forecast track parameters. Ideally the latter might be derived from a forecast product (e.g. TCLAPS) but more likely it will be a combination of a parametric wind and pressure field (e.g. Harper and Holland 1999) with merged forecast and/or observation data. Using this approach, $[\eta]_t$ will be obtained directly for all nominated sites, subject to sufficient forecast time being available to run the numerical model in real-time at the desired level of resolution. This direct method is more sensitive to equipment and/or systems failure than (b) or (c) and requires much longer forecast lead times.

(b) Parametric storm surge modelling

This would be an analytic approximation to the site specific storm surge response derived from a series of pre-computed numerical storm surge model simulations (e.g. MMUSURGE as above). The predicted $[\eta]_t$ would be obtained by direct substitution of the forecast track parameters into a site specific response function. The response functions would be derived using techniques similar to that below for the "traditional" MEOW database approach but not utilising the raw data directly. This method offers ease of direct application with very low computational needs but potentially sacrifices some degree of accuracy relative to (a).

(c) Traditional MEOW database

This would involve a real-time data recovery and (linear) interpolation of the forecast track parameters from, as per (b) above, a pre-computed set of discrete numerical model results for the region, i.e.

$$[\eta]_t = \mathbf{I}\,[\, p_0^{\,p}, R^r, B^b, X^x, V_{fm}{}^v, \theta_{fm}{}^\theta, \ldots\,]_t \qquad \text{(G.4)}$$

where $\mathbf{I}$ is an interpolation operator within the n-dimensional parameter space defined by the range of discrete parameter values $\{p, r, b, x, v, \theta, \ldots\}$ obtained from a series of systematic numerical model results. This method can become cumbersome in terms of on-line data and recovery requirements and is necessarily truncated by the available parameter space. It potentially represents comparable accuracy to (b) but with much greater system overheads.[11]

Combined Surge plus Tide Level $[\Phi]_t$

The next step is to combine the $[\eta]_t$ storm surge series with the corresponding tidal anomaly and astronomical tide water levels $[\zeta]_t$, the phasing of which will be dependent on the predicted time of landfall t_l, conceptually:

$$t_l = \boldsymbol{f}\,[V_{fm}, \theta_{fm}] \qquad \text{(G.5)}$$

where $\boldsymbol{f}$ incorporates the (pre-specified) geometric function describing the "coastline" for the purpose of defining "landfall", or closest-approach, intersecting with the forecast vector storm track dependent on the supplied track fixes (t,ϕ,λ)[12].

[11] The US approach here is to retain only maximum $[\eta]_t$ and simplify by removing firstly the variation due to X and then due to V_{fm}, θ_{fm} to produce a MOM. This may result in significant loss of detail for Australian conditions with highly variable coastal features and high tidal range.

[12] In the forecasting context the relative storm fixes and their variability in space at a given time is all that is required to define this geometry. The forecast parameter variation in V_{fm}, θ_{fm} is likewise calculated from the fix.

The phase aligned surge plus tide water level sequence is then:

$$[\Phi]_{t'} = \Delta + [\zeta]_{t''} + [\eta]_{t'} \qquad \text{(G.6)}$$

where t' indicates t phase-aligned at time t_l.

Wave Setup $[\psi]_t$

Analogous to storm surge, wave setup is also a complex function **f** of the incident tropical cyclone parameters combined with the localised bathymetry of the coastal site, but additionally highly sensitive to stillwater level $\Phi_{t''}$ i.e.

$$[\psi]_{t''} = \mathbf{f}\ [\ p_0, R, B, V_{fm}, \theta_{fm}, X, \ldots\ , \Phi]_{t'} \qquad \text{(G.7)}$$

Similarly, wave setup can be estimated by a range of data sources (a), (b) or (c) by substituting the hydrodynamic model with a spectral or other type of wave prediction model, for example, WAMGBR substituted for MMUSURGE.

Combined Storm Tide Level $[\xi]_t$

The total storm tide elevation time series is then:

$$[\xi]_{t'} = [\Phi]_{t'} + [\psi]_{t'} \qquad \text{(G.8)}$$

and the MEOW is accordingly given by Eq (G.2).

G.5 Incorporating Forecast Uncertainty

The above development is based on a single "best track" scenario which is now expanded within the MEOW philosophy to incorporate forecast parameter uncertainty. Within the multiple scenario forecast environment, the MEOW data source module must provide a range of, for example, storm surge levels for the site in question formed by the $n \times m$-dimensional parameter space e.g.

$$[\eta_i]_t = \mathbf{F}\ [\ p_{0i}, R_i, B_i, X_i, V_{fmi}, \theta_{fmi}, \ldots\ ]_t \qquad \text{(G.9)}$$

which is the original n-dimensional parameter space additionally with i=0,1,2,3,... for each of m parameter scenarios.

The multiple parameter cases are determined by expanding the specified forecast uncertainty bounds of each parameter $[\chi] = \{\ p_{0i}, R_i, B_i, X_i, V_{fmi}, \theta_{fmi}, \ldots\}$, viz

i =	0 = expected or mean parameter value	$[\chi]$
	1 = upper bound parameter value; say	$[\chi + \varepsilon_i(\chi)]$
	2 = lower bound parameter value; say	$[\chi - \varepsilon_i(\chi)]$ etc

where $\varepsilon_i(\chi)$ is the parameter error value having cumulative non-exceedance probability $P_i(\chi)$.

An example would be, say, for the uncertainty in forecast central pressure to be assumed to be distributed normally about the mean and an estimate of the standard deviation alone used as the measure of parameter dispersion:

p_{0i}	i=0	940	expected pressure at landfall (hPa)
	i=1	945	based on one standard deviation upper bound $\rightarrow [\varepsilon_1(p_{01}), P_1(p_{01})]$ of [5.0 , 0.8413]
	i=2	935	based on one standard deviation lower bound $\rightarrow [\varepsilon_2(p_{02}), P_2(p_{02})]$ of [5.0 , 0.1587]

This can be extended to as many *i* ordinates as deemed necessary in describing the probability of non-exceedance function for that parameter. In practice, it is unlikely that more than 2 or 3 probability limits per parameter would be chosen but it may be desirable to include skewness (unequal upper and lower intervals etc) depending on the particular forecast trends. If the information can be related to climatology then a more detailed set of probability ordinates could be used as the defaults.

The above is extended to include variability in regard to the time of landfall, thus providing a range of phase alignments with the storm surge, as well as wave setup. The MEOW at a single site then becomes:

$$[\xi_i]_{t=tmax} = \max \{ ([\xi_i]_t)_{t=t1,t2} \}_{i=0,m} \quad \text{(G.10)}$$

Assuming independence of each parameter uncertainty, the marginal probability of each scenario is then retained and accumulated as Π, the multiplicative sum of each component probability, such that:

$$Prob\,[\xi_i]_{t=tmax} = \Pi\{ P_i(\xi_i) \}_{i=0,m} \quad \text{(G.11)}$$

Graphing of $\{ [\xi_i]_{t=tmax}$ versus $Prob[\xi_i]_{t=tmax} \}$ will then permit consideration of the probabilistic variability in the storm tide predictions, for example, the extent to which the MEOW is more or less likely than a range of other water levels on that day. This will enable a degree of judgement to be exercised in addition to the single MEOW level being forecast for a site.

G.6 References

AMS (2000) Policy issues in hurricane preparedness and response. Proc of The Weather Channel Forum, Developed by the *Atmospheric Policy Program of the American Meteorological Society*, Sept.

FEMA *et al.* (1999) Northwest Florida hurricane evacuation study. *Prep by FEMA, NOAA, State of Florida and US Army Corps of Engineers*, July.

Foreman M.G.G. (1977) Manual for tidal heights analysis and prediction. Report 77-10, *Institute of Ocean Sciences*, Patricia Bay.

Harper B.A. and Holland G.J. (1999) An updated parametric model of the tropical cyclone. Proc. 23rd Conf. Hurricanes and Tropical Meteorology, *American Meteorological Society*, Dallas, Texas, 10-15 Jan.

Jarvinen B.R. and Lawrence M.B. (1985) An evaluation of the SLOSH storm-surge model. *Bull. Am. Met. Soc.*, 66(11),1408-1411.

Jelesnianski C.P, Chen J. and Shaffer, W.A. (1992) "SLOSH" sea, lake and overland surges from hurricanes. NOAA tech Report, *Dept of Commerce*, NOAA.

Nickerson J.W. (1971) Storm Surge Forecasting. *Navy Weather Research Facility*, Tech Report 10-71.

Sanderson B., Tang Y.M., Holland G., Grimshaw R. and Woodcock F. (1995) A tropical cyclone maximum envelope of waters (MEOW) technique. *Bureau of Meteorology*, BMRC Res. Rep. No. 51, Oct, 19pp.

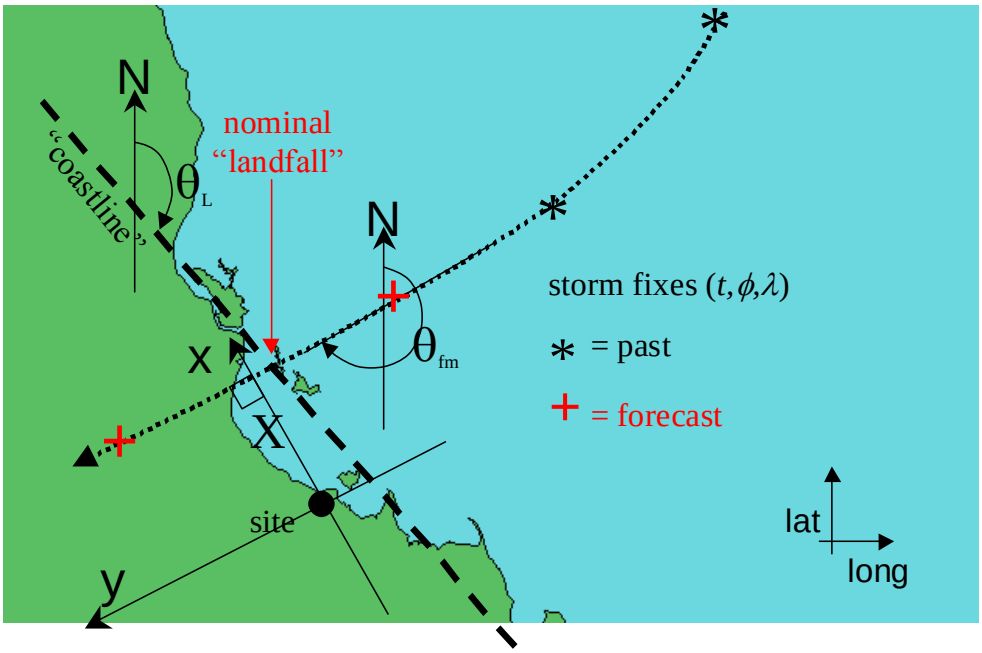

Figure G.1 Definition of storm proximity X, landfall position and coastline.

Appendix H MEOW Database Requirements and Storage Costs

This appendix addresses workscope Item A-4 and is based on the development of MEOW data generation scenarios in Section 11.5.

H.1 Storage Requirements and Indicative Costs

The "desirable" Scenario 2 suggests order-of-magnitude data storage would be 550 GB for a **B** grid resolution 24 h duration MEOW for the whole Queensland coast, storing only data within 10 grid points of the shore. If all data points were to be stored this would increase to the order of 7000 GB.

Whilst the data storage even for the recommended 550 GB case is non-trivial, the data relationships are relatively simple and information retrieval is unlikely to rely on the use of a complex database system (refer next section). Nevertheless, it may be more convenient to simply adopt Bureau of Meteorology standard (e.g. netCDF™ or Oracle™) interfaces and post-process the surge model data to suit. It is not presently possible to estimate whether this post-processing activity itself might represent any significant CPU requirement.

Notwithstanding the above, not all of the 550 GB of data would be required at any one time and only the data sets specifically relevant to the forecast problem need be retrieved from an archive storage medium (e.g. DAT tape or DVD). This could reduce the online data requirements to the order of 150 GB or possibly less, assuming a target domain and the two adjacent domains' data were to be retrieved. Hence, assuming off-line storage requirements are of the order of 500 GB, present readily available DAT technology of 40 GB/tape would require only 12 tapes but with (say) 2 backup copies, totalling 36 tapes. Retrieval time of the 500 GB would be approximately 1 days at 20 GB/h. Assuming the online requirement at any one time is only 150 GB, retrieval time would be less than 7 h to establish the immediate domain requirements. Online storage would be by (say) 40 GB SCSI HDD, requiring 4 in total.

Assuming a dedicated workstation is desirable for operational purposes, the following hardware costs are indicative:

Base workstation	$ 5000
DAT facility	$10000
HDD online	$10000
Total:	$25000

Duplication of at least the DAT facility and HDD storage (e.g. RAID) would also be recommended for operational purposes, yielding an overall facility capital expenditure of the order of **$50000**. The DAT archive would require ongoing maintenance throughout its life, probably requiring transfer to DVD at some future time to preserve data quality. As noted in Section 11.5, it is likely a dedicated Bureau officer would also be required to oversee the production.

An alternative to the above "in-house" production option would be to seek external supply under contract, which would ensure Bureau resources are not diminished during this phase.

H.2 Suggested Data Base Structure

It is recommended that MEOW data sets be retained as a simple series of flat data files, identified by a systematic filenaming convention. Each model simulation will represent the result of a given set of MEOW parameters for a particular domain. Each set of results can then logically be retained in a directory with the domain name as the principal or key "data base" identifier.

Each MEOW file will need to retain a timeseries of "snapshots" of (time-stamped) water levels covering the output sub-set of the domain (i.e. within 10 grid points of shore) at the chosen space and time resolution. For **B** grids this will be 2.8 km and a chosen multiple of 900 s, say 1800 s.

It is proposed that a unique filename be constructed based on the point estimates of the various parameters describing each simulation, viz

The parameters envisaged (as per Appendix G) are:

$p_0{}^p$	central pressure (or pressure deficit)	hPa
R^r	radius to maximum winds	km
B^b	wind field peakedness	-
X^x	distance from target	km
$V_{fm}{}^v$	forward speed	m s^{-1}
$\theta_{fm}{}^\theta$	track bearing	°
$\theta_{max}{}^{\theta'}$	wind field asymmetry (if adopted)	°

The resulting filename would then be, for example,:

$p\_r\_b\_x\_v\_\theta\_\theta'$.meow

where each of the above (*p,r,b,* etc) would be substituted by the specific point parameter used.

A typical path and filename under these rules might be:

Hervey_Bay/40_30_1_100_2_180_65.meow

Alternatively, each parameter point value could be allocated a simple index (1,2,3 etc) and the filename again concatenated in the same sequence, e.g.

Hervey_Bay/2_2_1_4_1_9_1.meow

where the first index (2) refers to the 2nd point value of *p* for the Hervey Bay domain.

The latter naming method would facilitate name generation and retrieval whereas the former would suit visual identification.

To reconstruct the MEOW forecast, as described in Appendix G, a number of data files would need to be retrieved and the time series of stored data overlaid with tidal data to construct the actual MEOW forecast.